PETROGENESIS OF NI-CU ORE BODIES, THEIR HOST ROCKS AND COUNTRY ROCKS AT SELEBI-PHIKWE, EASTERN BOTSWANA

By Peter James Brown 1987

UNIVERSITY OF SOUTHAMPTON

ABSTRACT

FACULTY OF SCIENCE
GEOLOGY

Doctor of Philosophy

PETROGENESIS OF NI-CU ORE BODIES, THEIR HOST ROCKS AND COUNTRY ROCKS AT SELEBI-PHIKWE, EASTERN BOTSWANA

by Peter James Brown

The Phikwe, Selebi and Selebi North Ni-Cu sulphide deposits occur in highly deformed and metamorphosed Archaean gneisses near the north margin of the Central Zone of the Limpopo Belt. The ores and host rocks have suffered all the phases of deformation that have affected the enclosing gneisses. Nappes and thrusts formed during the first deformation period, during which granulite facies conditions of 800° C and 10 kbar (accompanied by minor partial melting) were attained. Sheets of anorthosite were thrust into the sequence during late D1 time.

The main components of the Selebi-Phikwe sequence are hornblende gneiss, grey leucocratic gneiss and anorthositic gneiss. Granitic gneiss represents post-D1 granitic intrusions, not a basement or a sandstone unit as previously proposed. The hornblende gneiss has the geochemistry of a suite of variably altered fractionated tholeiitic basalts and Ti-rich ferrobasalts. Low-Ca biotite gneiss associated with hornblende gneiss represents a variety of basalt-derived rocks ranging from in situ alteration products to volcaniclastic and pelitic sediments. Lithological associations indicate that the hornblende gneiss represents both extrusive and high-level intrusive basalt. The grey gneiss has the geochemistry of a calc-alkaline suite. The mineralogical and chemical variation shown by the grey gneiss indicate a volcano-sedimentary rather than an intrusive origin. The protoliths of the anorthositic gneiss were gabbroic plagioclase-clinopyroxene cumulates. Ultramafic lenses within the sequence were olivine and clinopyroxene-rich cumulates. Minor components of the gneiss sequence are magnetite quartzite representing chemically precipitated silica-iron oxide sediment and associated cummingtonite-actinolite amphibolites representing mixtures of Mg-clays and carbonate.

The three Ni-Cu ore bodies are intimately associated with a layer of hornblende-plagioclase amphibolite plus minor pyroxenite within grey gneiss. The ore bodies consist of Ni-rich massive sulphides and Cu-rich disseminations. Metamorphism of the host rocks was mainly isochemical. Localised shearing resulted in higher contents of Ti, K, P, Nb, Rb, Y and Zr and lower contents of Ca. Fe-rich garnet amphibolite resulted from reaction between sulphide and silicate. The variation in host rock chemistry between the three ore bodies can be modelled in terms of mixtures of cumulus olivine and plagioclase, basaltic liquid and syngenetic immiscible massive and disseminated sulphide. The host amphibolite represents a tholeiitic intrusive mush. Chemical variation within the host body was due to a combination of flow differentiation during mush emplacement and later gravitational settling. Deformation resulted in physical remobilisation of massive sulphides and chemical mobilisation of Cu, Ni and S relative to Fe.

The subeconomic Ni-Cu sulphide-bearing ultramafic rocks at Dikoloti and Lentswe were tholeiitic cumulates, which were intruded or thrust into the sequence. The Selebi-Phikwe and Dikoloti-Lentswe host rocks and sulphides were comagmatic with the country-rock hornblende gneiss (tholeiitic basalts and ferrobasalts). The concentration of S in the ore bodies was due to magmatic processes in periodically replenished tholeiitic magma systems. The rocks at Selebi-Phikwe are more like those of a greenstone belt than a high-grade quartzite-marble-anorthosite association. They have affinities with oceanic crust.

ACKNOWLEDGEMENTS

This project was undertaken while I was in receipt of a N.E.R.C. research studentship.

Thanks are due to all those past and present employees at BCL who helped me with my work in Botswana.

I am grateful for the assistance given by members of the technical and other staff in the Department of Geology at the University of Southampton. Special thanks are due to Keith Gosden (geochemistry), Barry Marsh (photography) and Bob Jones, Clive Balcombe and Jane Hill (thin and polished sections). Pete Harvey at Nottingham made facilities available for repeat analyses. Andy Tindle at the Open University was very helpful with probe-work. An award from the Institution of Mining and Metallurgy (G. Vernon-Hobson bequest) which enabled me to go on a field excursion in South Africa is gratefully acknowledged.

Discussions about the project were held with people too numerous to acknowledge individually. Their encouragement was invaluable. I would like to thank Nick Badham who conceived and supervised the project and reviewed the thesis. I would also to thank Bob Nesbitt for reviewing the thesis.

List of Contents

CHAPTER 4 GEOCHEMISTRY AND ORIGIN OF THE SELEBI-PHIKWE GNEISSES

CHAPTER 5 THE SELEBI-PHIKWE NI-CU ORE BODIES

CHAPTER 6 THE SELEBI-PHIKWE SULPIDES

List of Figures

List of Tables

Frontispiece

(A) Contact of massive sulphide layer (Type 2) with grey gneiss, Phikwe - Zone E.

(B) "Durchbewegung" - host amphibolite inclusions in massive sulphide (Type 2), Phikwe -Zone E. Note chalcopyrite in pressure shadows.

(C) Vein quartz inclusions in massive sulphide, Phikwe - Zone E.

(D) Tongue of host amphibolite into massive sulphide (Type 2), Selebi. Upper Body.

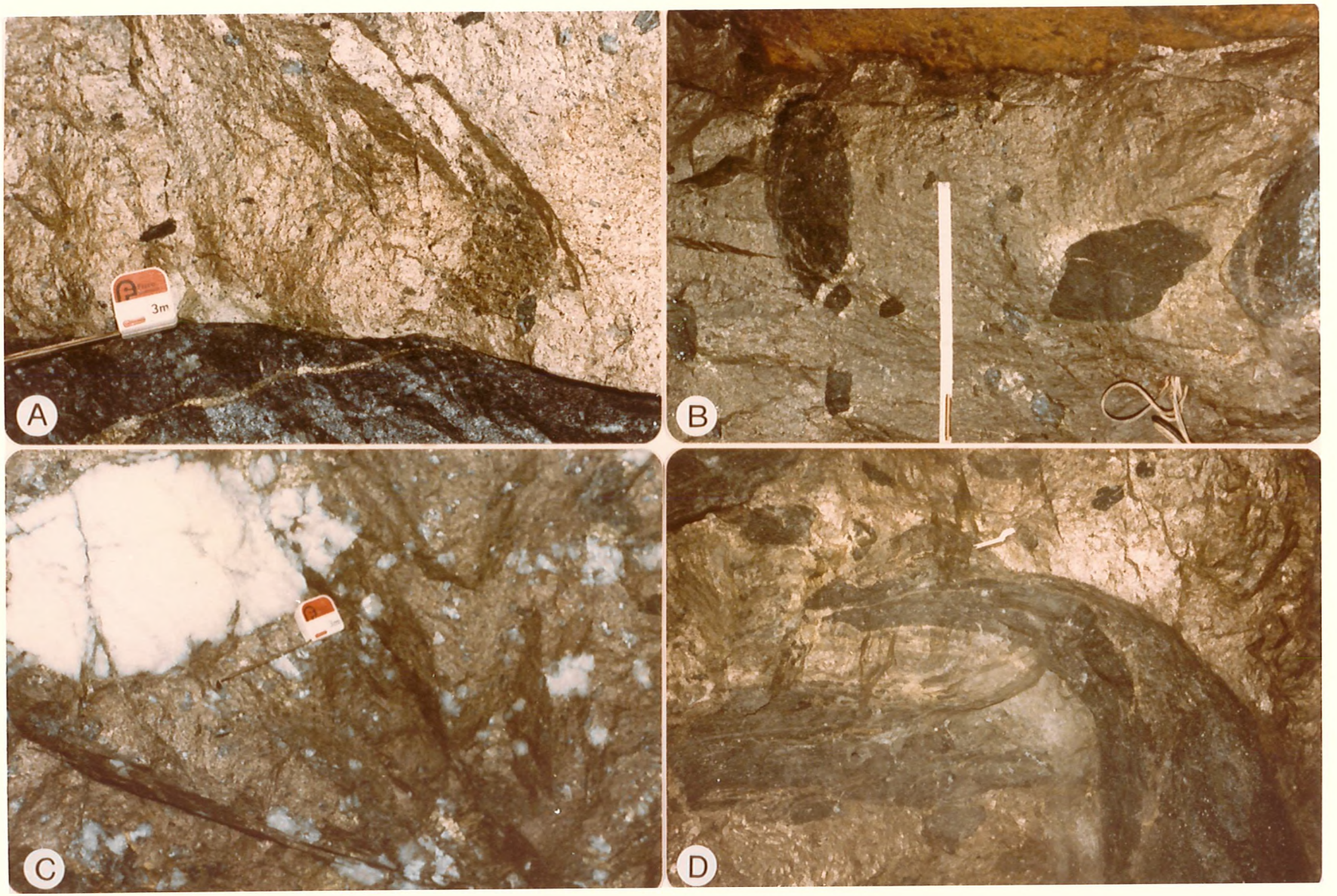
3m
A
B
C
D

CHAPTER ONE INTRODUCTION

1.1 INTRODUCTION

This thesis deals with the nickel-copper deposits of eastern Botswana, principally the Selebi-Phikwe ore bodies - Selebi, Phikwe and Selebi North, the only ones currently being mined (Fig. 1.1). The Selebi deposit (Gordon 1973) and a smaller occurrence at Dikoloti (Marsh 1978), were discovered by BCL - Bamangwato Concessions Limited (BotswanaRST) in late 1962 during reconnaissance soil geochemistry. Systematic soil sampling led to the discovery in 1966 of the Selebi North and Phikwe deposits, respectively 7.5 and 14.5 km northeast of Selebi, and the Lentswe prospect. Ni-Cu mineralisation was also discovered at about the same time at Phoenix, Selkirk and Tekwani (Fig. 1.1) during a reinvestigation of old gold prospects (Key 1976; Baldock et al. 1976). These prospects were evaluated by Sedge Botswana (Pty.) Limited, a subsidiary of Anglo American.

The establishment of the Phikwe and Selebi mines has rapidly changed a remote, sparsely populated area, which previously supported only cattle herding and subsistence agriculture, into Botswana's third town. Underground exploration development started at Phikwe and Selebi in 1967, with underground and open-cast production commencing at Phikwe in late 1973. Opencast production at Phikwe ceased in 1981. Underground production at Selebi started in 1976. Underground exploration development started at Selebi North in 1981.

The climate of eastern Botswana is dry subtropical with average maximum summer and winter temperatures of 32 and 27 C. The annual rainfall varies greatly but averages 419 mm, with most falling during thunderstorms in the summer months from October to April. The topography of the Selebi-Phikwe area is a flat, sand-covered pediment, 870 m above sea level, broken only by inselbergs and koppies of more resistant granitoid gneisses (Key 1976). Exposure is poor, apart from inselbergs and in some of the usually dry drainages. The vegetation is mainly mopane and acacia bush and woodland. Relatively large flat exposures are often hidden from view by thick bush. Despite poor exposure, photogeological expression is very good, due to slight changes in soil and vegetation (Plate 1). Access within the area is by a network of small tracks, best suited to 4-wheel drive vehicles.

1.2 PREVIOUS WORK

The geology of eastern Botswana has been investigated by three

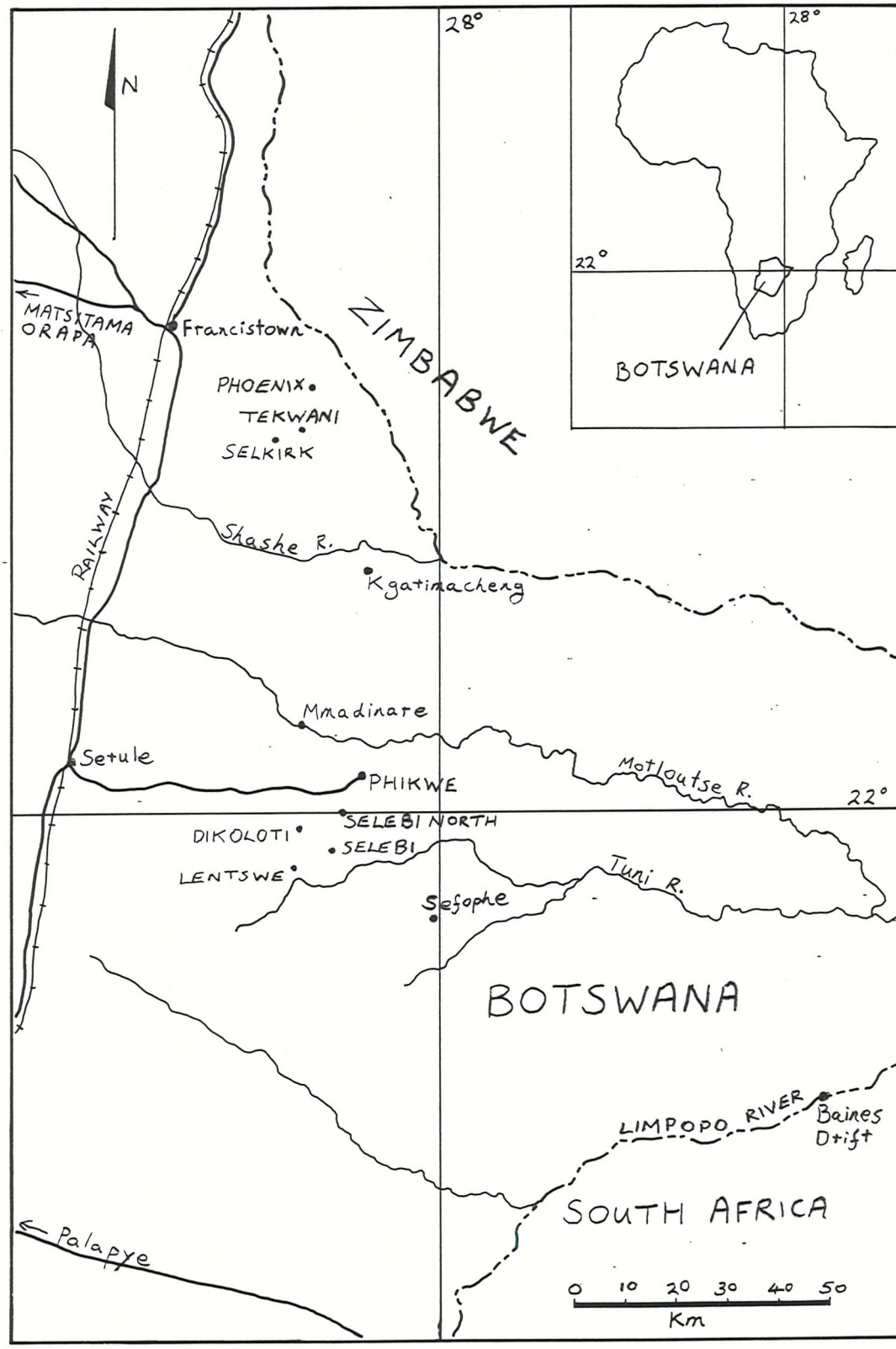

Fig 1.1 SELEBI-PHIKWE LOCALITY MAP

groups: the Botswana Geological survey, BCL and Leeds University.

The Botswana Geological survey has mapped eastern Botswana, from the Archaean granite-greenstone terrain of the Rhodesian Craton in the north, to the highly metamorphosed and multiply deformed rocks of the Limpopo Belt in the south (Figs 1.2 & 1.3), in a variety of detail (Key 1977). (The geological term "Rhodesian Craton" has been retained instead of converting to "Zimbabwean Craton".) The most relevant reports of their early work are those by Thomas (1970) on the Selebi area and Bennett (1971a) on the Magogaphate area. This early work has been synthesised by Bennett (1970, 1971b, 1972, 1973). A thesis by Mason (1970) covers the geology from Francistown to Mmadinare and includes the Selebi-Phikwe area. Key (1976) remapped the same area as part of the Survey's "Eastern Geotraverse" (Litherland & Key 1974; Key et al. 1976), from the Vumba greenstone belt of the Rhodesian Craton, through the Northern Marginal Zone, to the Central Zone of the Limpopo Belt (Figs. 1.2 & 1.3). Key (1976) briefly described the Phikwe ore body of the Limpopo Belt and the Phoenix, Selkirk and Tekwani prospects of the Tati greenstone belt, including 4 chemical analyses of the Selkirk and Tekwani host metagabbros.

Geologists of BCL have mapped in eastern Botswana from Kgarimacheng in the Tati greenstone belt in the north to the Limpopo River during the course of mineral exploration. Lear (1971) described several ultramafic bodies found in the Central Zone, and included a short discussion on the host rocks to the Ni-Cu mineralisation at Selebi-Phikwe and Dikoloti. The Selebi North deposit has been described by McKechnie (1971). The first published description of the Selebi-Phikwe deposits was by Gordon (1973), who thought that all three Selebi-Phikwe ore bodies are hosted by the same sill-like body of amphibolite, repeated by folding. Gordon (1973) published 4 chemical analyses of the host rocks. Lear (1977, 1979) briefly described the mineralogy of the Selebi-Phikwe ores and discussed the origin of the ore bodies. Marsh (1978) described the Dikoloti and Lentswe occurrences, including 3 analyses of their host rocks which, in contrast to the amphibolite at Selebi-Phikwe, are mainly metapyroxenite and metaperidotite. Marsh (1978) concluded that the host rocks and sulphides at Dikoloti and Lentswe did not have a common magmatic origin with those at Selebi-Phikwe and that they were not related. Recently BCL geologists (Gallon 1986) have suggested that the gneisses at Selebi-Phikwe were mainly sedimentary in origin, with some of the granitic gneisses having been arkosic sandstones, anorthositic

gneisses having been calcareous sediments and the host amphibolite possibly having been sedimentary.

The Leeds group (Coward and co-workers) have concentrated on the structure of the Limpopo Belt, particularly the northern margin (Coward et al. 1973, 1976a; Wright 1973, 1974). The deformation pattern of the Tati greenstone belt has been described by Coward (1973) and Coward & James (1974). Coward et al. (1976b) and Wright (1977) have constructed successions at several localities from the Limpopo Belt to the Rhodesian Craton, particularly at Sefhope, Phikwe and Kgarimacheng.

The most relevant of the Leeds work is by Wakefield (a former BCL employee), who studied the structural and metamorphic history of the Selebi-Phikwe area (Wakefield 1971, 1972, 1974, 1977a, 1977b), and described the Phikwe deposit. He included 4 new chemical analyses of Phikwe host rocks (Wakefield 1973, 1974, 1976). These indicated that the Phikwe host amphibolite has a troctolitic composition. Dumbbell-shaped sulphide blebs in a small ultramafic pod in the host amphibolite led Wakefield (1973, 1974, 1976) to conclude that the ore was emplaced as an immiscible sulphide magma along with an olivine mush into the pre-existing troctolite. The host amphibolite and associated sulphides subsequently suffered all the high-grade tectono-metamorphic events of the Limpopo Belt (Wakefield 1974, 1976).

Van Breemen and co-workers from Leeds found evidence for two widely separated isotopic events in the Limpopo Belt of eastern Botswana, about 2,700 and 2,000 Ma (Van Breemen et al. 1966; Van Breemen 1970; Van Breemen & Dodson 1972; Hickman & Wakefield 1975; Hickman 1976). They also recorded a metamorphic age of 2630* $\pm$ 70 Ma for the Selkirk volcanics in the Tati greenstone belt. Hickman & Wakefield (1975) working on gneisses from Selebi-Phikwe related these ages to tectono-metamorphic events in the area, with the first metamorphism at 2720* $\pm$ 40 Ma. (Unless otherwise stated, ages quoted in this thesis are Rb-Sr whole-rock isochron ages using 1.42 as the decay constant of Rb87. Ages indicated * have been recalculated using 1.42).

1.3 THE LIMPOPO BELT

1.3.1 Introduction

The Limpopo Belt was first recognised by Macgregor (1953) as a major east-northeast-trending zone of high-grade metamorphic tectonites in Botswana, Zimbabwe and South Africa, separating the

Archaean granite-greenstone terrains of the Rhodesian and Kaapvaal Cratons (Figs 1.2 & 1.3). The Belt had a long tectono-metamorphic history from its initiation in the early Archaean (3570 Ma suggested by Barton & Key, 1981) to approximately 2000 Ma (Hickman & Wakefield 1975; Watkeys 1983). Included within the Limpopo Belt are the oldest recognised rocks in Africa, the Sand River Gneisses, which have yielded a metamorphic age of 3790 $\pm$ 61 Ma (Barton et al. 1978, 1983b; Fripp 1981, 1983). The Belt is approximately 700 km long and up to 250 km wide (Watkeys 1983). However the main Limpopo deformation extends well into the flanking cratons (Coward 1976; Key et al. 1976), as far as the Gwanda greenstone belt to the north (Wright 1974) and Murchison to the south (Graham 1974). The limiting boundaries are arbitrarily taken to be the orthopyroxene isograds (Fig. 1.2).

Both ends of the Belt are obscured by later sedimentary sequences. In the west the Belt either extends under Kalahari and Karoo sequences to the Kalahari and Makgadikgadi Lines in Central Botswana (Fig. 1.3) (Reeves 1976; Barton & Key 1981; Barton 1983a) or expires just a short distance into the Kalahari Basin (Reeves & Hutchinson 1975; Key & Hutton 1976). In the east after disappearing under Proterozoic and Phanerozoic sedimentary cover, the Belt is overprinted by the Pan-African Mozambique Belt. It is possible that further portions of the Limpopo Belt exist to the east in Dronning Maud Land, Antarctica (Barton 1983a) and Madagascar.

1.3.2 Subdivision of the Belt

The tectonic subdivision of the Limpopo Belt into Northern and Southern Marginal Zones, with predominantly east-northeast-trending structures, separated by a Central Zone of north-trending structures (Cox et al. 1965) was later rationalised with lithostratigraphic differences by Mason (1973) (Fig. 1.3). These works have provided a valuable framework, although the symmetry implied can be disputed. Highly metamorphosed equivalents of the flanking Archaean granite-greenstone terrains comprise the Northern Marginal Zone (Robertson 1973, 1974; Key 1976; Key et al. 1976) and the Southern Marginal Zone (Du Toit & Van Reenan 1977; Du Toit et al. 1983). Between them is the Central Zone with a different Archaean stratigraphy, including supracrustal cover sequences and layered igneous complexes (Key 1977; Barton et al. 1979a; Fripp 1983; Watkeys et al. 1983).

Of the recent reviews of the Limpopo Belt (Robertson & Du Toit 1981; Barton & Key 1981; Light 1982; Tankard et al. 1982), the

Legend for Figure 1.2

Map based on Watkeys 1983

Shear

Thrust

Fault-only a few selected

Orthopyroxene Isograd

Tectonic Fabric

Kalahari sands

Cretaceous sandstones

Nuanetsi Igneous Complex c.190 Ma

Karoo Carboniferous to Triassic intracratonic sediments overlain by Jurassic volcanics

Waterberg, Soutpansberg, Palapye and Umkondo Groups Mid-Proterozoic red beds and volcanics

Bushveld Complex c.2100 Ma BC
Great Dyke c.2500 Ma GD

Mahalapye Complex c.2200 Ma
granites
migmatites

Porphyroblastic granites and gneisses inc. Bulai c.2700 Ma

Limpopo Gneisses containing meta. supracrustals and anorthosites, Beit Bridge, Baines Drift and G2 Gneisses younger in Botswana ?

Sand River Gneisses c.3800 Ma
Zanzibar Gneisses basement ?

Limpopo Belt Central Zone

Younger Granites porphyroblastic

Greenstones

Shamvian sediments c.2650 Ma

Upper Bulawayan, Tati c.2700 Ma

Lower Bulawayan, Tutume c.2900 Ma

Sebakwian c.3500 Ma
undated in the Kaapvaal Craton

Older Gneisses various granites and tonalitic-granitic gneisses from pre-Sebakwian? to Bulawayan

high grade in Marginal Zones

low to medium grade

Rhodesian and Kaapvaal Cratons
Marginal Zones of the Limpopo Belt

Locations

A Alldays
B Bulai
BB Beit Bridge
BD Baines Drift
F Francistown
K Kgarimacheng
M Messina
Mh Mahalapye
Mk Matok
P Phoenix
Pa Palapye
S Selkirk
Se Sefhope
SP Selebi-Phikwe
SR Sand River
Z Zanzibar

Greenstone Belts

G Gwanda
Ma Matsitama
Mu Murchison
Pi Pietersburg
Su Sutherland
T Tati
V Vumba

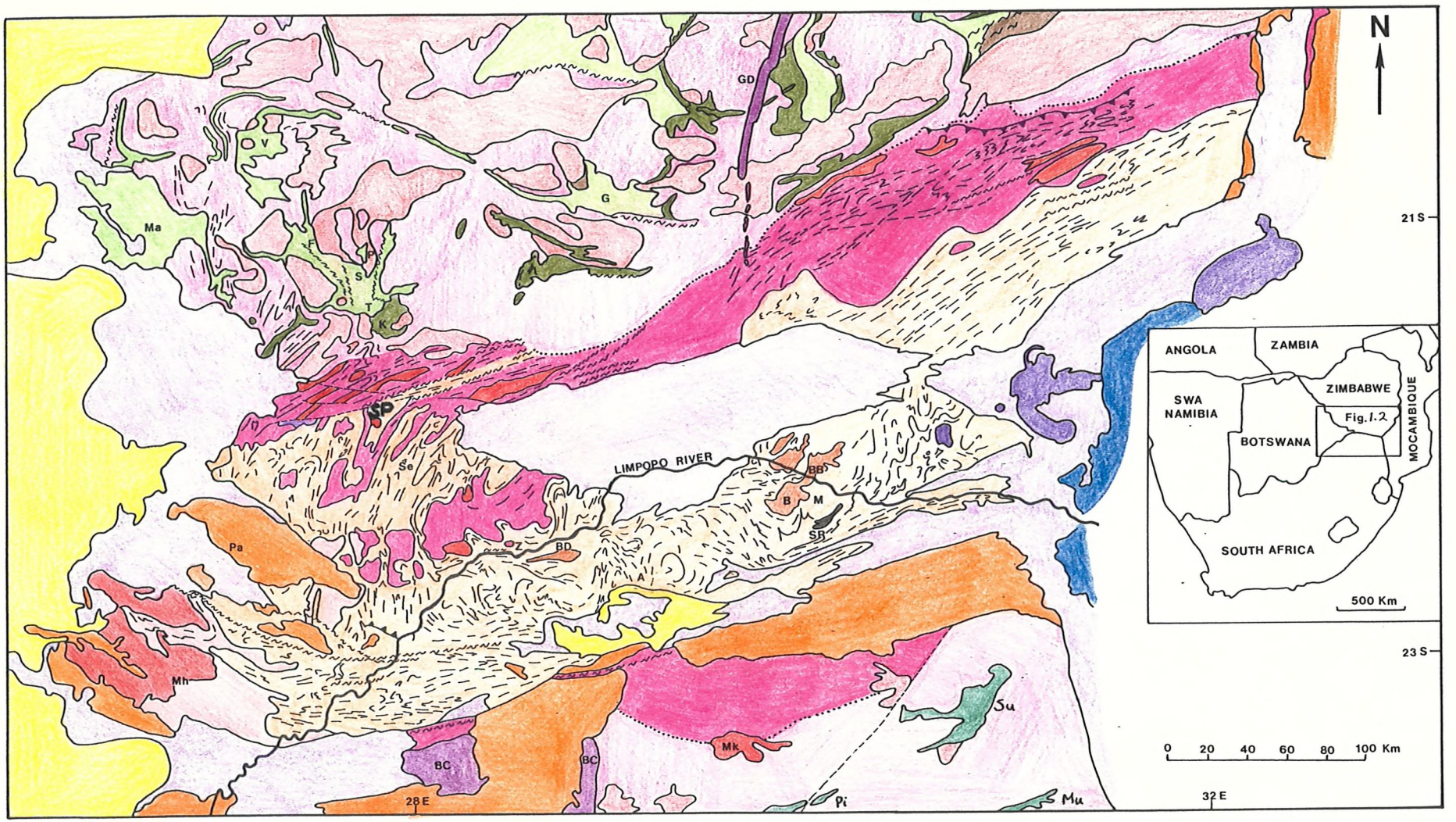

Figure I.2 Geological Map of the Limpopo Belt

approach of Watkeys (1983) is regarded here as both the simplest and potentially most rewarding. Watkeys (1983) subdivided the belt into seven tectono-stratigraphic domains, each with its own internal stratigraphic, structural and metamorphic histories (Fig. 1.3). Domain I, adjacent to the Rhodesian Craton, consists of high-grade equivalents of the granite-greenstone terrain. It has been interpreted as a wide ductile shear zone (Coward et al. 1976). In the west, a gradational structural contact is apparent through the Tuli-Sabi Straightening Zone (Bennett 1970; Key & Hutton 1976). Within Domain II the lithologies of the Central Zone and the Rhodesian Craton are juxtaposed in a wide dextral straightening zone (Light et al. 1977). Watkeys (1983) has shown Domain III, in which the Selebi-Phikwe ore bodies are situated, as consisting of Central Zone Limpopo gneisses and high-grade equivalents of the "Older Gneisses" of the Rhodesian Craton. Both Domains II and III seem to merge into Domain IV through the disappearance of the cratonic lithologies (Watkeys 1983). Domain V is a sinistral shear zone (Bahnemann 1972), which was reactivated to form post-Limpopo sedimentary troughs (Jansen 1975). Domain VII, the southernmost portion of the Limpopo Belt, consists of high-grade lithologies that have been correlated with the Kaapvaal Craton. Domain VII may coalesce with the lower-grade cratonic rocks by a decrease in metamorphic grade, without any structural discontinuity, as represented by the Hout River Transition (Du Toit & Van Reenen 1977). However the contact is possibly a sinistral shear zone (Watkeys 1983).

1.3.3. The Central Zone in the Messina-Beit Bridge Area

The Central Zone supracrustal gneisses including those in Domain III which host the Selebi-Phikwe ore bodies are generally grouped together as though they are all the same suite and the same approximate age (e.g. 3.3-3.5 Ga, Barton & Key 1981). However there has been little comparative work between different areas of the Central Zone and it is possible that the Central Zone supracrustals vary significantly in lithology, setting and age. The Selebi-Phikwe gneisses need to be compared to those in the rest of the Central Zone, particularly in the key Messina-Beit Bridge (M-BB) area, and to the greenstone belts to the north.

The Central Zone has been best studied in Domain IV, particularly the M-BB area (Fig. 1.2), where it is characterised by ancient basement, well-developed supracrustal sequences and major anorthositic igneous complexes, all metamorphosed to granulite or amphibolite

facies (Sohnge 1945; Bahnemann 1972) (Table 1.1). Undisputed basement has only been mapped in the Sand River area southeast of Messina (Fripp 1981, 1983). The basement Sand River Gneisses (3790 Ma, Barton et al. 1983b) are tightly infolded and possibly thrusted within the supracrustal Beit Bridge Gneisses (BBG). The Sand River Gneisses are cut by deformed and metamorphosed mafic dykes of two distinct ages, 3570 Ma and 3060 Ma (Barton et al. 1977).

The supracrustal BBG and similar lithological groups further west form most of the Central Zone in Domain IV. There are no reliable way-up criteria and there is much duplication by isoclinal folding and imbricate thrusting. Table 1.1 is only a pseudo-stratigraphic column. Conspicuous within the BBG are a quartzite-pyroxene amphibolite association and a pelitic gneiss-banded iron formation association and minor calc-silicate gneiss and marble (Jacobsen 1974; Brandl 1983; Fripp 1983). However much of the area is composed of less prominent variably garnetiferous quartzofeldspathic gneiss (Barton 1983a). Calc-silicate gneiss and marble are abundant near the southern margin of the Central Zone, whereas banded iron formation occurs more commonly near the centre (Horrocks 1983a). The BBG are thought to represent a relatively thin, predominantly sedimentary sequence deposited in a broad basin under shallow water (Sohnge et al. 1948; Bahnemann 1972; Mason 1973; Coward et al. 1976b; Light & Watkeys 1977). However the association of basic volcanism (now represented by amphibolite and hornblende gneiss), cherts (some of the thinner quartzites) and banded iron formation suggests an oceanic environment (Fripp 1983). The origin of the various volumetrically significant quartzo-feldspathic gneisses is an important problem (Barton 1983a). For example the Singelele Gneiss has been interpreted as either representing felsic volcanic or volcaniclastic rocks (Fripp et al. 1979; Fripp 1983) or as being a granitic intrusive derived by partial melting of the basement (Sohnge 1945; Bahnemann 1972, 1973; Barton 1983a; Watkeys et al.1983).

Conformable sheets of metamorphosed anorthosite and leucogabbro (Hor et al. 1975) are intimately associated with the BBG, often near their contact with the Sand River Gneisses. (The description metamorphosed and the prefix "meta" will be omitted for convenience, when describing the Limpopo anorthosites, gabbros and associated ultramafic rocks.) Minor layers and pods of pyroxenite and serpentinised peridotite and dunite occur adjacent to and concordant with the layers of anorthosite and leucogabbro. Barton et al.(1979a) included them all in their Messina Layered Intrusion (MLI). However similar pyroxenites

and serpentinites also occur within the BBG without any associated anorthosites and Light et al. (1977), Brown (1981a,b) and Watkeys et al. (1983) noted the association of this ultramafic suite with banded iron-formations. Light et al. (1977) and Light & Watkeys (1977) still included these ultramafic rocks along with anorthosites in a layered igneous complex. However Brown (1981a,b) and Watkeys et al. (1983) tentatively suggested that this separate ultramafic suite has affinities with komatiites which are typical of Archaean greenstone belts.

The last major unit within Domain IV in the M-BB area is the Bulai Gneiss, a grouping which includes several syntectonic plutons composed of porphyroblastic granitic gneiss (Sohnge 1945; Watkeys et al. 1983).

The relationships between these various units in the M-BB area are not clear and their isotopic ages are seldom discriminatory. The contacts between the basement Sand River Gneisses, the supracrustal BBG and the MLI are planar and tectonic. None of the older 3570 Ma dykes has been found cutting the BBG (Barton 1983a). The BBG are usually assumed to have been deposited unconformably on the already deformed Sand River Gneisses (Barton 1983a; Watkeys et al. 1983). However it is possible that the Sand River Gneisses were thrust into contact with the BBG and that they are not the true basement upon which the BBG were deposited (Fripp 1981; Barton 1983a). Xenoliths of possible supracrustal quartzite in the MLI indicate that it was intruded into both the Sand River and Beit Bridge Gneisses (Barton 1983a). However Fripp (1983) regards this as inconclusive and suggests that the MLI is older than the BBG.

In the rest of the Central Zone the direct correlation of the Limpopo Gneisses with those in the M-BB area and their subdivision into equivalent basement and supracrustal cover has proven difficult. Rare slivers of basement equivalent to the Sand River Gneisses have only been mapped to the north in Zimbabwe (Watkeys et al. 1983). BBG can be traced westwards in Domain IV, past Alldays (Brown, unpub. data 1976). Further west in Domain IV in Botswana, similar supracrustal and anorthositic gneisses have been mapped as the Baines Drift Formation by Mason (1967) who was the first to include quartzo-feldspathic gneiss as well as obvious metasediments into a Limpopo supracrustal group. Nearby at Zanzibar, Key (1977) recognised a basement to the supracrustal gneisses, which consisted of foliated pale-grey tonalite gneisses with pink adamellite anatectite phases and mafic stringers, all cut by mafic dykes that are apparently absent from the Baines

TABLE 1.1 Principal Archaean Lithostratigraphic Units and Lithologies in the Messina-Beit Bridge area (modified from Tankard et al. 1982)

Bulai Gneiss:	Porphyroblastic granitic gneiss interlayered with tonalitic-granodioritic gneiss. Intruded 2700 Ma (Van Breemen 1970, Van Breemen & Dodson 1972; Barton et al. 1979b).	
Messina Layered Intrusion:	Metamorphosed anorthosite and leucogabbro with subordinate gabbro, pyroxenite, dunite, magnetitite and chromitite. Dated at 3279 ± 105 Ma (Pb-Pb whole rock isochron, Barton 1983b), possibly as old as 3350 Ma (Barton 1979, 1981).	
Beit Bridge Gneisses:	Rb-Sr age 3375 Ma ? (Ryan et al. 1983)	
Messina-Nulli Metamorphic Suite:	Metaquartzite with calc-silicate and mafic granulite Aluminous Gneiss Magnetite-grunerite iron formation (plus serpentinite) with mafic granulite, amphibolite and hornblende gneiss Migmatitic garnetiferous leucogneiss throughout	Some basic dykes (3060 Ma)
Shanzi-Diti Metamorphic Suite:	Singelele Gneiss: Quartz-feldspar leucogneiss Quartz-feldspar-biotite-garnet leucogneiss with calc-silicate rock and marble, plus minor aluminous gneiss, iron formation, metaquartzite, amphibolite and basic dykes (3060 Ma)	
Basement: Sand River Gneisses:	Nebulitic layered granodioritic and quartz dioritic gneisses with basic dykes. Metamorphic, combined whole-rock Rb-Sr age of 3790 ± 61 Ma (Barton et al. 1983b). Causeway dykes dated at 3570 + 100 Ma, Stockford dykes at 3060 + 80 Ma (Barton et al. 1977; Fripp 1981, 1983).	

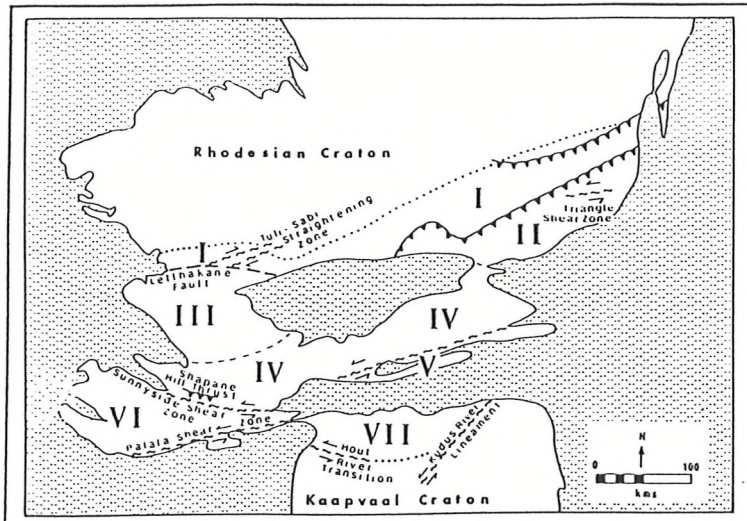

DOMAIN	Structural Zone	Stratigraphic Zone
I	NORTHERN MARGINAL	NORTHERN MARGINAL
II	NORTHERN MARGINAL	CENTRAL (2a)
III	CENTRAL	CENTRAL (2a)
IV	CENTRAL	CENTRAL (2b)
V	SOUTHERN MARGINAL	CENTRAL (2b)
VI	SOUTHERN MARGINAL	CENTRAL (2c)
VII	SOUTHERN MARGINAL	SOUTHERN MARGINAL

ORTHOPYROXENE ISOGRAD
GRADATIONAL CONTACT
SHEAR ZONE (with sense of movement)
THRUST ZONE (teeth in upper plate)
FAULT ZONE
COVER

Fig. 1.3 Tectono-stratigraphic domains of the Limpopo Belt. (after Watkeys 1983).

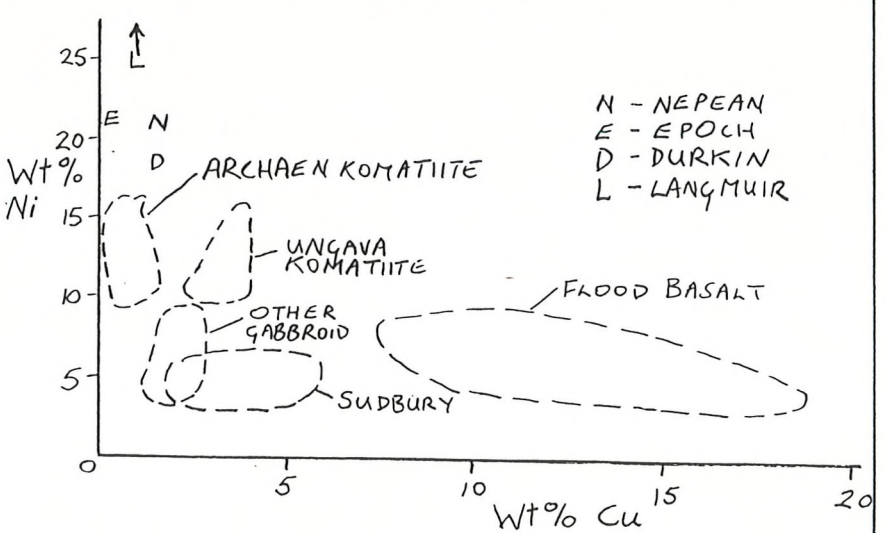

Fig. 1.4 Ni and Cu contents of Ni-Cu sulphide deposits (on a 100% sulphide basis, after Naldrett 1981).

Drift supracrustal rocks. The unique occurrence of mafic dykes is the only criterion for regarding them as basement (Key 1977). This "basement" gneiss has been dated as at least 3230 Ma old (a presumed metamorphic Rb-Sr age) and the intrusive age of the mafic dykes as 2960 ± 89 Ma (Barton & Key 1983). However Barton & Key (1983) also decided that the "basement" Zanzibar Gneisses are equivalent to the Sand River Gneisses and that the Baines Drift supracrustal rocks are equivalent to the BBG. They therefore concluded that the 2960 Ma-old dykes should be found in the supracrustal Baines Drift rocks. The evidence is that the Baines Drift supracrustal and anorthositic gneisses are lithologically similar to the BBG and MLI. The rocks near Malahapye in Domain VI in the far west, are stated by Barton & Key (1981) (referring to Ermanovics 1977) to be quite different to those in Domain IV and probably a new and younger succession. However the dominantly pelitic gneisses near Mahalapye appear to be the structurally upper part of a typical Domain IV supracrustal assemblage (Ermanovics 1977).

1.3.4. The Central Zone in the Selebi-Phikwe Area

In Botswana in Domain III a distinction has been made between extensive tracts of photogeologically homogeneous granitic gneisses and a varied well-banded supracrustal assemblage of hornblende gneisses and amphibolites, quartzofeldspathic grey gneisses, anorthositic and gabbroic gneisses, and minor metasediments (quartzites, marbles and banded iron formations), characterised by abundant photogeological trend-lines (Thomas 1970; Bennett 1971, 1973; Gordon 1973; Mason 1973; Wakefield 1974; Key et al.1976; Watkeys 1983). This supracrustal assemblage contains Ni-Cu sulphide ore bodies in the Selebi-Phikwe area (Gordon 1973). Thomas (1970), Mason (1973), Wakefield (1974) and Key et al. (1976) regarded the granitic gneisses as a basement to the supracrustal assemblage and Watkeys (1983) compiled them as the high-grade equivalents of the "Older Gneisses" of the Rhodesian Craton. However Bennett (1973) thought that there is a gradational contact between the two assemblages and doubted whether any stratigraphic significance should be attached to the distinction. Wright (1977) concluded that a large proportion of these granitic gneisses are strongly deformed, post-supracrustal intrusives.

An association between the amphibolites and hornblende gneisses of the supracrustal assemblage and the anorthosites has been suggested (Mason 1967, 1970, 1973; Key 1976, 1977; Wright 1977). For example Key

(1977) states that amphibolites of basaltic composition grade into anorthosites and therefore represent mafic sheeted intrusions. He further found no evidence to suggest an extrusive origin for the amphibolites and argued that extrusive rocks are confined to the greenstone belts of the Rhodesian Craton to the north. Only Gordon (1973) has suggested an extrusive origin for the amphibolites. The quartzofeldspathic gneisses are commonly regarded as metasedimentary because of their association with definite metasediments (Mason 1967; Key 1976, 1977; Key et al. 1976). However Mason (1973) suggested that some might be acid-intermediate volcanics and Wright (1977) believed many to be intrusive granitoids. The anorthositic and gabbroic gneisses are similar to those in the M-BB area (Mason 1973). However Barton & Key (1981) state that those in the Selebi-Phikwe area are anomalously rich in quartz and Barton (pers. comm. 1981) doubts that they are equivalent to the MLI (Messina Layered Intrusion).

Hickman & Wakefield (1975) obtained a metamorphic age of 2720* Ma from quartzofeldspathic and anorthositic gneisses at Selebi-Phikwe. The greenstone belts of the Rhodesian Craton are of three ages, 3.5, 2.9 and 2.7 Ga approximately (Wilson et al. 1978; Wilson 1979) (Fig. 1.2 and Table 1.2). Before Barton and co-workers obtained the very ancient dates in the Messina area the supracrustal gneisses of the Central Zone were generally regarded as the high-grade, shallow-water equivalents of the 2.7 Ga-old greenstone belts to the north (the Matsitama and Tati greenstone belts or the slightly older Tutume Group) (Bennett 1970; Van Breemen & Dodson 1972; Litherland 1973; Mason 1973; Coward et al. 1976a,b; Key et al. 1976; Saggerson & Turner 1976; Coomer et al. 1977; Key 1977). The Central Zone supracrustals are currently regarded as all being 3.3-3.5 Ga old (Barton & Key 1981; Barton 1983a). The combining of all the Central Zone supracrustal gneisses into one group is not justified. The BBG and MLI can be traced westwards to the possibly equivalent, lithologically similar Baines Drift supracrustal and anorthositic gneisses. However the gneisses in Domain III to the north contain more amphibolite (Key 1976; Barton & Key 1981) and less-obvious metasediments than the Beit Bridge-Baines Drift gneisses in Domain IV and are separated from them by granitic gneisses (Watkeys 1983). The age of the supracrustal gneisses of Domain III is problematic. They could be the equivalents of the 2.7 or 2.9 Ga-old greenstone belts to the north, or the 3.3-3.5 Ga-old BBG to the south, or neither (Table 1.2).

1.3.5 Structure and Metamorphism

The Limpopo Belt has suffered a long and complex deformational history and many complicated and conflicting accounts of the deformation have been published. However a pattern that can be seen throughout the Central Zone is one of early recumbent folds and refolds (nappes) and thrusts that were later deformed into the periclinal interference structures that are typical of the Central Zone. These deformation events and fabrics produced were probably not synchronous throughout the belt (Coward et al. 1976a). The Limpopo deformation lasted from at least 3200 to 2500 Ma in the M-BB area in Domain IV (Barton 1983a; Fripp 1983; Watkeys et al. 1983); whereas in the Selebi-Phikwe area in Domain III the first recognisable deformation and formation of the regional fabric at granulite facies has been dated as 2720* Ma (Hickman & Wakefield 1975). This is very broadly coeval with the development of fold nappes and imbricate thrust faults that took place about 2600 Ma in the majority of the greenstone belts in the southwestern part of the Rhodesian Craton (Wright 1974; Coward 1976; Coward et al. 1976a,b; Cooper et al. 1977). The later events that formed the typical dome and basin interference pattern of the Selebi-Phikwe area have been dated as late as 2100-2000 Ma (Hickman & Wakefield 1975). Coward et al. (1976a), working only in the northern half of the Limpopo Belt, concluded that the early and late deformation resulted from two intracratonic movements, widely separated in time, with movement taking place obliquely to the trend of the belt and producing shear zones.

Rocks in the Limpopo Belt have undergone granulite-facies metamorphism, although present mineralogies typically reflect retrograde amphibolite-facies conditions. There was an early pre-3570 Ma granulite event that only affected the Sand River basement gneisses Fripp (1980). Horrocks (1980), Barton (1983a) and Watkeys et al. (1983) view the later metamorphism of the Central Zone in the M-BB area as having taken place in one long metamorphic P-T loop of burial, uplift and erosion, beginning with the deposition of the supracrustal rocks and ending about 2000 Ma. The detailed shape of the loop is uncertain but granulite facies conditions were reached about 3100 Ma (Horrocks 1980, 1983a,b; Barton & Key 1981) when the supracrustal rocks were at a depth of about 35 km during recumbent folding (Watkeys et al. 1983). Amphibolite conditions existed at about 2700 Ma (Horrocks 1980) when rapid uplift resulted in decompression, the introduction of water and anatexis (the Bulai Gneiss) (Watkeys et al. 1983). Barton & Key (1981)

RHODESIAN CRATON — LIMPOPO BELT — KAAPVAAL CRATON

NORTH MARGINAL ZONE

CENTRAL ZONE

DOMAIN III SELEBI-PHIKWE

DOMAIN IV

SOUTH MARGINAL ZONE

1800 Ma

Umkondo Group

Palapye Group

Soutpansberg Group

Waterberg Group

1900 Ma

2000 Ma

widespread Rb-Sr mineral-rock ages c.2000 Ma
Limpopo Belt near present level ?

Lethlakane shear zone

D3 M greenschist upper amphib.

domes and basins

D2

Rb-Sr 2000-2100 Ma interpretation ? 7

2100 Ma

Bushveld Complex

2200 Ma

Rb-Sr 2200 Ma
Mahalapye Complex

D4 periclinal interference folds age ? 5

2300 Ma

Dykes
undeformed
unmetamorphosed

2400 Ma

Dykes
age ?

D4 M4 greenschist 8

2500 Ma

Great Dyke

Satellite dykes of Great Dyke
undeformed, unmetamorphosed

Rb-Sr 2560 Ma
Granite 7

Rb-Sr 2660 Ma
regional gneiss fabric

D3 M1 granulite

D2 Limpopo fabric D1

D1 nappes 5

D3 M3 hydration

Rb-Sr 2456 Ma
Palmietfontein gr.
undef. unmeta.

D4
D3
D2
M hydration-retrogress. later upper amphib. 2 granulite events
D1

2600 Ma

Shamvian sediments
Late Bulawayan Greenstones
Tati Schist Belt
Selkirk-Phoenix Ni-Cu deposits

Equivalent Greenstones ?

M2 low pressure granulite 8

Rb-Sr 2620 Ma
Matok gr.
porphyroblastic 1

Bulai Gneiss
anatexis, rapid uplift

2700 Ma

2800 Ma

= ?

2900 Ma

Early Bulawayan Greenstones

Greenstones
highly deformed, granulite facies
probably equivalent of E.Bulawayan

D2

Rb-Sr 2960 Ma
Dykes 4

3000 Ma

= ?

age ?

Selebi-Phikwe supracrustals
amphibolite, leucocratic gneiss, anorthosite and minor metasediment
Ni-Cu ore bodies

Pongola Supergroup
Mozaan Group
Nsuze Group

3100 Ma

Rb-Sr 3060 Ma
Dykes 2

M1 high pressure granulite

D1 nappes 8

Granitic Gneisses
basement, intrusive or underlying sedimentary unit ?

3200 Ma

= ?

3300 Ma

Pb-Pb 3270 Ma
Messina Layered Intrusion

3400 Ma

Baines Drift supracrustals and anorthosites

= ?

Rb-Sr 3375 Ma
Beit Bridge Gneisses
MLI before BBG ? 8

unconformity or tectonic contact ?

Rb-Sr 3570 Ma
Dykes 2

Greenstones
Bandelierkop Fm
highly deformed granulites
age ?

Baviaanskloof gneiss
granitic basement ?
age ?

undated greenstone belts
Sutherland
Pietersburg
Murchison

Barberton Greenstone Belt

3500 Ma

Sebakwian Greenstones
on older gneisses ?

Equivalent Greenstones
possibly minor ?

Rb-Sr 3230 Ma
Zanzibar gneiss 4

Ancient Gneiss Complex
Mkhondo Valley supracrustals
Dwalile supracrustals
Bimodal Gneiss Suite

3600 Ma

= ?

3700 Ma

Rb-Sr 3790 Ma
M granulite 3

Sand River Gneisses

3800 Ma

3900 Ma

1 Barton et al. 1983a
2 Barton et al. 1977
3 Barton et al. 1983b
4 Barton and Key 1983
5 Coward et al. 1976a
6 Fripp 1983
7 Hickman and Wakefield 1975
8 Watkeys et al. 1983

Table 1.2

have stated that the grade of metamorphism is apparently lower in the western Central Zone in Botswana, possibly reflecting a higher crustal level than at M-BB. However the metamorphic facies in Botswana is also typically amphibolite and relict granulite (Wakefield 1974; Ermanovics 1977; Key 1977).

The Southern Marginal Zone rocks were subjected to similar conditions of granulite-facies metamorphism followed by retrogression and hydration (Van Reenen & Du Toit 1977, 1978; Du Toit et al. 1983; Van Reenen 1983). In the North Marginal Zone, granulite-facies conditions (Robertson 1968) were reached at about 2900 Ma (Hickman 1976, 1978; Robertson & Du Toit 1978). A large wedge of granulites occurs in this zone in Zimbabwe. Further west in Botswana amphibolite-facies rocks are present, due either to retrogression during later shearing (Mason 1973) or because they represent a higher crustal level within this major shear zone (assuming later tilting) (Coward 1983).

1.3.6. Models for the Evolution of the Limpopo Belt

The relationship of Archaean high-grade terrains to adjacent low-grade granite-greenstone terrains is controversial. Three simplistic options have been suggested (Windley 1976, 1977; Condie 1976a, 1981):

1) Adjacent high-grade and low-grade terrains are unrelated and differ in age and tectonic setting (Hunter 1974).
2) High-grade terrains represent the uplifted and eroded root zones of low-grade terrains - a vertical relationship in which the high-grade terrain is younger (Glikson 1976).
3) Adjacent high and low-grade terrains are the same age but reflect different tectonic settings - a lateral relationship (Windley 1976, 1977).

Condie and Windley favour the third option, stressing that supracrustal rocks in high-grade terrains (including the Limpopo Belt) do not represent high-grade equivalents of greenstone belts, but are composed instead of quartzites, pelitic gneisses, carbonates and anorthosites. Similarly most overviews of the evolution of the Limpopo Belt treat the rocks of the Belt as a completely separate domain from those of the adjacent granite-greenstone terrains. Tectonic models by Barton & Key (1981), Light (1982), Fripp (1983) and Burke et al. (1985) are examples of this separate treatment. The intracratonic model of Barton and Key (1981) and Barton (1981) is the simplest and stresses the importance of the ancient Sand River Gneisses. In this model the Limpopo Belt formed as a graben in a proto-craton that was

neither the Kaapvaal nor the Rhodesian Cratons. The Limpopo Gneisses are the sediments filling the graben. The deformation of the Belt occurred as a result of differential movement between the portions of the proto-craton on either side of the graben. The granite-greenstone terrains of the Kaapvaal and Rhodesian Cratons formed in back-arc basins at the edge of the proto-craton and were accreted on to it.

Light (1982), Fripp (1983) and Burke et al. (1985) have interpreted the Limpopo Belt in modern plate-tectonic terms, involving an accreting continential margin and the destruction of significant amounts of oceanic crust. Some workers (e.g. Kröner 1981 and Condie 1982) doubt that modern plate tectonic regimes can be applied to the Archaean (see Burke et al. 1976 for an Archaean plate-tectonic view). Light (1982) and Burke et al. (1985) view the Belt as the product of continent-continent collision between an Atlantic-type margin of the Rhodesian Craton and an Andean-type margin of the Kaapvaal Craton. The subduction zone dipped under the Kaapvaal Craton and over 1000 km of oceanic crust was subducted before collision (Light 1982). Burke et al. (1985) present no new evidence and their model is essentially that of Light. Granites and anorthosites, not andesites, were produced during partial melting of this subducted oceanic crust (Light 1982). Fripp (1983) sees the M-BB area as representing a convergent plate-margin, including a vague magmatic arc, back-arc basin and continental margin. He believes the MLI formed in a marginal continental rift (also stressing the importance of the very old Sand River Gneisses) before the BBG which formed in the resulting back-arc basin.

Earlier workers in the north of the Limpopo Belt have presented similar though less elaborate plate-tectonic models involving northwards subduction of the Central Zone under the Rhodesian Craton (Robertson 1973; Key 1977). A non-uniformitarian plate-tectonic view is that the Limpopo Belt and adjacent granite-greenstone terrains have evolved as part of the same continental plate, with the Belt situated over a convective mantle downcurrent and the greenstones forming in continental rifts (Condie 1976a).

One of the main problems of the Limpopo Belt is its apparently very long history, with features that are supposedly definitive of the Belt spanning 1 billion years. The BBG which are regarded as a key component of the Belt and are commonly thought of as being an assemblage of quartzites, pelitic gneisses, carbonates and anorthosites (Shackleton 1976; Sutton 1976; Windley 1976,1977; Condie 1976a) were deposited 3.3-3.5 Ga. The metamorphism of the Belt, which is regarded

as its most definitive aspect by workers in the Southern Marginal Zone, has been dated in that area at 2626 Ma (Barton et al. 1983a). The deformation within the Belt has been used to define and subdivide it (Cox et al. 1965; Key & Hutton 1976; Watkeys 1983). However the main Limpopo fabric is found in 2.7 Ga greenstones belts of the Rhodesian Craton (Wright 1974; Coward et al. 1976a,b). The regional fabric and main metamorphism in the Selebi-Phikwe area have been dated at 2720* Ma, with the characteristic dome and basin interference pattern forming possibly as late as 2100 Ma (Hickman & Wakefield 1975).

The recognition of the original nature of the Limpopo gneisses and their comparison with the adjacent granite-greenstone terrains is still of major importance to the understanding of the Limpopo Belt. This applies particularly to the Selebi-Phikwe area, in which Ni-Cu ore bodies are an integral part of the Limpopo Gneisses. An understanding of the original nature of the ore bodies is required before the original nature of the Limpopo Gneisses can be recognised and vice versa.

1.4 NICKEL DEPOSITS: A REVIEW

The Selebi-Phikwe Ni-Cu sulphide ore bodies have been described as being synvolcanic, of uncertain parentage, in a tectonically reworked terrain (Naldrett IGCP Project 1979). It is pertinent at this stage to consider the main types of Ni-Cu sulphide deposit.

Nickel production is dominated by only two types of deposit, both associated with mafic and ultramafic igneous rocks or their altered or metamorphosed equivalents. These are (a) nickeliferous laterite deposits, and (b) Ni-Cu sulphide deposits, on which this review will concentrate. Nickel also occurs in "Cobalt type" arsenide-vein deposits associated with cobalt and native silver (Stanton 1972) (e.g. the Noel deposit in Zimbabwe, Williams 1979, and in the uranium deposits of Saskatchewan, Gatzweiler et al. 1979). These hydrothermal deposits are not important in terms of nickel production. Economically attractive, unexploited concentrations of nickel and copper (>1.8% combined Ni & Cu) are found in deep-sea ferromanganese nodules of the Pacific equatorial zone (Heath 1981), with potentially recoverable reserves of nickel (Archer 1981) of the same order as estimates of land-based reserves (Buchanan 1982).

1.4.1 Nickeliferous Laterite Deposits

Laterite deposits account for 40% of current production of nickel (Ross & Travis 1981; Buchanan 1982). Nickel laterite deposits are the residual products of tropical chemical weathering of ultramafic rocks, particularly Mesozoic and Cenozoic ophiolitic peridotites in relatively mountainous, modern island arcs (e.g. New Caledonia) (Golightly 1981). The nickel is present along with important minor cobalt, either in goethite in the limonitic oxide zone at the top of the laterite profile, or more importantly (up to 4% Ni) in garnierite in the saprolite zone at the base where nickel, magnesium and silica are precipitated to form hydrous silicate ore (Golightly 1981; Buchanan 1982).

The source of the nickel in nickeliferous laterite deposits is forsteritic olivine (Golightly 1981) which typically contains 0.3-0.4% Ni (Simkin & Smith 1970; Fleet et al. 1977). The enrichment of nickel in olivine and to a lesser extent in pyroxene during the fractional crystallisation of basic-ultrabasic magma has been explained by crystal field theory, as due to nickel's high octahedral "site preference energy" (Burns & Fyfe 1966; Burns 1970).

1.4.2 Ni-Cu Sulphide Deposits

Ni-Cu sulphide deposits account for 60% (about 4000,000 tons annually) of present production of nickel, although they represent only half the nickel reserves of laterite (Ross & Travis 1981; Buchanan 1982). Laterite ores require 2 to 5 times the energy used with sulphide ores, for equivalent nickel production (Dasher 1976).

Ni-Cu sulphide ores have a simple mineralogy, they consist mainly of pyrrhotite, with variable amounts of pentlandite, chalcopyrite, pyrite, magnetite and chromite. Cobalt, platinum group elements (PGE) and gold are locally significant constituents.

1.4.2a Deposit types and their relative importance

Ni-Cu sulphide deposits have been classified (Naldrett & Gasparrini 1971; Naldrett 1973, IGCP Project 161 1979, 1981; Naldrett & Cabri 1976) in terms of the type, size and tectonic setting of the mafic and ultramafic bodies with which they are associated. These classifications only show that Ni-Cu sulphide deposits are associated with a variety of igneous, mainly intrusive bodies or their metamorphosed equivalents, of both tholeiitic or komatiitic parentage, in several tectonic settings. Ophiolites, mafic (as compared to ultramaf-

ic) lava flows, Alaskan-type bodies and alkaline ultramafic bodies (such as kimberlites) contain few significant Ni-Cu sulphide deposits (Naldrett 1981). Because it is often difficult to precisely place a deposit in these elaborate schemes, a simpler classification based on that of Marston et al. (1981) and Ross & Travis (1981) for Australian deposits is used in this thesis. Deposits are classified as being either komatiite-associated, gabbroid-associated, or in a few cases sedimentary-associated. The hydrothermal vein-arsenide association is of minor economic importance and will not be considered.

Ni-Cu sulphide deposits occur throughout geologic time, the most recent major deposits being the Triassic ore bodies at Noril'sk-Talnakh in Siberia (Glaskovsky et al. 1977). They are dominantly of Lower Proterozoic (e.g. the gabbroid-associated deposits of Sudbury in Canada) and Archaean (e.g. komatiite-associated deposits) age.

When the reserves or past production of the main nickel-producing classes of Ross & Travis (1981) are compared, the Sudbury intrusion's dominant position is very clear. However this is partly due to historical, economic and logistical factors. Of the original resources containing greater than 0.8% sulphide Ni, the gabbroid-associated Sudbury deposits contribute 39%; other gabbroid-associated deposits contribute 38% and komatiite-associated deposits account for 23% (Ross & Travis 1981). Original resources with less than 0.8% Ni are dominated by deposits in large layered gabbroid-associated intrusions. Sedimentary-associated deposits contribute less than 0.5% of original resources of sulphide Ni.

1.4.2b Description of deposit types

1) Komatiite-associated deposits

Ni-Cu sulphide deposits are associated with komatiites in Archaean greenstone belts of the Yilgarn Block in Western Australia (W.A.), the Rhodesian Craton and the Superior Province in Canada and the Lower Proterozoic Cape Smith fold belt in Ungava, Canada (Hynes & Francis 1982). Komatiite-associated deposits in Western Australia (Marston et al. 1981) and Zimbabwe typically occur near the base of a sequence of ultramafic volcanics, later eruptions in the sequence being less magnesian with minor or no sulphides. For example in Zimbabwe ore bodies are located at the base of the first volcanic unit of the Bulawayan Group (Williams 1979).

Komatiite-associated ore bodies are nickel rich (10-15% when

recalculated to 100% sulphide) and copper poor (0.5-1.5%) (Naldrett 1981) (Fig. 1.4). Deposits with even higher grades of nickel are either highly chemically altered; for example the talc-carbonate hosted Epoch deposit in Zimbabwe (Naldrett 1981), the magnetite-rich Langmuir 1 ore body in Ontario (Green & Naldrett 1981) and the supergene Durkin deposit (W.A.) (Ross & Keays 1979); or have suffered extreme dynamic metamorphism, for example the Nepean deposit (W.A.) (Barrett et al. 1976).

Komatiite-associated deposits occur in three situations:
(a) as thin layers of massive to disseminated sulphide at the base of individual komatiite lava flows (the volcanic peridotite-associated deposits of Marston et al. 1981). The deposits of Kambalda (W.A.) (Woodall & Travis 1969; Ross & Hopkins 1975; Gresham & Loftus-Hills 1981) are the main examples. Others include the Damba-Silwane deposits in Zimbabwe (Williams 1979) and the Langmuir (Green & Naldrett 1981) and Alexo (Naldrett 1973) deposits of the Abitibi Belt, Canada. Flow-hosted ore bodies are generally small (1-5 million tons), with high nickel grades (1.5-3.5% Ni) (Naldrett 1981).
(b) in intrusive ultramafic bodies (usually toward the base) intimately associated with komatiitic volcanics. The deposits of the Ungava Ni-belt (e.g. the Katiniq sill deposit, Wilson et al. 1969) and the Shangani ore body in Zimbabwe are of this type. The intrusions acted as feeders for eruptions, for example the Shangani host peridotite has been interpreted as a volcanic neck or vent (Williams 1979) or a subvolcanic magma chamber (Viljoen et al. 1976). These obviously subvolcanic, komatiite-associated ore bodies are intermediate in type, grade and size between flow-hosted deposits and intrusive dunite-associated deposits.
(c) as dominantly disseminated sulphides in large intrusive lenses of variably serpentinised dunite locally with peripheral peridotite (the intrusive dunite-associated deposits of Marston et al. 1981). Examples are the Six-Mile (Naldrett & Turner 1977), Mt. Keith (Burt & Sheppy 1975) and Agnew (Perseverance) (Martin & Allchurch 1975; Billington 1984) deposits of the Leonora-Wiluna Belt (W.A.) and the Dumont deposit in Quebec (Eckstrand 1975; Duke 1980). The deposits of the highy deformed and metamorphosed Thompson Belt in Manitoba (Zurbrigg 1963; Peredery 1979; Peredery et al. 1982) are possibly of this type. Intrusive dunite-associated ore bodies occur in more deformed terrains than flow-hosted deposits and are less obviously related to komatiitic volcanism than the subvolcanic deposits. The

dunitic lenses have been interpreted as either subvertical bodies, dynamically emplaced after initial deformation, or as relics of sill-like feeder chambers for komatiitic volcanics (Marston et al. 1981). Disseminated intrusive dunite-associated deposits are large (up to 250 million tons) and mainly low grade (0.6% Ni) (Naldrett 1981).

2) Gabbroid-associated deposits

Gabbroic mafic-ultramafic intrusive complexes hosting Ni-Cu sulphide deposits vary from very large layered intrusions to small irregular intrusions. They appear to have crystallised from basaltic rather than ultrabasic (komatiitic) magmas, though the affinity of the parent magmas of these intrusions is not always clear. For example various estimates have been made of the composition of the early magmas of the Bushveld Complex in South Africa (Wager & Brown 1967; Vermaak 1976; Cawthorn & Davies 1982; Irvine & Sharpe 1982). Some deposits are in intrusions related to and possibly feeders for flood basalts, for example the Noril'sk-Talnakh deposits, hosted in differentiated gabbroic sills (Glaskovsky et al. 1977), and the unexploited deposits of the Late Proterozoic Duluth Complex in Minnesota (Weiblen & Morey 1980), a large layered troctolite-anorthosite complex associated with Keewanawan basalts.

The class includes the Sudbury Nickel Irruptive, a medium-sized differentiated intrusion, whose ore bodies have dominated sulphide nickel production. Sudbury will be treated as a separate subclass of gabbroid-associated deposits due to its enormous original resources and widely accepted, impact-related origin (Dietz 1964). However it must be stressed that Sudbury has many features in common with other gabbroid-associated deposits.

Gabbroid-associated ore bodies have simple mineralogies, similar to those of komatiite-associated deposits. However they have lower Ni:Cu ratios (Fig. 1.4) and usually much higher PGE (particularly Pt and Pd) (Naldrett et al. 1979) than those associated with komatiites. Flood basalt-related deposits are rich in copper and have very low Ni:Cu ratios (Naldrett 1981).

(a) Deposits in large layered intrusions

Ni-Cu sulphide deposits in these are characteristically extensive, low-grade, stratiform and undeformed, with relatively high concentrations of PGE. Large layered intrusions, such as the Bushveld Complex (Von Gruenewaldt 1979) and the Stillwater Complex in Montana

(Page & Simon 1978; McCallum et al. 1980) are significant in early to mid-Proterozoic rocks, when major cratons were first stabilised (Windley 1977).

(b) Deposits in small to medium mafic-ultramafic gabbroic intrusions

These mineralised intrusions vary from layered sills to irregular intrusions which are only partially layered or zoned. This diversity is due partly to tectonism. Many of the deposits occur in deformed terrains and proposed temporal relationships include pre-, syn-, and post-tectonic emplacement of host intrusions. Some host intrusions include a range of rock types from gabbro to peridotite, and others consist only of mafic rocks. Where ultramafic rocks are present, they occur either at the base of the intrusion (e.g. the Dumbarton-Bird River sill deposit, Karup-Moller & Brummer 1971, Coates et al. 1979, and the Lynn Lake deposit, Scoates 1971, both in Archaean differentiated gabbroic sills in Manitoba, and the Jinchuan deposit in China (Ross & Travis 1981; Yin Dezhi, pers. comm. 1986), or in the central portion (e.g. the host to the Empress deposit in Zimbabwe, and the synorogenic concentrically zoned Rana intrusion hosting the Bruvann deposit of the Norwegian Caledonides, Boyd & Mathiesen 1979).

Deposits in small to medium gabbroic intrusions are of higher grade and consist of more-massive sulphides than those in large layered intrusions. Sulphides are commonly concentrated toward the base of the host intrusion (e.g. in the Jurassic Insizwa Complex in the Transkei, South Africa, Scholtz 1936). However many of the deposits occur in deformed intrusions in which sulphides have been mobilised into tectonic zones to form tectonic ore bodies (e.g. some of the ore at Dumbarton and Lynn Lake, Naldrett & Gasparrini 1971). At Carr Boyd (W.A) and Giant Mascot (British Columbia) sulphides are associated with a pegmatoidal troctolitic phase in layered intrusions (Purvis et al. 1972; Nesbitt, pers. comm. 1987).

Mineralised intrusions typically occur in basaltic volcanic terrains, for example the early Proterozoic Pechenga deposits in the Kola Peninsula, U.S.S.R. (Glaskovsky et al. 1977), hosted by deformed stratified mafic-ultramafic intrusions associated with thick basaltic lavas of greenstone belt affinity in a graben (Grachev & Fedorovsky 1981). However exceptions include the mid-Proterozoic (Svecokarelian) Kotalahti deposits in Finland (Papunen et al. 1979; Gaal 1981), hosted in synorogenic differentiated intrusions without any obvious associated basic volcanics.

(c) Sudbury

The Ni-Cu sulphide deposits at Sudbury are a special case of deposits hosted by gabbroic intrusions. The norite-gabbro-micropegmatite units that form the majority of the basin-like Sudbury Nickel Irruptive represent a differentiated intrusion of one or more pulses of relatively siliceous, basic magma (Souch et al. 1969; Naldrett et al. 1970; Peredery & Naldrett 1975). The massive and disseminated ore bodies are associated with a sublayer at the base of the Irruptive (Souch et al. 1969) and with dyke-like bodies of sublayer (offsets) radiating outwards from the Irruptive. The sublayer consists of norite, breccia and sulphides (Pattison 1979).

There is now general concensus (see Card & Hutchinson 1972 and Fleet 1979a for the main alternative view that Sudbury was a major volcanic centre) that the Sudbury structure and its associated intrusions were triggered off by the impact of a large meteorite about 1800 Ma. This was first suggested by Dietz (1964) who described shatter cones in quartzites to the south of the Irruptive. Additional evidence was provided by French (1967, 1972), who noted shock metamorphic effects in country-rock quartz and feldspar grains, and Peredery (1972), who interpreted the Onaping Formation (directly overlying the Irruptive) as impact fall-back breccia (suevite).

One of the main problems of Sudbury geology has been the relationship of the sublayer to the main Irruptive. Early workers thought that the sublayer is the basal differentiate of the main norite-micropegmatite body (Coleman 1926). However there is an almost complete absence of pyrrhotite and pentlandite from the main Irruptive and Naldrett & Kullerud (1967) and Souch et al. (1969) have proposed that the sulphide-bearing sublayer is not the basal differentiation of the main Irruptive, but rather a series of late intrusions along the base of the Irruptive and in the offsets, concentration of immiscible sulphides having taken place at a deeper level. Pattison (1979) concluded that the norites, breccias and sulphides of the sublayer are pre-main Irruptive and suggested that the sublayer resulted from direct emplacement of sulphide-enriched impact melt along the walls of the crater (the splash emplacement of Dietz 1972) and that the offset deposits formed by forceful injection into impact-induced fractures. However this coincidentally requires pre-impact concentrations of Ni and Cu sulphides at the impact site. In support of this, Sudbury lies in a belt from Duluth to Cobalt, that contains numerous Ni-Cu sulphide-bearing basic intrusions (Guy-Bray 1972).

3) Sedimentary-associated deposits

A few small Ni-Cu sulphide deposits are associated with (meta-) sediments. The best documented are the Redstone deposit in the Abitibi Belt (Robinson & Hutchinson 1982) and the Sherlock Bay deposit in the Pilbara Block (W.A.) (Carr 1974; Miller & Smith 1975). At Redstone a layer of Ni-rich massive sulphides occurs within altered dacitic volcanisediments associated with a sulphide-facies iron formation, near the contact with overlying komatiitic flows. At Sherlock Bay Ni-Cu sulphides are concentrated in carbonate, sulphide and oxide-facies iron formations within a calc-alkaline metavolcanic sequence, with no obvious relationship to komatiites.

Ni-rich sulphide ores occur within interflow metasediments associated with more typical komatiitic flow-hosted deposits in the Yilgarn Block (W.A.), at Kambalda (particularly Jan Shoot) (Bavington 1981), Windarra (Seccombe et al. 1977; Groves et al. 1979) and Wannaway (McQueen 1979). The metasediments are banded albitic and sulphidic cherts.

The highly deformed and metamorphosed Thompson Belt deposits are hosted dominantly by serpentinised ultramafics of probable komatiite parentage (Peredery 1979). However 25% of the ore in the Thompson Belt occurs in metasediments, particular in association with pelites and iron formation at the Thompson mine and with dolomite and diopsidic skarn at Pipe 2 mine (Peredery et al. 1982).

1.4.2c The genesis of Ni-Cu sulphide deposits

Ni-Cu sulphide deposits have long been regarded as magmatic (Coleman 1926; Scholtz 1936; Hawley 1962). According to the traditional magmatic theory they result from (1) the formation of droplets of immiscible sulphide liquid within a basic or ultrabasic silicate magma; (2) the partitioning of Ni, Cu and PGE into these droplets; and (3) the subsequent concentration of the sulphides (Naldrett 1981). An origin by hydrothermal replacement has also been suggested, particularly for Sudbury (Wandke & Hoffman 1924; Phemister 1937; Fleet 1977, 1979b; Fleet et al. 1977). The discovery of komatiite flow-hosted deposits has led to the suggestion that this type formed by hydrothermal volcanic-exhalative processes (Lusk 1976a,b; Hutchinson 1982, 1983).

The evidence for a magmatic origin of most Ni-Cu sulphide deposits is formidable:

(1) All Ni-Cu sulphide deposits (excluding Sherlock Bay) are associated with mafic and ultramafic igneous rocks or their altered or metamorphosed equivalents.

(2) The metal and sulphur contents of Ni-Cu sulphide ores (Fig. 1.4) (Naldrett 1981) and the correlation between the Ni:Cu ratio of a deposit and the composition of the magma from which its host rock formed (Wilson & Anderson 1959; Rajamani & Naldrett 1978) are consistent with the Ni and Cu contents of basic and ultrabasic magmas (Duke 1979) and the coefficients that govern the partitioning of Ni, Cu and Fe between sulphide and silicate melts (Maclean & Shimazaki 1976; Rajamani & Naldrett 1978; Boctor 1981, 1982). The high Cu content of flood basalt-related deposits has been attributed (Naldrett 1981) to basalt magmas with exceptionally high Cu (400 ppm, Prinz 1967) (supported by the lava-hosted Keewanawan Cu deposits, Robertson 1975), or alternatively to post-emplacement processes, such as fractional crystallisation and the blending of successive magma batches (Rao & Ripley 1983).

(3) Immiscibility textures have been described in ores, for example at Sudbury (Hawley 1962).

(4) Most Ni-Cu sulphide ore bodies are concentrated towards the base of their mafic or ultramafic host (e.g. Kambalda). Gravitational settling is presumed (Naldrett 1979) to have concentrated dense immiscible sulphide (density 3.9 g/cc, as compared to silicate magma with a density of 2.6 to 3.0 g/cc) at some stage in the formation of these basal deposits. However the exact time of formation of the immiscible sulphides is often in doubt. In several cases, for example the Sudbury sublayer, estimates of the solubility of sulphur in basic-ultrabasic magmas indicate that in situ sulphide immiscibility and gravitational settling could not have taken place. Segregation and concentration of immiscible sulphides within a larger magma pool, prior to final emplacement of host rocks and sulphides has been invoked for the Sudbury sublayer (Naldrett & Kullerud 1967; Souch et al. 1969).

(5) Metallurgical observations of the formation of immiscible sulphide melts during smelting (Skinner & Barton 1973 and references therein).

(6) The direct observation of the precipitation of immiscible sulphide globules during the crystallisation of basaltic magma (Skinner & Peck 1969).

The hydrothermal replacement origin of Sudbury ores has been

based mainly on minor details of mineral alteration, for example the local occurrence of blue sodic amphibole adjacent to sulphide (Fleet 1977). Naldrett (1979, 1981) has effectively criticised the experimental data of Fleet et al. (1977) and the hydrothermal replacement hypothesis, except as a process which modified pre-existing ore, for example at Strathcona, Sudbury (Naldrett & Kullerud 1967).

A hydrothermal volcanic-exhalative origin seems probable for the minor deposits of Redstone and Sherlock Bay. It is feasible that exhalative Ni sulphides formed where sea floor hydrothermal circulation affected Ni-rich komatiitic lavas (Hutchinson 1982). However at Kambalda and Windarra where examples of this possibly occur, physical remobilisation of komatiite-hosted massive sulphide and hydrothermal diffusion and migration of Ni and Cu into adjacent sulphidic sediments during deformation and metamorphism has been invoked for the sediment-hosted ores associated with more typical flow-hosted deposits (Paterson et al. 1984; Schmulian 1984).

The idea of Lusk (1976a,b) that komatiitic flow-hosted deposits were actually volcanic-exhalative Ni deposits that have coincidentally been partially melted by, and incorporated into, immediately overlying komatiite lava flows has been strongly countered by Groves et al. (1976, 1979) and Groves & Hudson (1981) who argue convincingly that most of the features used by Lusk to indicate an exhalative origin are actually of metamorphic derivation. Barrett et al. (1977) suggested that komatiitic flow-hosted massive sulphides could have been generated from more dissemin-ated mineralisation during metamorphism and deformation. However Groves et al. (1979) concluded that though this happened locally, for example at Nepean (Barrett et al. 1976), it was usually pre-existing magmatic sulphides that had been modified and remobilised. The association of sulphides with metasediments in the Thompson Belt is probably due to deformation which moved the sulphides away from their komatiitic hosts (Nesbitt, pers. comm. 1986).

Basic and ultrabasic magmas are capable of supplying the metals to form Ni-Cu sulphide deposits. However concentration of magmatic sulphide is not the normal consequence of the generation, emplacement and crystallisation of basic or ultrabasic magma (Naldrett 1981). The sulphur content of basalt magma immediately prior to eruption rarely exceeds 0.16% (Moore & Fabbi 1971; Anderson 1974; Czamanske & Moore 1977). Sulphur saturation and the production of minor immiscible sulphide globules occurs during the quenching of the magma (Fleet et al. 1977). Most komatiites, even those from sequences containing Ni-

Cu deposits have sulphur contents (<0.05%) (Cameron et al. 1971; Groves et al. 1979) considerably below the saturation levels of 0.3% determined by Shima & Naldrett (1975). The key to the formation of ore is the availability of sulphur (Naldrett & Macdonald 1980). Only when a high supersaturation content of sulphur is present in a magma can the process of immiscibility and partitioning proceed efficiently. This must take place under critical conditions and at a critical time so that sulphides can concentrate undiluted by silicates.

Excess sulphur in the magmas that formed the host rocks and their associated Ni-Cu sulphide deposits could have originated either:

(a) internally, by the supersaturation of magmatic mantle-derived sulphur,

(b) externally, by sulphurisation, for example by assimilation of sulphur from country rocks, or

(c) a combination of both.

With respect to the first case, namely supersaturation of magmatic sulphur, experimental work has shown that the solubility of sulphur in a silicate melt decreases with falling temperature (Haughton et al. 1974) and with falling pressure (Mysen & Popp 1980). The sulphur-carrying capacity of a basic-ultrabasic silicate melt has been experimentally reduced by increasing the silica or alkalies content (Shamazaki & Clark 1973; Haugton et al. 1974), by reducing the iron or the Fe/Mg ratio (Fincham & Richardson 1954), and by oxidation (Shima & Naldrett 1975, Buchanan & Nolan 1979). Possible examples of these effects producing ore by the supersaturation of magmatic sulphur are:

(1) the reduction of sulphur solubility in komatiite magma due to falling temperature and pressure and possibly oxidation during rapid rise of the magma from the base of the lithosphere, for the formation of komatiite-associated deposits (Lesher et al. 1981). Processes proposed for the genesis and transport of komatiite magma however are equivocal (Arndt 1977; Arth et al. 1977; Bickle et al. 1977; Naldrett & Turner 1977; Nesbitt et al. 1979; Walker et al. 1980; Nisbet 1982). The possible extrusion of some komatiites with high contents of immiscible sulphides compounds the problem. Naldrett (1973) and Naldrett & Cabri (1976) have suggested that the source of the sulphur in komatiite-associated deposits was sulphur-rich mantle at 200 km depth (enriched in sulphur due to the melting of sulphides in the mantle below 100 km and their downward percolation).

(2) reduction of sulphur solubility in a basic-ultrabasic magma

due to an increase in silica and alkalies by:
(a) assimilation of salic country rocks, to produce Sudbury (Irvine 1975), the PGE-rich sulphides of the Stillwater Complex (Barker 1975), the Sally Malay deposit (W.A.) (Thornett 1981), the Madziwa deposit in Zimbabwe (Buchanan, pers. comm. 1981), and the Insizwa mineralisation (Lightfoot et al. 1984). Naldrett & Macdonald (1980) have suggested that sulphur saturation and the precipitation of immiscible sulphides at Sudbury without silicate crystallisation resulted from the assimilation of hot fractured siliceous rocks of the impact zone by rising impact-triggered basic magma (25-50% assimilation, Naldrett et al. 1986). The relatively siliceous nature of the Irruptive supports this. Field relationships (Pattison 1979) and magmatic, low 34S values (Naldrett 1981) rule out a sedimentary derivation of the sulphur at Sudbury (Cheney & Lange 1967).
(b) mixing and blending with a more siliceous magma (Irvine 1977). Irvine & Sharpe (1982) and Irvine et al. (1983) proposed that the PGE-rich sulphides of the Merensky Reef of the Bushveld Complex and the Stillwater J-M Reef precipitated during the mixing of sulphur-carrying anorthositic magma and boninitic magma carrying the PGE, Ni and Cu.

(3) the Merensky Reef. Lee (1983) suggested that the sulphides of the Merensky Reef were the consequence of two opposing trends in a normally differentiating basic magma, variously described as being sulphur-poor (Willemse 1969; Liebenberg 1970; Vermaak 1976). Lee (1983) proposed that the dissolved sulphur content of the residual Bushveld magma increased as it became enriched in FeO during fractional crystallisation. However at the Merensky Reef stage after which plagioclase crystallisation became dominant, the rapid increase in silica and alkalies in the residual melt reduced sulphur solubility resulting in the formation of immiscible sulphides. Lee & Fesq (1985) have also suggested a role for chromite crystallisation in the supersaturation of magmatic sulphur.

With respect to the second case, namely sulphurisation, sulphur isotope studies and field relationships indicate that introduction of sulphur from sedimentary country rocks at the magmatic stage contributed significantly to sulphur availability in the formation of several gabbroid-associated deposits:

(1) the Noril'sk-Talnakh deposits, the sulphides of which are anomalously heavy in sedimentary 34S (Godlevski & Grinenko 1963);

country rocks include extensive Devonian evaporites (Mainwaring & Naldrett 1977; Naldrett & Macdonald 1980).

(2) the deposits of the Duluth Complex (Mainwaring & Naldrett 1977). Ripley (1981) and Rao & Ripley (1983) suggested that sulphides and hydrous minerals of the underlying Virginia Formation sediments were broken down by the heat from the intrusion and sulphur introduced as an H20-rich volatile phase.

(3) the Platreef at the base of the Bushveld Complex. Buchanan et al. (1981) suggested incorporation of sedimentary sulphur into Bushveld magma from anhydrite in the floor rocks. Buchanan & Rouse (1984) later suggested multiple contamination, with increased contents or iron and carbon from the assimilation of banded iron-stones and organic material resulting in a higher sulphur-carrying capacity of the magma, as well as sedimentary-derived sulphur.

Sulphurisation has also been proposed for komatiite-hosted deposits (Naldrett 1966 for Alexo, retracted 1973; Pinder 1970; Hopwood 1981). The similarity of high S/Se ratios and sulphur isotope values for metasediments and ores from a number of flow-hosted deposits, particularly Windarra (Seccombe et al. 1977) and Langmuir led Groves et al. (1979) and Groves & Hudson (1981) to suggest that some sulphur was derived via contamination from a crustal source, more likely at a high-level magma chamber stage than <u>in situ</u> after eruption. Assimilation of sulphur from sulphidic sediments by komatiite lavas during flow has recently suggested, particularly for the Kambalda deposits, by Lesher et al. (1984) and Huppert et al. (1984), who respectively interpret the linear troughs which the ores occupy as pre-existing topographic channels down which the lavas were channelled, or as thermal erosion channels. Both groups of authors use the mutually exclusive relationship between the ores and stratig-raphically equivalent sulphidic metasediments as evidence for the localised assimilation of these sediments to form ore. However the high, undepleted Ni contents of olivines in mineral-ised flows (Groves & Hudson 1981) argues against the post-eruptive extraction of Ni from komatiite magma into immiscible sulphides. It is unlikely that magmatic Ni could have been efficiently scavenged by assimilated sulphur during flow and later rapid cooling. The occurrence of disseminated ore bodies in intrusive dunites also argues against post-eruptive sulphurisation as the major source of sulphur. The idea of Lusk (1976a,b) that komatiite flow-hosted deposits derived both their sulphur and nickel by assimilation of underlying volcanic

exhalative Ni deposits is also unlikely (Groves et al. 1976, 1979; Groves & Hudson 1981).

At Mt. Keith, Groves & Keays (1979) concluded that external sulphur had been added during progressive serpentinisation, and they suggested that the increase in sulphide volume during alteration possibly represents an important initial stage in the formation of metamorphic ores in highly strained and metamorphosed environments. Serpentinisation can also result in the release of silicate Ni and the upgrading of the Ni content of sulphides, most notably in weakly mineralised intrusive dunites, for example at Dumont (Eckstrand 1975) and Six-Mile (Naldrett & Turner 1977).

Accept in the few cases where sulphur isotopes and field relationships indicate sulphurisation, there is little agreement on the relative roles of sulphurisation and magmatic sulphur in the formation of Ni-Cu sulphide ore bodies (e.g. for komatiite-hosted ores). The Sudbury and Merensky sulphides appear to be of magmatic sulphur, although the actual processes for magmatic sulphur super-saturation in them are still highly debated.

In conclusion, the great majority of Ni-Cu sulphide deposits are of magmatic origin, caused by the formation of immiscible sulphides in basic to ultrabasic magma, the partitioning of Ni and Cu into these sulphides and the subsequent concentration of the immiscible sulphides. Basic to ultrabasic magmas are able to provide the Fe, Ni, Cu and PGE to form the deposits. The key to their formation is the availability of sulphur. Excess sulphur can be of magmatic mantle-derived origin, or may be assimilated from country rocks, or a combination of both. Supersaturation of magmatic sulphur may be caused by a variety of physical and chemical processes. Some mantle-derived magmas, particularly Archean komatiites, possibly have high initial sulphur contents. The preponderance of Ni-Cu sulphide deposits in the Archaean and early Proterozoic may reflect sulphur depletion of the upper mantle caused by many cycles of plate tectonics or similar processes (Naldrett 1981). The only large Ni-Cu sulphide deposits that are younger than mid-Proterozoic, Duluth (1115 Ma) and Noril'sk (Triassic), both probably acquired most of their sulphur by assimilation of sedimentary sulphur in an intracontinental setting.

Hydrothermal replacement has not played an important role in the formation of Ni-Cu sulphide deposits, except to modify and concen-trate pre-existing magmatic sulphides. Similarly deformation

and metamorphism (particularly serpentinisation) have been locally important in the formation of more massive sulphides from disseminated magmatic sulphides. Hydrothermal volcanic exhalative processes may have formed at least two minor deposits, and exhalative ores possibly occur adjacent to more-important magmatic komatiite flow-hosted deposits. The Sudbury deposits, although essentially magmatic, remain enigmatic. Although a role for meteorite impact in the formation of the world's largest occurrence of Ni-Cu sulphides has been accepted, there is (as yet) no evidence for, or acceptance of a cosmogenic origin (Dietz 1964, 1972) for all or some of the Ni, Cu and S. High contents of magmatic mantle-derived sulphur, high degrees (up to 50%, Naldrett 1986) of sialic crustal contamination, and pre-impact concentrations of Ni-Cu sulphides have all been proposed.

1.5 AIMS AND METHODS OF RESEARCH

The main aims of the research recorded in this thesis were to study the nature of the host rocks and mineralisation at the Selebi-Phikwe Ni-Cu mines, to elucidate the geochemical nature of the host-rock (e.g. are they komatiitic or tholeiitic ?) and to evaluate the relationships between host and ore. (Are the ores syngenetic?)

Secondary aims, with a direct bearing on the primary aims were:

a) to study the nature of the nearby Dikoloti-Lentswe Ni-Cu deposits (Are they similar and related to Selebi-Phikwe?); and
b) to investigate the nature and geochemistry of the Limpopo gneisses in the Selebi-Phiklwe area, as to the setting of the Ni-Cu deposits and in a more regional sense, to contribute to the understanding of the Limpopo Belt. (What were the gneisses originally? Are they high-grade equivalents of granite-greenstone terrains or do they represent a completely separate setting?)

By-products of the research are a better knowledge of aspects of the structure and metamorphism of the area, particularly the deformation suffered by the Selebi-Phikwe ore bodies.

The field of work for the research was carried out in two periods of three months during the winters of 1980 and 1981. Information on the Selebi, Selebi North and Phikwe ore bodies and the

Dikoloti-Lentswe prospects was obtained by relogging and sampling diamond drill core. (Surface exposure of the mineralisation is non-existant). Underground observation and sampling were carried out at the Selebi and Phikwe mines. Mapping and sampling were carried out in the Selebi-Phikwe area to increase understanding of particular problems (e.g. the original nature of the granitic and supracrustal gneisses). However poor exposure meant that a lot of information and samples had to be gathered from diamond drill core. This had the advantage of providing complete fresh sections. Two regional traverses from Selebi-Phikwe were made to the Sefhope area to the southeast and to Kgarimacheng to the north. The Phoenix and Selkirk deposits in the Tati greenstone belt 70 km to the north of Selebi-Phikwe were examined and the limited amount of available core was logged and sampled. A week was spent in the Messina area examining key exposures in order to compare with the Selebi-Phikwe area. Information was also gained from the author's previous employment for BCL in the Matsitama area from 1973 to 1975 and in the Messina-Beit Bridge area for Johannesburg Consolidated Investments during 1975 and 1976. Petrological and geochemical analysis of samples were carried out at Southampton University. Mineral probe data were obtained at the Open University and Imperial College.

CHAPTER 2 THE GEOLOGICAL SETTING OF THE SELEBI-PHIKWE NI-CU DEPOSITS

2.1 INTRODUCTION

The Selebi-Phikwe area, located near the north margin of the Central Zone of the Limpopo Belt in Botswana (Figs 1.2 & 1.3), has been mapped by BCL geologists (Gordon 1973; Gallon 1986), Wakefield (1974) and Key (1976). It was not the intention of this research to remap the area but rather to concentrate on areas of possible extension of the Ni-Cu mineralisation, particularly the Dikoloti-Lentswe horizon, and on specific problems such as the nature of the "basement" granitic gneisses and the anorthosites, given the present view by BCL geologists at Selebi-Phikwe that these gneisses are of sedimentary origin. Exposure is poor. The more resistent granitic gneisses, anorthosites and hornblende gneisses are the best exposed lithologies. Drill core provided complete sections through the gneisses.

The gneisses of the Selebi-Phikwe area can be conveniently sub-divided into photogeologically homogeneous granitic gneisses and a photogeologically well-banded assemblage including hornblende gneiss, grey quartzo-feldspathic gneiss, anorthosite and metasediments (Plate 1, Fig. 2.1). A section without obvious major repetitions occurs to the south of Phikwe and is seen in the deepest drill holes at Phikwe (Fig. 2.2). Wakefield (1974) and Wright (1977) have proposed from limited structural evidence that the Phikwe section is upside down. Figure 2.3 is a pseudostratigraphic column for the Selebi-Phikwe area. The gneisses above the Selebi ore body, although similar to those at Phikwe, can not be exactly correlated with those at Phikwe, possibly because of repetition due to early folding at Selebi.

2.2 GRANITIC GNEISSES

Granitic gneisses comprise about 40% of the Selebi-Phikwe area. They occur at the top of the deepest holes at Phikwe (Fig. 2.2). The granitic gneisses include a variety of lithologies. The three main types and their proportions are:

Plate 1, overleaf. Air photo montage of the Selebi-Phikwe area. PD-Phikwe Dome, SB-Selebi Basin, MR-Motloutse River, LF-Lethlakane Fault, P-Phikwe ore body, S-Selebi ore body, SN-Selebi North orebody.

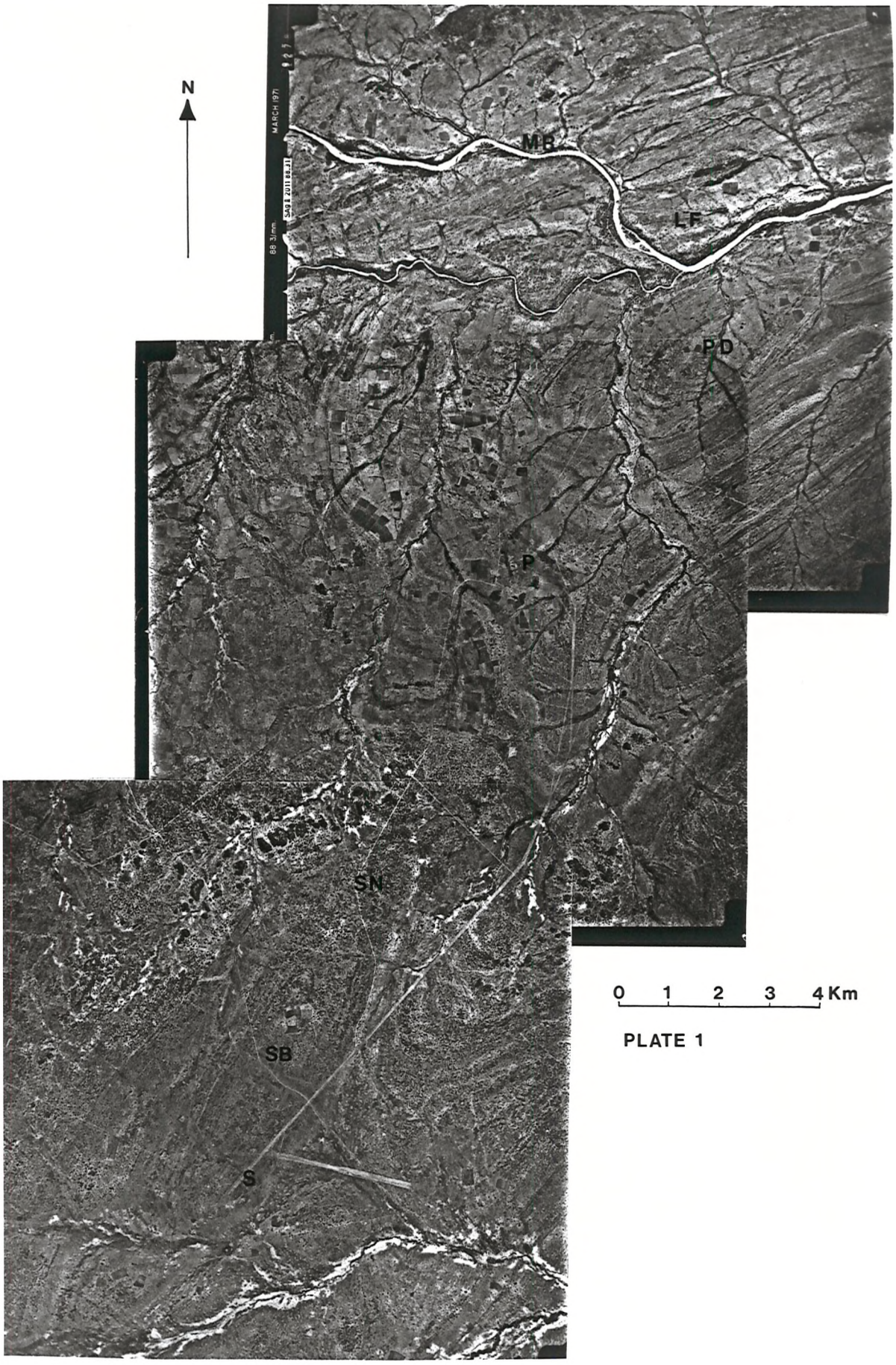

PLATE 1

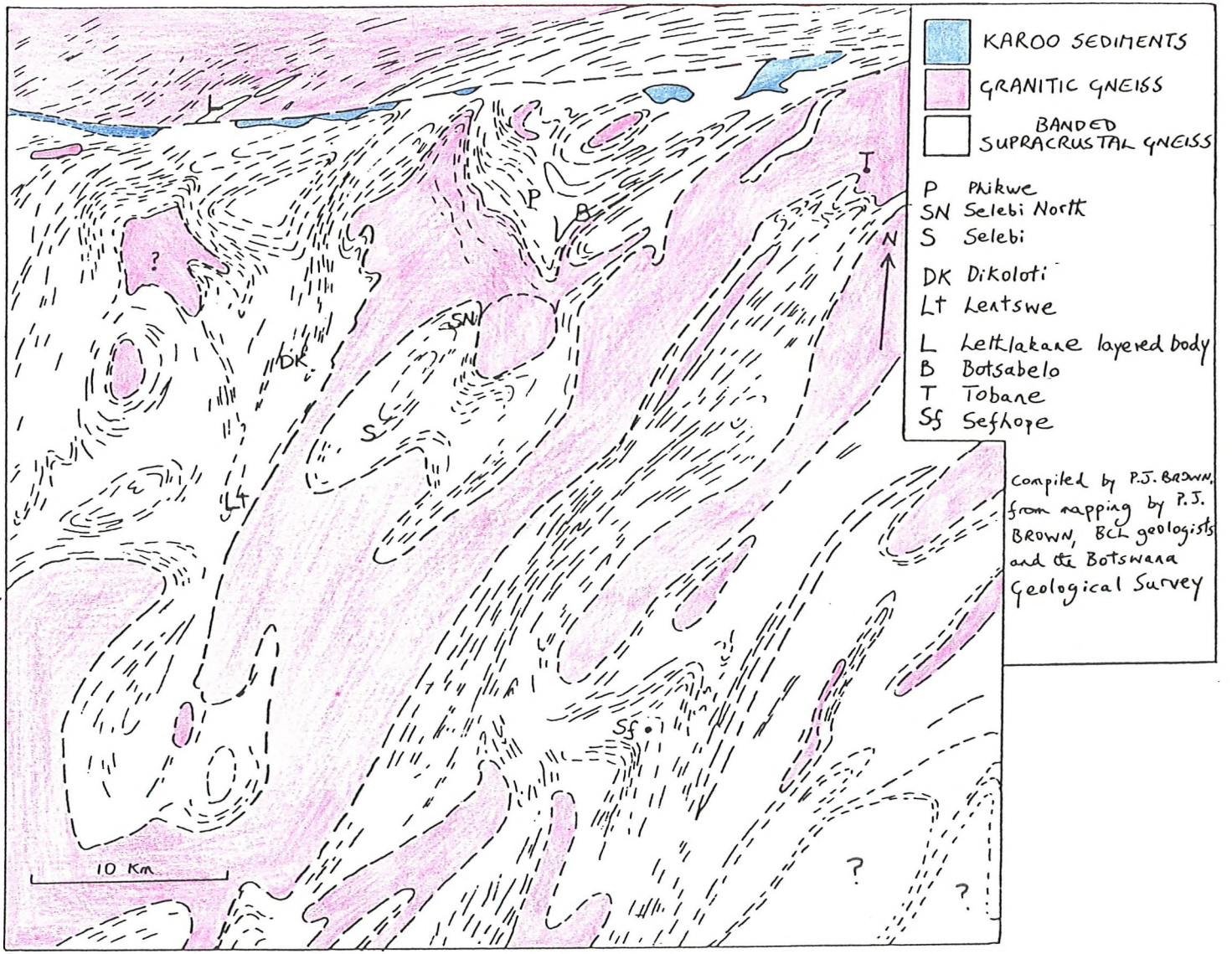

Fig. 2.1 GEOLOGICAL MAP OF THE NORTH MARGIN OF THE CENTRAL ZONE OF THE LIMPOPO BELT IN BOTSWANA.

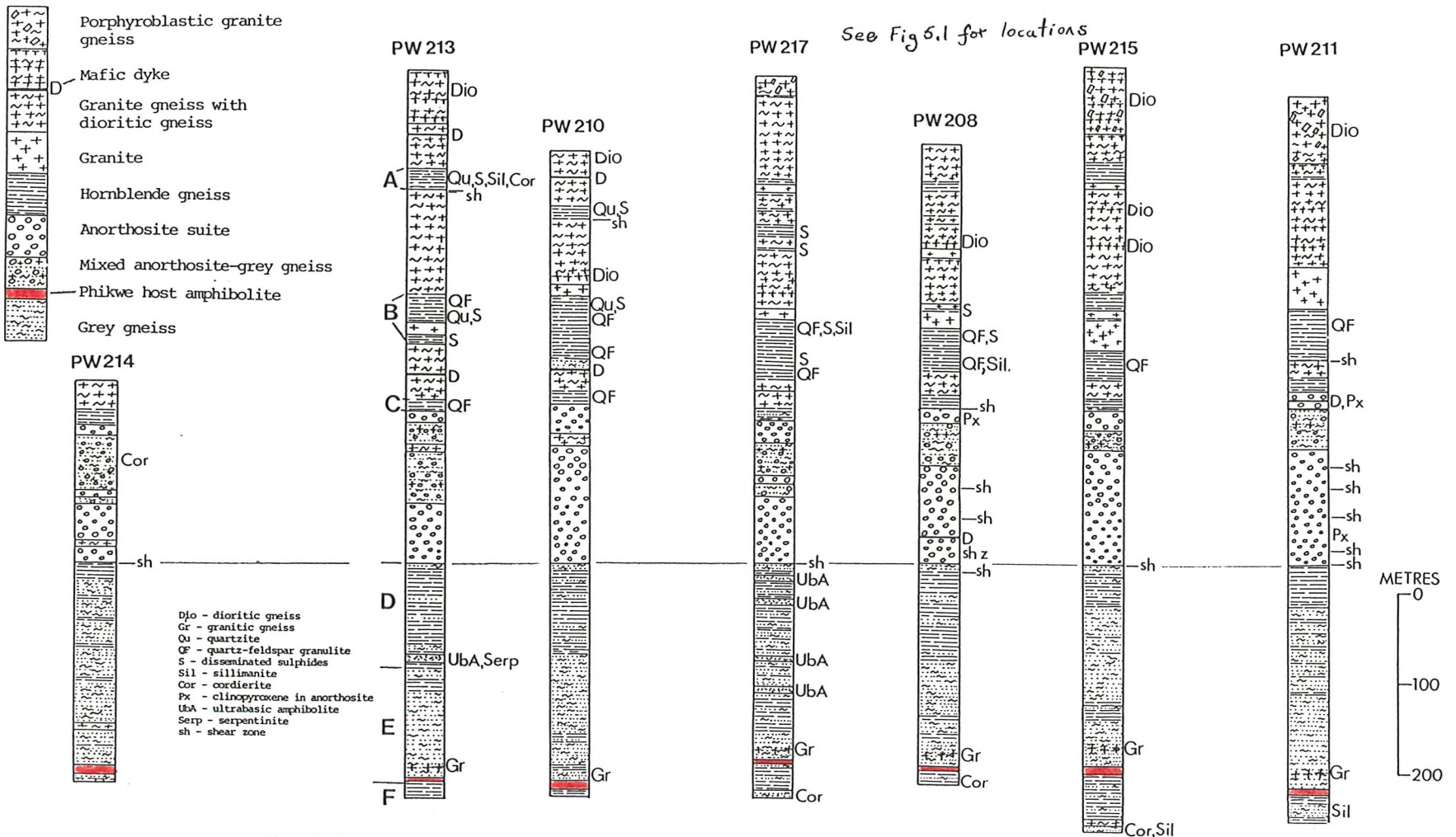

Fig. 2.2 Lithologies intersected in the deepest holes at Phikwe

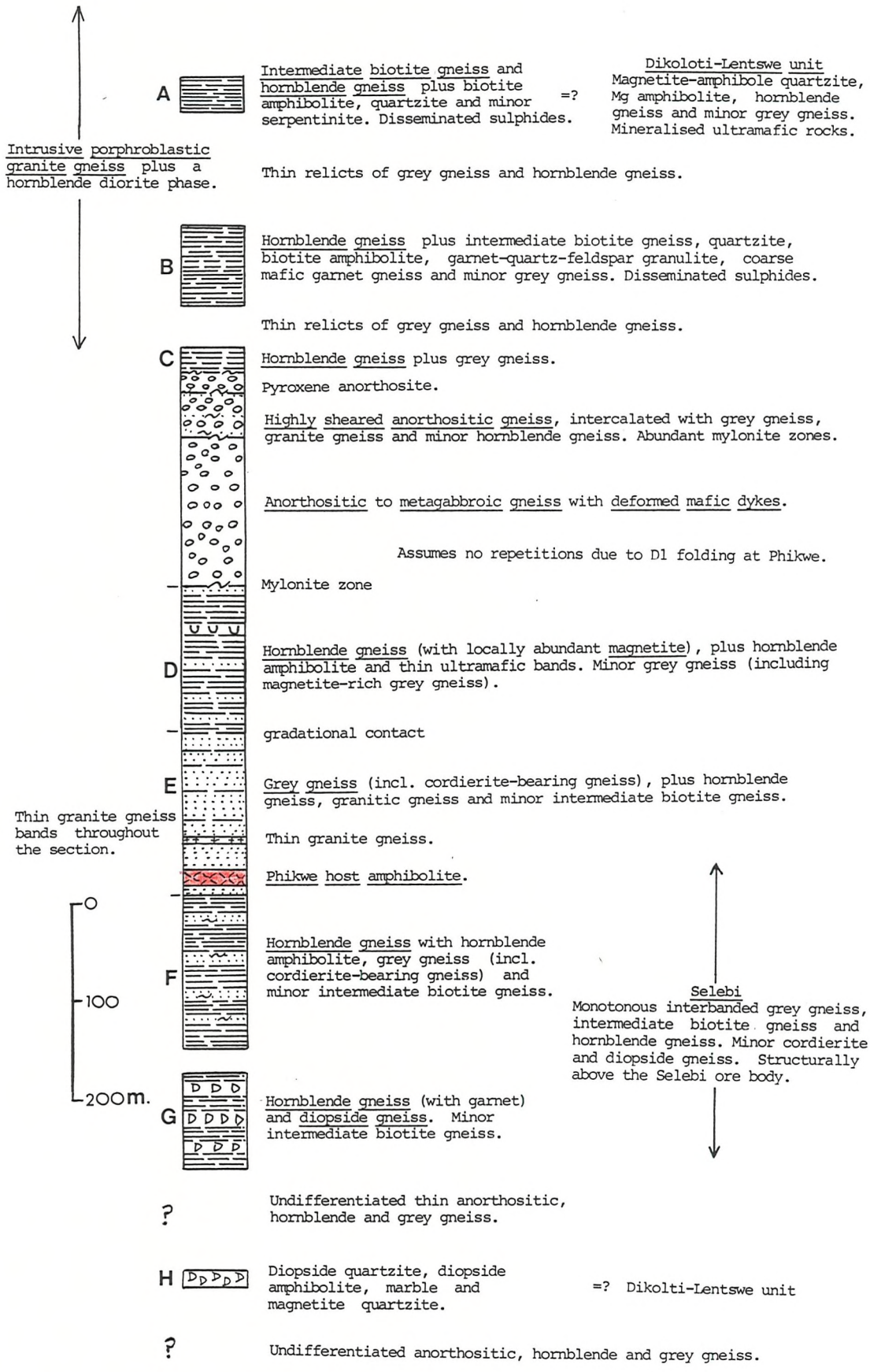

Fig. 2.3 "Stratigraphic" column of the Phikwe area

a) coarse porphyroblastic, dark pink, biotite granite gneiss (65%);
b) medium grained, granoblastic, pink quartzofeldspathic granite gneiss (15%); and
c) migmatitic, well-banded, pink and grey granitic gneisses, often highly deformed (20%).

The most common granitic lithology is a moderately coarse porphyroblastic granitic gneiss, which is either massive or has a faint segregation foliation. A good fabric indicated by biotite is present. Good examples occur in the intrusive body north-east of Phikwe (Plate 3c & d) and in the koppies forming the rim of the Selebi structural basin northwest of Selebi North and between the rim and the Dikoloti-Lentswe unit further west (Plate 3a & b).

The medium-grained granoblastic granitic gneiss (b) is homogeneous and massive to very weakly foliated. It contains less biotite than the porphyroblastic gneiss. Good examples occur in the rim to the Selebi basin, within the basin in contact with anorthositic gneiss (Plate 11e) and in the core of the early fold closure to the east of Botsabelo (Plate 3e).

Both porphyroblastic and granoblastic granitic gneiss are cut by deformed quartz-feldspar veins (Plate 13e). Both contain rare diffuse hornblende-rich patches and schlieren which are regarded as xenoliths (Plate 3e). No intrusive contacts between the two types were found. In the rim to the Selebi basin northwest of Selebi North, granoblastic granitic gneiss grades into coarse porphyroblastic gneiss going westwards. There are few obvious intrusive contacts between the granitic gneisses and the supracrustal assemblage. Granoblastic granitic gneiss intrudes and cuts across the fabric of banded hornblende and grey gneisses and anorthositic gneiss in the Selebi basin, just west of Selebi North. The porphyroblastic gneiss bodies to the northeast of Phikwe and northeast of the Selebi basin appear on air photographs to have intrusive dome relationships with the surrounding supracrustal gneisses. Thin granitic bands occur throughout the well-banded supracrustal gneisses. Their sharp margins and homogeneous coarser-grained unbanded granitic appearance within finely banded gneisses suggest these bands are intrusive rather than *in situ* partial melts. One particularly prominent granitic gneiss band up to 15 m thick occurs 6 to 20 m above the Phikwe ore body (Fig. 2.2).

Hornblende-bearing dioritic gneiss is associated with the granitic gneisses, particularly with porphyroblastic gneiss, and is well seen in the Phikwe core-section and near Tobane (Plate 2g). In the

Phikwe section this dioritic gneiss occurs as homogeneous unbanded layers within porphyroblastic granitic gneiss and is cut by abundant pink quartz-feldspar veins.

The third type (c) varies from well-banded gneiss consisting of biotite-bearing grey gneiss cut by pale pink quartz-feldspar gneiss, to ptygmatically folded, nebulously migmatitic gneiss (Plate 13a,b,f, & h). Locally the biotite-bearing portion of the migmatites resembles the grey gneiss of the supracrustal assemblage (Plate 13c & d). This is well seen in the Phikwe section where well-banded granitic and grey gneisses occur between the coarse porphyroblastic gneiss and the supracrustal assemblage below (Fig. 2.2). Near Tobane there is a thin strip of highly deformed and sheared migmatitic gneiss with abundant mafic shlieren (Plate 2). This strip occurs within weakly deformed porphyroblastic granitic gneiss associated with more-mafic finer-grained hornblende-bearing gneiss (Plate 2g & h). Adjacent koppies to the west consist of nebulously migmatitic granitic gneiss (Plate 13h). The contact of the weakly deformed granitic gneiss with the migmatites is a thin diffuse pegmatitic zone (Plate 2f). Thin veins of granite gneiss intrude into the migmatites. There is no doubt that the highly deformed migmatites were intruded by the weakly deformed granitic gneiss. The contact between the porphyroblastic and mafic gneiss was not seen and their precise relationship is not known. The migmatitic gneisses near Tobane appear to have suffered more deformation than the supracrustal assemblage and the typical granitic gneisses. They are possibly a sliver of older basement in which the mafic schlieren represent presupracrustal dykes. However their apparently higher deformation could also be the result of localised higher strain.

Bands of the supracrustal assemblage, most obviously hornblende gneiss bands, occur within the granitic gneisses (e.g. Unit A, Fig. 2.2). The Dikoloti-Lentswe unit of supracrustal gneisses (Chapter 8) occurs within porphyroblastic granitic gneiss.

Current thinking by BCL geologists is that much of the granitic gneiss at Selebi-Phikwe is metamorphosed arkosic sandstone (Fig.2.4c, Gallon 1986). They claim to have found evidence which they interpret as sedimentary structures (e.g. current bedding) in the granoblastic biotite-poor granitic gneisses. However in the writer's opinion these structures are produced by thin intersecting quartz and quartz-feldspar veins and minor shears and are not sedimentary structures. The massive to poorly foliated granitic gneisses (Plate 3) have the

appearance of massive granitic intrusives rather than metasediments.

Regional traverses were made from Selebi-Phikwe to the Sefhope area and to Kgarimacheng (Figs 1.1 & 1.2). The rocks between Selebi and Sefhope are dominately porphyroblastic granitic gneiss. A prominent band of granitic augen gneiss (Plate 3f) occurs 2 km east of Sefhope. It appears to mark a zone of increased deformation. Granitic gneiss comprises the majority of the terrain between the Lethlakane Fault and Kgarimacheng. Porphyroblastic and migmatitic granitic gneisses predominate. Porphyroblastic granitic gneiss immediately north of the Lethlakane Fault is variably augened with differential development of augens in adjacent bands (Plate 3h). A later granite nearby has a brecciated appearance (Plate 3g). Cataclastic granitic gneiss occurs in the Lethlakane Fault zone (Plate 16a-f).

The granitic gneisses have been interpreted as being a basement to the supracrustal assemblage (Wakefield 1974), as granitic intrusives into the supracrustal assemblage (Wright 1977) and as metasandstones (Gallon 1986). A similar sedimentary hypothesis in which a huge thickness (up to 20 km) of dominantly granitised arkose underlies the Vumba and Tati schist belts (the Tutume Group) has been proposed by Litherland 1973 and Key et al. 1976. Similar granitic gneisses in the Mmpatse area, east of Matsitama, have been identified as meta-arkoses by Key (Brown unpub. report 1974). The majority of the granitic gneisses at Selebi-Phikwe were regarded by the writer during field-work as having been intrusive granites rather than metasediments. The granitic gneisses are not a basement to the well-banded gneisses, although minor slivers of highly deformed granitic gneiss could be older than the supracrustal gneisses.

2.3 BANDED GNEISSES

The banded gneisses are dominately composed of hornblende gneiss, grey quartzo-feldspathic gneiss and anorthositic gneiss in the approximate proportions of 6:3:2. Gradational relationships exist between some of the lithological divisions, e.g. between hornblende gneiss and intermediate biotite gneiss.

2.3.1 Hornblende Gneisses

Mafic hornblende-rich gneiss occurs throughout the area. Hornblende gneiss is best exposed by sand pits in the Motloutse River, northeast of Phikwe (Plates 4 & 14d), and on the southeast side of the Phikwe dome (Plates 5d & 15d & e). In the section at Phikwe

hornblende gneiss forms a significant component of the non-granitic gneiss units (Fig. 2.2).

Hornblende gneiss varies from massive 100% hornblende amphibolite to well-banded hornblende-feldspar gneiss containing 50% hornblende. It is typically a medium-grained weakly banded speckled gneiss containing 70% hornblende and 30% feldspar. Locally hornblende gneiss contains bright red garnets (particularly in Unit G), magnetite (particularly in Unit D), biotite or disseminated sulphides (particularly in Units A and B, Plate 5b).

Hornblende gneiss is interbanded with grey quartzo-feldspathic gneiss throughout the Phikwe section on all scales. Bands of hornblende gneiss vary from centimetres to 10 metres in thickness. The contacts of individual hornblende gneiss bands are usually sharp. The gradational contact between units, particularly that between Unit D and E, is due to the gradational decrease in the number of hornblende gneiss bands. Hornblende gneiss is also interbanded with intermediate biotite-bearing gneiss and quartzite, for example in the Motloutse River exposure (Plate 4c & d) and in Units A and B (Plate 5a & b) and with diopside gneiss in Unit G. Several hornblende gneiss bands (0.5 to 3 m thick) within grey gneiss in Units E and F of the Phikwe core section show a gradation from a coarse-grained mafic hornblende-rich structural base to a finer-grained less mafic top. Apart from a spotted appearance of hornblende gneiss at Dikoloti, this mineralogical gradation is the only possible original feature seen within the hornblende gneisses. No original textures are preserved. Hornblende gneiss was regarded in the field as metamorphosed mafic igneous rock. It was speculated by the writer that the protolith of hornblende gneiss that is interbanded with quartzite, diopside gneiss or biotite gneiss was a mafic extrusive rock.

2.3.2 Grey Gneisses

Variable medium-grained grey quartzo-feldspathic banded gneisses occur throughout the supracrustal assemblage and comprise the majority of Unit E in the Phikwe section. They form the hanging and footwall gneisses at Selebi-Phikwe (Plates 14a & b, 15a,b,c, & f) and are present at the margins of the Dikoloti-Lentswe unit. Exposure of grey gneiss is usually poor. Grey gneiss is commonly interbanded with hornblende gneiss and lesser intermediate gneiss. However, unlike hornblende gneiss, grey gneiss was never found in association with quartzite or diopside gneiss. The main variation within grey gneiss

is the variable quantities of biotite and hornblende which give the banded appearance of the order of centimeters to one metre. This banding was regarded in the field as possibly representing original compositional differences in grey gneiss protoliths, e.g. in sediments or volcanics. This is the only possibly original feature seen in grey gneiss. No original textures were seen. Garnet and minor sillimanite are common. Garnet is conspicuous in grey gneiss immediately above and below the Selebi ore body. Locally the grey gneiss has a blue tinge due to altered cordierite, particularly in Unit F below the Phikwe ore body and at Selebi. Grey gneiss locally contains thin leucocratic bands (Plate 27c & g). All gradations exist between banded grey gneiss and migmatitic gneiss (Plate 13c & d). However thick sections of banded variable grey gneiss occur without significant leucocratic banding. The leucocratic bands were regarded in the field as having a variety of origins including partial melting (both intrusive locally derived partial melts and *in situ* partial melts), metamorphic segregation and original compositional differences.

2.3.3 Intermediate Biotite Gneisses

The distinction of intermediate biotite gneisses was made for those quartz-feldspar-biotite-amphibole gneisses that could not be clearly assigned to the suites of hornblende gneiss or grey gneiss. Initially the distinction was made in core, but intermediate biotite gneisses are also found in outcrop, for example interbanded with hornblende gneiss and quartzite in the Motloutse River, northeast of Phikwe. Two types of biotite gneiss are recognised, a quartz-rich type and a quartz-poor type. Garnet and cordierite are common components, particularly of the quartz-rich type. Disseminated sulphides are conspicuous in biotite gneiss in Units A and B (Plate 5a-c). Biotite gneisses are usually found interbanded with hornblende gneiss, particularly in Units A and B. They are less commonly distinguished within grey gneiss (usually the quartz-rich type). They also occur interbanded with diopside gneiss of Unit G. Some thin homogeneous bands of intermediate biotite gneiss mineralogy are distinctly finer grained (0.5mm) than typical biotite and grey gneiss.

2.3.4 Anorthositic Gneisses

Anorthositic gneiss outcrops relatively well throughout the area. In the Phikwe section there is a single composite layer of

anorthositic gneiss up to 200 m thick. The base of the anorthositic layer is approximately 250 metres above the Phikwe ore body (Fig. 2.2), a fact which can obviously be used to predict the depth of the highly sheared and thinned ore body in the deepest holes (Brown 1980). It is not known whether it is the same single layer that is repeated by folding and thrusting throughout the area or if there is more than one layer. Anorthositic gneiss is usually found near the contacts of major porphyroblastic granitic gneiss layers with supra-crustal gneisses.

The anorthositic gneisses are coarse-grained plagioclase-rich rocks with lesser hornblende. The plagioclase content varies from 100% (anorthosite) to 60% (metagabbro), but is typically 80 to 90% (hornblende anorthosite) (Plate 9). A higher than average proportion of metagabbro occurs in the anorthosite-metagabbro body, just north of the Lethlakane Fault (Plate 10). In outcrop the distinctively off-white, coarse to medium-grained anorthositic gneisses are massive to moderately foliated. Hornblende occurs as coarse patches and thin laminae (Plate 9). Locally the hornblende occurs as "ophitic" patches enclosing coarse plagioclase porphyroblasts, which gives the rock an igneous cumulate appearance. Patches of coarse pegmatitic hornblende anorthosite also occur within normal anorthosite (Plates 9h & 12f). Coarse porphyroblastic plagioclase occurs in the Lethlakane anorthosite-gabbro body. Usually the anorthosites are poorly layered, although bands of anorthosite, hornblende anorthosite and metagabbro with both gradational and sharp contacts are seen in core sections (Plate 11h). An important exception is the Lethlakane body, in which distinct bands of anorthosite, hornblende anorthosite and metagabbro and thin minor bands of weathered ultramafic rock occur (Plate 10e).

Anorthositic gneiss contains bands of grey gneiss and minor hornblende gneiss and granitic gneiss. This is well seen south of Selebi North and in core (Plate 11h). Highly interbanded and sheared anorthositic, grey and hornblende gneisses are concentrated in the upper part of the anorthosite layer in the Phikwe section (Fig. 2.2) Hornblende and grey gneisses immediately below the anorthosite layer at Phikwe are also highly sheared. Thin (>20 cm) garnetiferous quartz -rich mylonite zones, parallel to the banding, occur throughout the anorthosite section (Plates 11f & 20d), but are concentrated at Phikwe within the upper interbanded zone and at the base of the anorthosite layer (Fig. 2.2). Garnet only occurs in these siliceous zones. It does not occur in typical anorthosite.

Quartz is locally abundant in the anorthositic gneisses as coarse quartz-rich patches. It is this high quartz-content and the included grey gneiss bands that has led BCL geologists (Gallon 1986) to regard the anorthosites as metasedimentary. However the quartz can be shown to be secondary (see Ch. 3.4). For example quartz occurs at the contact of anorthosite with granitic gneiss (like a reaction rim) and as a diffuse network of undeformed quartz veins cutting the anorthosite (Plate 11a-e). Massive quartz-palgioclase anorthosite appears to replace and transgress weakly foliated hornblende anorthosite in core sections. Grey gneiss appears to have been tectonically interbanded with anorthositic gneiss during thrusting. The anorthositic gneisses were regarded in the field as metamorphosed igneous cumulates. This proposal is tested petrochemically in Chapters 3 and 4. The main alternative is that they are aluminous calcareous metasediments (Bahnemann 1972). No intimate relationship between anorthositic gneiss and hornblende gneiss was seen. Hornblende gneiss, particularly hornblende gneiss that is interbanded with quartzite and biotite gneiss, was easily distinguished from coarse-grained hornblende anorthosite and metagabbro.

2.3.5 Other Lithologies

Other lithologies present in the Selebi-Phikwe supracrustal assemblage include metasediments, calc-silicate gneiss and quartz-feldspar granulite, diopside gneiss, ultramafic rocks (including the host rocks to the mineralisation at Selebi-Phikwe and Dikoloti-Lentswe) and deformed mafic dykes.

2.3.5a Metasediments

Rocks regarded as undisputed metamorphosed sediments occur as a very small fraction of the supracrustal assemblage at Selebi-Phikwe. They include magnetite quartzite and marble. They are individually much thinner and volumetrically much less important than similar rocks in the Messina-Beit Bridge area. An intermittent but persistent magnetite quartzite-bearing unit has been mapped to the west of Selebi-Phikwe (Fig. 2.1) and has a N-S strike length of 40 km. The Dikoloti and Lentswe prospects occur within this unit. Most conspicuous is a finely laminated magnetite quartzite from 0.5 to 2 m thick. However more common is a well-banded quartz-amphibole rock with or without magnetite (Plates 6 & 7). These banded rock are associated with a massive light-green to red-brown weathering amphibolite (up to

5 m thick). The amphibolite contains thin bands composed of quartz with very minor amphibole (Plates 6e, 7c & d). Small isolated pods of serpentinite and lesser pyroxenite,including the mineralised serpentinised peridotites and amphibole pyroxenites at Dikoloti, Lentswe and Phokoje (Ch. 8), intermittently outcrop along the entire length of this magnetite quartzite-amphibolite unit (Fig. 8.1). The unit has not been recognised in the Selebi-Phikwe area before. It is the most extensive single unit mapped in the area.

Similar magnetite quartzite is not found in the Phikwe section. However the occurrence of quartzites and serpentinous gneisses, both with significant pyrrhotite, in Unit A (Figs 2.2 & 2.3) suggests that Unit A could be the equivalent at Phikwe of the Dikoloti-Lentswe horizon. This is reinforced by mapping the position of the Dikoloti-Lentswe horizon round the open late folds to Phikwe (Fig 2.4d) and by the exposure of a pod of serpentinite in the Selebi-Phikwe township within Unit A. Alternatives to this are that the Dikoloti-Lentswe unit is equivalent to Unit H or that it is a part the Phikwe section does not contain the whole of the Selebi-Phikwe sequence.

Thin quartzites containing pyrrhotite, sillimanite and feldspar, associated with hornblende gneiss and intermediate biotite gneiss occur in Unit B in the Phikwe section (Plate 5b) and in the Motloutse River exposure (Plate 4d). A thin diopside quartzite associated with diopside amphibolite (Unit H) outcrops in the Phikwe dome, northeast of Phikwe. A thin marble was mapped by Wakefield (1974) along the continuation of this horizon. However its location is now covered by the Phikwe tailings dam.

2.3.5b Calc-silicate Gneiss and Quartz-Feldspar-Garnet Granulite

Thin bands (usually less than one m) of calc-silicate gneiss and garnetiferous quartz-feldspar granulite outcrop between the anorthosite unit and the main granitic gneiss unit, for example east of Botsabelo where both lithologies occur in a tight early antiform, adjacent to granitic gneiss in the core. The calc-silicate gneiss is a fine to medium-grained greasey-looking quartz-feldspar-hornblende gneiss. It is usually finely banded and contains variable amounts of hornblende, but is usually quite felsic (Plate 8a-c). It has not been recognised in the Phikwe core-section. Calc-silicate gneiss is easily distinguished from grey gneiss because of its greasey siliceous appearance and lack of biotite. The lithology was initially difficult to distinguish from nearby anorthosites, and has been misidentified

as anorthosite by Key (1976) (see Plate 14, Key 1976) and Gallon (1986), the latter using its finely banded siliceous nature as further evidence that the anorthosites are metasedimentary.

Where the rock contains no hornblende it has been termed a quartz-feldspar granulite. The pale-pink quartz-feldspar granulite usually contains a few scattered bright-red garnets and is more feldspathic and less-banded than the calc-silicate gneiss (Plate 8d). Quartz-feldspar granulites are conspicuous in the Phikwe core-section within and immediately above Unit B associated with hornblende gneisses (Fig. 2.2, Plate 5c). Here they have the appearance of intrusive granitoids, but minor garnet-rich bands (Plate 20c) and traces of sillimanite argue against this. Garnetiferous quartz-feldspar granulite forms only a small portion of the assemblage at Selebi-Phikwe. However in the Messina-Beit Bridge area, similar rocks are more important, for example at Mount Shanzi (Brown unpub. report 1976; Watkeys et al. 1983). Although the calc-silicate gneiss and garnetiferous quartz-feldspar granulite at Selebi-Phikwe have been grouped together, it is was thought in the field that they could represent significantly different protoliths, e.g. sediments, felsic volcanics, felsic intrusives and mylonites (see Chs 3.4 & 4.4).

2.3.5c Diopside Gneiss

Diopside gneisss outcrops in the koppies immediately northwest of Phikwe and in the Lethlakane River near its junction with the Motloutse River. Up to 85 m of diopside gneiss (Unit G) occurs below the Phikwe ore body (Fig. 2.3). The diopside gneiss consists of coarse weakly-foliated diopside-feldspar gneiss (up to 7 m thick) and highly banded diopside-feldspar-hornblende gneiss, in about equal proportions. Individual bands in the highly banded gneiss are 2-5 cm thick and some appear to be mineralogically graded. The two types of diopside gneiss occur interbanded with each other and together occur interbanded with garnetiferous hornblende gneiss and lesser biotite gneiss. Similar banded (and mineralogically graded) diopside-feldspar -hornblende gneiss was found associated with hornblende gneiss in the large gently plunging folds 13 km to the east of Sefhope (Fig. 1.2). The origin of the diopside gneiss was thought in the field to be intimately related to that of the hornblende gneiss.

2.3.5d Ultramafic Rocks including Host Rocks to Ni-Cu Mineralisation

Ni-Cu sulphide mineralisation at Phikwe, Selebi and Selebi North

is associated with a similar layer (from 1 to 25 m thick) of hornblende-rich amphibolite with lesser pyroxenite and minor peridotite at approximately the same "stratigraphic" position (Figs 2.2 & 2.3 and Chs 5, 6 & 7). The host amphibolite is conformable with the surrounding grey quartzo-feldspathic gneiss. Ni-Cu mineralisation also occurs in serpentinised peridotite and amphibole pyroxenite at Dikoloti and Lentswe (Ch. 8). Isolated thin pods and bands (from 1 to 8 m thick) of ultramafic rocks with very minor or no disseminated sulphide occur throughout the supracrustal assemblage and particularly within the hornblende gneisses of Unit D (Fig. 2.2 & 2.3). These ultramafic pods consist of amphibole pyroxenite, variably serpentinised peridotite and amphibolite, either as composite or single-lithology pods. Pyroxenite pods have amphibolite margins. The ultramafic rocks, particularly the pyroxenites, are coarse-grained and massive. However some of the amphibolites are schistose and have a good fabric picked out by phlogopite, e.g. some of the ultramafic amphibolites at Dikoloti-Lentswe. Except for minor ultramafic bands in the layered Lethlakane anorthosite-metagabbro body, the anorthositic gneisses are not associated with ultramafic rocks.

2.3.5e Deformed Dykes

Deformed and metamorphosed mafic dykes are found in the Selebi-Phikwe gneisses, particularly in the anorthosites (Plate 12a-e). In the Phikwe core section they mainly occur near the top of the anorthosite layer. The dykes consist of fine to medium-grained hornblende-feldspar gneiss or amphibolite. Recognition of them in core is difficult. However some deformed mafic dykes within anorthosites and granitic gneisses have been distinguished by their fine-grained nature, relative thinness, sharp contacts and unbanded appearance. They are more easily recognised in anorthosites and granitic gneisses than in hornblende gneiss units. However the observation that they mostly occur within anorthosites is thought to be valid.

Undeformed and unmetamorphosed dykes trending between east and northeast (i.e. parallel to the ENE Limpopo trend) are easily recognised and are of Waterberg and Karoo age (Mason 1969).

2.4 STRUCTURE AND METAMORPHISM OF THE SELEBI-PHIKWE AREA

The structure of the Selebi-Phikwe area has been studied by Wakefield (1974, 1977), Key (1976) and Wright (1977) and placed in

the regional framework of the northern margin of the Limpopo Belt by Coward et al. (1976a,b). The structural history outlined here is a simpler version of these accounts and agrees most closely with that of Wright. The deformation suffered by the Selebi-Phikwe gneisses has been divided into two major periods, early (D1) and late (D2) (Fig. 3.4).

The major early folds were flat-lying structures (nappes). Wright (1977) has differentiated the early deformation into F1 and F2. However the early deformation is treated here as a continuous event with later folds refolding the earliest ones. Examples of major early closures are those at Selebi and Selebi North (Fig. 2.4). The regional gneissic foliation was formed during the early episode. The foliation is axial planar to the earliest folds, for example as defined by biotite at Selebi (Plate 14b). A rodding lineation formed parallel to the early fold axes (Plate 13g, Fig. 5.3a). Examples of early minor folds are shown in Plates 7f & g, 8b and 14. The development of flat-lying mylonites (Plate 14f) due to thrusting and imbricate stacking was important during the early episode, particularly during late D1. Flat-lying mylonites and cataclasites were also formed in the Sefhope area (Plate 16g & h). It was not always straight forward to distinguish between D1 and D2 minor folds, particularly in the migmatitic granitic gneisses (Plate 13e-f). The folding in the migmatitic gneisses is thought to be mainly late D1 and lesser early D2.

There are no reliable younging criteria at Selebi-Phikwe. Regional work by Wright (1977) indicates the Phikwe section is inverted. This is weakly reinforced at Phikwe by the location of the massive sulphide usually at the structural top of the host amphibolite (see Chs 5, 6 & 7). No definite major D1 folds nor any minor D1 folds were found in the anorthositic gneisses. The contacts of the anorthositic units are mylonite zones and the upper portion of the anorthosite unit at Phikwe is interbanded with grey and granitic gneiss and is highly mylonitised. It is thought possible that slices of anorthosite were thrust into the Selebi-Phikwe sequence during the late D1. Somewhat similarly, post-F1 intrusion of anorthosite was suggested by Key (1976) and Light and Watkeys (1977) but later rejected (Key 1977; Watkeys et al. 1983) for pre-F1 in situ intrusion. The practice of regarding the anorthosites at Selebi-Phikwe as a single "stratigraphic" marker in the construction of cross-sections (Fig. 2.4a-c) is questionable. Some calc-silicate

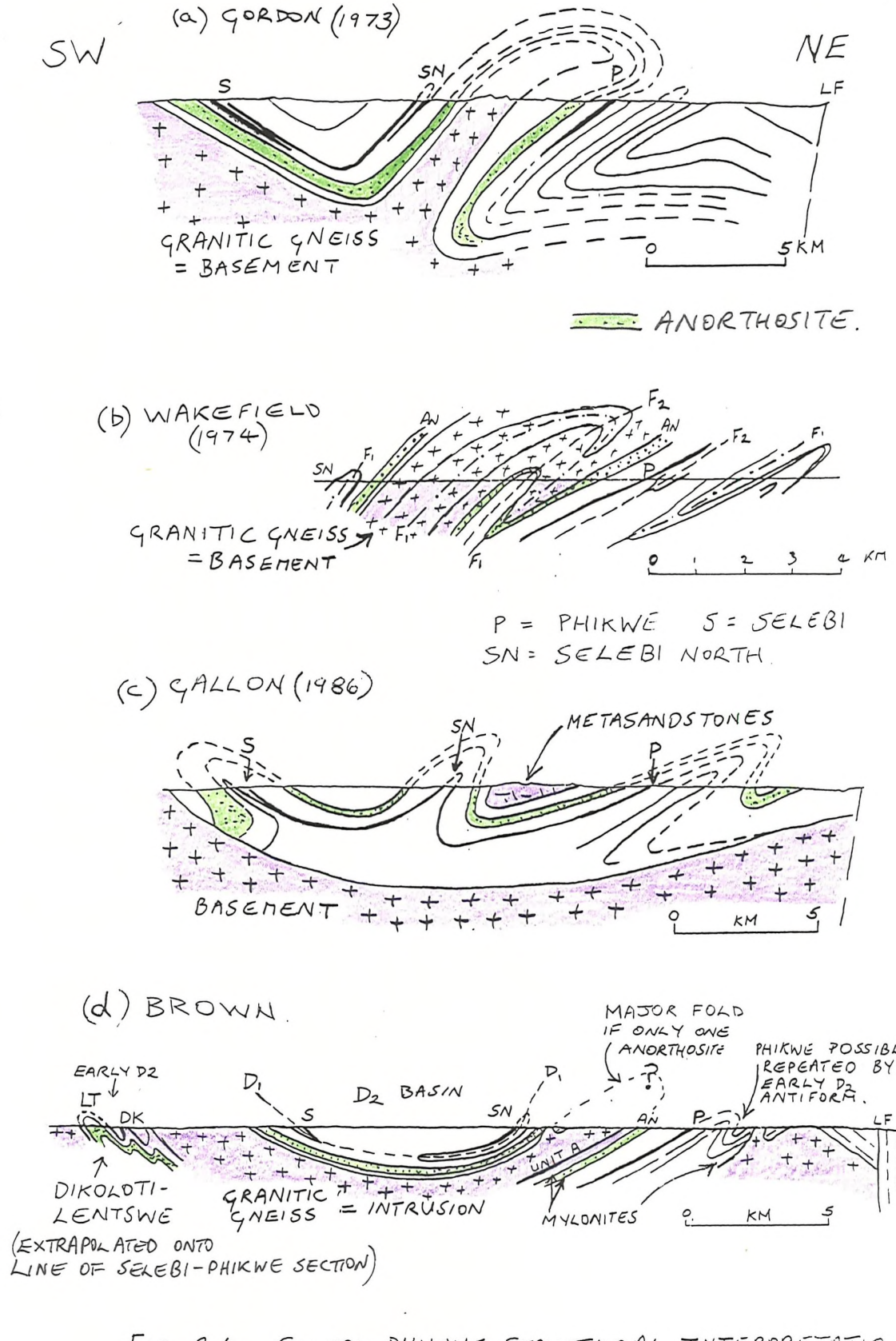

FIG. 2.4. SELEBI-PHIKWE STRUCTURAL INTERPRETATIONS

gneiss bands have been mistaken for anorthosites in these sections. A simpler less-interpretative section is preferred (Fig. 2.4d). The gneisses in the Selebi basin above the Selebi ore body can not be precisely correlated with those below the Phikwe ore body (Fig. 2.3), possibly because of D1 repetition at Selebi. It is therefore not possible to conclude that there is only one anorthosite layer and hence the anorthosite layer cannot be used as a "stratigraphic" marker (Fig. 2.4d, in which Dikoloti and Hentswe have been extrapolated).

The Selebi ore body is a complex early structure (Figs 5.4 & 5.5). Brown (1980, 1981b) showed that the repetition of the Upper body was due to D1 folding (Plate 14b). Shearing and possible complete attenuation of a middle antiform has taken place. The antiformal closure at Selebi North is possibly the same early fold structure as Selebi and both are possibly part of a major early nappe (Fig. 2.4d). If the alignment of the Selebi, Selebi North and Phikwe ore bodies is more than coincidence, it means that a Selebi-Selebi North early nappe is more likely and that the early nappe closure should be repeated at Phikwe. However no evidence of an early closure was found at Phikwe. Possibly Phikwe is a sheared limb of an attenuated early structure. However major early closures are difficult to find. Soil geochemistry rather than conventional mapping found the closure at Selebi. There appears to be a section without repetitions at Phikwe.

The later deformation period (D2) produced the open dome and basin structures (Figs 2.1 & 2.4). Major examples are the Selebi basin and the Phikwe dome (Plate 1). Wakefield (1974) thought that these structures were produced by interference of F3 folds (trending approximately NW) and F4 folds (approximately NE). However it is thought that these structures possibly formed during one continuous event of combined compression and shearing (Wright, pers comm 1986). 1967). Early D2 folds are recumbent. Later D2 folds are upright. Good examples of D2 minor folds are found in the footwall of the Phikwe ore body (Plates 15a, 26b & c, Fig. 5.3). Phikwe lies on the southwest limb of an early D2 anitform (Fig. 2.4). The possible repetition of Phikwe in this antiform to the northeast is an important exploration target (Brown 1980). Other examples of D2 minor folds are shown in Plates 15 and 28g. Associated with D2 is the development of cataclasites and mylonites, particularly well seen in the Phikwe ore body (Plates 26g & h, 27a-d). Shearing was localised in the Selebi-Phikwe ore bodies during both D1 and D2. The role of deform-

ation and metamorphism in the location of sulphides at Selebi-Phikwe is discussed in detail in Chapters 5 and 6.

Immediately north of the Lethlakane Fault at Selebi-Phikwe, there is a 10 km wide, ENE-trending strip of highly sheared, dominantly granitic gneisses with thin zones of intense cataclastic deformation (Plate 3h). This is the western continuation of the Tuli-Sabi Straightening Zone (Figs 1.2 & 1.3). The southern margin of this strip is a prominent zone of cataclastic granitic gneiss up to 100 m wide on either side of the later Lethlakane Fault (Plate 16a-f). The Lethlakane Fault is marked by pseudotachylitic veins cutting the granitic gneisses (Plate 16e & f). The Lethlakane Fault has had repeated post-Limpopo movements, with at least 20 m post-Karoo downthrow to the south (Hart, pers. comm. 1974). Small outliers of flat-lying Karoo sediments unconformably overlie the Selebi-Phikwe gneisses, particularly along the south side of the Lethlakane Fault, for example northeast of the Phikwe dome. The swing of the F4 axial traces from N38E in the south to N56E immediately south of the Lethlakane Fault indicates late dextral movement along the Tuli-Sabi Straightening Zone. Much of the deformation in this zone was synchronous with the later deformation period at Selebi-Phikwe (Table 1.2).

Granitic gneisses, the great majority of which are regarded as intrusive, have suffered varying degrees of deformation and are of a variety of ages. Some appear to have been deformed during the D1, for example the migmatitic granitic gneisses. Thick sheets of granite were probably intruded between D1 and D2. The granitic bodies northeast of Phikwe and the Selebi basin appear to be associated with D2. The body northeast of Phikwe has cataclastic margins (Plate 3c).

The metamorphism of the Selebi-Phikwe area will be discussed along with the detailed petrology of the Selebi-Phikwe gneisses in Chapter 3. It is sufficient to indicate here that the supracrustal gneisses at Selebi-Phikwe have a complex metamorphic history with rocks of the transition from amphibolite to granulite facies preserved. Sillimanite, corundum and later cordierite formed in the grey quartzo-feldspathic gneisses and biotite gneisses. The ultramafic rocks contain metamorphic olivine and pyroxene. Sapphirine occurs in a feldspathic amphibolite at Dikoloti.

2.5 SUMMARY

The highly deformed and metamorphosed gneisses at Selebi-Phikwe

can be split up into granitic gneisses and a well-banded supracrustal assemblage of hornblende gneiss, grey quartzo-feldspathic gneiss and anorthositic-metagabbroic gneiss with minor calc-silicate gneiss, metasediment, quartz-feldspar granulite and ultramafic rock (including the hosts to Ni-Cu mineralisation at Selebi-Phikwe and Dikoloti-Lentswe). I believe that the majority of the granitic gneisses were intrusive granites into the well-banded gneisses rather than a basement to the well-banded gneisses or metasandstones. (This is in agreement with Wright (1977).) Minor slivers of highly deformed granitic gneiss could be older than the supracrustal gneisses. The anorthositic gneisses were regarded in the field as metamorphosed feldspathic igneous cumulates rather than metasediments. No relationship between anorthosite and hornblende gneiss was seen, in disagreement with the observations of Key (1977) and Wright (1977). The deformation suffered by the Selebi-Phikwe gneisses can be simply split into an early period (D1) of flat-lying isoclinal folds and refolds (nappes) with imbricate thrusting and a later period (D2) of domes and basins and cataclastic deformation (see Fig. 3.4). The Selebi-Phikwe ore bodies and host rocks have suffered the earliest phase of deformation that can be recognised in the Selebi-Phikwe gneisses. It is possible that the anorthosites were tectonic slices emplaced during late D1 rather than <u>in situ</u> pre-D1 intrusions. Granites were mainly intruded in the interval between D1 and D2. Migmatitic granitic gneiss locally formed during late D1.

PLATE 2 (overleaf)

Migmatitic gneisses near Tobane

(A) - (E) Highly deformed migmatitic gneisses with mafic schlieren.

(F) Contact of migmatitic gneiss with massive weakly deformed granitic gneiss (at top of photo).

(G) Fine-grained weakly deformed hornblende-bearing dioritic gneiss.

(H) Coarse-grained weakly deformed porphyroblastic granitic gneiss.

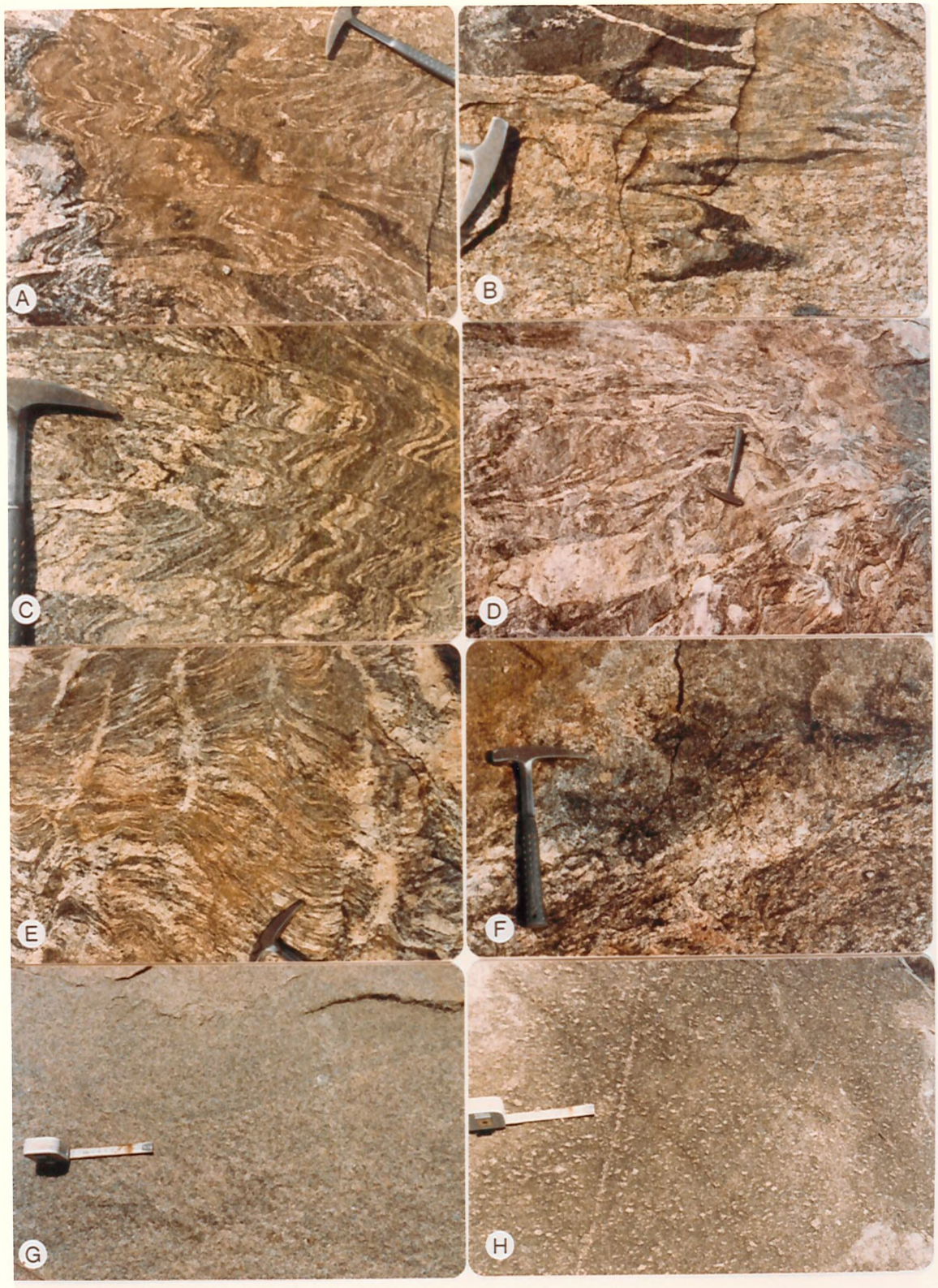

PLATE 2

PLATE 3
Granitic gneiss

(A) Moderately foliated granitic gneiss, Phokoje North.

(B) Weakly foliated porphyroblastic granitic gneiss, Phokoje South.

(C) Porphyroblastic granitic gneiss (see D). Microcline porphyroblasts in matrix of quartz, microcline and minor biotite. Cataclastic texture. Northeast of Phikwe, Sample # 31-7-3. FV = 6 mm.

(D) Porphyroblastic granitic gneiss, northeast of Phikwe.

(E) Coarse-grained weakly foliated granitic gneiss with mafic xenolith, east of Botsabelo in core of D1 antiform.

(F) Granitic augen gneiss, Sefhope.

(G) Coarse-grained porphyroblastic (brecciated ?) granodioritic gneiss, Segodi immediately north of the Lethlakane Fault.

(H) Sheared and augened granitic gneiss, Segodi immediately north of the Lethlakane Fault.

PLATE 4
Hornblende gneiss in the Motloutse River, northeast of Phikwe

(A) Coarse-grained homogeneous hornblende gneiss. Folded leucocratic veins with more mafic hornblende gneiss at their margins.

(B) Banded hornblende gneiss.

(C) Banded hornblende gneiss and intermediate biotite gneiss (both quartz-poor and quartz-rich types).

(D) Banded hornblende gneiss and intermediate biotite gneiss (both quartz-poor and quartz-rich types) with minor quartzites (meta-cherts ?).

PLATE 5

(A) & (C) Unit B in PW 210 (continuous section from A to C, top of is towards top of hole). Variable interbanded hornblende gneiss, intermediate biotite gneiss (QRIB, QPIB, ARIB and GRHG) and quartz-feldspar granulite plus minor grey gneiss. Disseminated pyrrhotite and traces of chalcopyrite in hornblende gneiss and intermediate biotite gneiss.

(B) Unit A in PW 213. Interbanded hornblende gneiss, intermediate biotite gneiss (mainly QRIB plus GRHG) and quartzites (meta-cherts ?). Disseminated sulphides (mainly pyrrhotite) throughout.

(D) Feldspathic hornblende gneiss with quartz bands (deformed veins ?), Phikwe dome.

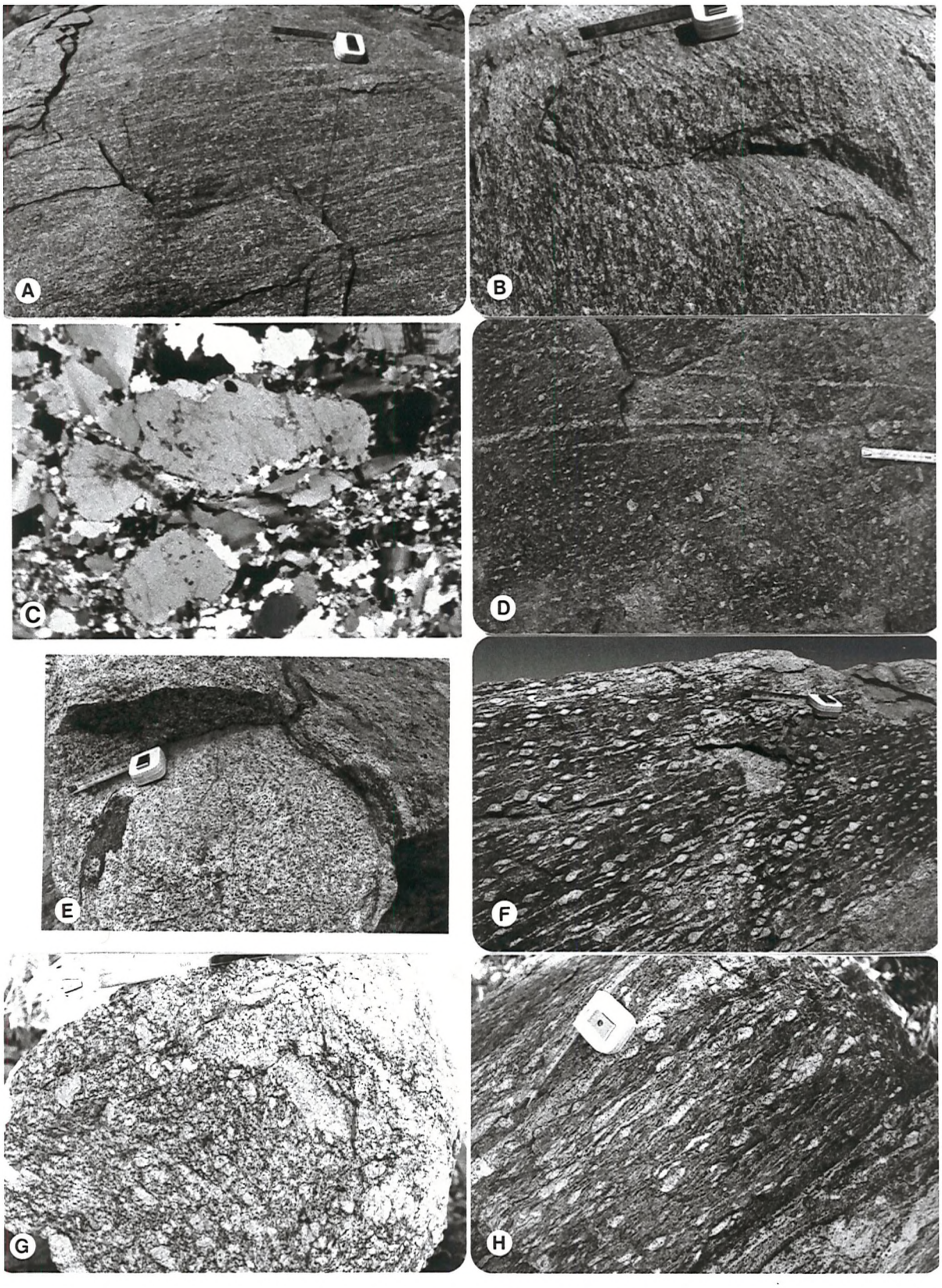

PLATE 3

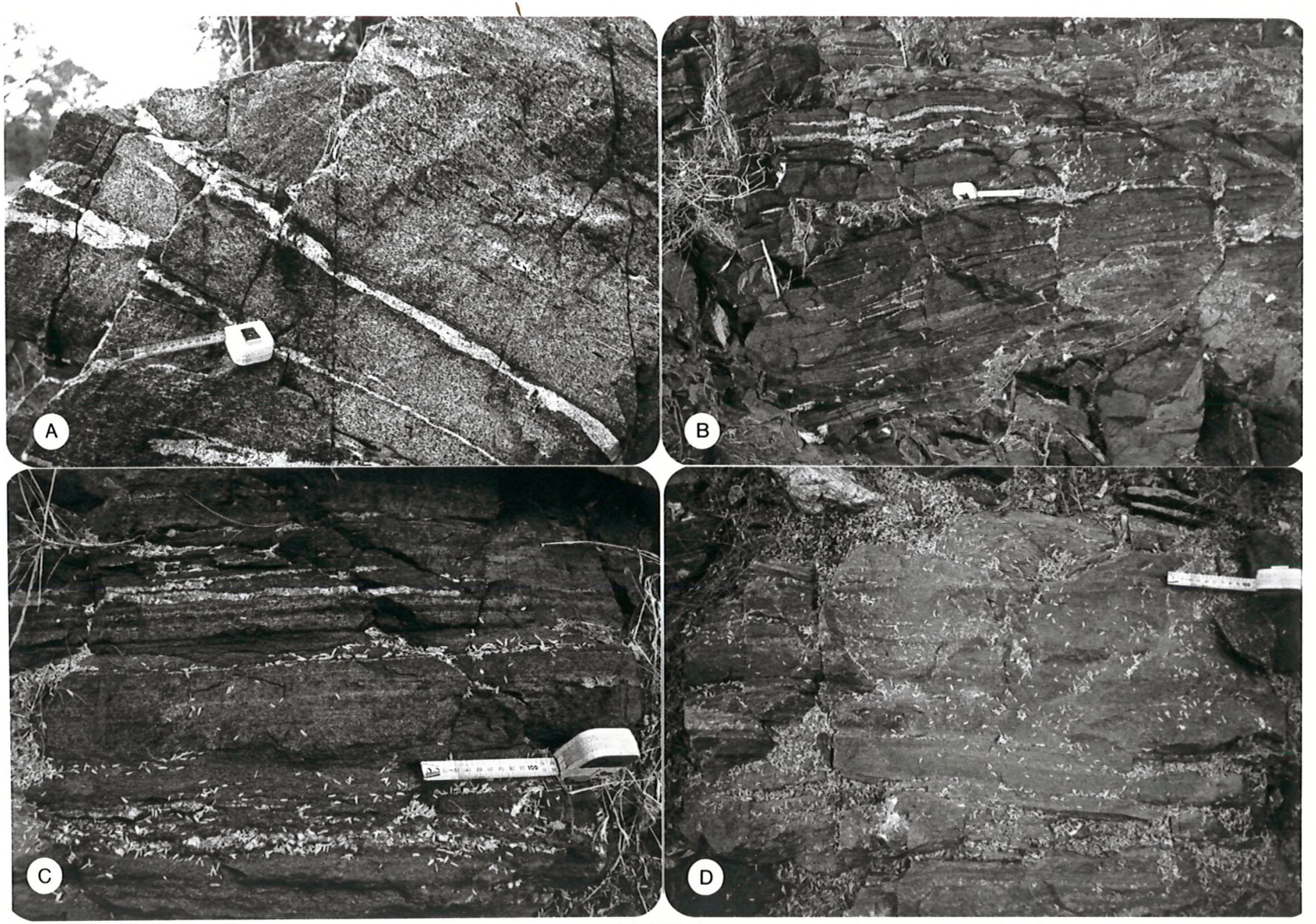

PLATE 4

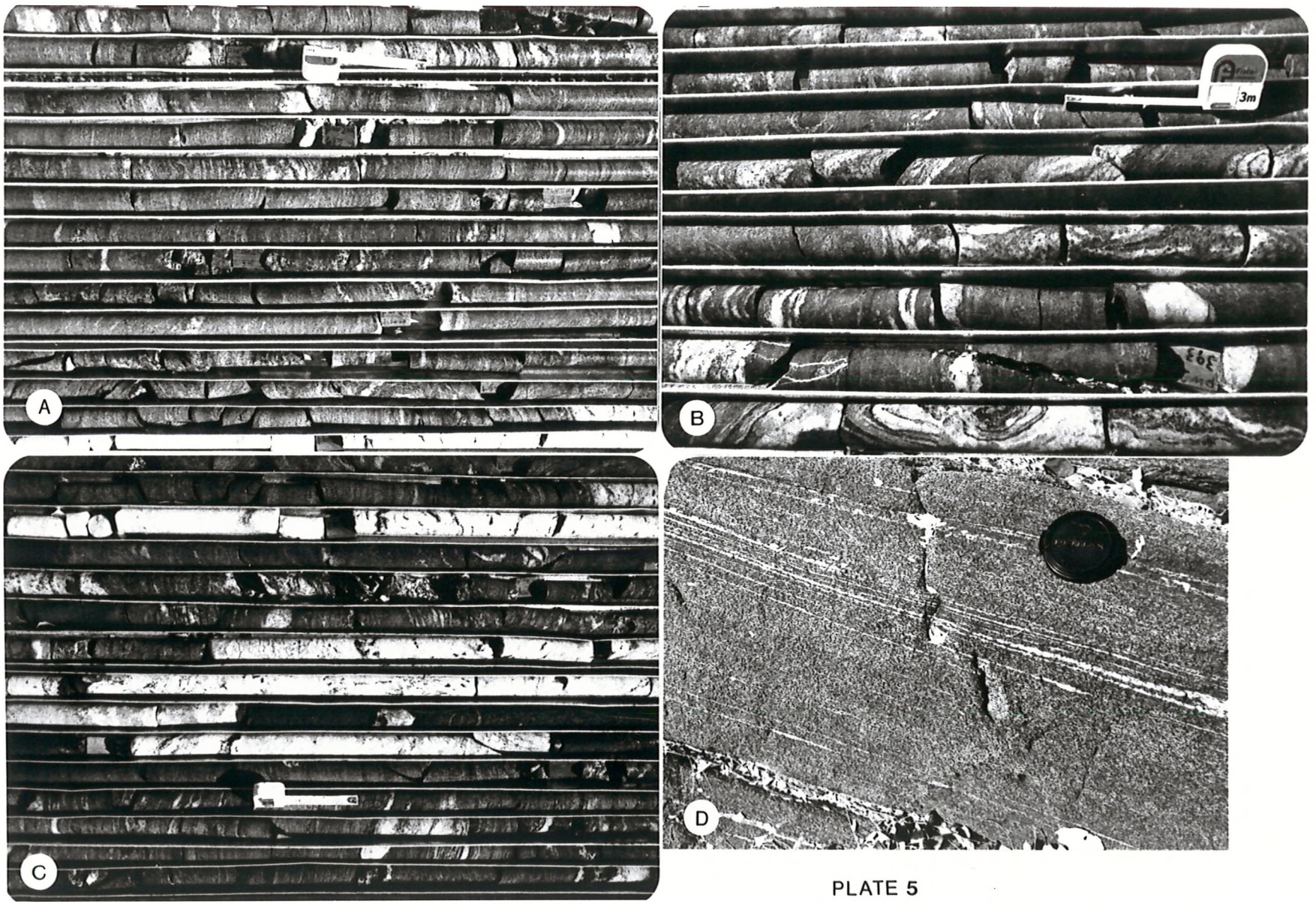

PLATE 5

PLATE 6

The morphology of amphibolites associated with magnetite quartzite

(A) Siliceous magnetite-amphibole quartzite, Seloka North (see Fig. 8.1 for locations).

(B) Banded actinolite amphibolite and quartzite (with minor actinolite and magnetite), Mogolodi.

(C) Banded cummingtonite amphibolite and quartzite, Lethlakane S.

(D) Cummingtonite amphibolite with quartzite laminae, Lethlakane South.

PLATE 7

The regional nature of the amphibolite-quartzite association.

(A) Siliceous magnetite-amphibole quartzite, Khurumella.

(B) Siliceous magnetite-amphibole quartzite with amphibolite bands, Mogolodi.

(C) Banded actinolite amphibolite and quartzite, Lethlakane.

(D) Banded quartzite-amphibolite (early D2 folding ?), Lethlakane South.

(E) Massive cummingtonite amphibolite, Phokoje.

(F) Siliceous magnetite-amphibole quartzite, Seloka North

(G) Detail of (F) showing amphibolite in core of D1 interference fold.

PLATE 8

Calc-silicate gneiss and quartz-feldspar granulite

(A) Banded plagioclase-hornblende-quartz gneiss, east of Botsabelo.

(B) Siliceous quartz-hornblende-plagioclase gneiss, with D1 minor fold, east of Botsabelo.

(C) Banded hornblende-plagioclase-quartz gneiss, near Selebi North.

(D) Spotty garnetiferous quartz-plagioclase granulite, east of Botsabelo.

PLATE 9

Morphology of Selebi-Phikwe Anorthosites (1)

(A) & (B) Banded hornblende anorthosite, Phikwe.

(C) Banded hornblende anorthosite, Dikoloti-Lentswe.

(D) (E) Banded hornblende anorthosite, Khurumella. Folding and shearing in (E).

(F) Sheared cataclastic anorthositic gneiss, Lethlakane immedately south of Lethlakane Fault.

(G) Anorthosite with "ophitic" hornblende patches, towards Tobane

(H) Zone of coarse-grained banded (sheared ?) plagioclase-hornblende gneiss in massive hornblende anorthosite, southwest of Selebi North.

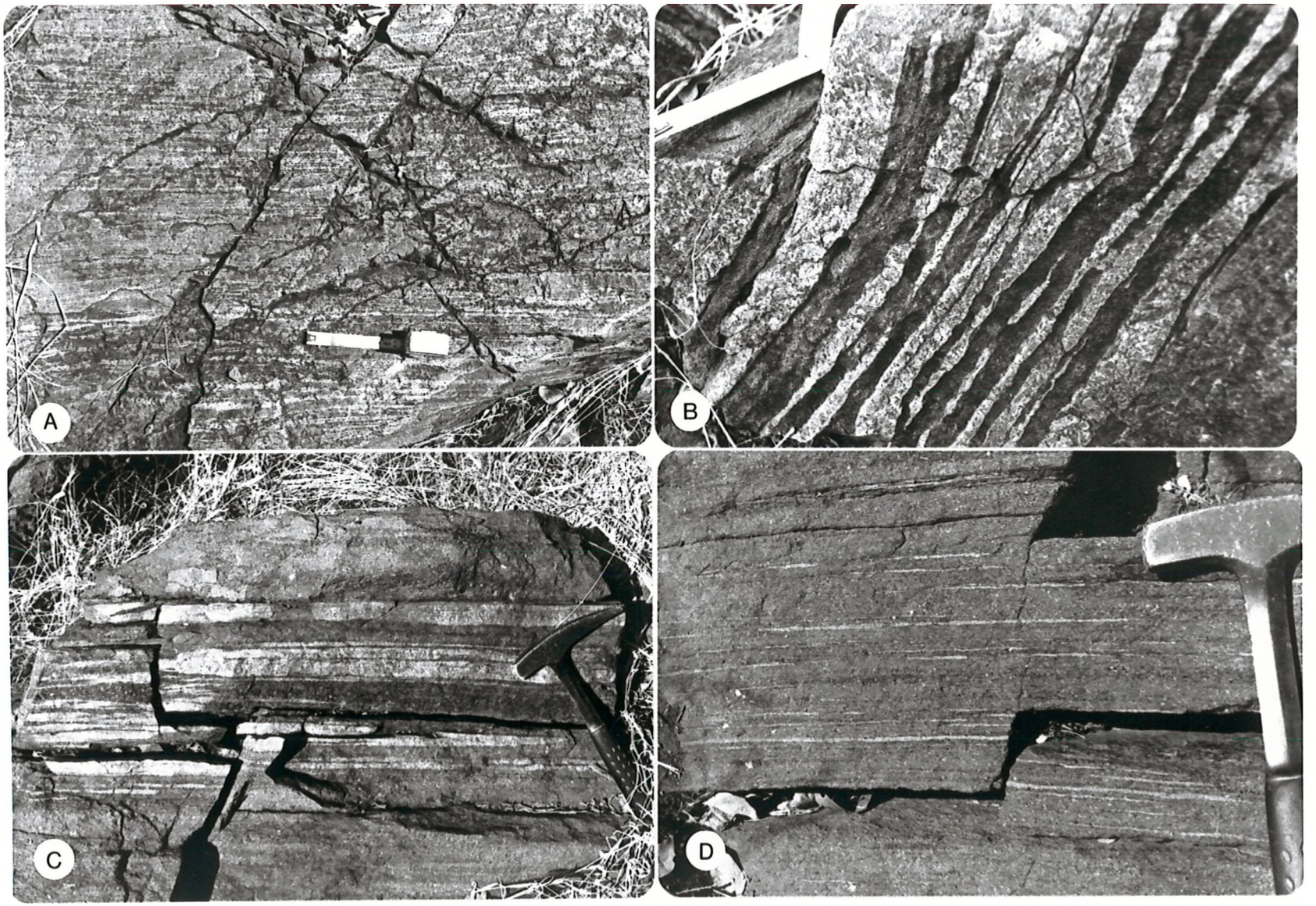

PLATE 6

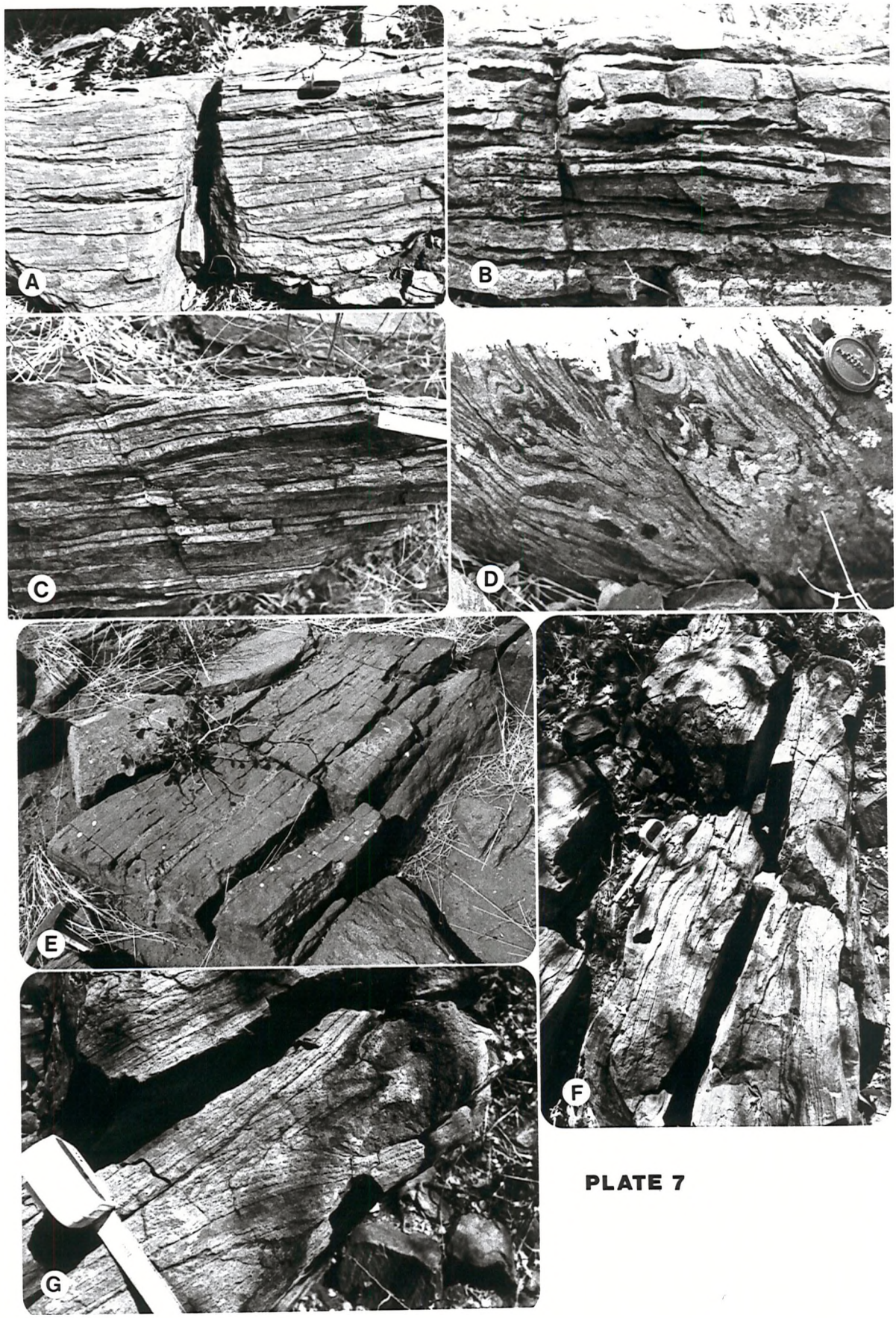

PLATE 7

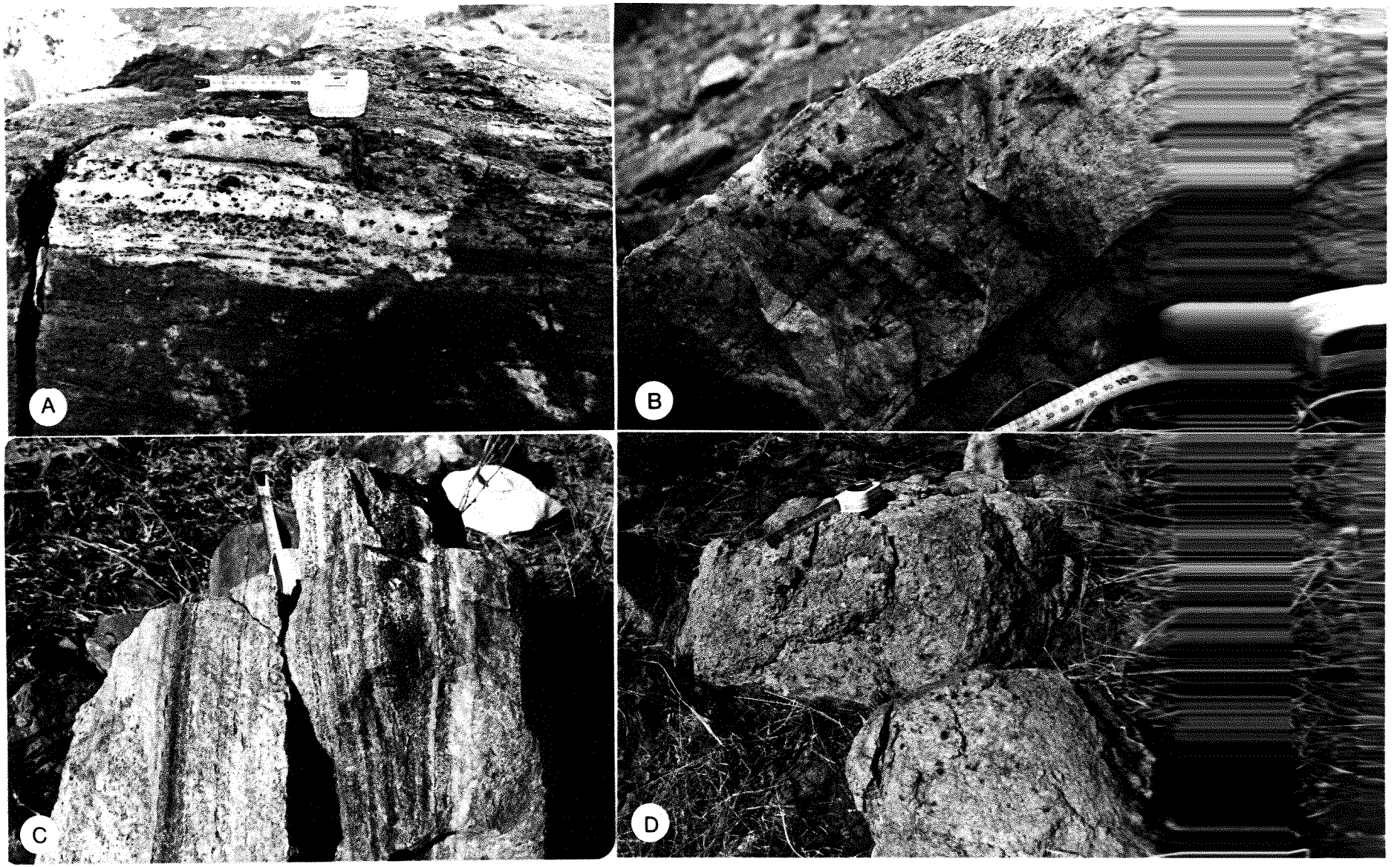

PLATE 8

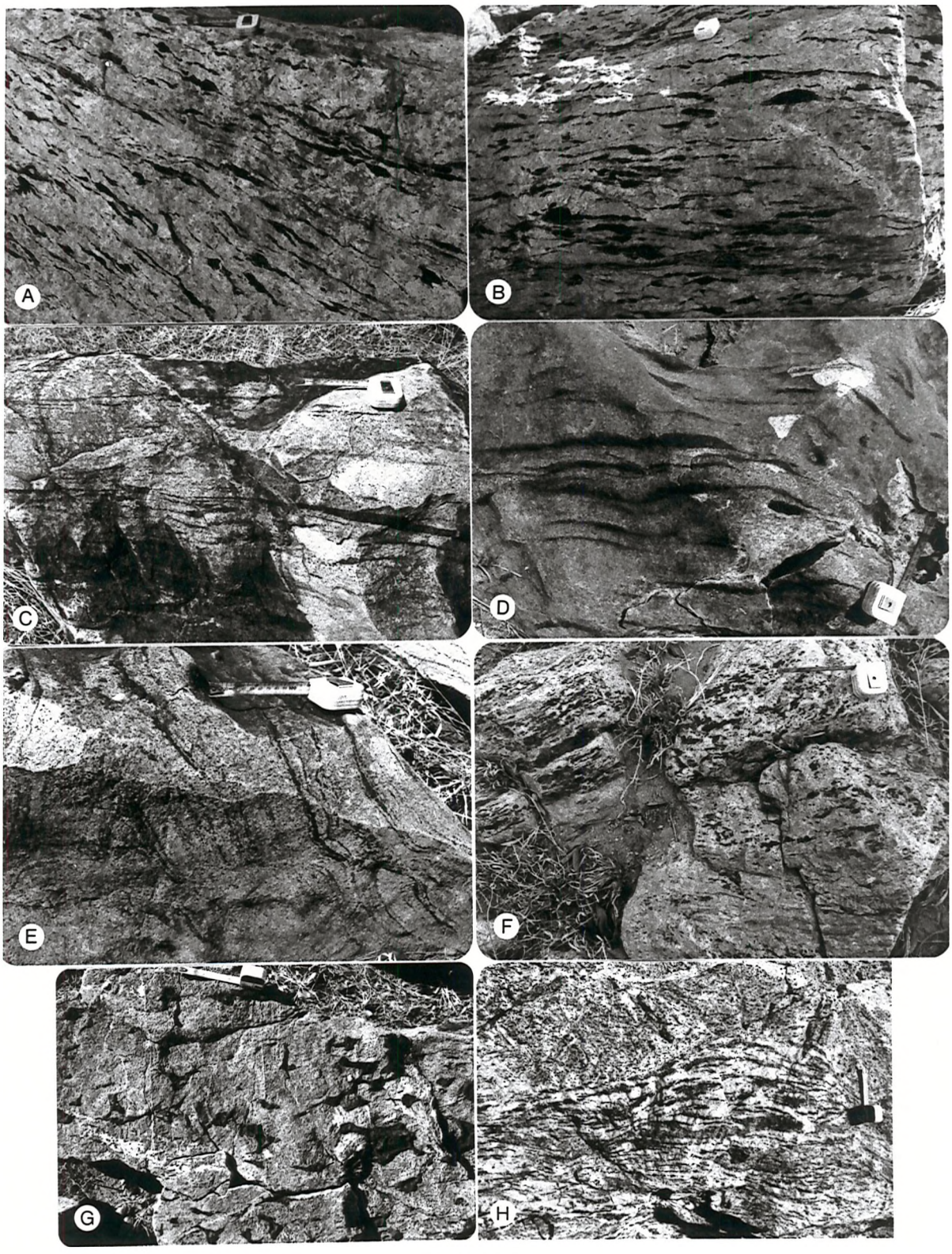

PLATE 9

PLATE 10

Lethlakane anorthosite-metagabbro body immediately north of the Lethlakane Fault

(A)-(D) Range of textures in hornblende anorthosites from: coarse-grained "ophitic" texture (A) without signs of Tuli-Sabi shearing, sheared foliated hornblende anorthosite (B), to porpyroblastic plagioclase texture (C & D).

(E) Sharp contact of anorthosite and metagabbro.

(F) & (G) Porphyroblastic metagabbro.

(H) Porphyroblastic metagabbro with silicified anorthosite bands.

PLATE 11

Morphology of Selebi-Phikwe Anorthosites (2)

(A)-(E) Highly folded siliceous contact of anorthosite with grey gneiss and granitic gneiss, southwest of Selebi North. Note siliceous rims of quartz anorthosite to anorthosite boudins in (B), (C) and (D) and siliceous veinlets and patches of quartz anorthosite within anorthosite. Late D1 - early D2 folding.

(F) Mylonite band "M" in hornblende anorthosite, PW 211.

(G) Contact of anorthosite with hornblende gneiss "H" of Unit C. Clinopyroxene porphyroblast "P" rimmed by hornblende, PW 208.

(H) Typical section of hornblende anorthosite. Note metagabbro band "G" and grey gneiss band "GG".

PLATE 12

Deformed dykes in anorthosite

(A)-(E) Deformed crosscutting mafic dykes (hornblende gneiss) in anorthosite, southwest of Selebi North.

(F) Coarse-grained "pegmatitic" hornblende-rich anorthosite, southwest of Selebi North.

PLATE 13

Migmatitic grey and granitic gneiss

(A) & (B) Highly deformed, sheared migmatitic gneiss, east of Lentswe. Late D1 - early D2 deformation.

(C) & (D) Highly folded migmatitic grey gneiss, east of Botsabelo. Late D1 - early D2 folds.

(E) Ptygmatically folded (early D2) quartz vein in granitic gneiss, southwest of Selebi North. Note development of axial planar quartz-ribbon fabric.

(F) Sheared migmatitic gneiss, east of Botsabelo.

(G) D1 rodding lineation in grey gneiss, southwest of Selebi North.

(H) Nebulous migmatitic granitic gneiss, near Tobane.

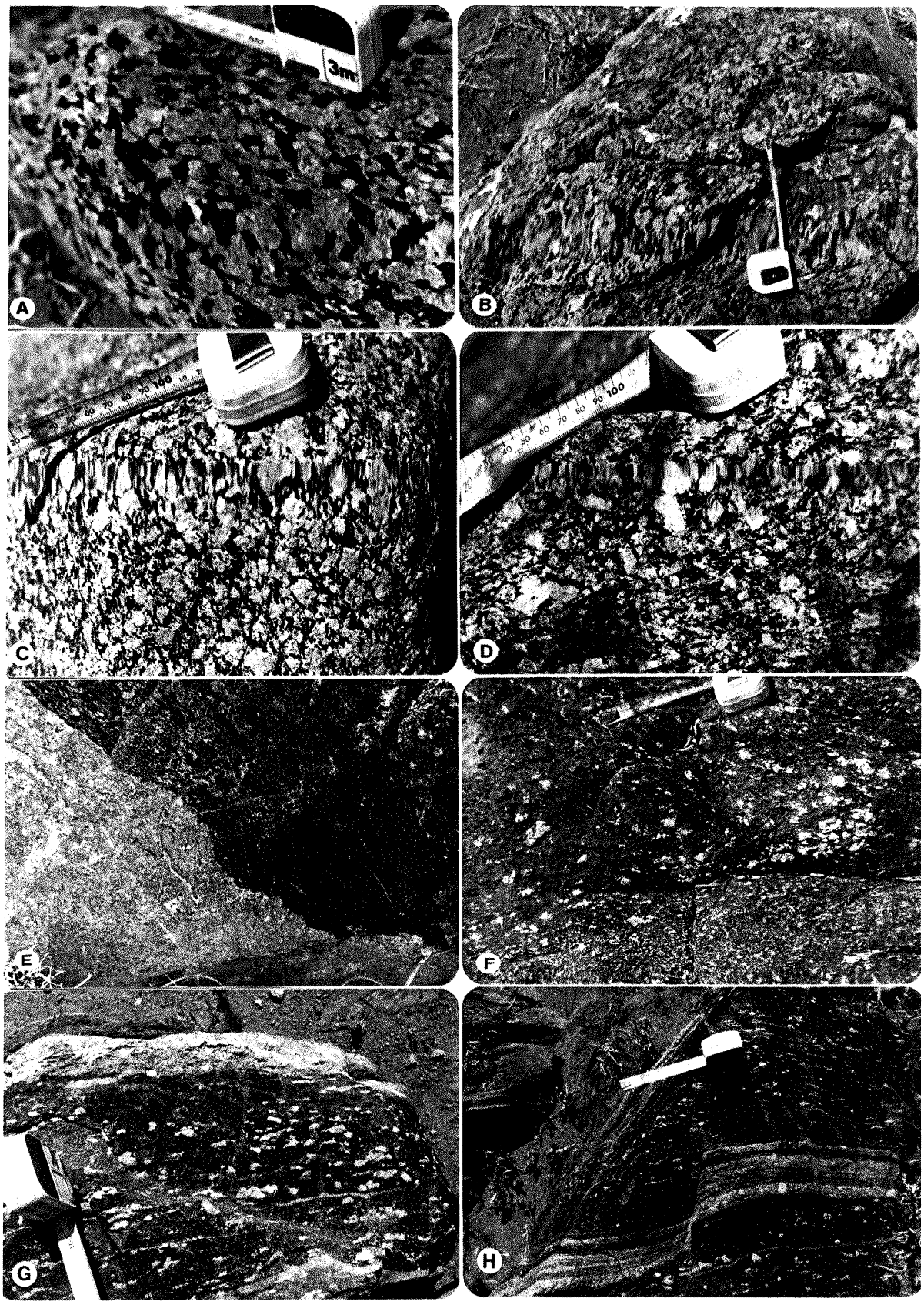

PLATE 10

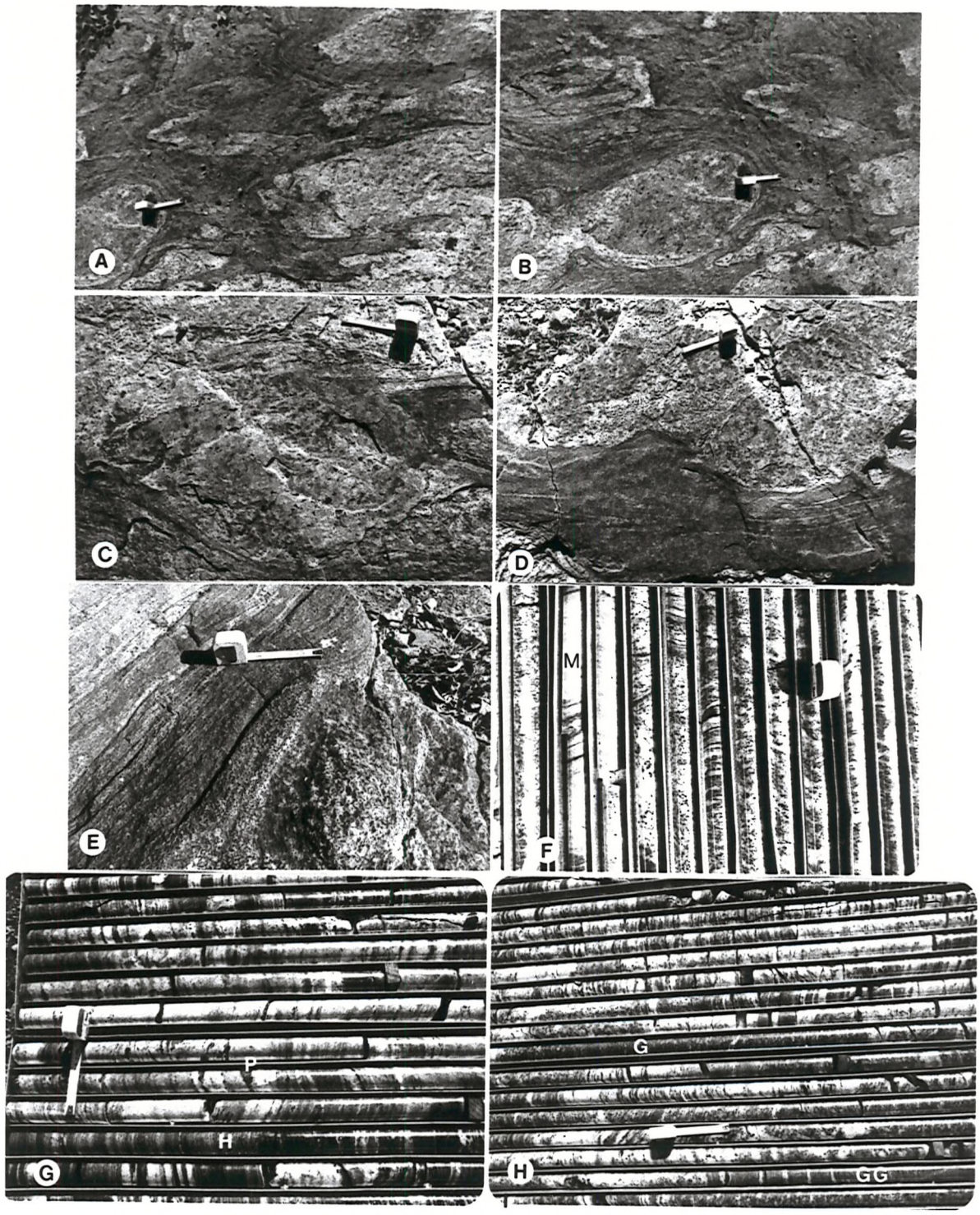

PLATE 11

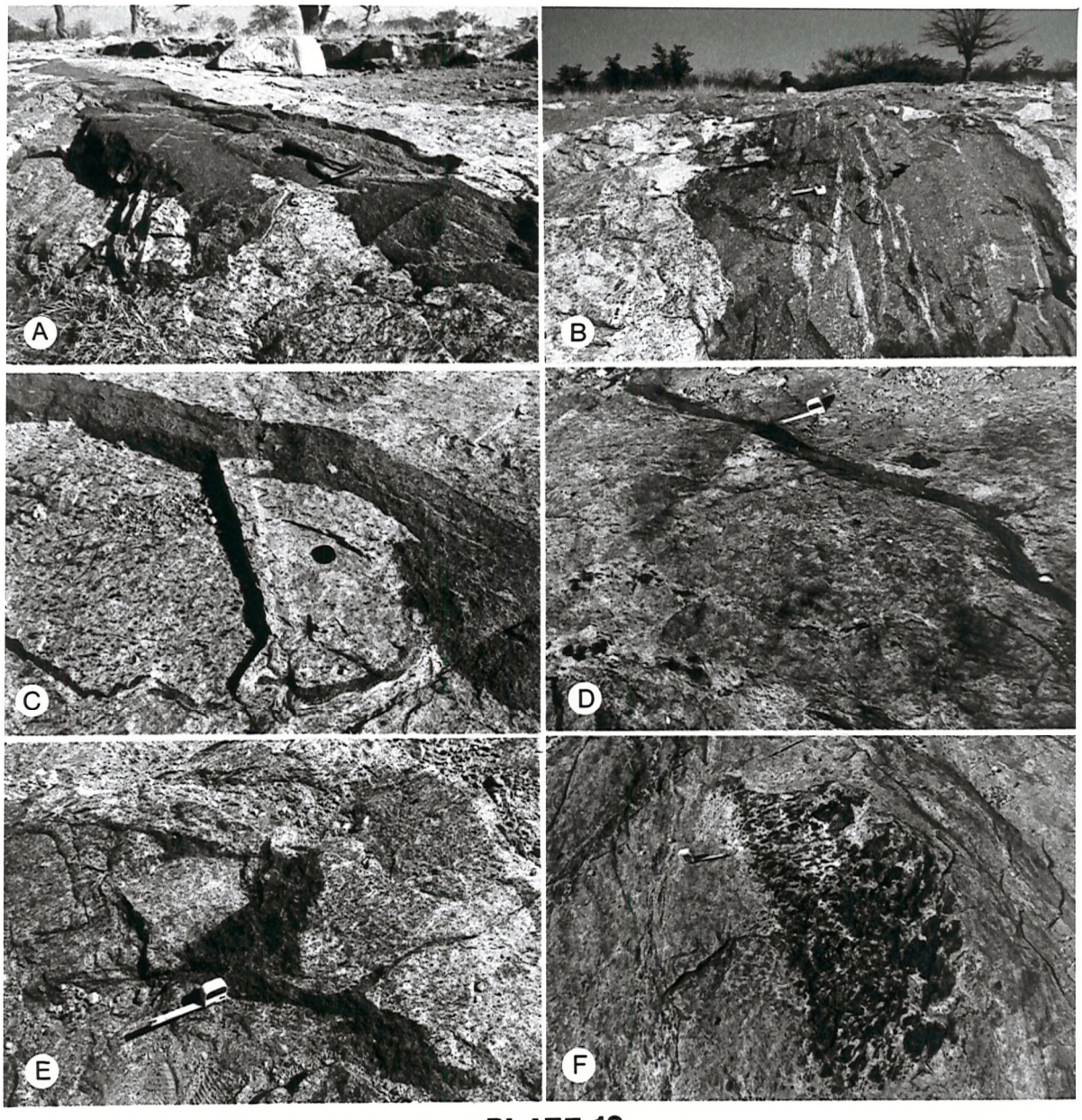

PLATE 12

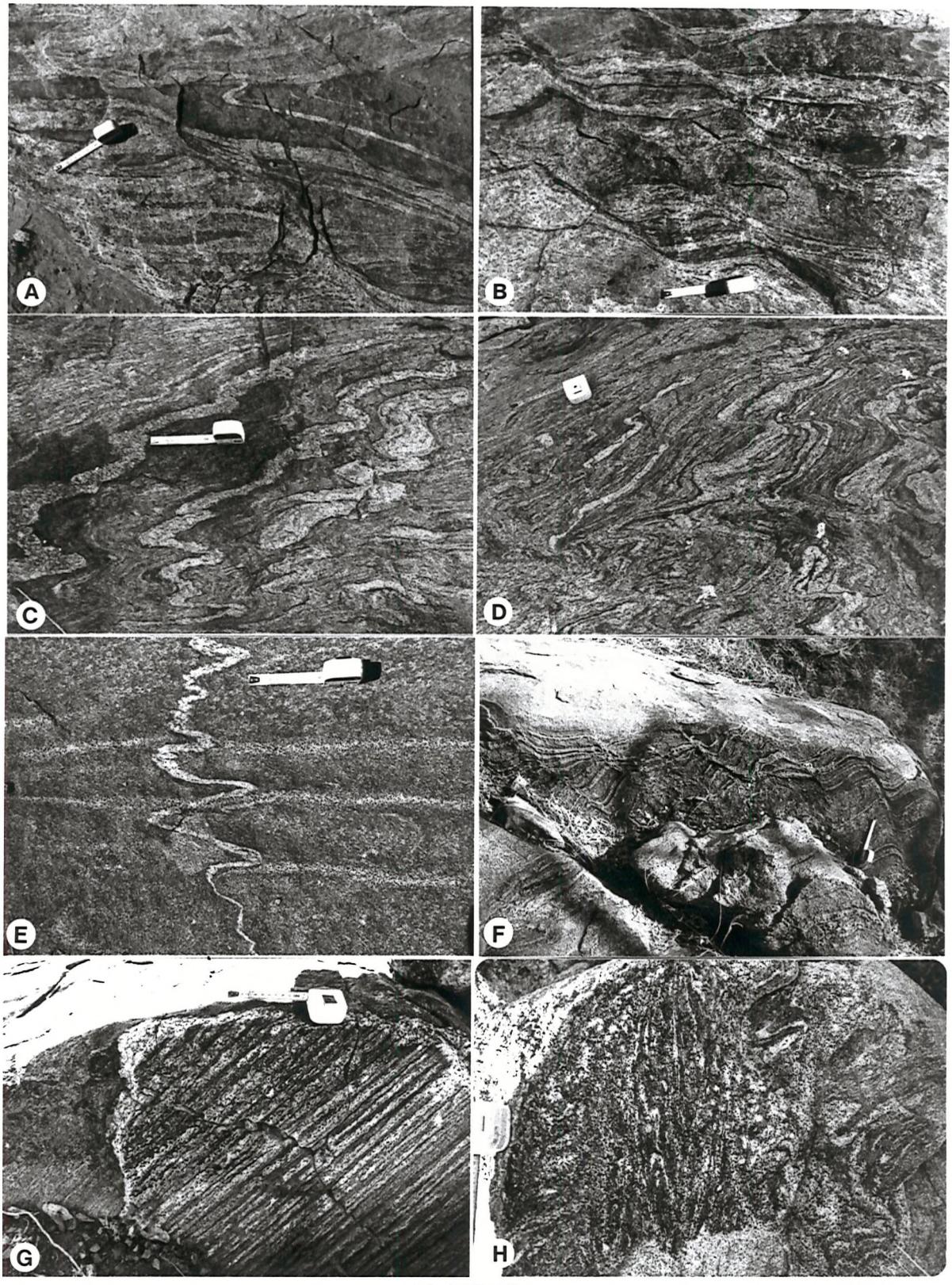

PLATE 13

PLATE 14
D1 structures

(A) D1 folds in grey gneiss below Selebi ore body.

(B) D1 fold in grey gneiss at Selebi. "A" = Upper A amphibolite with disseminated sulphides. Upper B amphibolite just in photo in bottom right corner.

(C) Folded Mg-amphibolite - quartzite (correction - probably early D2 folding), Lethlakane South.

(D) D1 fold in hornblende gneiss in Motloutse River northeast of Phikwe.

(E) D1 fold in hornblende gneiss, east of Sefhope.

(F) & (G) D1 mylonites, east of Botsabelo.

(H) D1 folds in migmatitic grey gneiss associated with D1 mylonites, east of Botsabelo.

PLATE 15
D2 structures

(A) D2 folds (early F3) in "platey" grey gneiss in the footwall of the Phikwe ore body, Phikwe open pit.

(B) D2 fold (F4) in grey gneiss below massive sulphide, Selebi ore body.

(C) Open D2 fold (F4) in grey gneiss at Selebi ore body. Note band of cataclastic gneiss.

(D) D2 fold (F3) in hornblende and grey gneiss, northeast of Phikwe.

(E) Boudins (D2 - early F3 ?) of hornblende gneiss/amphibolite in grey gneiss, northeast of Phikwe.

(F) D2 (early F3) folding and boudinage of pegmatitic quartz-feldspar band within grey and hornblende gneiss in the footwall of the Phikwe ore body.

PLATE 16
Lethlakane Fault Zone - D2 Tuli-Sabi deformation

(A) D2 cataclastic granitic gneiss in the Lethlakane Fault zone, in Motloutse River northeast of Phikwe.

(B)-(D) D2 cataclastic gneiss in the Lethlakane River, immediately south of the Lethlakane anorthosite-metagabbro body.

(E) & (F) Pseudotachylyte veins in cataclastic gneiss, Lethlakane Fault immediately south of Lethlakane anorthosite-metagabbro body.

(G) & (H) Cataclastic gneiss and pseudotachylyte veins, east of Sefhope.

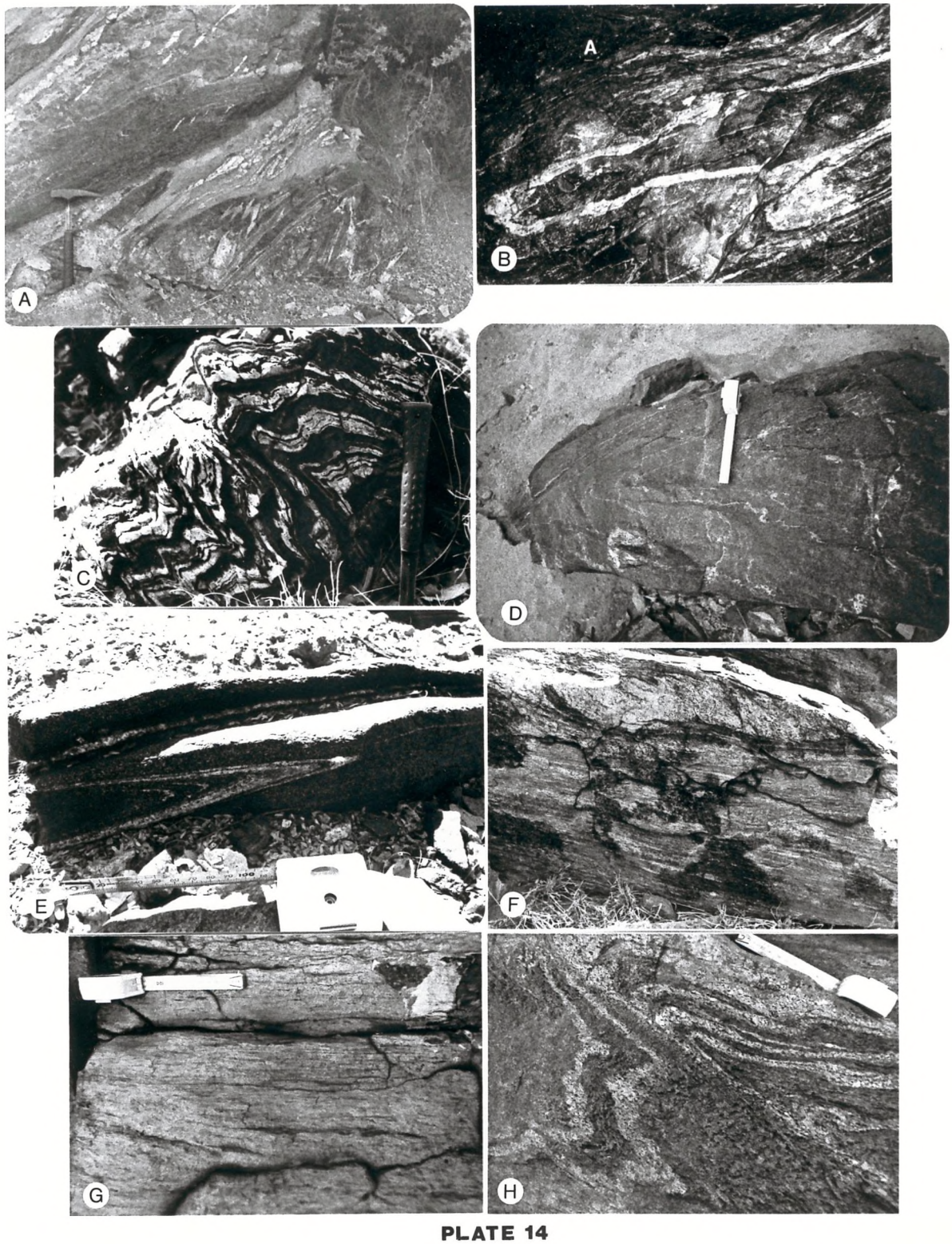

PLATE 14

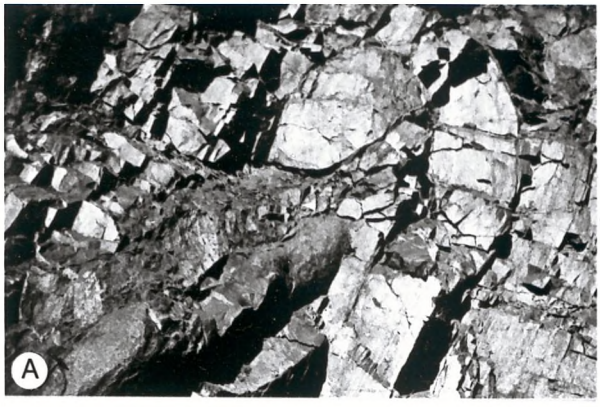

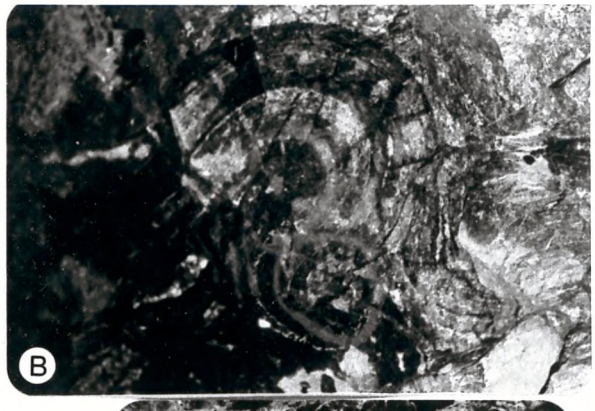

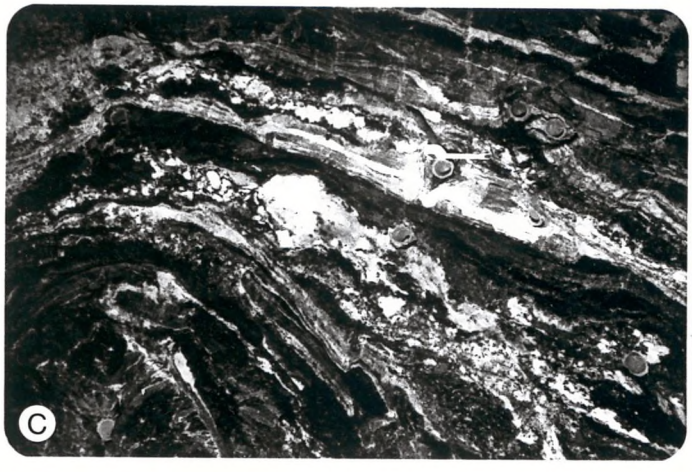

PLATE 15

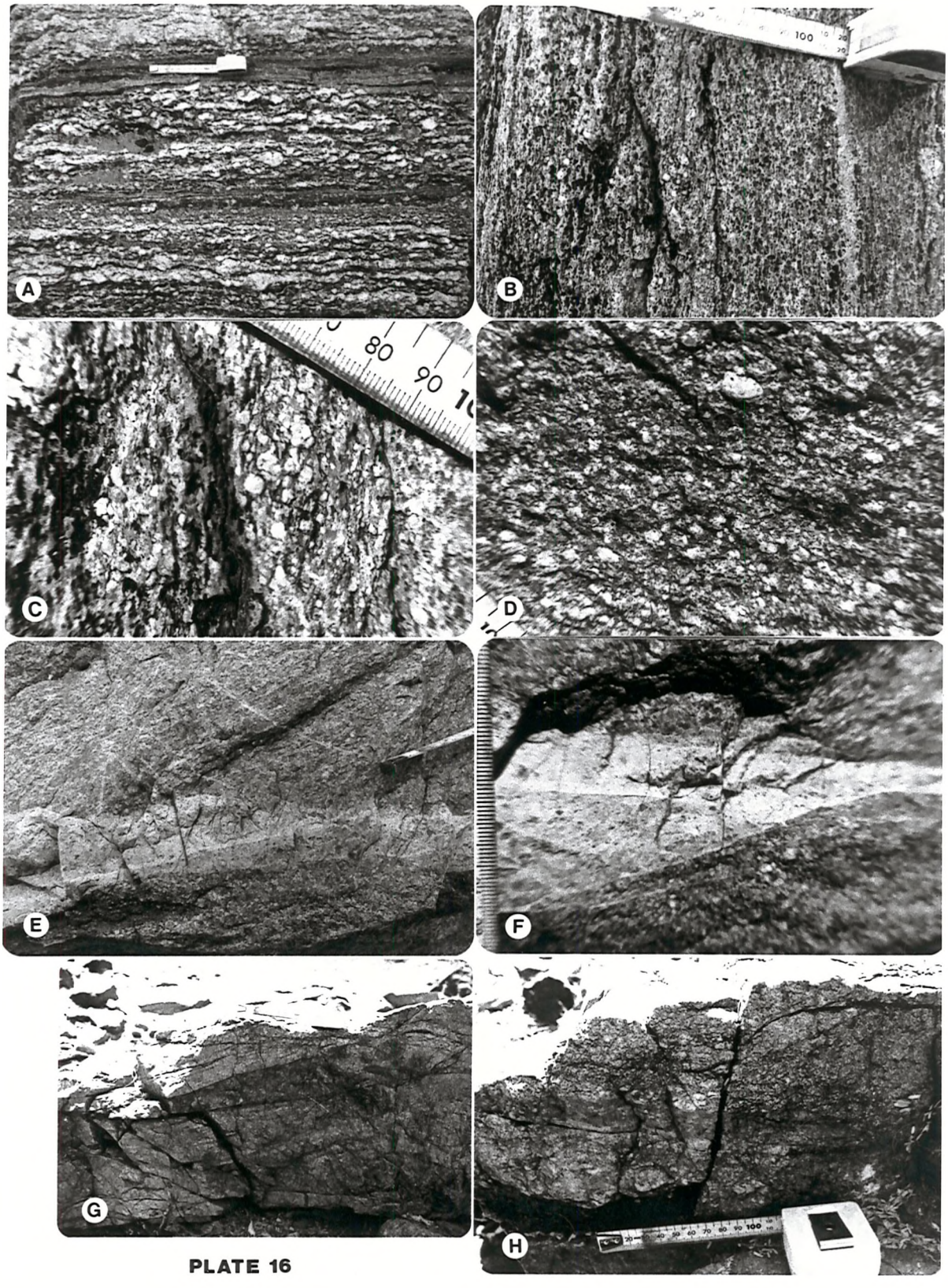

PLATE 16

CHAPTER 3 DETAILED PETROGRAPHY AND METAMORPHIC HISTORY OF THE SELEBI-PHIKWE GNEISSES

This chapter deals with the petrography of the Selebi-Phikwe gneisses and their metamorphic history. The geochemistry of the gneisses along with a discussion of their protoliths are discussed in Chapter 4. Since the majority of the granitic gneisses are regarded as being intrusive into an already deformed Selebi-Phikwe sequence (see Ch.2.2), they are described after the Selebi-Phikwe banded gneisses. The metamorphic assemblages are simply subdivided into M1 and M2 assemblages (see Fig. 3.4).

3.1 HORNBLENDE GNEISSES

The various hornblende gneisses have simple mineralogies and textures. They consist of hornblende and plagioclase (labradorite) with lesser biotite, quartz, clinopyroxene, garnet, magnetite and apatite. They have been divided into three major gradational mineralogical groups:

a) Hornblende-plagioclase gneiss (HGN) - the most typical;
b) Hornblende-plagioclase-magnetite gneiss (HGF); and
c) Hornblende-plagioclase-clinopyroxene-quartz gneiss (HGC).

The distinction between HGN and HGF was initially made while mapping and sampling. Although minor pyroxene was noted while sampling, the distinction of a separate group was not made until after thin-section work and geochemistry had been completed. The three groups occur throughout the Selebi-Phikwe banded gneisses. However HGF occurs mainly in Unit D of the Phikwe section (in which it is the most common hornblende gneiss). HGC is common in Units B and F (Table 4.4).

Typical medium-grained HGN consists of hornblende with slightly less plagioclase (Plate 17a). Minor quartz, biotite, iron oxide and rare garnet may be present. The rock has a decussate granoblastic texture with a weak foliation shown by hornblende. Biotite if present is usually randomly orientated. This granoblastic M1 assemblage is typical of the majority of the mafic gneisses in the Selebi-Phikwe area and is designated M1m. The subidioblastic hornblende is strongly coloured and pleochroic, dominantly green and unzoned. The smaller plagioclase is usually twinned and is unzoned with a composition of labradorite. Locally the M1m hornblende-plagioclase is altered to a M2 assemblage of fine clinozoisite and chlorite, particularly in D2 shear zones. Coarse-grained rocks with more plagioclase (feldspathic

amphibolites with weakly zoned plagioclase) or more hornblende (up to 100% amphibole) occur interbanded with typical hornblende gneiss and are part of the HGN group. Hornblende gneisses (HGG) that are rich in garnet but do not have significant magnetite (Plate 17e) are associated with the diopside gneisses of Unit G.

HGF is similar to HGN but with the addition of magnetite (up to 7% is common) plus garnet and minor apatite. The high Ti content of HGF (Ch. 4.1.2b) indicates that the magnetite is probably titano-magnetite. The magnetite occurs at hornblende grain boundaries, rather than as an included phase or replacement. Coarse porphyroblasts of magnetite (up to 5 mm) locally occur, particularly in HGF of Unit D. As in HGN, minor biotite or quartz may be present. HGF hornblende is more brown than that of HGN. Garnets vary from small idioblastic crystals to large xenoblastic poikiloblasts including hornblende and magnetite (Plate 17b). Some garnets are rimmed by plagioclase. Rare bands containing coarse garnets (1 cm) with pyrrhotite in pressure shadows occur in hornblende-rich HGF.

The mineralogically graded hornblende gneiss bands in Units E and F generally consist of hornblende-rich HGN at their base and less mafic magnetite-bearing HGN or HGF at their top. Both HGN and HGF occur in the hornblende gneiss envelope to the Dikoloti-Lentswe ultramafic rocks. Spotted HGF at Dikoloti contains sub-round patches (4 mm) of labradorite with fine included idioblastic hornblende. It is impossible to deduce whether these spots represent an original feature (e.g. amygdales in a basaltic volcanic rock) or are a metamorphic recrystallisation phenomenon. The latter is preferred because no other original textures appear to have been preserved in these highly strained rocks.

HGC contains up to 20% clinopyroxene as well as slightly more labradorite than hornblende. Magnetite and quartz are always present (quartz locally up to 15%). Biotite is rare. The clinopyroxene varies from small grains or aggregates within the granoblastic plagioclase-hornblende fabric to rare xenoblastic porphyroblasts enclosing hornblende, plagioclase and iron oxide (Plate 17c). The included hornblende is idioblastic and does not replace pyroxene. The clinopyroxene is not a relict mineral. Magnetite typically occurs adjacent to clinopyroxene (Plate 17d).

Minor disseminated sulphides (pyrrhotite and lesser chalcopyrite with pyrite in later veinlets) are found in the hornblende gneisses, particularly in HGC and HGF, and particularly those in Units A and B.

3.2 GREY QUARTZO-FELDSPATHIC GNEISSES

Grey quartzo-feldspathic gneisses are massive to well-banded medium-grained rocks consisting of a M1 assemblage of essential quartz, plagioclase and biotite, with minor hornblende, garnet, magnetite, microcline, cordierite or sillimanite. Locally M2 clinozoisite and chlorite are developed. They contain no sulphides except where adjacent to the Selebi-Phikwe ore bodies from which minor sulphides appear to have been mobilised. Their texture is granoblastic, with a tendency towards a "mortar-like" texture of coarser plagioclase rimmed by finer quartz and plagioclase. Any fabric is picked out by aligned biotites (Plate 18a).

In the less siliceous gneisses both hornblende and biotite are present in varying amounts. The more mafic grey gneisses contain hornblende with only minor biotite (Plate 18b). As the quartz content increases, the ratio of hornblende to biotite decreases. The plagioclase is andesine and is usually twinned and unzoned. Rare, embayed and coroded plagioclase poikiloblasts occur. They are zoned and strained and commonly have round quartz inclusions (Plate 18c). These inclusions appear to have grown during recrystallisation after the coarse plagioclase and are not an earlier included phase. It is not possible to deduce whether the coarse plagioclase is a relict from an earlier metamorphic assemblage (M1e, see Fig. 3.5) or a premetamorphic assemblage. Isolated irregular poikiloblastic garnets occur but do not include biotite. Magnetite content varies from commonly a trace to more than 5%. This rare magnetite-rich grey gneiss (FRGG) is finely interbanded with hornblende gneiss in Unit D and at Dikoloti (Plate 19f).

In the more siliceous gneisses there is no hornblende and the amount of biotite is less than in the less siliceous grey gneiss (Plate 18d). The feldspar is mainly oligoclase, but there is also minor microcline with distinctive tartan twinning. A lot of the feldspar however is untwinned. Coarser quartz shows undulose extinction. The development of lobate growths of myrmekite (symplectic vermicular quartz and plagioclase) from plagioclase into usually untwinned feldspar is conspicuous (Plate 18e). Sparse garnets occur (Plate 18f) in siliceous grey gneiss but there are only traces of magnetite. Blue-tinged siliceous gneisses (SCGG) contain large xenoblastic poikiloblasts of M1m cordierite. The cordierite includes trains of fibrolitic sillimanite, usually only in the core (Plate 18g). Fine blue-green spinel was noted along with sillimanite in one

cordierite core. The sillimanite and spinel are regarded as forming at about the peak of M1 metamorphism (M1p, see Figs 3.4 & 3.5) prior to the development of the main M1 assemblage (M1m). Plagioclase is not common in cordierite-bearing grey gneiss. If microcline is present it occurs at the margins of the cordierite as a rim (Plate 18h). Biotite is always present. The cordierite is commonly and distinctively altered, either completely or partially along cracks and at its rim, to M2 pinnite (giving the rock a blue colour) (Plate 18h).

Finely banded grey gneisses form the majority of Unit E in which the main varieties of grey gneiss (quartz-poor, quartz-rich and quartz-cordierite) are completely interbanded with each other and with hornblende gneiss and biotite gneiss.

3.3 INTERMEDIATE BIOTITE GNEISSES

The umbrella-term of intermediate biotite gneiss was initially used to indicate biotite-bearing gneisses that could not readily be placed into the hornblende gneiss groups by virtue of containing more biotite than either of these two groups. The original splitting of the biotite gneisses into a quartz-poor group and a quartz-rich group has been confirmed by detailed petrology and geochemistry (Ch. 4.1).

3.3.1 Quartz-poor Biotite Gneisses

The fine to medium-grained quartz-poor biotite gneisses (QPIB) have a simple M1 mineralogy of plagioclase, biotite, green hornblende, quartz and minor magnetite, plus locally clinopyroxene, garnet and disseminated sulphides. They vary from rocks which are texturally and mineralogically similar to typical granoblastic hornblende gneiss with just the addition of biotite and quartz to feldspathic biotite schists (Plate 17f). The plagioclase has the composition of andesine to labradorite, usually andesine. Quartz occurs as fairly coarse grains throughout (cf. the fine quartz that occurs as a late recrystallisallisation product in some grey gneisses). Clinopyroxene occurs locally as (M1p ?) relicts altered to hornblende, along with rare relicts of altered plagioclase. Garnet is rare, although coarse idioblastic helicitic garnets (M1e ?) were found in a plagioclase-magnetite-rich biotite gneiss (Plate 17h). This rare coarse-grained (1 cm.) garnet-rich biotite gneiss (GRHG) commonly contains cordierite as well as essential magnetite and is only found as thin bands within hornblende gneiss.

Biotite amphibolite (ARIB) with only minor plagioclase and

quartz occurs in Unit B. The amphibole is typically non-calcic and is either clinoamphibole (well-twinned cummingtonite, Plate 17g) or orthoamphibole (gedrite).

The similarity of the mineralogy of QPIB to that of the hornblende gneisses with which they are commonly interbanded suggests a genetic relationship between the two. QPIB is commonly finer grained and more finely banded than the associated hornblende gneiss.

3.3.2 Quartz-rich Biotite Gneisses

Quartz-rich biotite gneisses contain essential biotite and quartz. Where biotite is abundant the rock is a schist. Thin (>5 cm) bands of 100% biotite schist locally occur in the grey gneisses. However some of the thin biotite schists are considered to have a tectonic origin, for example the biotite-magnetite schists at Dikoloti -Lentswe. Disseminated pyrrhotite and chalcopyrite are locally abundant in QRIB, particularly the QRIB that is interbanded with hornblende gneiss in Units A and B. Cordierite (M1m) is a very common constituent along with lesser plagioclase and sparse garnets. Fibrolitic sillimanite (M1p) is included in the cordierite, either in the cores along with minor green spinel or throughout spongey poikiloblasts along with quartz and biotite (Plate 19a & b). Plagioclase occurs in quartz-biotite plagioclase schist/gneiss with or without cordierite. However if cordierite is present the amount of plagioclase is minor. Isolated poikiloblastic garnets are found in the cordierite gneisses and in this case plagioclase only occurs rimming the garnets. Myrmekitic quartz intergrowths that have grown outwards from the garnet are conspicuous in the garnet-rimming plagioclase (Plate 19c). If amphibole is present, it is calcium-poor. Orthoamphibole occurs in gedrite-biotite-quartz bands in a cordierite-bearing gneiss and clinoamphibole in a cummingtonite-quartz-biotite-plagioclase-apatite gneiss (Plate 19d & e).

In a banded cordierite-biotite schist within grey and biotite gneisses 150 m above the Selebi ore body, cordierite occurs as nodular M1 aggregates of small grains surrounded by biotite (Plate 19g). The aggregates coalesce in one band to form a cordierite band 0.5 m wide. Skeletal corundum occurs in the cores of the fine-grained polygonal granoblastic cordierite aggregates (Plate 19h). Relatively coarse subidioblastic sillimanite (as compared to the more common fibrolite) also occurs in the cordierite aggregates. The corundum in each aggregate consists of several skeletal crystals, as indicated by their

extinction positions. The skeletal corundum branches are located at cordierite grain boundaries. The corundum and cordierite appear to have crystallised at the same time. The relationship of the sillimanite to the cordierite and corundum is less clear. Corundum never occurs adjacent to sillimanite. In one case corundum surrounded by cordierite is enclosed within relatively coarse sillimanite. However this is possibly a section effect. In more typical cordierite gneiss, early fibrolitic M1p sillimanite is included in later porphyroblastic M1m cordierite. It is suggested that the coarse subidioblastic sillimanite possibly owes its form to replacement of earlier andalusite or kyanite. However Chinner (1961) has shown that when sillimanite forms in a rock containing andalusite or kyanite, it nucleats within biotite. The cordierite and corundum were recognised with difficulty. The fine alteration of the cordierite to pinnite along cracks is distinctive. However conclusive identification was provided by X-ray diffraction. The metamorphic corundum-cordierite nodules either represent original Al-rich aggregates in a biotite gneiss protolith, or the concentration of Al during metamorphism. A similar problem is posed by the corundum-spinel-sapphirine aggregates in the Dikoloti feldspathic amphibolite (Chs 3.9 & 8.6.2).

The mineralogy of the quartz-rich biotite gneisses shows obvious gradational similarities to the grey gneisses. The biotite gneisses contain more biotite, more cordierite at lower quartz contents, non-calcic amphibole and disseminated sulphides.

3.4 CALC-SILICATE GNEISS, QUARTZ-FELDSPAR GRANULITE and ANORTHOSITE

Calc-silicate gneiss and quartz-feldspar granulite will be considered in the same section as the anorthositic gneisses as they have similarities in their mineralogies. Calc-silicate gneiss and anorthosite have been grouped together as anorthosites (Key 1976) or as metasediments (Gallon 1986).

3.4.1 Calc-silicate Gneiss and Quartz-Feldspar Granulite

Calc-silicate gneisses consist of quartz, plagioclase and hornblende in a granoblastic texture. They are banded due to variations in the quartz-plagioclase content and hornblende laminae. At Botsabelo calc-silicate gneiss contains poikiloblastic porphyroblasts of green pleochroic hornblende (M1e ?). Clinopyroxene (M1p) rims occur around the hornblende porphyroblasts (Plate 20a). The hornblendes contain abundant quartz inclusions, often in their core

with an outer inclusion-free zone or in a weak spiral pattern. The age relationship between the hornblende and the clinopyroxene is opposite to that in the anorthosites in which Mlm hornblende and actinolite-quartz intergrowths form rims to Mlp clinopyroxene porphyroblasts (Plate 21d & e). The felsic matrix of the calc-silicate gneiss consists of plagioclase and quartz with minor clinopyroxene and amphibole and significant idioblastic sphene. The texture is even fine-grained polygonal granoblastic (Plate 20b). Plagioclase is slightly coarser than quartz although in more siliceous gneiss the quartz grain-size increases. The plagioclase has cores of bytownite (An81) and margins of labradorite (average An70) (Table 3.1 & p.A.3). The range in plagioclase composition is similar to that in the anorthosites although the latter appear to have had a more complicated history. The clinopyroxene is a calcic salite, very similar in composition to the clinopyroxene porphyroblasts in the anorthosites, although the calc-silicate gneiss clinopyroxene contains slightly more Ca, Al, Fe and Na and slightly less Mg (Table 3.1 & p.A.2). The hornblende is edenitic to ferroan pargasitic hornblende (Fig. 3.1). Scapolite was considered a possible constituent of the calc-silicate gneiss assemblage but none was identified. Overall the compositions of the calc-silicate gneiss minerals are very similar to those of the anorthosites.

Interbanded with hornblende-bearing calc-silicate gneiss at Botsabelo are garnetiferous quartz-feldspar granulite. They vary from well-banded gneisses due to variations in quartz-plagioclase content to massive unbanded rocks. Their fine-grained granoblastic matrix is similar to that of the calc-silicate gneisses. However the plagioclase is albite-oligoclase. The small subidioblastic garnets are in bands or scattered throughout. Sphene is a significant constituent. Where finely-banded, the granoblastic quartz-feldspar granulite has a mylonitic appearance.

The garnetiferous quartz-feldspar granulites that are associated with hornblende gneiss in Unit B are similar to the Botsabelo rocks, but with a more complex granoblastic felsic matrix which contains minor microcline. Quartz occurs as coarse polygonal grains and as small round inclusions in both feldspars. The plagioclase is albite. Bright red almandines occur either as isolated crystals or concentrated in bands (Plate 20c). The garnets are idioblastic to subrounded with few inclusions. Minor sillimanite, biotite and rarely magnetite in thin laminae parallel to the garnet bands also occur. One garnet-

Calc-silicate Gneiss

	a	b	c	d
	cpx	hor	plg	plg
SiO2	51.29	42.81	47.77	50.11
TiO2	0.17	0.68		
Al2O3	2.09	10.50	32.82	31.00
FeO	9.03	14.29		
MnO	0.18	0.13		
MgO	12.38	12.66		
CaO	24.11	12.25	16.63	14.40
Na2O	0.49	1.42	2.18	3.39
K2O	0.01	1.95	0.06	0.08
Cr2O3	0.01	0.00		
NiO		0.02		
Total	99.7	96.71	99.46	98.98
			An 81	An 70
No. of analyses	2	2	2	2

Sample 30-7-1d plagioclase-hornblende-quartz-pyroxene granulite Botsabelo

See Plate 20b for 30-7-1d

a Clinopyroxene rimming hornblende porphyroblast 30-7-1d

b Hornblende porphyroblast 30-7-1d

c Matrix plagioclase - core 30-7-1d

d Matrix plagioclase - margin 30-7-1d

See appendix A.2 & 3 for all analyses

Anorthosite

	e	f	g	h	i	j	k	l	m
	cpx	act	hor	plg	plg	plg	plg	plg	gnt
SiO2	53.79	53.07	49.78	51.76	54.42	52.57	46.89	52.03	38.41
TiO2	0.11	0.12	0.55						0.39
Al2O3	1.19	4.41	6.75	31.23	30.11	30.32	33.54	31.32	14.62
FeO	6.81	10.32	10.36			0.09		0.09	12.54
MnO	0.22	0.27	0.15						0.08
MgO	13.95	16.19	15.42						0.08
CaO	22.90	12.53	11.93	14.17	12.70	12.93	16.68	14.11	33.03
Na2O	0.36	0.49	0.88	3.55	4.36	4.24	1.86	3.75	
K2O	0.00	0.31	0.34	0.09	0.12	0.13	0.01	0.08	
Cr2O3	0.01	0.03	0.03						0.00
NiO	0.02	0.02	0.06						
Total	99.36	97.76	96.25	100.80	101.71	100.28	98.98	101.38	99.15
				An 69	An 62	An 63	An 83	An 67	
No. of analyses	6	3	6	2	2	2	2	3	20

e Clinopyroxene porphyroblast 549 & 572

f Actinolite intergrown with quartz, rimming clinopyroxene 572

g Matrix hornblende 549 & 572

h Zoned plagioclase porphyroblast, core 572

i Zoned plagioclase porphyroblast, margin 572

j Unzoned polygonal plagioclase 572

k Unzoned polygonal plagioclase 549

l Fine intergranular plagioclase, average of An 73, 72, & 62 572

m Zoned garnets, average of core to rim 546 & 566

Samples 549 & 572 hornblende-pyroxene anorthosite from PW 208 & PW 211

Samples 546 & 566 plagioclase-quartz-garnet zones in anorthosites from PW 213 & PW 211

See Fig. 2.2 for PW 208, PW 211 & PW 213. See Plates 21 for 549 & 572, 20h for 566

TABLE 3.1 AVERAGE MINERAL ANALYSES -- CALC-SILICATE GNEISS AND ANORTHOSITE

poor quartz-feldspar granulite band contains scattered fibrolite knots and grades into a quartzite at its base. Other coarse-grained white quartz-oligoclase bands (particularly the band at the top of Unit B, Fig. 2.3) without garnet or sillimanite have a granitic intrusive appearance.

3.4.2 Anorthosite

The anorthositic gneisses are medium to coarse-grained, granoblastic plagioclase-rich rocks, with variable amounts of hornblende, clinopyroxene and quartz. Plagioclase occurs in at least four generations. The most common generation is equigranular, polygonal, well twinned and unzoned (Plate 21a). Polygonal plagioclase composition varies between samples from calcic bytownite to sodic labradorite, although intrasample variation is small. Calcic labradorite however is by far the most common polygonal plagioclase (Table 3.1 and p.A.2). Rare labradorite porphyroblasts that occurr within the medium-grained polygonal fabric are irregular, typically untwinned (Plate 21b) and zoned with more calcic cores. They are interpreted as the earliest generation seen. Fine-grained plagioclase between polygonal plagioclase grains is calcic labradorite-bytownite. It is interpreted as the third generation, having formed by granulation and recrystallisation at polygonal plagioclase margins. The fourth generation is andesine porphyroblasts which only occur adjacent to quartz in coarse quartz-anorthosites (Plate 21g).

Hornblende is usually present in the anorthositic gneisses and is the main mafic phase. Metagabbroic rocks within the anorthosites simply have a higher hornblende content (Plate 21c). The foliation in the anorthosites is due to thin hornblende-rich bands and laminae. The granoblastic hornblende (actinolitic to magnesio-hornblende, Table 3.1 & p.A.2, Fig. 3.1) forms part of the polygonal fabric and is interpreted as being in equilibrium with and the same generation as the polygonal plagioclase. Clinopyroxene porphyroblasts occur within the anorthosites, usually near the structural top of the anorthosite unit at Phikwe (Plate 11g, Fig. 2.3). They are aligned parallel to the anorthosite foliation. The clinopyroxene is a calcic salite. The clinopyroxene porphyroblasts are aligned parallel to the hornblende foliation and are usually rimmed by hornblende grains. Fine sphene commonly occurs with the rimming hornblende. A few unrimmed clinopyroxene poikiloblasts which include fine idioblastic hornblende and plagioclase (Plate 21f). Some clinopyroxene porphyroblasts are

Fig. 3.1 SELEBI-PHIKWE CALCIC AMPHIBOLES

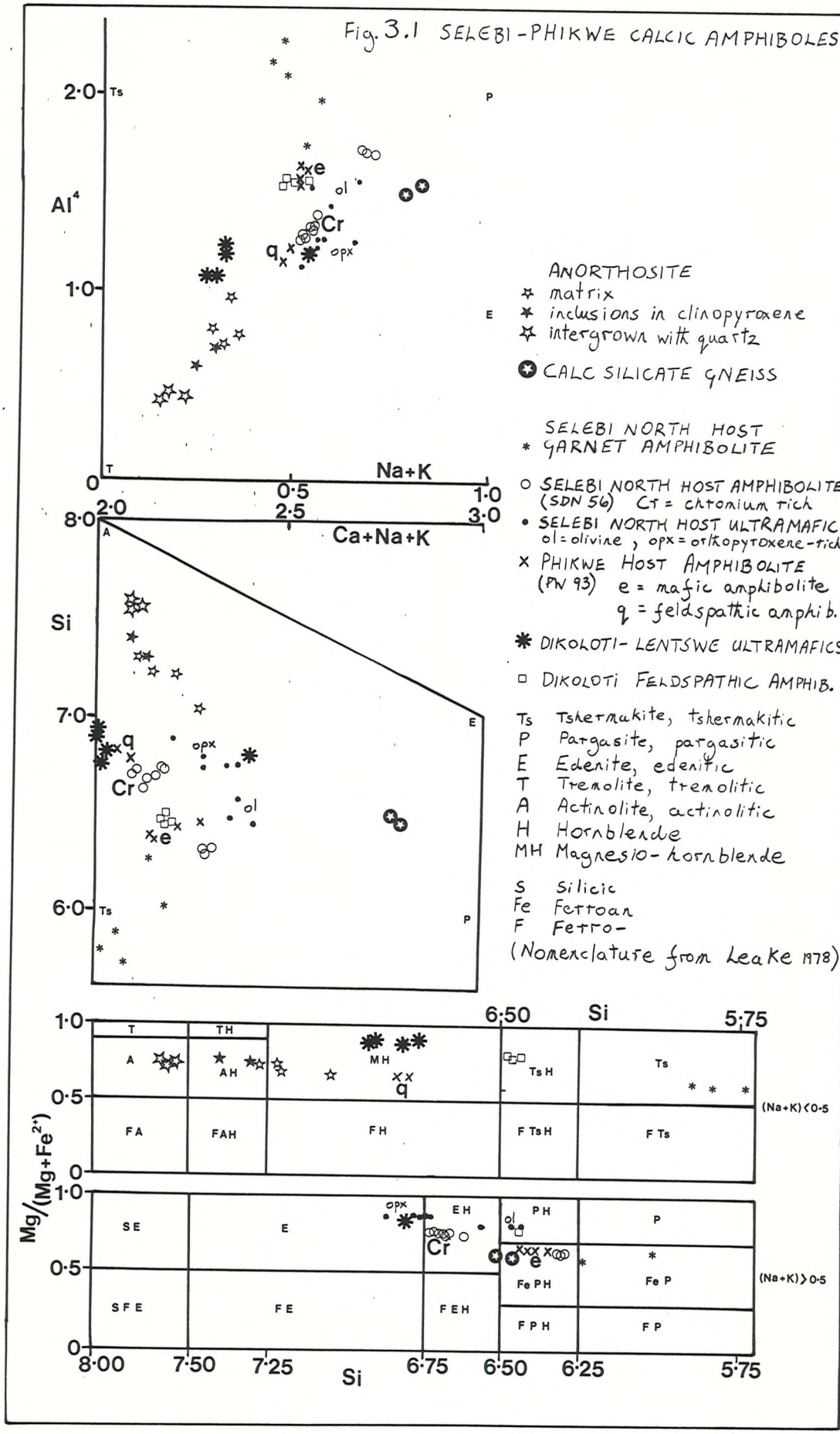

rimmed by a coarse actinolite-quartz intergrowth (Plate 21d & e). Fine clinozoisite forms a thin mantle between the intergrowth and the surrounding plagioclase. It is difficult to balance the hydration reaction which formed the actinolite-quartz intergrowth. Some plagioclase is required to have been consumed to provide the Al for the actinolite:

calcic salite + labradorite + H2O --> actinolite + quartz + clinozoisite + Ca

The very thin rim of clinozoisite is insufficient to account for the excess Ca produced in the formation of the intergrowths and Ca was possibly removed from the system. The plagioclase surrounding the actinolite-quartz intergrowth was not probed and any possible change in its anorthite component could not be determined.

Quartz is usually only a minor intergranular constituent of the anorthosites. However quartz locally forms large patches, typically in hornblende-poor anorthosites. Rare magnetite rimmed by biotite occurs with these coarse quartz patches (Plate 21g).

The ultramafic bands that form a minor component of the layered Lethlakane anorthosite-metagabbro body are pyroxenites with irregular olivine porphyroblasts in a granular clinopyroxene-olivine matrix (Plate 21h).

The granoblastic polygonal labradotite-hornblende assemblage is the main M1 assemblage (M1m). The question arises whether the clinopyroxene porphyroblasts and early zoned labradorite porphyroblasts are a metamorphic or relict premetamorphic assemblage (i.e. igneous if the proposal in Ch. 2.3.4 is correct, see Ch. 4.4). The poikiloblastic nature of some of the clinopyroxenes, the alignment of the clinopyroxenes in the anorthosite foliation and their high calcium content show that the clinopyroxenes are metamorphic (M1p). The nature of the early labradorite porphyroblasts is more difficult to determine. No conclusive original textures are seen. Ellipsoidal aggregates of labradorite surrounded by "ophitic" hornblende suggest recrystallised cumulate plagioclase megacrysts. However the minerals are all metamorphic. The metamorphic nature of the clinopyroxenes suggests that the early labradorites are also metamorphic and both are regarded as an M1p assemblage that formed at the peak of M1. Minor hornblende that is included in M1p clinopyroxene is the result of prograde metamorphism (M1e) during M1. However it is not known whether all the matrix M1m

hornblende formed from M1p clinopyroxene or whether the M1p assemblage only formed locally within the M1m assemblage at the peak of M1. The third and fourth generations of plagioclase are tentatively regarded as M2 assemblages.

Significant amounts of quartz would have been produced in the formation of matrix hornblende at the expense of clinopyroxene. This quartz could have been redistributed to form the quartz anorthosites. However the high quartz contents at the margins of the anorthosite body (Plate 11b,d & e) were possibly formed by transfer of Si from adjacent siliceous grey and granitic gneisses. The higher Ti content of the granoblastic matrix hornblende than of the actinolite intergrown with quartz possibly suggests that the former formed at a higher metamorphic grade than the latter (Raase 1974). However there is also a strong control by whole-rock Ti contents on amphibole Ti contents, for example in the hornblendes of the Phikwe host amphibolite and the chromium-rich hornblendes of the Selebi North host amphibolite (Table 5.2 & Fig. 7.7). The actinolite-quartz intergrowth is thought to be later than the matrix M1m hornblende and its coarsely symplectic nature suggests a relatively rapid decrease in pressure during late M1 (Leyreloup et al. 1975).

Thin (>20 cm) quartz-garnet-plagioclase bands are found in the anorthosites parallel to their foliation. They are of two types in about equal proportions:

Type (a) - composite bands with garnet-quartz-plagioclase-sphene cores and banded quartz-plagioclase-sphene-minor biotite marginal zones (Plate 20d). The planar margins are parallel to the anorthosite foliation and weakly gradational. The marginal banding is due to lenses and laminae of coarsely recrystallised quartz (Plate 20e). The sphene occurs in lensoid aggregates parallel to the banding. The plagioclase in the marginal zones is labradorite, the same as in the immediately adjacent anorthosite. The marginal banding is thought to be an early D1 mylonitic fabric that was statically recrystallised during M1 to a granoblastic garnet-bearing M1b assemblage (see Sutton & Watson 1959). Some of these recrystallised mylonite bands have acted as the sites for later D2 shearing in which a M2 greenschist facies assemblage developed. The yellow-green garnets have been broken and partially altered to chlorite (Plate 20g) and clinozoisite, epidote and minor anthophyllite have grown in the marginal quartz-plagioclase zones (Plate 20f).

Type (b) -homogeneous quartz-garnet-plagioclase-sphene-minor epidote bands with very sharp irregular "intrusive-like" contacts with the anorthosite. The subidioblastic garnets are colour zoned with yellow-green cores and darker green margins (Plate 20h). The garnets occur in aggregates typically with sphene at the core of the aggregate. The garnets are grossular-andradites (Table 3.1 & p.A.2). There is little chemical difference between garnet cores and margins, although the margins are slightly poorer in Ca and Al. The colour zoning is possibly due to variation in the Zr and Y contents of the garnets (see Fig. 4.14).

The similarities between the mineralogies of the two types of garnetiferous band in the anorthosites suggest they are genetically related. Type (a) are thought to have been either D1 mylonitised and metasomatised anorthosites or early D1 veins/intrusives which acted as the sites of shearing and became mylonitised. The mylonites recrystallised during M1. Type (b) were veins or alteration zones that were not sheared or in which a mylonitic fabric was not developed. It is thought that a banded mylonitic fabric would not have been destroyed during recrystallisation. The nature of the recrystallised mylonites (Type-a) and possible element mobility during shearing is discussed in Chapter 4.

Hor (1972), Wakefield (1974) and Hor et al. (1975) concluded in a detailed study of a complete core section (PW 75) through the anorthosite layer that there was no systematic variation in the plagioclase composition. However they failed to recognise the highly deformed nature of the anorthosite layer and interpreted all the siliceous bands within it as intrusive granitoids. Wright (1977) reinterpreted these siliceous bands as granite that had been intruded along thrusts within the anorthosite and concluded that the anorthosite layer was made up of at least seven overturned imbricate thrust slices. He suggested that within each thrust slice the plagioclase composition varied systematically, with the more calcic plagioclase at the structural top of each slice. Wright (1977) regarded this variation as due to igneous differentiation in a layered intrusion which was later overturned and imbricated. The mylonitic garnetiferous bands and the mixed siliceous gneiss-anorthosite zones recorded in this current study confirm the highly sheared, probably imbricately repeated nature of the composite anorthosite layer. However there is no evidence for any systematic variation in the plagioclase composition and hence no "way-up". Hor and Wakefield's

data show wide variations in plagioclase compositions within individual samples and Wright has been very selective in the analyses he used to define a differentiation trend. The andesine porphyroblasts recorded by Hor and Wakefield and in this study are obviously relatively late and along with coarse quartz replace the typical polygonal labradorite. It is thought here that the variation in plagioclase composition is metamorphic and not an original igneous feature.

The anorthosites in the Selebi-Phikwe area are mineralogically similar to those of the Messina area. The latter however contain thin bands of chromitite and magnetite. (Barton et al. 1979a) have included the minor peridotites and pyroxenites which occur immediately adjacent to the anorthosites in their anorthositic Messina Layered Intrusion. Barton & Key (1981) considered that the Selebi-Phikwe anorthosites contain much more quartz than those at Messina and for this reason Barton (pers. comm. 1981) doubts that they are lithologically equivalent. Barton & Key (1981) believe that the quartz in the Selebi-Phikwe anorthosites is due to hydrothermal alteration. However the higher content of the Selebi-Phikwe anorthosites is possibly related to a more pervasive amphibolite-facies retrogression as compared to the typical granulite facies at Messina. The Selebi-Phikwe anorthosites also appear to be more highly imbricated and mixed with siliceous gneisses. Although the Selebi-Phikwe anorthosites (metamorphic age -2720 Ma, Hickman & Wakefield 1975) are possibly significantly different in age to the Messina anorthosites (metamorphic age - 3279 Ma, Barton 1983b) (Table 1.2), they are definitely similar in mineralogy and texture. A geochemical comparison is made in Chapter 4.4. The Selebi-Phikwe and Messina anorthosites have similar mineralogies and settings to anorthosite-gabbro complexes in other high-grade Archaean terrains (Windley et al. 1981), for example in West Greenland (Windley et al. 1973; Windley & Smith 1974; Steele et al. 1977), in southern India (Subramaniam 1956; Bose 1979) and Labrador (Collerson et al. 1976; Wiener 1981).

The mineralogical differences between the Selebi-Phikwe anorthosites and calc-silicate gneisses are subtle. The ranges of plagioclase composition and the highly calcic clinopyroxenes in each lithology are similar. Calcic amphibole in the anorthosites ranges from magnesio-hornblende to actinolite, whereas that in calc-silicate gneiss is edenitic to ferroan pargasitic hornblende (Fig. 3.1). Calc-silicate gneisses have much higher quartz contents. Their quartz-

plagioclase banding is thought to be a primary feature, whereas the coarse quartz patches in the anorthosites are secondary and transgress the hornblende foliation. A geochemical comparison between the anorthosites and calc-silicate gneisses is made in Chapter 4.1.

3.5 MAGNETITE QUARTZITE AND ASSOCIATED AMPHIBOLITES

The main occurrence of magnetite quartzite is in the Dikoloti-Lentswe unit, where it is associated with banded and massive amphibolites. Four lithologies are recognised; the first three are intergradational:

a) finely banded magnetite quartzite;
b) finely banded magnetite-amphibole quartzite;
c) thinly banded quartz-amphibole rock (bands from 1-25 cm, usually 10 cm); and
d) massive amphibolite up to 5 m thick with few or no quartz bands.

The magnetite quartzite is a finely banded rock (Plate 22a). The variation in grain-size between adjacent bands is related to magnetite content. Magnetite-rich bands contain coarser idioblastic magnetite grains (Plate 22b). The magnetite grain-size also increases if the magnetite quartzite occurs immediately adjacent to ultramafic rocks (e.g. at Lentswe and Phokoje). Finely banded magnetite-amphibole quartzite with minor amphibole scattered throughout or more usually concentrated in the magnetite-rich bands is the most common type of quartzite (Plate 22c). The amphibole is clinoamphibole and both weakly pleochroic actinolite and highly twinned cummingtonite are present even in the same band. Actinolite is the more common of the two. The fine banding of the quartzites is frequently cut by a D1 cleavage formed by magnetite trains, aligned amphiboles and quartz grain-boundaries (Plate 22c). The fine banding is regarded as a primary feature.

Thinly banded quartz-amphibole rock is a common component of the association. The amphibole bands can be either actinolite (Plate 22d), cummingtonite or less frequently hornblende (Plate 22e). Actinolite bands are the most common. The hornblende bands were only found immediately adjacent to the ultramafic rocks at Lentswe. The amphibole bands usually contain only one amphibole. Rare thin cummingtonite laminae occur within some actinolite bands (Plate 22f). The amphibole bands usually contain minor disseminated quartz and magnetite. At Lentswe disseminated pyrrhotite occurs in both the amphibole and quartz bands (Plate 22g). Quartz bands contain scattered magnetite

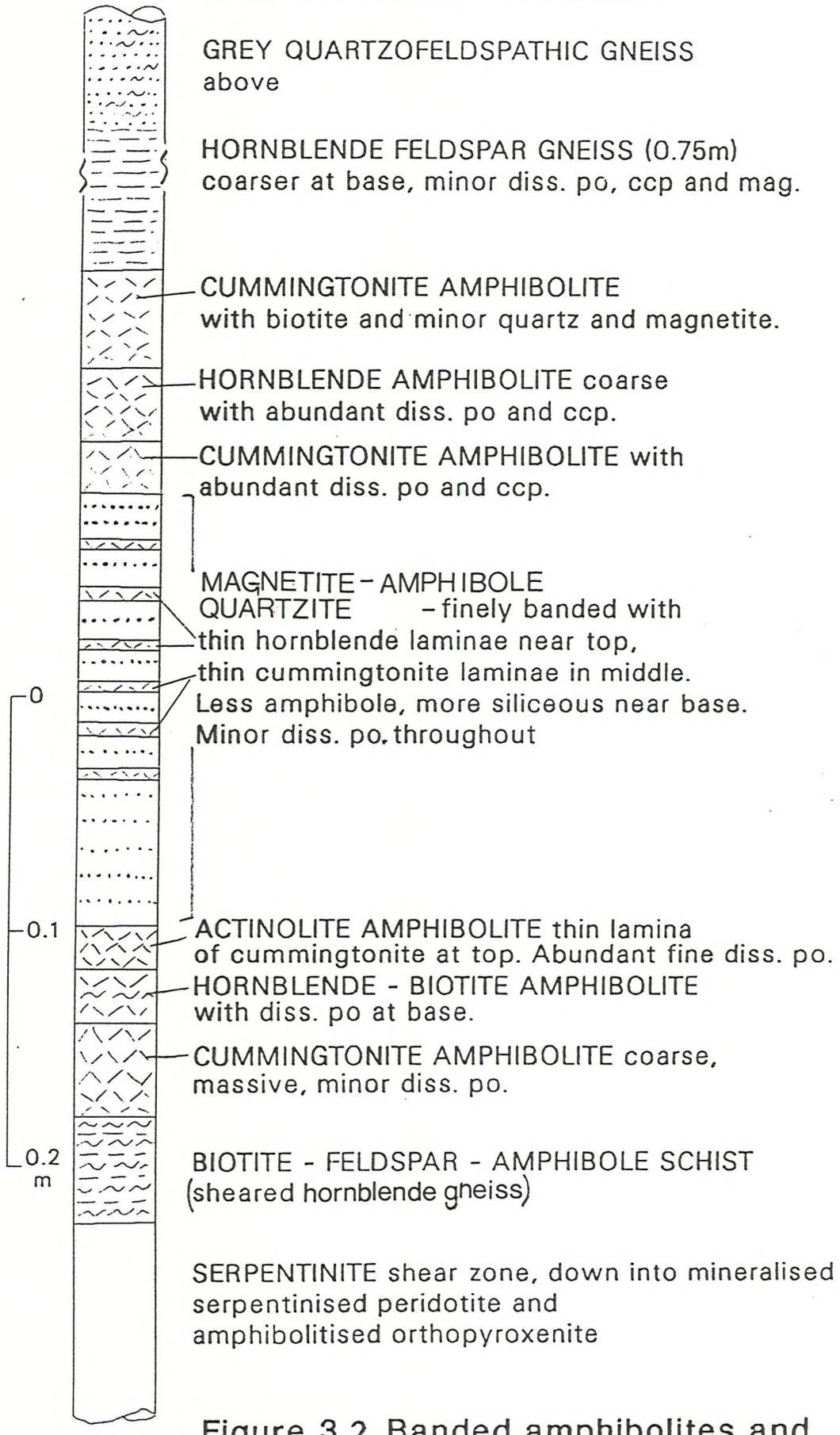

Figure 3.2 Banded amphibolites and Quartzite in LT 31.

and amphibole, locally both cummingtonite and actinolite in the same quartz band. The hornblende bands at Lentswe have sharp with adjacent actinolite-bearing quartz bands (Plate 22e).

A detailed example of banded amphibolites and magnetite quartzite from LT 31 is shown in Figure 3.2. (Diamond drill holes at Phikwe, Selebi, Selebi North, Dikoloti and Lentswe are prefixed PW, SD, SN, DK and LT respectively.) In LT 26 & 27 (Fig. 8.5) well-banded quartz-amphibole rocks below the mineralised ultramafic rocks contain thin cummingtonite, actinolite and hornblende-biotite-cummingtonite amphibolite bands. The amphibole in the quartz bands in this case is mainly cummingtonite (see p.A.3). Fine disseminated pyrrhotite occurs throughout but particularly in the hornblende amphibolite which contains thin orthopyroxene-quartz-pyrrhotite laminae (Plate 22h).

The banding in the quartz-amphibole rocks is regarded as a primary feature. However the presence of Mg-amphibolites in magnetite quartzites adjacent to ultramafic rocks could possibly be due to Mg-metasomatism, possibly during shearing. These alternatives are tested geochemically in Chapter 8.

The thick massive amphibolites are dominantly cummingtonite amphibolites. Thick actinolite amphibolites are less common. The cummingtonite amphibolites often contain thin laminae of hornblende. The actinolite amphibolites contain minor disseminated quartz. As a generalisation, the amphibole in thinly banded quartzite-amphibolite is actinolite; that in thick massive amphibolite is cummingtonite.

3.6 OTHER QUARTZITES

Thin quartzites are associated with hornblende and biotite gneisses, particularly in Units A and B of the Phikwe section. Some are monomineralic quartz bands, but normally they are feldspathic (up to 30% albite-oligoclase) with only minor magnetite. The quartzites usually contain laminae of sillimanite and/or biotite (Plate 23a) or minor hornblende (with relicts of clinopyroxene being replaced by hornblende, Plate 23b). Quartzite in Unit B contains laminae of fibrous sillimanite and pyrrhotite (Plate 23c).

Well banded magnetite quartzite and associated amphibolites are not found at Dikoloti. They are represented by a finer grained, more siliceous and magnetite-rich facies of grey and biotite gneisses and plagioclase quartzites. For example in DK 23, fine-grained plagioclase quartzite within grey and hornblende gneiss adjacent to mineralised ultramafic rocks contains thin bands that are rich in plagioclase and

magnetite plus either (a) hornblende with minor cummintonite, or (b) cummingtonite, garnet and biotite. This quartzite is similar to the plagioclase quartzites that occur in Units A and B at Phikwe.

A thin unit of interbanded diopside quartzite and diopside amphibolite occurs in the Phikwe dome (Unit H). The quartzite contains scattered diopside (salite ?) and actinolite (Plate 23g). The actinolite occurs as separate prisms, not as a replacement of diopside. The amphibolite is dominantly coarse-grained actinolite with relicts of diopside (salite ?) and very fine-grained aggregates of an epidote-group mineral or saussurite (possibly after plagioclase although no plagioclase was found, Plate 23h). Quartz is a minor constituent and minor carbonate occurs between grains. The contact of the amphibolite with the quartzite is a thin zone of epidote. Marble (Wakefield 1974) and minor magnetite quartzite (Key 1976) occur at the same structural position in the Phikwe dome as the diopside amphibolite and quartzite.

3.7 DIOPSIDE GNEISSES

Diopside gneisses occur in Unit G, structurally below the Phikwe ore body, associated with fine-grained garnetiferous hornblende-rich gneisses (HGG) and biotite gneisses. (The clinopyroxene was assumed during field work to be diopside. However whole-rock analyses indicate that it is Fe-rich, i.e. ferrosalite. The term diopside gneiss however has been retained.) The diopside gneisses are of three types, interbanded with each other and with HGG. In order of decreasing abundance, they are:

a) Weakly-banded coarse-grained granoblastic clinopyroxene-plagioclase gneiss with minor sphene. The weak banding is due to the variation in clinopyroxene and plagioclase content. The plagioclase is calcic labradorite.

b) Well-banded rocks: - hornblende-plagioclase bands and clinopyroxene -plagioclase bands with minor magnetite and a trace of carbonate (Plate 23d). The banding is on the scale of 2-5 cm and has sharp margins. Clinopyroxene (Mlp ?) is locally replaced by hornblende. However the majority of the clinopyroxene, hornblende and plagioclase occurs in an equilibrium Mlm assemblage.

c) Similar to b, but with mineralogically graded and size-graded bands in which an upper assemblage of coarse-grained clinopyroxene-garnet-plagioclase-minor magnetite-carbonate grades down into a lower hornblende-plagioclase assemblage (Plate 23e). The base of the band is hornblende-rich and sharp, not gradational.

Similar mineralogically graded diopside-plagioclase-hornblende gneisses occur east of Sefhope (Plate 23f).

These banded gneisses are mineralogically and morphologically similar to the striped amphibolites of Connemara (Evans & Leake 1960) and Sirohi, India (Bhattacharyya & Mukherjee 1984). The nature of the banding (e.g. grading) of the Selebi-Phikwe diopside-bearing rocks and the lack of leucocratic segregations indicate that the banding is not due to metamorphic differentiation or partial melting. The banding is considered to be an original feature, probably accentuated by tectonic flattening. This conclusion can be contrasted with that of Evans & Leake (1960) for the Connemara amphibolites (i.e. banding due to tectonic and metamorphic processes).

3.8 ULTRAMAFIC ROCKS

Thin ultramafic bands and pods occur throughout the well-banded Selebi-Phikwe gneisses particularly Unit D and include the host rocks to Ni-Cu mineralisation at Dikoloti-Lentswe (Ch. 8) and some of the host rocks at Phikwe and Selebi-North (along with less mafic amphibolites, Chs 5 & 7). The ultramafic rocks of Unit D contain traces of disseminated sulphide, mainly pyrrhotite.

3.8.1 Mineralogy of Unit D Ultramafic Rocks

The full range of ultramafic bands is seen in Unit D and consists of variably retrogressed peridotites, amphibole pyroxenites and amphibolites, usually as single-lithology bands but also as composite bands. The unretrogressd ultramafic rocks consist of various proportions of olivine, green spinel, amphibole (hornblende to tremolite) and pyroxene (Plate 24c). The pyroxene is usually orthopyroxene. Olivine-two pyroxene rocks are rare at Selebi-Phikwe. The most common lithologies are actinolite amphibolites and hornblende pyroxenites. Actinolite amphibolites (Plate 24d) may contain orthopyroxene and olivine (Plate 24e) but lack green spinel. Hornblende pyroxenite consists of porphyroblasts of orthopyroxene (highly included with hornblende) in a matrix of hornblende and minor olivine and green spinel. All gradations also exist between dunite and orthopyroxenite (Plate 24a & b). The olivine is typically interstitial to, and wraps around, the orthopyroxenes in the pyroxenites (Plate 24b & c). Olivine also includes hornblende. Magnetite networks locally surround and cut across unaltered olivines in unserpentinised rocks. Green spinel usually occurs as inclusions in olivine (Plate 24c).

Olivine-rich ultramafics have commonly been retrogressed to M2 assemblages of mainly serpentine with chlorite, phlogopite, magnetite and talc. Amphibole pyroxenites are less altered, except where they have suffered D2 shearing. Orthopyroxene is locally replaced by (M2a ?) cummingtonite and phlogopite (Plate 24f). More extensive retrogression has developed cummingtonite-rich amphibolites with abundant phlogopite and orthoamphibole and rare relict calcic clinoamphibole (Plate 24g).

Serpentine also occurs in a thin highly sheared orthoamphibole-serpentine-biotite-pyrrhotite-quartz schist (Plate 24h) in Unit A. This serpentine-schist is associated with hornblende gneiss and amphibolite, garnet-biotite schist and feldspathic and sillimanitic quartzite, all with minor disseminated pyrrhotite. It is possibly a highly sheared and attenuated equivalent in the Phikwe section of the Dikoloti-Lentswe unit.

3.8.2 Interpretation of Ultramafic Assemblages

The olivines, orthopyroxenes and green spinels of the ultramafic rocks in Unit D are either metamorphic or relict igneous assemblages. The textures between olivine, pyroxene and calcic amphibole are equivocal although the olivine is typically interstitial to orthopyroxene, a feature of metamorphic ultramafic assemblages (Evans 1977). The calcic amphiboles were initially thought by the author to postdate and replace orthopyroxenes. However the amphibole that would be expected from the isochemical retrogression of orthopyroxene is anthophyllite or magnesio-cummingtonite, not hornblende or actinolite (Evans 1982). A retrograde (M2) assemblage of cummingtonite, orthoamphibole and phlogopite replacing the orthopyroxene and calcic amphibole assemblage is in fact developed. Hornblende is locally included in olivine and appears to be in metamorphic equilibrium with it, not replacing it. Therefore the actinolite-orthopyroxene-olivine assemblage and the hornblende-orthopyroxene-olivine-green spinel assemblage are thought to be prograde M1 metamorphic assemblages that do not contain relict igneous minerals. These two assemblages are respectively typical of those that form in ultramafic rocks at the middle amphibolite facies and upper amphibolite-granulite facies transition (Trommsdorf & Evans 1974; Evans 1977, 1982). The networks of magnetite locally surrounding unaltered olivines are tentatively suggested as being derived from the iron oxide produced during serpentinisation of original igneous

olivine-bearing assemblages (cf. Eckstrand 1975).

Further evidence for the metamorphic nature of the olivine-orthopyroxene-green spinel-calcic amphibole assemblage comes from the mineralised ultramafic rocks (to be discussed in Chapters 5 & 8). The evidence includes the variety of Cr-bearing spinels in a single rock and the low nickel-contents of the olivines (Evans 1977). Theoretical and experimental studies on ultramafic systems (Trommsdorf & Evans 1974; Evans 1977: Lieberman & Rice 1986) indicate that the calcic amphibole-bearing M1 assemblages formed at metamorphic conditions of about 725-825° C at 3-8 kbar (Fig. 5.7). The higher grade hornblende and green spinel-bearing assemblage near the upper limit of this estimate at the transition from amphibolite to granulite facies. These temperatures and pressures are broadly in agreement with those deduced from the corundum-pleonaste-sapphirine assemblage (see Ch. 3.9).

The variable nature of the resulting prograde M1 assemblage (actinolite-bearing or hornblende-green spinel-bearing) in the ultramafic rocks is possibly due to bulk chemical variations and water content. Juxtapositioning of apparently different metamorphic grades is also seen at Lentswe. Monomineralic actinolite and cummingtonite M1m amphibolites (indicative of low to middle amphibolite facies conditions) without any obvious relict prograde metamorphic minerals (Ch. 3.5) occur immediately adjacent to Lentswe ultramafic rocks with a typical amphibolite-granulite facies transition assemblage of olivine, orthopyroxene, green spinel and hornblende and rarely an olivine-two pyroxene M1p assemblage (Ch. 8.2). This juxtapositioning could be due to a retrogressive metasomatic origin of the actinolite and cummingtonite amphibolites. However it is suggested that this juxtapositioning of apparently different metamorphic grades is more likely to be due to rapid chemical variations between lithologies (Stanton 1982a, 1982b) and possibly the high original water-contents of the amphibolites (Stanton, pers. comm. 1976).

3.9 SAPPHIRINE-BEARING DIKOLOTI FELDSPATHIC AMPHIBOLITE

3.9.1 Mineralogy of Sapphirine-bearing Dikoloti Amphibolite

At Dikoloti a gabbroic feldspathic amphibolite is associated with mineralised ultramafic rocks. The amphibolite contains an important metamorphic assemblage which it is appropriate to discuss here. The geochemistry and protolith of the amphibolite will be discussed in Chapter 8. Sapphirine (Table 3.2 & p.A.4) occcurs in the

Dikoloti feldspathic amphibolite in two situations:
a) Subround aggregates (5-50 mm) of spinel, sapphirine and corundum. Each aggregate is surrounded by a corona of fine-grained alteration products (dominantly clinozoisite plus chlorite and sericite) and coarse orthoamphibole (Plate 40a).
b) Thin bands and laminae (<10 mm) of the corona minerals with minor sapphirine and spinel (Plate 40b).

The aggregates consist dominantly of dark green spinel with lesser sapphirine grains (Plate 40d). The sapphirine appears to rim the spinel. Corundum only occurs in the cores of the largest aggregates where it occurs as coarse subidioblastic grains (Plate 40e). This coarse corundum is surrounded by a rim-like aggregate of spinel. This spinel is locally rimmed by and appears to be altering to sapphirine (Plate 40f & g). The coarse corundum is also replaced by sapphirine. Opaque anastomising veinlets of unknown mineralogy and composition surround the granular aggregates of corundum, spinel and sapphirine at the margins of coarse corundum (Plate 40f & g). The sapphirine is distinctively pale blue and pleochroic. The spinel is pleonaste showing little variation in composition (Table 3.2 & p.A.4). The more-aluminous sapphirine (663) is associated with the least-aluminous pleonaste. There appears to be a limited range of solid solution by Mg-Fe substitution in the pleonaste and (Si,Mg)-Al substitution in the sapphirine.

The aggregates are each surrounded by a corona of fine-grained granular and radiating minerals in light and dark patches (Plate 40a & d). Microprobe analysis (Table 3.2 & p.A.4) shows them to be dominantly zoisite/clinozoisite plus mixtures of this and chlorite, sericite and gedrite with no chemical difference between the light and dark patches. Minor relicts of anorthite occur in the corona and plagioclase multiple twinning is mimicked by the fine-grained clinozoisite. Cordierite with twinning and minor kyanite and ortho-pyroxene were tentatively identified in the coronas. The contact of the spinel-sapphirine aggregates with the coronas is marked by a thin rim of high Al-Mg chlorite (corundophilite) on the spinels (Plate 40d). A similar corundum-sapphirine-corundophilite assemblage has been described from Mount Painter, Australia (Oliver & Jones 1965). The outer margin of the corona against feldspathic amphibolite is marked by relatively coarse tangential fibrous orthoamphibole extensively replaced by (or intergrown with) chlorite. The sapphirine-bearing laminae and bands consist of a similar minerlaogy to the fine-grained

but
coronas with higher proportions of coarse orthoamphibole and chlorite and only minor spinel and sapphirine grains (a higher sapphirine/spinel ratio also) (Plate 40h). The coarse fibrous minerals grow randomly across the bands. The amphibolite that hosts the sapphirine-bearing aggregates and bands has a very simple (M1m) mineralogy of coarse-grained granoblastic tshermakitic hornblende (Fig. 3.1) and anorthite (Plate 40c) which are unzoned, unaltered and show no compositional variation (Table 3.2 & p.A.4).

The corundum-pleonaste-sapphirine aggregates at Dikoloti are similar to the corundum-pleonaste-anorthite aggregates found in the Selebi host amphibolites, although the latter have a simpler coronitic texture (Ch. 5.2.2, Plate 32b & c). The pleonastes from the two occurrences are very similar chemically (Table 5.2).

Sapphirine-bearing assemblages have been described from elsewhere in the Central Zone of the Limpopo Belt by Schreyer and Abraham (1976), Horrocks (1983), Schreyer and Horrocks (1984) and Windley et al. (1984) and from the North Marginal Zone by Robertson (1977). However the other occurrences in the Central Zone are only loose piles of pegmatitic material near to anorthosite exposures. No precise field relations are known. The importance of the Dikoloti occurrence is that core provides a complete section of the sapphirine-bearing rocks.

3.9.2 Discussion of Dikoloti Sapphirine-bearing Assemblage

The assemblages found in the Dikoloti feldspathic amphibolite indicate a complicated metamorphic history and many mineral reactions can be proposed to have occurred in the Al-rich, Si-poor aggregates (see Windley et al. 1984). The complicated history of the aggregates is in contrast to the apparently simple mineralogy of the M1m assemblage of hornblende and anorthite in the amphibolite. The corundum at both Dikolti and Selebi apppears to be the oldest phase in the aggregates and is thought to have formed at the peak of M1 metamorphism (M1p) possibly from a highly aluminous precursor. M1p magnesium-bearing phases that have possibly been consumed include garnet. The coronas particularly the simple ones at Selebi are thought to be M1 and M2 retrogresssion coronas around an M1p corundum nucleus within a hornblende-anorthite amphibolite (Leyreloup et al. 1975). A generalised reaction for the formation of the coronas of spinel and sapphirine can be expressed as:

Corundum + An-rich Plagioclase + Hornblende ---> Sapphirine + Spinel

Subsiduary reactions possibly involving localised Si metasomatism also took place, for example:

Pleonaste + SiO2 -----> Sapphirine (Robertson 1977)

Sapphirine + SiO2 -----> Cordierite (Robertson 1977; Droop & Bucher-Nurminen 1984)

Later reactions during late M1/early M2 involved hydration, for example the formation of corundophilite from spinel and:

Cordierite + H2O ---> Gedrite + Kyanite + SiO2 (Van Reenen & Du Toit 1977)

Thermodynamic calculations for the reactions in similar sapphirine-bearing assemblages of Horrocks (1983), Droop & Bucher-Nurminen (1984) and Windley et al. (1984) indicate metamorphic conditions of approximately 10 kbar and 800°C during the formation of M1p corundum, followed by almost isothermal decompression (possibly during rapid uplift) down to about 4 kbar at 700°C during late M1 (Fig. 3.3) for the Dikoloti corona assemblages. Sapphirine possibly formed at Dikoloti rather than at Selebi because of a higher degree of Si metasomatism (cf. Herd et al. 1969) or higher Mg activity (cf. Yardley & Blacic 1976) in the former. However sapphirine could possibly have been formed at Selebi but have been destroyed in later spinel and corundum-forming reactions (Droop & Bucher-Nurminen 1984; Windley et al. 1984).

Further cooling, decompression and hydration (plus localised K metasomatism) during M2 led to the development of fine-grained clinozoisite, chlorite and sericite in the outer plagioclase-rich (+ cordierite) corona.

The geochemistry and origin of the of the corundum-spinel-bearing amphibolites at Dikoloti and Selebi is dealt with in Chapters 7.2, 8.2.2 and 8.6.2. The original nature of the corundum-spinel aggregates of the Dikoloti feldspathic amphibolite and Selebi host amphibolite is problematic. An origin by metamorphism of aluminous xenoliths or hydrothermally altered patches seems the most likely. However the effects of metamorphism (e.g. exsolution of corundum in anorthite) and metasomatism can not be ruled out.

	Amphibolite		Spinel-Sapphirine Aggregate				Corona		
	a	b	c	d	e	f	g	h	i
	plg	hor	spi	sap	cor	chl	zoi/clz	ser	ged
SiO2	43.92	45.69	0.06	12.86	0.03	25.85	39.24	46.75	45.14
TiO2		0.08	0.02	0.03	0.02	0.02	0.02	0.02	0.05
Al2O3	35.58	15.34	65.23	63.43	97.79	25.99	32.70	37.72	17.26
FeO	0.09	7.19	17.37	5.59	0.38	4.15	0.54	0.35	10.67
MnO		0.15	0.13	0.07	0.02	0.03	0.04	0.02	0.31
MgO		16.07	16.76	17.09	0.00	27.97	0.01	0.04	21.17
CaO	19.51	11.30	0.02	0.03	0.01	0.28	24.25	0.07	0.83
Na2O	0.41	1.62			0.02	0.01	0.08	0.20	1.53
K2O	0.00	0.25				0.00	0.01	11.08	0.00
Cr2O3		0.00	0.01	0.01	0.00	0.00			
NiO		0.09	0.20		0.00				
Total	99.51	97.66	99.80	99.11	98.27	84.30	96.89	96.25	96.96
	An 96								
No. of analyses	3	4	6	8	3	5	4	1	1

Feldspathic Amphibolite
a Anorthite 660
b Hornblende 660 & 663

See appendix A.4 for all analyses

Spinel-Sapphirine Aggregate
c Pleonaste 660 & 663
d Sapphirine 660 & 663
e Corundum 660
f Corundophilite rimming pleonaste 663

Corona rimming Spinel-Sapphirine Aggregate
g (Clino)zoisite 660 & 663
h Sericite 660
i Gedrite 663

Samples 660 and 663 from DK 23 See Plate 40 for 660 & 663

TABLE 3.2 - AVERAGE MINERAL ANALYSES -- DIKOLOTI FELDSPATHIC AMPHIBOLITE

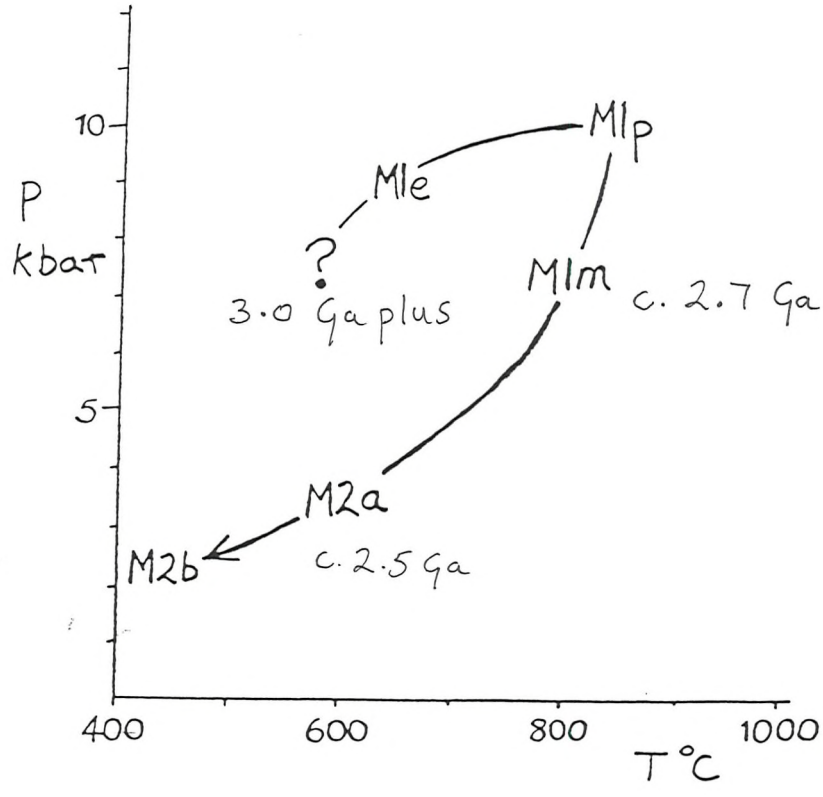

Fig. 3.3 P-T path of the Selebi-Phikwe Rocks

3.10 GRANITIC GNEISSES

The typical porphyroblastic granitic gneiss contains microcline, quartz, plagioclase and minor fine biotite. The porphyroblasts are microcline with tartan twinning or less-commonly microcline perthite in a matrix of quartz, plagioclase and microcline in a weak "mortar-like" granoblastic texture (Plate 25a). Evidence for weak early-D2 cataclasis is common in the granitic gneisses and textures vary from porphyroblastic granoblastic to porphyroclastic. Plagioclase (oligoclase) is always a minor component. Myrmekite penetrating into microcline is well developed in both granoblastic and cataclastic types (Plate 25b). The porphyroblastic granitic gneiss body to the northeast of Phikwe has a highly cataclastic margin (Plate 3c). In its core the body contains microcline porphyroblasts surrounded by large areas of fine-grained microcline and quartz, locally in a graphic-like intergrowth. The hornblende-bearing dioritic gneisses associated with the porphyroblastic granitic gneisses are plagioclase-dominated granoblastic rocks with quartz, hornblende and biotite (Plate 25c). The plagioclase is andesine and is unaltered, unzoned and well twinned. These hornblende-bearing gneisses do not have cataclastic textures and do not appear to have been highly deformed.

3.11 MYLONITES AND CATACLASITES

Thin zones interpreted as recrystallised mylonites occur throughout the Selebi-Phikwe well banded gneisses (Plate 25e & d). They are most common at the margins of and within the anorthositic gneiss layers, in which D1 mylonites have been recrystallised to M1 quartz-feldspar granulites (see Ch. 3.4).

Important mylonites and cataclasites occur in the Selebi-Phikwe ore bodies. At least three phases of typically superimposed shearing have effected the Phikwe ore body. The earliest shearing is represented by banded quartz-plagioclase-garnet M1m granulites which occur at the base of the massive sulphide in Zone C and as relicts in later thick M2a cataclastic gneisses in Zone F (Fig. 5.2). These banded granulites are thought to represent recrystallised D1 mylonites. There are no signs of early shearing having been preserved within the host amphibolite.

Most of the apparent shearing at Phikwe is related to early-D2 deformation during which finely banded M2a blastomylonites (Plates 27b & 34e & h) with subround plagioclase and minor microcline porphyroclasts were developed in the immediately adjacent footwall and

hanging wall grey gneisses, particularly the latter. These commonly contain broken and altered garnets (Plate 25g & h) which are interpreted as relicts of recrystallised D1 mylonites. Highly sheared and thinned host amphibolite is represented by thinly banded, fine-grained mafic and felsic zones. The mafic zones consist of ellipsoidal plagioclase porphyroclasts, rare hornblende porphyroclasts and cracked garnets in a matrix of fine biotite and minor felsics (Plate 25f). The roundness of the plagioclase porphyroclasts increases as the mica content increases. This early-D2 shearing is most conspicuous where the host amphibolite and sulphides are thin or missing. Superimposed on the early-D2 cataclasites are thin late-D2 shear zones (Plates 26g & 27a). These are located exactly at the ore body horizon. Their effect on the ore body is not as great as the early-D2 shears and they appear to have been significantly developed only where the ore body was already absent. They consist of a fine-grained finely banded M2b assemblage of chlorite, felsics and minor epidote and calcite with highly altered plagioclase porphyroclasts (Plates 25g, 26h & 27b-d). These mylonites are typically crosscut by coarse calcite and pyrite veins.

The Phikwe ore body has repeatedly acted as a zone of shearing. The most important shearing appears to have been associated with early -D2 folding during which the ore body acted as a zone of decollement.

The other major development of M2a cataclasites during early D2 is in the granitic gneisses. The majority of granite bodies were intruded during the interval between D1 and D2, although some were intruded during D2.

3.12 SUMMARY of METAMORPHIC HISTORY of the SELEBI-PHIKWE AREA

The mineral assemblages in the Selebi-Phikwe gneisses can be simply divided into M1 and M2. The M1 minerals show little zoning either optically or chemically. No relict premetamorphic minerals are recognised. For example the clinopyroxenes of the anorthosites and hornblende gneisses are metamorphic. The olivines, pyroxenes and spinels of the ultramafic rocks are thought to be metamorphic rather than igneous. The earliest recognisable minerals (M1e) are relict prograde porphyroblasts with syntectonic rotational structures that grew during D1. The highest grade assemblages (M1p) occur as possible relicts in the main M1m assemblages. The granulite facies M1p assemblages indicate temperature and pressure conditions of about 800° C and 10 kbar. They are thought to have formed at the end of D1

deformation, when tectonic burial to about 35 km had taken place. The great majority of the assemblages are simple unaligned granoblastic M1m amphibolite-facies assemblages as exemplified by the hornblende-plagioclase assemblages of the hornblende gneisses and the anorthosites. Cordierite porphyroblasts including sillimanite (M1p) are characteristic of M1m in the grey and biotite gneisses. There is evidence from the corundum-spinel-sapphirine assemblage in the Dikoloti feldspathic amphibolite for rapid, almost isothermal, uplift to conditions of about 700°C and 4 kbar (c. 10 km) during late M1. The common hornblende plagioclase assemblage appears to have been stable over a wide variety of metamorphic conditions. M2 assemblages are greenschist facies and indicate a pervasive hydration. M2 assemblages are important in D2 shear zones (e.g. in the Phikwe ore body). Where structural data allow, the M2 assemblages can be subdivided into early M2a and later M2b.

The porphyroblastic granitic gneisses are regarded as having been mainly intruded during the interval between the two main deformation periods. Although it is difficult to estimate to what degree the textures seen in the porphyroblastic gneisses are plutonic modified by metamorphism or if they are entirely metamorphic, they do not appear to have suffered the M1 conditions. Many show dynamic cataclastic effects (M2a granulation and recrystallisation) that occured during D2. Very limited partial melting of the Selebi-Phikwe gneisses probably took place during late M1 to produce some of the thin granitic bands seen in the Selebi-Phikwe gneisses. However formation of the grey gneisses as extensive partial melts of a mafic-gneiss dominated sequence as suggested by Wakefield (1974) did not take place (see Ch. 4 for the likely protoliths of the grey gneisses).

The relationship of the three metamorphic stages to the two main deformation periods is shown in Figure 3.4. A possible P-T time-path is shown in Figure 3.3. The peak of M1 took place at P-T conditions of approximately 800°C and 10 kbar. This shows that metamorphic grade reached in this northwest portion of the Central Zone was as severe as in the rest of the Central Zone and not of a lower grade as suggested by Barton & Key (1981). It is not known whether (a) the amphibolite-facies M1m assemblages all formed by retrogression of granulite-facies M1p assemblages, i.e. the M1p assemblages are simple relicts, or (b) the M1p assemblages only developed locally within the M1m assemblage at the peak of metamorphism. It is tentatively thought that the textures indicate the latter case. It is therefore possible that

Fig. 3.4 Summary of the structural and metamorphic history of the Selebi-Phikwe area

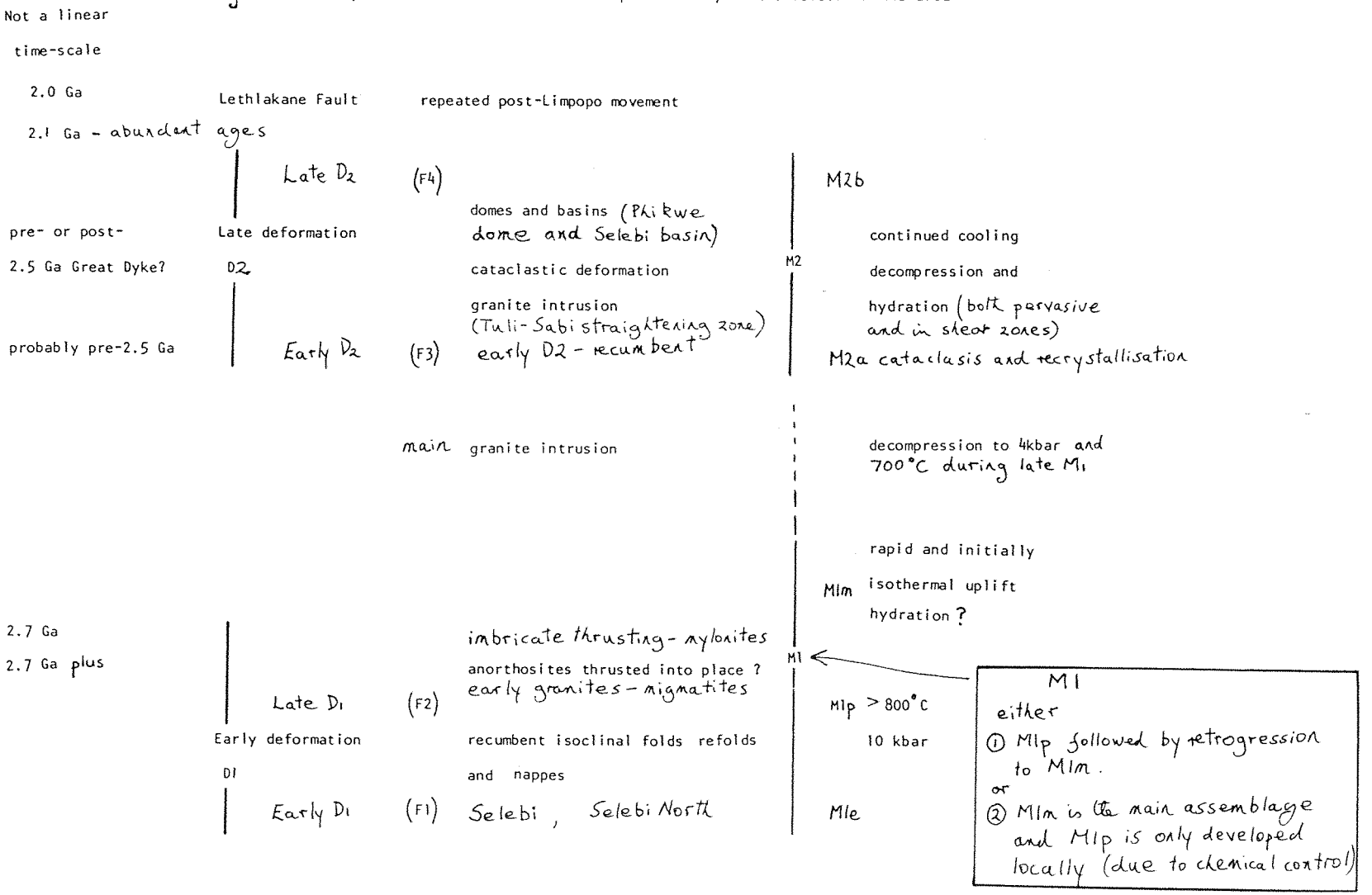

severe metamorphic conditions at Selebi-Phikwe were attained for a much shorter time than in the rest of the Central Zone.

The ages of the deformation and metamorphism are not well known. Widespread Rb-Sr mineral ages show that the Limpopo deformation had ceased by 2.0 Ga and that the rocks of the Selebi-Phikwe and the rest of the Limpopo Belt were near to their present erosion level by then (Van Breemen & Dodson 1972; Hickman & Wakefield 1975). The isotopic work of Hickman and Wakefield (1975) indicates that the main Mlm metamorphic assemblages formed approximately 2.7-2.6 Ga. Hickman and Wakefield (1975) argue that the dome and basin interference folds were formed as late as 2.1-2.0 Ga. However major deformation in the North Marginal Zone had ceased by the time of intrusion of the Great Dyke at 2.5 Ga. Although the undeformed Great Dyke does not intrude the Central Zone it is thought here that significant major deformation did not take place in the Selebi-Phikwe area (on the northern boundary of the Central Zone and immediately adjacent to the westward continuation of the main North Marginal Zone) after 2.5 Ga.

PLATE 17 (overleaf)

Mafic Amphibole-rich Gneisses (mainly Hornblende Gneiss)

(A) HGN. Hornblende, labradorite and trace of quartz. Phikwe Unit B (LK 2), Sample # 560. FV = 6 mm.

(B) HGF. Garnet poikiloblast (G) with included magnetite, quartz and hornblende. Phikwe Unit D (PW 195), # 275. FV = 6 mm.

(C) HGC. Clinopyroxene poikiloblast (P) with included hornblende, plagioclase and magnetite. Phikwe Unit B (PW 210), # 535.FV = 6mm.

(D) HGC. Granular clinopyroxene (P) associated with magnetite. Granoblastic hornblende (H) and plagioclase matrix. Phikwe Unit D (PW 210), # HG3. FV = 3 mm.

(E) HGG. Garnet porphyroblast in hornblende-plagioclase gneiss. Phikwe Unit G (PW CAM 38/1), # 634. FV = 6 mm.

(F) QPIB. Biotite-plagioclase-hornblende-quartz-pyrrhotite schist. Relicts of pyroxene (Mlp ?) altering to hornblende and biotite. Phikwe Unit B (PW 210), # 547. FV = 3 mm.

(G) ARIB. Cummingtonite-biotite-plagioclase-quartz amphibolite/ schist. Phikwe Unit B (PW 210), # 533. FV = 6 mm.

(H) GRHG. Idioblastic helicitic garnet (Mle ?). Phikwe Unit D (PW 149), # 12. FV = 6 mm.

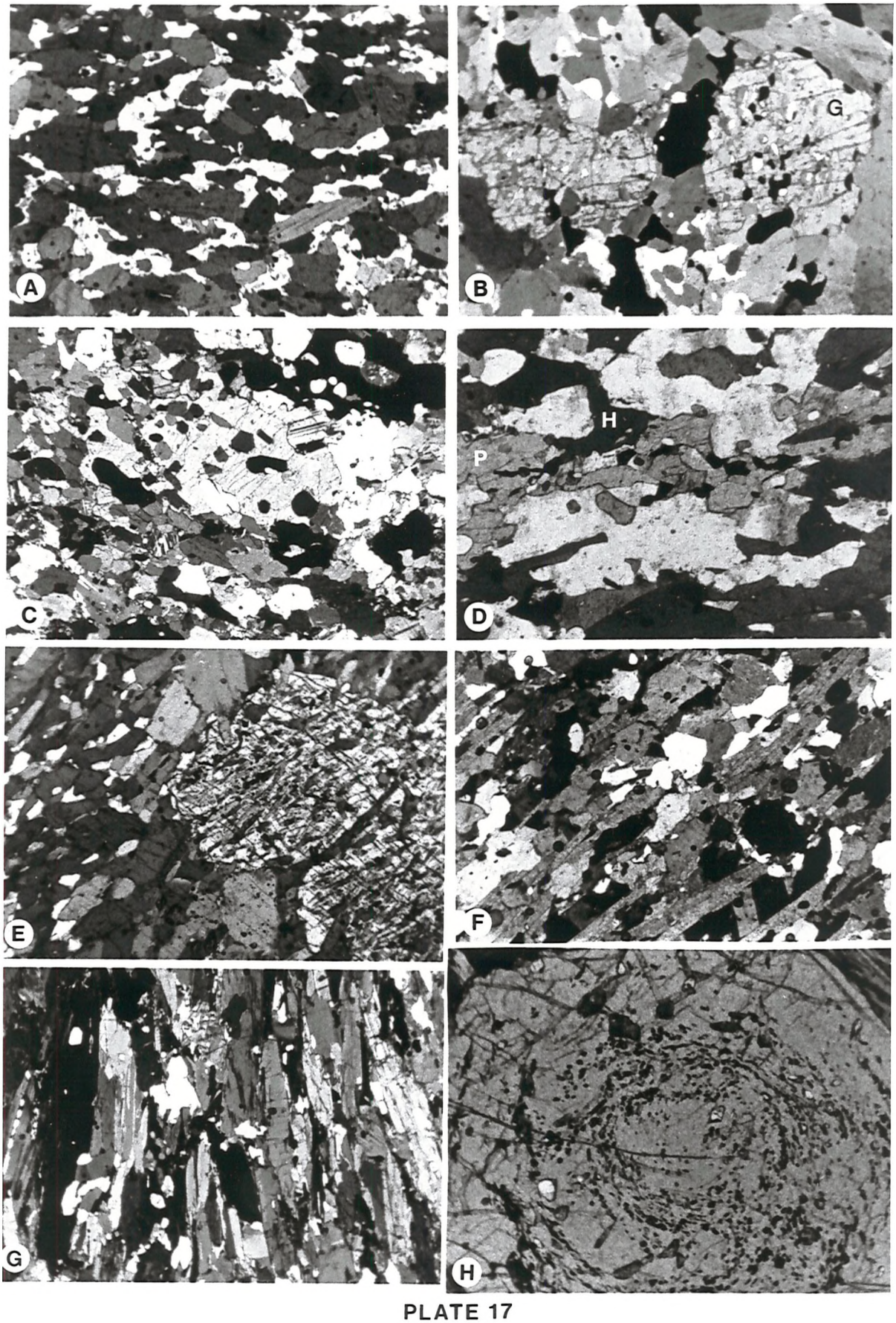

PLATE 17

PLATE 18

Grey Gneiss

(A) Typical garnetiferous quartz-plagioclase-biotite(B) grey gneiss (low-Si). Phikwe Unit E (PW 210), # GG3 FV = 6 mm.
(B) Mafic plagioclase-hornblende(A)-quartz-minor biotite grey gneiss (low-Si). Phikwe Unit F (PW 188), # 56, FV = 3 mm.
(C) Round quartz inclusions in corroded plagioclase. Selebi Unit E/F (SD 80), # 102. FV = 3 mm.
(D) Granoblastic oligoclase-quartz-biotite(B)-minor microcline grey gneiss (med.-Si). Phikwe Unit (PW 210), # GG5. FV = 3 mm.
(E) Symplectic vermicular quartz and plagioclase (?). Phikwe Unit E (PW 93), # 34. FV = 1.5 mm.
(F) Garnetiferous siliceous grey gneiss. Note minor myrmekite. Same as (E) above. FV = 3 mm.
(G) SCGG. Cordierite poikiloblast(C) with sillimanite in core. Phikwe Unit F (PW 208A), # 705. FV = 3 mm.
(H) SCGG. Cordierite altered to pinnite at margin. Microcline rim to cordierite. Selebi North Unit E/F (SDN 51), # 525. FV =3 mm.

PLATE 19

Intermediate Biotite Gneiss

(A) QRIB. Green spinel and sillimanite in core of cordierite. Selebi Unit E/F (SD 80), # 103. FV = 1.5 mm.
(B) QRIB. Quartz and sillimanite in spongey poikiloblastic cordierite. Phikwe Unit A (PW 213), # 541. FV = 3 mm.
(C) Vermicular quartz in plagioclase rimming garnet in (A) above. FV = 3 mm.
(D) Gedrite(G)-biotite-quartz band in (A) above. FV = 3 mm.
(E) QRIB. Cummingtonite-quartz-biotite-plagioclase-apatite gneiss. Phikwe Unit B (PW 210), # 529. FV = 3 mm.
(F) FRGG. Quartz-plagioclase-biotite-magnetite bands in hornblende gneiss. Dikolti (DK 17), # 658. FV = 3 mm.
(G) Skeletal corundum in aggregate of cordierite surrounded by biotite. Selebi (SD 79), # 177b. FV = 6 mm.
(H) Detail of (H). S = sillimanite. FV = 3 mm.

PLATE 20

Calc-silicate Gneiss & Garnetiferous Quartz-feldspar Granulite

(A) Calc-silicate gneiss. Hornblende porphyroblast (Mle ?) with spiral of included quartz. Clinopyroxene (Mlp ?) rims the outer inclusion-free hornblende. East of Botsabelo, # 30/7/1d. FV = 6 mm.
(B) Typical polygonal granoblastic plagioclase(bytownite)-quartz matrix of (A). FV = 6 mm.
(C) Garnetiferous quartz-feldspar granulite. Band of almandines in quartz-albite-minor microcline matrix. Phikwe Unit B (PW 208), # 574. FV = 6 mm.

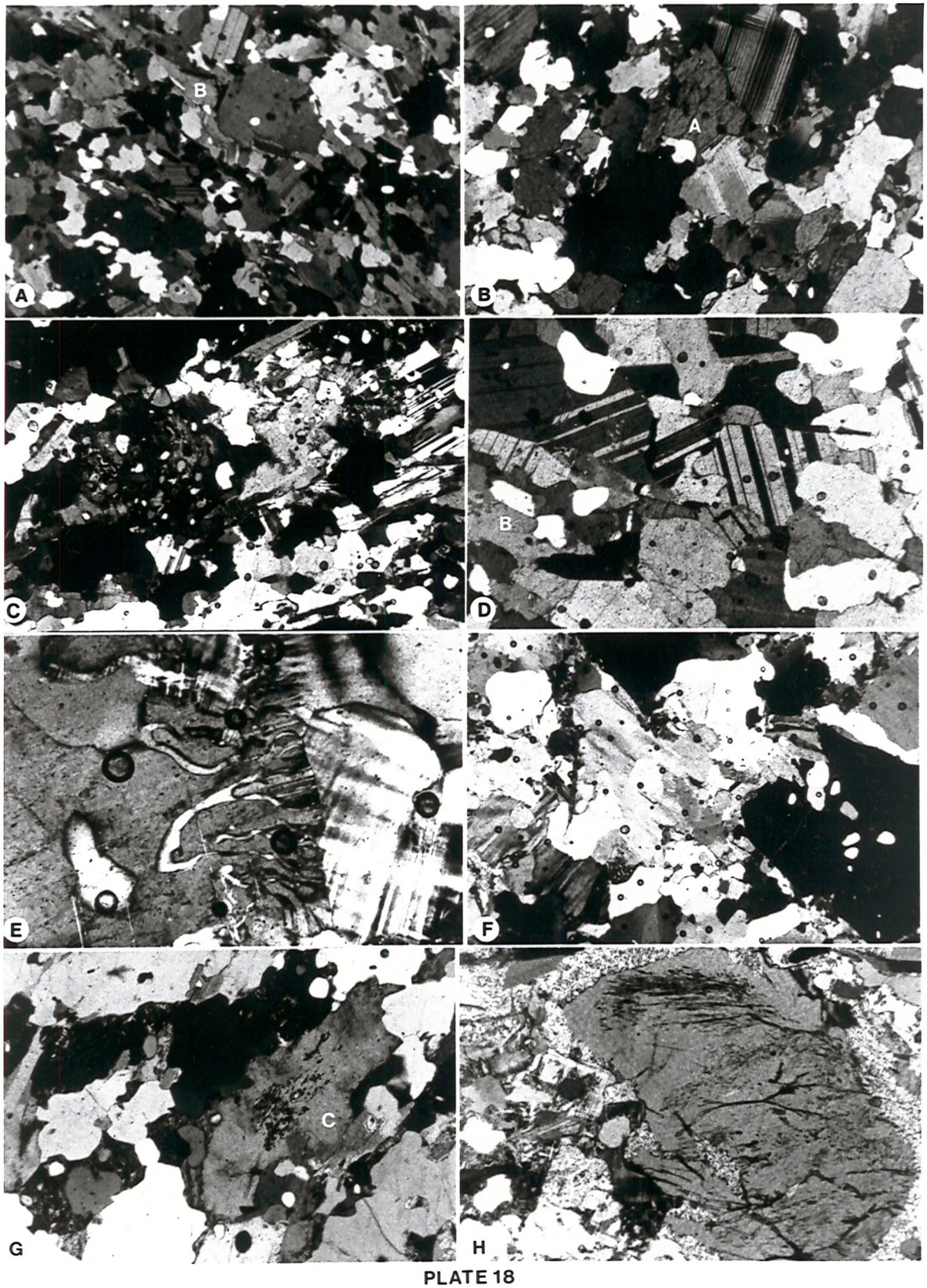

PLATE 18

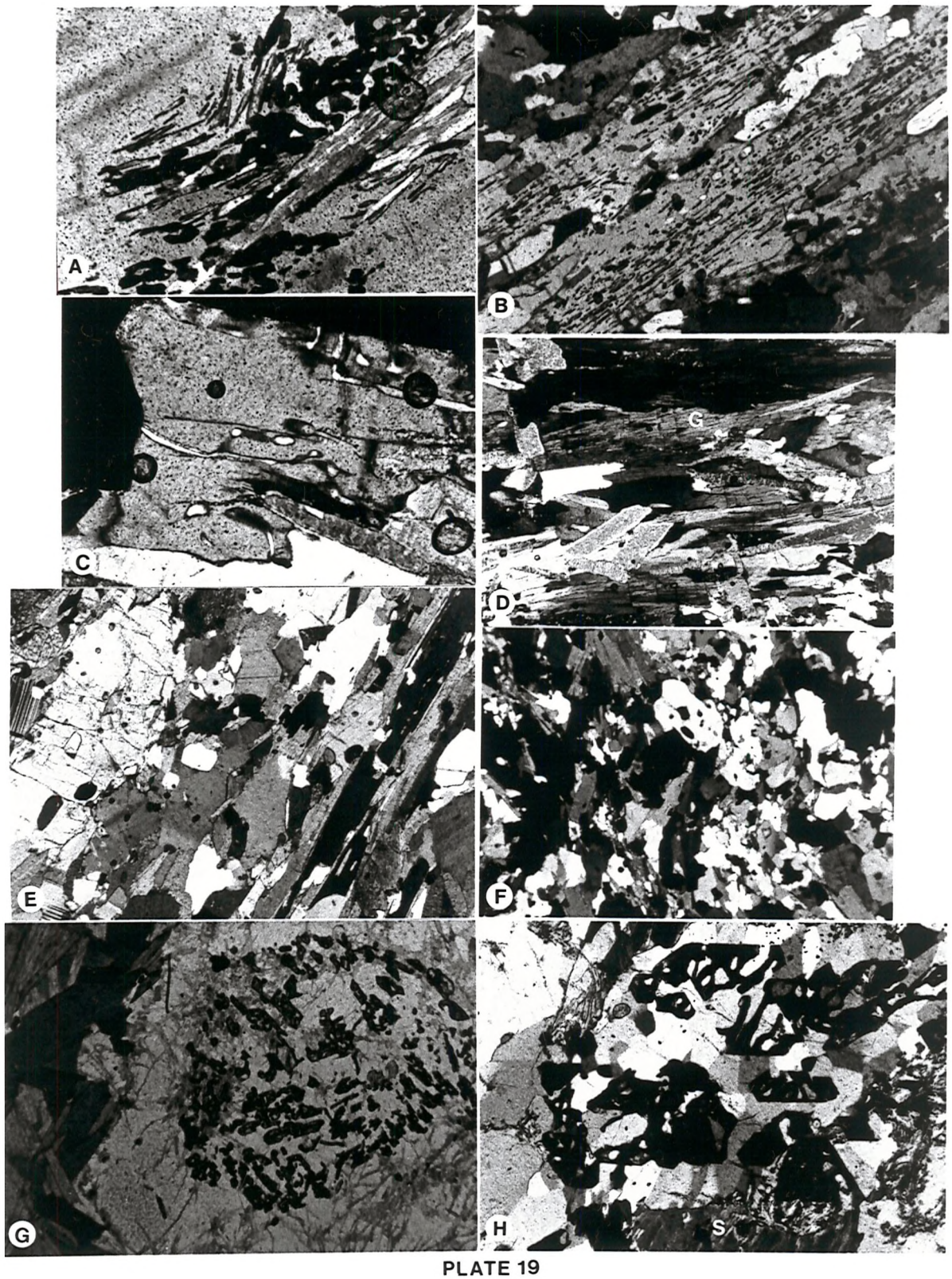

PLATE 19

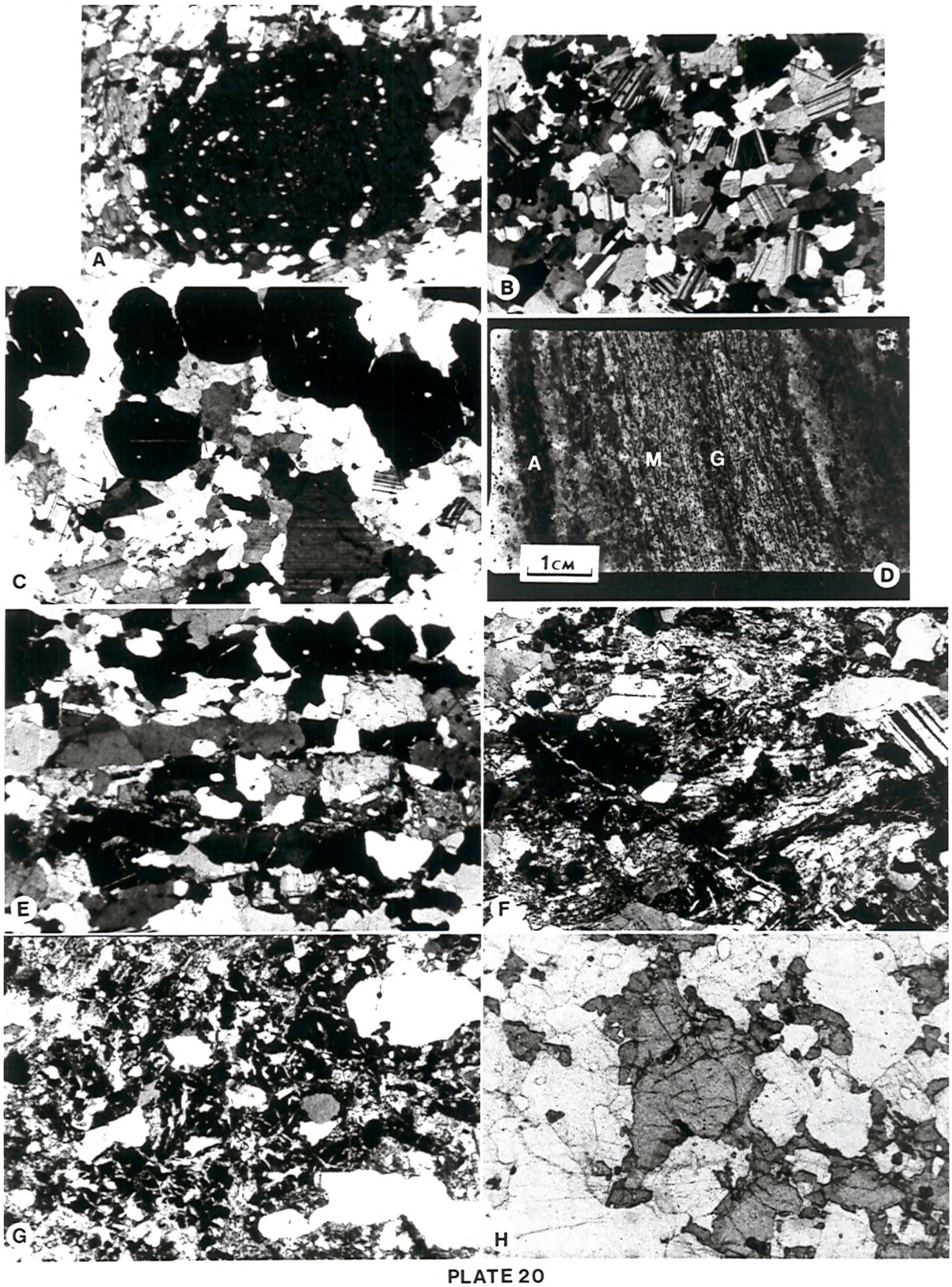

PLATE 20

Plate 20 (continued)

Mylonites in Anorthosite

(D) Recrystallised D1 mylonite band in anorthosite - Type (a). A = anorthosite; M = finely banded mylonitic quartz and plagioclase; G = garnetiferous zone in centre of band. Phikwe (PW 208), # 576.

(E) Type (a).Banded recrystallised (M1m) mylonitic texture of quartz and plagioclase with biotite. Phikwe (PW 211), # 570. FV = 6 mm.

(F) Type (a). D2 shear superimposed on D1 recrystallised mylonite. Development of M2 chlorite, clinozoisite, epidote (?) and anthophyllite (?). Phikwe (PW 208), # 575. FV = 3 mm.

(G) Type (a). D2 shear superimposed on D1 recrystallised mylonite. Broken M1m garnets altered to M2 chlorite. Phikwe (211), # 569, FV = 3 mm.

(H) Type (b). Colour zoned garnets in unbanded quartz-plagioclase matrix. Phikwe (PW 211), # 566. FV = 3 mm.

PLATE 21

Anorthosite

(A) Polygonal granoblastic unzoned plagioclase, 2nd generation. Phikwe (PW 208), # 549. FV = 6 mm.

(B) 1st generation zoned plagioclase in 2nd generation granoblastic plagioclase matrix. Phikwe (PW 211), # 572. FV = 6 mm.

(C) Granoblastic hornblende-plagioclase of metagabbro. Phikwe (PW 208), # 553. FV = 6 mm.

(D) & (E) Altered M1p clinopyroxene (P) surrounded by actinolite-quartz intergrowth. Same as (B). FV = 6 mm.

(F) M1p clinopyroxene porphyroblast including M1e (?) hornblende and plagioclase. Phikwe (PW 211), # 561. FV = 6 mm.

(G) Quartz-anorthosite with 4th generation plagioclase (andesine) and magnetite (M) rimmed by biotite. Phikwe (PW 211), # 559. FV = 6 mm.

(H) Olivine porphyroblast in granular clinopyroxene-olivine matrix. Lethlakane clinopyroxenite, # 992/8. FV = 6 mm.

PLATE 22

Magnetite Quartzite and Associated Amphibolites

(A) Finely banded magnetite quartzite with minor actinolite and trace of pyroxene (?). Note D1 foliation marked by magnetite and actinolite cutting across primary banding. Lentswe (LT 30), # 667. FV = 6 mm.

(B) Finely banded magnetite quartzite with minor actinolite. Note magnetite grain-size variation. Phokoje (PJ 1),# 332. FV = 6mm.

(C) Magnetite quartzite. Note actinolite in the magnetite bands and cross-cutting D1 foliation marked by quartz. # 4-9-1a.FV = 6mm.

(D) Banded actinolite amphibolite (A) and magnetite quartzite. Phokoje (PJ 1), # 331. FV = 6 mm.

(E) Banded hornblende amphibolite (H) and actinolite quartzite in a banded quartz-amphibole rock. Lentswe (LT 25), # 664. FV = 6 mm.

(F) Laminae of cummingtonite (C) in actinolite amphibolite band (A). Same as (E). FV = 6 mm.

(G) Disseminated pyrrhotite in actinolite band. Lentswe (LT 27), # LT 27-30a. FV = 6 mm.

(H) Orthopyroxene-quartz-pyrrhotite-biotite-cummingtonite laminae in hornblende amphibolite. Interbanded with (G). FV = 6 mm.

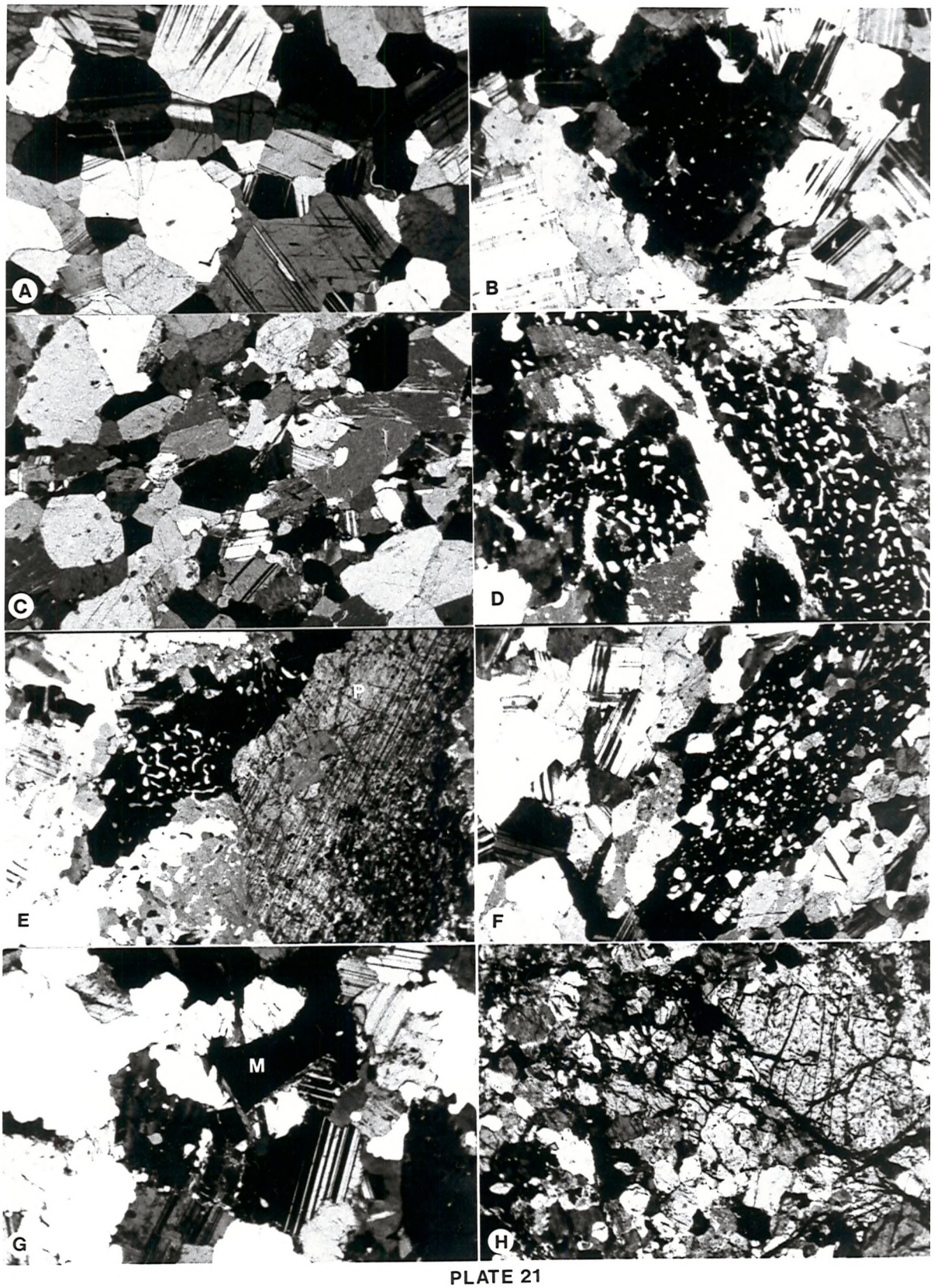

PLATE 21

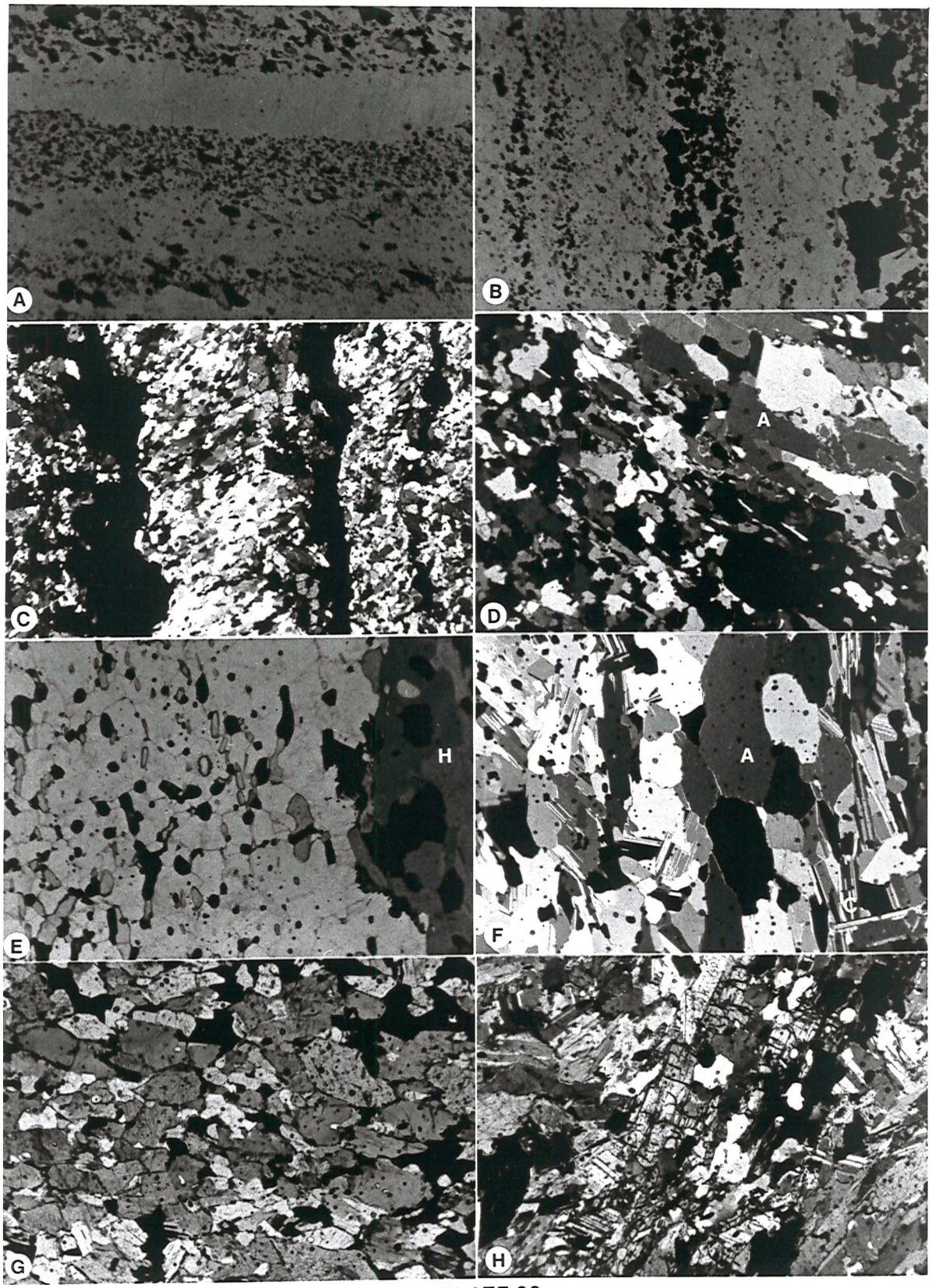

PLATE 22

PLATE 23

Quartzites and Diopside-bearing Gneisses

(A) Fibrolite knots in plagioclase-biotite quartzite. Phikwe Unit A (PW 213), # 539. FV = 3 mm.

(B) Plagioclase-hornblende quartzite with relicts of clinopyroxene (M1p ?) altering to hornblende. Plagioclase is altered. Phikwe Dome - Unit H, # 31-7-1b. FV = 3 mm.

(C) Sillimanite(S)-pyrrhotite quartzite. Phikwe Unit B (PW 210), # 530. FV = 6 mm.

(D) Well-banded diopside gneiss (Type b). Diopside(D)-plagioclase and hornblende(A)-plagioclase bands. Phikwe Unit G (CAM 38/1), # 640. FV = 6 mm.

(E) Well-banded diopside gneiss (Type c). Hornblende(A)-plagioclase base of band and diopside(D)-plagioclase-garnet(G) top. Phikwe Unit H (CAM 38/1), # 638. FV = 3 mm.

(F) Sefhope diopside(D)-hornblende(A)-plagioclase gneiss. # 2-8-6a. FV = 6 mm.

(G) & (H) Diopside(salite ?)-actinolite quartzite in (G) and diopside(D, salite?)-actinolite amphibolite with quartz, epidote and carbonate in (H). Phikwe Dome - Unit H, # 31-7-5b. FV = 3mm.

PLATE 24

Ultramafic Rocks

(A) Serpentinised dunite. Olivine altering to serpentine. Minor pyroxene. Phikwe Unit D (PW 213), # 213-2. FV = 6 mm.

(B) Peridotite. Pyroxene porphyroblast including olivine in olivine-rich groundmass. Phikwe Unit D (PW 213), # 213-2, FV = 6 mm.

(C) Peridotite. Olivine(O) with included green spinel and hornblende wrapping around pyroxene porphyroblast(P). Selebi (SD 97),# 157. FV = 6 mm.

(D) Actinolite amphibolite. Phikwe Unit D (PW 217),# 217-1.FV = 6mm.

(E) Actinolite amphibolite with pyroxene(P). Olivine is included in the pyroxene. Phikwe Unit D (PW 217), # 217-2. FV = 6 mm.

(F) Retrogressed hornblende orthopyroxenite. Development of M2 cummingtonite and phlogopite. Phikwe Unit D (PW 213),# 14. FV = 6mm.

(G) M2 cummingtonite-orthoamphibole-phlogopite amphibolite with relict M1 hornblende.Phikwe Unit D (PW 213), # 213-1. FV = 6 mm.

(H) Orthoamphibole-serpentine-biotite-pyrrhotite-quartz schist. Phikwe Unit A (PW 210), # 527. FV = 6 mm.

PLATE 25

Granitic Gneiss

(A) Granitic gneiss. Vermicular quartz in plagioclase penetrating into microcline. East of Botsabelo, # 30-7-1k. FV = 3 mm.

(B) Vermicular quartz in plagioclase penetrating into microcline. North-east of Phikwe, # 31-7-1c. FV = 1.5 mm.

(C) Dioritic gneiss. Plagioclase (andesine), quartz, hornblende and biotite.Phikwe (PW 208), # 700. FV = 3 mm.

Mylonite

(D) - (E) Mylonite. Quartz ribbons and perthitic microcline porphyroblast in quartz-plagioclase-microcline-myrmekite groundmass (mylonitised granite gneiss ?). East of Botsabelo, # 30-7-6c. FV = 6 mm.

(F) M2a mylonite. Relict garnet(G) and ellipsoidal plagioclase porphyroblasts in biotite-felsics matrix. Phikwe ore body - Zone C, # 188. FV = 6 mm.

(G) & (H) Superimposed shearing. Broken garnets (D1-M1m) in early D2-M2a quartz-plagioclase mylonite. Cross-cutting late D2-M2b mylonite consisting of chlorite, felsics, epidote and carbonate in lower half of (G). Phikwe ore body (PW 202),# 515. FV = 6 mm.

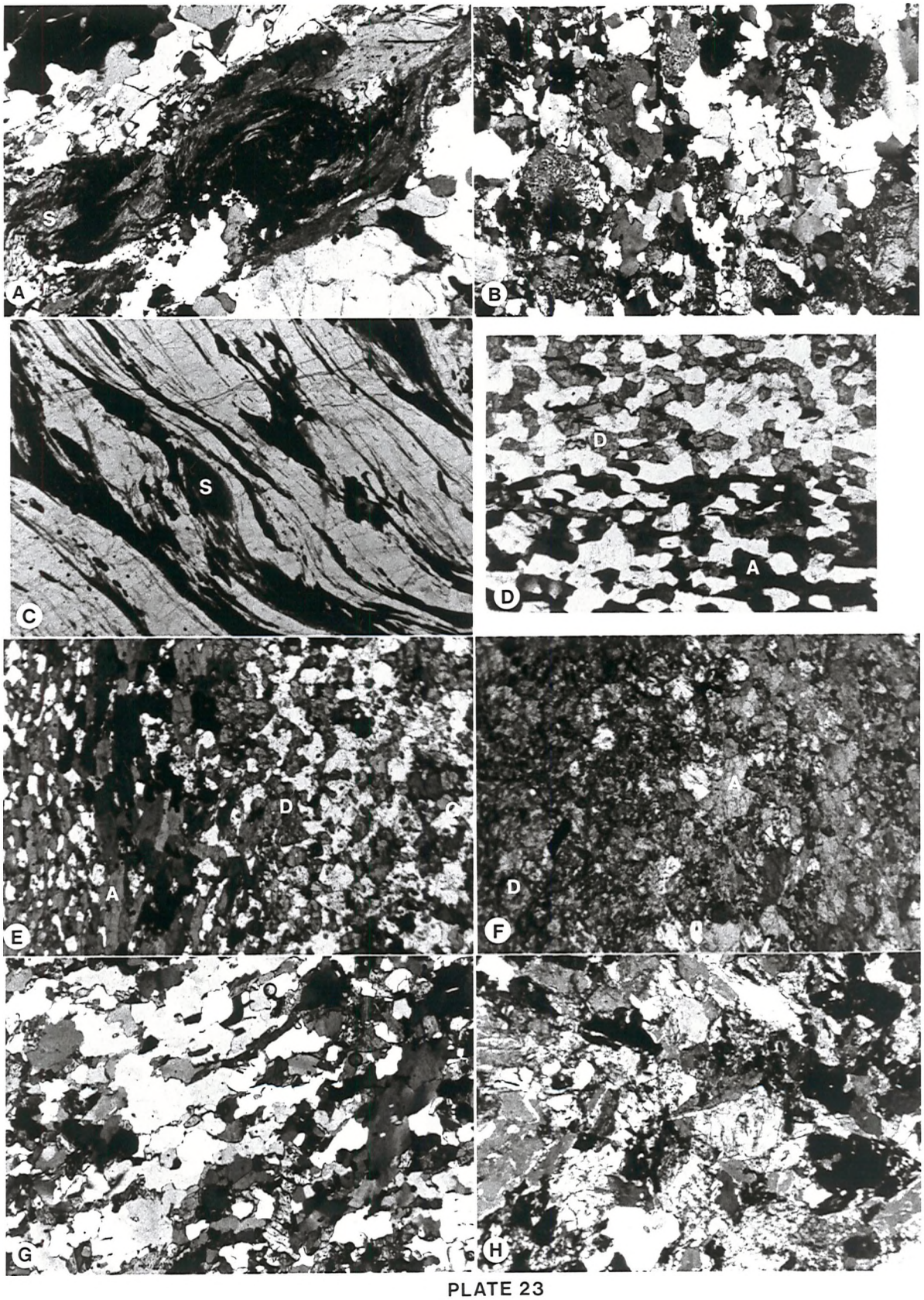

PLATE 23

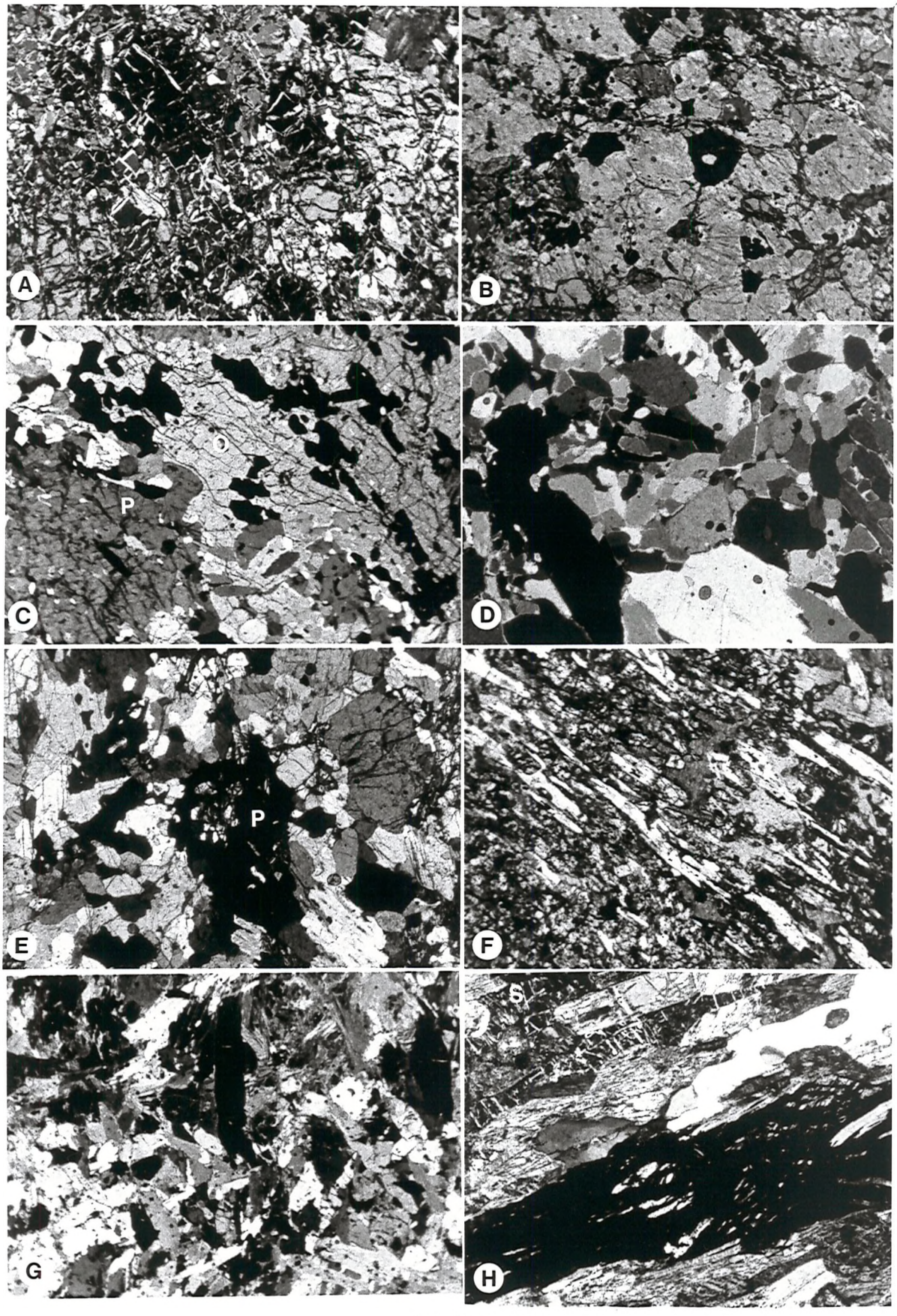

PLATE 24

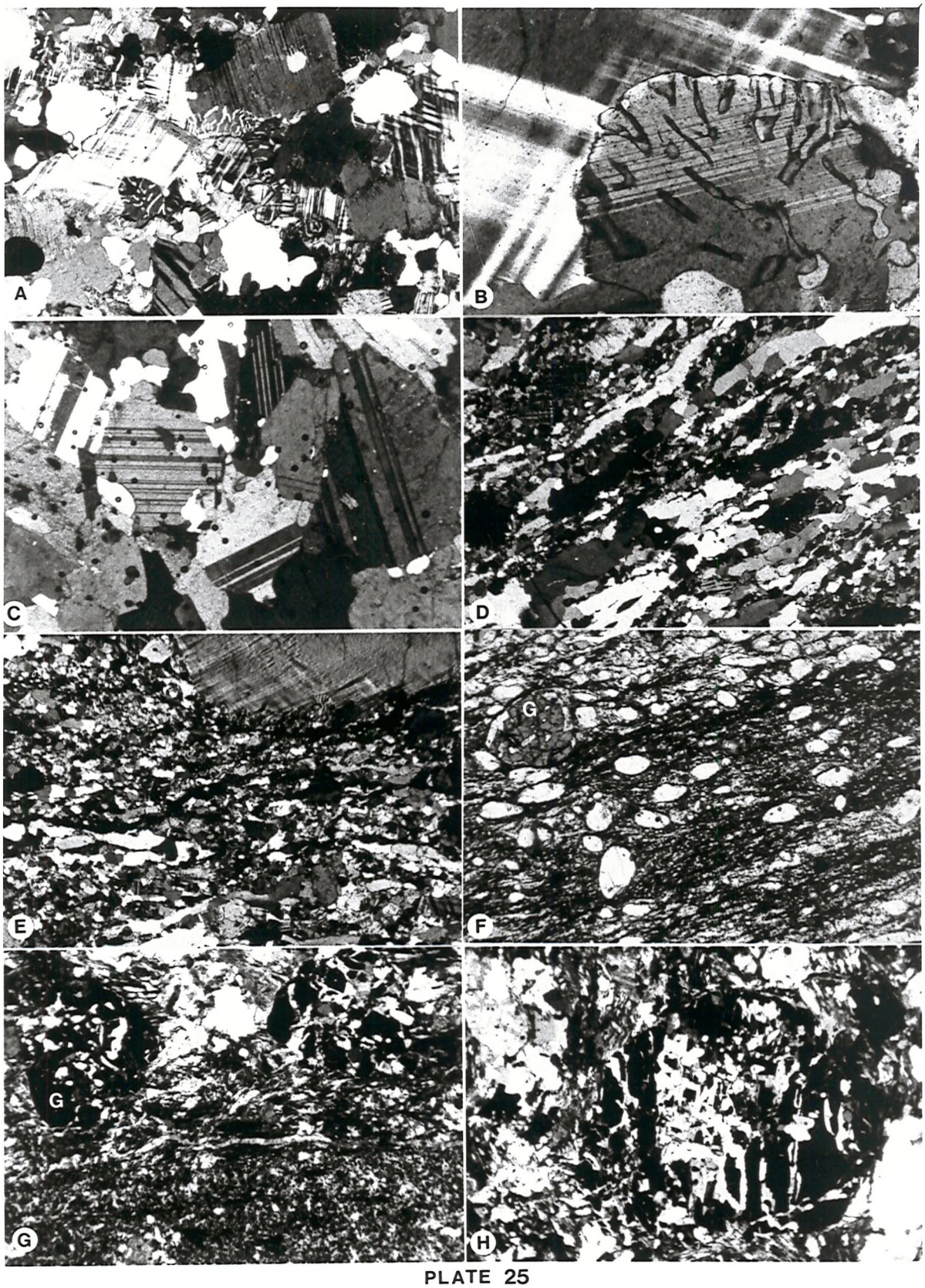

PLATE 25

CHAPTER 4 GEOCHEMISTRY AND ORIGIN OF THE SELEBI-PHIKWE GNEISSES

4.1 GEOCHEMISTRY OF THE SELEBI-PHIKWE GNEISSES

4.1.1 Intoduction

Geochemistry is used in this thesis as a major tool in the unravelling of the original nature of the gneisses, because of the high metamorphic grade of the Selebi-Phikwe gneisses and the absence of original textures. Analytical techniques are described in the Appendix where all analyses are listed. Core samples were fresh. Field samples were also relatively fresh, due to the arid climate (e.g. typically unaltered metamorphic feldspar and ferromagnesium minerals). Recent weathering is therefore considered to have played a negligible role in the chemical alteration of the sampled rocks.

4.1.2 Hornblende Gneiss and Intermediate Biotite Gneiss

4.1.2a Major subdivision by Ca content

These gneisses were initially split during field work by their essential mineralogy. The initial subdivisions were confirmed by thin section work (Ch. 3.1 & 3.3). Geochemistry has also confirmed the original subdivisions. The assignment of samples to geochemical groups has not resulted in significant changes to the original subdivisions. The mineralogical-geochemical groups are intergradational.

The major geochemical subdivision, that can be made of the mafic hornblende gneiss and the intermediate biotite gneiss, is into high-Ca and low-Ca gneiss (Figs 4.1-4.3). The average and range of chemical compositions of the mafic and intermediate gneisses are shown in Tables 4.1 (high-Ca) and 4.2 (low-Ca). The high-Ca gneiss has CaO contents of 5-12 wt% (typically >8 wt%). The low-Ca hornblende and intermediate gneisses have CaO contents below 3 wt%. The high-Ca gneiss includes the HGN, HGG, HGC, and HGF hornblende gneisses and the quartz-poor type of intermediate biotite gneiss (QPIB, see Ch.3.3). QPIB has relatively low CaO contents (5-9 wt%). The low-CaO gneiss includes the coarse garnet-rich mafic gneiss (GRHG), the quartz-rich type of intermediate biotite gneiss (QRIB) and the (non-calcic) amphibole-rich type of intermediate biotite gneiss (ARIB).

Major and trace element contents of the hornblende and intermediate biotite gneisses (and ultramafic rocks in the sequence)

have been plotted against a fractionation index-FeO/(FeO+MgO) (total Fe as FeO, Figs 4.2, 4.4, 4.5 & 4.6a). Lines have been drawn joining samples from the structural top and bottom of two mineralogically graded layers of hornblende gneiss (see Chs 2.3.1 & 3.1).

4.1.2b High-Ca hornblende and intermediate biotite gneisses

The high-Ca gneisses show a marked fractionation trend towards increasing Fe content (Fig. 4.1a). The low-Ca mafic and intermediate gneisses and the high-Ca intermediate gneiss have higher K contents than typical high-Ca hornblende gneiss (Tables 4.1 & 4.2, Fig. 4.3), which accounts for the spread towards the alkali apex of the AFM diagram. The geochemical characteristics of the various high-Ca hornblende gneisses are as follows:

HGN, the main type of hornblende gneiss (hornblende-plagioclase with minor magnetite and clinopyroxene), has a wide variation in fractionation index, which reflects the wide range in mineralogy from plagioclase-rich to hornblende-rich. HGN can be split chemically (Table 4.1) and mineralogically into HGN1 (hornblende-plagioclase) and HGN2 (hornblende-rich). HGN1 is Al-rich (13-17 wt% Al_2O_3) and shows a wide variation in fractionation index. Al, (Ca), Mg, Ni and Cr decrease with increasing fractionation index. Fe, Ti, P, (Cu), Y and Zr increase with increasing fractionation index (Figs 4.2, 4.4, 4.5 & 4.6a). HGN2 is Al-poor (5-10 wt% Al_2O_3) with high MgO contents (12-18wt%). HGN2 has significantly higher Cr, Ni and Ca/Al and K/Rb than HGN1. (Element contents and relative differences which are regarded as particularly significant are indicated thus Mg; elements which show small differences are shown as (Mg).)

HGG, the garnetiferous hornblende-plagioclase-minor magnetite gneiss, is the dominant hornblende gneiss in Unit G. HGG (Tables 4.1 and 4.5-C) has higher contents of Ti, Al, Fe, (Mn), Na, P, (Cu), (Nb), (S), (Sr), (V), Y and Zr, and lower contents of Si, Mg, Ca, K, Cr and Rb than average HGN1. Compared to HGC, HGG has higher contents of Al, Fe, Mg and Na and lower contents of Si, Ti, K, Cu, Nb, (Rb), S, V, Y and (Zr). In terms of Ti and Mg, HGG is intermediate between HGN1 and HGC (Fig. 4.7). However it has significantly higher contents of Fe and lower contents of Si than both groups. One sample (HGGX, Table 4.5-D) has higher contents of Si, Fe, Mn, P, Nb, S, Rb, Y and Zr, similar Ti, and lower Al, Mg, Ca, Na, Cr, Ni, Sr and V than typical HGG. The HGG samples lie on a line of Rb-enrichment relative to K (K/Rb = 52, Fig. 4.3b).

	HGN1		HGN2		HGG		HGC	
SiO2	51.32	50.0-53.0	52.28	49.7-53.8	47.26	46.9-47.6	50.64	47.1-53.5
TiO2	0.73	0.19-1.54	0.70	0.40-1.26	1.60	1.5-1.8	2.02	1.7-2.4
Al2O3	14.89	13.6-16.9	7.27	5.1-10.0	15.47	15.1-16.1	13.91	13.1-16.7
Fe2O3	11.07	8.9-14.4	10.63	9.8-11.3	15.10	14.2-15.6	14.64	13.8-16.2
MnO	0.18	0.14-0.21	0.23	0.17-0.36	0.22	0.16-0.29	0.19	0.15-0.21
MgO	8.24	6.6-10.1	15.59	12.5-18.4	6.98	6.5-7.6	5.34	4.7-6.4
CaO	10.07	7.5-12.2	11.50	10.3-12.4	9.87	9.0-10.5	9.93	9.6-10.6
Na2O	2.44	1.4-4.0	1.06	0.65-1.77	2.91	2.8-3.1	2.37	1.6-2.9
K2O	0.91	0.51-2.26	0.43	0.15-0.80	0.33	0.31-0.35	0.67	0.43-1.31
P2O5	0.10	0.03-0.23	0.12	0.06-0.25	0.23	0.22-0.24	0.27	0.06-0.46
Cr2O3	0.05	0.02-0.08	0.19	0.08-0.39	0.03	0.02-0.03	0.02	0.00-0.07
	100.00		100.00		100.00		100.00	
Cr	339	122-552	1260	560-2600	168	160-173	156	19-484
Cu	30	nd-68	104	nd-348	46	12-89	187	11-431
Nb	4.9	3-7	5	3-7	6.7	6-7	8.5	3-16
Ni	124	103-162	300	158-430	114	111-117	93	57-121
Rb	36	12-114	8	4-15	11	6-15	22	7-14
S	247	nd-1196	204	65-344	338	nd-959	912	427-1269
Sr	108	83-145	31	13-60	137	75-187	145	100-197
V	185	115-264	169	113-258	248	220-266	399	239-671
Y	20	7-27	17	13-21	28	23-33	37	31-49
Zr	57(79)	15-110 (259)	38	28-56	104	97-114	129	66-187
N-Samples	9		4		3		6	

	HGF1		HGF2		QPIB	
SiO2	49.14	46.9-51.9	44.37	43.3-45.8	57.12	54.9-60.7
TiO2	2.57	2.0-3.3	3.72	3.3-4.4	1.29	0.36-2.55
Al2O3	12.92	12.5-13.8	11.02	9.5-12.4	15.19	12.0-17.3
Fe2O3	16.77	15.7-19.0	21.57	19.1-22.8	11.01	9.6-12.8
MnO	0.27	0.21-0.55	0.22	0.21-0.24	0.17	0.14-0.24
MgO	5.26	3.9-6.0	6.40	5.4-7.4	4.66	3.6-6.1
CaO	9.56	8.4-10.3	10.38	9.8-10.7	6.91	5.1-9.1
Na2O	2.18	1.3-3.0	1.48	1.3-1.8	2.14	1.2-3.4
K2O	0.88	0.70-1.24	0.75	0.67-0.84	1.14	0.53-1.89
P2O5	0.43	0.23-0.91	0.08	0.04-0.14	0.36	0.10-1.05
Cr2O3	0.02	0.01-0.02	0.01	0.01-0.02	0.01	0.00-0.02
	100.00		100.00		100.00	
Cr	106	43-154	95	68-131	42	5-108
Cu	94	37-277	223	70-353	114	5-350
Nb	10	7-17	6.3	2-13	8.5	4-14
Ni	63	56-67	66	39-87	203	13-890
Rb	20	7-78	11	6-16	70	19-129
S	1560	360-2720	4850	1360-9440	3130	nd-7260
Sr	110	80-172	63	41-78	106	47-166
V	349	286-415	1232	1178-1323	202	77-359
Y	42	36-58	21	12-38	51	26-104
Zr	151	79-273	37	21-62	128	29-266
N-Samples	8		3		6	

Table 4.1 Average chemical composition (wt% and ppm) of High-Ca hornblende gneiss and intermediate biotite gneiss. Analyses recalculated to 100% on an anhydrous and sulphide-free basis. Average and range are quoted.

HGC, the clinopyroxene-bearing hornblende-plagioclase-minor magnetite gneiss, has a narrower range of composition than HGN. HGC typically has higher contents of Ti, Fe, P, Cu, Nb, (Sr), V, Y and Zr and lower contents of (Si), (Al), Mg, (Cr) and (Ni) than average HGN1.

HGF, the magnetite-rich hornblende-plagioclase gneiss, can be geochemically subdivided into HGF1 and HGF2. The main mineralogical difference is the higher proportion and coarser grain size of magnetite in the latter. HGF1 and HGF2 are both characterised by high Fe and Ti contents. HGF1 has lower contents of (Si), (Al), (Mg), (Ca), (Cr) and Ni and higher contents of Ti, Fe, Mn, P, Nb, Y, and Zr and higher K/Rb than both HGN1 and HGC. HGF2 differs from HGF1 by having even higher Fe (21 wt% Fe2O3) and Ti (3.7 wt% TiO2) contents and higher Mg, Ca and V, but lower Si, Al and Na, and significantly lower P, Nb, Y and Zr (Table 4.1).

QPIB, the quartz-poor intermediate biotite gneiss, has higher Si and lower Ca than the other high-Ca mafic gneisses. The contents of Ti, P, Cu, Ni, S, Y and Zr in QPIB are very variable. QPIB typically has higher contents of Si, Ti, Al, Fe, (K), P, Cu, Nb, Ni, Rb, S, Y and Zr, similar contents of Na, and lower contents of Mg, Ca and Cr and lower K/Rb ratios than average HGN1, after allowing for the effect of simple dilution due to increased Si. The Mg contents of QPIB are more like those of HGC and HGF1 than HGN1 (Fig. 4.10b).

D, deformed hornblende gneiss bands that crosscut foliation are regarded as deformed mafic dykes. They are most prominent within the anorthosites. Deformed dykes in the anorthosites (Table 4.6-E) are characterised by high contents of Al, P, Nb, Y and Zr, moderate Ti (1.4 wt% TiO2), and low contents of Mg and Cr.

4.1.2c Low-Ca hornblende and intermediate biotite gneisses

QRIB, the quartz-rich biotite gneiss of the intermediate biotite gneiss group, is characterised by high Si (60 wt% SiO2), low Ca (1 wt% CaO) and relatively high Mg (8 wt% MgO) (Table 4.2). QRIB has higher contents of Si, K, Nb, Rb and (S) and lower contents of Ca, Sr, Na and Mn than all the high-Ca gneisses. Compared to average HGN1, QRIB also has higher contents of (P), (Cu), Y and Zr, similar contents of Ti, Fe, Mg and V, and lower contents of (Al), Cr and (Ni) and lower K/Rb ratios. The degree of enrichment in P, Y and Zr is, however, highly variable (Figs 4.5, 4.6 & 4.11). QRIB has similar Si and Ti contents to the low-Si grey gneiss (Fig. 4.10a). However

	QRIB		ARIB		GRHG	
SiO2	60.03	55.9-64.2	52.70	50.0-54.3	48.07	46.9-51.4
TiO2	0.77	0.37-1.45	1.46	0.67-2.94	1.34	0.53-2.87
Al2O3	14.40	13.0-16.7	10.05	7.9-12.4	18.61	13.2-23.0
Fe2O3	11.37	9.1-16.6	16.16	14.0-17.5	15.31	11.3-19.1
MnO	0.09	0.05-0.13	0.23	0.15-0.31	0.17	0.12-0.21
MgO	8.19	5.6-10.3	14.04	11.8-16.4	10.65	9.9-11.3
CaO	1.18	0.34-3.0	2.23	1.1-3.2	1.25	0.37-2.41
Na2O	0.95	0.29-2.32	1.29	0.41-1.89	0.81	0.33-1.70
K2O	2.78	0.23-4.55	1.70	0.44-3.29	3.59	1.8-6.1
P2O5	0.21	0.05-0.82	0.10	0.05-0.17	0.16	0.03-0.45
Cr2O3	0.03	0.00-0.06	0.04	0.01-0.09	0.04	0.01-0.09
	100.00		100.00		100.00	
Cr	188	32-425	284	63-587	297	90-557
Cu	79	5-167	439	12-1282	196	6-441
Nb	12.6	5-32	9.0	6-14	10.5	8-13
Ni	92	58-235	194	151-239	112	68-148
Rb	155	14-277	162	33-342	154	84-229
S	1640	nd-6780	2210	nd-4420	14250	23-32640
Sr	39	9-92	38	10-66	18	9-30
V	180	61-579	121	74-195	209	126-259
Y	32	9-76	33	32-35	42	13-69
Zr	134	78-331	139	77-220	105	43-178
N-Samples	10		3		4	

Table 4.2. Average chemical compositions (wt% and ppm) of Low-Ca mafic gneiss and intermediate biotite gneiss.

	A		B	C
SiO2	51.47	49.6-53.5	51.10	42.47
TiO2	0.38	0.29-0.60	0.37	0.13
Al2O3	4.21	3.4-5.2	6.41	2.84
Fe2O3	9.80	7.6-14.5	9.92	11.15
MnO	0.14	0.10-0.21	0.22	0.15
MgO	22.11	20.9-23.2	25.83	39.47
CaO	10.50	5.1-12.6	1.93	2.10
Na2O	0.56	0.47-0.61	0.20	0.32
K2O	0.29	0.11-0.66	3.08	0.26
P2O5	0.05	0.04-0.06	0.05	0.05
Cr2O3	0.49	0.36-0.60	0.89	1.06
	100.00		100.00	100.00
Cr	3290	2420-3980	5960	6830
Cu	137	10-477	14	10
Nb	3	nd-4	4	2
Ni	618	476-915	998	1550
Rb	9	4-21	125	13
Sr	13	11-16	7	10
S	2380	nd-7140	nd	90
V	127	97-152	62	54
Y	9	5-14	6	3
Zr	31	23-43	73	21
N-Samples	4		1	1

Table 4.3. Average chemical compositions (wt% and ppm) of ultramafic rocks in Unit D. Analyses recalculated to 100% on an anhydrous and sulphide-free basis.

QRIB has much higher contents of Mg (Fig. 4.10b) and Cr, and lower contents of Ca and Na (Fig. 4.9b) than low-Si GG.

ARIB, the (non-calcic) amphibole-rich intermediate biotite gneiss, is characterised by low Ca (2 wt% CaO) and high Mg (14 wt% MgO) and Fe (16 wt% Fe2O3). The Mg contents are similar to those of HGN2. Compared to both HGN1 and HGN2, ARIB has higher contents of Ti, Fe, K, Cu, Nb, Rb, S, Y and Zr, similar contents of Si, and lower contents of Ca, Cr and V. The contents of Ti and Zr in ARIB are highly variable (Fig. 4.11b). K/Rb ratios are relatively low (87, Fig.4.3b).

GRHG, the coarse garnet-rich mafic biotite gneiss, is characterised by low Ca (1 wt% CaO) and Si (48 wt% SiO2) and high Al (18 wt% Al2O3), Fe (15 wt% Fe2O3), Mg (10 wt% MgO) and K (3 wt% K2O) and Rb. GRHG has similar Al/Mg ratios to those of HGN1 (Fig. 4.1b). Contents of Ti, P, S, Y, and Zr are relatively high but highly variable (Figs 4.5, 4.6, & 4.11).

The proportions of the main types of hornblende gneiss in the units at Phikwe, along with the main types of intermediate biotite gneiss in each unit, are shown in Table 4.4.

Unit A - poorly sampled, 100% HGF1, abundant intermediate biotite gneiss (particularly QRIB), minor quartzite.
Unit B - 50% HGN1, 50% HGC, abundant intermediate biotite gneiss (QPIB, QRIB, ARIB, CGHG), minor quartzite.
Unit C - not sampled.
Anorthosites - deformed dykes D.
Unit D - 18% HGN1, 9% HGN2, 9% HGC, 27% HGF2, 27% HGF1.
Unit E - poorly sampled, 100% unaltered HGG, mainly grey gneiss.
Unit F - 44% HGN1, 11% HGN2, 22% HGC, 22% HGF1, minor QPIB.
Unit G - 100% HGG, significant diopside gneiss, some QPIB and QRIB.

Table 4.4. The various high-Ca hornblende gneiss types,expressed as the percentage of total high-Ca hornblende gneiss in each unit.

4.1.3 Diopside Gneisses

Diopside-rich gneiss occurs, along with hornblende gneiss (HGG) and minor QPIB and QRIB, in Unit G (see Ch.3.7). The thick

	A massive		B banded-graded		C HGG	D HGGX	E
SiO2	49.00	47.8-50.2	49.28	48.6-49.9	47.26	52.71	53.06
TiO2	0.58	0.47-0.69	1.66	1.5-1.8	1.60	1.60	0.14
Al2O3	9.22	7.9-10.6	16.38	16.4	15.47	10.41	11.07
Fe2O3	13.93	13.5-14.3	11.87	11.3-12.4	15.10	19.82	4.95
MnO	0.56	0.53-0.58	0.27	0.27	0.22	0.63	0.13
MgO	2.54	2.3-2.8	3.03	3.0-3.1	6.98	5.46	11.61
CaO	23.00	20.2-25.8	13.58	13.0-14.2	9.87	7.38	16.49
Na2O	0.71	0.40-1.02	3.34	3.1-3.6	2.91	1.00	0.96
K2O	0.11	0.08-0.14	0.30	0.29-0.31	0.33	0.45	1.53
P2O5	0.35	0.34-0.36	0.25	0.23-0.27	0.23	0.54	0.03
Cr2O3	0.00	0.00	0.04	0.03-0.04	0.03	0.00	0.03
	100.00		100.00		100.00	100.00	100.00
Cr	8	5-11	221	172-270	168	11	213
Cu	38	19-57	66	43-89	46	48	15
Nb	13	12-14	8	8	6.7	13	5
Ni	10	10	108	98-118	114	19	54
Rb	8	7-9	9	8-9	11	30	54
S	1320	518-2120	3295	2840-3750	338	6830	2390
Sr	56	52-59	124	111-137	137	27	146
V	11	11	248	239-256	248	20	68
Y	64	51-76	38	35-41	28	75	13
Zr	241	194-287	116	109-122	104	272	168
N-Samples	2		2		3	1	1

Sefhope	F massive		G graded	H mafic
SiO2	45.68	45.3-46.5	48.59	50.61
TiO2	1.45	0.85-2.63	1.09	0.97
Al2O3	14.34	13.7-15.0	15.82	15.42
Fe2O3	10.82	9.1-13.4	11.60	11.23
MnO	0.29	0.27-0.30	0.20	0.17
MgO	5.44	4.5-5.9	6.17	6.97
CaO	20.77	18.8-22.8	13.72	11.79
Na2O	0.55	0.33-0.89	2.32	2.37
K2O	0.41	0.07-0.90	0.33	0.33
P2O5	0.23	0.17-0.28	0.11	0.10
Cr2O3	0.02	0.01-0.03	0.05	0.04
	100.00		100.00	100.00
Cr	153	46-207	323	269
Cu	24	13-37	25	42
Nb	7.3	4-11	6	6
Ni	116	45-158	135	132
Rb	18	2-38	8	9
Sr	177	112-262	146	149
S	2400	2400		161
V	255	166-407	279	244
Y	29	21-45	26	27
Zr	97	67-151	73	76
N-Samples	3		1	1

Table 4.5. Average chemical compositions (wt% and ppm) of the diopside-rich rocks of Units G and H, and Sefhope. Analyses recalculated to 100% on an anhydrous ans sulphide-free basis.

massive diopside-plagioclase bands are characterised by high contents of Ca, (Fe), Mn, P, Nb, Y and Zr, and low contents of Mg, Na, K, Cr, Ni and V and relatively low K/Rb (114) (Table 4.5-A). The thin, locally graded, bands (diopside-garnet-plagioclase to hornblende-plagioclase) are characterised by high contents of Ca, (Al) and Na, and low contents of Mg (Table 4.5-B). The thinly banded and graded diopside gneiss (B) was initially thought to be a mixture of the massive diopside-rich gneiss (A) and hornblende gneiss (HGG, Table 4.5-C). In terms of Ca, Mg, Mn, (K), (P), Nb, Ni, Sr, Y and (Zr), this could be possible. However (B) has lower contents of Fe and higher contents of Si, Ti, Al, Na, Cr and Cu, than both (A) and (C).

A similar suite of diopside and hornblende-bearing gneiss was found to the east of Sefhope (Figs 1.1 & 1.2) during a reconnaissance traverse. The suite includes massive diopside-plagioclase gneiss (Table 4.5-F), banded and graded diopside-plagioclase-hornblende gneiss (G) and mafic hornblende-rich gneiss (H).

The diopside amphibolite of Unit H (Table 4.5-E) is characterised by high Ca, Mg and (Cr), and low Fe, Ti and Cu.

4.1.4 Ultramafic Rocks

Thin lenses of unmineralised ultramafic rock occur as a minor constituent throughout the Selebi-Phikwe gneisses but are most prominent in Unit D. The analysed ultramafic rocks in Unit D are of three types (Table 4.3): (A) olivine and pyroxene-bearing actinolite amphibolite with 22 wt% MgO, 4 wt% Al2O3 and variably high CaO (average 11 wt%); (B) retrogressesed (M2) amphibolite (both ortho- and clinoamphibole) with 26 wt% MgO, 6 wt% Al2O3, and 2 wt% CaO; and (C) serpentinised peridotite with 39 wt% MgO, 3 wt% Al2O3, and 2 wt% CaO (Fig. 4.1b). There is an inverse relationship in types (A) and (B) between K content and Ca/Al ratio (Fig. 4.3). The Cr and Ni contents are high but variable (Fig. 4.4) and increase along with Mg from (A) to (C). Ti contents are low and decrease from (A) to (C) (Fig. 4.5). Ultramfic type (A) has chemical similarities to HGN2 (Table 4.1) and the clinopyroxenite bands in the Lethlakane layered body (Table 4.6-D).

4.1.5 Grey Gneisses

A suite of representative grey gneiss was sampled from drill core at Selebi-Phikwe. Relatively homogeneous bands without leucocratic metamorphic segregations were sampled. The analysed grey

gneiss has been subdivided into typical grey gneiss, siliceous cordierite-rich grey gneiss (SCGG) and magnetite-rich grey gneiss (FRGG, see Ch. 3.2).

The suite of typical grey gneiss (quartz-plagioclase-biotite-hornblende gneiss) is characterised by a wide range of SiO2 contents (58-72 wt%) and high Al (14.0-17.5 wt% Al2O3, Table 4.6). Grey gneiss is Na and Ca-rich (3.0-4.7 wt% Na2O, 6.9-2.6 wt% CaO) and K-poor (0.9-2.7 wt% K2O) (Fig. 4.9b). The typical grey gneiss has been subdivided mineralogically and geochemically into low-Si GG (58-64 wt% SiO2), medium-Si GG (66-68 wt% SiO2) and high-Si GG (70-72 wt% SiO2). Low-Si GG can be further subdivided into high-Ca (6-7 wt% CaO) and low-Ca (4-5 wt% CaO). Low-Si grey gneiss is volumetrically the most important type, followed by high-Si GG.

As the Si content increases from low-Si to high-Si grey gneiss, all major elements, except Na and K, decrease in content (Fig. 4.10). The increase in Na and K, along with only a small increase in the Fe/Mg ratio defines a good trend on an AFM diagram (Fig. 4.9a). The decrease in Al content with increasing Si content is less than would result by simple dilution due to increasing Si and high-Si grey gneiss plots near the Al apex of an ACM diagram (Fig. 4.1b). The decrease in Fe, Mg and Ca is more than would result by dilution due to increasing Si. The suite of typical grey gneiss shows marked increase in Zr and Y with increasing Ti content (Fig. 4.11). Two separate trends of increasing Zr and Y can be discerned for (a) low-Si GG; and (b) medium and high-Si GG. The field of Ti v. Y for the low-Si GG is a more diffuse trend than the good trends of Ti v. Y for medium to high-Si GG and Ti v. Zr for both groups. Grey gneiss, particularly high-Si GG, has a high Ni content, when compared to tonalites or felsic volcanics. The high Ni in high-Si GG is partly due to one sample, 0.3 m. above the Phikwe host amphibolite, with a Ni content of 90 ppm. This grey gneiss is porphyroclastic and has been sheared. Ni was possibly mobilised from the host amphibolite. After allowing for this anomolous sample, the Ni content of high-Si GG (not adjacent to the Selebi-Phikwe ore bodies) is still relatively high (26 ppm, cf. Condie 1981; Bhatia & Crook 1986).

The blue siliceous cordierite-rich grey gneiss (SCGG, Table 4.6) is characterised by high contents of Si, Mg (Figs 4.8, 4.9a & 4.10b) and K, low contents of Ti, Ca, Na, Cr, Ni and V (Figs 4.1b & 4.9b), and variable Y (Fig. 4.11). In terms of Mg, Ca and Na, SCGG has more in common with QRIB than high-Si GG. However the Ti/Y and

	Low-Si GG		Med.-Si GG		High-Si GG	
SiO2	61.30	58.0-64.2	66.97	66.2-67.8	71.11	70.3-71.7
TiO2	0.81	0.60-1.14	0.60	0.42-0.79	0.36	0.22-0.44
Al2O3	16.32	15.0-17.5	15.52	15.2-15.9	14.19	14.0-14.7
Fe2O3	7.42	6.3-8.7	5.15	4.5-5.8	4.00	3.4-4.8
MnO	0.08	0.04-0.13	0.05	0.05-0.06	0.05	0.02-0.12
MgO	3.22	1.8-4.4	1.46	1.35-1.58	1.29	0.85-2.38
CaO	5.37	4.1-6.9	4.52	4.5-4.5	3.00	2.6-3.4
Na2O	3.72	3.0-4.4	3.85	3.8-3.9	4.04	3.7-4.7
K2O	1.54	0.87-2.12	1.74	1.5-2.0	1.88	1.1-2.7
P2O5	0.21	0.14-0.32	0.14	0.12-0.17	0.08	0.05-0.10
Cr2O3	0.01	0.00-0.01	0.00	0.00-0.00	0.00	0.00-0.00
	100.00		100.00		100.00	
Cr	41	7-83	18	8-29	9	nd-31
Cu	34	5-162	13	11-15	17	9-21
Nb	11.5	8-14	14.5	13-16	10.6	8-13
Ni	50	11-78	20	12-28	39	14-90
Rb	71	43-107	76	73-79	74	46-114
Sr	172	125-202	163	147-179	146	125-160
V	87	56-124	40	35-44	30	26-34
Y	32	18-41	51	37-64	25	12-41
Zr	206	112-339	382	220-544	186	93-242
N-Samples	10		2		5	

	SCGG cordierite-rich		FRGG Fe-rich GG	
SiO2	73.92	73.8-74.0	58.75	57.2-60.3
TiO2	0.25	0.22-0.28	0.60	0.45-0.75
Al2O3	14.31	13.6-15.0	14.24	12.2-16.3
Fe2O3	2.24	1.9-2.6	15.78	12.4-19.2
MnO	0.04	0.04-0.04	0.10	0.06-0.14
MgO	5.21	5.2-5.3	3.00	2.6-3.4
CaO	0.22	0.05-0.40	2.80	1.8-3.8
Na2O	0.71	0.63-0.80	2.76	2.7-2.8
K2O	3.08	2.3-3.8	1.87	0.97-2.78
P2O5	0.02	0.02-0.03	0.09	0.04-0.14
Cr2O3	0.00	0.00-0.00	0.01	0.00-0.01
	100.00		100.00	
Cr	6	5-6	52	28-76
Cu	10	7-12	37	6-68
Nb	10.5	8-13	5.5	5-6
Ni	12	11-13	64	39-89
Rb	112	84-140	139	29-248
Sr	47	29-642	155	71-239
V	12	9-14	76	64-87
Y	42	14-70	15	8-22
Zr	146	137-154	113	82-143
N-Samples	2		2	

Table 4.6. Average chemical compositions (wt% and ppm) of grey gneiss. Analyses recalculated to 100% on an anhydrous and sulphide-free basis.

Ti/Zr ratios are more like those of high-Si GG.

The magnetite-rich grey gneiss (FRGG,Table 4.6) is characterised by high contents of Fe and (Na) and low contents of Si and Ca (Figs 4.1 & 4.9). It has similarities with several lithologies and can also be described as a high-FeNa, low-Mg type of QRIB, or as an Fe-rich, Si-poor leucogneiss or plagioclase quartzite.

4.1.6 Plagioclase-rich Gneisses

The plagioclase-rich gneisses include the anorthositic-metagabbroic suite, the hornblende-bearing calc-silicate gneiss and the garnetiferous quartz-feldspar granulite.

4.1.6a Anorthositic-metagabbroic suite

There is little compositional difference between the anorthositic-metagabbroic rocks at Selebi-Phikwe and the Lethlakane layered body, except that there is a higher proportion of mafic rocks at Lethlakane (Figs 4.12 & 4.13). The two groups are therefore treated together. The anorthositic-metagabbroic suite has been subdivided (Table 4.7) into: (A) anorthosite and hornblende anorthosite, (B) gabbroic anorthosite and meta gabbro; (C) quartz-rich anorthosite, and (D) Lethlakane clinopyroxenite. The anorthositic-metagabbroic suite is charaterised by high Al and Ca and low Ti. The main difference between (A) and (B) is the increase in Mg and Fe at the expense of Al. The suite defines a good trend of increasing Mg/Al at relatively constant Ca/(Mg+Al) on an ACM diagram (Fig. 4.12b) and on a plot of Al v. Mg (Fig. 4.13). The suite also defines a good trend of increasing alkalies at relatively constant Fe/Mg (Fig. 4.12a). The quartz-rich anorthosite is characterised by high Si, relatively high Ti, Al and Fe (Fig. 4.12a) and low Ca (Table 4.7-C). The Lethlakane clinopyroxenites are characterised by high Mg, Fe, Ti and Cr, and relatively low Al.

Some of the high-Ca hornblende gneiss (particularly the coarser, more aluminous ones) resemble metagabbro of the anorthosite-metagabbro suite. The chemistry of the two lithologies slightly overlaps (i.e. aluminous low-Ti HGN1 is similar to metagabbro) but is usually distinctly different (e.g. incompatible elements). The textures and lithological associations of the two rock types are also distinctive.

	A		B		C	
SiO2	51.21	47.6-55.8	49.62	47.6-51.8	71.47	63.4-79.3
TiO2	0.11	0.01-0.35	0.23	0.14-0.36	0.31	0.14-0.41
Al2O3	27.20	24.0-32.2	19.11	11.6-24.3	14.34	11.7-18.0
Fe2O3	3.22	1.0-6.6	6.74	3.8-10.0	3.45	0.95-5.00
MnO	0.04	0.01-0.08	0.12	0.04-0.21	0.03	0.01-0.04
MgO	1.80	0.31-3.58	7.81	5.4-11.5	1.12	0.60-1.53
CaO	12.63	9.8-16.4	13.84	11.6-16.8	6.30	3.8-9.45
Na2O	3.16	1.7-4.1	1.88	1.2-2.8	2.52	1.8-2.9
K2O	0.57	0.04-1.41	0.52	0.06-2.08	0.40	0.30-0.58
P2O5	0.05	0.02-0.12	0.11	0.03-0.71	0.06	0.04-0.09
Cr2O3	0.01	0.00-0.03	0.02	0.01-0.03	0.00	0.00
	100.00		100.00		100.00	
Cr	43	6-177	130	43-238	14	6-25
Cu	10	nd-25	65	nd-298	36	14-62
Nb	4.5	3-9	4.4	nd-10	5.7	5-6
Ni	38	9-79	148	95-218	27	20-32
Rb	26	4-74	14	4-33	15	8-25
S	10	nd-96	50	nd-473	nd	
Sr	257	151-455	188	80-394	172	144-226
V	38	nd-129	131	55-215	13	nd-25
Y	12	nd-32	9	6-24	17	10-28
Zr	27	12-88	21	9-62	139	29-330
N-Samples	10		10		3	

	D		E		F	
SiO2	48.03	46.8-49.7	50.12	46.4-53.2	58.04	47.5-66.9
TiO2	1.67	1.6-1.8	1.40	0.78-1.95	0.51	0.06-1.14
Al2O3	5.35	3.5-7.1	16.64	12.3-19.2	19.27	13.9-26.5
Fe2O3	15.14	14.5-15.5	12.96	10.2-17.8	5.61	4.2-6.5
MnO	0.22	0.20-0.24	0.19	0.15-0.26	0.05	0.03-0.06
MgO	16.68	15.9-17.1	4.78	3.7-6.1	0.81	0.25-1.94
CaO	11.60	11.4-11.8	9.80	8.5-12.2	14.51	10.4-17.1
Na2O	0.93	0.26-1.35	2.32	2.0-2.5	0.68	0.43-1.02
K2O	0.15	0.12-0.22	1.33	0.42-1.93	0.30	0.16-0.45
P2O5	0.04	0.04-0.04	0.45	0.23-0.70	0.22	0.05-0.59
Cr2O3	0.19	0.18-0.20	0.01	0.01-0.02	0.00	0.00-0.01
	100.00		100.00		100.00	
Cr	1267	1206-1346	81	46-145	23	7-48
Cu	193	167-229	139	24-205	127	10-243
Nb	6	5-7	16	13-21	8.3	3-15
Ni	682	679-688	71	41-120	46	21-62
Rb	8	3-16	45	8-83	13	10-15
S	163	nd-252	164	117-211	850	nd-2175
Sr	224	88-354	153	90-216	329	225-432
V	234	215-257	208	58-388	21	nd-50
Y	17	15-20	54	34-88	29	11-58
Zr	38	34-43	288	129-537	501	14-1009
N-Samples	3		3		4	

Table 4.7. Average chemical compositions (wt% and ppm) of the Selebi-Phikwe and Lethlakane anorthosite-metagabbro bodies. A - anorthosite to hornblende anothosite; B - gabbroic anorthosite to metagabbro; C - quartz-rich anorthosite; D - Lethlakane clinopyroxenite; E - deformed dykes in anorthosite; and F - mylonites in anorthosite. Analyses recalculated to 100% on an anhydrous and sulphide-free basis.

4.1.6b Mylonite bands in anorthosite

Geochemical sections across two mylonite bands, from anorthosite to the centre of the mylonite, are shown in Figure 4.14. The average chemical composition of the mylonites is listed in Table 4.7-E. Section (A) is of a D1 mylonite with a recrystallised M1*m* assemblage, within a quartz-rich anorthosite. Section (B) is of a repeatedly sheared zone, in which M1*m* recrystallised mylonite has been partly replaced by a M2 assemblage associated with D2 shearing. Both mylonites are enriched in Fe (relative to Mg and alkalies, Fig. 4.12a) and in Ca (Fig. 4.12b). The middle of the mylonite band in Section (A) is enriched in Ca, Fe, P, Ti, Ce, Nb, Y and Zr, and significantly depleted in Al, Mg, Na, Cl and Cr compared to the quartz-anorthosite. The middle of the mylonite band in Section (B) is enriched in Ca, P, Sr and Rb and significantly depleted in Mg, Na, Ti, Ce, Cl and Zr.

4.1.6c Hornblende-bearing calc-silicate gneiss

The hornblende-bearing calc-silicate gneiss (CSG, Table 4.8) is characterised by high but variable Si (Fig. 4.10a), Al, Ca and Sr contents, and low Ti (Figs 4.10a & 4.11), Fe, Mg and K (Fig. 4.9b). The Ca/Al ratio is constant (Fig. 4.12b), but the Ca/Na ratio is highly variable (Fig. 4.9b). Zr and Y contents are also highly variable, but are generally inversely proportional to Si content.

The quartz-rich anorthosites are chemically similar to the hornblende-bearing calc-silicate gneiss. The former are slightly higher in Ti, Fe and Mg, and lower in Ca.

4.1.6d Garnetiferous quartz-feldspar granulite

The two analysed garnetiferous quartz-feldspar granulites (GQFG, Table 4.8) occur as: (a) bands within hornblende gneiss in Unit B; and (b) interbanded with hornblende-bearing calc-silicate gneiss. They are both characterised by high Si (Fig. 4.10a), Al, Mn, Na (Fig. 4.9a), Nb and Y, and low Ti (Figs 4.10a & 4.11), Ca, Fe and Mg. The Nb and Y contents are particularly high but variable. Sample 30-7-4 (associated with calc-silicate gneiss) contains 158 ppm Nb, 49 ppm Y, and 0.08 wt% MnO. Sample 574 (associated with hornblende gneiss in Unit B) contains 32 ppm Nb, 401 ppm Y and 1.61 wt% MnO. The variably high Y and Nb are contained in the spessartine-rich garnets.

Compared to high-Si GG, garnetiferous quartz-feldspar granulite has lower contents of Ti, Fe and Mg, and a lower Ca/Na ratio.

	A		B	
	CSG		GQFG	
SiO2	71.40	59.6-87.2	75.59	72.1-79.1
TiO2	0.14	0.04-0.24	0.01	0.01-0.01
Al2O3	15.44	7.9-22.5	13.35	12.5-14.2
Fe2O3	1.72	0.16-3.62	2.32	0.45-4.19
MnO	0.01	0.01-0.02	0.85	0.08-1.61
MgO	0.38	0.01-1.26	0.27	0.11-0.44
CaO	9.09	2.1-12.5	1.09	0.92-1.26
Na2O	1.62	0.57-2.72	5.45	5.3-5.5
K2O	0.14	0.03-0.26	1.05	0.84-1.25
P2O5	0.06	0.03-0.08	0.02	0.02-0.03
Cr2O3	0.00	0.00-0.00	0.00	0.00-0.00
	100.00		100.00	
Cr	8	nd-14	nd	
Cu	14	9-17	23	20-26
Nb	12.5	3-24	95	32-158
Ni	23	9-35	26	19-34
Rb	6	nd-20	39	26-52
Sr	330	216-422	24	12-35
V	16	6-36	6	nd-8
Y	28	7-39	225	49-401
Zr	142	42-247	52	17-86
N-Samples	8		2	

Table 4.8. Average chemical compositions (wt% and ppm) of (A) calc-silicate gneiss and (B) garnetiferous quartz-feldspar granulite.

	A	B	C	
SiO2	80.06	80.24	75.42	60.2-84.5
TiO2	0.04	0.67	0.02	0.00-0.03
Al2O3	12.69	9.32	0.77	0.49-1.15
Fe2O3	0.86	4.14	19.79	8.0-36.4
MnO	0.01	0.05	0.05	0.01-0.10
MgO	0.28	3.30	2.48	1.2-4.8
CaO	1.97	0.98	1.34	0.83-1.95
Na2O	3.53	0.67	0.05	0.00-0.12
K2O	0.54	0.53	0.02	0.00-0.03
P2O5	0.02	0.06	0.06	0.03-0.08
Cr2O3	0.00	0.04	0.00	0.00-0.00
	100.00	100.00	100.00	
Cr	4	191	15	7-22
Cu	7	216	172	39-378
Nb	3	5	2	nd-4
Ni	33	166	286	107-475
Rb	34	19	5	4-8
Sr	84	27	4	4-5
S	nd	47360	7220	554-17500
V	9	108	23	21-25
Y	9	10	6	6-7
Zr	86	43	6	6-6
Samples	1	1	3	

Table 4.9. Chemical compositions of quartzites: (A) typical sodic plagioclase quartzite of Unit A; (B) sillimanite-pyrrhotite quartzite of Unit B; and (C) magnetite quartzite of Dikoloti-Lentswe unit. Analyses recalculated to 100% on an anhydrous and sulphide-free basis.

4.1.7 Quartzites

Analysed quartzites (Table 4.9) include: (A) a typical albite-sillimanite quartzite; (B) a sillimanite-pyrrhotite quartzite; and (C) magnetite quartzite (from the Dikoloti-Lentswe unit).

The albite-sillimanite quartzite is characterised by low Ti, Fe, Mg, Cr and S. It has a high Zr content (86 ppm). The pyrrhotite quartzite has a higher contents of Ti, Fe (on a sulphide-free basis), Mg, Cr, Cu and Ni than the typical quartzite.

The main chemical variation in the magnetite quartzite is in Si and Fe, reflecting variation in magnetite content. The Mg and Ca contents relect the minor amphibole component. Sulphide is also an important minor component. The magnetite quartzite has a relatively high Ni and Cu content (286 & 172 ppm respectively, cf. Groves et al. 1978; Bavinton 1981).

	A		B	C	D	E	
SiO2	73.89	72.7-75.0	59.29	74.96	73.25	73.93	72.3-75.3
TiO2	0.17	0.16-0.18	1.00	0.01	0.13	0.20	0.16-0.26
Al2O3	14.22	13.7-15.0	15.03	14.08	15.19	13.51	13.1-13.8
Fe2O3	1.54	1.1-1.9	10.18	0.11	1.12	2.18	1.3-3.0
MnO	0.03	0.02-0.04	0.12	0.02	0.03	0.01	0.01-0.02
MgO	0.37	0.29-0.50	2.75	0.05	0.32	0.66	0.46-0.81
CaO	1.60	1.4-1.9	5.91	0.58	3.63	1.48	1.2-1.7
Na2O	4.08	3.3-4.7	3.35	2.85	4.65	3.18	2.6-3.8
K2O	4.05	3.8-4.3	1.94	7.33	1.63	4.82	4.2-5.3
P2O5	0.05	0.04-0.06	0.42	0.01	0.05	0.03	0.03-0.04
Cr2O3	0.00	0.00	0.01	0.00	0.00	0.00	0.00
	100.00		100.00	100.00	100.00	100.00	
Cr	4	nd-8	64	7	9	nd	nd
Cu	16	13-17	45	8	10	15	6-22
Nb	9.7	4-14	15	25	13	10.3	5-15
Ni	24	19-32	40	22	26	13	3-22
Rb	180	108-239	89	361	73	108	102-114
Sr	195	79-416	151	58	109	103	74-120
S	198	198	nd	nd	nd	162	162
V	14	12-174	135	6	10	16	13-317
Y	22	3-39	54	20	18	32	12-43
Zr	134	115-158	263	21	52	158	119-234
N-Samples	3		1	1	1	3	

Table 4.10. Chemical composition (wt% and ppm) of granitic gneisses. (A) to (D) - porphyroblastic granite gneiss suite; (A) - porphyroblastic granite gneiss; (B) - dioritic gneiss; (C) - granitic vein; (D) - tonalitic vein; and (E) - thin granite gneiss bands within grey gneiss. All analyses recalculated to 100% on an anhydrous and sulphide-free basis.

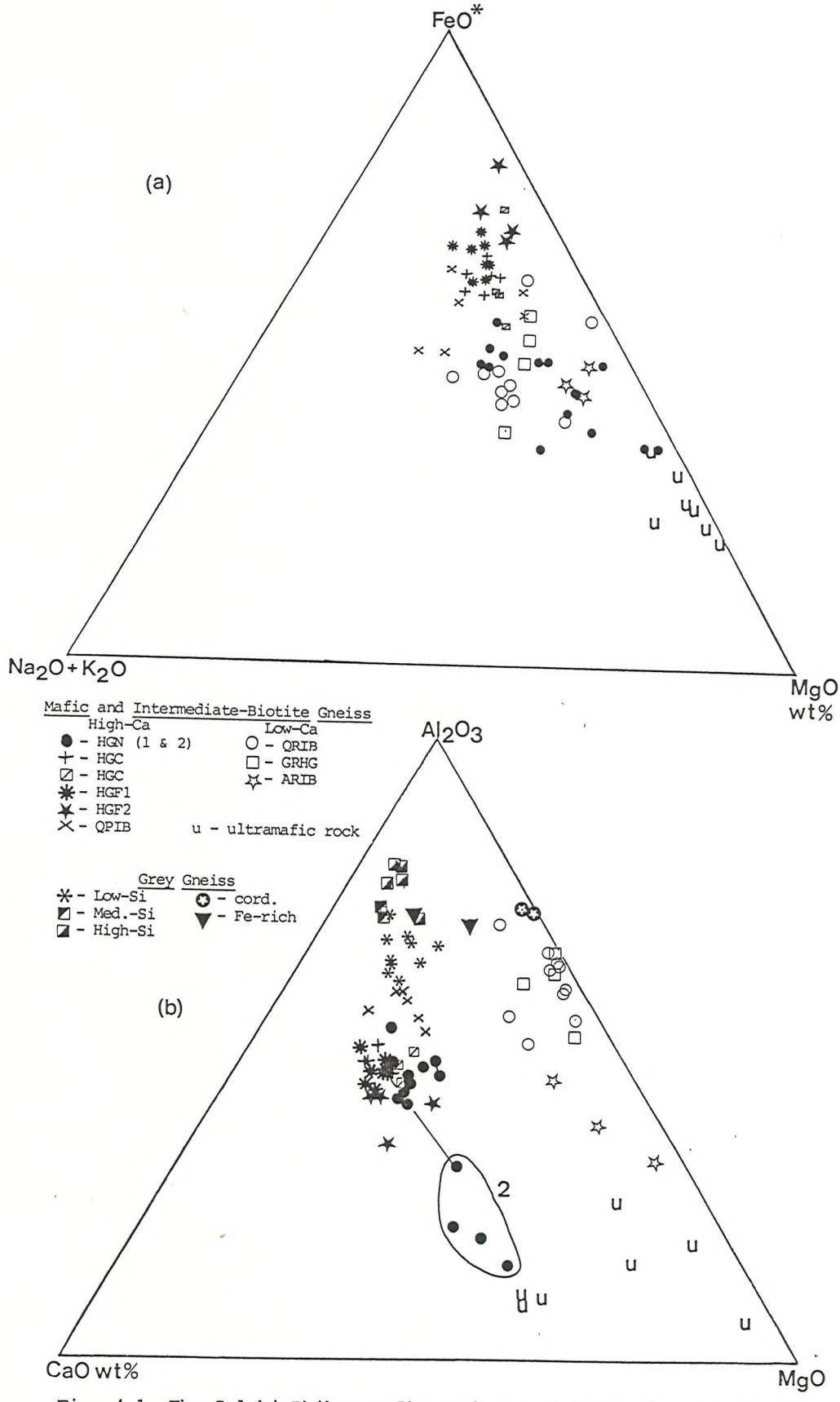

Fig. 4.1. The Selebi-Phikwe mafic gneisses: (a) AFM diagram of mafic and intermediate gneiss and ultramafic rock (FeO* -total Fe as FeO). (b) ACM diagram of mafic, intermediate, and grey gneiss and ultramafic rock.

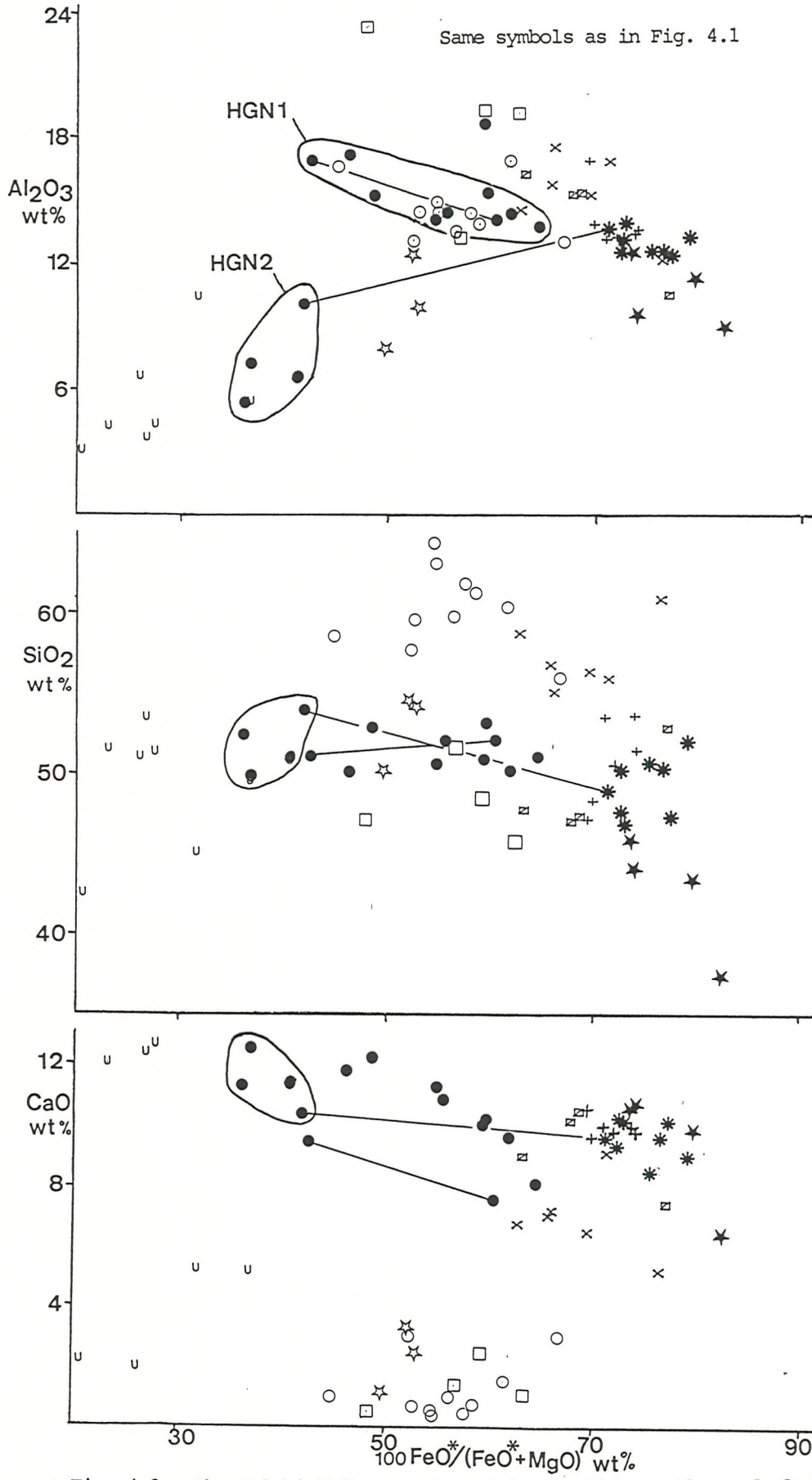

Fig. 4.2. The Selebi-Phikwe mafic and intermediate gneiss and ultramafic rock; Al, Si and Ca contents.

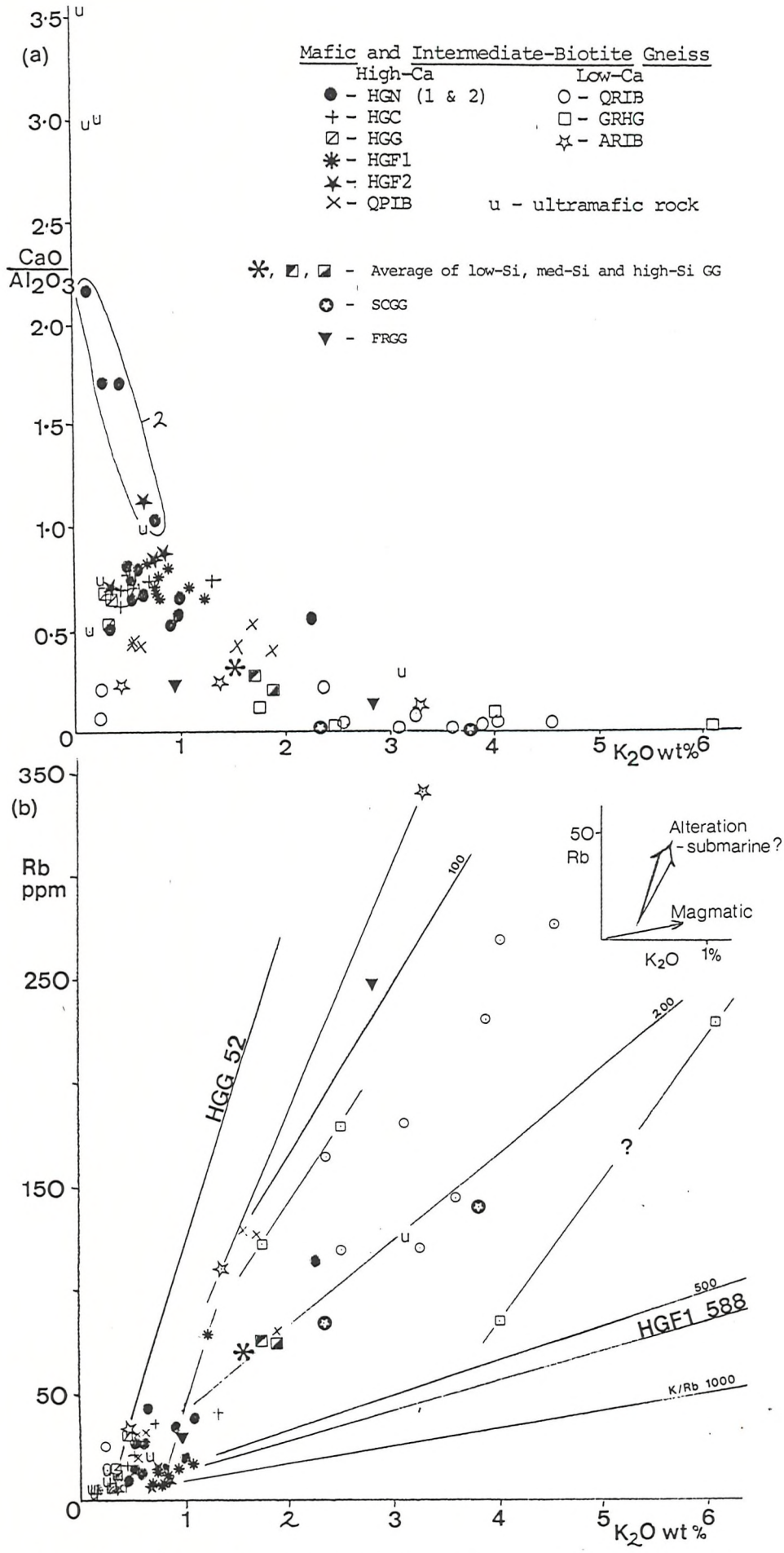

Fig. 4.3 The Selebi-Phikwe mafic and intermediate gneiss and ultramafic rock; K and Rb contents and Ca/Al ratios.

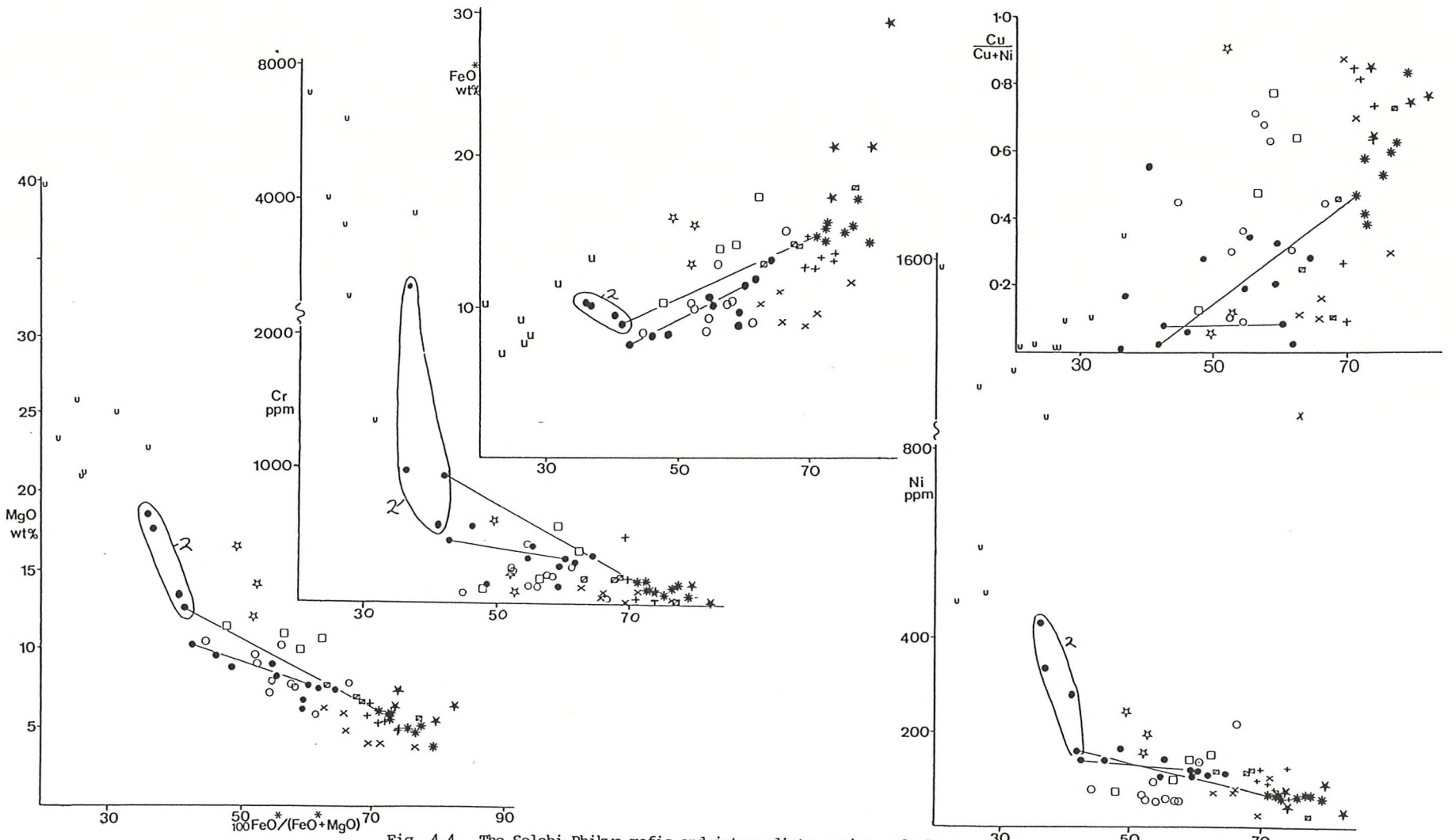

Fig. 4.4. The Selebi-Phikwe mafic and intermediate gneiss and ultramafic rock; Mg, Cr, Fe, Ni and Cu contents. Same symbols as Fig. 4.3.

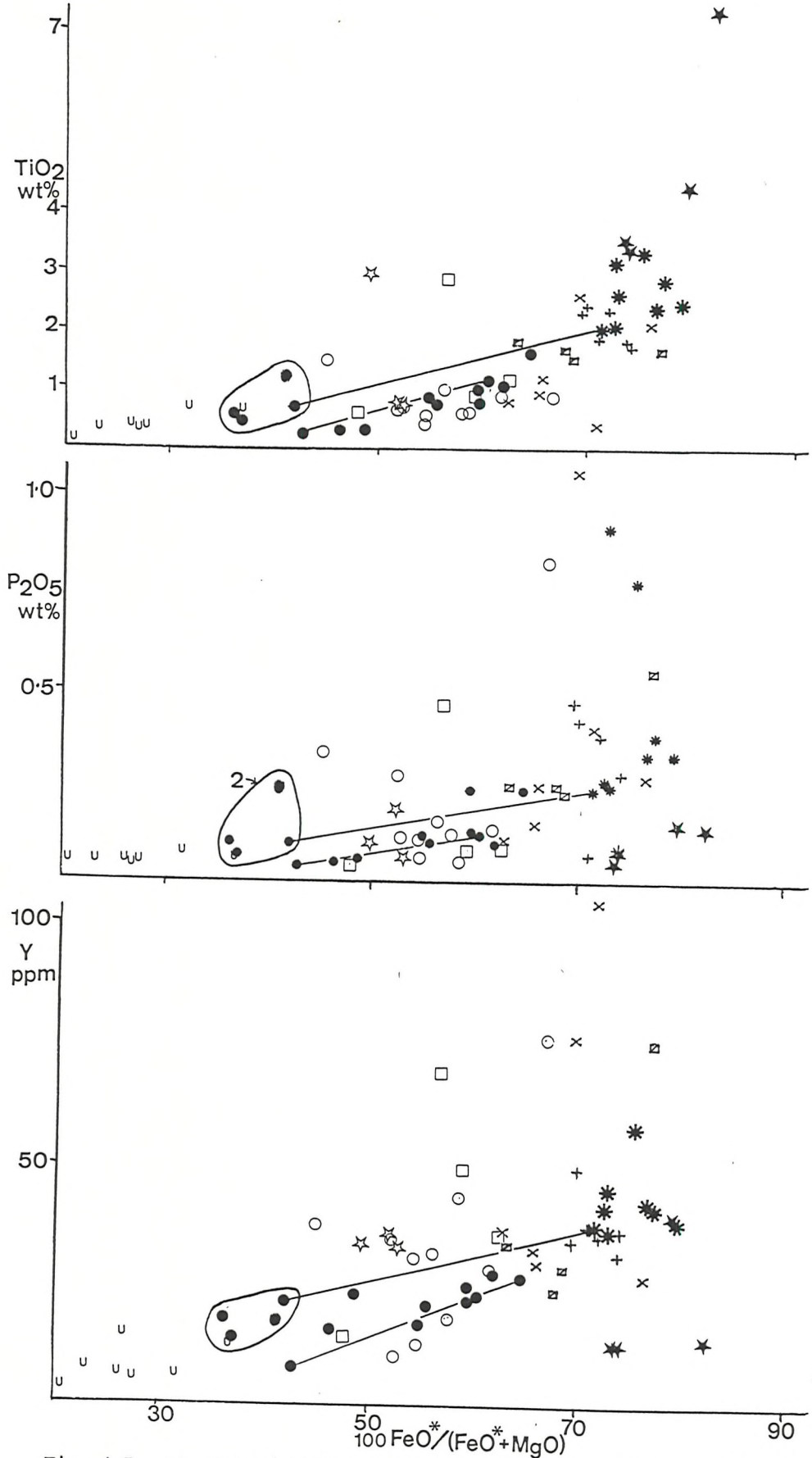

Fig. 4.5. The Selebi-Phikwe mafic and intermediate gneiss, and ultramafic rock; Ti, P, and Y contents. Same symbols as Fig. 4.3.

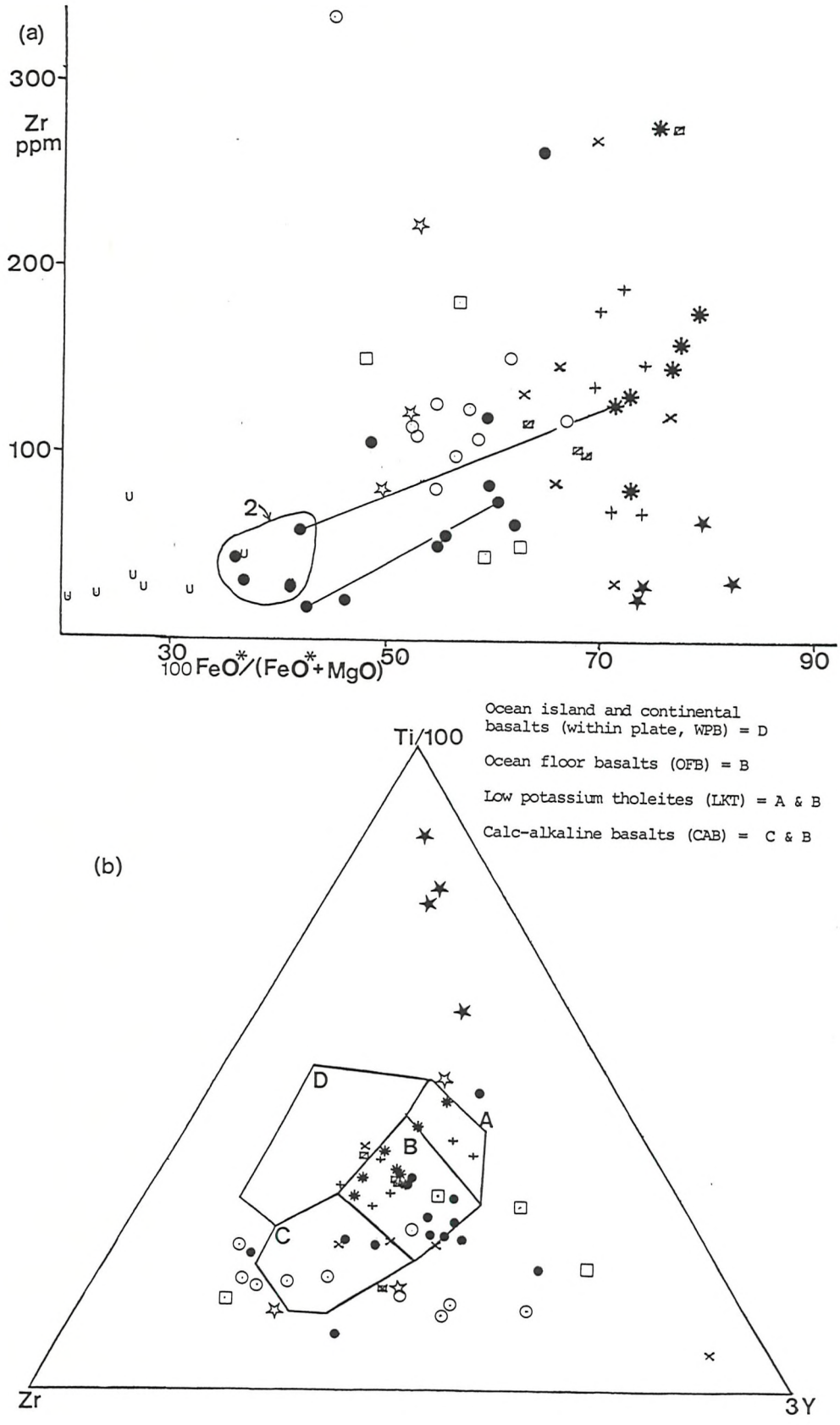

Fig. 4.6. The Selebi-Phikwe mafic and intermediate gneiss and ultramafic rock: (a) Zr contents; (b) Ti-Zr-Y variation diagram. Fields after Pearce & Cann (1973). Same symbols as Fig. 4.3.

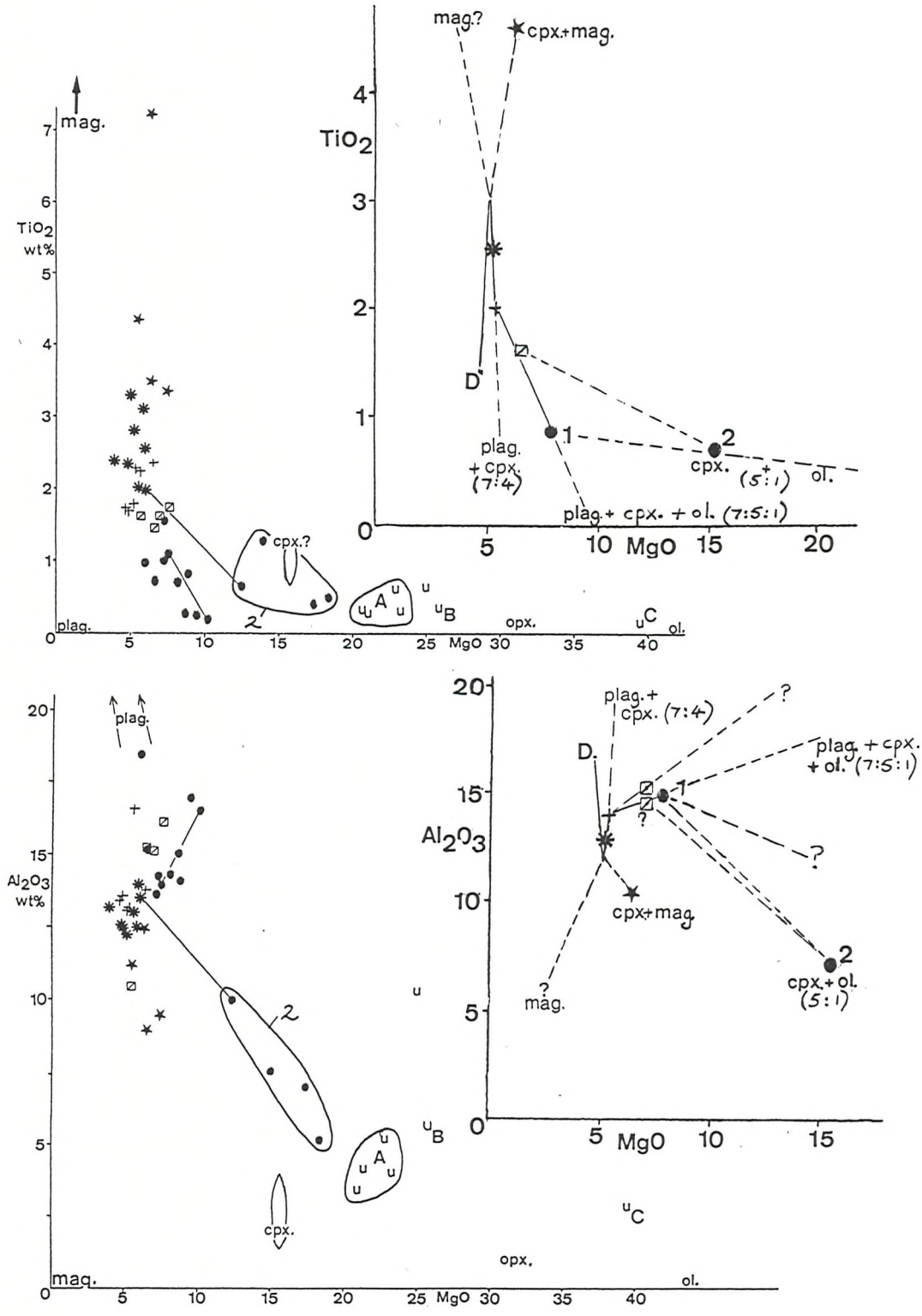

Fig. 4.7. Crystal fractionation and the evolution of the Selebi-Phikwe basalts (least altered samples only). Ti, Al, and Mg contents. Same symbols as Fig. 4.3.

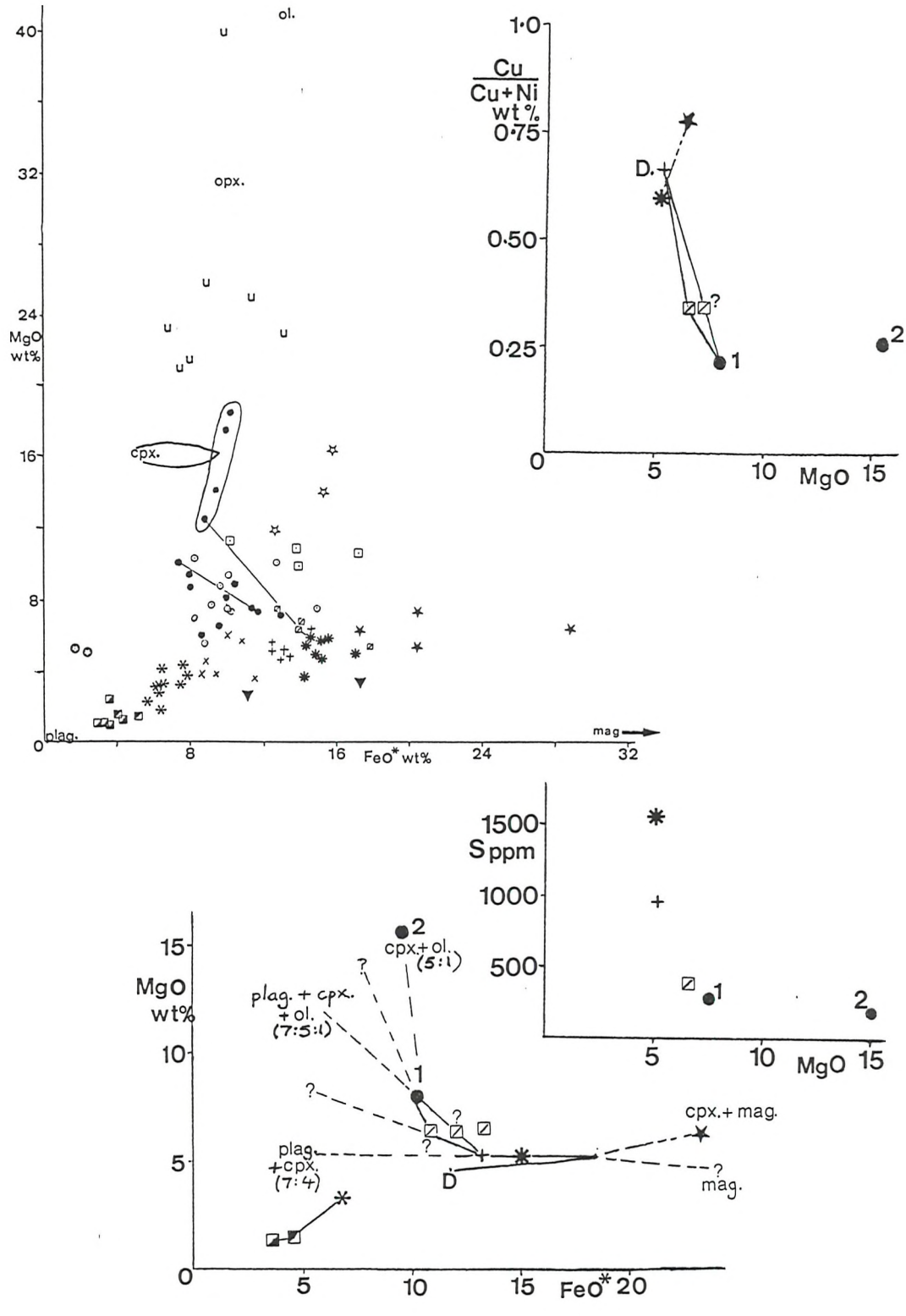

Fig. 4.8. Crystal fractionation and the evolution of the Selebi-Phikwe basalts (least altered samples). Fe-Mg contents and Cu/(Cu+Ni) ratios. Same symbols as Fig.4.1.

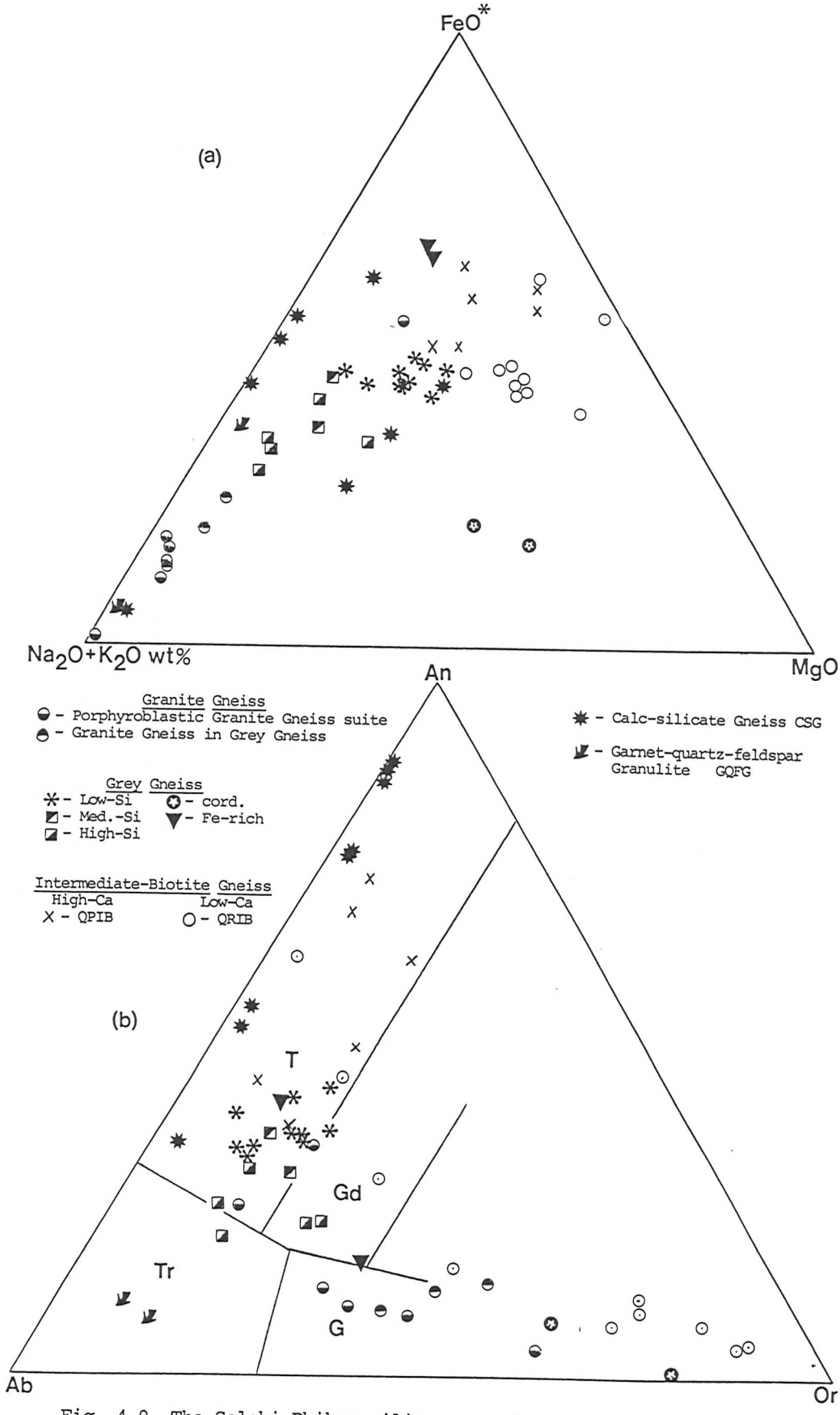

Fig. 4.9. The Selebi-Phikwe siliceous gneisses: (a) AFM diagram of grey gneiss, granitic gneiss and calc-silicate gneiss. (b) An-Ab-Or diagram. Fields from Barker (1979) after O'Connor (1965): T - tonalite, Tr -trondhjemite, Gd -granodiorite, G -granite.

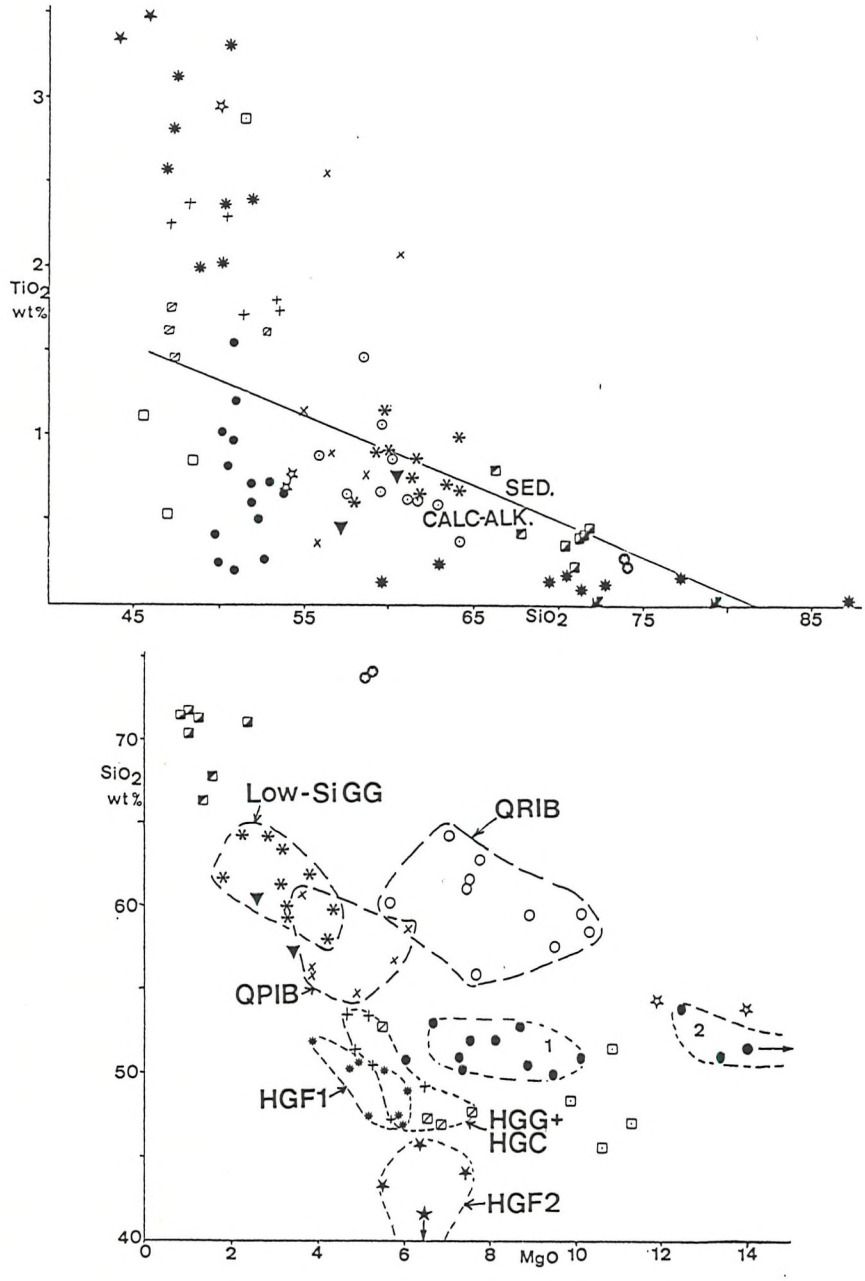

Fig. 4.10. The Si, Ti, and Mg contents of the Selebi-Phikwe gneisses: (a) TiO2 v. SiO2. Diagonal line separating calc-alkaline igneous rocks from clastic sediments, after Tarney (1976). (b) SiO2 v. MgO. Same symbols as Fig. 4.3; CSG (calc-silicate gneiss) - *; GFQG (garnet-quartz-feldspar granulite) - ⧓.

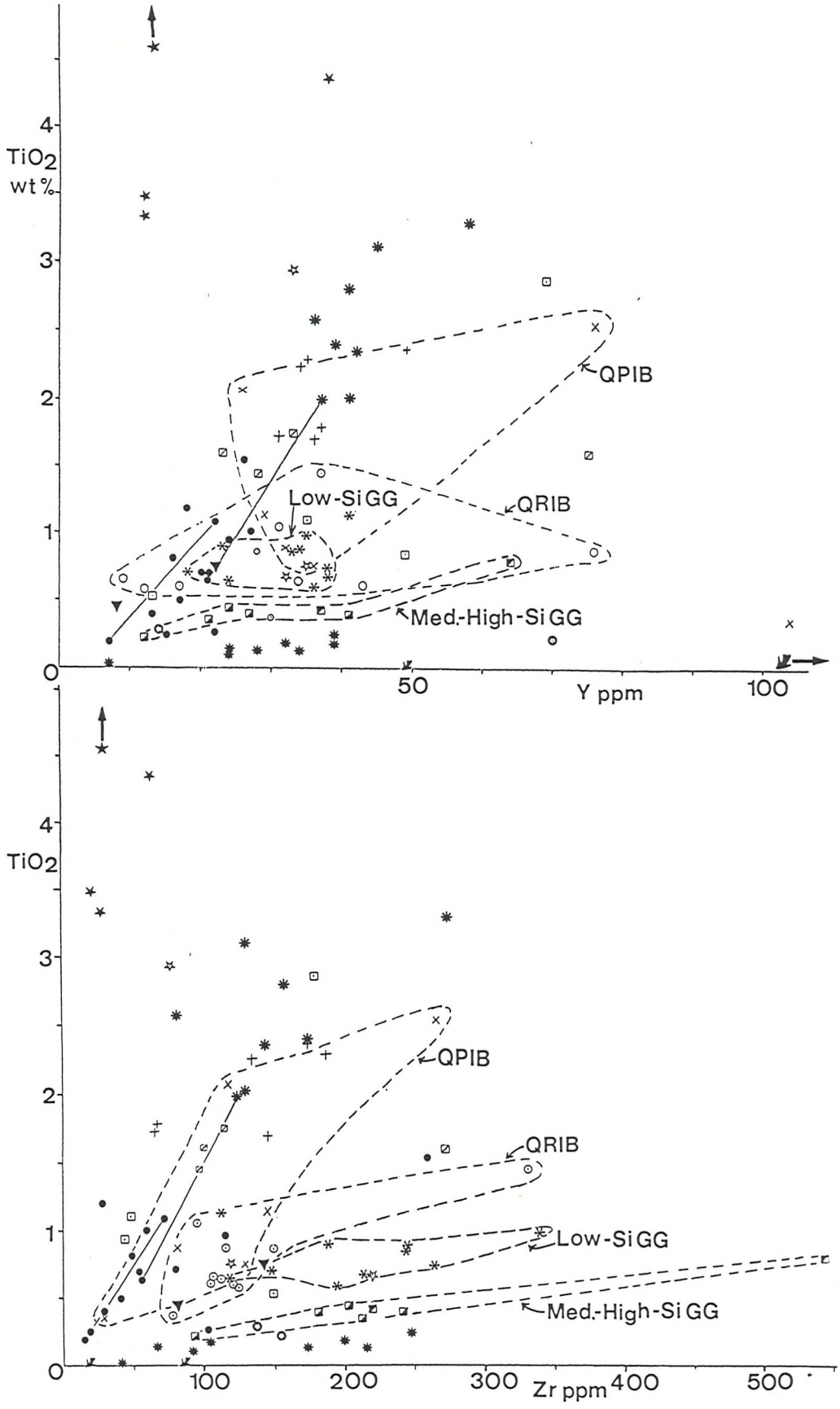

Fig. 4.11. The Ti, Y and Zr contents of the Selebi-Phikwe gneisses: (a) TiO2 v. Y; (b) TiO2 v. Zr. Same symbols as Fig. 4.10.

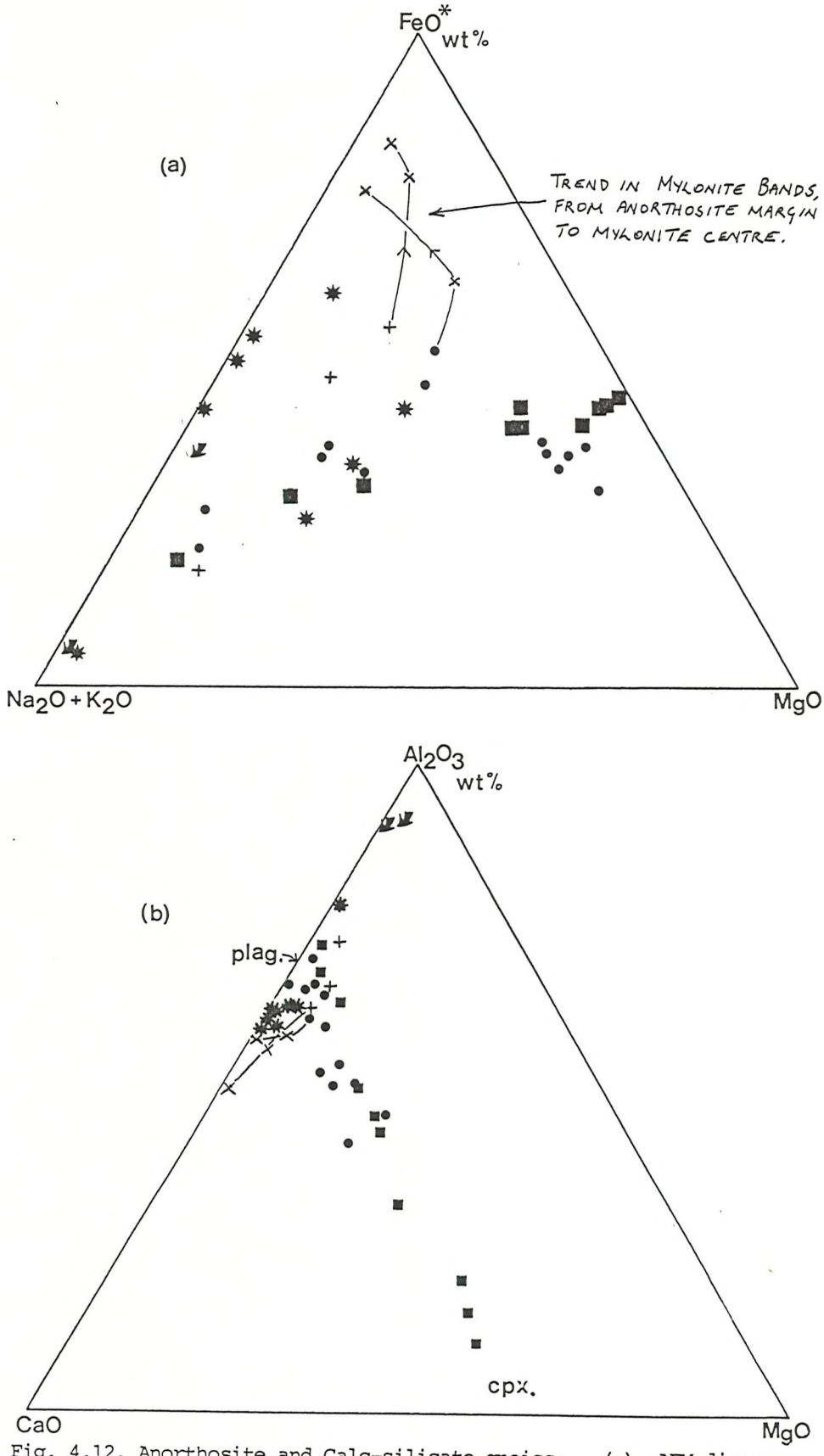

Fig. 4.12. Anorthosite and Calc-silicate gneiss: (a) AFM diagram; (b) ACM diagram. Selebi-Phikwe anorthosite: anorthosite, hornblende anorthosite and metagabbro - ● ; quartz-rich anorthosite - + ; mylonite bands in anorthosite - × ; Lethlakane layered body - ■. Calc-silicate gneiss (hornblende-bearing) - ✸; Garnet-quartz-feldspar granulite - ◤.

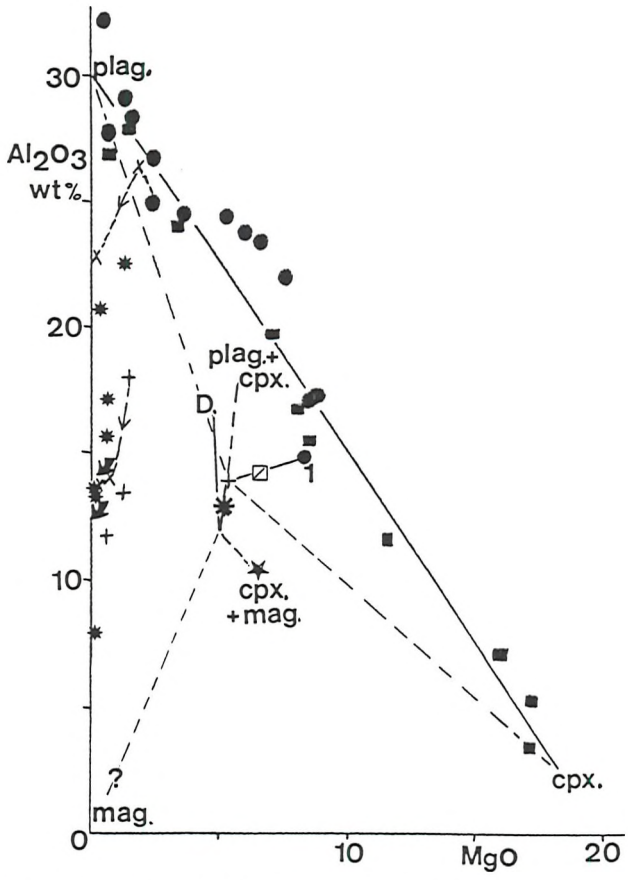

Fig. 4.13. Anorthosite and Calc-silicate gneiss; Al2O3 v. MgO. Same symbols as Fig. 4.12. Trend of evolution of Selebi-Phikwe basalts also shown.

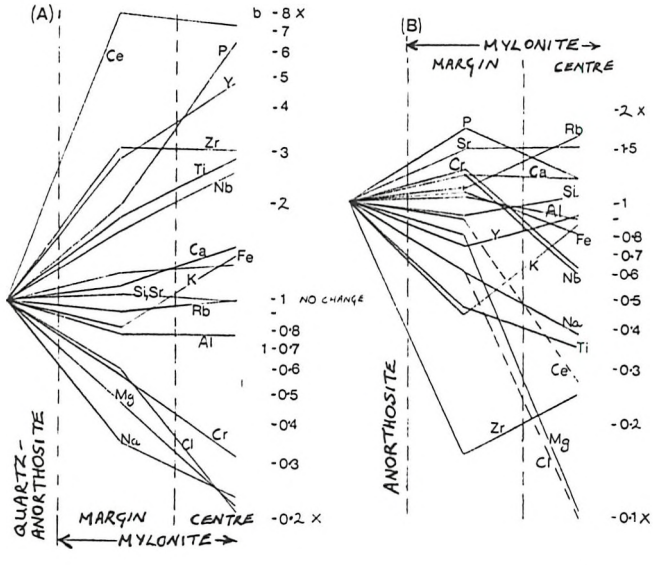

Fig. 4.14. Recrystallised mylonites in anorthosite. Relative chemical changes going from anorthosite to centre of mylonite band (6-12 cm). (A) D1-M1m assemblage; (B) superimposed D2-M2 assemblage on D1-M1m.

4.1.8 Granitic Gneisses

Little geochemistry has been done of the volumetrically important granitic gneiss of the Selebi-Phikwe area. The granitic gneiss has been subdivided into the porphyroblastic granitic suite which occurs as a major unit within the Selebi-Phikwe gneiss (e.g. at the top of the section at Phikwe) and thin granitic gneiss bands that occur within the sequence of grey and hornblende gneiss (Fig. 4.9). As well as typical porphyroblastic granitic gneiss, the porphyroblastic suite also includes dioritic gneiss and relatively undeformed quartz-sodic plagioclase and quartz-microcline bands. The granitic gneiss, with its high K contents, is easily distinguished from the grey gneiss (Table 4.10). There is little difference between the thick porphyroblastic granitic gneiss and the thin bands of granitic gneiss. The dioritic gneiss is similar to low-Si GG, but the high Fe, P, Nb, V and Y are outside the range of low-Si GG.

4.2 DISCUSSION - THE ORIGINAL NATURE OF THE HORNBLENDE AND INTERMEDIATE GNEISSES AND ULTRAMAFIC ROCKS

4.2.1 The High-Ca Hornblende and Intermediate Biotite Gneisses

4.2.1a HGN1, HGG, HGC, HGF1 and D

The major element trends and the trace element signatures (e.g. Cr & Ni) of the high-Ca hornblende gneisses (high-Ca HG) suggest that they have been derived from basic igneous rocks rather than from sediments. The HGN1, HGC, HGG and HGF1 hornblende gneisses and deformed mafic dykes (D) have major element compositions of basalt-gabbro (Gill 1979). In terms of Si and (Na + K) contents, the high-Ca HG (except HGG) has the composition of a sub-alkaline basic suite (Macdonald & Katsura 1964). Their enrichment in Fe, Ti and V and their Ti/Zr (77-102) and Zr/Y (2.8-3.7) ratios are characteristic of the tholeiitic magma series (Pearce & Cann 1973). HGC and HGF1 are best described as Ti-rich ferrobasalts or ferrogabbros (high Ti, Fe & V).

The Selebi-Phikwe high-Ca HG represent either metamorphosed extrusive basalts or intrusive basalts/gabbros. During field work it was thought that the intimate interbanding of some hornblende gneiss layers with quartzites, diopside gneiss, QRIB, QPIB, ARIB and CGHG possibly indicates that these hornblende gneiss layers represent

metamorphosed mafic extrusive rocks (see Ch. 2.3.1). This suggestion is developed further in Chapter 4.7.1 after the nature of the protoliths of the other Selebi-Phikwe gneisses has been discussed. It should be borne in mind at this stage that some of the hornblende gneiss bands probably represent metamorphosed extrusive basalts.

4.2.1b QPIB

High-Ca quartz-poor intermediate gneiss mainly occurs in hornblende gneiss-rich units (e.g. Unit B). In terms of Si and the ACM diagram (Figs 4.1b & 4.10a), QPIB is intermediate between the high-Ca HG and the low-Si grey gneiss. However on the AFM diagram QPIB has distinct affinities with high-Ca hornblende gneiss (Fig. 4.1a). The wide range of Ti (Fig. 4.10a) contents is also similar to that of the hornblende gneiss. The Zr and particularly Y contents of QPIB are very variable. However when Zr and Y are plotted against Ti (Fig. 4.11), the widespread fields of QPIB are more like the trend in the high-Ca HG, particularly Ti v. Zr, than those in grey gneiss. Also on the Ti-Zr-Y plot (Fig. 4.6b), QPIB mainly plots near the high-Ca hornblende gneiss field, although the QPIB field is more widespread. Low-Si grey gneiss would plot nearer to the Zr apex on the Ti-Zr-Y plot. It is considered that QPIB is a siliceous type of high-Ca hornblende gneiss rather than a mafic type of grey gneiss.

When compared to all the main types of high-Ca HG (HGN1, HGG, HGC, and HGF1), QPIB has lower contents of Ca, Mg and Cr, and higher Si, K, Rb, S and Y contents. These chemical differences, plus the widespread fields on the plots of Ti, Y and Zr (Fig. 4.11), suggest that QPIB was derived from tholeiitic rock (now represented by high-Ca HG) by such processes as alteration, weathering or sedimentation rather than by igneous fractionation. The wide range of Ti contents of QPIB suggests that it was derived from the whole range of litholgies represented by HGN1 to HGF1 (Fig. 4.10a). QPIB could represent altered in situ basalt or altered basaltic volcaniclastics. The high Si content could be the result of silicification or, if QPIB were a volcaniclastic, could alternatively be due to epiclastic quartz. The banded nature of the QPIB and its interbanding in Unit B with QRIB, ARIB, CGHG, thin quartzites, HGN1 and HGC suggest that a volcaniclastic origin is more likely. This would mean that some of the variabilty in chemistry could be due to sedimentary processes. For example, a minor component of QPIB could have been grey gneiss protolith (volcaniclastics of andesitic to rhyodacitic composition,

see Ch. 4.3). The protolith of QPIB is tentatively regarded as having been moderately altered tholeiitic rock, possibly of volcaniclastic origin (e.g. tuffs).

4.2.1c Layered bodies and the original nature of HGN2 and HGF2

A mineralogically graded HGN1 layer (4.4 m. thick) occurs in Unit F. It consists of Al & Mg-rich, Ti-poor HGN1 at the base and Ti-rich, Al & Mg-poor HGN1 at the top. These major element variations are matched by trace element variations (Figs 4.2, 4.4, 4.5 & 4.6a). The base of the layer is interpreted as HGN1 enriched in cumulus olivine and plagioclase (Fig. 4.7 & 4.8). The top of the layer is interpreted as residual HGN1 liquid. The layer is regarded as a right way-up differentiated tholeiittic sill (or flow, cf. Arndt 1977; Arndt et al. 1977) of Ti-rich HGN1.

The high Mg content (15.6 wt% MgO) of HGN2 suggests that HGN2 might have been basaltic komatiite. The CaO (11.5 wt%), Al_2O_3 (7.3 wt%), Cr (1260 ppm) and Zr (37 ppm) contents, and CaO/Al_2O_3 (1.6) and Al_2O_3/TiO_2 (10.4) ratios of HGN2 are similar to those of aluminium-depleted basaltic komatiites from Barberton, although CaO/TiO_2 (16.4) is chrondritic and TiO_2/P_2O_5 (5.8) is low (Nesbitt et al. 1979). An alternative interpretation is that HGN2 are basalts, rich in cumulus clinopyroxene and olivine (or orthopyroxene). This interpretation is supported by the occurrence of HGN2, interpreted as tholeiitic basalt enriched in cumulus clinopyroxene and olivine (Fig. 4.7 & 4.8) at the base of a mineralogically graded hornblende gneiss layer (0.3 m. thick) in Unit E. The hornblende gneiss at the top of the layer is typical HGF1, interpreted as residual liquid. The layer is regarded as a right way-up differentiated sill (or possibly a layered flow), with an approximate overall composition of HGG. It is therefore concluded that HGN2 represents cumulus clinopyroxene and olivine-enriched HGG (and HGN1), rather than basaltic komatiite.

The way-up inferred from these two differentiated layers is consistent and is opposite to that concluded by Wakefield (1974) and Wright (1977).

HGF2 only occurs in Unit D, intimately associated with HGF1. The very high Fe and Ti contents, but relatively low P, Y, and Zr, (Fig 4.11) suggest that there is a significant cumulate component in HGF2 (cf. Graham 1976). The much higher Fe, Ti and V, the slightly higher Mg and Ca, and the lower Al of HGF2 compared to HGF1 suggest that the cumulate component is titanomagnetite/ilmenite and low-Ca

clinopyroxene (Figs 4.7 & 4.8). HGF2 has chemical similarities with some of the high-Ca ultramfic rocks that occur in Unit D (Table 4.3-A) and the clinopyroxenites of the Lethlakane layered body (Table 4.7-D). It is concluded that HGF2 represents cumulus clinopyroxene and titanomagnetite-enriched HGF1.

4.2.2 Diopside Gneiss

The massive and banded diopside gneiss of Unit G is intimately interbanded with HGG-type hornblende gneiss. This interbanding is thought (see Ch. 2.3.1) to indicate an original relationship between the diopside gneiss and the hornblende gneiss and that the hornblende gneiss in Unit G was possibly extrusive HGG-type basalt rather than intrusive tholeiitic rock (see also Ch. 4.7.2).

In order to gain an insight into the original nature of the diopside and hornblende gneisses of Unit G, geochemical comparisons can be made with geochemically similar suites of rocks. For example, a suite of middle Proterozoic amphibolites, including pillowed amphibolite and banded high-Ca amphibolite, from Rajasthan in India (Bhattacharyya & Mukherjee 1984), has a similar compositional range as the suite of diopside and hornblende gneisses in Unit G. Some of the Dheli Supergroup massive amphibolites are chemically similar to HGG and some of the pillowed amphibolites are similar to the banded and graded diopside gneiss (B). The banded high-Ca amphibolites (including one sample with 55 wt% SiO_2, 0.4 TiO_2, 9.3 Al_2O_3, 7.9 Fe_2O_3, 0.5 MnO, 2.9 MgO, 23.2 CaO, and 0.6 NaO) are chemically similar to the massive diopside-plagioclase gneiss (A). The main differences are the higher Nb, Y, and Zr contents and lower Sr of the massive diopside-plagioclase gneiss (56 ppm Sr : 301 ppm Sr).

The massive diopside-plagioclase gneiss (A) is also chemically similar to epidotised tholeiitic basalt from the Barberton greenstone belt (Table 4.11-P, Condie et al. 1977), particularly with respect to their high contents of Ca, Fe and Zr and low Mg, Na, K and Cr. (The main difference again is in Sr.)

The highly banded (and graded) diopside gneiss (B) is chemically similar to a greenschist-facies altered mafic tuff from the Penhalonga Mixed Formation in the Tati greenstone belt (Table 4.11-N; Brown, in prep.), particularly the Si, Al, Fe, Mg, Ca, Cr, Cu, Nb, Ni, Sr, V and Zr contents. Type B also has similarities to an altered greenschist-facies pillow margin (Table 4.11-O; Gelinas et al. 1982) from the Abitibi greenstone belt.

	A	B	C	D	E	F	G	H
SiO2	50.2	49.5	49.94	58.9	55.4	59.7	68.4	67.90
TiO2	0.94	1.49	2.07	0.65	0.81	0.70	0.25	0.34
Al2O3	15.5	15.2	12.95	15.5	17.6	17.1	14.8	15.19
Fe2O3	1.63	2.80		1.5	3.4	2.8	1.20	1.30
FeO	9.26	9.17	13.36	4.5	6.1	3.8	2.85	1.74
MnO	0.22	0.18	0.20		0.21	0.12	0.08	0.05
MgO	7.53	6.82	5.84	4.5	4.3	3.2	1.58	1.69
CaO	11.6	8.79	10.59	5.1	9.1	6.6	3.20	3.29
Na2O	2.15	2.70	2.59	4.0	2.7	3.3	4.00	5.16
K2O	0.22	0.69	0.15	1.9	0.43	1.5	1.65	1.73
P2O5	0.10	0.17	0.20		0.16	0.19	0.25	0.12
H2O	1.62	2.04		3.0	0.78	1.0	1.25	
Cr	490	250		88			40	
Cu	110	100		36			15	
Ni	140	125		60			20	
Rb				75				48
Sr	100	190		580			320	519
V	260	365					20	
Y	20	30		35			32	
Zr	53	135		190			260	

	I	J	K	L	M	N	O	P
SiO2	63.3	58.8	70.7	57.4	60.41	48.85	54.57	46.6
TiO2	0.56	1.06	0.64	0.59	0.84	1.08	0.85	0.73
Al2O3	13.3	17.1	14.0	13.3	14.18	16.52	16.49	15.5
Fe2O3	1.0	1.9	1.4	12.2	8.97	10.79	2.56	9.63
FeO	4.9	5.5	3.1				3.43	3.0
MnO	0.1	0.15	0.10	0.11	0.14	0.18		0.21
MgO	3.7	3.6	2.0	6.2	14.53	3.77	4.09	3.58
CaO	3.4	5.8	2.7	0.94	0.35	15.99	11.82	18.9
Na2O	2.9	4.1	3.1	0.99	0.09	0.64	2.44	1.09
K2O	2.1	1.6	1.9	2.3	0.25	1.86	0.00	0.19
P2O5	0.15	0.26	0.16	0.1	0.18	0.28	0.04	0.05
H2O	2.0						2.05	0.7
Cr				>800	397	276		68
Cu					7	50		56
Nb					8	6		5.6
Ni				586	180	113		76
Rb					8	46		3.2
Sr					11	108		1800
V				200	120	218		
Y					18	22		nd
Zr				105	159	115		199

Table 4.11. Chemical compositions (wt% and ppm) of some possible equivalents of the Selebi-Phikwe gneisses: A & B -The most common types of Archaean tholeiitic basalt (TH1 & TH2, Condie 1976b, 1981); C - Ferro-basalt from Galapagos (Anderson et al. 1975); D - Archaean andesite (Type II, Condie 1976b, 1981, 1982); E & F - Orogenic andesites, low-K basic (E) and med-K acid (F) (Gill 1981); G - Archaean rhyodacite (FII Condie 1976b, 1981); H - Tonalite diapirs, Ancient Gneiss Complex, Swaziland (Hunter 1974); I-Composite Archaean greywacke (Condie 1976b, 1981); J & K -Sandstones of oceanic island arcs (J) and continental island arcs (K) (Bhatia 1983); L - Fig Tree shales, Barberton greenstone belt (Condie et al. 1970; McLennan et al. 1983b); M & N -Tuff from bedded coarse (andesitic?) lapilli tuffs (M) and green chlorite-feldspar-quartz schist (altered mafic flow/tuff) (N), Penhalonga Mixed Formation, Tati greenstone belt (Brown in prep.); O-Margin of altered greenschist-facies mafic pillow, Abitibi belt (Gelinas et al. 1982); P - Epidotised tholeitic flow, Barberton belt (Condie et al. 1977).

The elements in the diopside gneisses that show the most variation from contents in HGG (the main lithology with which they are interbanded are:

(1) in (A), + Ca, Mn, P, (Fe), Nb, Y and Zr; -Ti, Mg, Na, K, Cr, Ni, Sr and V.

(2) in (B), + Ca, Na and (Al); - Mg (see Table 4.5).

The above chemical comparisons plus the interbanding of the diopside gneiss with HGG-type hornblende gneiss (that is thought to have had an extrusive origin) are considered to be evidence that the diopside gneiss represents highly altered HGG-type tholeiitic volcanics or HGG-derived volcaniclastics. The high Ca and low Mg contents of the diopside gneiss suggest highly epidotised tholeiitic volcanics or volcaniclastics. The migration of Ca during epidotisation is typically accompanied by Sr-enrichment (Humphris & Thompson 1978). The lack of Sr-enrichment possibly indicates a low fluid/rock ratio during alteration (Ludden et al. 1982). The very high Ca content of the massive diopside gneiss (A) is possibly also due to an original carbonate component. This is supported by the traces of carbonate in well-banded diopside gneiss and the occurrence of marble in Unit H. Highly effective metamorphic decarbonation reactions (cf. Klein 1973) have possibly taken place. The epidotised rock could have been highly altered in situ HGG-lava or volcanic detritus (e.g. pillow breccia and hyalotuff). Thick hyalotuffs can form by the reworking of lava detritus in shallow water, followed by transportation into deeper water by turbidity currents (Dimroth et al. 1978). In deeper water they could mix with deep water argillite or carbonate. The banding of the well banded diopside gneiss with alternate diopside and hornblende-rich bands is considered to reflect an original feature of the gneiss. The well banded diopside gneiss and the mineralogically graded diopside gneiss could indicate highly altered pillows that have been deformed during D1 (cf. Ehlers 1976; Myers 1978; Holland & Norris 1979). It is speculatively suggested that the mineralogically graded diopside gneiss may also possibly represent altered, graded hyalotuffs (Dimroth et al. 1978).

The suite of diopside and hornblende gneisses at Sefhope is also considered to represent altered tholeiitic pillow basalt and volcanic detritus.

The diopside amphibolite associated with quartzite and marble in Unit H is possibly a mixture of dolomite, Mg-Al clay and altered tholeiitic volcanic detritus, that has suffered decarbonation.

4.2.3 Low-Ca Intermediate Gneiss - QRIB, ARIB and GRHG

QRIB has higher Si, K, Nb, Rb and S, and lower Ca, Mn, Sr and Na (Table 4.2), than all the main types of high-Ca HG (HGN1, HGG, HGC, & HGF1). However Ti, Al, Fe and Mg contents are within the range of the above hornblende gneiss and are particularly similar to those in HGN1. The composition of QRIB is such that it could not represent unaltered igneous rock. The relatively high Mg suggests QRIB is not related to low-Si grey gneiss. QRIB is thought to be derived from tholeitic basalt, now represented by high-Ca HG. The highly banded nature of QRIB and its interbanding with other lithologies (as with QPIB) indicates a sedimentary origin for the tholeite-derived QRIB, rather than in situ alteration/silicification. The relatively high but variable K content and the low Ca and Na contents (Figs 4.3 & 4.9b) suggest a clay component. The relatively high Si content possibly indicates detrital quartz or silicification.

QRIB has similar major element chemistry to the Fig Tree shales of the Barberton greenstone belt (McLennan et al. 1983b), except for the high Cr and Ni of the latter (Table 4.11-L). McLennan et al. (1983a) have suggested that the high Cr and Ni of some Archaean shales is due to a secondary enrichment process, such as adsorption of Cr and Ni on chlorite or its precursor.

QRIB is thought to be a pelitic/semi-pelitic sediment derived mainly from altered tholeitic basalt or tholeitic volcaniclastics. QRIB possibly consisted of Mg-Al smectite or other Mg-Al clays such as the fibrous magnesium clays (palygorskite, attapulgite and sepiolite). Other components could have been chlorite, illite, phillipsite, epiclastic quartz and andeistic volcaniclastics (see grey gneiss protoliths in Ch. 4.3).

ARIB: The low Ca and Cr and high Mg contents of ARIB indicate that it can not be an unaltered igneous rock. The high Mg (14 wt% MgO, Table 4.2) content suggests that ARIB could be altered basaltic komatiite. The low Ca and relatively high K are indicative of alteration. However the high Ti, Al, Cu, Nb, Y, Zr and Cu/(Cu+Ni) and low Cr and Ni are so unlike those of basaltic komatiite (Nesbitt et al. 1979) that an origin for ARIB by in situ alteration (even extreme alteration) of basaltic komatiite is thought unlikely.

The following features are thought to be important in the interpretation of the original nature of ARIB:

(a) The high Ti, Nb, Y and Zr, which suggest a relationship to

basalt (particularly HGC and HGF1);
(b) The low Ca content and relatively high Al and K, which indicate a clay component or K-feldspar;
(c) The high Mg (14 wt% MgO) content, but relatively low Cr (284 ppm) and Ni (194ppm);
(d) The high Si content which possibly indicates a detrital quartz component or silicification;
(e) The interbanded nature of ARIB with QPIB, QRIB, CGHC, quartzite and high-Ca hornblende gneiss in Unit B; and
(f) The chemical similarity of ARIB to magnesiopelites of the Murchison greenstone belt (Pearton 1982) and tuffaceous volcaniclastics within andesitic volcanics in the Tati greenstone belt (Brown, in prep; Table 4.11-M).
It is thought that ARIB represents altered volcaniclastic sediment, rather than in situ altered basalt. The high Mg content possibly indicates a high content of the alteration products of olivine or orthopyroxene, perhaps by the weathering of HGN2 or ultramafic rocks (cf. the serpentinous tuffs of Pharaoh 1985). However the low Cr and Ni contents of ARIB suggest that an alternative explanation for the high Mg content is Mg-rich clay. Clay and zeolite-rich sediments (e.g. a montmorillonite-phillipsite assemblage) possibly formed by devitrification of volcanic ash and were then enriched in Mg by absorption from seawater or hydrothermally fluids (cf. Hathaway & Sachs 1965; Bonatti & Joensuu 1968; Couture 1977; Desprairies 1982). Alternatively Mg-rich clay may have formed by direct precipitation from Mg-saturated seawater or hydrothermal solution reacting with seawater (cf.Bowles et al. 1971; Jeans 1978; Natland & Mahoney 1982).

It is concluded that ARIB was semipelitic sediment, derived mainly from alteration of basaltic rocks and containing Mg-rich clay.

GRHG: Similar chemical considerations as those applied to the other intermediate biotite gneisses (QPIB, QRIB and ARIB) imply that GRHG was derived form highly altered tholeitic basalt. The occurrence of GRHG within hornblende gneiss, rather than with (sedimentary ?) QPIB and QRIB, the high-Al and S contents (Table 4.2), and the coarse garnet-dominated mineralogy (cf. Hutchinson 1983), suggest that GRHG possibly represents in situ hydrothermally altered tholeiitic basalt. An alternative possibility is that the GRHG (containing garnet, hornblende, cordierite, biotite and pyrrhotite) is the residue of partial melting of hornblende gneiss (cf. Winkler 1979).

When compared to high-Ca HG, the intermediate biotite gneiss

(QPIB, QRIB, ARIB, GRHG) are characterised by lower Ca and higher K and higher but highly variable (P), Nb, S, Y, Zr and Cu/(Cu+Ni) ratio. The intermediate biotite gneiss are thought to represent a variety of lithologies derived from the alteration of tholeitic basalt. They possibly span a range from in situ alteration to volcaniclastic and pelitic sediments. Some of the metasediments possibly contain a minor grey gneiss precursor component.

4.2.4 Ultramafic Rocks

The high Mg of the ultramafic rocks in Unit D suggests that they could possibly be komatiites. However their high and variable Cr contents, their Ca and Al contents and CaO/Al2O3 ratios (either too high - 2.5 in Type A, or too low - 0.3 in Type B), and their low Ti contents, are more like those of ultramafic cumulates, than typical ultramafic extrusives (Nesbitt et al. 1979). Type A has similar Ca/Al and Al/Ti ratios to the Badplass basaltic komatiites from the Barberton greenstone belt (Viljoen & Viljoen 1969). The Badplas komatiitic basalts may not represent a liquid composition and may be clinopyroxene-rich cumulates (Nesbitt et al. 1979).

The major element contents suggest that the ultramafic rocks in Unit D were originally cumulus mixtures of clinopyroxene, olivine, orthopyroxene and minor plagioclase (Figs 4.7 & 4.8). It is thought that Type A was clinopyroxene-rich (plus olivine), Type C was olivine-rich, and Type B was possibly orthopyroxene-rich with some plagioclase. The Ca, Al and K contents of Type B indicate however significant alteration and loss of Ca. Type B could also have been clinopyroxene-bearing. Type (B) and (C) occur together in the same (4 m. thick) layer, with (B) in the top half and (C) in the bottom lower half. The main alternative to a cumulate origin, suggested by the highly variable Ca and Al contents, is that the ultramafic rocks are highly altered komatiites. The absence of original (e.g. spinifex) textures means that this suggestion is speculative (Brooks & Hart 1974; Nesbitt et al. 1979) .

4.3 DISCUSSION - THE ORIGINAL NATURE OF THE GREY GNEISS

4.3.1 Typical Grey Gneiss

The possible protoliths of the typical grey gneiss suite are thought to be:

(a) tonalitic intrusives,

(b) intermediate-felsic volcanics, or

(c) sediments.

No intrusive contacts of grey gneiss were found. Given the high deformation suffered by the Selebi-Phikwe gneisses and lack of exposure, this is not surprising. The main morphological feature of the grey gneiss is its banding. The banding, due to variation in amounts of the major components -quartz, plagioclase, hornblende and biotite, is on all scales. Within the typical grey gneiss, there are thin bands that are rich in either garnet, sillimanite, magnetite, cordierite, or corundum. Although leucocratic metamorphic segregations can be found, the main banding is not thought to be a tectono-metamorphic product. The banding is regarded as reflecting original compositional differences. This banding is regarded as major evidence for a dominantly volcanic-sedimentary origin for the grey gneiss suite, rather than a tonalitic intrusive origin. The main alternative for the banding is that it is tectonometamorphic. For example, a biotite-rich band with corundum, cordierite and sillimanite (Plate 19g & h) could represent either a highly aluminous protolith or the residue from the extraction of a partial melt (Green 1976; Winkler 1979). Limited partial melting (see Ch. 4.7.4) would still have been controlled however by original compositional differences.

The typical low-Si to high-Si grey gneiss of the Selebi-Phikwe area define a good calc-alkaline trend on an AFM diagram (Fig. 4.9a) and in terms of SiO2 v. FeO/MgO (not figured), which contrasts with the tholeiitic Fe-enrichment trend in the high-Ca hornblende gneiss (Fig. 4.1a). The grey gneiss has the major element geochemistry (Fig. 4.9b) of tonalite, plus minor granodiorite and trondhjemite (O'Connor 1965; Le Maitre 1976; Barker 1979). The volcanic equivalents, in terms of Si and Ca-Na-K (not figured), are andesite, dacite and rhyodacite.

The low-Si grey gneiss has the major element geochemistry of orogenic (i.e. at convergent plate boundaries) andesite (e.g. medium-K acid orogenic andesite - Table 4.11-E, Gill 1981). When compared to the range of andesite compositions, low-Si grey gneiss is relatively high in Si, Na, Y and Zr and low in Ca and V. Compared to oceanic (anorogenic at divergent boundaries, Gill 1981) andesite, low-Si grey gneiss is significantly lower in Fe and Ti, but has similar contents of V, Y and Zr (Byerly et al. 1976; Gill 1981; Hekinian 1982). Condie

(1976, 1981, 1982) states that Archaean andesites (Table 4.11-C) differ from modern andesites in terms of their low Al contents and their high Fe, Mg, Cr, Ni and Y. Low-Si grey gneiss has slightly higher Si, Ti, Al and Fe, and lower Mg, Cr and Sr contents than the Archaean andesite quoted. In terms of Cu, Ni, Rb, Y and Zr, they are identical.

The medium-Si and high-Si grey gneiss have major element compositions of dacite and rhyodacite respectively and are similar to Archaean felsic volcanics (Condie 1981). A typical Archaean rhyodacite (Condie 1976, 1981) is tabulated for comparison (Table 4.10-F). The main differences are the higher Ti content and lower Cr and Sr of both medium and high-Si grey gneiss, and the high Y and Zr contents of the medium-Si grey gneiss. The higher Ti/Y and Ti/Zr ratios (Fig. 4.11) of low-Si grey gneiss compared to the medium to high-Si grey gneiss suggest that the grey gneiss does not represent a single magmatic suite. However if the grey gneiss represents sediments, this could be a sedimentary feature (e.g. sorting and concentration of zircons in more siliceous detritus).

If the grey gneiss suite protoliths were andesitic to rhyodacitic volcanics, their major and trace element contents (e.g. Fe and Mg, Fig. 4.8, cf. Jolly 1975) and proportion (c. 1:2 - grey gneiss: hornblende gneiss) compared to high-Ca hornblende gneiss indicate that the calc-alkali grey gneiss suite was not derived by continued low-pressure fractional crystallisation of tholeiitic HGF1. The production of HGF1 from HGN1P by low-pressure crystal fractionation required approximately 75% crystallisation of HGN1P (see Ch. 4.2.5). The QPIB protolith could have been basic andesite (cf. Table 4.11-E), intermediate between high-Ca hornblende gneiss and low-Si GG (Figs 4.1b, 4.8, 4.9a, 4.10b). However, as concluded in Chapter 4.2.1b, the wide variation of Ti, Y and Zr in QPIB suggest that it was derived from tholeiitic basalt by alteration-sedimentation processes (Figs 4.10a, 4.11).

The main alternative to a volcanic origin for the grey gneiss is a sedimentary one. In terms of Na-K-(Fe + Mg) (not plotted), the grey gneiss suite has the composition of greywacke (Blatt et al. 1972; cf. average Archaean greywacke in Table 4.11-I, Condie 1981) Maynard et al. (1982), Bhattia (1983) and Bhattia & Crook (1986) have correlated the chemical compositions of sandstones and the tectonic settings of their respective sedimentary basins. In terms of Si/Al and K/Na, the grey gneiss suite is similar to modern deep-sea sands

from active rather than passive plate-tectonic settings and in particular forearc basins (Maynard et al. 1982). Using Bhattia's parameters, low-Si grey gneiss has the major element composition of sandstone (greywacke) from oceanic island arcs and high-Si grey gneiss has the composition of sandstone from continental island arcs (Table 4.11-J & K). These results are hardly surprising, given that island arc sandstones are dominantly derived from andesites, and continental island arcs from felsic volcanics. The thin biotite-rich bands and laminae (not analysed) within the grey gneiss suite possibly represent argillites of greywacke-argillite couplets of turbidity current origin. The grey gneiss suite could represent submarine calc-alkaline volcaniclastic turbidites or debris flows (cf. Fisher 1984; Carey & Sigurdson 1984; Suthren 1985).

In order to determine the premetamorphic nature (sedimentary or igneous) of high-grade quartzofeldspathic gneiss, Shaw (1972) derived a discriminant function:

$$DF = 10.44 - 0.21\ SiO2 - 0.32\ Fe2O3\ (\text{total Fe}) - 0.98\ MgO + 0.55\ CaO + 1.46\ Na2O + 0.54\ K2O \quad \text{wt\%}$$

Positive DF values generally suggest an igneous parentage, whereas negative values point to a sedimentary origin. On application of the function to the typical grey gneiss suite, the majority have a positive DF (+ve 1 to 3). The main group with negative (-ve 2 to 0) or low positive (<+0.5) DF are the low-Si grey gneiss with lower Ca contents. The high-Si cordierite-rich grey gneiss (-ve 8) and the Fe-rich grey gneiss (-ve 2) are distinctively negative. The granitic gneiss bands within grey gneiss have a positive DF (+ve 1 to 2).

The TiO2-SiO2 distribution of the grey gneiss (Fig. 4.10a) also suggests that grey gneiss protoliths were both sedimentary and calc-alkali igneous, although predominantly the latter (cf. Tarney 1976).

The suite of typical grey gneiss is concluded to be metamorphosed andesitic to rhyodacitic volcanics and/or little-altered volcaniclastic sediments derived from andesitic to felsic volcanics. It is not thought to be a tonalitic intrusive suite. Volcano-sedimentary grey gneiss precursor could also have been a minor component in the intermediate biotite gneiss. The results of detailed petrology and geochemistry at Selebi-Phikwe in this thesis confirm the speculations of Mason (1973) based on mapping that the grey gneiss are psammitic and semipelitic metasediments with possible

minor acid-intermediate volcanics.

4.3.2 Siliceous Cordierite-rich Grey Gneiss

SCGG does not have an igneous composition. The occurrence of SCGG within grey gneiss rather than high-Ca hornblende gneiss suggests an an origin by alteration of grey gneiss protolith. The high Mg and Si contents suggest that SCGG may have been derived by chloritic alteration of typical grey gneiss protolith (calc-alkali volcanics or volcaniclastics). However the protolith of SCGG could also have been a sediment partly composed of altered mafic detritus (derived from high-Ca HG protoliths). SCGG has more in common with QRIB and ARIB than typical grey gneiss. SCGG, QRIB and ARIB have similar K-Ca-Na ratios (Fig. 4.9b) and a clay component in SCGG is indicated. If sufficient silica were added to QRIB, a similar rock to SCGG would be obtained but with too little Al and too much Fe compared to SCGG. It is suggested that the protolith of SCGG possibly consisted of a mixture of silica and Al-Mg clays. The clay could have been an Al-Mg clay (e.g. smectite, palygorskite or attapulgite) or a mixture of Al-rich (e.g. beidellite, kandite or illite, or zeolites, e.g. phillipsite or clinoptilolite) and Mg-rich (e.g. sepiolite, chlorite or even talc). The relatively high K content could be due to the mobility of K during regional metamorphism. Alternatively it indicates an original K-bearing phase (e.g. illite or phillipsite). As with ARIB, the clays could have been derived either by (a) devitrification of volcanic ash, along with enrichment in Mg by reaction with sea water or hydrothermal fluids, or (b) direct precipitation from seawater or hydrothermal fluids. The low Cr and Ni contents of SCGG possibly indicate direct precipitation of clay rather than by hydrothermal alteration of altered volcanic detritus. The silica could be precipitated or detrital. The high Zr content of SCGG possibly suggests a detrital zircon (and hence quartz) component.

The protolith of SCGG is considered to have been either chloritised andesitic-rhyodacitic volcanics/volcaniclastics or a mixture of detrital or precipitated silica and Al-Mg clay minerals (such as the fibrous magnesian clays - palygorskite, attapulgite or sepiolite, or Mg-rich smectite). Modern clays rich in palygorskite, attapulgite and sepiolite and zeolites such as phillipsite and clinoptilite have been reported from the Atlantic ridge and abyssal plain by Hathaway and Sachs (1965), Bonatti and Joensuu (1968) and Bowles et al. (1971) and the Mariana trough and arc-trench system in

the Pacific (Stonecipher 1978; Desprairies 1982; Natland & Mahoney 1982).

4.3.3 Fe-rich Grey Gneiss

FRGG presents similar problems in deducing its protolith as QRIB, ARIB and SCGG. It has similarities with a wide variety of lithologies: low-Si GG (Figs 4.1b, 4.9b, 4.10ab), HGF1 (Fig. 4.9a), HGN (Fig. 4.11a), QPIB (Figs 4.9a, 4.10b), and QRIB (Figs 4.9b, 4.11b).

The association of FRGG with high-Fe HGF1 gneiss is thought to be significant. If FRGG were derived by alteration of HGF1, substantial loss of Ti, Mn, Mg, Ca, Cr, Nb, V and Y and addition of Si and K would have been required. FRGG could be a siliceous closed-system differentiate of HGF1, e.g. an icelandite (Gill 1981) or oceanic andesite (Hekinian 1982). However the extreme Fe content and low Ti and Ca indicate that FRGG could not have been unaltered igneous rock. FRGG could be an Fe-enriched type of low-Si GG, e.g. Fe-rich volcaniclastic sediment. If FRGG has a sedimentary origin, the low Ti and V indicate the Fe-enrichment could not have been in the form of detrital iron oxide, but more likely as an Fe-rich clay (e.g. nontronite, Fe-saponite or Fe-beidellite). FRGG could therefore be the Fe-rich equivalent of ARIB and QRIB.

It is thought that FRGG possibly represents a semipelitic sediment of mixed intermediate (andesitic) and mafic source with significant Fe (in the form of Fe-rich clay) derived ultimately from alteration of HGF1, via altered volcanic detritus or hydrothermal fluids. The Fe-rich clay could be a direct precipitate. Hydrothermal Fe-rich clay is common in oceanic sediments (Weaver & Pollard 1973), for example nontronite in the East Pacific rise (Hekinian et al. 1980) and Fe-saponite and beidellite in the Marianna trough (Desprairies 1982). The main alternative is that FRGG is an Fe-enriched altered andesite.

4.4 DISCUSSION - THE ORIGINAL NATURE OF THE PLAGIOCLASE-RICH GNEISSES

4.4.1 Anorthosite-metagabbro Suite

Previous workers have suggested that the Selebi-Phikwe anorthosites (Hor 1972; Wakefield 1974; Wright 1977) are metamorphosed plagioclase-rich layered igneous rocks. The anorthosites in the Messina area (Hor et al. 1975; Barton et al. 1979a; Windley et al.

1981) are typical of Archaean high-grade anorthosite complexes of igneous origin. The occurrence of thin chromite and magnetite seams within the Messina anorthosites would appear to put an igneous origin beyond doubt. However at Selebi-Phikwe a sedimentary origin for the anorthosites (and the rest of the Selebi-Phikwe gneisses) has been preferred recently (Gallon 1986a,b). Gallon has grouped together the typical anorthositic gneiss and mineralogically similar, finer grained, highly banded calc -silicate gneiss. The main point of further geochemical analysis of the anorthositic gneisses in this thesis was initially to compare the geochemistries of these two lithologies.

The good trends on the ACM diagram (Fig. 4.12b) and for Al v. Mg (Fig. 4.13) suggest that the composition of the anorthositic-metagabbroic suite is a refection of original variable proportions of cumulus plagioclase and a Ca-Mg phase, i.e. clinopyroxene. A good linear plot of increasing Fe with Mg (not figured) indicates that magnetite was a not a significant cumulus phase. A linear but more diffuse trend of increasing Ca with Al (not figured) indicates that olivine and orthopyroxene were not significant phases, and that Ca was mobile during metamorphism. The trend on the AFM diagram (Fig. 4.12a) is not a calc-alkaline trend (see Windley 1977 for a contrasting conclusion for the Fiskenaesset Complex). It merely represents the original variation in proportion of calcic plagioclase (with Na and minor K) to a single magnesium phase (clinopyroxene with negligible Na and K) (see Myers 1975).

The anorthositic-metagabbroic suite at Selebi-Phikwe is concluded to be plagioclase-rich, plagioclase-clinopyroxene cumulates. A similar conclusion was eventually made for the anorthositic to gabbroic cumulates of the Fiskenaesset Complex (Weaver et al. 1981), although it had previously been considered that hornblende had possibly been a cumulus phase (Steele et al. 1977). Estimates of the original cumulus mineral compositions can be made from Figures 4.12b and 4.13. The plagioclase was a bytownite-calcic labradorite (An 76-68). The clinopyroxene, indicated by the Lethlakane clinopyroxenite, was a subcalcic ferroaugite with approximately 11.3 wt% CaO and 18.2 wt% MgO. It is not known whether the range of plagioclase compositions is due to metasomatism or original cryptic variation.

The metamorphism appears to have been largely isochemical. Some redistribution of Ca took place during the breakdown and recrystallisation of igneous plagioclase and clinopyroxene, particu-

larly loss of Ca in the monomineralic anorthosites (Fig. 4.12b). Although a wide range of metamorphic plagioclase compositions was produced, the metamorphic plagioclase generally has a slightly lower Ca content to that proposed for the original igneous plagioclase. The metamorphic (M1p) clinopyroxene (salite) had a higher Ca content than the proposed igneous clinopyroxene.

Barton et al. (1979a) suggested that the less calcic nature of plagioclase in hornblende anorthosites at Messina, compared to pure anorthosite, was due to the formation of secondary hornblende at the expense of the anorthite component of plagioclase. In the Fiskenaesset complex a similar relationship has been attributed to transfer of Na from amphibole (some of which has been regarded as premetamorphic, Steele et al. 1977) to plagioclase during metamorphism (Windley et al. 1981). At Selebi-Phikwe it can be seen that the formation of the M1p metamorphic assemblage of lower-Ca plagioclase and higher-Ca salite is the control on the mineralogy of the M1m plagioclase-hornblende assemblage. Much of the Si in the quartz-rich anorthosites was derived by the breakdown of metamorphic (M1p) salite to form calcic amphibole.

The interpretation of the mylonite sections is complex. The original nature of the mylonite bands is not known (Are they simply the result of shearing and metasomatism of anorthosite or do they represent mylonitised intrusive bands at the site of shearing ?). It is thought that at least some of the chemical changes from anorthosite to mylonite are the result of processes during shearing. D1 shearing has possibly resulted in significant enrichment of Ti, P, Ce, Nb, Y and Zr in Section A. This enrichment is thought to be due to addition from metasomatic shear-zone fluids, rather than concentration as residual immobile elements during depletion of Mg, Cr and Na. In the case of section B, either D1 shearing was highly variable in its effects or D2 shearing has redistributed the effects of D1 shearing.

The anorthositic-metagabbroic suite at Selebi-Phikwe is essentially the same as that in the Messina area in terms of major and trace elements. Barton et al. (1979a) have modelled the major element composition of the Messina Layered Intrusion magma using plagioclase and olivine fractionation trends. They have not accounted for clinopyroxene fractionation. Their data can be reinterpreted in terms of plagioclase (An 70), clinopyroxene and only minor, if any, olivine fractionation. Olivine was not a significant

cumulus mineral in the Messina anorthosites and gabbros.

The inclusion by Barton et al. (1979a) of all ultramafic rocks in the Messina area within the anorthositic Messina Layered Intrusion suite is questionable. The majority of the ultramafic lenses in the Messina area are spatially unrelated to the anorthosites. No ultramafic rock occurs within the Messina anorthosites. The juxtaposition of ultramafic rocks to the anorthosites is possibly tectonic. At Selebi-Phikwe, the only ultramafic rocks that are considered to be both comagmatic and coeval with the anorthosites are the Lethlakane clinopyroxenites.

The origin of the anorthosite-metagabbro suite as plagioclase (An 76-62) - subcalcic ferroaugite cumulates can be related to the evolution of the high-Ca hornblende gneiss. Cumulus plagioclase (approx. An 70) and low-Ca clinopyroxene are the phases that are thought to have controlled the evolution of HGF1 from HGC (see 4.2.5). It is interesting to note that the average composition (20.8 wt% Al_2O_3 and 6.3 wt% MgO) of the unaltered anorthosite-metagabbro-clinopyroxenite suite (average of Table 4.6-A,B & D weighted by number of samples) is very similar (Fig. 4.13) to the cumulus product (20.6 wt% Al_2O_3 and 6.6 wt% MgO) of the fractional crystallisation of plagioclase and clinopyroxene in HGC in the proposed proportion of 7:4 (see 4.2.5). It is therefore suggested that the anorthosite-metagabbroic suite were the cumulates produced during the low-pressure crystal fractionation of plagioclase plus lesser low-Ca clinopyroxene in the evolution of HGF1 from HGC (Figs 4.7, 4.8 & 4.13). The deformed mafic dykes cutting the anorthosites are thought to be the evolved liquids from further low-pressure crystal fractionation of low-Ca clinopyroxene and magnetite (producing HGF2) in evolved HGF1.

4.4.2 Hornblende-bearing Calc-silicate Gneiss

CSG is chemically similar to the quartz-rich anorthosites and the mylonite bands within the anorthosites. The morphology and textures of the lithologies are the main difference between them (see Ch. 3.4). The high Ca and Si of CSG are such that it could not be unaltered igneous rock. The highly variable quartz content but constant Ca/Al ratio (Fig.4.12b) suggest a sedimentary detrital origin or variable silicification. CSG could have been a mixture of detrital calcic plagioclase and quartz (although there is an excess of Ca). A more likely protolith is thought to be siliceous or

silicified calcareous argillite (although the K content is low). The possible occurrence of scapolite, the Al, Ca, Na and Sr (I.West, pers. comm. 1987) contents of CSG suggest an evaporitic component (cf. Ramsay & Davidson 1970).

4.4.3 Garnetiferous Quartz-feldspar Granulite

A sedimentary origin of GQFG is suggested by its local gradation into quartzite, minor sillimanite laminae, and chemically similar plagioclase quartzites (Table 4.9-A) elsewhere in the section. The major element chemistry of GQFG is essentially that of sodic sandstones (Marston 1978). The high Mn content is similar to that of some arkoses (Pettijohn 1963). The very high but eratic contents of Nb and Y could indicate detrital heavy minerals, such as sphene, garnet, rutile and apatite.

In terms of Si and Ca-Na-K (Fig. 4.9b), GQFG is a quartz keratophyre or trondhjemite (O'Connor 1965). GQFG is chemically similar to some volcanic rocks, e.g. high-Si dacites of Fiji (Gill & Stork 1979). These have the added similarity of high but variable Y contents (up to 560 ppm), although with very low Nb contents (<2ppm). The sodic plagioclase plus quartz mineralogy also suggests a keratophyre. The high-Na, relatively low-K character is possibly the result of low-temperature hydrothermal alteration of intermediate to siliceous lava involving seawater (cf. Amstutz 1974). However Coleman and Donato (1979) regard some keratophyres in ophiolitic sequences as being the volcanic equivalents of ophiolitic plagiogranite. CQFG (574) (p.A.14) has the approximate major element composition of plagiogranite (Coleman & Donato 1979). For example the relatively high Fe content indicates that 574 follows a tholeiitic rather than calc-alkali trend (Fig. 4.9a). The high Y content (401 ppm) is hard to explain. The field relations of 574 are worth noting. Sodic plagioclase-quartz gneiss with minor garnet is conspicuous in Unit B, interbanded with hornblende gneiss (interpreted as tholeiitic basalt). Quartzite and the semipelitic alteration products of basalt weathering (QPIB, QRIB & ARIB) are the other main components of Unit B. This suggests a volcanogenic origin for GQFG, along with the extrusion of basalt. Keratophyre may occur within basalt in ophiolite complexes as small plugs, parallel dykes or flows (Coleman & Donato 1979). An alternative explanation for the intimate nature of GQFG and hornblende gneiss in Unit B is partial melting of basalt. Helz (1976) found that melting of tholeiite at PH2O=5 kbar produced quartzo-

feldspathic liquids of tonalite to trondhjemite composition (i.e. similar to GQFG). The occurrence of CGGH (containing coarse garnet plus hornblende, cordierite, biotite and pyrrhotite) within the more typical hornblende gneiss of Unit B possibly supports an anatectic origin of GQFG. CGHG could be the residue of partial melting of hornblende gneiss (cf. Winkler 1979). (The main alternative for CGHG is that it is metamorphosed hydrothermally altered tholeiitic basalt.) However once again the high Y (and low Ti) content of 574 is hard to explain. The high Y and Nb contents of GQFG can possibly be equated with the high Y and Nb in some garnetiferous pegmatites (Deer et al. 1966, Condie 1981).

Diverse protoliths are possibly represented by garnetiferous sodic plagioclase-quartz gneiss. One (574) is intimately associated with hornblende gneiss (basalt) in Unit B, whereas the other (30-7-4) is associated with CSG in a sedimentary unit.

The origin of garnetiferous quartz-plagioclase granulite remains unsolved. Although a minor component of the Selebi-Phikwe gneisses, similar garnetiferous quartz-sodic plagioclase gneiss is volumetrically significant in the gneisses of the Messina area. Their origin has been suggested to be: argillaceous fedspar-rich arkose (Brandl 1983); sedimentary/volcano-sedimentary (Fripp et al. 1979); metamorphic high-pressure anatectic melt derived from pelite (Fripp 1983); or an acid intrusive phase associated with the anorthosite-metagabbro suite (Watkeys et al. 1983).

4.5 DISCUSSION - THE ORIGINAL NATURE OF THE QUARTZITES

The thin quartz bands associated with hornblende gneiss possibly represent metamorphosed cherts, although it is virtually impossible to distinguish these from deformed early quartz veins. The oligoclase-sillimanite quartzite is most easily explained as a metamorph-osed feldspathic argillaceous sandstone. It is also possible however that the high Si is not due to detrital quartz, but could be due to silicification. The Na content of albite-sillimanite quartzite might also indicate an evaporitic component (although no scapolite was positively identified). The mineralogy of the albite-sillimanite quartzites shows similarities to the finely laminated quartz-albite-(± sulphide) rocks associated with mineralised komatiites in the Yilgarn Block. The latter have been interpreted as mixed volcaniclastic/exhalative metasediments (Groves et al. 1978). The Selebi-Phikwe quartzites are typically massive to weakly banded.

The finely laminated pyrrhotite-sillimanite quartzite of Unit B is similar to some of the sulphidic sediments at Kambalda (Bavinton 1981; Paterson et al. 1984). The fine pyrrhotite laminations are thought to indicate precipitation of sulphide during exhalative hydrothermal activity, with some Cu and Ni derived by hydrothermal leaching of basalt. Alternatively the sulphide could have been diagenetic or mobilised during regional tectono-metamorphism.

The weakly banded albite-sillimanite quartzites are tentatively regarded as having been (silicified ?) volcaniclastic argillites or tuffs. The finely laminated quartzites with sillimanite and sulphide indicate mixed volcaniclastic and exhalative components. Thin quartz bands could be metamorphosed cherts. Unlike the Messina area, there are no thick orthoquartzites at Selebi-Phikwe.

The Fe content of the typical finely laminated magnetite quartzite of the Dikolti-Lentswe unit is too low to regard them as Algoma-type banded iron formation. However their origin is thought to be similar (i.e. as the metamorphic products of chemically precipitated silica-iron oxide sediments, Klein 1973). The relatively high Ni and Cu in the magnetite quartzite could have been leached from mafic-ultramafic rocks and precipitated. However it is also possible that Ni and Cu were metasomatically mobilised from adjacent ultramafic rocks during regional tectonometamorphism. The rare instances of minor Ni-Cu enrichment in grey gneisses immediately adjacent to massive Ni-Cu sulphides at Selebi-Phikwe suggest that the Ni and Cu in the magnetite quartzites was probably precipitated during the hydrothermal exhalative activity. The original nature of the magnetite quartzites is intimately related to that of the cummingtonite and tremolite amphibolites with which they are interbanded. The origin of these amphibolites is discussed in Chapter 8, because of their similarities to the adjacent Dikoloti-Lentswe ultramafic rocks hosting Ni-Cu sulphides. It is tentatively concluded in Chapter 8 that the protoliths of the cummingtonite and tremolite amphibolites were various mixtures of Mg,Fe-rich, Al-poor clays and carbonate, which were intimately associated with chemically precipitated silica-iron oxide sediments. They are not thought to be derived from, or related to, the Dikoloti-Lentswe ultramafic rocks.

4.6 DISCUSSION - THE ORIGIN OF THE GRANITIC GNEISS

In terms of Si and (Ca-Na-K, Fig. 4.9b), the porphyroblastic granite gneiss is granite (Barker 1979) and the thin granite gneiss

bands within the Selebi-Phikwe gneiss are granite-quartz monzonite (O'Connor 1965). There is very little chemical variation in the three porphyroblastic granite gneiss samples (Table 4.10-A), which were taken from widely spaced locations (the Phikwe section, the intrusive body north of Phikwe, and near Tobane, Fig. 2.1). The low variation in the K content and the ubiquitous occurrence of microcline porphyroblasts suggest that the porphyoblastic nature is not due to late K-metasomatism.

The dioritic phase of the porphyroblastic granite gneiss suite is particularly Fe-rich (Table 4.10-B). It is chemically similar to ferrodiorites that are part of a late Fe-rich intrusive suite within the Amitsoq gneiss of West Greenland (Nutman et al. 1984). The quartz -sodic plagioclase and quartz-microcline veinlets cutting the porphyroblastic granite gneiss (and as a minor phase throughout the Selebi-Phikwe gneisses) are late tonalitic and granitic minimum melts (Winkler 1979).

In Chapters 2 and 3, it was concluded on morphological, mineralogical and textural grounds that the porphyroblastic granite gneiss suite is a weakly deformed granitic intrusive suite (cf.Wright 1977), intruded mainly between D1 and D2 and during D2, rather than a previously deformed and metamorphosed basement to the Selebi-Phikwe gneisses (Wakefield 1974; Key et al. 1976), or a thick meta-arkose unit (Gallon 1986). The limited geochemistry supports an intrusive granite origin. The genetic relationship of the ferrodiorite to the porphyroblastic granite is not known. The ferrodiorite magma could have been coeval with the granite magma (e.g. as an immiscible phase which separated from a felsic magma, cf. Wiebe 1979), or the ferro-diorite could have been incorporated into the granite magma (e.g. as contaminated highly evolved residual liquid of the tholeiitic rocks, or as partially digested hornblende gneiss inclusions).

4.7 FURTHER DISCUSSION AND SUMMARY OF CONCLUSIONS

4.7.1 High-Ca Hornblende Gneiss - Intrusive or Extrusive ?

There are no original textures remaining in the highly metamorphosed and deformed high-Ca hornblende gneiss (high-Ca HG). Therefore it is impossible to conclude unequivocally that high-Ca HG was either intrusive or extrusive. However it is thought that rock-associations can be used to give an insight into the original nature of these tholeiitic rocks.

The intimate association of HGG with variable diopside gneiss and minor QPIB and QRIB suggest that HGG were submarine lava flows.

The intimate interbanding of high-Ca HG with quartzite (metacherts ?), QRIB (and in the case of Unit B, also with QPIB, ARIB and CGHG) indicates that the protoliths of the high-Ca hornblende gneiss of Units A and B were possibly extrusive.

Unit E is dominated by grey gneiss. The relatively thin high-Ca HG bands occur within the grey gneiss without any other associated rocks (i.e. without quartzites, QRIB, ARIB, diopside gneiss etc.). It is concluded that the high-Ca HG of Unit E are more likely to have been high-level intrusives (i.e. dykes or sills) than extrusives. This is supported by the occurrence of the differentiated HGN1 basalt layer (sill ?) in Unit E. (The degree of flattening suffered by the Selebi-Phikwe gneisses means that the recognition of the crosscutting nature of dykes is very difficult and impossible in core sections.)

The interbanding of high-Ca HG in Unit F with QPIB and grey gneiss including SCGG indicates that some high-Ca HG in Unit F may have been extrusive. When compared to Units A and B, however, the quantity of basalt-derived volcaniclastic-pelitic rocks is much less in Unit F. It is therefore concluded that some of the high-Ca HG in Unit F may also have been high-level intrusives. This is supported by the ocurrence of the differentiated HGG layer (sill ?) in Unit F.

The thickest occurrence of high-Ca hornblende gneiss is in Unit D, which consists of a variety of interbanded high-Ca hornblende gneiss, but particularly of Fe-rich HGF1 and HGF2. Bands of grey gneiss including FRGG are only a very minor component of Unit D. Another minor but significant component of Unit D is ultramafic rock (mainly bands of metamorphosed clinopyroxene-olivine cumulate). No bands of quartzite, diopside gneiss or intermediate biotite gneiss were noted in Unit D. It is tentatively concluded that Unit D is more likely to have been an intrusive unit.

It is concluded that the high-Ca hornblende gneiss represent both extrusive tholeiitic basalts and their high-level intrusive equivalents.

4.7.2 The Origin of the Geochemical Variation within the High-Ca Hornblende Gneiss Suite

The range of high-Ca hornblende gneiss compositions, from HGN1 via HGG and HGC to HGF1, exhibits a marked tholeiitic Fe-enrichment fractionation trend (Figs 4.1 & 4.4). This is accompanied by

pronounced enrichment in Ti, P, S, Nb, V, Y and Zr, an increase in Cu/Ni, and depletion in Mg, Cr and Ni. This suggests that the Selebi-Phikwe high-Ca hornblende gneisses represent a comagmatic suite of fractionated basalts. However some of the differences could be due to alteration rather than to original igneous processes. Alternatively the various types of hornblende gneiss could be unrelated, e.g. products of separate partial melting events in the mantle.

4.7.2a The problem of alteration

In terms of virtually all analysed major and trace elements, HGN1 is similar to the most common volcanic rock in greenstone belts, a tholeiitic basalt (Table 4.11-A; Condie 1976, 1981). The only elements that are significantly different are Ca and Cu which are lower in HGN1 and K and Rb which are higher. HGC compares remarkably well with a modern ferrobasalt from the Galapagos spreading centre (Anderson et al. 1975; Table 4.11 -C). As in the comparison of HGN1 with typical Archaean tholeiite, the Ca content of HGC is lower and the K content is higher than that of the ferrobasalt example. These differences in Ca and K content could be fundamental (i.e. due to igneous processes) or imposed (e.g. due to alteration). Alteration would have begun immediately after emplacement and would have proceeded gradually to a condition controlled by regional metamorphism. The high metamorphic grade of the Selebi-Phikwe gneisses means that it is not possible to conclude whether any alteration occured before or during regional metamorphism. The limitation of the differences to minor loss of Ca and increase in K (Fig 4.3) is consistent with the geochemical changes that take place during regional metamorphic transition of gabbroic rocks to amphibolites at upper amphibolite to hornblende granulite facies (Elliott 1973; Field & Elliott 1974).

In terms of Ti, Al, and Mg, HGG is similar to the second most common type of Archaean tholeiitic basalt (Table 4.11-B). HGG has however lower contents of Si and Cr and higher contents of Fe and P. Comparisons of HGG with HGN1 and HGC indicate that HGG is relatively enriched in Fe, Na and P and depleted in Si and Cr. In terms of Si and (Na & K), HGG is an alkali basalt (Macdonald & Katsura 1964). It has been suggested that the interbanding of HGG-type hornblende gneiss with diopsidic gneiss in Unit G possibly indicates an extrusive origin for the hornblende gneiss. Some of the differences between HGG and HGN1-HGC could be the result of original igneous processes (e.g. higher Ti, Nb, V, Y and Zr and lower Mg in HGG than

in less-fractionated HGN1, see Ch. 4.7.2b). The differences in Fe, Na, P and Si however are the same as the relative changes that take place in basalt undergoing low-temperature submarine alteration (Miyashiro et al. 1969; Hart 1970; Shido et al. 1974; Aumento et al. 1976; Scott & Hajash 1976; Smith et al. 1984) and higher temperature spilitisation (Cann 1970; Pearce & Cann 1973; Hart et al. 1974; Floyd & Winchester 1975). None of the assemblages in the gneisses of Unit G postdates the main M1b metamorphic fabric. Post-M1 alteration (Condie et al. 1977; Condie 1981) can therefore be ruled out. Submarine alteration would be consistent with the suggested extrusive origin for HGG and the original nature concluded for the diopside gneiss (see Ch. 4.2.2). (This is a somewhat circular arguement because it has been proposed that the protoliths of the diopsidic gneiss resulted from high degrees of submarine alteration of HGG-type extrusive basalts. The main evidence for an extrusive origin is the intimate interbanding with lithologies of possible sedimentary origin.)

It is suggested that the the alkali character of HGG is due to alteration and that the geochemistry of HGG is consistent with submarine alteration of a slightly fractionated type of HGN1. It is also suggested the geochemistry of HGGX (Table 4.5-D) represents extreme submarine alteration that resulted in very high contents of Fe, Mn, P, Nb, Rb, Y and Zr and lower Al, Mg, Ca, Na, Cr, Ni, Sr and V and K/Rb. Ti was unaffected. The difference in behaviour of Na (addition in moderate alteration, depletion in extreme alteration) could be due to higher temperatures and higher water/rock mass ratios in the extreme alteration (Seyfried & Bischoff 1977, 1979). The low K/Rb ratio of HGGX and the trend of Rb-enrichment in the HGG rocks indicates significant enrichment in Rb relative to K. Similar Rb and K contents and low K/Rb ratios due to preferential absorbtion of Rb by smectite have been found in highly altered submarine basalts (Dasch 1973; Menzies & Seyfried 1979). It is interesting to note that cumulate-enriched HGN2 and HGFF2 (see Ch. 4.2.1c) have the highest K/Rb ratios of the hornblende gneiss suite (see Ch. 8.6.5).

The very high contents of Y (75 ppm) and Zr 272 ppm) in HGGX indicate that Y and Zr can not be unquestionably treated as immobile elements in high-Ca hornblende gneiss. The high Y and Zr contents are thought to represent addition of Y and Zr, rather than concentration by removal of other elements. This possibly explains why there is a wide variation in Ti/Zr ratios (HGN1-77, HGN2-110, HGG-92, HGGX-35, HGC-94, HGF1-102, QPIB-60) and Zr/Y ratios (HGN1-2.85, HGN2-2.24,

HGG-3.71, HGGX-3.63, HGC-3.49, HGF1-3.60, QPIB-2.51) (cf. Sun et al. 1979).

It is concluded that the extrusive and intrusive tholeiitic basalts, ferrobasalts, cumulate-enriched tholeiitic basalts and tholeiitic volcaniclastics (?) represented by high-Ca hornblende (and intermediate) gneiss have suffered various degrees of alteration, some of which can be attributed to early submarine alteration of extrusive basalt and some to regional metamorphism. HGG is thought to represent extrusive basalt that has suffered submarine alteration, during which Ti was relatively immobile and Y and Zr were enriched. The slight alteration that is thought to hav been suffered by HGN1, HGC, and HGF1 (and HGN2, HGF2 and D) is consistent with alteration during regional metamorphism. An alternative explanation for the apparently little altered nature of high-Ca HG in Unit E is that if the grey gneiss protoliths were rapidly deposited volcaniclastic sediments (e.g. debris flows), extensive submarine alteration of basalt lava may have been suppressed by rapid burial.

4.7.2b The comagmatic nature of the high-Ca HG suite

The range of compositions shown by the Selebi-Phikwe high-Ca hornblende gneiss is similar to that of the basalts of the Galapagos Spreading Centre (Clague & Bunch 1976). Clague and Bunch modelled the evolution of the Galapagos basalts in terms of low-pressure, closed system crystal fractionation of olivine (Fo 86), plagioclase (An 71-68) and augite in a single parent magma with the same Ti and Mg contents as HGN1. (HGN1 has slightly higher Fe and lower Al.) Evolved basalt similar to HGG was produced after 34% crystallisation, basalt similar to HGC required about 58% crystallisation and basalt similar to HGF1 required about 68% crystallisation (5% olivine, 36% plagioclase and 27% clinopyroxene).

The two-element variation diagrams (Figs 4.7 & 4.8) indicate that the evolution of HGC form HGN1 was controlled by crystal fractionation of plagioclase, augite and olivine (and possibly orthopyroxene) in the proportions 7:5:1. Further evidence of low-pressure crystal fractionation is provided by the differentiated HGN1-HGN1 and HGF1-HGN2 layers. HGN2 is thought to be HGN1 and HGG tholeiitic basalt enriched in cumulus clinopyroxene and olivine. Further evolution of HGF1 from HGC was controlled by plagioclase and low-Ca clinopyroxene in the proportion of 7:4. The evolution-path of HGN1 to HGG, the nature of HGN2 and the nature of the dominant type

of ultramafic rock in Unit D indicate the relatively early crystallisation of clinopyroxene and that clinopyroxene rapidly joined plagioclase on the liquidus following olivine.

Calculations using Figures 4.7 and 4.8 and the partition coefficients of Pearce and Norry (1979) for Ti (considered to be relatively immobile in Ch. 4.2.1d) and assuming closed system crystal fractionation of olivine (Fo 86), plagioclase (An 75) and clinopyroxene (En37.5 Wo25 Fs37.5) indicate that HGC would have required about 66% crystallisation of HGN1 (5% olivine, 33% plagioclase and 28% clinopyroxene) and that HGF1 would have required about 75% crystallisation of HGN1 (5% olivine, 39% plagioclase and 31% clinopyroxene). Significantly lower degrees of fractionation result using the Nb, Y and Zr contents (i.e. 60% crystallisation for HGF1 using Y and 62% using Zr). This is thought to be due to their mobility relative to Ti during alteration (see 4.2.1d). These discrepancies mean that the use of more detailed fractionation models (cf. Stern 1979) would not be worthwhile. The mineral compositions were estimated from the variation diagrams and are consistent with the melting experiments of Bender et al. (1978) and Walker et al. (1979).

HGG is thought to be an evolved type of HGN1 (higher Ti, P, Nb, Y and Zr and lower Mg, Cr and Ni) which has suffered significant submarine alteration, resulting in higher contents of Fe, (P) and Na, and lower Si, K and (Cr). Because of the alteration suffered by HGG it is not clear whether HGG represents a higher degree of early olivine fractionation in HGN1 or whether HGG is simply an altered intermediate product of HGN1-HGC plagioclase-clinopyroxene-olivine crystal fractionation (see Figs 4.7 & 4.8).

Significant titanomagnetite would have started to crystallise when the Ti content in evolved HGF1 reached about 3.3 wt% TiO2 (the highest Ti content in HGF1, cf. Wager 1960, Wager & Brown 1968, Hunter & Sparks 1987, for the onset of crystallisation of magnetite in the Skaergaard intrusion, the textbook example of closed-system fractional crystallisation of basalt). Crystal fractionation of low-Ca clinopyroxene and titanomagnetite in HGF1 would have resulted in cumulus-enriched HGF2 and liquid of the composition of the dykes cutting the anorthositic-gabbroic suite (D, Figs 4.7 & 4.8).

The numbers of analysed samples of the different types of high-Ca hornblende gneiss (total = 37) are HGN1-9, HGN2-3, HGG-5, HGC-6, HGF1-7, HGF2-4, D-3. Attempts were made to make the sampled and analysed suites representative, although inevitably it is

slightly biassed towards minor types (e.g. D within anorthosite). The proportions of analysed samples indicates that the fractionated ferrobasalts are not a minor component of the basalt suite. HGF (HGF1 + HGF2) represents about 30% of the analysed suite. This is generally consistent with the modelling in which HGF1 results from continued crystal fractionation of HGC after about 66% crystallisation of HGN1 has already taken place.

There are no proven komatiites in the Selebi-Phikwe gneiss. The most primitive magma at Selebi-Phikwe appears to have been HGN1 and there seems to have been no primary magma variation component (cf. Pearce & Flower 1977). The differentiated HGN1 body (see Ch. 4.2.1b) is important because it shows that the range of HGN1 compositions are not just the cumulus olivine and plagioclase enriched-liquids of crystal fractionation in a tholeiite with a high Ti (c. 1.5 wt% TiO2) content. Instead, diffentiated HGN1 layer indicates that the range of HGN1 compositions represents the range of both evolved liquids and cumulus olivine and plagioclase-enriched liquids, produced by low-pressure crystal fractionation of olivine, plagioclase and clinopyroxene in HGN1 basalt with a TiO2 content of <1 wt% (c. 0.6-1.0 wt% TiO2). A reasonable estimate for the primary Selebi-Phikwe basalt (HGN1P) is 0.8 wt% TiO2, 14.9 wt% Al2O3 and 8 wt% MgO (Mg number = 45).

Walker et al. (1979) and Bender et al. (1978) disagree whether high-FeTi basalts could result from low-presssure crystal fractionation of a single parent in a magma chamber without replenishment or would require replenishment and mixing of magma (possibly of different-percentage partial melts from a single source) in an open magma chamber. The early crystallisation of clinopyroxene possibly indicates that the magma system was relatively closed (Walker et al. 1979). However Pallister & Gregory (1983) suggested that the nearly simultaneous appearance of clinopyroxene and plagioclase on the liquidus following olivine is a feature of repeatedly replenished systems. The conclusion in Chapter 4.2.1d, 4.2.2 and 4.7.1 that some of the high-Ca hornblende gneiss (HGG) was extrusive, indicates that the Selebi-Phikwe magma system was at least open to eruption. It is likely, therefore, that some replenishment also took place (see Ch. 8.6.9).

An important feature of the evolution of the Selebi-Phikwe basalts is the increase in the S content and Cu/(Cu+Ni) ratio going from HGN1 to HGF1 (Fig. 4.8, Tables 4.1 & 8.8). The possible

relevance of this to the formation of the Selebi-Phikwe and Dikoloti-Lentswe Ni-Cu sulphide deposits is discussed in Chapter 8.6.9.

It is concluded that there is a tholeiitic FeTi-enrichment series from HGN1 to HGF1, via HGG and HGC. It is thought that although various types of alteration have modified the high-Ca hornblende gneiss chemistry, alteration would not have produced the consistent chemical trends (see Figs 4.7 & 4.8). It is concluded that that the series from HGN1 to HGF1 is a genetically related series, controlled by simple low-pressure fractional crystallisation. The evolution of the series from HGN1 to HGC is thought to be due to crystal fractionation (66% if in a closed-system) controlled by plagioclase, clinopyroxene and olivine in the proprtion 7:5:1 (Figs 4.7 & 4.8). (Mg-rich phase could also have been orthopyroxene.)

The evolution of HGF1 from HGC was controlled by plagioclase and lesser clinopyroxene fractionation (in the proportion of 7:4). HGF1 represents the evolved liquid resulting from about 75% crystal fractionation of HGN1 (if in a closed system). HGF2 is thought to represent evolved HGF1 magma, enriched in cumulus clinopyroxene and titanomagnetite. HGN2 is thought to be HGN1 and HGG tholeiitic basalt enriched in cumulus clinopyroxene and olivine. The nature of the main ultramafic cumulate in Unit D (i.e. clinopyroxene plus minor olivine) and the proportion of clinopyroxene-rich ultramafic cumulate to olivine (+opx.)-rich cumulate in Unit D is consistent with the proportion of clinopyroxene to olivine (5:1) calculated in the modelling of the evolution of HGC from HGN1. The olivine (+opx.)-rich cumulate is thought to have crystallised from primary HGN1, whereas the clinopyroxene-rich cumulate crystallised from evolved HGN1 and HGG. The order of crystallisation in HGN1 was early olivine (plus orthopyroxene ?) follwed by plagioclase and clinopyroxene. Plagioclase and clinopyroxene dominated the crystallisation.

It is thought that the proposed crystal fractionation took place at low pressure and shallow depth (cf. O'Hara 1977; Walker et al. 1979). There is no need to resort to high pressure fractionation (cf. Bender et al. 1978) or variable degrees of partial melting or mantle source heterogeneities (cf. Scheidegger 1973) to explain the compositional variation shown by the Selebi-Phikwe high-Ca hornblende gneiss. The development of highly evolved ferrobasalts at Selebi-Phikwe probably took place in a magma system that was periodically replenished.

4.7.2c The "stratigraphic" evolution of the high-Ca HG suite

The inferred way-up from the differentiated HGN1-HGN1 and HGN2-HGF1 layers indicates that the sequence of gneisses at Phikwe is the right way-up. There is a general increase in the proportion of fractionated basalt going up from Unit G to Unit A (particularly from Unit G to Unit D, see Table 4.4), although the trend is not clear. There are several reasons why a smooth trend would not be expected:

(a) Some of the basalts were intrusive and could have been intruded into earlier less-evolved basalts.

(b) The basalts may have been tapped from different portions of a fractionating magma chamber (e.g. some may be intercumulus liquid from crystal mush areas, whereas some may represent fractionated magma from the roof zone, cf. Siroky et al. 1985).

(c) Periodic magma replenishment probably took place in the Selebi-Phikwe magma system, with mixing of primary basalt with more evolved basalt. For example, Unit B contains less-evolved basalt than Unit D. Unit A contains evolved ferrobasalt. Major replenishment between Units D and B is indicated.

(e) More than one magma chamber possibly existed in the Selebi-Phikwe magma system.

(f) The sequence in Tables 2.1 and 4.4 is only a pseudostratigraphy. The possibility of unidentified D1 repetitions remains. The way-up evidence from the differentiated layers is also flimsy.

(g) Although it is thought that the Selebi-Phikwe basalts represent a single type of primary basaltic magma (HGN1P) and its low-pressure fractionation products, it is also possible that separate tholeiitic melts produced by different percentages of mantle melting could have formed the high-Ca hornblende gneiss suite.

4.7.3 The Tectonic Setting of the Selebi-Phikwe Basalts

The high-Ca hornblende gneiss suite is characterised by marked enrichment in Fe and Ti, but with little variation in Si content (cf. Miyashiro 1975). Marked Fe-Mg fractionation in tholeiitic suites can occur in a variety of crustal environments including island arc and continental margin suites, continental rifts, oceanic islands and to a lesser extent in oceanic crust at mid-ocean ridges and back-arc basins. Marked Ti-enrichment is not however typical of island arc or continental margin suites (Miyashiro 1975; Shervais 1982). In terms of Ni, Cr and V contents and Ti/Zr and Ti/V ratios the hornblende

gneiss suite is most like fractionated MORB and quite different to continental tholeiites and particularly island arc tholeiites (Pearce & Cann 1973; Pearce 1975; Condie 1976a; Rogers 1982; Rogers et al. 1984; Shervais 1982). The majority of the high-Ca hornblende gneiss falls in the plate margin fields (Pearce & Cann 1973) on the Ti-Zr-Y plot (Fig. 4.6b) and in the MORB field on the Ti-Zr-Sr plot (not figured). However it must be borne in mind that Zr and Y cannot be regarded as having been completely immobile during alteration and metamorphism (see Ch. 4.2.1). The hornblende gneiss suite has higher K contents than modern low-K tholeiites (including MORB) (Condie 1976a). This is thought to be due to alteration and the high-grade of metamorphism that has affected the Selebi-Phikwe rocks. The Selebi-Phikwe hornblende gneiss suite appears to lack the minor components of alkali basalts that commonly occur in oceanic island and continental rifts. HGG has an alkaline character due to its low Si content. However this is interpreted as being due to alteration.

Further evidence of the possible tectonic environment of the hornblende gneiss suite can be obtained by the lithological associations in which it occurs. Hornblende gneiss (HGG) is intimately associated with diopside gneiss in Unit G. The protoliths of the well-banded diopside gneiss were possibly pillow lavas. The chemistry of HGG is also comparable to tholeiitic basalt that has undergone submarine alteration. Hornblende gneiss is commonly associated (particularly in Units A and B) with QRIB and ARIB of the intermediate biotite gneiss suite and FRGG. The compositions of QRIB, ARIB and FRGG (and SCGG within grey gneiss) are characterised by relatively high Mg (or Fe in the case of FRGG). Their range of compositions are similar to the range in compositions of oceanic volcaniclastic/hydrothermal exhalative sediments (cf. Desprairies 1982). Other intermediate biotite gneisses, QPIB and GRHG, are thought to represent less altered tholeiitic volcaniclastics and <u>in situ</u> altered basalt. Hornblende gneiss is also associated with thin quartzites in Units A and B. The quartzites are interpreted as having been cherts and silicified aluminous sediments with a minor localised exhalative hydrothermal component. In contrast to the Messina area, there are no thick orthoquartzites or carbonates in the Selebi-Phikwe area. The above evidence indicates that some of the hornblende gneiss at Selebi-Phikwe was extrusive in a submarine (oceanic ?) environment.

It is tentatively concluded from the geochemistry and lithological associations that the hornblende gneiss suite has most

in common with fractionated oceanic basalts from a mid-ocean ridge or back-arc basin. The primary Selebi-Phikwe basalt (HGN1P) has similarities to primary MORB resulting from a high degree (25%) of mantle melting (cf. Sun et al. 1979), although the Mg content and Mg number of HGN1P is lower and the Fe content higher. This is possibly due to a general weak depletion of Mg in the high-Ca hornblende gneiss due to alteration, or a magmatic feature. These differences are in agreement with the observations of Gill (1979) and Condie (1981) that Archaean tholeiites typically have higher Fe contents and are more fractionated than MORB. Therefore caution should be applied when comparing the possible tectonic environments of formation of Archaean magmas with those of modern magmas. Gill and Bridgewater (1976), Gill (1979) and others have questioned the use of chemical parallels with modern volcanic suites to identify Archaean crustal environments, since modern magma chemistry reflects the attributes of the mantle source region, as much as crustal type. The problem of possible alteration of highly metamorphosed rocks exacerbates this situation.

Such fractionated tholeiitic suites as occur at Selebi-Phikwe (with the formation of Ti-rich ferrobasalt - HGF1) are not common in typical modern mid-ocean ridge basalts in the Atlantic, but do occur in fracture zones off the main spreading centre in the Atlantic (Shibata et al. 1979). They are more common in the Indian Ocean (Bryan & Moore 1976) and the East Pacific; for example the fractionated MORB suites of the East Pacific Rise (Kay et al. 1970; Scheidegger 1973; Clague & Bunch 1976); the Juan de Fuca Ridge (Clague & Bunch 1976; Vogt & Byerly 1976; Delaney et al. 1981); the Galapagos Spreading Centre (Anderson et al. 1975; Byerly et al. 1976); and the Galapagos Rise (Rhodes et al. 1976). High-FeTi basalts (along with alkali basalts) also occur in aseismic ridges (e.g. the Cocos and Carnegie Ridges, Hekinian 1982) and isolated oceanic islands and seamounts. The aseismic ridges and isolated oceanic islands are possibly "hot spots" generated by mantle plumes (Miyashiro 1975; Hekinian 1982).

A range of basalts from primitive basalts to highly evolved ferrobasalts also occurs in some ophiolitic complexes, including the Bay of Islands Complex in Newfoundland (Siroky et al. 1985), the Sariamento Complex in Chile (Saunders et al. 1979; Stern 1979) and the ophiolites of the Western Mediterranean, e.g. of the Northern Appenines (Ferrara et al. 1976) and Corsica (Beccaluva et al. 1977).

Serri (1980) has classified these ophiolites as high-Ti ophiolites, as compared to the low-Ti Troodos and Vourinos ophiolites (see also Sun & Nesbitt 1978).

The formation of highly fractionatated Ti-rich tholeiites in the East Pacific has commonly been regarded as being due to fast spreading rates (Nisbett & Pearce 1973) and the formation of relatively closed-system, unreplenished, rarely tapped magma chambers distal from the ridge axis (Clague & Bunch 1976; Delaney et al. 1981; Hey & Sinton 1979), whereas the less fractionated basalts of the Atlantic have been attributed to long-lived magma chambers undergoing repeated periodic replenishment (O'Hara 1977; Bryan et al. 1979; Walker et. al. 1979). Conversely however Flower (et al. 1977,1981), Pearce & Flower (1977) and Robson and Cann (1982) have suggested that slow-spreading ridges would be underlain by small, often semi-permanent magma chambers, whereas fast-spreading ridges would have a large permanent magma chamber.

A situation somewhat analogous to that in the Juan de Fuca Ridge of the East Pacific is envisaged in which maximum fractionation occurs in intermediate magma chambers of intermediate duration with periodic magma mixing. These magma chambers coexist with small short-lived magma chambers and long-term steady-state magma chambers with continual replenishment coexist (cf. Delaney et al. 1981).

Little geochemistry has been done of hornblende gneiss from elsewhere in the Limpopo Belt. The hornblende gneiss of the Messina area is chemically similar to HGN1, HGG and HGC and has been interpreted as basalts of intrusive and/or extrusive origin (Fripp 1983). Fripp has tentatively suggested that some of the hornblende gneiss, particularly that associated with quartzites, may be oceanic spreading-centre basalts (mid-ocean ridge or back-arc basin). He concluded that bands of slightly Fe-enriched basalt within pelitic gneiss were dykes, although no cross-cutting relationships were found. HGF1-type ferrobasalts have not been found in the Messina area. It remains to be seen whether ferrobasalts are a feature of the Selebi-Phikwe area alone.

4.7.4 Partial Melting

The maximum pressure and temperature conditions during M1a of 10 kbar and 800°C suggest that partial melts may have formed in the Selebi-Phikwe gneisses (Winkler 1979). Within the Selebi-Phikwe region, areas of migmatitic gneiss (see Ch.2.2 & 2.3.2) suggest that

partial melting was locally significant. At Selebi-Phikwe minor coarse leucocratic bands occur in the grey gneiss and intermediate biotite gneiss and are interpreted as partial melts. A biotite-rich band with corundum, cordierite and sillimanite possibly represents a residue from partial melting (cf. Green 1976). However thick sections of banded variable grey gneiss occur without leucocratic granitic or tonalitic segregations. It is proposed (see Ch. 3.12) that the grey gneisses at Selebi-Phikwe have not been significantly affected by partial melting and that they are essentially palaeosomes (Winkler 1979).

The amount of partial melting produced in melting experiments is suppressed by a lack of sufficient water (Winkler 1979). Also if a situation of inadequate amounts of water exists then the amount of partial melt produced is decreased by an increase in pressure. The temperature of the beginning of anatexis is increased by a higher An content of plagioclase in a gneiss and the amount of partial melting produced at any P and T is decreased by a lower alkali feldspar content (Winkler 1979). Loss on ignition analysis (LOI <0.7 wt%) of the grey gneiss suite suggests that the water content of the grey gneiss is low. Although rocks of the composition of grey gneiss (Ab/An 1.5) with 2% water would start to melt at about 700° C, temperatures in excess of 1000° C at 10kbar would be required for complete melting.

It is concluded that although some partial melting of grey gneiss and intermediate biotite gneiss precursors took place and locally produced significant migmatites, the amount of partial melting of grey and intermediate gneiss at Selebi-Phikwe was typically low, because of lack of sufficient water. Weakly deformed granite gneiss bands do occur in the grey gneiss. These are regarded as intrusive granites related to the porphyroblastic granite gneiss intruded between D1 and D2 and during D2 rather than *in situ* partial melts. These granites were possibly produced by anatexis of Selebi-Phikwe-type gneiss at greater depth during relatively isothermal decompression (Figs 3.3 & 3.4).

The mafic hornblende-bearing gneiss is typically devoid of leucocratic segregations and it can be concluded that partial melts have not formed in them. The exception is the hornblende gneiss in Unit B, which is associated with garnetiferous quartz-feldspar granulite. The origin of GQFG is a problem. Partial melting of high-Ca hornblende gneiss is a possibility. Helz (1973, 1976) found that

melting of tholeiite at PH2O=5 kbar produced liquids of tonalite to trondhjemite composition. CGHG bands (coarse garnet plus hornblende, cordierite, biotite and pyrrhotite) in the hornblende gneiss of Unit B could therefore be residues of partial melting, rather than representing hydrothermally altered basalt. It is possible that the presence of water was the controlling factor in the production of partial melts in Unit B. Ringwood (1977) has stressed the importance of water in generating more siliceous magmas from mafic rocks. The corundum-sapphirine-spinel aggregates in the Dikolti feldspathic amphibolite (see Chs 3.9 and 8.6.2) are also possible residues of partial melting (cf. Cartwright & Barnicoat 1986).

4.7.5 Summary of Conclusions

Conclusions as to the original nature of the Selebi-Phikwe gneisses have been made, based mainly on geochemistry (geochemical comparisons with known rock types), lithological associations, gross morphological features (e.g. banding) and minor textural evidence. The conclusions should all be viewed with caution. Geochemical comparisons can not provide unequivocal answers. Original field relations have been obliterated and original textures are absent. Given these caveats, the conclusions are made with a variety of degrees of confidence. Perhaps the most speculative conclusion is that the grey gneiss suite represents a relatively little altered, andesitic to rhyodacitic volcanic-sedimentary suite.

The main types of hornblende gneiss (HGN1, HGG, HGC & HGF1) are concluded to have been tholeiitic basalt and Ti-rich ferrobasalt. The basalts have suffered varying degess of alteration, some of which can be attributed to submarine alteration and some to regional metamorphism. The basalts now represented by high-Ca hornblende gneiss are thought, based on lithological associations and type of alteration and alteration products, to have been both submarine extrusives and high-level intrusives (dykes and sills). HGN2 and HGF2 were cumulus-enriched basalts. HGN2 formed by accumulation of clino-pyroxene and olivine in HGN1 and HGG. HGF2 formed by accumulation of titanomagnetite and clinopyroxene in HGF1. The range of chemical compositions of the suite of tholeiitic basalt, ferrobasalt and cumulus-enriched basalt is satisfactorarily explained by low-pressure crystal fractionation dominated by plagioclase and clinopyroxene. The order of crystallisation was olivine, (orthopyroxene), plagioclase,

clinopyroxene, titanomagnetite. The early crystallisation of clinopyroxene suugests that the Selebi-Phikwe magma system was a relatively closed system. The evolution of HGC from HGN1P was controlled by fractionation of plagioclase, clinopyroxene and olivine in the proportions 7:5:1 and required about 66% crystallisation. The evolution of HGF1 from HGC was controlled by fractionation of plagioclase and clinopyroxene in the proportion of 7:4 and required a further 25% crystalliation of HGC (75% total crystallisation of HGN1). The differentiated basalt layers (sills or flows) indicate that the Phikwe sequence is the right way-up. There is a general increase in the evolved nature of the basalt from Unit G at the base to Unit A at the top of the Phikwe sequence.

The typical grey gneiss suite represents a little-altered calc-alkaline suite, dominated by rocks of andesite and rhyodacitic composition. Due to their high variability (e.g. their banding and local concentration of garnet, sillimanite, cordierite, magnetite and corundum), the typical grey gneiss suite is thought to represent a volcanosedimentary suite of calc-alkaline affinity, rather than a tonalitic intrusive suite. The grey gneiss could be volcanics, volcaniclastic sediments, or a mixture of both. The calc-alkaline grey gneiss is thought to be unrelated to the tholeiitic hornblende gneiss suite.

The intermediate biotite gneiss plus the low-Ca hornblende gneiss, the siliceous cordierite-rich grey gneiss and magnetite-rich grey gneiss are thought to represent a variety of lithologies derived from the alteration of tholeiitic basalt. They possibly span a range from in situ alteration to volcaniclastic and pelitic sediments. Mg-clays (Fe-rich clays in the case of FRGG) are thought to have been an important component. Some possibly contain a minor grey gneiss volcaniclastic component.

The diopside-bearing gneiss of Unit G is regarded as having been derived form altered tholeiitic basalts (HGG). The chemistry of the massive diopside gneiss suggests epidotisation and a possible carbonate component. The massive diopside gneiss bands are regarded as thick hyalotuffs or highly epitodised in situ basalt. The banded and mineralogically diopside-hornblende gneiss is regarded as deformed pillow basalts.

The ultramafic rocks of Unit D are mainly clinopyroxene-olivine cumulates (derived from evolved HGN1 and HGG) and lesser olivine (and orthopyroxene ?) cumulates (derived from primary HGN1).

The anorthosite-metagabbro suite represents plagioclase-clinopyroxene cumulates. They are thought to be the cumulus products of the crystal fractionation that formed the high-Ti ferrobasalts of the high-Ca hornblende gneiss suite. The conclusion that the Selebi-Phikwe high-Ca hornblende gneiss suite represents extrusive and high-level intrusive basalts contrasts with the conclusions of Mason (1973), Key (1977) and Wright (1977). They concluded that the hornblende gneisses of the Central Zone in Botswana are mafic portions of layered anorthositic complexes, rather than mafic extrusives. Key (1977) states that basaltic amphibolites grade into anorthosite and therefore represent layered intrusions. He also stated that there is no evidence of pillows or other features to suggest extrusives. In this thesis it has been shown that the high-Ca hornblende-plagioclase gneiss represents a suite of fractionated extrusive tholeiitic basalt and their high-level intrusive equivalents. The superficially similar, but chemically distinct, metagabbros of the anorthosite-metagabbro suite are part of a layered cumulus plagioclase-clinopyroxene body, which is comagmatic with the evolved basalts (HGC & HGF1).

The hornblende-bearing calc-silicate gneiss are thought to be metasedimentary, possibly as siliceous or silicified calcareous argillite. It has been speculated that they may have had an evaporitic component.

The origin of the garnetiferous quartz-felspar granulite is equivocal. Diverse protoliths, including clastic sediment, volcanic quartz-keratophyre and partial melt of tholeiite, are possibly represented by GQFG.

The albite-sillimanite quartzites are thought to represent silicified aluminous sediments, which locally had a minor exhalative hydrothermal component. The protolith of the finely laminated magnetite quartzite is thought to be a chemically precipitated silica -iron oxide sediment.

The weakly deformed porphroblastic granite gneiss suite is regarded as intrusive granites, intruded between D1 and D2 and during D2. Only limited partial melting of the Selebi-Phikwe gneiss is thought to have taken place.

The suggestion of Gallon (1986) that the granitic gneiss, anorthositic gneiss and hornblende gneiss are all metamorphosed sediments is untenable.

It is suggested that the suite of tholeiitic basalt, including the ferrobasalt and cumulus-enriched basalt, the ultramafic rocks in the gneiss sequence and the anorthosite-metagabbro suite were all comagmatic and formed by low-pressure crystal fractionation of tholeiiitc magma. The primary magma at Selebi-Phikwe was chemically similar to MORB. The Selebi-Phikwe magma system is tentatively regarded as an open system with periodic magma replenishment. The role that the fractionating tholeiitic magma may have played in the formation of Ni-Cu sulphide deposits at Selebi-Phikwe is discussed in Chapters 7.4.6 and 8.6.9.

A speculative synthesis of the original tectonic environment of Selebi-Phikwe indicated by the proposed protoliths for the Selebi-Phikwe gneisses is made in Chapter 9.

CHAPTER FIVE THE SELEBI-PHIKWE NI-CU ORE BODIES

Each of the Phikwe, Selebi North and Selebi Ni-Cu sulphide ore bodies is associated with an amphibolite layer which occurs within grey gneiss and lesser hornblende gneiss of Unit E of the Selebi-Phikwe sequence (Plate 1 & Fig. 2.1). The ore reserves in 1971 (Gordon 1973) and 1981 (Murray 1981) are shown in Table 5.1.

	Million tonnes		Grade (1971)		Cu/(Cu+Ni)
	1971	1981	%Ni	%Cu	
Phikwe	31.1	36.8	1.36	1.12	0.45
Selebi	12.6	16.9	0.74	1.50	0.67
Selebi North	1.9	1.9	0.86	0.97	0.53

Table 5.1 Selebi-Phikwe Ore Reserves.

This chapter deals with the form and structure of the ore bodies and the petrology of their host rocks. Chapter 6 deals with the sulphides, their mineralogy, their relationship to the host rocks and their tectono-metamorphic history. Chapter 7 discusses the geochemistry and origin of the mineralised host rocks.

5.1 THE MORPHOLOGY AND STRUCTURE OF THE SELEBI-PHIKWE ORE BODIES

The main aim of this thesis is not to unravel the complex deformation suffered by the Selebi-Phikwe ore bodies. However some assessment of the deformation and its effects, particularly those on the relationships between the host rocks and their sulphides, is necessary before conclusions about the origin of the ore bodies can be made.

The sulphide occurrences have been subdivided into either massive, disseminated or occasionally stringer sulphides. The main distinction is between massive and disseminated sulphide. Massive sulphide bodies consist dominantly (usually >70%) of sulphide with the remainder being small silicate inclusions. Disseminated sulphides consist of typically finely disseminated sulphide (usually < 30%) within host rock. Problems arose particularly when logging core if the massive sulphide contained more silicate inclusions than sulphide (massive inclusion sulphide) or if the disseminated sulphides in the

host amphibolite occurred as abundant coarse segregations, typical in garnet amphibolite. The textures of the sulphides and the sharp margins of the massive inclusion sulphide bodies enabled the distinction into massive or disseminated sulphide to be made. Stringer sulphides are thin (< 10 cm) veins which typically crosscut the foliation in the host amphibolite.

5.1.1 Phikwe

Phikwe has the most extensive underground development of the three ore bodies and apparently the simplest structure. Its form and structure are discussed in detail. The host amphibolite is a conformable layer within grey gneiss (Fig. 5.1a). It is usually less than 25 metres thick, averaging 11 metres (Fig. 5.1c) (Gordon 1973). The Phikwe ore body consists of disseminated sulphides within the host amphibolite and massive sulphide layers. The main massive sulphide layer either occurs within the host amphibolite in the northwest or within grey gneiss without any associated amphibolite in the southeast. The Phikwe ore body can be subdivided laterally into 6 zones (Figs 5.1b & 5.2) based on host amphibolite thickness and sulphide mode of occurrence. This subdivision was made from underground observations by the author between the 210 and 330 metre mine levels, where mining in progress provided the freshest sections. The zones from northwest to southeast are:

Zone A - host amphibolite with only weak sulphide disseminations.
Zone B - thin host amphibolite with disseminated sulphides and two or more thin massive sulphide bands.
Zone C - thick host amphibolite with abundant disseminated sulphides and one main massive sulphide layer near the top of the amphibolite.
Zone D - a thick massive sulphide layer (locally up to 12 m thick) above thin host amphibolite with only weak sulphide disseminations.
Zone E - a thick massive sulphide layer in locally cataclastic grey gneiss without any associated host amphibolite.
Zone F - very weakly disseminated sulphides (mainly pyrite) in highly cataclastic grey gneiss.

More rapid changes in amphibolite thickness are superimposed on the above zonation. These more abrupt changes are mainly due to D2 folding and shearing. Observations of the Phikwe ore body below the 330 m level were limited to diamond drill cores. The lateral variation

Fig. 5.1 PHIKWE ORE BODY GEOLOGY

Fig. 5.1a GEOLOGICAL MAP OF PHIKWE AREA (COMPILED FROM MAPPING BY BCL)

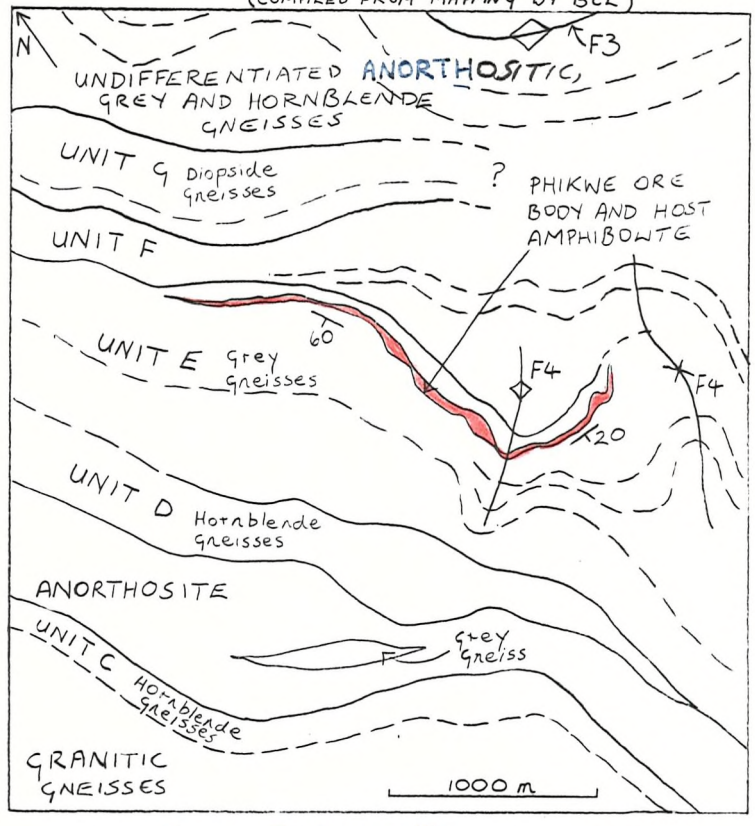

F3 = EARLY D2
F4 = LATE D2

Fig 5.1b ZONATION OF PHIKWE ORE BODY

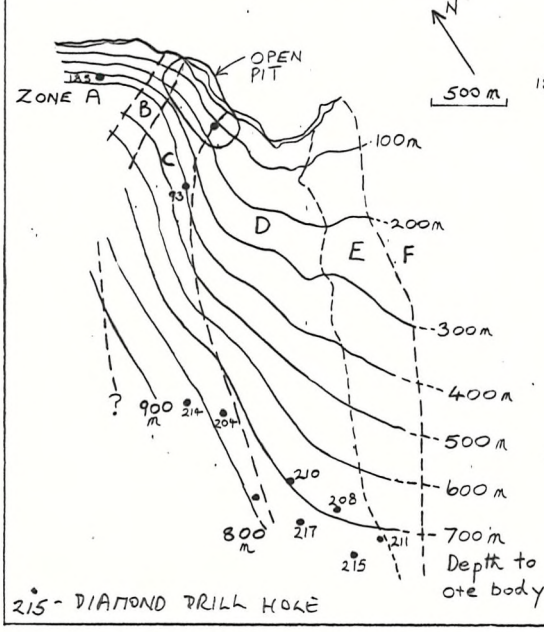

Fig. 5.1c HOST AMPHIBOLITE THICKNESS

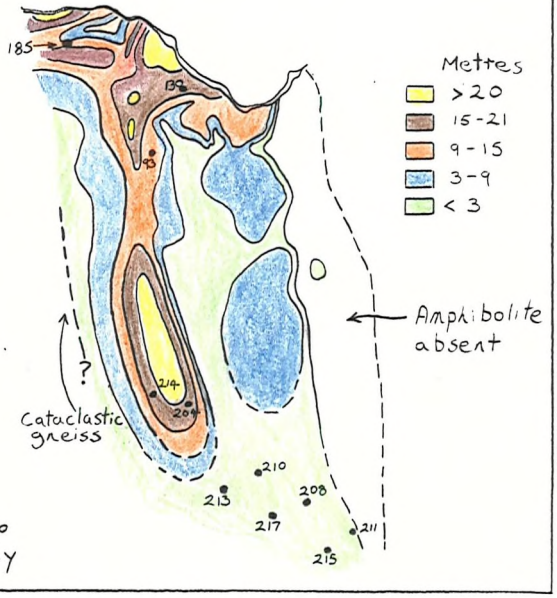

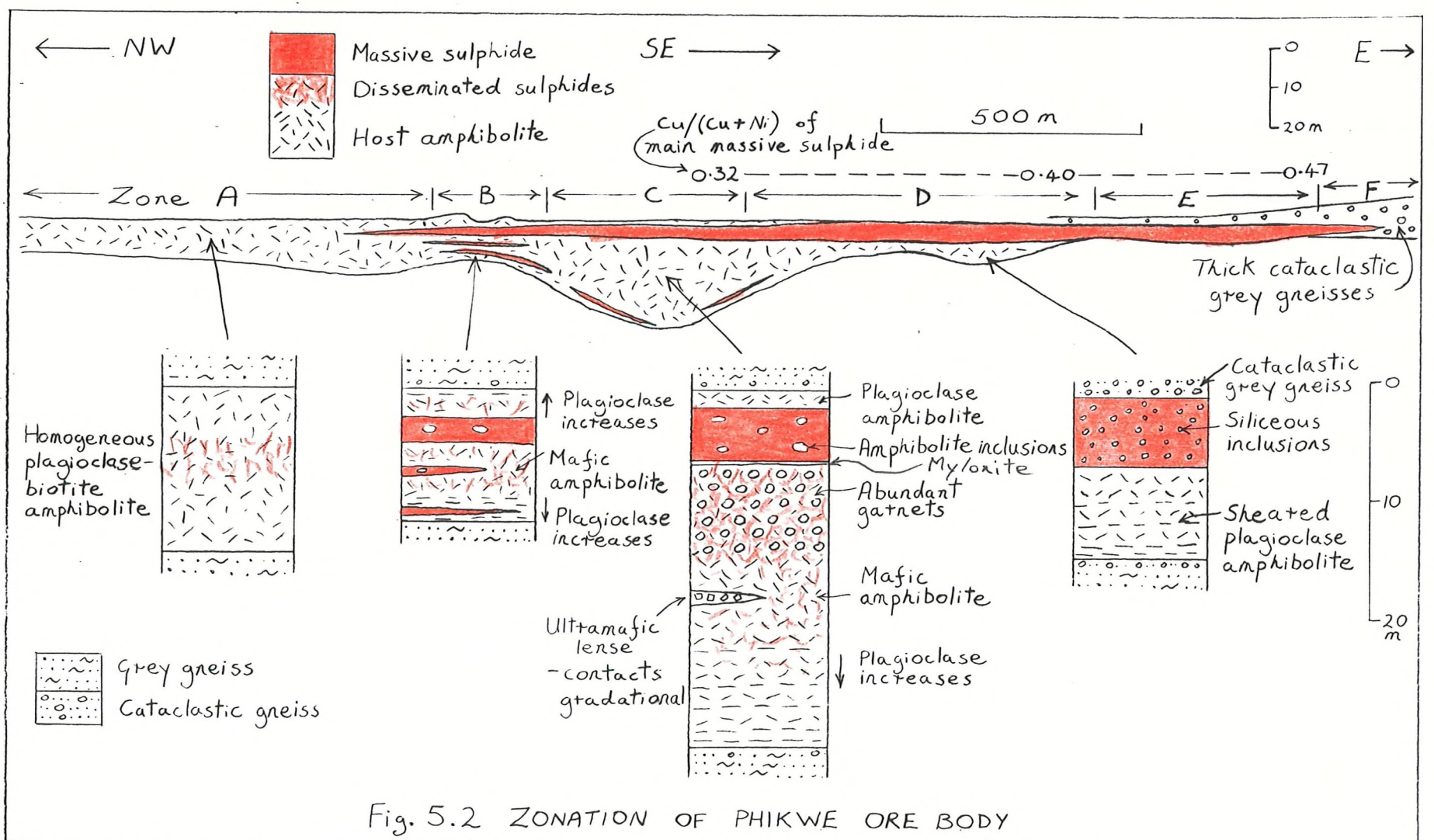

Fig. 5.2 ZONATION OF PHIKWE ORE BODY

from thick mineralised host amphibolite of Zone C to very weakly mineralised cataclastic gneiss of Zone F appears to be partly mirrored going down dip from the 330 m level. In the deepest exploratory holes at Phikwe (e.g. PW 214) only a thin inclusion-rich massive sulphide, weakly mineralised cataclastic grey gneiss or very thin amphibolite are found (Fig. 5.1c).

The structure of the ore body appears to be controlled by D2 folding and shearing. The layer of mineralised amphibolite has the form of an open late-D2 antiform which dies out down plunge (Fig. 5.1b). Dips are gentle (10-30^{o})on the southeast limb and steeper on the northwest limb (25-60^{o} and locally vertical). The top of the ore body is relatively planar and usually only folded by open late-D2 folds. There are few early-D2 folds in the immediate hanging wall grey gneisses. The base of the host amphibolite and the immediate footwall grey gneiss are highly folded by early-D2 folds which gently plunge to the northwest (Plates 15a & f & 28f & g). Locally early and late-D2 folds interfere to form domes in the immediate footwall gneiss and at the base of the host amphibolite. The early-D2 structures are particularly prominent in the open pit where the axial planes of early-D2 folds in the footwall grey gneiss are curved and become overturned towards the host amphibolite (Plate 26a,b & c & Figs 5.3a & b). A small difference in the angle of dip between the ore body and the hanging wall gneiss, which dips at a shallower angle, can also be seen in the open pit. The Phikwe ore body appears to lie on the limb of a major early-D2 antiform to the northeast (Fig. 5.1a) and not on the overturned limb of a recumbent synform as suggested by Wakefield (1974,1976).

D1 folds are uncommon in the hanging wall and footwall grey gneiss and have not been definitely recognised within the host amphibolite. D1 lineations and rare D1 minor folds in the grey gneiss at Phikwe plunge at approximately 20^{o} to the southwest (Figs 5.3a). In Zone B more than one thin massive sulphide band is present within relatively thin host amphibolite and the development of a footwall massive sulphide near the base of the host amphibolite is particularly notable. Initially these thin massive sulphide bands were thought by the author to be due to splitting of the thicker main massive sulphide layer of Zone C. Mining below the open pit however has shown that locally within Zone B the usually flat, unfolded contact of host amphibolite and hanging wall grey gneiss is highly folded and the foliation in the amphibolite is locally vertical (Plate 28a & b). At

least some of the development of thin massive sulphide near the base of the host amphibolite is therefore considered to be due to repetition of the main massive sulphide layer by recumbent isoclinal folding within the host amphibolite (Fig. 5.3c). The age of the folding within the host amphibolite in Zone B is problematic. The folds appear to be the extreme development of the early-D2 folds seen in the open pit above, rather than D1 folds. No other major folds or repetitions were seen within the other zones of the Phikwe ore body. However, the possibility of isoclinal folding within the host amphibolite has implications for the interpretation of the vertical mineralogical and geochemical variations in the host amphibolite (Chs 5.2.1 and 7.4.4). The localised development of the isoclinal folds within the host ampibolite in Zone B is possibly due to pre-D2 thinning of the amphibolite combined with a high proportion of massive sulphide to amphibolite.

The Phikwe ore body has repeatedly acted as a zone of shearing and at least three superimposed phases of shearing have affected it (Ch. 3.11). The M1m mylonite assemblage is thought to represent recrystallised D1 mylonite. The M2a and M2b assemblages are correlated with early-D2 and late-D2 folding and shearing respectively. The most important shearing appears to have been associated with early-D2 folding, during which the ore body acted as a zone of decollement. The late-D2 shears are thin zones located exactly at the ore body horizon. Their effect on the ore body is not as great as the early-D2 shears and they appear to be most conspicuous in the grey gneiss where the ore body was already absent due to previous deformation.

The orientation of the zonation of the ore body, particularly the zone of thickest amphibolite (Zone C) and the cataclastic margin of the ore body at the transition between Zones E and F, trends to the southwest and is approximately parallel to the D1 lineations and to the late-D2 folds. Late D2 folding produces very open folds and late-D2 shearing is responsible for only localised minor changes in thickness of the ore body. Therefore it is thought that the zonation is unrelated to late D2. The zonation could be related to D1. For example, the zone of thick amphibolite could be a D1 boudin. The main alternative is that the thick amphibolite zone and the orientation of the margins of the ore body are original predeformation features.

5.1.2 Selebi

Early drilling at Selebi revealed the presence of two mineral-

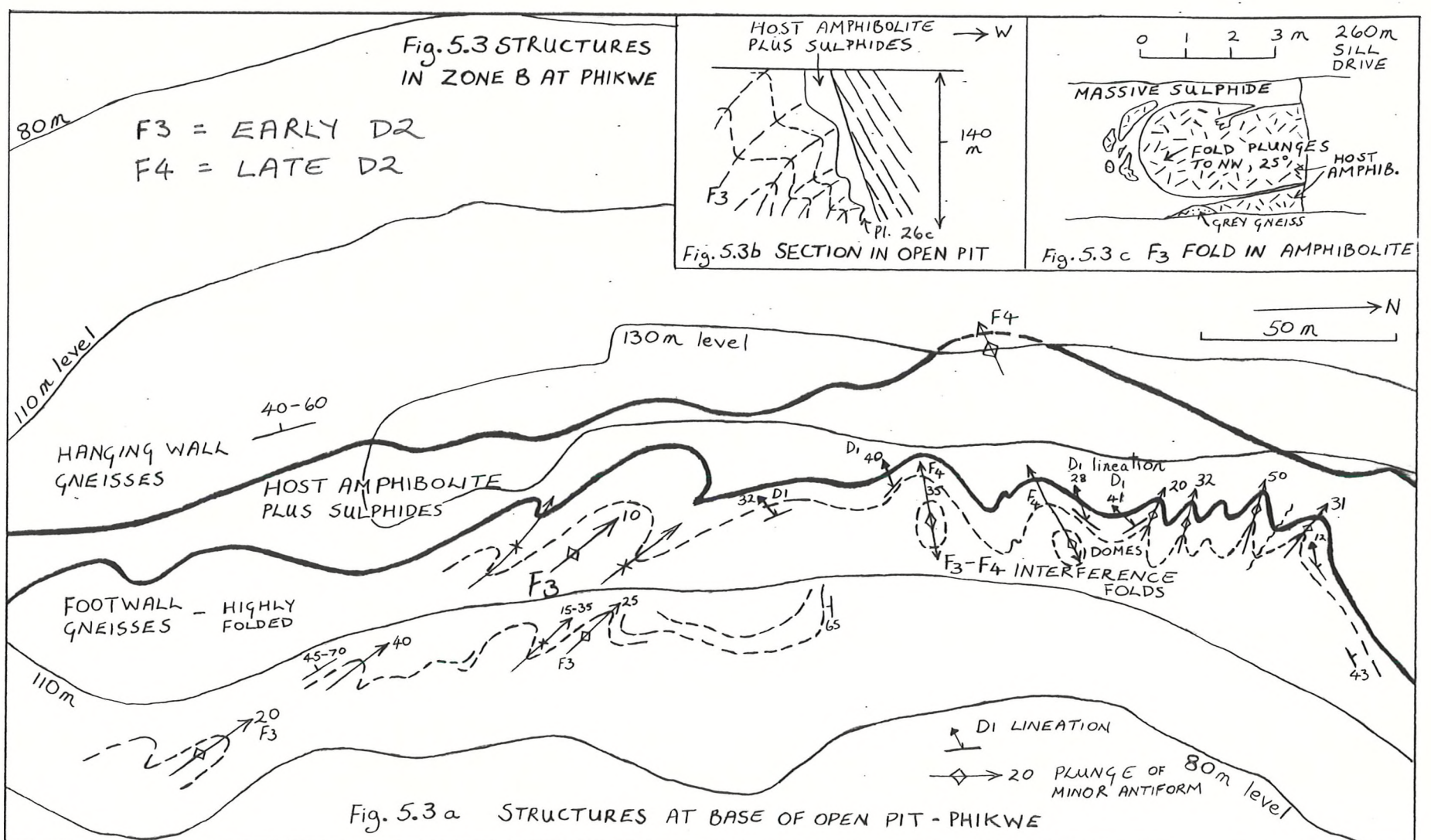

Fig. 5.3b SECTION IN OPEN PIT

Fig. 5.3c F_3 FOLD IN AMPHIBOLITE

Fig. 5.3a STRUCTURES AT BASE OF OPEN PIT - PHIKWE

ised amphibolite layers separated by about 12 m of grey gneiss, which dip to the west at 35° (Fig. 5.4a). The mineralisation consists of abundant disseminated sulphides and highly variable and irregular massive sulphides within host amphibolite. Thick tabular massive sulphide is not developed at Selebi, unlike Phikwe. The most westerly exploration holes at Selebi seeking deep mineralisation failed to intersect any host amphibolite and the structure was tentatively interpreted as a tight early synform plunging to the north (Gordon 1973). Interpretation was complicated by the presence of three amphibolite layers in some holes.

Underground development has revealed the presence of three mineralised amphibolites, a Lower body and an Upper body that was split into an Upper A and an Upper B body (Figs 5.4 & 5.5). The splitting of the Upper body eventually dies out to the north. Before 1980 the splitting of the Upper body was speculatively regarded as the result of folding or shearing, or as an original intrusive feature (Gallon, pers. comm. 1980; Gallon 1986). Brown (1980, 1981b) found evidence that the repetition of the Upper body was due to D1 isoclinal folding (Plate 14b). The lack of intersections in the most westerly drill holes suggest the Upper and Lower bodies join in a tight D1 isoclinal synform plunging to the north at 20° (Fig. 5.4). The contacts of the host amphibolite with the surrounding grey gneiss are conformable but typically sheared, with the development of abundant mica locally in the host amphibolite and coarse cataclastic textures in the grey gneiss (Plate 29a). However the early D2 (M2a) shearing that is prominent at Phikwe is much less conspicuous at Selebi.

The average amphibolite thickness is about 13 m at Selebi (Gordon 1973). The Upper amphibolite is thicker than the Lower amphibolite but its thickness is highly variable, from 1 to 27 m. The Lower amphibolite is thin (always less than 10 m), lenticular and locally absent. It is however the more persistent horizon. There is marked thickening in the synformal closure of the Upper and Lower bodies. The upper limit of the Upper body plunges to the north parallel to the D1 axis (Fig. 5.4a). The pinching and swelling (Figs 5.4b & 5.5) of the ore body is thought to be mainly due to D1 boudinage, rather than being either an original feature or a result of D2 folding. D2 folding (mainly late-D2) has produced only small flexures of the ore body (Plates 15b & c & 29a & b). Locally D2 deformation has caused massive sulphide to invade the grey gneiss, cutting across their foliation (Plate 29f & g).

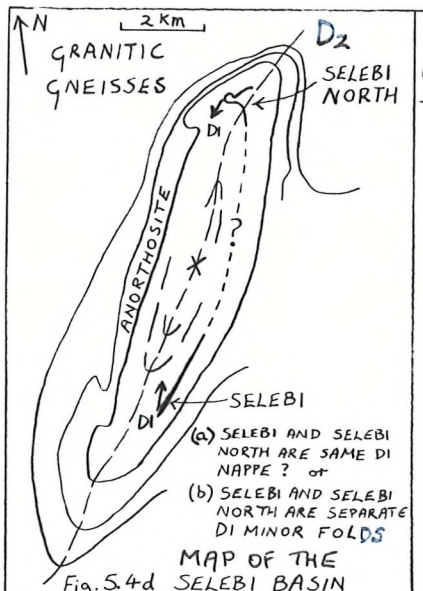

Fig. 5.4d MAP OF THE SELEBI BASIN

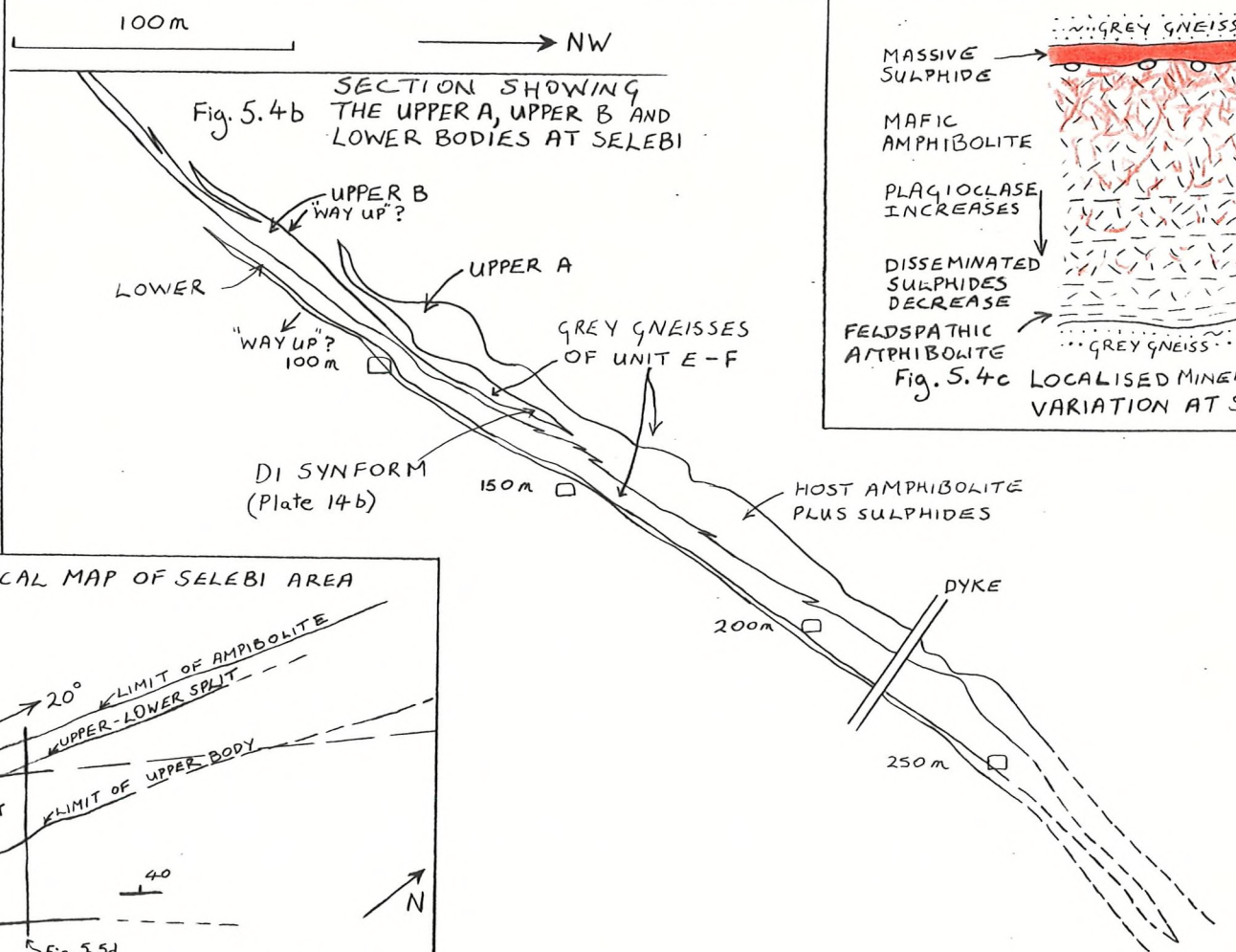

Fig. 5.4b SECTION SHOWING THE UPPER A, UPPER B AND LOWER BODIES AT SELEBI

Fig. 5.4c LOCALISED MINERALOGICAL VARIATION AT SELEBI

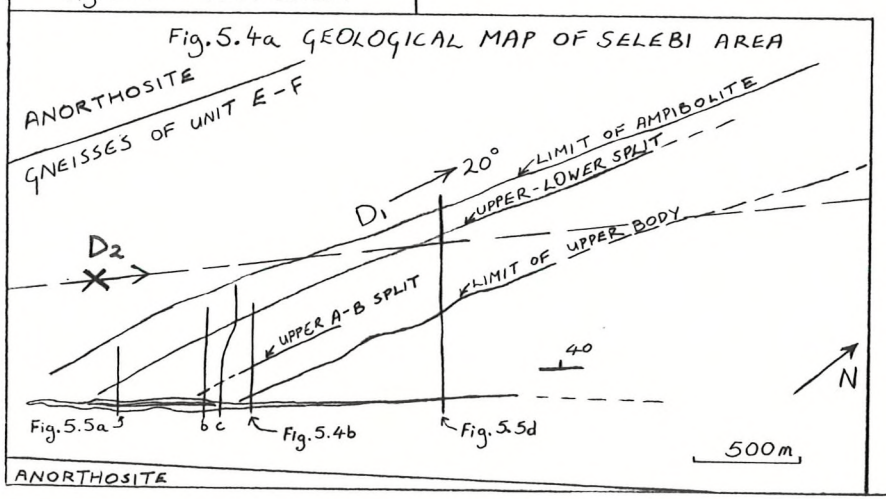

Fig. 5.4a GEOLOGICAL MAP OF SELEBI AREA

Fig. 5.4 SELEBI ORE BODY GEOLOGY

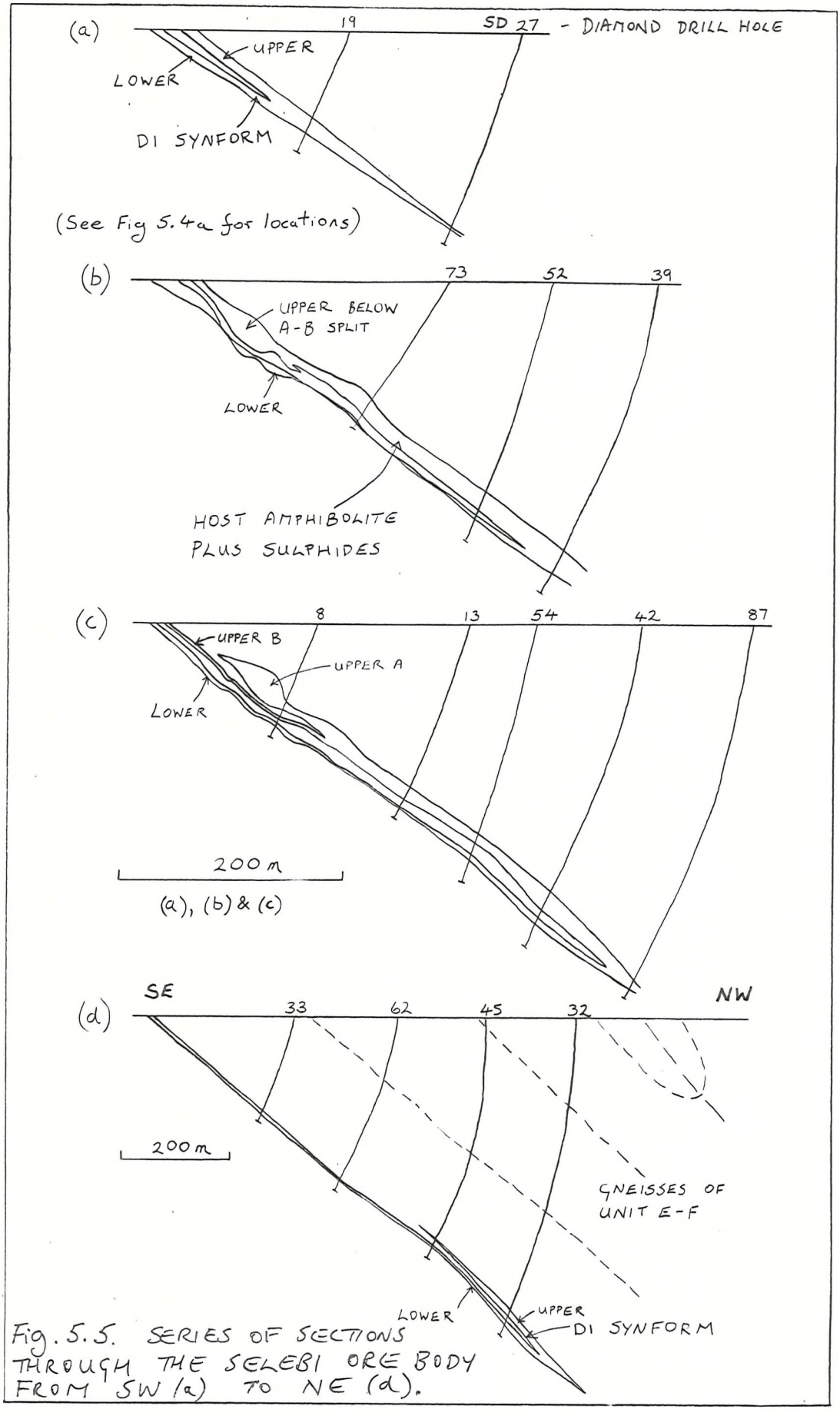

Fig. 5.5. SERIES OF SECTIONS THROUGH THE SELEBI ORE BODY FROM SW (a) TO NE (d).

The origin of the structure of the Selebi ore body is obviously complex and is poorly understood (see Chs 5.2.2 & 7.4.4 & Fig. 7.15 for tentative way-up information obtained from the mineralogical and geochemical variations in the Upper B and Lower bodies). The geometry of the body suggests a control by thrusting and shearing (Wright, pers. comm. 1986).

5.1.3 Selebi North

The Selebi North ore body was only examined in diamond drill core. Only limited underground development has taken place. The ore body consists of disseminated sulphides and thin massive sulphides in a host amphibolite that has been folded into a moderately tight, overturned D1 antiform. The host amphibolite is conformable with the surrounding grey gneiss. The antiform at the surface plunges towards the south-southwest at 50° (Fig. 5.6). At depth the antiform becomes tighter and the axial plane dips less steeply to the south. There is a persistent minor fold on the north limb, which is either a synchronous drag fold of the main antiform, or an earlier D1 closure that has been refolded by the main Selebi North closure (later D1). There is marked thickening of the host amphibolite and more abundant sulphide in the main antiform core. As at Selebi, there has been much less early-D2 shearing than at Phikwe.

The main antiform is refolded by an open late-D2 synform (Fig. 5.6a). The northern overturned limb can not be traced further than this late-D2 closure. The southern limb is more persistent and can be traced toward Selebi. A deep well between Selebi and the southern limb at Selebi North intersected thick (>50 m) highly sheared cataclastic grey gneiss but no host amphibolite. It is impossible to tell whether a once continuous amphibolite body between Selebi and Selebi North has been stretched and pulled apart, or whether the Selebi and Selebi North bodies have always been completely separate. It is possible that the closure at Selebi North is the same closure as the D1 synform at Selebi (Figs 2.4d & 5.4d). Both Selebi and Selebi North main closures appear to plunge towards the centre of the Selebi structural basin and towards each other. Ideas about the relationship of the structures at Selebi and Selebi North are speculative (see Ch. 7.4.4 for structure derived from the geochemical way-up).

5.1.4 Structural Relationship of Phikwe, Selebi North and Selebi

It is impossible to prove that the host amphibolites of each

Fig. 5.6 SELEBI NORTH ORE BODY GEOLOGY

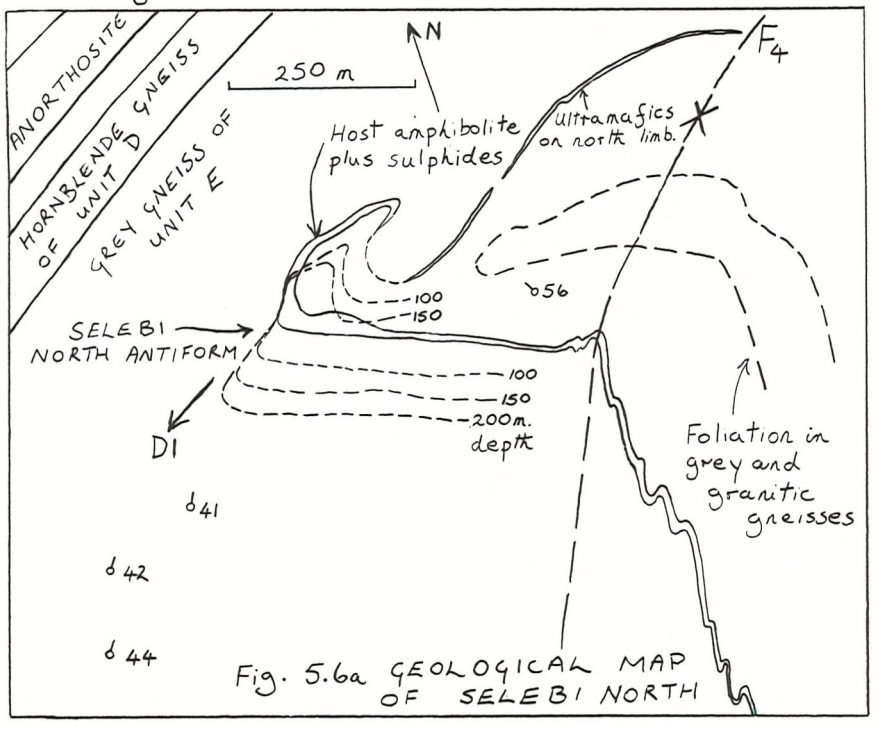

Fig. 5.6a GEOLOGICAL MAP OF SELEBI NORTH

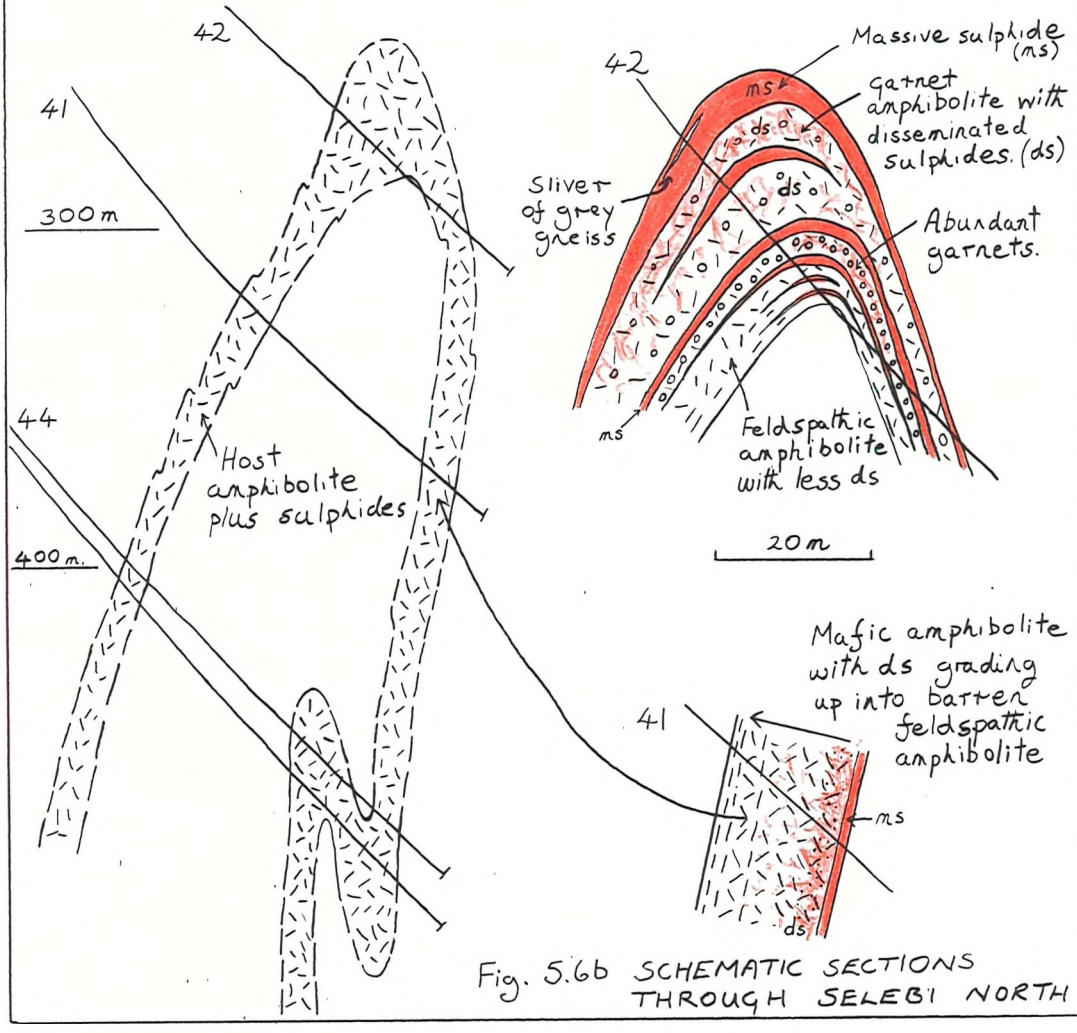

Fig. 5.6b SCHEMATIC SECTIONS THROUGH SELEBI NORTH

ore body are at exactly the same "stratigraphic position". This is due to the lack of a detailed "stratigraphy" that can be applied throughout the Selebi-Phikwe area and because one of the main mappable units is one or more layers of anorthosite, which were possibly thrust into the sequence after the earliest deformation event (Fig. 2.3). It is likely however that the host amphibolite of each ore body is at the same approximate "stratigraphic" position within the gneiss sequence.

The Selebi, Selebi North and Phikwe ore bodies are aligned in a southwest direction (Plate 1 & Fig.2.1). If this is more than coincid-ence, the alignment is probably a D1 feature and an early fold closure might be expected at Phikwe. There is as yet no sign of this. Phikwe may lie on a sheared limb of an attenuated early structure (Fig. 2.3). It is easier to think of the alignment of the ore bodies as being a D1 feature if the main closures at Selebi and Selebi North are the same major D1 nappe refolded during D2 rather than if they are two separate minor D1 closures.

Gallon (1986) thought that all three ore bodies were linked at depth. The lack however of host amphibolite in deep exploration holes between Selebi and Selebi North and the paucity of deep holes between Phikwe and Selebi North mean that it is impossible to conclude whether the three ore bodies were originally connected or were separate. The high strain suffered by the Selebi-Phikwe gneisses means that the original shape of the host bodies is difficult to determine. It is feasible that they were originally stock-like bodies that have been completely flattened. The host rocks to the Empress Ni-Cu deposit in Zimbabwe for example are a subvertical wedge-shaped plug of gabbroic amphibolite with a core of peridotite and pyroxenite (Mander, unpub. report 1982). The present form of the Selebi-Phikwe host rocks as discrete layers within unrelated grey gneisses suggests that they were originally sill-like bodies (or part of one sill). This remains the most plausible assumption.

5.2 THE PETROLOGY OF THE SELEBI-PHIKWE HOST AMPHIBOLITES

5.2.1 The Phikwe Host Amphibolite

The Phikwe host amphibolite is a variable hornblende-feldspar-gedrite-mica amphibolite with disseminated sulphides. Lateral variations in the amphibolite thickness and mineralogy are shown in Figures 5.1c and 5.2. Sections through the host amphibolite that have been studied geochemically are shown in Figures 7.1 - 7.4.

5.2.1a Large-scale variations in the Phikwe host amphibolite

A generalised section through the host amphibolite of Zone C, the thickest and most variable part of the host amphibolite is shown in Figure 5.2. At the top of this section above the massive sulphide layer there is a variable thickness of weakly mineralised hornblende-feldspar amphibolite. The contact with the grey gneiss is sharp. A thin band of quartz-feldspar-garnet granulite (M1m assemblage) is locally developed at the base of the massive sulphide. This is interpreted as a recrystallised D1 mylonite. Below the massive sulphide there is a coarse garnetiferous hornblende-rich amphibolite associated with abundant coarsely disseminated sulphide. The base of the garnet amphibolite is rapidly gradational into a massive hornblende-gedrite-mica amphibolite and coincides with an abrupt decrease in the amount of dissseminated sulphide. Further below, the hornblende-gedrite amphibolite gradually becomes more feldspathic, micaceous and foliated and takes on a sheared appearance. The basal contact of the host amphibolite is usually sharp against strongly banded grey gneisses with abundant quartz-rich segregations (Plate 28g). Locally this contact appears gradational, particularly if the grey gneiss is hornblende-bearing and relatively mafic. Locally at the base of the host amphibolite there is a highly micaceous sheared amphibolite. Rare lenses of ultramafic rock with disseminated sulphide occurs in the thicker sections of mineralised host amphibolite, typically near the centre of the amphibolite layer within the hornblende-rich zone. The host amphibolite rapidly grades over a distance of approximately two cm into ultramafic rocks, which consist of amphibole pyroxenite with minor patches and bands of serpentinised peridotite.

Along strike to the northwest in Zone B the host amphibolite thins. The massive sulphide layer also thins and two or more thin irregular massive sulphides are locally developed (Fig. 5.2). The garnetiferous amphibolite decreases in thickness and disappears going from Zone C to Zone B. The centre of the host amphibolite is hornblende-rich with minor gedrite, mica and garnet and little feldspar. The upper and lower zones of the amphibolite gradually increase in feldspar and mica content towards the margins and become more foliated.

Further to the northwest in Zone A the host amphibolite thickens again before eventually thinning in the extreme northwest. The host amphibolite becomes less variable and consists of weakly foliated, relatively homogeneous hornblende-feldspar-mica amphibolite

with only minor sulphide disseminations. The main variation within this amphibolite is the development of porphyroblastic (plagioclase) amphibolite and minor hornblende-feldspar gneiss at its margins (Fig. 7.4).

Southeast of Zone C the mineralised amphibolite becomes thinner along strike. The garnetiferous amphibolite zone with its associated abundant disseminated sulphides rapidly thins and disappears. The main massive sulphide layer (up to 10 m thick) directly overlies weakly mineralised hornblende-gedrite amphibolite with more feldspathic and foliated amphibolite below (Zone D, Fig. 5.2). Where the host amphibolite is thin massive sulphide overlies basal feldspathic amphibolite only. The thin amphibolite above the massive sulphide is not present in Zone D and the massive sulphide is in contact with highly cataclastic grey gneiss (Plate 34e). The lack of disseminated ore in Zone D is probably a combination of original disseminated sulphide distribution in the host body and the effects of shearing. Some host amphibolite has possibly been sheared out and disseminated sulphides have possibly been mobilised into the massive sulphide layer (see Ch. 6.4). Further to the southeast the massive sulphide layer occurs within cataclastic grey gneiss, without any associated host amphibolite (Zone E, Fig. 5.2).

5.2.1b Detailed mineralogy of the Phikwe host amphibolite of Zone C

The mineralised amphibolite of Zone C has a much more variable mineralogy than that of Zone A (Figs 5.2, 7.1 & 7.2). The hornblende-feldspar amphibolite above the massive sulphide is similar to the homogeneous amphibolite of Zone A. It typically contains abundant labradorite (50%), rare disseminated sulphide and no biotite and has a decussate granoblastic texture. The labradorite is usually zoned with slightly more-calcic cores. The contact with the massive sulphide layer is sharp and locally marked by a thin vein of quartz and chlorite (Plate 34c).

The garnet amphibolite zone below the massive sulphide contains garnet, hornblende, minor gedrite, rare biotite and abundant dissem-inated sulphide. The bright red garnets occur as single porphyroblasts or aggregates up to three cm across. They comprise 10-15% of the garnetiferous amphibolite and are evenly distributed throughout it. Similar probed garnets from Selebi North are almandines (Table 5.2 & p.A.6). The almandines are poikiloblastic and contain abundant inclusions of hornblende and minor biotite (Plate

32e). Locally the hornblende inclusions have rims of quartz. Sulphides rarely occur in the almandines but are abundantly disseminated both within the surrounding amphiboles and at their grain boundaries. Gedrite has not been observed in contact with the almandines. Plagioclase is absent from the garnetiferous zone. Garnet amphibolite occurs as inclusions within the massive sulphide layer and some contain in excess of 50% garnet. In one highly garnetiferous inclusion from Zone E hornblende porphyroblasts occur in a matrix of fine granular garnet (Plate 32g). The majority of the amphibolite inclusions within the massive sulphide however are garnet-free. The formation of garnet-bearing amphibolite at Phikwe appears to be intimately related to the occurrence of disseminated ore. The geochemistry and origin of the garnetiferous amphibolite are discussed in Chapter 7.2 and 7.4.2.

The mafic amphibolite below the garnetiferous amphibolite consists of hornblende, gedrite and phlogopite with lesser amounts of disseminated sulphide. The hornblende is ferroan pargasitic hornblende in composition (Table 5.2, Fig. 3.1). Gedrite occurs as both a coarse idioblastic and a fine-grained matrix mineral (Plate 31b). In the mafic hornblende-rich amphibolite the mica is commonly phlogopite whereas in garnetiferous or hornblende-feldspar amphibolite the mica is biotite. Minor orthopyroxene (usually altered to fine amphibole, Plate 31d) typically occurs in the mafic amphibolite. Fine-grained, dark green spinel occurs as inclusions within hornblende (Plate 31c).

The rare lenses of amphibole pyroxenite that occur in the central hornblende-rich amphibolite of Zone C, consist of coarse-grained idioblastic orthopyroxene, rare olivine and green spinel in a matrix of finer pale green clinoamphibole (hornblende) (Plate 33b). Sulphides occur as disseminations in the silicates and at grain boundaries. The orthopyroxene contains inclusions of fine hornblende. Locally orthopyroxene occurs as corroded relicts in a cummingtonite -gedrite-phlogopite-hornblende matrix. Rare patches and bands of serpentine with minor relict olivine occur in the amphibole pyroxenite. One round xenolithic patch (4 cm across) of chromitite was noted in the serpentinite (Plate 33h).

The central hornblende-rich amphibolite of Zone C increases in plagioclase content going downwards (Fig. 5.2) and the host amphibolite gradually changes from a massive hornblende-gedrite-phlogopite amphibolite to a weakly foliated hornblende-plagioclase-biotite-gedrite amphibolite with up to 50% plagioclase and a variable but typically low content of disseminated sulphide (see Plate 31g). The

PHIKWE

	a	b	c	d
	hor	ged	hor	plg
SiO2	43.70	44.62	48.03*	54.69*
TiO2	0.09	0.06	0.50	
Al2O3	14.89	15.54	11.73	30.46
FeO	12.05	16.54	12.55	
MnO	0.22	0.40	0.18	
MgO	13.44	17.51	14.04	
CaO	10.86	1.08	10.48	12.78
Na2O	1.61	1.61	1.52	4.50
K2O	0.28	0.01	0.33	0.03
Cr2O3	0.01	0.00	0.09	
Total	97.15	97.37	99.45*	102.46*
				An 61
No. of analyses	4	4	2	3

Host amphibolite samples 34e and 34q from PW 93

See Figure 7.2 for PW 93 section

See Plate 31b for sample 34e

a Fine matrix hornblende 34e

b Elongate idioblastic and fine matrix gedrite 34e

c Moderately coarse hornblende 34q

d Matrix plagioclase 34q

* SiO2 too high (See appendix A.5 & 6 for all analyses)

SELEBI

	Spinel Aggregates				Amphibolite	
	e	f	g	h	i	j
	spi	plg	zoi/clz	phl	plg	ged
SiO2	0.07	44.05	39.75	38.24	44.36	44.66
TiO2				0.67		0.18
Al2O3	64.99	35.86	32.44	17.88	36.07	17.65
FeO	19.33		0.46	6.14		11.33
MnO	0.08			0.05		0.30
MgO	15.89		0.07	21.33		21.25
CaO	0.03	19.77	23.47	0.00	19.81	0.95
Na2O	0.09	0.38	0.08	0.89	0.67	2.10
K2O	0.01	0.02	0.15	8.18	0.00	0.00
Cr2O3	0.03			0.03		0.09
Total	100.52	100.08	96.42	93.41	100.91	98.51
		An 97			An 94	
No. of analyses	4	2	3	1	3	1

Samples 112 & 113 from SD 82

See Plate 32b for 112

e Pleonaste 112 & 113

f Plagioclase associated with pleonaste 112 & 113

g Clino?zoisite surrounding aggregate 112 & 113

h Phlogopite at margin of clinozoisite rim 113

i Plagioclase of host amphibolite 112 & 113

j Gedrite of host amp. 113

SELEBI NORTH

	Cr-Amphibolite		Garnet Amphibolite	
	k	l	m	n
	hor	hor	hor	gnt
SiO2	42.83	46.36	42.86	39.40
TiO2	1.32	0.51	0.20	0.02
Al2O3	14.48	11.58	15.47	22.14
FeO	12.75	8.96	13.68	25.28
MnO	0.22	0.21	0.22	1.66
MgO	12.70	15.87	12.10	8.64
CaO	10.38	10.45	10.71	4.19
Na2O	2.17	1.78	1.60	0.04
K2O	0.32	0.20	0.28	0.01
Cr2O3	0.04	0.86	0.08	0.02
Total	97.21	96.78	97.20	101.40
No. of analyses	3	7	5	13

Samples 56-16 & 56-17 from SDN 56

See Figure 7.7 for SDN 56 section

Samples 129 & 133 from SDN 42

See Figure 5.6b for SDN 42 section

See Plate 32h for 56-17, 32d for 129

k Moderately coarse hornblende of hornblende-(feldspar) amp. 56-16

l Cr-hornblende, average of coarse to fine-grained hornblendes of hornblende-(feldspar) amp. 56-17

m Hornblende of gnt amp. 129 & 133

n Garnet of gnt amphibolite 129 & 133

TABLE 5.2 AVERAGE MINERAL ANALYSES -- SELEBI-PHIKWE HOST AMPHIBOLITE

actual base of the host amphibolite is usually a granoblastic feldspathic amphibolite (Plate 31e) or occasionally a highly micaceous amphibolite. The sulphides typically occur at hornblende-plagioclase grain boundaries (Plate 31e) and are more abundant where plagioclase is altered to clinozoisite. The plagioclase of the basal feldspathic amphibolite of Zone C is labradorite in composition (Table 5.2 & p. A.5). The hornblende is a magnesio-hornblende (Fig. 3.1) with higher Cr and Ti contents than the hornblende in the mafic amphibolite above. Chlorite (and minor anthophyllite) and clinozoisite locally replace amphibole and plagioclase respectively (see Plate 31h) and the amphibolite appears sheared. This new assemblage occurs either in thin shear zones subparallel to the massive sulphide layer or may locally pervade the whole lower feldspathic amphibolite.

The thin host amphibolite of Zone D is a weakly mineralised, foliated feldspathic amphibolite and is similar to the lower amphibolite of Zone C. It is typically sheared with abundant chlorite, anthophyllite and clinozoisite. The weakly mineralised, homogeneous amphibolite of Zone A is a granoblastic decussate hornblende (50%) - plagioclase (40%) rock with minor randomly orientated biotite and gedrite crystals (similar to Plate 31a). The plagioclase is unzoned or very weakly zoned and is labradorite in composition.

5.2.1c Summary and discussion of the Phikwe amphibolite assemblage

The Phikwe host amphibolite shows the greatest mineralogical variation in Zone C, where it is thickest and contains the highest contents of disseminated sulphide. The weakly mineralised amphibolite of Zone A is a homogeneous hornblende-plagioclase amphibolite. The amphibolite of Zone D is similar to the basal part of Zone C. The upper part of Zone D amphibolite may have been removed by shearing.

The main granoblastic, dominantly unaligned hornblende-plagioclase-mica-gedrite assemblage of the Phikwe host amphibolite can be correlated with the typical Mlm assemblage observed in mafic Selebi -Phikwe gneisses. Almandine and hornblende of the garnet amphibolites associated with abundant disseminated sulphide are also thought to be a Mlm assemblage. The rare orthopyroxene and green spinel in the amphibolite and the orthopyroxene, olivine and green spinel of the ultramafic lenses are regarded as a metamorphic assemblage (Ml) and not as original igneous minerals (see Chs 5.3.2 & 8.2.5). The chlorite-anthophyllite-clinozoisite assemblage is a typical M2 assemblage.

5.2.2 The Petrology of the Selebi Host Amphibolite

5.2.2a The mineralogy of the Selebi host amphibolite

The Selebi host amphibolite is similar to that at Phikwe but is more feldspathic and shows less mineralogical variation. It is typically a homogeneous granoblastic hornblende-plagioclase amphibolite with minor mica (biotite or phlogopite), gedrite and disseminated sulphide. The amphibolite is weakly banded reflecting changes in plagioclase content. It also contains rare feldspathic bands of hornblende anorthosite up to one metre thick (Fig. 7.5).

Garnets are rare in the Selebi host amphibolite compared to the Phikwe amphibolite. At Selebi they occur either as rare porphyroblasts randomly distributed in the less feldspathic amphibolite or at the contact of massive sulphide with hornblende-rich amphibolite (Plate 30 & Fig. 5.4c). In the second case inclusions within the massive sulphide are garnet-rich aggregates with only minor hornblende. A thin rim of chlorite occurs around the garnet-rich inclusions. The lack of a distinct garnetiferous amphibolite zone at Selebi compared to Phikwe, appears to be related to the absence of a zone of abundant disseminated sulphides. At Selebi fine disseminated sulphides are evenly distributed throughout the host amphibolite, with lesser amounts in the feldspathic amphibolite. In contrast, at Phikwe abundant coarsely disseminated sulphides are concentrated in Zone C in the garnetiferous amphibolite immediately below the massive sulphide. The lower part of the Phikwe amphibolite is relatively barren.

Thin shear zones of more than one age are developed within the host amphibolite and particularly at the contacts of the amphibolite with the enclosing grey gneiss. Thin zones of phlogopite or porphyroclastic plagioclase in a biotite-rich matrix occur in the host amphibolite. Coarse porphyroclastic plagioclase is typically developed in the adjacent grey gneiss and the marginal amphibolite often comprises hornblende porphyroblasts in a sulphide-rich matrix (Plates 29a & 32a). These assemblages are correlated with the M2a assemblage at Phikwe. However at Selebi early-D2 shearing is less commonn than at Phikwe. Later zones containing an M2b assemblage of chlorite, anthophyllite and clinozoisite (Plate 31h) are superimposed on the earlier shear zones.

5.2.2b Localised vertical variation within the Selebi amphibolite

In parts of the Lower and Upper B bodies there is a gradation

from feldspathic hornblende-plagioclase amphibolite (50-60% plag.) at the base (Plate 31f), through less feldspathic hornblende-gedrite-biotite-plagioclase in the middle (Plate 31g), to hornblende-phlogopite amphibolite at the top (Figs 5.4c, 7.5 & 7.6). The granoblastic basal feldspathic amphibolite consists of polygonal, weakly zoned labradorite (Michel-Levy), green hornblende and minor quartz. It resembles the gabbroic and hornblende anorthosites. A thin irregular massive sulphide layer typically occurs at the top of the upper hornblende-rich amphibolite in contact with grey gneiss (Plates 29a & 30a). Garnet occurs locally at the contact of the host amphibolite and massive sulphide (Plate 30). Fine-grained disseminated sulphide occurs throughout the host amphibolite, except in the feldspathic amphibolite where it is rare. The vertical mineralogical variation seen in the Lower and Upper B bodies is similar, i.e. from feldspathic amphibolite at the base to hornblende-rich amphibolite at the top. If this variation is indicative of the original way-up of the Selebi host amphibolite (e.g. as it would be in a gravitationally differentiated igneous body), it may be of use in unravelling the complicated structure of the Selebi ore body (Fig. 5.4b). The origin of the geochemical variation accompanying the vertical mineralogical gradation in the Selebi host amphibolite is discussed in Chapter 7.4.

5.2.2c Spinel-rich aggregates in the Selebi host amphibolite

Spinel-rich areas occur in the centre of the host amphibolite of the Upper Body (below the A-B split). They either occur as rounded aggregates (1-2 cm across) of spinel with a rim of clinozoisite (Plate 32c) or as larger more diffuse aggregates of spinel and clinozoisite. The boundary between the clinozoisite rim and enclosing amphibolite is marked by coarse-grained tangential phlogopite. Anorthite (An 97) (Table 5.2 & p.A.5) occurs interstitially within the spinel aggregates (Plate 32c). Locally a porphyroblast of corundum occurs at the core of the spinel aggregates (Plate 32b). Surrounding amphibolite contains hornblende, anorthite and minor gedrite. The variation in the plagioclase composition from anorthite to labradorite within the Selebi host amphibolite is thought to be due to variation in bulk chemistry, not differing metamorphic conditions. The spinel is pleonaste and is very similar chemically to the pleonaste of the Dikoloti feldspathic amphibolite (Tables 3.2 & 5.2 & Fig. 8.7), but is richer in Fe. The mimetic preservation of plagioclase twinning in fine-grained clinozoisite rims shows that clinozoisite (regarded as M2) has replaced

plagioclase. Anorthite occurring interstitially within spinel aggregates has been protected from this alteration.

The Selebi corundum-spinel-anorthite aggregates are thought to consist of M1p relicts of corundum, surrounded by M1 amd M2 retrogression coronas. They are similar to the corundum-spinel-sapphirine aggregates of the Dikoloti feldspathic amphibolite and reflect a similar, though mineralogically less complex metamorphic history. Due to the high strain suffered by the Selebi host amphibolite the concentric zonation from corundum at the core, through rims of pleonaste, plagioclase (altered to clinozoisite) and finally phlogopite does not represent premetamorphic chemical zonation. It formed by diffusion of Al, Mg and Ca around a corundum-rich core within hornblende-anorthite amphibolite during retrogression after the peak of M1 (Leyreloup et al. 1975). The more complex sapphirine-bearing Dikoloti assemblage mat have formed as a result of higher Mg activity (Yardley & Blacic 1976) than at Selebi, or minor Si and K metasomatism (Herd et al. 1969). It is also possible however that sapphirine in the Selebi assemblage was destroyed in spinel and corundum-forming reactions (Droop & Bucher-Nurminen 1984; Windley et al. 1984). The geochemistry of the spinel-rich amphibolite at Selebi and the origin of its aluminous aggregates are dealt with in Chapters 7.2 and 8.6.2.

5.2.2d Summary

The Selebi host amphibolite differs from the Phikwe host amphibolite in a number of ways:

1) The Selebi amphibolite is more feldspathic than the Phikwe amphibolite.
2) There are no ultramafic rocks within the Selebi host amphibolite and no orthopyroxene was found in the host amphibolite.
3) At Selebi there is no distinct garnetiferous zone and disseminated sulphides are more evenly distributed throughout the Selebi amphibolite.
4) Corundum-pleonaste-anorthite aggregates occur in the Selebi host amphibolite.
5) Early-D2 shearing at Selebi is uncommon and the M2a assemblage is only weakly developed.

5.2.3 The Petrology of the Selebi North Host Amphibolite

The Selebi North host amphibolite was only examined from diamond drill core. It is typically a hornblende-plagioclase-mica-

gedrite amphibolite and is generally similar to the Phikwe and Selebi host amphibolites. Variations in the mineralogy of the host amphibolite occur between the limbs of the early antiform, the core of the early antiform and the eastwards continuation of the northerly limb where ultramafic rocks are associated with the host amphibolite (Figs 5.6 & 7.7).

5.2.3a The mineralogy of the Selebi North host amphibolite of the southern limb and antiformal core

The host amphibolite of the limbs of the early antiform is a relatively homogeneous hornblende-plagioclase-mica-gedrite amphibolite. However a systematic variation has been observed in some sections. The southern limb locally shows a mineralogical gradation from a dark hornblende-rich amphibolite containing minor phlogopite at the structural base, through a hornblende-plagioclase-biotite-gedrite amphibolite in the middle, to a feldspathic plagioclase-hornblende amphibolite at the top (Fig. 5.6b). The plagioclase is labradorite in composition (Michel-Levy). Abundant apatite was noted in a sheared and altered hornblende-chlorite-clinozoisite amphibolite but was not found in the Phikwe or Selebi amphibolites. Thin massive sulphide bands occur within the lower outer margin of the mafic amphibolite and in the immediately surrounding blastomylonitic grey gneiss. Weakly disseminated sulphides occur in the rest of the host amphibolite, mainly in the lower more-mafic part. The same mineralogical gradation and sulphide distribution occurs in parts of the northern overturned limb near to the antiformal core. This mineralogical gradation and sulphide distribution is similar to that seen locally at Selebi (Fig. 5.4c).

In the core of the early antiform there is a trend towards the development of more feldspathic amphibolite at the base. However this gradation is less obvious than on the southern limb and is obscured by the development of garnet amphibolite, associated with zones of abundant disseminated sulphide (Fig. 5.6b). Sulphides, both as massive sulphide bands and disseminated zones, are abundant in the core of the early antiform. As at Phikwe, the association of garnet amphibolite with abundant disseminated sulphide is common. However at Selebi North this association occurs in zones throughout the antiformal core, whereas at Phikwe the association mainly occurs immediately below the massive sulphide layer in Zone C. The garnet-hornblende amphibolite at Selebi North is very similar to that at Phikwe. The poikiloblastic (Mlm) almandine garnets (Plate 32d) have a composition of Alm 58 -Pyr

27 -Gro 11 - Sp 4 (Table 5.2). The almandine is chemically homogeneous, except for its MnO content which varies from 2.2% at the margin to 1.3% in the core (p. A.6). The surrounding hornblende is low in Si and has a composition ranging from tschermakite to ferroan pargasite (Fig. 3.1, Table 5.2 & p.A.6). Idioblastic inclusion-free garnets occur in an unmineralised section of well-banded hornblende-plagioclase host amphibolite associated with ultramafic rocks. The inclusion-free garnets are surrounded by coarse kelyphitic rims of intergrown hornblende and plagioclase (Plate 32f). The groundmass is typical M1m granoblastic hornblende and plagioclase. The kelyphitic rims are thought to be due to late M1 retrogression of M1p relicts of inclusion-free garnets.

5.2.3b Selebi North ultramafic rocks

Ultramafic rocks occur within typical hornblende-plagioclase-mica-gedrite host amphibolite along the eastern continuation of the northern overturned limb (Fig. 5.6a). This is the largest occurrence of ultramafic rocks within the Selebi-Phikwe host amphibolite. Ultramafic rocks occur in several ways: (1) interbanded with typical host amphibolite; (2) in the centre of the amphibolite section; or (3) at the top of the overturned limb (Fig. 7.7). The contacts between host amphibolite and ultramafic rock are gradational over two c

The ultramafic rocks are similar to those within the Phikwe host amphibolite and mainly comprise massive amphibole pyroxenite with gradations between orthopyroxenite and amphibolite. Highly serpentinised peridotite bands (up to 20 cm) and pods occur within the amphibole pyroxenite. The amphibole pyroxenite consists of coarse-grained idioblastic orthopyroxene (< 3 cm) in a matrix of fine to medium-grained green hornblende (Plate 33f & g). The orthopyroxene contains abundant inclusions of randomly orientated fine-grained hornblende. Minor elongate idioblastic gedrite occurs at the margins of orthopyroxene grains (Plate 33f). Rare olivine with inclusions of green spinel occurs in the amphibole pyroxenite (Plate 33c & d). Olivine is also found as inclusions in hornblende. Locally orthopyroxene is corroded and occurs in a cummingtonite-gedrite-phlogopite-hornblende matrix. Cummingtonite-rich amphibolite, with minor phlogopite and gedrite, is rare. Serpentinised peridotite consists of relict olivine and orthopyroxene (altered to talc) in a serpentine-talc-chlorite-phlogopite matrix. Weak sulphide disseminations occur throughout the ultramafic rocks, both as inclusions within silicates and at grain

boundaries. They are more abundant where a retrogressive cummingtonite -rich or serpentine-rich assemblage is developed.

Analyses of orthopyroxene in typical hornblende orthopyroxenite show that it is bronzite (En 85) (Table 5.3 & p.A.7). The matrix hornblende ranges in composition from edenite to edenitic hornblende (Fig. 3.1) with an average Mg/Mg+Fe ratio of 0.86 and a relatively high Cr content (0.9% Cr_2O_3). There is little compositional difference between the fine-grained hornblende inclusions within orthopyroxene and the coarse-grained matrix hornblende. Orthopyroxenes are locally Ca and Na-rich (Table 5.3). This may be an effect of fine-grained hornblende inclusions in the orthopyroxene. Analyses of olivine in a hornblende orthopyroxenite show that it is chrysolite with a composition of Fo 80 and a relatively low Ni content (0.12% Ni). The associated orthopyrox-ene is bronzite (En 80) and matrix hornblende varies in composition from pargasitic to edenitic hornblende with an average Mg/Mg+Fe ratio of 0.81. The similarity in Mg/Mg+Fe ratios of coexisting olivine, orthopyroxene and hornblende is striking.

A wide variety of spinel is found in the ultramafic rocks of Selebi North (Fig. 8.7). Green spinel (pleonaste) with fine-grained magnetite inclusions is the most common. Pleonaste occurs more commonly as inclusions in olivine, than in orthopyroxene or commonly as inclusions in olivine, than in orthopyroxene or hornblende. The pleonaste inclusions have a variable size and Cr content. Fine-grained Cr-bearing pleonaste (Table 5.3 & p.A.7) is locally concentrated as indistinct bands of inclusions within olivine, orthopyroxene and hornblende (Plate 33c). Within orthopyroxene Cr-rich pleonaste occurs in trains of elongate hornblende inclusions and forms a definite fabric. Elsewhere coarse-grained pleonaste with a very low Cr content is found as inclusions in olivine in a coarse-grained hornblende-phlogopite-pleonaste-olivine orthopyroxenite (Plate 33d). Pleonaste inclusions in olivine are typically rimmed by phlogopite, whereas relict pleonaste in serpentine is rimmed by chlorite. Minor laminae and lenses of fine-grained (1 mm.) granoblastic orthopyroxene associated with grains of picotite (Table 5.3 & p.A.7) and magnetite occur in porphyroblastic amphibole orthopyroxenite. The picotite contains small blebs of magnetite and pyrrhotite at its margins. The fine-grained granular orthopyroxene is geochemically similar to porphyroblastic orthopyroxene (Table A.7). Apatite (Table 5.3) occurs along with serpentine, olivine and hornblende in a sheared ultramafic rock (Plate 33e). Its formation appears to be related to the shearing.

Amphibole-Olivine Pyroxenite

	a	b	c	d	e	f
	olv	opx	hor	spi	spi	apa
SiO2	39.22	55.07	44.89	0.09	0.10	0.11
TiO2	0.01	0.05	0.57	0.07	0.37	0.04
Al2O3	0.00	1.59	12.08	57.64	34.65	0.01
FeO	19.07	12.63	7.15	22.57	35.95	0.16
MnO	0.24	0.36	0.08	0.17	0.35	0.01
MgO	42.01	29.63	17.12	14.58	8.13	0.17
CaO	0.01	0.23	11.51	0.01	0.01	54.62
Na2O	0.00	0.02	1.97	0.04	0.02	0.11
K2O	0.00	0.00	0.22		0.00	0.01
Cr2O3	0.03	0.12	0.34	5.89	20.26	0.06
NiO	0.15	0.03	0.05		0.04	
P2O5						46.91
Total	100.74	99.73	95.98	101.06	99.88	102.21
	Fo 80	En 80				
No. of analyses	3	5	3	1	2	2

a Small olivine relict in serpentine of amphibole olivine pyroxenite 56-5

b Orthopyroxene, average of fine granoblastic and coarse idioblastic opx 56-5

c Fine matrix hornblende 56-5

d Cr-pleonaste w/ olivine 56-5

e Picotite associated with fine granoblastic opx 56-5

f Apatite associated with serpentine 56-5

See appendix A.7 for all analyses

Amphibole Pyroxenite

	g	h	i	j
	opx	opx	hor	spi
SiO2	55.34	56.63	47.62	0.06
TiO2	0.07	0.07	0.52	0.05
Al2O3	1.71	1.45	9.92	61.49
FeO	10.14	9.44	5.29	21.96
MnO	0.19	0.22	0.09	0.09
MgO	31.88	28.07	18.91	15.46
CaO	0.17	0.51	11.43	0.01
Na2O	0.00	0.25	1.90	0.02
K2O	0.00	0.00	0.13	0.00
Cr2O3	0.14	0.20	0.88	0.16
NiO	0.04	0.07	0.08	0.25
Total	99.68	96.91	96.77	99.55
	En 85	En 84		
No. of analyses	2	2	5	1

g Core of coarse idioblastic orthopyroxene of amphibolitised pyroxenite 56-7

h Core of coarse orthopyroxene altered ? 56-7

i Average of hornblendes of matrix and included in orthopyroxene 56-7

j Coarse pleonaste of coarse hornblende-phlogopite-pleonaste-olivine pyroxenite 506

Samples 56-5 and 56-7 from SDN 56
Sample 506 from SDN 45

See Figure 7.7 for SDN 56 section
See Plate 33c & e for 56-5, 33d for 506

TABLE 5.3 AVERAGE MINERAL ANALYSES -- SELEBI NORTH HOST ULTRAMAFIC ROCKS

5.2.3c Chromium in hornblende in the Selebi North host amphibolite

In the ultramafic section studied in most detail (SDN 56, Fig. 7.7) ultramafics occur at the structural top of the overturned limb above hornblende-plagioclase amphibolite. The hornblende-plagioclase amphibolite becomes increasingly feldspathic towards the base. A high-Cr hornblendite zone (3.5% Cr2O3) occurs within the lower feldspathic amphibolite (Fig. 7.7). Within this zone the Cr content of Cr-bearing hornblende varies from 0.7% Cr2O3 in coarse-grained hornblende to 1.1%

in adjacent finer-grained intergranular hornblende (Plate 32h, p.A.6). Elsewhere in this zone hornblende is low in Cr (<0.05% Cr2O3). The Cr-bearing hornblende is edenitic hornblende in composition and the low-Cr hornblende is a ferroan pargasitic hornblende with a higher Ti content than the Cr-bearing hornblende (Table 5.2 & Fig. 3.1). This negative correlation between Cr and Ti is typical of calcic amphibole within individual metamorphosed ultramafic complexes (Evans 1982). There is no basis for the use of Ti content as a geothermometer (Evans 1982). The low-Cr hornblende contains aligned titanomagnetite inclusions defining an older fabric (D1-M1e ?), whereas the high-Cr hornblende does not contain opaque minerals. The highest measured Cr content of the hornblende is insufficient to account for the average Cr content of the zone. Either hornblende with a much higher Cr content is present or more likely, unobserved fine chromite occurs in the hornblendite. The variation in the hornblende major-element composition within the zone is due to subtle variations in whole-rock geochemistry. These whole-rock geochemical variations are thought to be original (see Ch. 7.4) and metamorphism is thought to have been essentially isochemical. The high variation in the Cr content of the hornblende of the zone is thought to be due to inherited bulk Cr variations. The concentration of Cr in the latest fine edenitic hornblendes indicates that localised Cr diffusion took place. The high Cr content of the whole zone suggests that the original Cr-bearing phase is more likely to have been chromite rather than a silicate (e.g. pyroxene).

5.2.3d The nature of the Selebi North ultramfic assemblage - igneous or metamorphic ?

The question arises as to whether the olivine, spinel and orthopyroxene at Selebi North are a metamorphic or igneous assemblage. Initially the amphibole pyroxenite was regarded by the author as consisting of relict orthopyroxene (of either igneous or metamorphic origin) in a retrograde amphibole matrix. The main assemblage and texture is one of orthopyroxene porphyroblasts in a hornblende matrix, the interpretation of which is equivocal. However the olivine-pleonaste-hornblende-orthopyroxene assemblage with hornblende inclusions in olivine appears to be in textural equilibrium (Plate 33c). The amphibole that would be expected to form from the isochemical retrogression of orthopyroxene is anthophyllite or magnesio-cummingtonite, not hornblende (Evans 1982). Abundant Ca and Al metasomatism would be required to form hornblende and there is no evidence

(e.g. zonation of the ultramafic bodies) for this. In addition, the fine-grained hornblende inclusions within orthopyroxene are identical in composition to matrix hornblende. The hornblende-orthopyroxene and olivine-pleonaste-hornblende-orthopyroxene assemblages are therefore thought to be equilibrium M1 metamorphic assemblages. The cummingtonite-gedrite-phlogopite assemblage, which is developed in (sheared) amphibole pyroxenites, is the retrograde assemblage (M2). Serpentine with lesser amounts of chlorite, phlogopite and talc is the M2 assemblage developed in olivine-rich rocks. The fabric of pleonaste-hornblende inclusions in orthopyroxene porphyroblasts is thought to be a D1-M1e metamorphic fabric rather than an original igneous fabric.

The assemblage olivine-green spinel-hornblende-orthopyroxene is the typical eqilibrium assemblage of metaperidotites at the transition between upper amphibolite and granulite facies conditions (Evans 1977, 1982). The amphibole of the Selebi North Ultramafic rocks, with its average Si content of 6.6 atoms per formula unit and edenitic hornblende composition, is typical of these conditions (Evans 1982). During progressive metamorphism, magnesio-hornblende replaces tremolite through complex substitutions of the tschermakite and pargasite end-members at this high temperature facies (Frost 1975, 1976; Misch & Rice 1975; Evans 1977). The transformation can be represented by the following equilibrium reaction:

2 Tremolite + 5 Spinel + 2 Na + H_2O
= 2 Hornblende + 3 Forsterite + 3 Enstatite + 2 H

The porphyroblastic texture of Selebi North orthopyroxene is typical of metamorphic rocks (Evans 1977). The orthopyroxene has an average CaO content of 0.2%, which is characteristic of the amphibolite-granulite facies transition (Evans 1982). However the orthopyroxene plots close to the boundary of the fields for igneous and metamorphic pyroxenes in a (Mg + Fe)-Al diagram (Bhattacharyya 1971; Medaris 1972). The minor lenses and laminae of fine-grained granular orthopyroxene associated with picotite are anomolous because of their texture and spinel composition. The granular texture is similar to a cumulate texture and picotites do occur in unmetamorphosed ultramafic rocks (Henderson 1975). It is possible therefore that the granular orthopyroxene-picotite assemblage is a relict, original igneous assemblage. Evans & Frost (1975) however have shown that during progressive meta-morphism of ultramafic rocks the range of spinel compositions

increases from Al-poor Cr-magnetite alone in low-grade serpentinites, and gradually includes ferrit-chromite, chromite, Al-chromite and Cr-Al spinel (picotite). Eventually the range includes green Mg-Al spinel close to the granulite facies transition. The picotite could therefore be of metamorphic origin. A metamorphic origin of the fine granular orthopyroxene-picotite assemblage, possibly synchronous with the formation of the early pleonaste fabric (D1-M1e), is preferred by the author. The variation in Cr content of pleonaste at Selebi North is probably due to variation in bulk rock geochemistry (Evans & Frost 1975; Medaris 1975).

Theoretical and experimental studies on ultramafic systems (Trommsdorf & Evans 1974; Evans 1977; Lieberman & Rice 1986) indicate that the olivine-spinel-edenitic hornblende-orthopyroxene assemblage at Selebi North lies above the curve for the univariant reaction:

Chlorite = Forsterite + Enstatite + Spinel + H2O (Fig. 5.7)

The presence of enstatite and spinel rather than cordierite places the assemblage above the curve for the reaction:

Enstatite + Spinel = Cordierite + Forsterite

The absence of clinopyroxene at Selebi North indicates that metamorphic conditions did not reach high enough temperatures and pressures for the reaction:

Forsterite + Tremolite = Diopside + Enstatite + H2O

These three reactions in the pure CaO-MgO-Al2O3-SiO2-H2O system constrain the metamorphic conditions of the Selebi North ultramafics to 725-825°C at 3-8 kbar (Fig. 5.7). The absence of plagioclase and the presence of hornblende rather than tremolite indicate that temperatures and pressures were close to the upper limits of this range (Frost 1976).

Fe/Mg fractionation between olivine and spinel is strongly temperature dependent (Evans 1977). Evans & Frost (1975) and Fabries (1979) have empirically calibrated the olivine-spinel geothermometer. The ferric iron content of the Selebi North spinels has been estimated stoichiometrically, although complete analysis, particularly of ferric iron in spinel, is required for the geothermometer. Comparison with

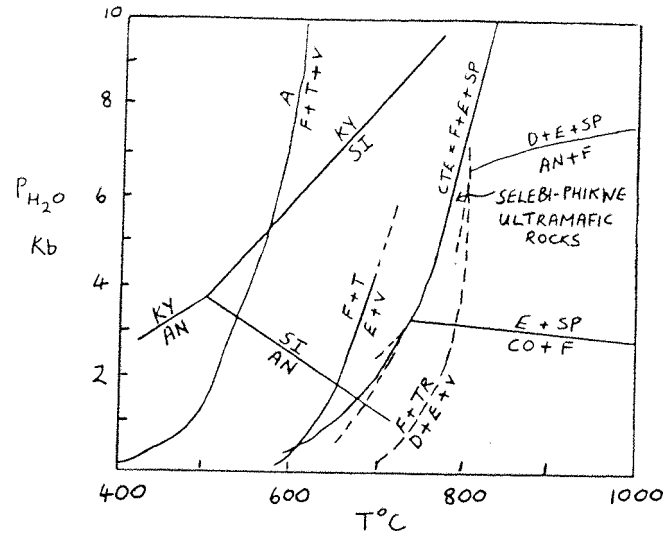

Fig. 5.7 PART OF THE P-T PHASE DIAGRAM FOR REACTIONS IN THE SYSTEM CaO-MgO-Al2O3-SiO2-H2O (Evans 1977). Full lines experimentally reversed, broken lines calculated or inferred. A, Antigorite; F, Forsterite; T, Talc; E, Enstatite; CTE, Chlorite; SP, Spinel; TR, Tremolite; D, Diopside; An, Anorthite; CO, Cordierite; V, Water Vapour. Superimposed Alumino-Silicate phase diagram from Holdaway (1971).

the above calibrations and that by Desmarais (1981) gives temperatures of around 750 $\pm$ 50 °C for olivine-spinel pairs at Selebi North. This estimate is consistent with the P-T estimate in Figure 5.7. and with with that made from the corundum-spinel-sapphirine assemblage (800 °C and 10 kbar) in Chapter 3.9.2.

The olivine, orthopyroxene and spinel occurring in the ultra-amafic rocks of Selebi North and Phikwe are regarded as M1 metamorphic minerals rather than original igneous minerals. The evidence for this can be summarised as follows:

(a) The olivine-green spinel-hornblende-orthopyroxene assemblage appears to be an equilibrium metamorphic assemblage rather than a disequilibrium assemblage of relict olivine, spinel and orthopyroxene with metamorphic amphibole.

(b) The variation in Cr content of pleonaste inclusions in olivine.

(c) The coarse-grained porphyroblastic nature of the orthopyroxene.

(d) The similar Mg/Fe ratios of coexisting olivine, orthopyroxene and hornblende.

(e) The nature of the typical amphibole, i.e. hornblende which is typical of the upper amphibolite to granulite facies conditions (Evans 1977), rather than anthophyllite or magnesio-cummingtonite which would

be expected to form from the isochemical retrogression of orthopyroxene (Evans 1982). The hornblende included within porphyroblastic orthopyroxene is the same as that as forming the matrix to it.
(f) The metamorphic fabric formed by hornblende and pleonaste inclusions in orthopyroxene.

The view that the olivine and pleonaste of the ultramafic rocks at Phikwe and Selebi North are metamorphic rather than relict igneous is contrary to that of Wakefield (1974, 1976). Wakefield observed relict igneous olivine, pleonaste, magnetite and sulphide in metamorphic orthopyroxenite at Phikwe and suggested that igneous olivine was replaced by metamorphic orthopyroxene. He also observed subspherical, occasionally dumbbell-shaped blebs of sulphide within olivine. He regarded this as of fundamental importance in proving the magmatic origin of the Selebi-Phikwe ore bodies. No evidence was found in this study of orthopyroxene replacing olivine. The olivine, orthopyroxene and pleonaste in the Selebi-Phikwe host rocks are all regarded as metamorphic. Contrary to the conclusion of Wakefield (1974, 1976), the rounded form of inclusions of sulphide in a mineral (in this case in olivine interpreted by Wakefield as relict igneous and by this author as metamorphic) does not necessarily mean that the sulphides are original immiscible droplets. The rounded form of sulphide inclusions could be due to the lack of gross orientation effects and to negligigible differences in interfacial energies between positions within, and at the grain boundary of, the host mineral (Stanton 1964).

5.2.3e Relationship of SN ultramafic rocks to SN host amphibolite

The mineralogical variation shown by the host body in SDN 56 (Fig. 7.7) from an ultramafic top to a feldspathic base suggests that tectonic overturning of an originally differentiated igneous body has occurred. This variation however is in the opposite direction of the previously mentioned gradation (in the same overturned limb near the antiformal closure to the west) from feldspathic amphibolite at the top to mafic amphibolite at the base (Fig. 5.6b). This apparent discrepancy could be because the Selebi North structure is more complex than envisaged or because the ultramafic rocks are unrelated to the host amphibolite. In other sections at Selebi North, ultramafic rocks occur in the middle of the section surrounded by typical host amphibolite or are interbanded with host amphibolite. Although it is accepted that unknown structural complexities probably exist at Selebi North, the section in SDN 56 (Fig. 7.7) is considered to be unrepres-

entative of the relationship of the ultramafics to the host amphibolite. Ultramafic rocks occur within the host amphibolite at Selebi North, but at no particular position. The gradational contacts between host amphibolite and ultramafic at Selebi North and Phikwe indicate that the ultramafic rocks are related to, and are an integral part of, the Selebi-Phikwe host amphibolite. This is contrary to the conclusion of Wakefield (1974, 1976), who regarded the contacts of ultramafic rocks with host amphibolite at Phikwe as sharp and intrusive. He therefore suggested that ultramafic rocks at Phikwe represent an intrusion into the host amphibolite protolith. Wakefield (1974, 1976) also concluded that the origin of the sulphides was intimately linked with these later ultramafic rocks. However the distribution of disseminated sulphide in the ultramafic rocks is similar to that in surrounding host amphibolite.

5.2.4 Summary of Conclusions

The mineralised host amphibolites at Selebi, Selebi North and Phikwe are essentially similar and comprise hornblende-rich amphibolites with variable amounts of plagioclase, gedrite, mica, garnet and disseminated sulphide. Locally there are systematic mineralogical gradations vertically through the host amphibolites. At Phikwe the amphibolite locally develops a mafic core with more feldspathic margins. At Selebi and Selebi North there is a gradation from mafic hornblende-rich amphibolite at one margin to feldspathic amphibolite at the other.

The host amphibolites are conformable with the surrounding Selebi-Phikwe gneisses and have suffered all the phases of deformation that have been recognised in the gneisses. The metamorphic assemblage that occurs in the host amphibolites can be correlated with those that formed in the surrounding gneisses. The amphibolites have been metamorphosed at conditions of the transition from upper amphibolite to granulite facies.

Ultramafic rocks are an integral part of the host amphibolites at Phikwe and Selebi North. The ultramafics are coeval with the host amphibolites and do not represent later intrusions. The assemblages in the ultramafics are metamorphic, not igneous.

The mafic hornblende-rich mineralogy of the Selebi-Phikwe host amphibolites, their association with Ni-Cu ores and their gradation into ultramafic rocks suggest an igneous origin for the host amphibolites.

PLATE 26
Morphology of Phikwe Ore Body (1)

(A) Phikwe Open Pit. Early-D2 folds in footwall (FW) gneisses plunge towards viewer. No early-D2 folds in hanging wall (HW) gneisses.

(B) Phikwe Open Pit. Early-D2 folds in footwall gneisses.

(C) Phikwe Open Pit. Early-D2 fold in footwall gneisses and ore body. Hanging wall gneisses dip less steeply than the ore body (OB). See Fig. 5.3b.

(D) "Durchbewegung" - amphibolite inclusions in massive sulphide. Zone D/E.

(E) Chalcopyrite-rich upper part (C) of the massive sulphide layer. Zone E.

(F) "Durchbewegung" - amphibolite inclusions in massive sulphide. Abrupt termination of massive sulphide against host amphibolite (A) which was in the process of being incorporated into the massive sulphide. Zone D/E.

(G) Late-D2 shear zone. Pyrite-bearing M2b mylonite. Host amphibolite and massive sulphide absent. Zone C.

(H) M2b mylonite from (G). Pyrite, chlorite and felsics. # 1600/315. FV = 3 mm.

PLATE 27
Morphology of Phikwe Ore Body (2)

Superimposed D2 shearing - Phikwe Ore Body, Zone D

(A) Superimposed early and late-D2 shearing. See. Fig. 6.1a.

(B) Late-D2 M2b mylonite of chlorite and felsics from (A) with relict phacoid of early-D2 M2a mylonite. # 1900/200d. FV = 6mm.

(C) M2b mylonite from (A) with veinlet of calcite. FV = 6 mm.

(D) Pyrite in M2b mylonite from (A). M2a mylonite in bottom right corner. FV = 6 mm.

(E) Amphibolite inclusion in massive sulphide. Note chalcopyrite in pressure shadow. Phikwe Zone E.

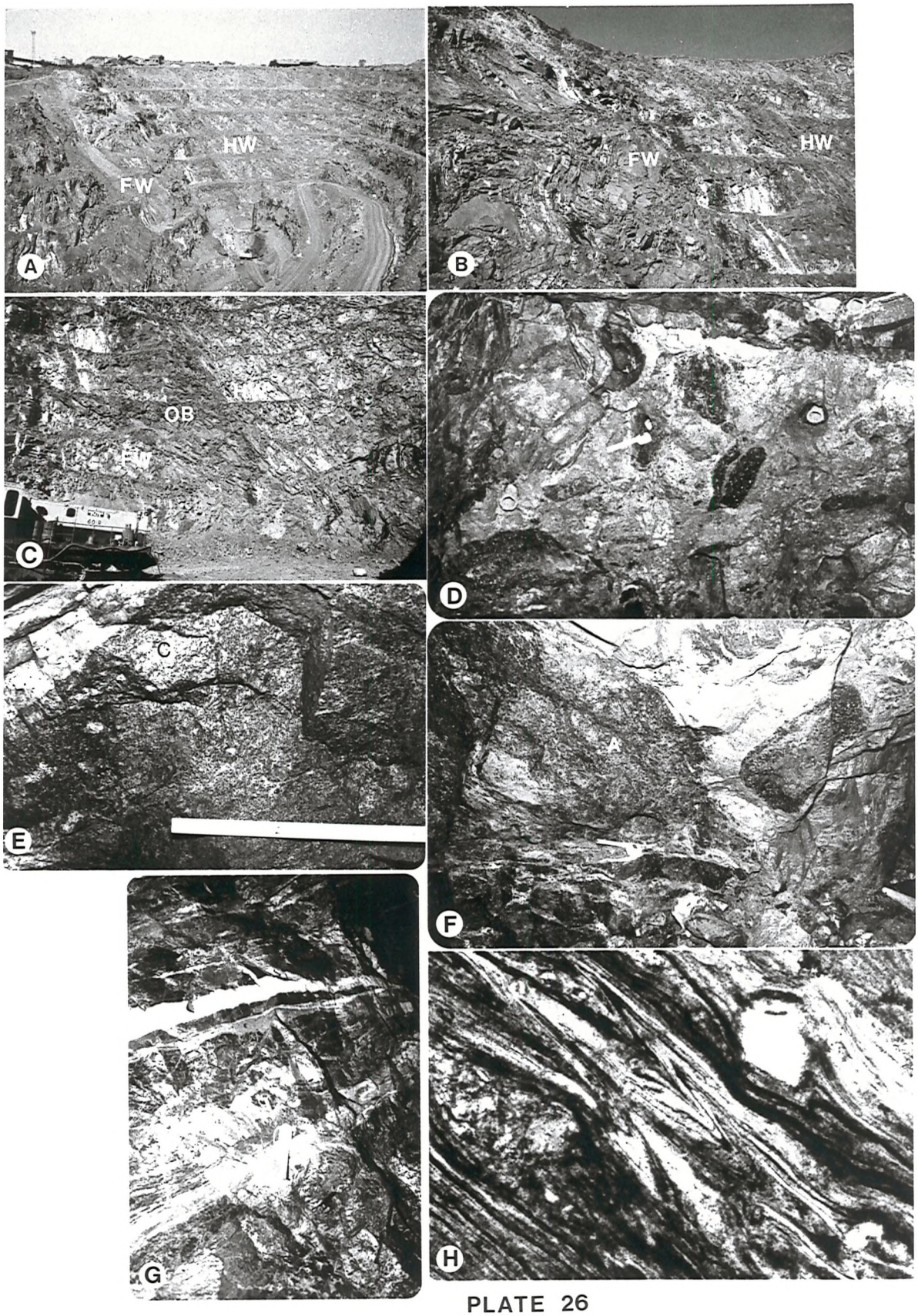

PLATE 26

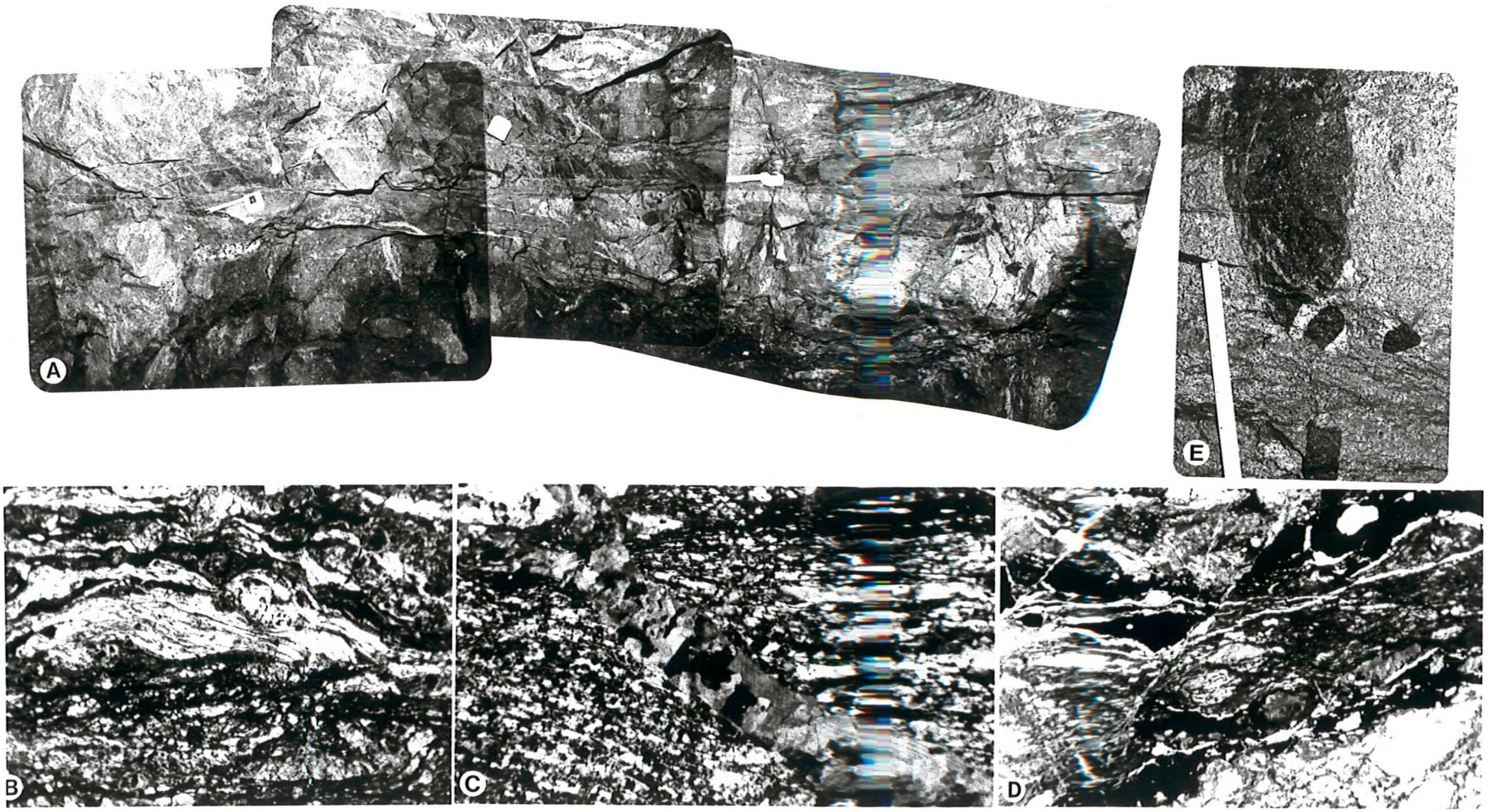

PLATE 27

PLATE 28

Morphology of Phikwe Ore Body (3)

(A) Zone B. Massive sulphide layer crosscutting steep foliation in host amphibolite.

(B) Zone B. Early-D2 tongue of host amphibolite which is becoming mixed with massive sulphide.

(C) & (D) Massive sulphide crosscutting footwall grey gneiss. Minor tongues and veinlets from massive sulphide into grey gneiss. Zone D/E.

(E) Zone D. The massive sulphide layer atypically below the host amphibolite (A).

(F) & (G) Massive sulphide crosscutting D2 folds in footwall gneisses. Grey gneiss has abundant quartz-rich segregations in (G). Zone D/E.

(H) Wedge of massive sulphide into host amphibolite. Chalcopyrite and quartz at edge of wedge. Zone C.

PLATE 29

Morphology of Selebi Ore Body

(A) & (B) Upper Body below A/B split. Thin irregular massive sulphide layer with "durchbewegung" at top of host amphibolite. See Fig. 6.1b.

(C) Wedge of massive sulphide intomhost amphibolite.

(D) End of Upper A body. See Fig. 6.1c.

(E) Atypical coarse-grained magnetite (M) and chalcopyrite-rich (C) ore.

(F) & (G) Selebi Upper B body. Tongues of massive sulphide into grey gneiss. See Fig. 6.1d.

PLATE 30

Garnetiferous host amphibolite at Selebi

(A) - (D). Thin irregular massive sulphide at top of host amphibolite in Upper B body. Garnets (Gnt) developed at contact of mafic host amphibolite (Amp) with massive sulphide. HWG = hanging wall gneiss. See Fig. 7.6.

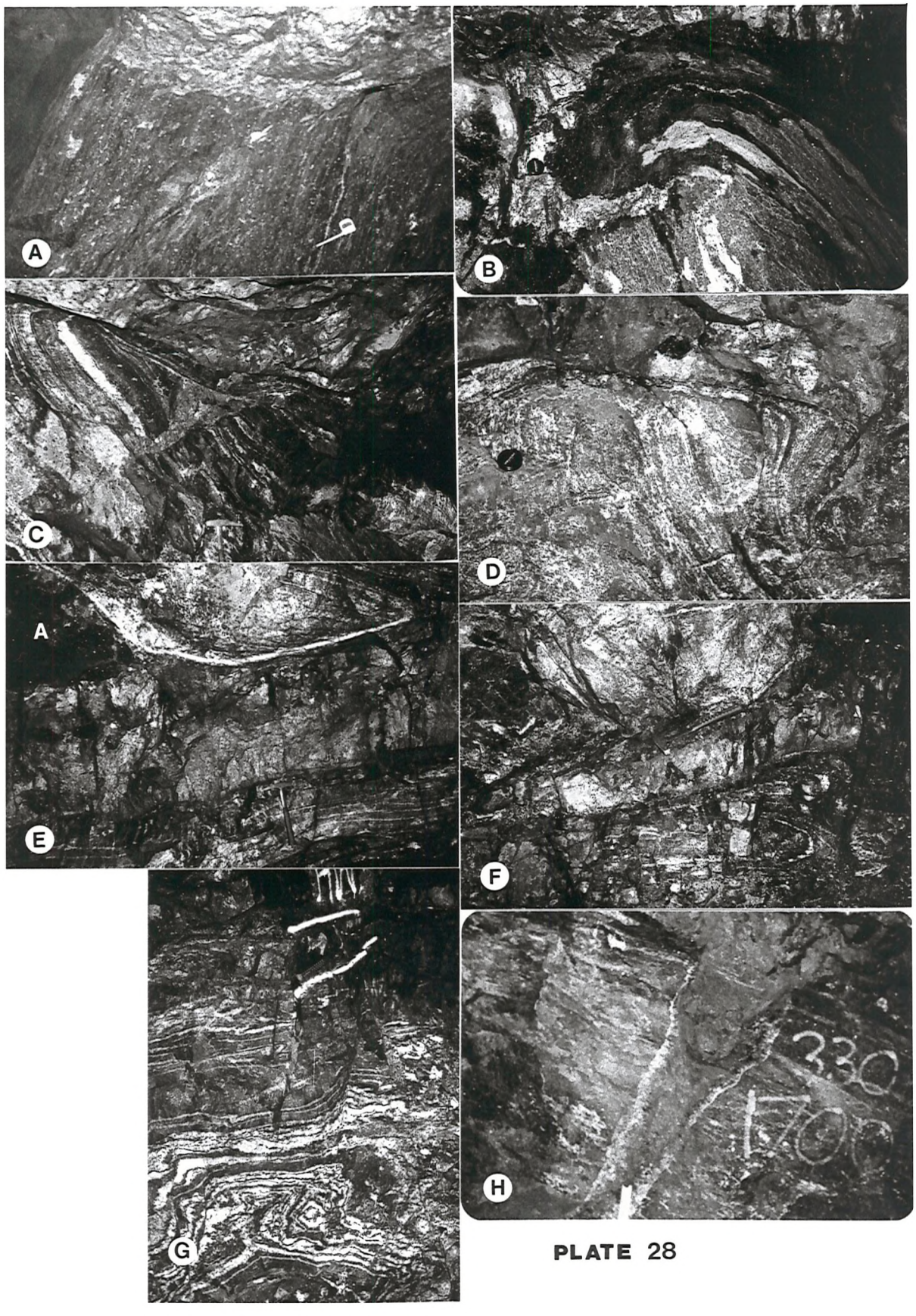

PLATE 28

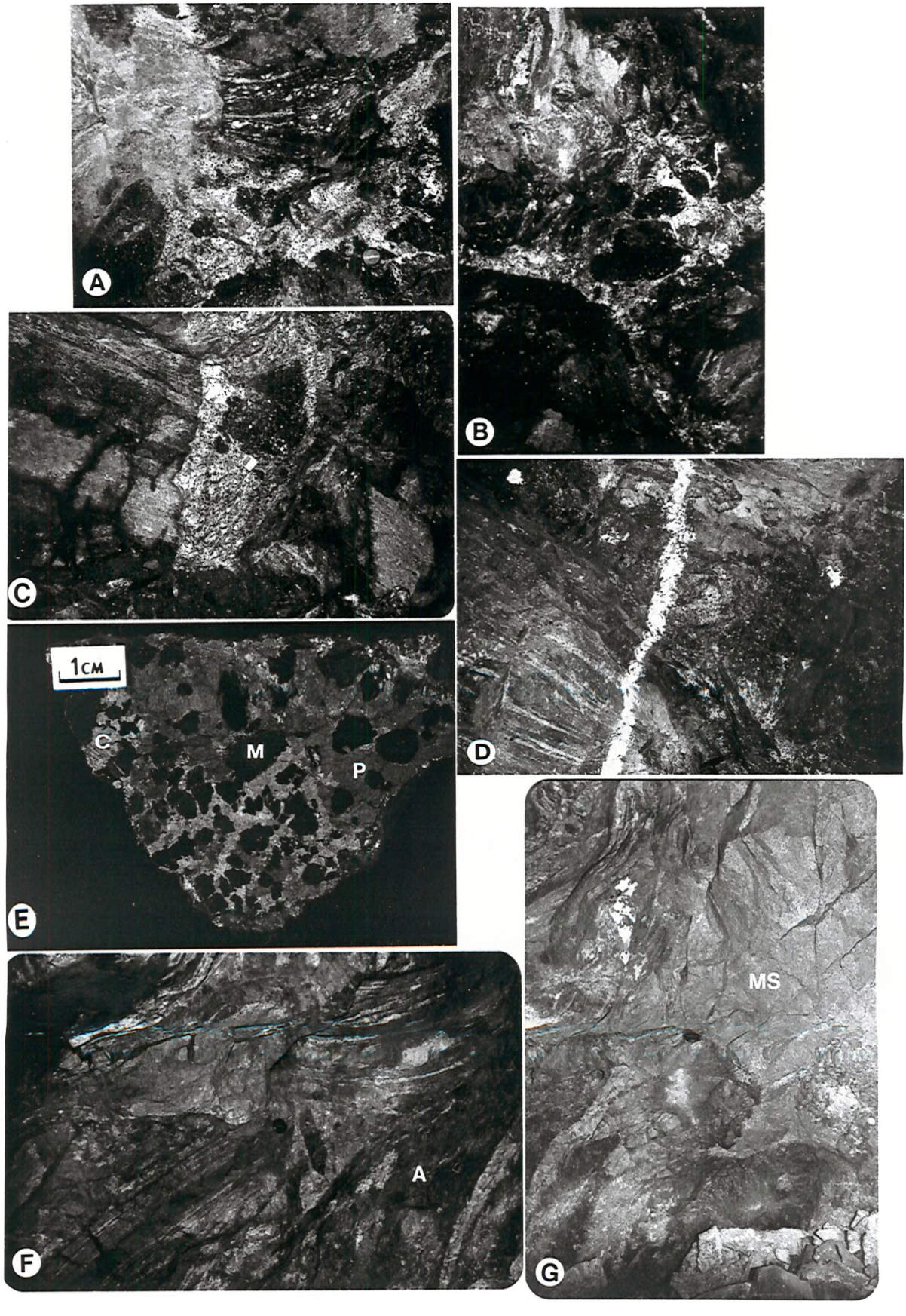

PLATE 29

PLATE 31

The Selebi-Phikwe Host Amphibolite (1)

(A) Typical host amphibolite of Zone A. A granoblastic decussate M1m hornblende-plagioclase rock with randomly orientated biotite. # 34c. FV = 6 mm.
(B) Idioblastic gedrite in matrix of hornblende and gedrite .# 34e. FV = 6 mm.
(C) M1p (?) spinel inclusions in hornblende. # 34f. FV = 3 mm.
(D) Altered relict of orthopyroxene (M1p?) surrounded by hornblende. # 34j. FV = 3 mm.
(E) Sulphide at hornblende-plagioclase boundaries. Phikwe, # 34k. FV = 3 mm.
(F) Feldspathic M1m hornblende-plagioclase amphibolite. Selebi, # Su 30. FV = 6 mm.
(G) Weakly foliated M1m hornblende-gedrite-plagioclase-biotite amphibolite. Selebi, # 268. FV = 6 mm.
(H) M2 assemblage in sheared amphibolite. Phacoid of relict plagioclase in chlorite, anthophyllite, clinozoisite and biotite. Selebi, # 254. FV = 6 mm.

PLATE 32

The Selebi-Phikwe Host Amphibolite (2)

(A) M2a assemblages at contact of host amphibolite with grey gneiss. M2a blastomylonitic plagioclase-rich grey gneiss. Hornblende porphyroblasts (clasts ?) in a sulphide-rich matrix in the host amphibolite. Phikwe, # 174. FV = 6 mm.

Selebi Spinel Amphibolite

(B) Corundum porphyroblast (M1p) at the core of the spinel (pleonaste) aggregate. Anorthite altering to M2 clinozoisite occurs at the bottom right corner. # 112. FV = 6mm.
(C) Edge of spinel aggregate within host amphibolite. Note anorthite within spinel. Spinel surrounded by mantle of clinozoisite after anorthite. # 153d. FV = 6 mm.

Phikwe and Selebi North Garnet Amphibolite

(D) M1m poikiloblastic spongey almandine including hornblende. Selebi North, # 129. FV = 6 mm.
(E) M1m poikiloblastic almandine including hornblende and biotite. Phikwe, # 180. FV = 6 mm.
(F) Kelyphitic M1m hornblende-plagioclase rim around inclusion-free M1p garnet. Selebi North, # 501. Fv = 3 mm.
(G) Hornblende porphyroblast in granular garnet matrix. Highly garnetiferous inclusion in massive sulphide, Zone E at Phikwe, # 272. FV = 6 mm.

(H) Cr-rich hornblende amphibolite. Cr is higher in fine-grained intergranular hornblende than in coarse-grained hornblende. Selebi North, # SN 56-17. FV = 6 mm.

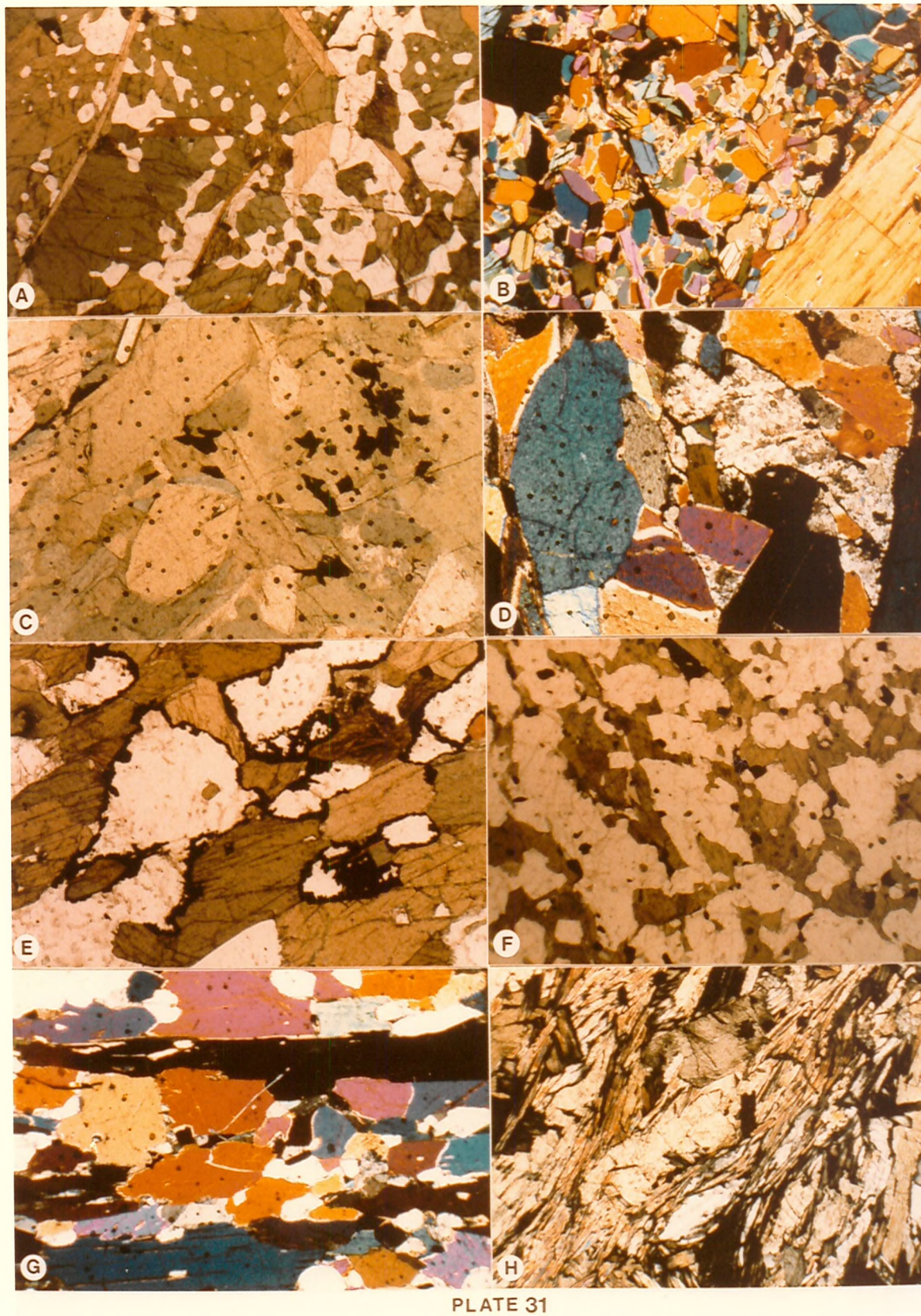

PLATE 31

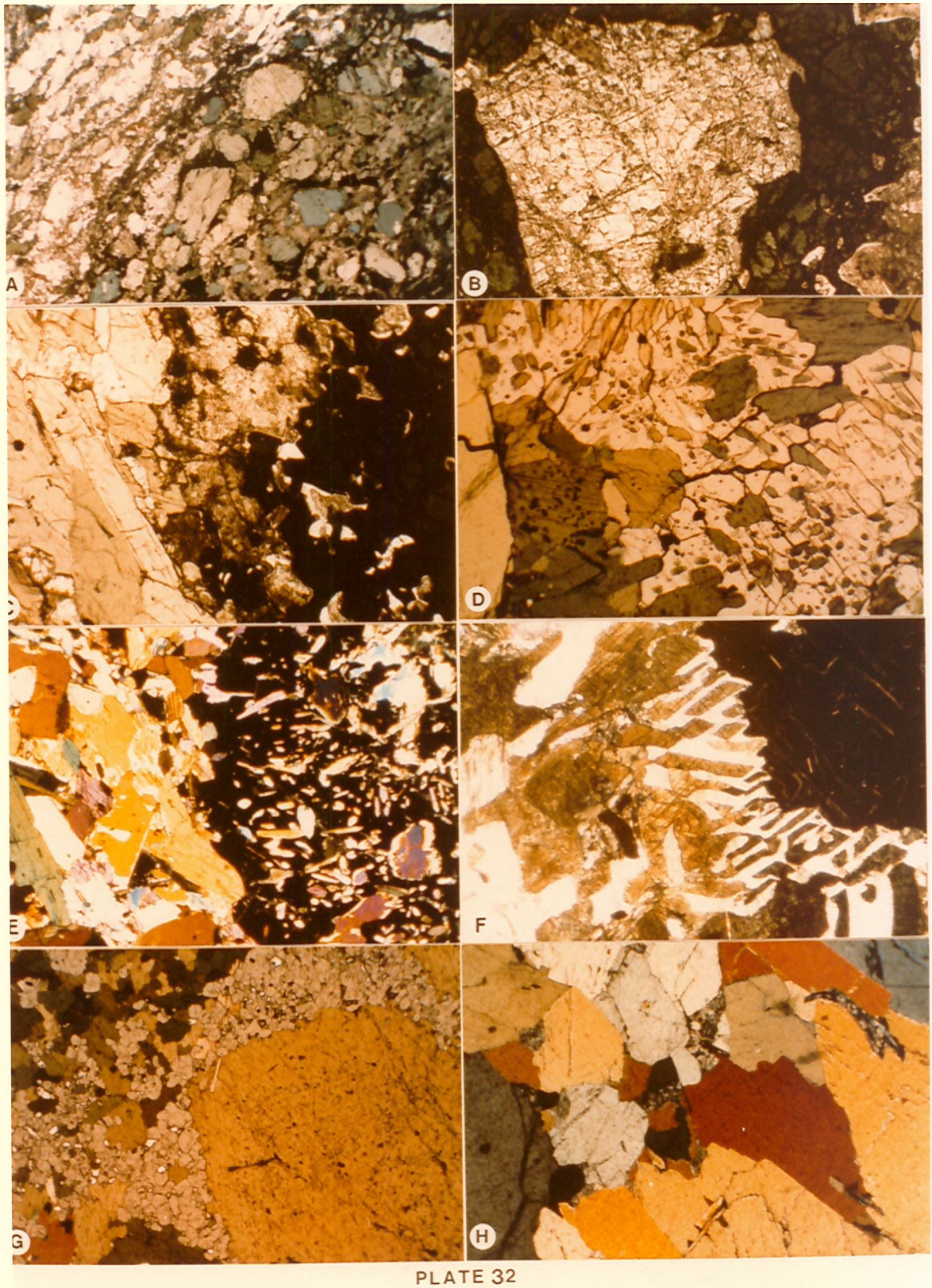

PLATE 32

PLATE 33

(A) Inclusion-rich Type 2 massive sulphide layer. Mainly biotite and plagioclase inclusions in pyrrhotite. Development of M2 myrmekite in area of fine-grained recrystallised quartz and feldspar at edge of plagioclase porrphyroclast. In situ stress-induced crystallisation. Phikwe, # 271. Fv = 3 mm.

Phikwe and Selebi North Host Ultramafic Rocks

(B) Hornblende orhopyroxenite. Equilibrium assemblage of spongey orthopyroxene porphyroblast with inclusions of hornblende in matrix of hornblende. Phikwe (PW 204a), # 520. FV = 6 mm.

(C) Olivine-hornblende orthopyroxenite. Olivine porphyroblast in hornblende matrix. Inclusions of hornblende in olivine. Mle fabric of trains of green spinel in both olivine and hornblende. Selebi North (SN 56), # SN 56-5. FV = 6 mm.

(D) Dark green spinel (pleonaste) rimmed by phlogopite in olivine porphyroblast in orthopyroxenite. Selebi North (SN 45),# 506. FV = 6 mm.

(E) Apatite (A) in hornblende in a hornblende-spinel-olivine rock (as C). Selebi North (SN 56), SN 56-5. FV = 6 mm.

(F) Hornblende orthopyroxenite. Gedrite (G) at margin of ortho-pyroxene porphyroblast. Matrix and inclusions in opx. are hornblende. Selebi North (SN 56),# SN 56-11. FV = 6 mm.

(G) Hornblende orthopyroxenite. Hornblende inclusions in orthopyrox-ene porphyroblast. Selebi North (SN 45),# 505. FV = 6 mm.

(H) Granular chrome-rich spinel (chromite ?) with unknown silicate. Phikwe, (PW 204a), # 522. FV = 3 mm.

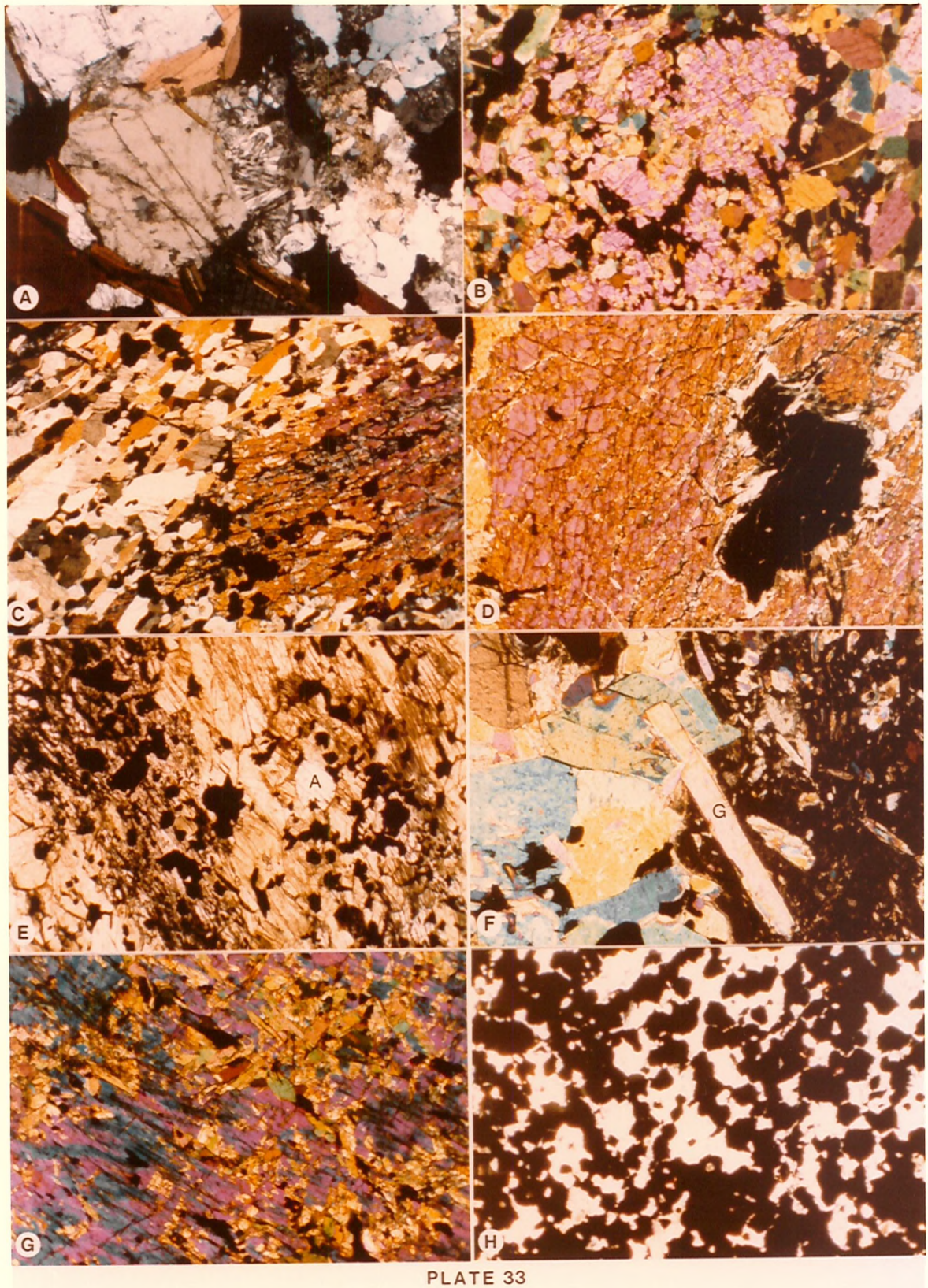

PLATE 33

CHAPTER 6 THE SELEBI-PHIKWE SULPHIDES

The primary sulphides of the Selebi-Phikwe ore bodies are mainly pyrrhotite with lesser pentlandite, chalcopyrite and pyrite. Magnetite is commonly associated with the sulphides. The products of near-surface oxidation processes in the upper levels of the ore bodies, which include pyrite, violarite, marcasite, bravoite, covellite and bornite (Gordon 1973, Lear 1979), are not considered in this thesis.

6.1 SULPHIDE DISTRIBUTION AND GROSS FEATURES

6.1.1 Phikwe

Sulphides at Phikwe occur either as pyrrhotite-rich massive sulphides or as disseminations in the host rocks (mainly amphibolite with minor ultramafic rock). The zonation of the Phikwe ore body has been described in Chapter 5.1 and is shown in Figures 5.1 and 5.2. There is a thick tabular massive sulphide at Phikwe. This massive sulphide occurs in cataclastic grey gneisses without any host amphibolite in Zone E; at the top of relatively barren host amphibolite in Zone D; and towards the top of host amphibolite with disseminated sulphides in Zones C. Towards the northwest end of Zone C and in Zone B the main massive sulphide layer thins and occupies a more central position within the host amphibolite. Its place is taken by several thin massive sulphides within the host amphibolite. Early D2 folding within the host amphibolite of Zone B has possibly caused the massive sulphide to be repeated. The main massive sulphide layer is typically 2-3 metres thick and is thickest in Zone D (up to 12 m). The massive sulphide layer locally thins (Plate 27f & g) and may be absent (Plates 26g & 27a, Fig. 6.1a) because of late D2 shearing. However it appears to be essentially the same continuous layer from Zone E to Zone C. The main massive sulphide layer locally crosscuts the foliation in the host amphibolite (particularly in Zone B, Plate 28a), and the foliation in the grey gneisses in Zones D and E (Plate 28c-f). The contacts of massive sulphide are sharp. There are no gradational contacts between massive sulphide and amphibolite hosting abundant disseminated sulphides (Plate 34d).

The Phikwe massive sulphides have been subdivided into magnetite-bearing massive sulphide with amphibolite inclusions (Type 1) and siliceous inclusion-rich massive sulphide without magnetite

(Type 2). There is a complete gradation between the two types. Type 1 massive sulphides occur in Zones B and C whilst in Zone C they grade into Type 2 massive sulphide of Zones D and E. At the eastern end of Zone E abundant pyrite is developed within Type 2 massive sulphide and overlying cataclastic gneisses (see Chapter 6.2.3).

Near the base of the host amphibolite a thin Type 1 massive sulphide is locally developed. Locally at the base of the massive sulphide layer there are wedges which project down into the host amphibolite (Plate 28h). These wedges were only found projecting into host amphibolite, never into grey gneiss. Chalcopyrite is concentrated at the margin of the wedge and there is an outer rim of quartz-rich pegmatite. The wedges are probably tensional features associated with late D2 open folding of the ore body.

Disseminated sulphides in the Phikwe host amphibolite are most common in Zones C and B. In Zone C disseminated sulphides are most abundant in garnet amphibolite immediately below the massive sulphide and their content decreases downwards in the host amphibolite. The disseminations in garnet amphibolite are typically coarse chalcopyrite -rich segregations. Sulphide stringers both parallel to the massive sulphide and randomly orientated are also common within the garnet amphibolite of Zone C. In Zone B disseminated sulphides typically occur in the middle of the host amphibolite and their content decreases towards both upper and lower margins of the amphibolite. Zones A and D contain only minor disseminated sulphide. Contrary to the conclusion of Wakefield (1974, 1976) disseminated sulphide is no more associated with the thin ultramafic lenses that occur in the middle of the host amphibolite in Zone C, than it is with typical surrounding host amphibolite.

Silicate inclusions are found in both Type 1 and Type 2 massive sulphide. There is a gradual change in inclusion lithology from amphibolite to siliceous grey gneiss, and a decrease in inclusion size going from Type 1 massive sulphide in Zone B to Type 2 massive sulphide in Zone E. In Zone B and C round inclusions (0.2 - 1 m) of hornblende-rich amphibolite and lesser garnet amphibolite are the most common (Plate 26d & f). These inclusions have gradational margins with the surrounding massive sulphide and appear to have been disrupted and replaced by sulphide. The inclusions typically have chalcopyrite and lesser pentlandite concentrated at their margins. Chalcopyrite disseminations are also abundant within amphibolite inclusions. Some amphibolite inclusions have the shape of detached

fold cores (cf. Vokes 1969). Thin trains of hornblendes trail out from these detached fold cores (Plate 34a) or pick out isoclinal folds within massive sulphide. This fabric of round inclusions is similar to the "durchbewegung" of German workers (Vokes 1969) and appears to have resulted from a thorough "kneading" of the massive sulphide in which rotational movements dominated.

Passing from Type 1 massive sulphides in Zone C to Type 2 in Zone D, siliceous inclusions of cataclastic grey gneiss and individual quartz, plagioclase or biotite crystals gradually become more common until in Zone E they are the most abundant type (Plate 34b, & f). At the eastern end of Zone E there are no amphibolite inclusions. The amount of siliceous inclusions relative to sulphide also increases, until at the eastern end of Zone E up to 80% of the Type 2 massive sulphide layer consists of single small (1-5mm) crystals (Frontispiece A). This inclusion-rich massive sulphide has the appearance of a sulphide-cemented breccia (cf. Vokes 1969). This texture is also found in thin Type 2 layers intersected by deep exploration holes at the extremities of the ore body (Fig.5.1). These Type 2 massive sulphides typically have a weak foliation picked out by biotite (Plate 34b). Some plagioclase inclusions have myrmekitic intergrowths at their margins. Some of these are myrmekitic porphyroclasts from the enclosing cataclastic grey gneisses that have been incorporated into the Type 2 massive sulphide. However some of the myrmekite is thought to have been an in situ stress-induced crystallisation where the sulphide content is low (Plate 33a). The development of myrmekitic exsolution during cooling would have been aided by internal dislocations, especially micro-cracks in the high temperature plagioclase (Hubbard 1968). Some amphibolite inclusions do occur in the Type 2 massive sulphide eastwards of the termination of host amphibolite in Zone D. These amphibolite inclusions in Zones D and E have much sharper margins than those to the northwest in Zones B and C. Chalcopyrite is concentrated in pressure shadows around the inclusions (Frontispiece B, Plate 27e), rather than within the inclusions. Locally in Zone E there are quartz veins at the top of the massive sulphide at the contact with cataclastic gneisses. Large inclusions of quartz vein have been incorporated into the massive sulphide (Frontispiece C).

Except for the lateral continuation of the main massive sulphide into Zone E there is very little sulphide in the immediately surrounding grey gneiss. Minor tongues and stringers of sulphide cut

Fig. 6.1a PHIKWE - SUPERIMPOSED D2 SHEARING - ZONE D

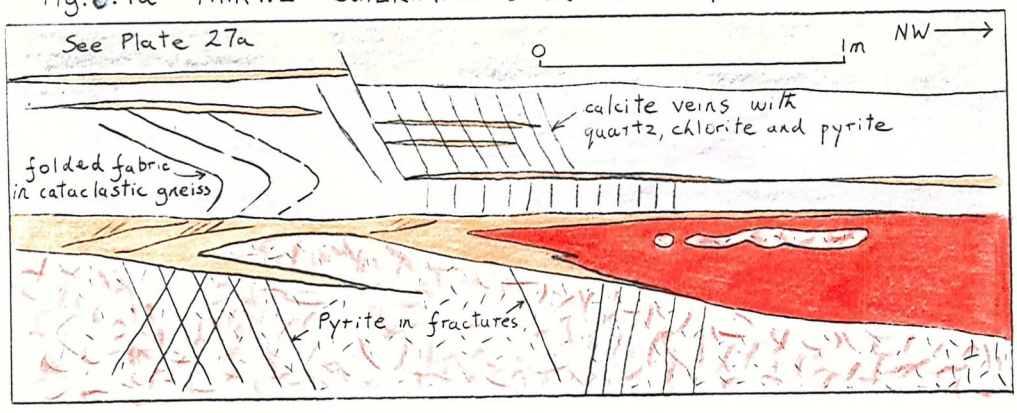

Fig 6.1b SELEBI - UPPER BODY - BELOW A/B SPLIT

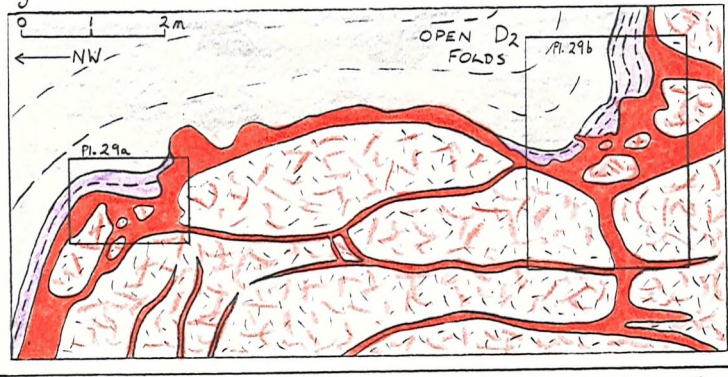

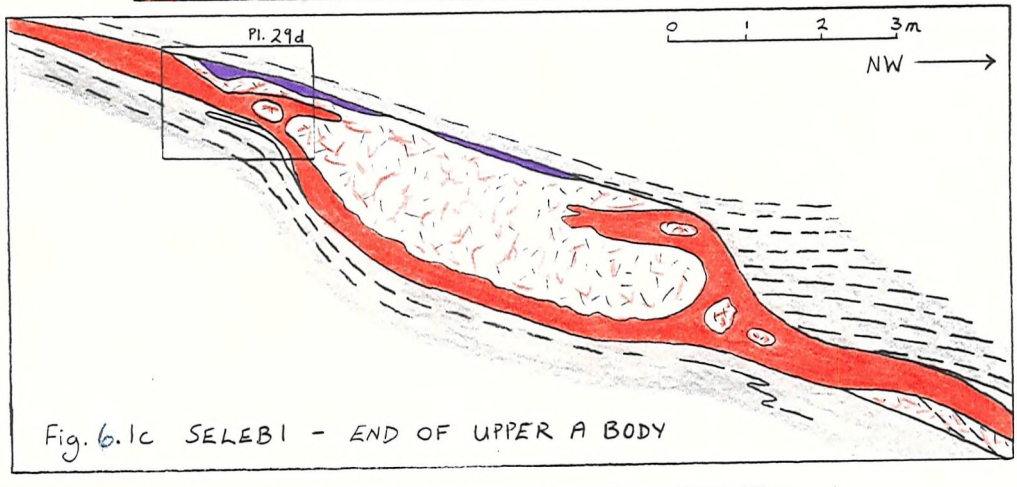

Fig. 6.1c SELEBI - END OF UPPER A BODY

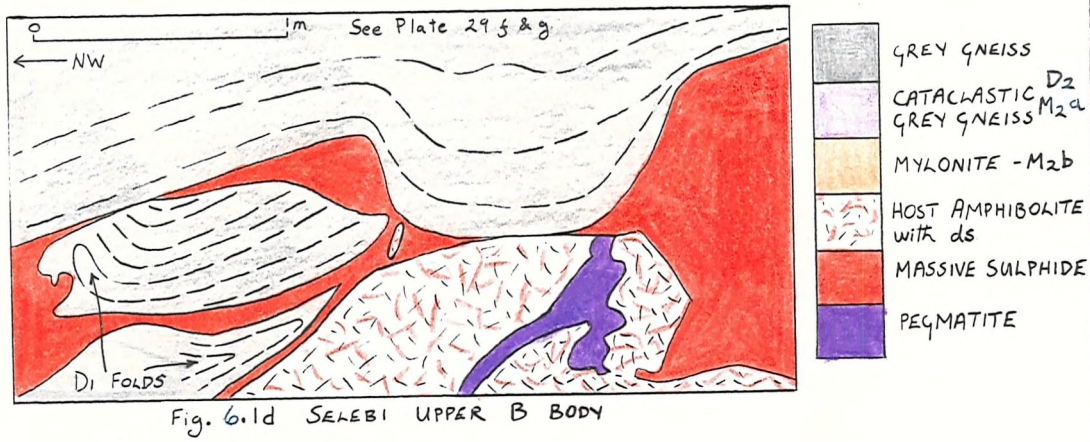

Fig. 6.1d SELEBI UPPER B BODY

Fig. 6.1 MASSIVE SULPHIDE RELATIONSHIPS AT PHIKWE AND SELEBI

across grey gneiss but only for short distances (Plate 28c & d). Locally there are minor sulphide disseminations in grey gneiss. However grey gneiss in contact with host amphibolite or massive sulphide is normally completely barren. The base of the Type 2 massive sulphide layer is usually sharp against weakly cataclastic grey gneiss (Frontispiece A). The base locally follows the minor D2 folds in the grey gneiss, but typically cuts across them (Plate 35a, Fig. 6.2).

6.1.2 Selebi

Sulphides at Selebi are similar to those at Phikwe in that they are either disseminated sulphides in the host amphibolite or massive sulphides. However at Selebi the proportion of disseminated to massive sulphide is much higher than at Phikwe (Table 6.1). The Selebi massive sulphides contain few siliceous inclusions and are dominantly Type 1. These Type 1 massive sulphides are thin and highly irregular in shape (Fig. 6.1b & c). There is no thick massive sulphide layer. Stringers of sulphide are more common at Selebi and commonly stem from massive sulphide as if in the process of incorporating amphibolite as inclusions into the massive sulphide (Plate 29a & b, Fig. 6.1b). Massive sulphides typically occur at both the upper and lower margins of the host amphibolite at Selebi (Plates 29a & b & 30a-c, Fig. 6.1b) and locally they cut across from host amphibolite top to bottom (Fig. 6.1c). However where a mineralogical and geochemical gradation from a feldspathic margin to a hornblende-rich margin is seen within the host amphibolite, the massive sulphide commonly occurs at the mafic margin and disseminated sulphides are more concentrated in the mafic portion adjacent to the massive sulphide (Fig. 5.4c). Locally the ore body (particularly the Lower body) is represented by a thin Type 1 massive sulphide without host amphibolite (e.g. SD 27, Fig. 6.4). Tongues of massive sulphide cut across and invade the surrounding grey gneiss to a greater extent at Selebi than at Phikwe (Plate 29f & g, Fig. 6.1d). Late tensional wedges of massive sulphide similar to those at Phikwe also intrude into the host amphibolite (Plate 29c). Amphibolite inclusions are common in the Selebi massive sulphides (Plate 29a-d) with a "durchbewegung" fabric. Tongues of amphibolite have locally been caught up in the massive sulphide (Frontispiece D).

Fine chalcopyrite-rich disseminated sulphides occur throughout the Selebi host amphibolite, although there are less in feldspathic

portions. Coarser chalcopyrite-rich segregations also occur in the host amphibolite. They are particularly found in the middle of the Upper body just below the A-B split, where they are parallel to the D1 axial plane.

6.1.3 Selebi North

Observations of the Selebi North ore body were only made from drill core. The sulphide type and distribution is similar to that at Selebi rather than Phikwe. Thin Type 1 massive sulphides typically occur at the margins of the host amphibolite, particularly the outer margin (Fig. 5.6b). Sulphides (thin Type 1 massive sulphides, stringers and disseminations) are concentrated in the thickened core of the D1 antiform. The mineralisation on the limbs of the antiform consists of thin massive sulphides and minor disseminations. There is a weak tendency for disseminated sulphides to decrease in content going inwards from the outer margin of the host amphibolite (Fig. 5.6b). The massive sulphides contain small amphibolite inclusions but few siliceous inclusions. There are few Type 2 massive sulphides at Selebi North.

The ultramafic rocks at Selebi North contain only minor sulphide disseminations. This is possibly because the ultramafic rocks only occur on the northern limb, whereas sulphides are concentrated in the antiformal core. However at Phikwe, disseminated sulphides are no more concentrated in ultramafic rock than they are in the immediately surrounding hornblende amphibolite. These observations refute the conclusion of Wakefield (1974, 1976) that the sulphides at Phikwe were not originally associated with the host amphibolite protolith but rather with later ultramafic rocks that were intruded into the host amphibolite protolith.

6.1.4 Sulphide Content of the Ore Bodies

Estimates of the amount of Fe-Ni-Cu sulphide in each of the Selebi-Phikwe ore bodies are shown in Table 6.1. Although factors such as the amount of barren host rock and the amount of amphibolite and grey gneiss inclusions in massive sulphide are taken into account, the estimates are crude. The estimate for Selebi North is the least reliable. However the estimates do indicate that the proportion of sulphide to host rock at Selebi-Phikwe is high. Phikwe has the highest sulphide content - 22 vol% (cf. the estimate of 50% for Phikwe by Wakefield, 1974).

	Volume % of Sulphide in ore body.	Proportion of massive to disseminated sulphide	
		ms	ds
Phikwe	22 vol%	70 %	30 %
Selebi North	12 vol% ?	25 %	75 %
Selebi	14 vol%	5 %	95 %

Table 6.1 The estimated volume percentage of Fe-Ni-Cu sulphides in the Selebi-Phikwe ore bodies.

Estimates of the proportion of massive to disseminated ore in each ore body are included in Table 6.1. These estimates are also very rough but they serve to show that massive sulphide is dominant at Phikwe, whereas Selebi is essentially a disseminated ore body.

6.2 SULPHIDE PETROGRAPHY

6.2.1 Massive Sulphides

Polished sections were only examined from Phikwe and Selebi. Massive sulphides at Selebi-Phikwe are irregular aggregates of pyrrhotite (aproximately 70-80% in inclusion-free Type 1 massive sulphide) with lesser pentlandite, chalcopyrite and pyrite. Magnetite varies from up to 15% in Type 1 massive sulphide to 0% in Type 2. The pyrrhotite is typically strain-free. Twinning (Plate 37e) and kink banding are not common. The pyrrhotite grain-size at Phikwe gradually decreases from about 5 mm. in Type 1 massive sulphide in Zones B and C (Plate 37a & b) to about 0.1 mm. in Type 2 sulphide in Zone E (Plate 37c & d). Selebi pyrrhotites are typically coarse, commonly up to 1 cm. (Plate 37g). Etching of Phikwe pyrrhotites with chromic acid (Naldrett & Kullerud 1967) revealed the presence of intimate lamellar intergrowths, interpreted as monoclinic pyrrhotite and hexagonal pyrrhotite (cf. Vaughan et al. 1971). The hexagonal phase occurs in the core of pyrrhotite grains and the monoclinic phase tends to occur at the margins of grains and adjacent

to intragranular cracks where it commonly envelopes flame pentlandite. There appears to be slightly more hexagonal than monoclinic pyrrhotite.

Pentlandite occurs as rims to pyrrhotite grains (Plate 37b & g), as granular aggregates (Plate 37e), as granular rims to magnetite and silicate inclusions (Plate 37a,c & f) and as exsolution flame pentlandite within pyrrhotite (Plate 37g & h). The exsolution flames occur scattered throughout pyrrhotite and vary from very thin flames to irregular masses up to 0.2mm. (Plate 37a,b & h). Locally they occur en echelon along intragranular cracks in pyrrhotite (Plate 37g). Flame pentlandite also occurs at the margins of coarser granular pentlandite. Flame pentlandite accounts for about 15% of the total pentlandite in the Type 1 massive sulphides in Zones B and C at Phikwe. However going laterally to Zone E (Type 2) the amount of pentlandite as flames and fine rims to pyrrhotite becomes negligigible and the pentlandite is either coarse granular aggregates, or rims and partial replacements of silicate inclusions (Plate 37c & d).

Chalcopyrite typically occurs as granular aggregates within pyrrhotite aggregates and as rims to magnetite (Plate 37a & f) and silicate inclusions. It is commonly associated with pentlandite. Chalcopyrite aggregates associated with pentlandite locally form thin (< 3mm.) lenses within pyrrhotite aggregates in Type 1 massive sulphide and impart a weak foliation. Chalcopyrite also accompanies pentlandite as rims to pyrrhotite grains in Type 1 massive sulphides. Chalcopyrite commonly corrodes and replaces silicate inclusions in massive sulphide and is commonly concentrated within amphibolite inclusions in Type 1 massive sulphide.

In the Type 2 massive sulphide layer at Phikwe chalcopyrite aggregates are concentrated at the top (Plate 26e) and bottom of the layer and in bands of fine siliceous inclusions (Fig. 6.3). Chalcopyrite is commonly associated with fine pyrite idioblasts in Type 2 massive sulphide (Plate 37c) in Zone E at Phikwe. At the extremity of the ore body in Zone E chalcopyrite occurs along with pyrite as crosscutting veinlets in Type 2 massive sulphide and the overlying pyritised cataclastic gneisses (Plates 35b & 36a, Fig. 6.2).

Pyrite is a minor constituent of the Selebi-Phikwe massive and disseminated sulphides and overall accounts for less than 1% of the sulphides. Most of the pyrite occurs at Phikwe. There is very little at Selebi and Selebi North. Pyrite occurs in the following

locations as:
(a) rare fine-grained idioblasts or rare replacements of silicate inclusions (Plate 37h) in Type 1 massive sulphide,
(b) abundant coarse-grained idioblasts (up to 1 cm) in some thin Type 1 massive sulphides and stringers (e.g. in the massive sulphide that occurs near the base of the Phikwe host amphibolite),
(c) veinlets in mylonites associated with late D2 shearing (Plates 26g & 27a & d) - particularly at Phikwe where the ore body and host amphibolite are thin or absent,
(d) thin crosscutting veinlets (post-D2),
(e) abundant idioblasts associated with chalcopyrite and replacement of silicate inclusions (Plate 37c & d) in Type 2 massive sulphide of Zone E at Phikwe,
(f) the matrix of cataclastic gneisses and replacements of silicate clasts at the eastern end of Zone E and in Zone F at Phikwe (Fig.6.2, see Ch. 6.2.3).

Magnetite is common (up to 15%) in Type 1 massive sulphide from Selebi, Selebi North and Zones B and C at Phikwe. Going laterally from Zone C at Phikwe to Zone E the magnetite content rapidly decreases to nothing. The magnetite occurs as rounded embayed crystals or idioblastic octahedra (up to 1 cm.). These are thought to represent two generations of magnetite. The rounded generation (concluded to be the earlier) locally contains round inclusions of pyrrhotite and has idioblastic magnetite overgrowths (Plate 37b). It is cracked and invaded by sulphides, particularly by chalcopyrite but also pentlandite and pyrrhotite (Plate 37f). Granular aggregates of magnetite associated with chalcopyrite occasionally occur at host amphibolite-Type 1 massive sulphide contacts. Locally within thick massive sulphide at Selebi there are patches of coarse octahedral magnetite and chalcopyrite (Plate 29e).

In summary, massive sulphides at Selebi-Phikwe are of two intergradational types:
(a) Type 1 - the typical magnetite-bearing massive sulphides at Selebi and Selebi North and the massive sulphides that occur at Phikwe in Zones B & C. They are usually relatively thin and inclusion -poor (only host amphibolite inclusions). They are pyrrhotite-rich and consist of up to 15% magnetite (normally about 10%). Pentlandite typically occurs as intergranular rims to pyrrhotite or as flames in pyrrhotite.

(b) Type 2 - inclusion-rich massive sulphides, the main example of which is the massive sulphide layer in Zones D & E at Phikwe. This massive sulphide contains abundant inclusions (up to about 80%). The inclusions are commonly of the surrounding siliceous grey gneiss and include cataclastic grey gneiss and mylonite. They contain relatively less pyrrhotite and relatively more pentlandite and pyrite and particularly more chalcopyrite than Type 1 massive sulphides. They contain no magnetite. Pentlandite typically rims the silicate inclusions.

The mineralogical changes in the main Phikwe massive sulphide layer that occur going laterally from Type 1 in Zone C to Type 2 in Zone E can be summarised as:

(a) a decrease in: (1) the pyrrhotite grain-size, (2) the proportion of pyrrhotite to both pentlandite and chalcopyrite, (3) the magnetite content, (4) the proportion of flame pentlandite to coarser intergranular pentlandite, and (5) the maximum size of the silicate inclusions.

(b) an increase in: (1) the proportion of chalcopyrite to pentlandite, (2) the pyrite content, (3) the degree to which all sulphides replace silicate inclusions, (4) the amount of inclusions relative to sulphide, and (5) the proportion of siliceous inclusions to amphibolite inclusions.

6.2.2 Disseminated Sulphides

Disseminated sulphides in the host amphibolites are the same as in the massive sulphides, namely pyrrhotite, pentlandite, and chalcopyrite with minor pyrite. The disseminated sulphides occur as intersilicate aggregates, particularly at silicate grain boundaries (Plate 32a), and also as fine blebs within silicate crystals. Within hornblende-plagioclase amphibolite sulphide typically occurs at hornblende-plagioclase grain boundaries (Plates 31e & 34d) rather than at hornblende-hornblende or plagioclase-plagioclase boundaries. Sulphides occur along cracks and cleavages in silicates. This is probably due to a combination of replacement and injection. Sulphides locally corrode and replace the silicates at their margins. Where disseminated sulphides are abundant, chalcopyrite is the most common sulphide. The chalcopyrite typically rims and replaces silicates (mainly hornblende), whereas pyrrhotite and pentlandite occur at interstitial sites with chalcopyrite forming an outer rim adjacent to silicate. Both granular pentlandite and flame pentlandite within

pyrrhotite occur in these interstitial sites. The proportion of flame (up to 25%) to granular pentlandite is higher than in Type 1 massive sulphide.

Disseminated sulphides are locally preferentially associated with the development of an M2 assemblage in host amphibolite or ultramafic rock, for example at the boundaries of plagioclase altered to clinozoisite or along with serpentine and chlorite in ultramafic rock.

6.2.3 The Development of Pyrite in Zone E at Phikwe

The main occurrence of pyrite at Selebi-Phikwe is at Phikwe, at the eastern extremity of the ore body in Zones E and F (Fig. 5.2). Here the upper part of the pyrrhotite-rich Type 2 massive sulphide layer (referred to here as the massive sulphide) gradually changes laterally into a pyrite-rich zone consisting of abundant pyritised fragments in a fine dark silicate-pyrite matrix, until eventually there is a pyritic layer above Type 2 massive sulphide (Fig. 6.2). Further east, as the whole sulphide-bearing zone thins, the proportion of pyritic rocks to Type 2 massive sulphide gradually increases (Plates 35b & 36a) until in Zone F the lateral equivalent of the ore body is a thin pyritic layer within thick cataclastic gneisses.

The basal contact of the pyritic layer with the massive sulphide is either rapidly gradational (over 2 mm., Plate 36e) or is a sharp, late-D2 shear plane. A thin pyrite stringer is typically developed at the shear (Plate 35a). The upper part of the massive sulphide is commonly chalcopyrite-rich (Plate 35a). The upper contact of the pyritic layer with highly cataclastic gneisses without pyrite is also either gradational or more commonly a late-D2 shear with a pyrite stringer. Whether or not this contact is sharp, the pyrite content of the pyritic layer gradually decreases upwards. Quartz veins are commonly developed at the upper and lower contacts of the pyritic layer. Locally these quartz veins have been disrupted and inclusions incorporated into the massive sulphide or pyritic layer, particularly the latter. Both the massive sulphide and particularly the pyritic layer are cut by chalcopyrite-pyrite veins (Plates 35a & 36a). These veins typically dip to the west between 35 and 60 and are approximately parallel to small thrusts in the massive sulphide layer further west in Zone E. Locally where only the pyritic layer is present, the chalcopyrite veins form a chaotic network (Plate 35b).

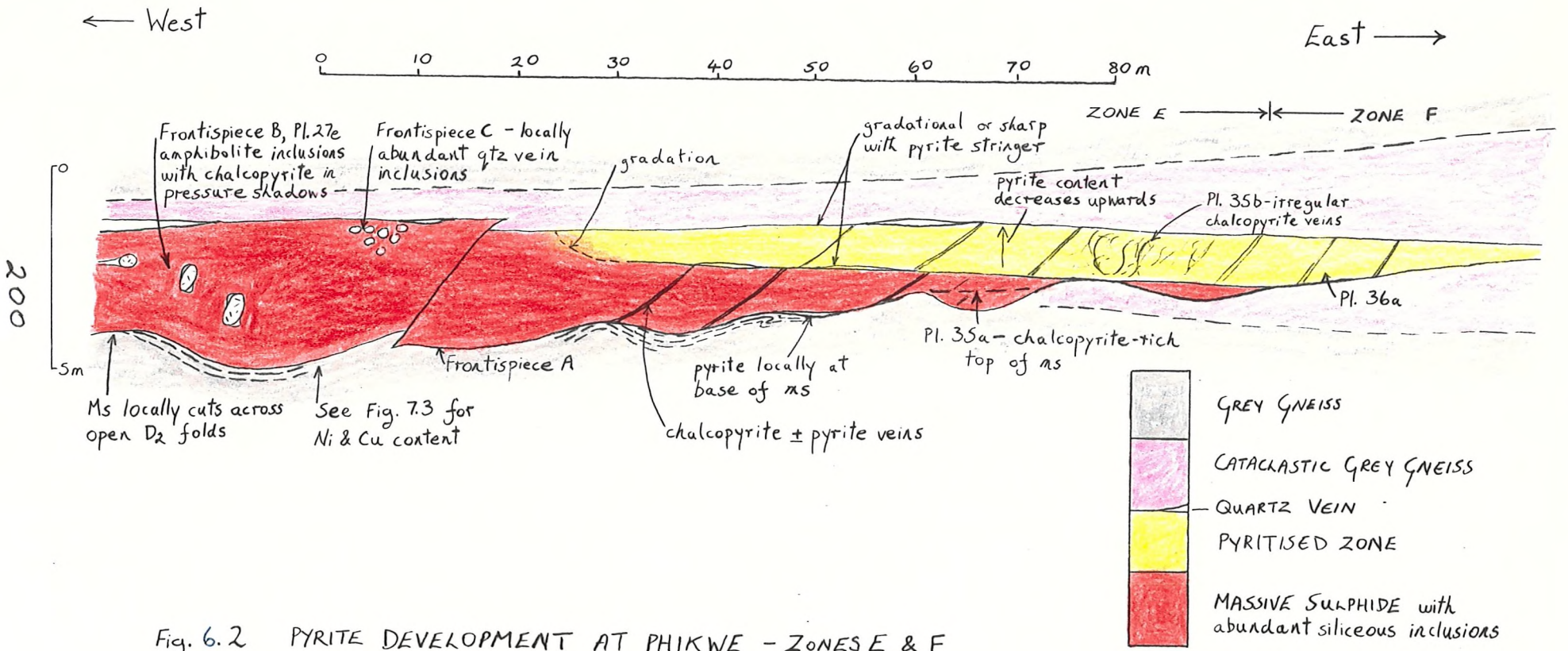

Fig. 6.2 PYRITE DEVELOPMENT AT PHIKWE - ZONES E & F

The massive sulphide below the pyritic layer represents the most extreme development of Type 2 massive sulphide. It consists of a high proportion of fine (typically 1-5 mm.) silicate inclusions (Frontispiece A, Plate 36e & g) in a matrix of fine (0.1 mm) unstrained polygonal pyrrhotite with abundant idioblastic pyrite associated with chalcopyrite (Plate 37c & d). There is no flame pentlandite and no magnetite. The inclusions are mainly siliceous, dominantly of quartz, but also of plagioclase and quartzofeldspathic gneiss. The few mafic inclusions are of chlorite. No amphibolite was found. Fine idioblastic pyrite locally replaces the siliceous inclusions (Plate 37c & d). Locally the inclusions have idioblastic overgrowths of quartz (Plate 36g) or thin chlorite rims.

The pyritic layer consists of variably pyritised mainly siliceous inclusions in a M2b matrix of very fine dark green-brown chlorite with minor pyrite (Plates 34g & h, and 36c, e & f). Inclusions are typically 1-5 mm. (Plate 36c & e). Single quartz crystals are the main inclusion type. Others are fragments of mylonite, cataclastic gneiss and plagioclase (Plates 34g & h, and 36c & d). Some inclusions have been completely pyritised (Plate 36e & f). Plagioclase and chlorite inclusions are highly pyritised by pyrite without any crystal faces (Plate 35c, d & e). One coarse, six-sided, highly pyritised chlorite inclusion (Plate 35c) possibly pseudomorphs a dodecahedral garnet. Quartz inclusions have a variable degree of replacement, but always with idioblastic pyrite (Plate 35c, e & f). Angular quartz inclusions without any pyrite replacement (Plate 36f) were presumably the last fragments to be incorporated into the layer. The inclusions may have thin rims of quartz and/or radiating chlorite (Plate 36d). Weakly pyritised cataclastic rock from Zone F contains abundant chlorite in the matrix (Plate 35g). Chalcopyrite occurs as veinlets rimmed by chlorite (Plates 35c & 36b) or occasionally as rims to pyritised inclusions. Other fine-grained sulphide phases were difficult to identify. Violarite, pentlandite and pyrrhotite are possibly present. (More work needs to be done on this.)

The cataclastic gneisses, some of which contain pyrite at the eastern end of the Phikwe ore body, are the result of repeated shearing, during D1 and particularly D2. This shearing was localised at the Phikwe ore body. The nature of the Type 2 massive sulphide indicates that Type 1 massive sulphide has been mobilised laterally due to this shearing and that it has incorporated fragments of

cataclastic gneiss. The pyrite in the pyritic layer occurs mainly as replacements of silicate inclusions. Two alternatives are thought possible for the origin of the pyritic layer: (1) alteration and pyritisation of massive pyrrhotite-rich sulphide; or (2) pyritisation of cataclastic gneiss. The gross form of the pyritic layer, its location above the massive sulphide, its upwards gradation into unpyritised cataclastic gneisses, its dominantly silicate matrix and replacement textures, all suggest that an origin by pyritisation of a cataclasitic grey gneiss is very likely. The undeformed nature of the pyrite suggests that much of the pyritisation took place during and after late D2 (see Ch. 6.4.2 for mobility of S). The deformational origin suggested here for the inclusion-rich Type 2 massive sulphide and pyritic layer of Zones E and F at Phikwe completley refutes the sedimentary origin suggested by Gallon (1986). He considered that the cataclastic grey gneisses were coarse detrital sediments that were extensively replaced by sulphide. However the textures of the cataclastic grey gneiss, particularly the development of mylonites, indicate an origin by shearing of typical grey gneiss.

6.2.4 Sulphide Mineral Analyses

No microprobe analyses of Selebi-Phikwe sulphides were made in this study and this remains an important part of future work. The limited amount of microprobe data that are available has been summarised by Lear (1979). The average Ni content of pyrrhotite at Phikwe is 0.4%, with two weakly distinguished phases containing 0.7% and 0.3% Ni respectively. The average nickel content of pyrrhotite at Selebi is possibly higher - 0.6%. Pentlandite at Phikwe and Selebi North contains 35-36% Ni and 2-3% Co.

6.3. THE BULK CHEMICAL COMPOSITION OF THE SULPHIDES

The Ni and Cu contents of a Ni-Cu sulphide deposit, particularly the Cu/Ni ratio (expressed here as the ratio - Cu/{Cu+Ni}), are important petrogenetic parameters (Naldrett & Cabri 1976; Rajamani & Naldrett 1978). Most of the information on the grade of mineralisation has been obtained from BCL sampling and assays. There are significant differences in the grades and Cu/(Cu+Ni) ratios between massive and disseminated sulphides and between ore bodies.

At Phikwe, Type 1 massive sulphide typically contains between

2.0-3.5 wt% Ni and 1.2-1.9% Cu (Cu/Cu+Ni ratio of 0.3-0.4), depending on the amount of amphibolite inclusions. Ni values exceeding 3.5% are rare. Type 2 massive sulphide commonly has ratios of 0.4-0.45, with Ni contents of about 2.0-2.5%. The main massive sulphide layer gradually contains more Cu going from Zone C (Type 1) to Zone E (Type 2) and the ratio changes from 0.32 to 0.47 (Figs 5.2 & 6.3). This agrees with the observation that as the amount of inclusions in the massive sulphide increases from Zone C to E, the pentlandite/pyrrhotite ratio and particularly chalcopyrite/pyrrhotite ratio also increase. Ni is more uniform than Cu in its distribution in both Type 1 and 2 massive sulphides (Fig. 6.3). There is little variation from top to bottom in the nickel content of the Type 2 massive sulphide layer of Zones D and E (typically 2.0-2.4%). However the Cu content is highly variable. The Cu content is typically high at the margins of the Type 2 massive sulphide layer, particularly the top, and also in bands of very fine inclusions within the massive sulphide. Locally there are thin massive sulphides/stringers with low copper contents and Cu/(Cu+Ni) ratios as low as 0.1, for example the thin massive sulphide that invariably occurs near the base of the host amphibolite (Fig. 6.3).

In Zones B and C at Phikwe disseminated ore is Cu-rich, with Cu/(Cu+Ni) ratios from 0.45-0.8. However the ratio is usually between 0.6 and 0.7. Cu is particularly abundant immediately below the massive sulphide layer in Zone C (Figs 6.3 & 7.2). Host amphibolite with only minor disseminated sulphide (e.g. in Zones A and D) is Cu-poor with ratios of 0.1-0.45 (typically 0.15 to 0.3) (Figs 6.3, 7.2-7.4 & 7.16).

The Type 1 massive sulphides within amphibolite at Selebi have similar ratios to Phikwe, usually 0.3-0.4. However the actual Ni and Cu grades are higher than at Phikwe and are both commonly over 3.5% (Fig. 6.4). As at Phikwe there are very minor thin massive sulphides and stringers that are Cu-poor (ratios down to 0.1). Type 1 massive sulphides that occur within grey gneiss without any host amphibolite are Cu-rich (e.g. in SD 27, Fig. 6.4). As at Phikwe, Ni tends to be more uniform than copper in its distribution within massive sulphide. The higher grades in Type 1 massive sulphide at Selebi compared to those at Phikwe are due to a combination of: (1) very few siliceous inclusions at Selebi; and (2) higher pentlandite (Lear 1979) and higher chalcopyrite contents relative to pyrrhotite at Selebi. Disseminated ores at Selebi are Cu-rich with ratios from 0.6 to 0.8

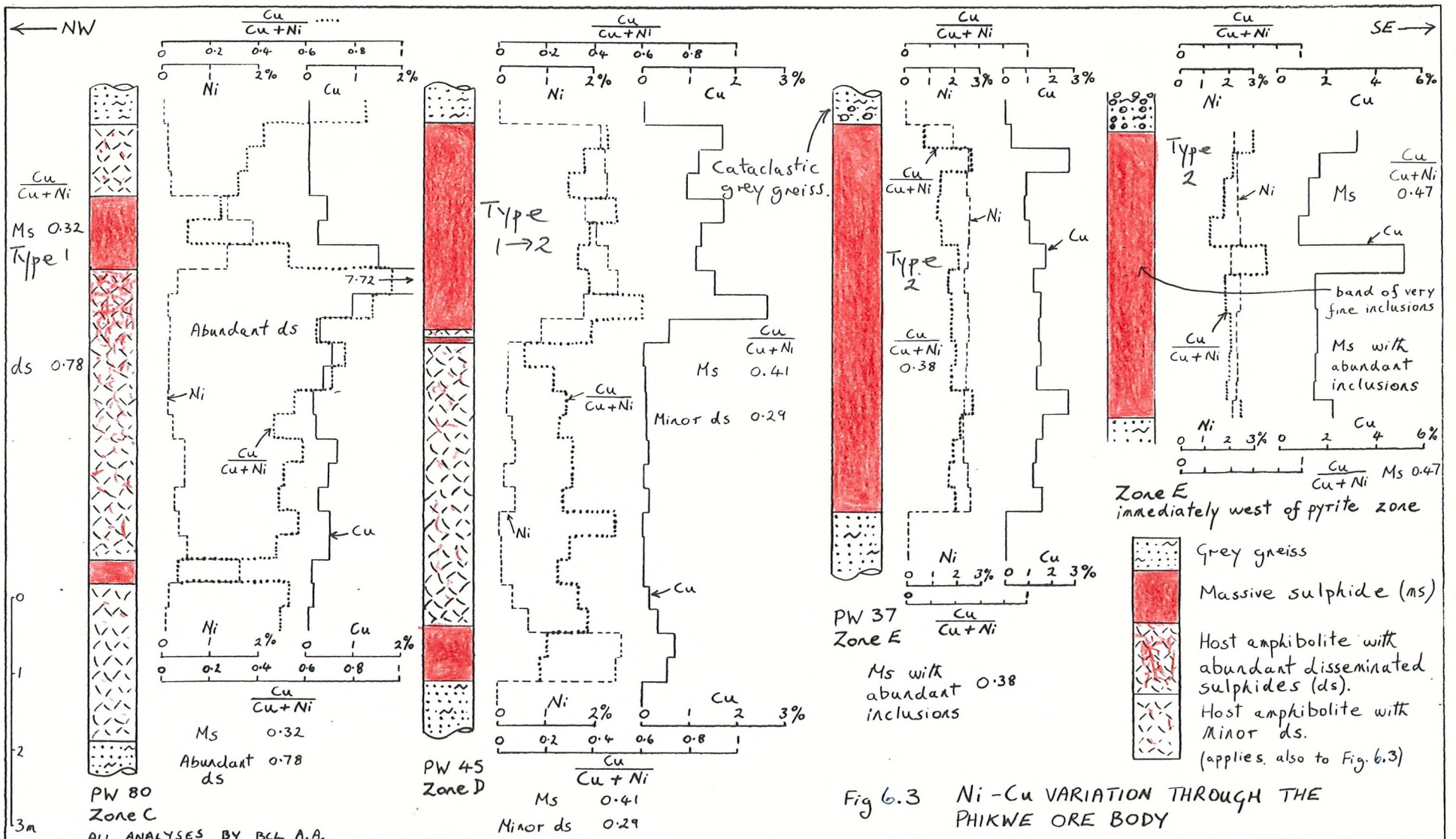

Fig 6.3 Ni-Cu VARIATION THROUGH THE PHIKWE ORE BODY

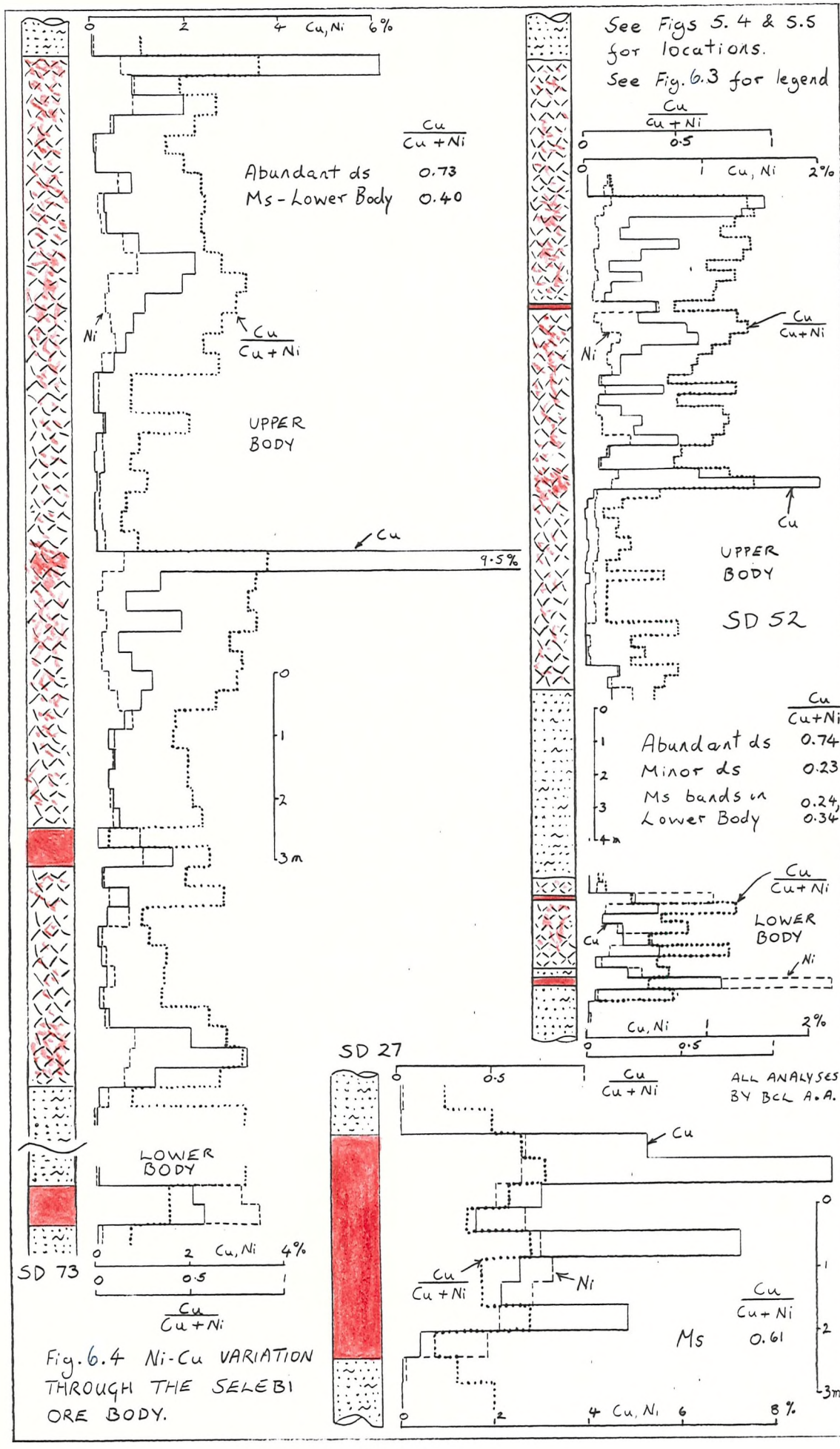

Fig. 6.4 Ni-Cu VARIATION THROUGH THE SELEBI ORE BODY.

(Fig. 6.4). As at Phikwe weakly mineralised amphibolite is Cu-poor with ratios of 0.15 to 0.3 (Figs 6.4 & 7.5).

The limited assessment in this study of the Selebi North massive sulphides indicates that they are more like those at Selebi than those at Phikwe, with both Ni and Cu commonly over 3.5%. Type 1 massive sulphides are Ni-rich with Cu/(Cu+Ni) ratios varying widely from 0.1 to 0.6 (mainly 0.3-0.4). As at Phikwe and Selebi thin massive sulphides tend to have the lowest ratios. Disseminated ores are Cu-rich with ratios from 0.5 to 0.8. Selebi North host ultramafic rocks with minor disseminated sulphides have a ratio of 0.24 and are essentially Cu-poor (Fig. 7.7). However adjacent hornblende-feldspar amphibolites with even less sulphides have a ratio of 0.08. The low Cu/(Cu+Ni) ratios of these weakly mineralised host rocks and those at Phikwe and Selebi appear to be related to their low sulphide content and are considered to be partly due to a high proportion of the Ni having been originally located in premetamorphic olivine (& opx., see Ch. 7.4.3). Some of this Ni is now in metamorphic silicates (e.g. hornblende) but some has probably been scavenged by the minor amount of disseminated sulphide (Ewers 1972; Eckstrand 1975).

	% Ni	% Cu	% Co
Thin massive sulphide with euhedral pyrite near the base of the host amphibolite in Zone C	0.93	0.05	0.13
Pyritised cataclastic rock from Zone E	1.40	0.68	0.19

Table 6.2 Co contents (wt %) of pyrite-bearing samples from Phikwe

The Selebi-Phikwe ore bodies contain significant Co. Within each ore body the Co content of pyrite-free Type 1 massive sulphide is proportional to the Ni content and the Co appears to be contained in pentlandite. The Ni/Co ratio at Phikwe is 18.5 and the typical maximum for Type 1 massive sulphide with 3.5% Ni is 0.19% Co. Hodkinson (unpub.report, 1979) thought that Selebi contains less Co and has a Ni/Co ratio of 27.7. However Lear (1979) concluded that the Ni/Co ratios of Phikwe, Selebi North and Selebi were approximately the same (about 18). Anomolously high Co contents are found in pyrite-bearing samples (Table 6.2). Co contents as high as 0.57%

(0.40% Ni) have been found in BCL sampling of the pyritised cataclastic gneiss of Zone E. It is not known whether the Co is contained within the pyrite or whether it is a separate exsolved phase (carrollite; King, pers. comm. 1981) associated with pyrite.

The estimated Ni-Cu-Fe-S-Co compositions (used in Fig. 6.5) of the main sulphide types at Selebi-Phikwe are shown in Table 6.3. They were estimated on a silicate and magnetite-free basis. The Ni, Cu and Co contents were recalculated from BCL assays (mainly by atomic adsorption). The Fe and S contents were estimated from BCL assays and from the mineralogies of the ores in unpublished BCL reports and Lear (1979). For the Type 1 massive sulphide, the highest grades (i.e. with the least inclusions) of typical mineralisation were used.

	Ni	Cu	Fe	S	Co	$\frac{Cu}{Cu+Ni}$
Type 1 massive	4.2	2.3	56.5	36.7	0.2 wt %	0.35
sulphide	3.1	1.6	44.7	50.5	atomic %	
Pyrite-bearing	5.0	4.1	53.0	37.9	0.2 wt %	0.45
Type 2 massive	3.8	2.8	41.6	51.8	atomic %	
sulphide (15% py)						
Disseminated	2.5	4.6	56.4	36.5	0.1 wt %	0.65
ore	1.9	3.2	44.6	50.3	atomic %	

Table 6.3 Chemical compositions of Selebi-Phikwe sulphide types

The composition, particularly the Fe and S content, of disseminated ore is more difficult to estimate than that of massive sulphide. The composition in Table 6.3 is only an approximation. Pentlandite/pyrrhotite ratios in disseminated ores are both higher and lower than in the Type 1 massive sulphides (Lear 1979). The loss of Fe from sulphide into silicates and to form magnetite and the removal of S from the system possibly occurred during complex metamorphic sulphide-silicate oxidation reactions (see Ch. 7.4.2). This has resulted in a local increase in the pentlandite/pyrrhotite ratio of the disseminated ores.

The best estimates of the overall Cu/(Cu+Ni) ratio of the ore

bodies are the published ore reserves: Phikwe 0.45, Selebi North 0.53 and Selebi 0.67 (Gordon 1973). The differences in Cu/(Cu+Ni) ratio between the three ore bodies are significant and are not seriously affected by the exclusion of low-grade uneconomic mineralisation. Host rocks with disseminated sulphides have a wide range of ratios. Disseminated ore is Cu-rich (ratio of c. 0.65). Weakly mineralised host rock is Cu-poor (ratios of 0.1-0.3). No major systematic differences in the Cu/(Cu+Ni) ratios of each of the three main types of sulphide mineralisation (Type 1 massive sulphide, Type 2 massive sulphide and disseminated ore) were found between the three ore bodies. Selebi disseminated sulphides are typically Cu-rich, with Cu/(Cu+Ni) ratios commonly over 0.7. These are within the range of Phikwe disseminated ores. The difference in the Cu/(Cu+Ni) ratios of the three ore bodies is essentially due to their differing proportions of the three sulphide types (Fig. 7.16). The Selebi ore body (ratio of 0.67) consists mainly of disseminated ore. Selebi North (0.53) consists of disseminated ore and Type 1 massive sulphide. Phikwe (0.45) consists of both Type 1 and Type 2 massive sulphide and disseminated ore.

6.4 DISCUSSION - THE EFFECTS OF DEFORMATION AND METAMORPHISM ON SULPHIDES AT SELEBI-PHIKWE

6.4.1 Mobilisation of Sulphides: Gross Features

The general form of the Selebi-Phikwe mineralised host rocks, the folding of the mineralised host rocks and massive sulphides by the early deformation (D1) and the virtual restriction of sulphides to the host rocks indicate that sulphides were intimately associated with the host rocks prior to deformation and metamorphism. The main alternative is that the ore bodies resulted from syn- or post-metamorphic replacement of host rocks by sulphide (Gallon 1986). However the high degree of replacement by sulphide that would be required and the virtual restriction of the sulphides to the host rocks implies that the replacement model is highly unlikely. Sulphides at Selebi-Phikwe are therefore considered to have suffered all the phases of deformation and metamorphism that have affected the host rocks and enclosing gneisses. The sulphides (their mineralogies, grade, distribution, crystallisation history etc.) can be considered as being the result of processes in two separate periods:

(a) Processes prior to deformation and metamorphism (e.g. possibly magmatic processes, see Ch. 7.4).
(b) Later tectono-metamorphic processes that modified preexisting sulphides.
The effects of deformation and metamorphism on pre-existing sulphides must be considered before the erection of models for the initial stage.

The sulphides at Selebi-Phikwe essentially occur as massive sulphides or disseminated sulphides. The question arises as to whether these represent modified original massive and disseminated sulphides or whether they, and in particular the massive sulphides, have been generated (Barrett et al.1976, 1977) by tectono-metamorphic processes from sulphide-bearing protoliths. The massive sulphides at Selebi-Phikwe have been divided into two types, magnetite-bearing Type 1 and inclusion-rich Type 2 massive sulphide. The generation of Type 2 massive sulphide, mainly from Type 1 massive sulphide but also from disseminated sulphide by tectono-metamorphic processes during repeated shearing, particularly during early D2, is indicated by:
(a) the gross form of the Type 2 massive sulphides,
(b) the occurrence of Type 2 massive sulphide at Phikwe in grey gneiss without any host rocks,
(c) the content and typically siliceous nature of inclusions in Type 2 massive sulphide,
(d) the gradation at Phikwe from Type 1 massive sulphide in Zone C to Type 2 massive sulphide in Zone E (see Fig. 6.3), and
(e) The association of Type 2 sulphides with D2 shearing.

The existence of massive sulphides (similar to Type 1) and disseminated sulphides as two separate forms of mineralisation prior to deformation and metamorphism, is indicated by:
(a) the D1 folding of Type 1 massive sulphides and disseminated sulphide bodies at Selebi and Selebi North,
(b) the sharp nontectonic contacts between host amphibolite containing disseminated sulphides and Type 1 massive sulphide,
(c) the relatively constant mineralogy of the Type 1 massive sulphides, and
(d) the differing Cu/(Cu+Ni) ratios of Type 1 massive sulphide (0.3-0.4) and disseminated ore (0.45-0.8).

Studies of the mineralogies of the rocks in the Selebi-Phikwe area (Chapter 3, Fig. 3.3) indicate that temperatures and pressures of at least 800^{o}C and 10 kbar were attained during the peak of

metamorphism (M1p). The compositions of the Type 1 massive sulphides (Table 6.3) are such that original massive sulphides would have homogenised at the peak of metamorphism to dominantly quaternary Cu-Fe-Ni-S monosulphide solution (MSS) with less than 10% magnetite and no pyrite (Fig. 6.5c & d) (Naldrett et al. 1967; Craig & Kullerud 1969). Thus the sulphide assemblages now found have crystallised from metamorphic MSS. Rapid diffusion (Gill 1960, 1969; McDougall et al. 1961; McDonald 1967) characterises the Cu-Fe-Ni-S system at the temperatures of metamorphism suffered by the Selebi-Phikwe sulphides.

At temperatures considerably below those of the metamorphic climax, the two main components of the ore bodies (i.e massive sulphides and disseminated ores) would have had contrasting strengths (Graf & Skinner 1970; Clark & Kelly 1973; Kelly & Clark 1975; Atkinson 1974, 1975; Roscoe 1975) and would have behaved as discrete entities during deformation. The massive ores (dominantly quaternary MSS) would have been highly ductile at the peak of metamorphism and would have been mobilised much more than the disseminated ores. Strain would have been concentrated in the very low strength massive ore layers. The mobility of the Type 1 massive ores is indicated by their concentration at Selebi and Selebi North in fold closures; by their "durchbewegung" fabric; by the isoclinal folds marked by amphibole inclusions within the massive sulphide; by the tongues of amphibolite within massive sulphide and by the crosscutting relationships of massive sulphide and host amphibolite. The occurrence of Type 1 massive sulphides at Selebi within grey gneisses without any host amphibolite (e.g. SD 27, Figs 5.5 & 6.4) indicates mass transport over tens of metres, probably by ductile flow of quaternary MSS. The Type 1 massive sulphides were mainly mobilised during D1 and early D2.

The continued high ductility of massive ore under cooler (M2) conditions is indicated by the generation of siliceous inclusion-rich Type 2 massive sulphide in Zones D & E at Phikwe during D2. Type 1 massive sulphides and adjacent disseminated sulphides at Phikwe had probably been mobilised laterally into the grey gneisses during D1. Further shearing during early D2 was localised along this mobilised massive sulphide. Sulphide was remobilised further along the zone of early D2 (M2a) blastomylonitic grey gneiss and formed Type 2 massive sulphide. Abundant fragments of cataclastic grey gneiss were incorporated into the Type 2 massive ore during flow. However at the eastern extremity of Zone E, where inclusions account for up to 80%

of the massive layer, the mobilisation mechanism was possibly solid-state stress-activated diffusion (Gill 1960, 1969), rather than ductile flow of sulphide. The typically unstrained polygonal annealed textures of both Type 1 and Type 2 massive sulphides indicate that the majority of the ductile deformation took place at temperatures above that of the unmixing of hexagonal and monoclinic pyrrhotite (at about 250°C, Kissin & Scott 1982). This agrees with the P and T estimates made from the assemblages in the surrounding gneisses (Fig. 3.3). D2 shearing is less important at Selebi and Selebi North and there is little Type 2 massive sulphide developed there. At Selebi open D2 folding has caused Type 1 massive sulphide to flow and cut across grey gneiss.

The above discussion has concentrated on the massive sulphides. Less information is provided by the disseminated sulphides. Apart from the overall control of the shape of host amphibolite with disseminated ores by regional structures, the disseminated ores usually show little internal evidence of deformation. Mobilisation of disseminated sulphides is less obvious than that of massive sulphides. However evidence of mobilisation of disseminated sulphides is provided by their concentration in the crest of the D1 antiform at Selebi North. There is no evidence of upgrading of originally disseminated ores to Type 1 massive ores, although disseminated sulphide adjacent to massive sulphide was probably mobilised to form a minor component of Type 2 massive sulphides. The lack of disseminated ore in Zone D at Phikwe is possibly due to a combination of the original sulphide distribution, the attenuation of the host amphibolite and the mobilisation of disseminated sulphide into Type 2 massive sulphide. The shape of the disseminated sulphide aggregates was controlled by the growth of metamorphic silicates and interfacial energies, for example the location of sulphide at plagioclase-hornblende rather than hornblende-hornblende or plagioclase-plagioclase boundaries. There is little evidence remaining for the original shape of sulphide aggregates. The round form of sulphide inclusions could be due to the lack of gross orientation effects and to negligible differences in interfacial energies between positions within and at the grain boundary of the host mineral (Stanton 1964), rather than to original sulphide immiscibility (cf. Wakefield 1974, 1976). The association of disseminated sulphides with the development of hydrous M2 assemblages indicates that localised hydrous redistribution of sulphides took place during D2.

There is little evidence from the distribution and form of the sulphide bodies for either significant in situ generation of Type 1 massive sulphides from disseminated sulphides or for the suggestion by Wakefield (1974) that the disseminated sulphides were generated by the mobilisation of chalcopyrite from massive sulphide into host amphibolite. Type 1 massive sulphide and disseminated ore are respectively thought to be the tectono-metamorphically modified equivalents of original massive and disseminated sulphides in the host amphibolite-ultramafic protoliths. Original massive sulphides were mobilised to varying degrees relative to the disseminated sulphides during deformation and metamorphism. Mobilised massive sulphides moved independently of disseminated sulphides and there was substantial relative movement between massive and disseminated sulphides. The majority of the ductile deformation of the sulphides is recorded in their gross structures, whereas the smaller scale structures and textures only record later deformation or annealing events at lower temperatures, i.e. when metamorphic quaternary MSS was not the dominant phase in the ores.

6.4.2 Mobility of Sulphide Elements

The distribution of chalcopyrite in massive sulphides at Selebi-Phikwe is more irregular than that of pentlandite. Chalcopyrite is commonly irregularly distributed in Ni-Cu sulphide deposits (McDonald 1967; Coats et al. 1976; Barrett et al. 1977; Patterson & Watkinson 1984a,b). The Cu content in the profiles through both Type 1 and 2 massive sulphide is highly variable, whereas the Ni content is uniform (Figs 6.3 & 6.4). The distribution of chalcopyrite appears to be related to mobility of Cu during both the mobilisation of the Type 1 massive sulphides and the generation of Type 2 massive sulphide. This is particularly well shown at Phikwe by the following features:

(a) the concentration of chalcopyrite at the margins of the Type 2 massive sulphide layer in Zones D & E (particularly near the top of the massive sulphide),

(b) the association of chalcopyrite with bands of very fine inclusions in Zones D & E,

(c) the occurrence of chalcopyrite in pressure shadows around amphibolite inclusions, and

(d) the gradual increase in the Cu/(Cu+Ni) ratio in the massive sulphide layer going from Type 1 massive sulphide in Zone C to Type 2

in Zone E.

The distribution of chalcopyrite in the massive sulphides is therefore indicative of migration of chalcopyrite and/or Cu during deformation and metamorphism, rather than original processes. The occurrence of the Type 2 massive sulphide layer at Phikwe in grey gneiss without any host amphibolite and the higher Cu/(Cu+Ni) ratio of Type 2 compared to Type 1 massive sulphides suggests that some of the Cu in Type 2 massive sulphide was derived from disseminated sulphide.

During the majority of D1 and early D2 deformation, the Type 1 massive sulphides and the disseminated sulphides would have been a quaternary MSS (Figs 3.3 and 6.5c & d). This fact plus the ore textures and the experimentally determined strengths of pyrrhotite and chalcopryrite (Kelly & Clark 1975) suggest that much of the distribution of chalcopyrite is controlled by repeated stress-induced diffusion of Cu in quatenary MSS rather than by the mechanical strength of chalcopyrite. Mechanical separation of chalcopyrite and pyrrhotite by shearing possibly took place during initial deformation and during late D2, but was much much more localised than stress-induced diffusion (e.g. the formation of thin lenses of chalcopyrite in massive sulphide).

The pentlandite/pyrrhotite ratio and hence Ni/Fe ratio of the main massive sulphide layer at Phikwe gradually increases as the inclusion content increases going from Type 1 massive sulphide in Zone C to Type 2 in Zone E (Fig. 6.3). This means that either there was Ni diffusion relative to Fe in the quarternary MSS above the metamorphic temperatures of about 600°C, below which pentlandite would become stable (Craig & Kullerud 1969, Hill 1984) or that significant mechanical segregation of pentlandite has taken place (Barrett et al. 1976, 1977). Mechanical segregation of pentlandite from pyrrhotite could have taken place during the earliest deformation, prior to the establishment of metamorphic temperatures above 600°C, or from MSS at decreasing metamorphic temperatures (from about 600°C down to 350°C, to form the thin pentlandite lenses in massive sulphide). However pentlandite is less ductile than pyrrhotite (Barrett et al. 1977; Marston & Kay 1980) and hence it is thought unlikely that mechanical pyrrhotite-pentlandite segregation during early deformation would have increased the Ni/Fe content of the Type 2 massive sulphide at the extremity of the Phikwe ore body in Zone E. The very uniform Ni contents in each of the profiles

through massive sulphide at Phikwe (Fig. 6.3) also rule out significant differential movement of pentlandite from cooling metamorphic MSS due to mechanical segregation. They are more in agreement with the stress-induced diffusion of Ni relative to Fe during D1 and early D2 mobilisation of massive sulphide as a quaternary MSS. This is contrary to the assumption of Barrett et al. (1977) and Patterson & Watkinson (1984b) that the diffusion rate of Ni is very similar to that of Fe. The correlation of the Co content of the massive sulphides with their Ni content indicates stress-induced diffusion of Co.

Although it is feasible that the premetamorphic precursor of Type 2 massive sulphide at Phikwe had higher Cu and Ni contents than those of Type 1 sulphide, it is proposed that the higher Cu and Ni contents of Type 2 massive sulphide than Type 1 are the result of stress-induced diffusion of Cu and Ni along the Phikwe ore body. The higher Cu/(Cu+Ni) ratio of Type 2 massive sulphides than Type 1 is a combination of the higher mobilty of Cu compared to Ni and the mobilisation of some of the Cu and Ni from Cu-rich disseminated sulphide adjacent to massive sulphide. The slightly higher pentlandite and chalcopyrite contents of inclusion-free Selebi Type 1 massive sulphides compared to those of Phikwe Type 1 are possibly due to lower diffusion rates at Selebi. Selebi is less sheared than Phikwe. The thin massive sulphides with very low Cu and lower than average Ni contents at Phikwe and Selebi are possibly the result of very high diffusion and removal of Cu and to a lesser extent Ni from typical Type 1 massive sulphide.

Pyrite is rare in Type 1 massive sulphides at Selebi-Phikwe. The compositions of the Type 1 massive sulphides are such (Table 6.3) that there would be no pyrite associated with the quaternary MSS during the majority of the metamorphism (Fig. 6.5c-e). The minor pyrite idioblasts in Type 1 sulphide probably exsolved from cooling MSS between 350 and 250°C (Fig. 6.5f). Pyrite is commonly associated with D2 shearing at Phikwe, particularly in Zones E and F where it occurs in massive sulphide associated with chalcopyrite and in cataclastic gneisses. The occurrence of the majority of the pyrite at Phikwe could be due to either sulphur migration or oxidation of pyrrhotite. The occurrence of pyrite without magnetite in the massive sulphide of Zone E suggests repeated stress-induced diffusion of S in quaternary MSS during D1 and early D2, rather than oxidation. Solid-state diffusion of sulphur is several orders of magnitude

slower than the diffusion of iron and nickel in the Fe-Ni-S system (Klotsman et al. 1963; Condit et al. 1974) so that solid-state diffusion of sulphur would not appear to be the main process. Sulphur diffuses much faster along fractures and in areas of high porosity than in massive sulphide in diffusion experiments. This is thought by Condit et al. (1974) to be due to vapour transport along grain boundaries.

The undeformed textures of the pyrite in the pyritised cataclastic gneisses of Zones E & F at Phikwe suggest replacement by pyrite at a relatively late stage in their metamorphic and deformation history. The association of pyrite with late D2 shearing, the replacement by pyrite of clasts in cataclastic gneisses, the calcite veinlets and the occurrence of quartz and/or chlorite rims to pyritised clasts indicate significant stress-induced sulphur migration in a fluid phase (cf. Lesher & Keays 1984; Seccombe et al. 1981) during late D2. This is supported by the hydrated nature of the M2 assemblages that occur throughout the Selebi-Phikwe gneisses and particularly in late-D2 shear zones. The occurrence of chalcopyrite-pyrite veins cutting the pyritised cataclastic gneisses and the high Co and significant Ni contents of the pyritised cataclastic gneisses indicate that Cu, Co and Ni were also transported in a fluid phase along with the sulphur. (More work needs to be done on the mineralogy of the Ni-bearing phase. It could be violarite.) Fluid-phase transport in metamorphosed sulphide deposits has been suggested by Lawrence (1967), McDonald (1967), Vokes (1971) and Mikkola & Vaisanen (1972). Lawrence (1967) and Vokes (1971) proposed that metahydrothermal fluids were the products of the partial melting of ores. However the Fe, S, Ni and Cu contents of the Type 1 massive sulphides and the metamorphic temperatures of about 800°C (even allowing for the effects of pressure) are such that melts (either Cu or Ni-enriched liquid, Fig. 6.5c) would not occur at the peak of metamorphism (Craig & Kullerud 1969). Sulphur diffusion appears to have taken place as repeated, high temperature, stress-induced diffusion in quaternary MSS during D1 and early D2 and as relatively low temperature and pressure fluid-phase diffusion during and after late D2. This fluid-phase diffusion was localised along thin zones of increased permeability produced by D2 shearing.

The alternative possibilty is that pyrite formed by oxidation of pyrrhotite, for example (Marston & Kay 1980):

$$12FeS + 6O_2 = 3Fe_3O_4 + 3FeS_2 + 6S$$

pyrrhotite magnetite pyrite

Similar equations can be postulated involving quaternary MSS, pentlandite and chalcopyrite. However the form and textures of the pyritised ores at Phikwe and their lack of associated magnetite suggest that in situ oxidation of pyrrhotite or MSS could not have been an important process in the formation of pyritic massive sulphide of Zone E. Another source of sulphur could have been the complex sulphide-silicate metamorphic oxidation reactions that resulted in the formation of garnetiferous host amphibolite (e.g. in Zone C at Phikwe, see Ch. 7.4.2). Sulphur generated by these oxidation reactions would have diffused via a fluid phase into disrupted zones (Condit et al.1974).

The disseminated ores are significantly more Cu-rich (Cu/Cu+Ni ratio of 0.5-0.8) than the massive sulphides (0.3-0.4) (Fig. 7.15). This could be an original premetamorphic feature of the two sulphide types or caused by tectono-metamorphic effects such as the stress-induced diffusion of Cu, mechanical separation of chalcopyrite or the formation of a Cu-enriched liquid at the peak of metamorphism. Although the coexistence of a Cu-enriched liquid with quaternary MSS is possible at temperatures above 850°C in the Cu-Fe-Ni-S system (Fig. 7.5c) (Craig & Kullerud 1969), it has already been concluded that this latter process was unlikely. The concentration of strain in the massive sulphides suggests that mechanical segregation of chalcopyrite or stress-induced diffusion of Cu would have taken place in the massive sulphide layers rather than in the host amphibolite. Locally (PW 80, Fig. 7.3) chalcopyrite is very high adjacent to massive sulphide and some mobilisation of Cu from massive sulphide into immediately adjacent host rocks could possibly have taken place. The high Cu and Ni contents of the host amphibolite immediately below the main massive sulphide in Zone C at Phikwe (Fig. 7.2) and the low Cu and Ni of the amphibolite inclusion or band within the massive sulphide indicate only limited mobilisation of Cu and Ni from massive sulphide into host amphibolite. The Cu content of the host rocks is typically independent of adjacent massive sulphides (Figs 6.3 & Fig. 6.4). There is therefore little evidence for the suggestion of Wakefield (1974) that the disseminated sulphides were generated by the movement of chalcopyrite from massive sulphide into the host

rocks. There is some evidence for the mobilisation of Cu from disseminated sulphide adjacent to massive sulphide into Type 2 massive sulphide. Locally chalcopyrite-rich zones have formed in the host amphibolite, particularly at Selebi (Fig. 6.4) where stringers below the A-B split are parallel to the D1 axial plane. However these occur in host amphibolites with overall higher Cu/(Cu+Ni) ratios than the massive sulphides and they are thought to result from mainly stress-induced diffusion of Cu within the amphibolite combined with some localised mechanical segregation of original chalcopyrite during early D1 and metamorphic chalcopyrite during D2. The higher Cu/(Cu+Ni) ratio of disseminated ore than that of Type 1 massive sulphide is therefore thought to be an original, pretectono-metamorphic feature.

Repeated (D1 and early D2) stress-induced diffusion Cu, S, (Ni?) and Co relative to Fe in quaternary MSS aided by later diffusion (late D2) of S, Cu, Co and (Ni?) via a fluid phase are thought to have been responsible for the mobilisation of the ore elements. The later diffusion is particularly significant at Phikwe and was concentrated in thin D2 shear zones at the margins of the massive sulphides and at the eastern extremity of the ore body.

6.4.3 The Formation of Magnetite

Type 1 massive sulphides typically contain up to 10% magnetite. The magnetite occurs as two generations: subround cracked resorbed magnetites and idiomorphic magnetites. In some cases partly resorbed magnetites have overgrowths of idioblastic magnetite. The subround resorbed magnetites are regarded as relicts of pre-metamorphic magnetites. The idiomorphic magnetites are regarded as metamorphic magnetites. Any magnetite that existed in the original massive sulphides prior to metamorphism would have partly dissolved in the quaternary MSS at the peak metamorphic temperatures (Naldrett 1969). Oxygen solubility in the metamorphic MSS would have resulted in the unmixing of metamorphic magnetite from cooling MSS (Groves et al. 1977). There is no magnetite in the Type 2 massive sulphides. The cracking of premetamorphic magnetites in Type 1 massive sulphide suggests that during the repeated deformation and mobilisation necessary to form the Type 2 massive sulphides the dissolution of all the magnetite into metamorphic MSS was aided by high degrees of magnetite comminution. The occurrence of abundant pyrite instead of magnetite in the Type 2 massive sulphides indicates high S activity

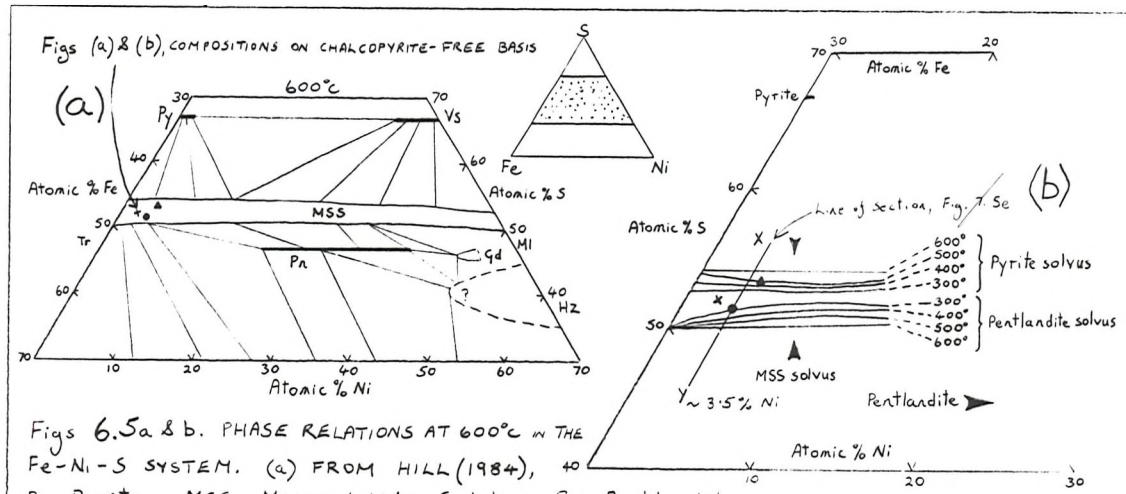

Figs 6.5a & b. PHASE RELATIONS AT 600°C IN THE Fe-Ni-S SYSTEM. (a) FROM HILL (1984), Py - Pyrite, MSS - Monosulphide Solution, Pn - Pentlandite. • SELEBI-PHIKWE MASSIVE SULPHIDES (TYPE 1), × DISSEMINATED SULPHIDES, ▲ PYRITE-BEARING TYPE 2 MASSIVE SULPHIDE (Table 7.). (b) FROM NALDRETT & KULLERUD (1967), SHOWING ISOTHERMS LIMITING SOLVUS OF Fe-RICH PORTION OF MSS.

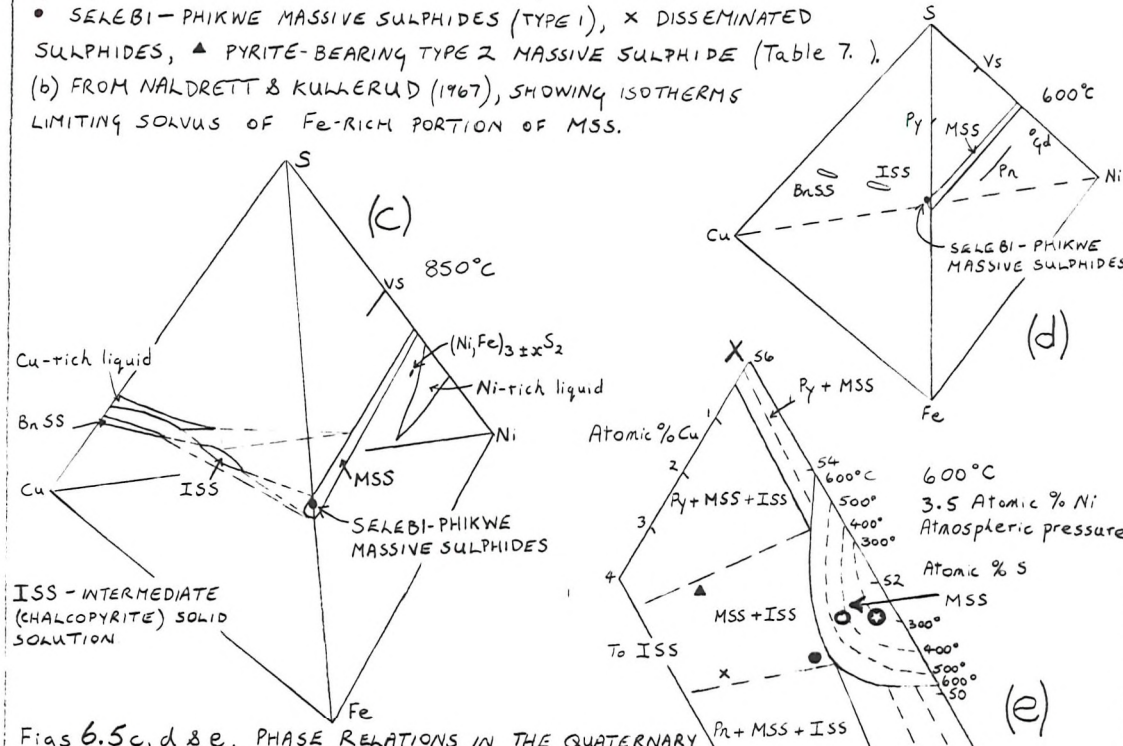

Figs 6.5c, d & e. PHASE RELATIONS IN THE QUATERNARY Cu-Fe-Ni-S SYSTEM, (c) AT 850°C FROM CRAIG & KULLERUD (1969), (d) AT 600°C FROM HILL (1984), (e) ESTIMATED AT 600°C IN THE NEIGHBOURHOOD OF MSS AT 3·5 ATOMIC % Ni.

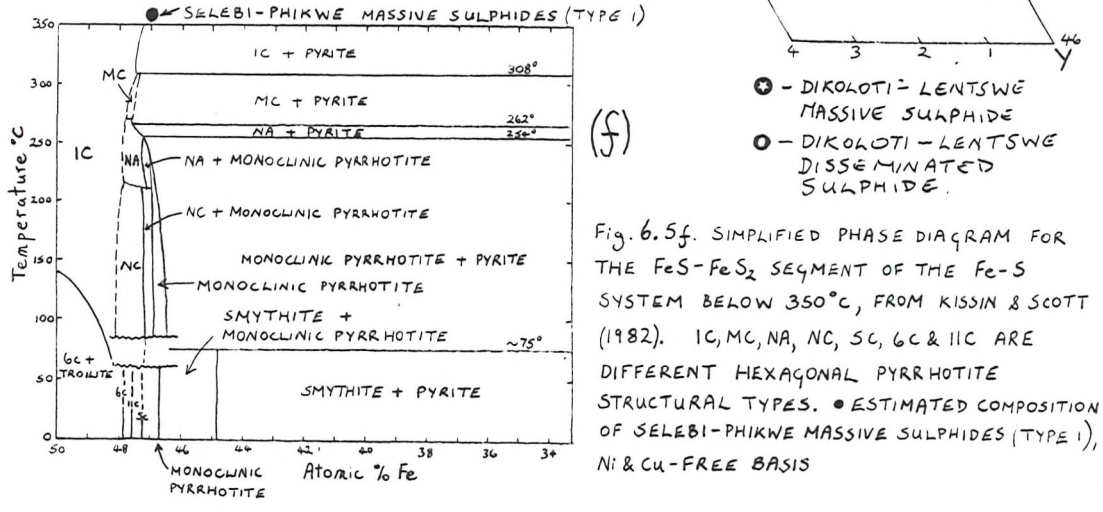

Fig. 6.5f. SIMPLIFIED PHASE DIAGRAM FOR THE FeS-FeS$_2$ SEGMENT OF THE Fe-S SYSTEM BELOW 350°C, FROM KISSIN & SCOTT (1982). IC, MC, NA, NC, 5C, 6C & 11C ARE DIFFERENT HEXAGONAL PYRRHOTITE STRUCTURAL TYPES. • ESTIMATED COMPOSITION OF SELEBI-PHIKWE MASSIVE SULPHIDES (TYPE 1), Ni & Cu-FREE BASIS

Fig. 6.5 PHASE RELATIONS IN THE Fe-Ni-S, Cu-Fe-Ni-S and Fe-S SYSTEMS

which is thought to result from stress-induced diffusion of S.

Ragged aggregates of magnetite locally occur at Type 1 massive sulphide-host amphibolite contacts and could have been derived by localised oxidation of pyrrhotite. Small changes in Eh and pH at the interface between sulphide-poor and sulphide-rich rocks may have controlled such magnetite deposition (Groves et al. 1977). However since no pyrite accompanies the magnetite, any pyrite or sulphur formed in the reaction must have been removed.

6.4.4 The Cooling History of the Metamorphic MSS

The compositions of the Type 1 massive sulphides (Table 6.3) are such that the original massive sulphides would have homogenised at the peak of metamorphism to dominantly quaternary Cu-Fe-Ni-S monosulphide solution (MSS) with less than 10% magnetite and no pyrite (Fig. 6.5c & d) (Naldrett et al. 1967; Craig & Kullerud 1969). The majority of the ductile deformation of the massive sulphides is recorded in their gross structures. The majority of the textures in the massive sulphides are unstrained polygonal fabrics. This indiccates static crystallisation from metamorphic MSS and annealing after the majority of the D2 deformation. If chalcopyrite is removed from considerations of the phase relationships, the compositions of the Type 1 massive sulphides plot (Fig. 6.5a & b) within the confines of the MSS field in the Fe-Ni-S system down to temperatures below 300 ^{o}C (Naldrett & Kullerud 1967; Craig 1973). However errors accompany this widespread practice of ignoring copper when considering the cooling history of primary magmatic Ni-Cu sulphides or metamorphic MSS (Hill 1984). Craig & Kullerud (1969) concluded that the stable coexistence of pentlandite and chalcopyrite solid solution (ISS) does not occur in the Cu-Fe-Ni-S system above 575 ^{o}C. Hill (1984) found however that there is stable coexistence of pentlandite and chalcopyrite solid solution over a wide compositional range in the quaternary system at 600 ^{o}C. A phase diagram (Fig. 6.5e) at atmospheric pressure, applicable to the compositions of the Selebi-Phikwe Type 1 massive sulphides, has been constructed by combining data in the Ni-free Cu-Fe-S system (Kullerud et al. 1969), the Cu-Fe-Ni-S system (Craig & Kullerud 1969) and the Cu-Fe-Ni S system with 10 atomic % Ni (Hill 1984). Assemblages have been projected at constant copper content and metal/sulphur ratio on to section X-Y through MSS shown in Figure 6.5b. The Cu contents (1.2-2.0 atomic%, Table 6.3) of the Type 1 massive sulphides are such that the great majority, if not

all, of the Cu was in the field of quaternary MSS until temperatures dropped to about 600° C, when chalcopyrite solid solution (ISS) started to exsolve (Fig. 6.5d & e). The effects of confining pressure (about 10° C/kbar, Bell et al. 1964, Craig & Kullerud 1969) on the phase relations have been taken into account in the temperature estimates. The Selebi massive sulphides have slightly higher Cu contents than those at Phikwe and started to exsolve ISS at slightly higher temperatures. Pentlandite started to exsolve from the MSS after the chalcopyrite solid solution, at a temperature between 600 and 500 °C. (A more exact estimate is not possible.) Exsolved lamellae of pentlandite coalesced to form pentlandite veinlets (Craig 1973). The great majority of the chalcopyrite and about 80% of the pentlandite is thought to have unmixed from the cooling metamorphic MSS between temperatures of 600 to 300° C.

The last major deformation that affected the Selebi-Phikwe gneisses, late D2 folding and shear-ing, is thought to have taken place at a temperature and pressure of about 400° C and 2 kbar (Fig. 3.3). The effects of D2 deformation on the unmixng MSS resulted in the localised redistribution of chalcopyrite and pentlandite. Segregation of thin chalcopyrite and chalcopyrite-pentlandite lenses took place and imparted a weak foliation on the massive sulphides. Chalcopyrite and to a lesser extent pentlandite were concentrated at the margins of magnetite and silicate inclusions. There was an increase in the grain-size of pentlandite and relatively coarse granular pentlandite formed.

At the cessation of deformation, the remaining MSS would have been disordered high-temperature hexagonal pyrrhotite (1c, Kissin & Scott 1982). Minor pyrite would have crystallised from the MSS between 350 and 250° C (Fig. 6.5f, Kissin & Scott 1982) to give the small random idioblasts seen in Type 1 massive sulphides. In view of the normally brittle behaviour of pyrite during deformation (Graf & Skinner 1970), the relatively late crystallisation of pyrite is confirmed by its undeformed appearance. About 20% of the pentlandite is found as flame pentlandite in pyrrhotite. The association of some of the flame pentlandite with tension cracks (due to the thermal contraction of pyrrhotite, Taylor 1970) and with envelopes of monoclinic pyrrhotite indicates that the flame pentlandite crystallised late in the cooling history of the metamorphic MSS after the final deformation. This probably occurred at and below about 250° C (Fig. 6.5f), the temperature of unmixing of monoclinic and low temperature

hexagonal (NC) pyrrhotite from the high temperature pyrrhotite (Kissin & Scott 1982; Taylor 1970). The development of twinning and kink banding in Selebi-Phikwe pyrrhotites is not common. The formation of the undeformed pyrrhotite-flame pentlandite assemblage in the massive sulphides at Selebi-Phikwe is consistent with the tectono-metamorphic history of the surrouding gneisses.

The cooling history of the Type 2 massive sulphides is more difficult to decipher and is a more complex interplay of repeated deformation, metamorphic homogenisation, repeated stress-induced diffusion and unmixing of metamorphic MSS during waning metamorphism. An increase in Cu plus S and Ni, due to repeated stress-induced diffusion during D1 and early D2, is thought to have taken place in the highly mobilised quaternary MSS that eventually formed the Type 2 sulphide. (Ni diffusion possibly took place only at the D1-M1 climax.) In metamorphic quaternary MSS enriched in Cu plus S and Ni (Table 6.3), chalcopyrite solid solution started to exsolve at a higher temperature than in typical Type 1 sulphide (possibly as high as 700° C, depending on the rate of Cu diffusion). Further cooling resulted in the exsolution of pyrite along with chalcopyrite (Fig. 6.5e) and eventually pentlandite. This sequence is in agreement with the textures observed in pyrite-bearing Type 2 massive sulphide. Continued D2 deformation mobilised the exsolved phases. Pentlandite, chalcopyrite and pyrite locally replaced silicate inclusions. Chalcopyrite was concentrated in zones of maximum stress within, and at the margins of, the Type 2 massive sulphide layer at Phikwe. The ratio of flame pentlandite to granular pentlandite is much less than in Type 1 massive sulphides. This is due to the higher Ni content and the effects of repeated deformation.

Original aggregates of disseminated sulphide had reverted to quaternary MSS aggregates by the peak of M1 metamorphism. The cooling history would have been similar to that of the Type 1 massive sulphides, except that chalcopyrite, the first phase to exsolve, would have exsolved at a higher temperature (possibly as high as 750°C, Fig. 6.5e). The increase in the ratio of flame pentlandite to granular pentlandite in the disseminated ores compared to the massive sulphides is because of the lower Ni contents of the former. A higher proportion of the Ni possibly remained in the cooling metamorphic monosulphide solution until after the final deformation. The lower strain suffered by the disseminated sulphides compared to the massive sulphides also possibly had an effect on the proportion of flame

pentlandite. The fact that the mineralogies and textures of the Selebi-Phikwe sulphides can be interpreted in terms of cooling metamorphic MSS is further evidence against the origin of the sulphides by syn-or postmetamorphic replacement of the host rocks.

6.5 SUMMARY OF CONCLUSIONS

The Selebi-Phikwe sulphides were associated with their host rocks prior to deformation and metamorphism. Replacement of silicate by sulphide has locally taken place, particularly replacement by pyrite in Zones E and F at Phikwe. An origin of the ore bodies by synmetamorphic or postmetamorphic replacement of the host rocks by sulphides (Gallon 1986) however is very unlikely. The Selebi-Phikwe sulphides are considered to have retained aspects of their original form and Ni-Cu contents. In contrast, the generation of purely tectono-metamorphic massive sulphides at Phoenix in the Tati greenstone belt (Fig. 1.1) by the complete redistribution of Selkirk-type sulphides resulted in major easily recognised changes in the form of the sulphide bodies and their Ni-Cu contents (Brown, in prep.).

Type 1 massive sulphides and the disseminated sulphides represent separate forms of mineralisation that existed prior to deformation and metamorphism. Original massive sulphides were mobilised to varying degrees relative to the disseminated sulphides during deformation and metamorphism. Type 2 massive sulphides were generated from mainly Type 1 massive sulphides but also disseminated sulphides by tectono-metamorphic processes during repeated shearing.

The bulk chemical compositions of the massive and disseminated sulphides are such that the original sulphides would have homogenised at the peak of metamorphism to dominantly quaternary Cu-Fe-Ni-S monosulphide solution (MSS) with less than 10% magnetite and no pyrite. Subround resorbed magnetites are relicts of premetamorphic magnetites. Idiomorphic magnetites are metamorphic magnetites. The sulphide mineralogies and textures can be interpreted in terms of cooling metamorphic MSS. The formation of the undeformed pyrrhotite-flame pentlandite assemblage in the massive sulphides at Selebi-Phikwe is consistent with the tectono-metamorphic history of the surrounding gneisses.

Repeated (D1 and early D2) stress-induced diffusion of Cu, S, (Ni?) and Co relative to Fe in quaternary MSS aided by later diffusion (late D2) of S, Cu, Co and (Ni?) via a fluid phase is thought to have been responsible for the mobilisation of the ore

elements. The later diffusion is particularly significant at Phikwe and was concentrated in thin D2 shear zones at the margins of the massive sulphides and at the eastern extremity of the ore body.

The difference in the Cu/(Cu+Ni) ratios of the three ore bodies is essentially due to their differing proportions of Type 1 and 2 massive sulphides and disseminated ore (Fig. 7.16). The Selebi ore body (ratio of 0.67) consists mainly of disseminated ore. Selebi North (0.53) consists of disseminated ore and Type 1 massive sulphides. Phikwe (0.45) consists of both Type 1 and Type 2 massive sulphides and disseminated ore. The difference in Cu/(Cu + Ni) ratios of the Type 1 massive sulphides (c. 0.35), host rocks with abundant disseminated sulphides (c. 0.65) and host rocks with minor disseminated sulphides (0.1-0.3) is thought to be an original, pretectono-metamorphic feature of the ore bodies, rather than a product of tectono-metamorphic processes. Tectono-metamorphic proceeses (e.g. diffusion) has only modified and blurred the original differences. The original nature of the Selebi-Phikwe sulphides is discussed in Chapter 7.4 along with the original nature of the host rocks.

Plate 34 (overleaf)

Inclusion-rich massive sulphides at Phikwe

(A) Type 1 massive sulphide. Bent hornblende inclusion. Footwall stringer, Zone C, # 678. FV = 3 mm.

(B) Type 2 massive sulphide with plagioclase and biotite inclusions. Biotite picks out foliation. Zone D (PW 194), # 271. FV = 6 mm.

(C) Contact of Type 1 massive sulphide with host amphibolite above marked by a thin veinlet of Ms quartz and chlorite. Zone C, # 187 (see Fig. 7.1b). FV = 3 mm.

(D) Contact between hornblende inclusion-rich massive sulphide (on right) and amphibolite with disseminated sulphides (on left). Note disseminated sulphide located within plagioclase at grain boundaries. (PW 76), # 6. FV = 6 mm.

(E) Contact of inclusion-rich Type 1 to 2 massive sulphide with M2a cataclastic grey gneiss above. Zone D, # 170. FV = 6 mm.

(F) Type 2 massive sulphide with abundant plagioclase porphyroclasts and finer grained quartz. Zone E (PW 175), # 30. FV=6 mm.

(G) & (H) Pyritised cataclastic gneiss. Plagioclase porphyroclast with marginal granulation and recrystallisation in (G), folded M2a mylonite clast replaced by pyrite in (H) in chlorite-minor pyrite matrix. Zone E, # 679. FV = 6 mm (G), 3 mm. (H).

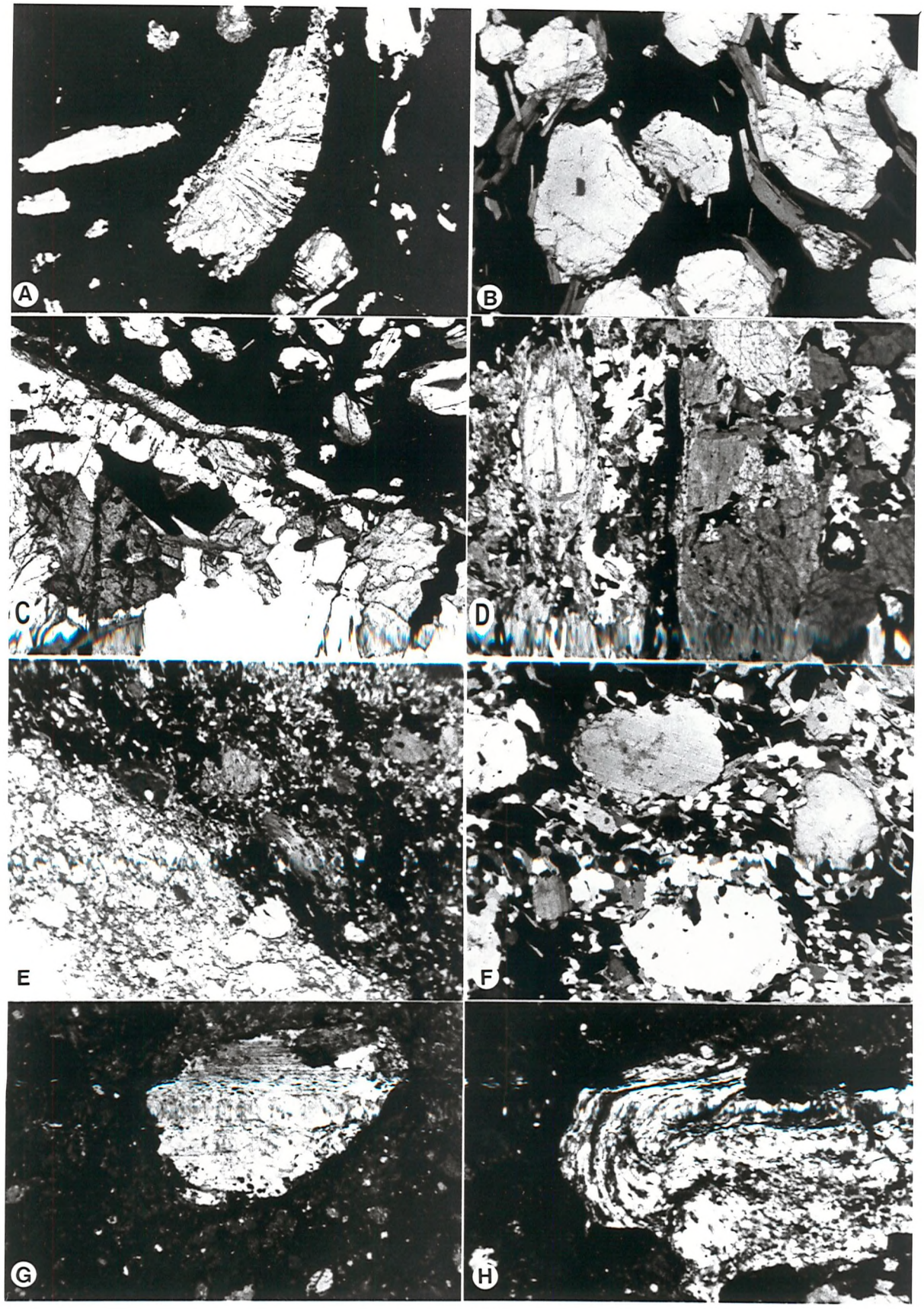

PLATE 34

PLATE 35

The development of pyrite in Zone E of Phikwe (1)

(A) Pyritised cataclastic gneiss (at top right) underlain massive sulphide. The sheared contact is marked by a pyrite stringer. Upper part of massive sulphide is chalcopyrite-rich (see Fig. 6.2). Note the chalcopyrite-pyrite veins in the massive sulphide.

(B) Chaotic network of chalocpyrite veins in pyritised cataclastic gneiss. No massive sulphide layer.

(C) Pyritised cataclastic gneiss. Note:- 6-sided pyritised (without crystal faces) chlorite inclusion (at right), after a dodecahedral garnet; veinlet of chalcopyrite rimmed by chlorite (top centre); and quartz inclusion partially replaced by idioblastic pyrite. FV = 6 mm.

(D) Pyritised cataclastic gneiss. Note:- Pyritised (without crystal faces) plagioclase fragment; and chalcopyrite veinlet rimmed by chlorite and quartz (bottom right). FV = 3 mm.

(E) Pyritised (cataclastic gneiss) inclusions in chlorite-rich matrix. Note:- idioblastic pyrite replacing quartz inclusion and pyrite (without crystal faces) replacing plagioclase (top right). FV = 6 mm.

(F) Pyritised cataclastic gneiss. Idioblastic pyrite replacing quartz inclusions. FV = 3 mm.

(G) Weakly pyritised cataclastic gneiss in Zone F. Note:- chlorite-rich matrix. FV = 6 mm.

PLATE 36

The development of pyrite in Zone E of Phikwe (1)

(A) Pyritised cataclastic gneiss layer without the massive sulphide layer. Note large cataclastic gneiss inclusions and chalcopyrite -pyrite veins.

(B) Pyritised cataclastic gneiss. Chalcopyrite veinlet with quartz and rim of chlorite. FV = 6 mm.

(C) Close-up of cataclastic gneiss inclusion in (A).

(D) Pyritised and chloritised edge of cataclastic gneiss inclusion in (A) & (C). FV = 6 mm.

(E) Gradational contact of Type 2 massive sulphide into pyritised cataclastic gneiss above.

(F) Pyritised cataclastic gneiss from (E). Note:- angular quartz inclusions with limited pyrite replacement and completely pyritised fragments in a matrix of chlorite and minor pyrite. FV = 6 mm.

(G) Type 2 massive sulphide from (E). Note:- silicate inclusions with subidioblastic overgrowths of quartz in a sulphide (pyrrhotite)-rich matrix. FV = 3 mm.

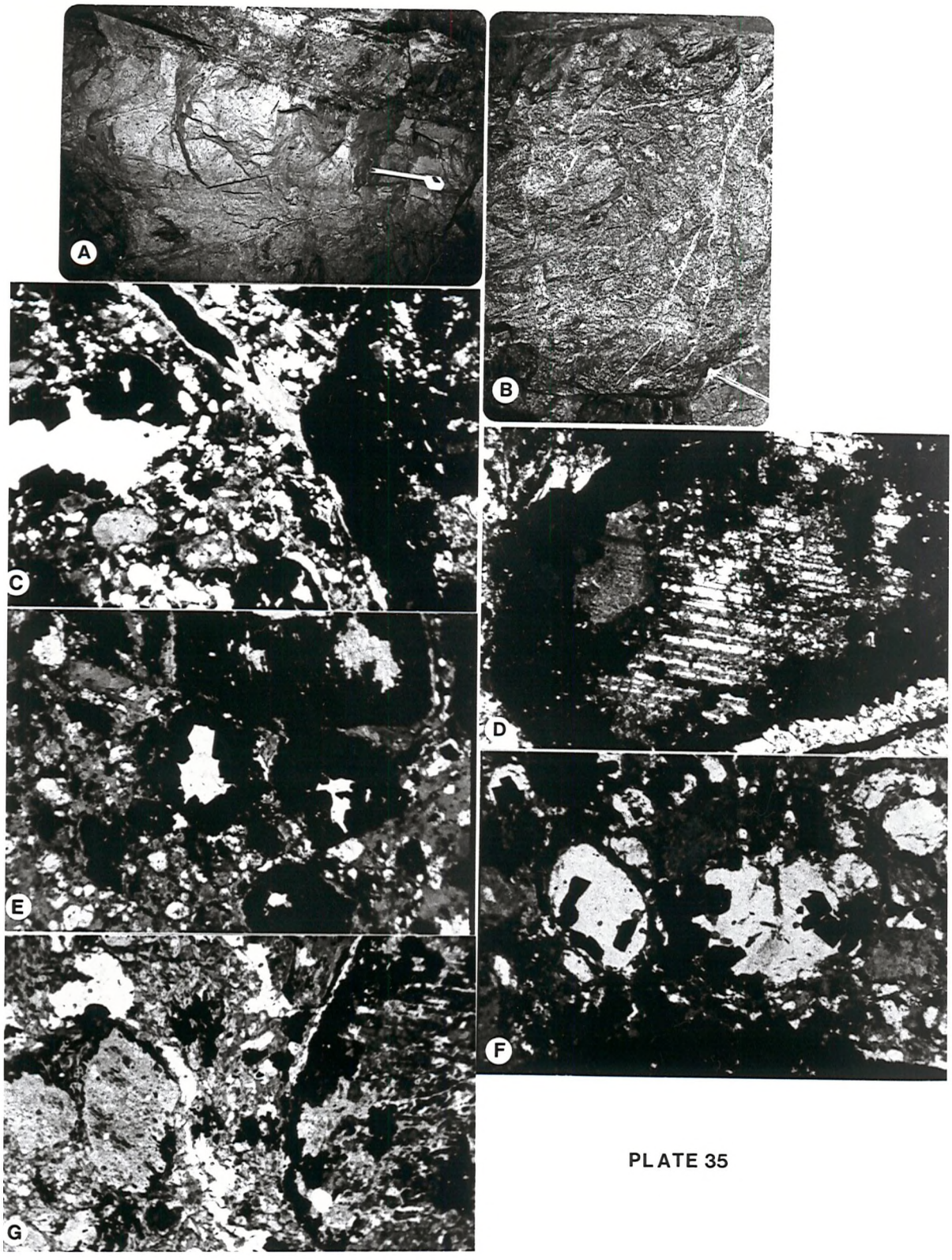

PLATE 35

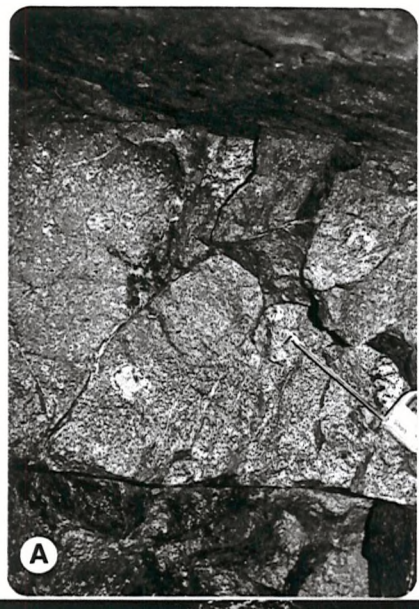

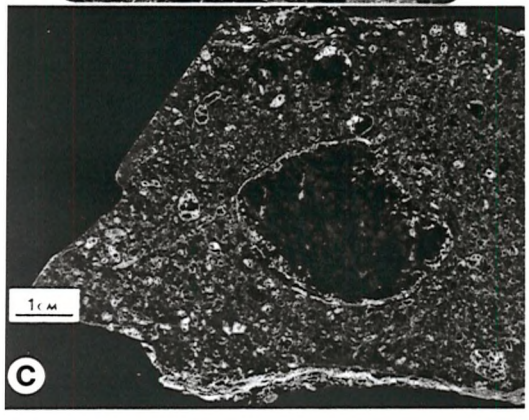

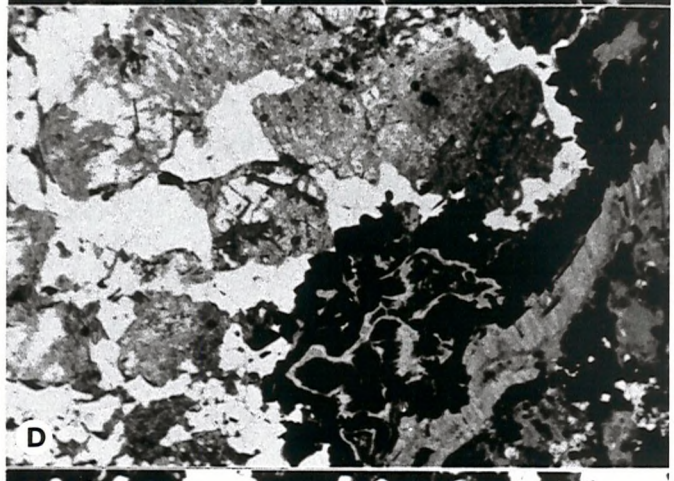

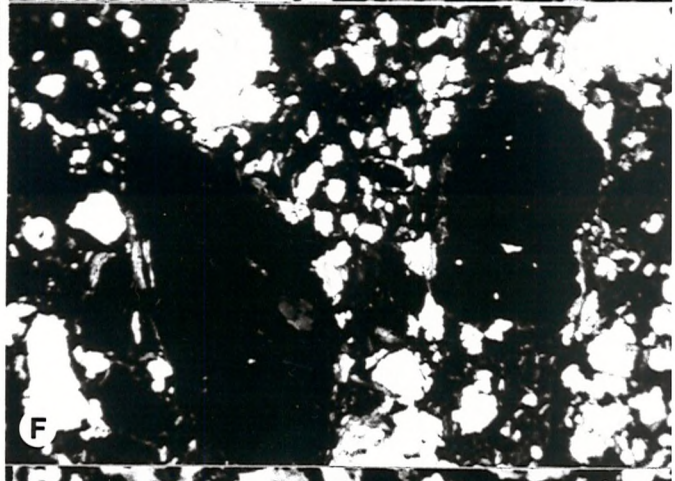

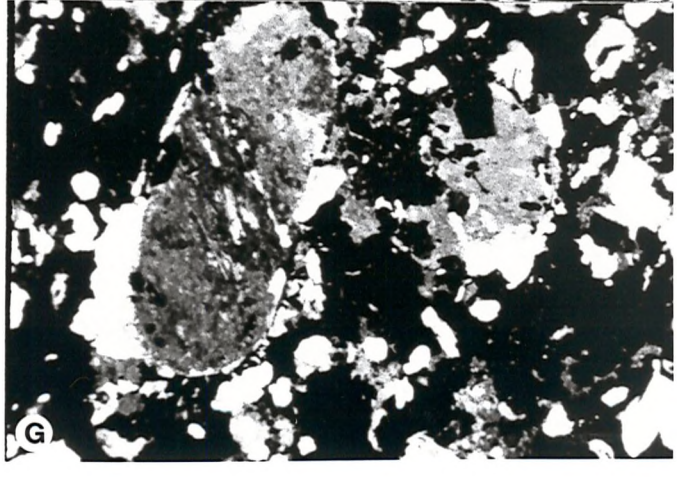

PLATE 36

PLATE 37

Selebi-Phikwe sulphides

(A) Type 1 massive sulphide. Idioblastic magnetite (later generation) with rim of chalcopyrite (Cp) and granular pentlandite (Pe) in a pyrrhotite-rich matrix. FV = 1 mm.

(B) Type 1 massive sulphide. Subround embayed magnetite with magnetite overgrowths in a pyrrhotite-rich matrix. Coarse irregular mass of exsolution pentlandite (Pe) at pyrrhotite grain margins. FV = 1 mm.

(C) Type 2 massive sulphide. Idioblastic pyrite (Py) associated with chalcopyrite within pyrrhotite-rich matrix (Po). Note:- pentlandite (Pe) rim to silicate inclusion. FV = 0.5 mm.

(D) Type 2 massive sulphide. Idioblastic pyrite (Py) replacing silicate inclusion and in pyrrhotite-rich matrix (Po). Note:- abundant pentlandite (Pe) rims tp oyrrhotite grains. FV = 1 mm.

(E) Type 1 massive sulphide. Twinning in pyrrhotite. Granular pentlandite (Pe), chalcopyrite (Cp). FV = 2 mm.

(F) Type 1 massive sulphide. Cracked and invaded magnetite (earlier generation) with round inclusions of pyrrhotite. FV = 2 mm.

(G) Type 1 massive sulphide. Pentlandite as granular rims to pyrrhotite grains and exsolution flames along intergranular cracks in pyrrhotite. FV = 2 mm.

(H) Type 1 massive sulphide. Pyrite replacing silicate inclusion. Note:- flame pentlandite in pyrrhotite and at inclusion margin. FV = 1 mm.

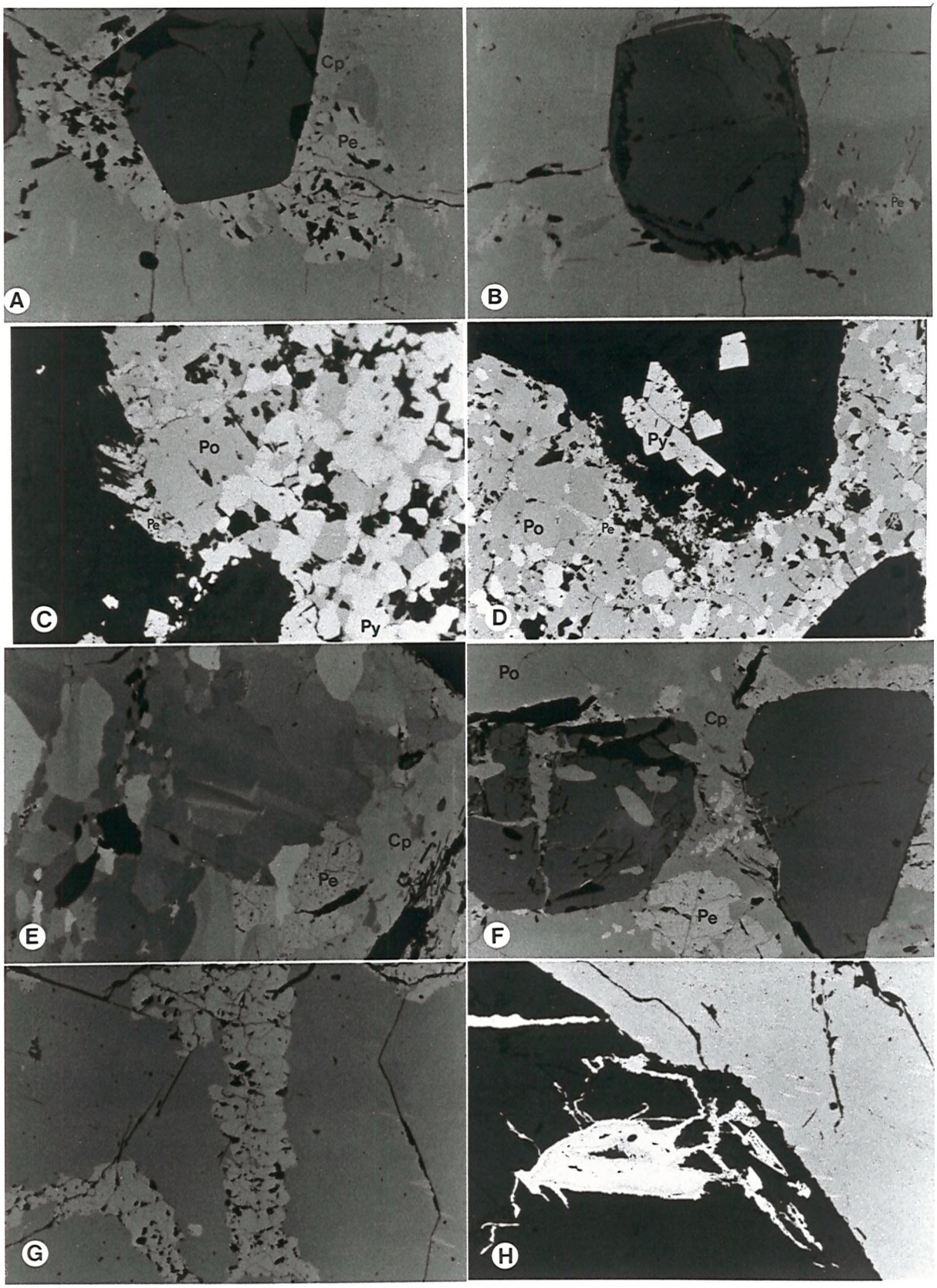

PLATE 37

CHAPTER 7 SELEBI-PHIKWE HOST ROCK GEOCHEMISTRY AND THE ORIGIN OF THE HOST ROCKS AND SULPHIDES

7.1 INTRODUCTION: SAMPLING AND TREATMENT OF DATA

Sections through the host rocks at Phikwe, Selebi and Selebi North were sampled and analysed for major and trace elements (see Appendix, p.A.18-p.A.25). A few individual host rock samples were also taken. The sampled sections were either from diamond drill core or from underground mining development. The sections were chosen on the basis of a combination of several factors: the availability of a core section or access to an underground section; the representative nature of a section; and the systematic mineralogical variation in a section. The host rocks contain significant but variable amounts of disseminated sulphide. In order to compare the major element chemistry of the host rocks on a sulphide-free basis, the Fe, S, Ni and Cu contained in the sulphides were subtracted from the totals. The recalculation involved the assumption that all the Ni in the amphibolite was in pentlandite with a Ni content of 36 weight %, that all the Cu was in chalcopyrite with a stoichiometric composition of CuFeS2 and that any sulphur that remained after the subtraction of the sulphur in the assumed pentlandite and chalcopyrite was in stoichiometric monoclinic pyrrhotite. All analyses have been recalculated to 100%, on an anhydrous and sulphide-free basis.

The geochemical variation in the host amphibolites has been displayed as profiles through the host amphibolites (Figs 7.1-7.7) and by variation diagrams (Figs 7.8-7.14).

7.2 THE AVERAGE CHEMICAL COMPOSITIONS OF THE SELEBI-PHIKWE HOST ROCKS

The average analyses and range of chemical compositions of the Selebi-Phikwe host rocks are tabulated in Table 7.1. The Selebi North host rocks have been subdivided into host amphibolite and host ultramafic rock. These averages include virtually all the host rocks that were analysed. The only samples that have not been included are two host ultramafics from Phikwe (a pyroxenite and a serpentinised peridotite), a hornblende anorthosite from Selebi and a highly sheared serpentinous rock from Selebi North (with anomolous Si,Ti, Al, Ca, P, Cr and Zr contents).

The Phikwe, Selebi and Selebi North host amphibolites are geochemically similar and are characterised by high Al2O3 and MgO contents. The Selebi North host ultramafic rocks are characterised by

	Phikwe		Selebi	
	Mean	Range		
SiO2	46.21	42.6-50.9	47.45	43.5-54.7
TiO2	0.33	0.08-1.67	0.44	0.08-1.64
Al2O3	16.29	11.1-19.2	16.89	3.9-22.3
Fe2O3	11.79	7.7-17.0	10.15	6.7-19.1
MnO	0.16	0.09-0.45	0.16	0.05-0.46
MgO	13.55	8.7-19.0	12.13	6.6-19.9
CaO	8.81	1.9-11.7	9.93	4.0-13.6
Na2O	1.51	0.7-2.7	1.56	0.4-3.0
K2O	1.26	0.2-6.4	1.16	0.09-3.37
P2O5	0.05	0.03-0.24	0.07	0.03-0.59
Cr2O3	0.04	0.01-0.14	0.06	0.02-0.41
	100.00		100.00	
Cr	300	89-990	392	108-2730
Nb	3.9	nd-18	4.6	2-15
Rb	50	6-279	49	5-137
Sr	80	9-237	102	8-276
V	87	32-159	111	42-212
Y	14	3-47	17	4-69
Zr	29	10-334	37	11-246
or	7.51		6.89	
ab	12.94		13.26	
an	34.26		35.97	
di	7.72		10.71	
hy	4.14		8.05	
ol	30.58		22.30	
mt	2.07		1.76	
il	0.62		0.84	
ap	0.12		0.16	
cr	0.04		0.06	
An	76		77	
Fo	74		75	
N-Samples	62		65	

	Selebi North Amphibolites		Selebi North Ultramafics	
SiO2	45.62	41.6-52.2	50.26	47.3-53.3
TiO2	0.65	0.16-3.37	0.27	0.22-0.31
Al2O3	14.05	4.4-19.4	5.73	4.8-9.9
Fe2O3	13.60	6.1-20.0	11.36	9.0-15.0
MnO	0.23	0.05-0.54	0.20	0.16-0.23
MgO	14.06	9.8-19.9	25.76	24.1-27.7
CaO	9.02	3.3-11.5	4.27	1.7-6.7
Na2O	1.38	0.4-2.7	0.64	0.4-1.0
K2O	0.91	0.05-4.25	0.16	0.05-0.67
P2O5	0.09	0.03-0.68	0.05	0.03-0.07
Cr2O3	0.39	0.03-4.08	1.30	0.20-2.63
	100.00		100.00	
Cr	2605	191-27090	8650	1280-16620
Nb	4.6	nd-10	4.0	3-5
Rb	33	3-188	8	3-32
Sr	63	7-271	8	nd-11
V	145	54-403	97	53-133
Y	17	8-48	9	7-13
Zr	45	10-175	23	18-32
or	5.45		0.94	
ab	11.84		5.50	
an	29.75		12.40	
di	12.12		6.87	
hy	7.48		53.12	
ol	29.15		17.25	
mt	2.37		1.97	
il	1.26		0.52	
ap	0.19		0.12	
cr	0.39		1.31	
An	75		79	
Fo	72		85	
N-Samples	30		10	

Table 7.1 Average chemical and normative compositions of Selebi-Phikwe host rocks.

All analyses have been recalculated to 100% on an anhydrous and sulphide-free basis. The Fe2O3/FeO ratio in the norm calculation is assumed to be 0.15 (Brooks 1976).

	Selebi North Host Amphibolites			
	AU - with ultramafic rocks		A - without ultramafic rocks	
SiO2	46.21	42.2-52.2	45.41	42.8-50.3
TiO2	0.73	0.27-1.39	0.42	0.16-1.51
Al2O3	13.14	4.4-19.4	14.77	7.5-17.6
Fe2O3	12.53	6.1-20.0	14.34	9.6-19.2
MnO	0.19	0.05-0.33	0.26	0.12-0.54
MgO	15.46	9.8-19.9	13.05	10.3-19.2
CaO	8.03	4.9-11.4	9.72	3.3-11.5
Na2O	1.41	0.4-2.7	1.36	0.5-2.4
K2O	1.38	0.05-4.25	0.56	0.20-1.76
P2O5	0.10	0.03-0.23	0.05	0.03-0.17
Cr2O3	0.82	0.04-4.08	0.06	0.03-0.26
	100.00		100.00	
Cr	5492	236-27090	402	191-1755
Nb	5.5	nd-10	3.5	nd-7
Rb	51	3-188	20	4-58
Sr	65	7-271	63	14-101
V	160	67-274	116	54-382
Y	20	8-48	13	9-41
Zr	57	20-99	28	10-85
N-Samples	13		16	

Table 7.2 Average chemical compositions of Selebi North Host Amphibolites: AU - Amphibolites associated with ultramafic rocks on the northern limb of Selebi North; A - Amphibolites without ultramafic rocks in the core of the antiform and on the southern limb. (A sample with very high TiO2 (3.37 wt%) and P2O5 (0.68wt%) has been omitted from AU.) Anhydrous and sulphide-free basis.

	Garnet Amphibolite		Selebi Spinel Amphibolite	
SiO2	43.61	42.6-45.5	44.28	43.5-44.9
TiO2	0.21	0.12-0.26	0.28	0.20-0.35
Al2O3	15.69	14.1-16.6	18.73	17.0-20.7
Fe2O3	16.80	15.9-19.2	9.10	8.3-10.3
MnO	0.39	0.24-0.54	0.13	0.12-0.15
MgO	12.34	10.6-13.7	14.25	13.8-14.6
CaO	9.16	7.4-10.7	11.37	10.4-12.0
Na2O	1.10	0.7-1.6	1.30	1.2-1.4
K2O	0.62	0.21-2.00	0.48	0.15-1.04
P2O5	0.04	0.03-0.04	0.05	0.04-0.06
Cr2O3	0.04	0.02-0.07	0.03	0.02-0.04
	100.00		100.00	
Cr	303	140-439	186	143-269
Nb	3.3	2-6	3.3	2-4
Rb	20	5-71	21	7-48
Sr	51	30-76	132	66-177
V	72	45-157	70	64-79
Y	13	4-30	16	14-17
Zr	15	10-20	23	13-29
N-Samples	8 - 4 from Phikwe - 4 from Selebi North		3	

Table 7.3 Average chemical compositions of Garnet Amphibolite and Selebi Spinel Amphibolite. Anhydrous and sulphide-free basis.

high MgO and relatively high SiO2 contents. The major differences in the three average amphibolites are their Ti, Al and Mg contents. The average Selebi North host amphibolite has significantly higher Ti, Mg, Cr, Zr and V than the Phikwe and Selebi host amphibolites. The higher Cr is mainly due to two high-Cr amphibolite samples (Fig. 7.7). The Selebi North host amphibolites have been further subdivided (Table 7.2) into those that are associated with ultramafic rocks on the northern limb (e.g. those in SDN 56, Fig.7.7) and those that occur without ultramafic rocks in the core of the antiform and on the southern limb (Fig. 5.6). The former have significantly higher Ti, Mg, P, Cr, Nb, V, Y and Zr than the latter.

The average chemical compositions of garnetiferous host amphibolite from Phikwe and Selebi North and the spinel-bearing host amphibolite from Selebi are also shown separately in Table 7.3. The garnetiferous amphibolites have significantly higher contents of Fe and Mn than the average host amphibolites. When compared to average Phikwe host amphibolite and allowing for the effect of simple addition of Fe and Mn to that average Phikwe amphibolite, the garnetiferous amphibol-ites also have relatively higher contents of Ca and to a lesser extent Al and lower contents of Ti, Na, K, Rb, Sr and Zr.

The spinel-bearing amphibolites from Selebi have higher contents of Al, Mg, Ca and Sr and lower contents Si, Ti, Fe, Na, K, P, Cr, Nb, Rb, V and Zr than the average Selebi host amphibolite.

7.3 GEOCHEMICAL VARIATION IN THE SELEBI-PHIKWE HOST ROCKS

7.3.1 Geochemical Profiles

7.3.1a Phikwe

Figures 7.1 and 7.2 show representative profiles through the mineralogically variable, garnet-bearing mineralised amphibolite in Zone C at Phikwe (see Ch. 5.2.1b). Figure 7.1 illustrates two underground sections. Figure 7.2 is a core section that has been sampled in more detail. The main features of these three profiles are:

(a) The gradual decrease in Fe and Mn from the garnet amphibolite immediately below the massive sulphide to near the base of the host amphibolite. Amphibolite inclusions (and bands ?; the distinction between silicate bands and inclusions is difficult in core sections.) in the massive sulphide are commonly rich in Fe and Mn.

(b) The low Mg contents at the top and base of the host amphibolite

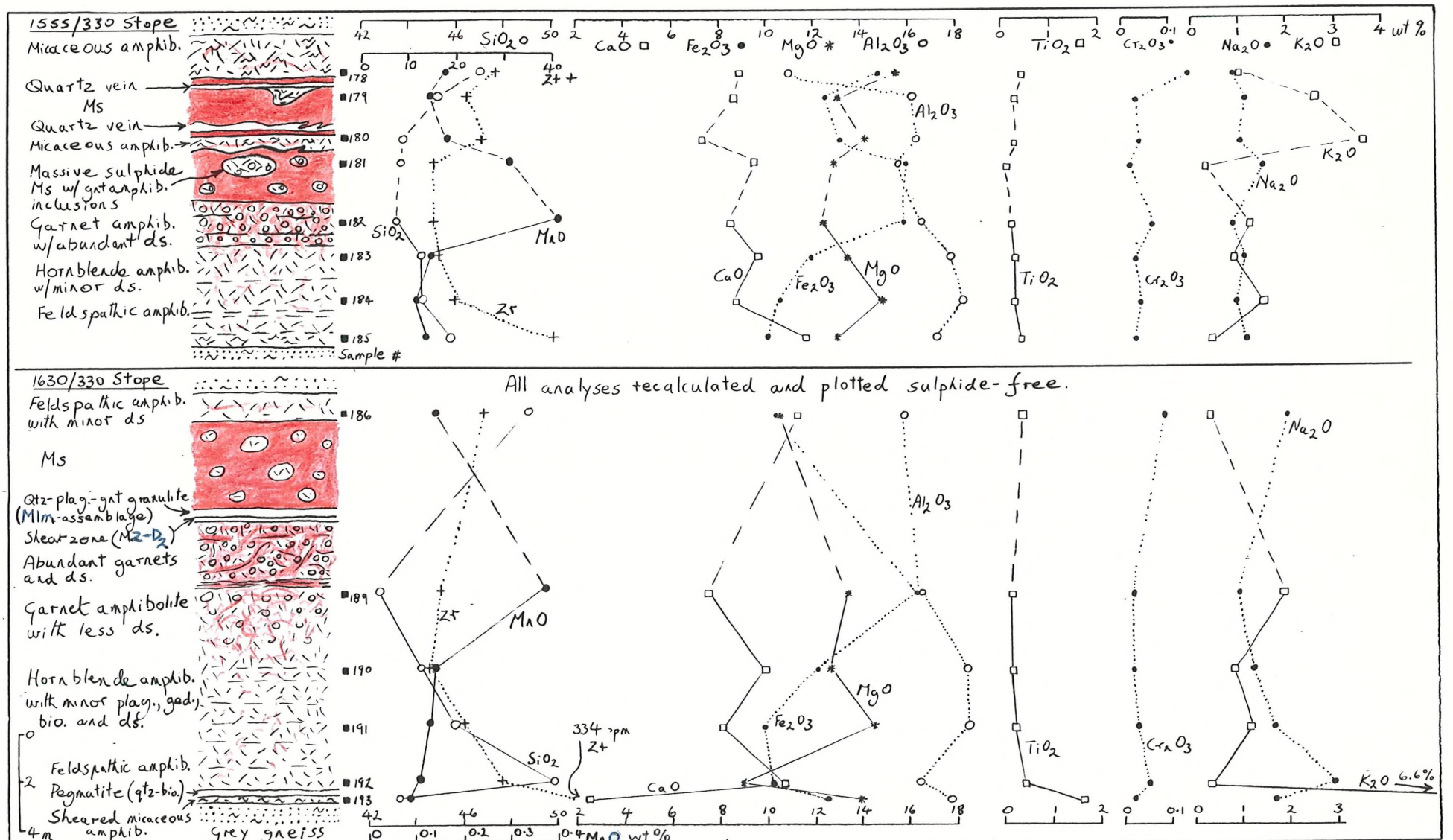

Fig. 7.1 GEOCHEMICAL VARIATIONS THROUGH THE PHIKWE HOST AMPHIBOLITE (UNDERGROUND, 330 m LEVEL) — ZONE C.

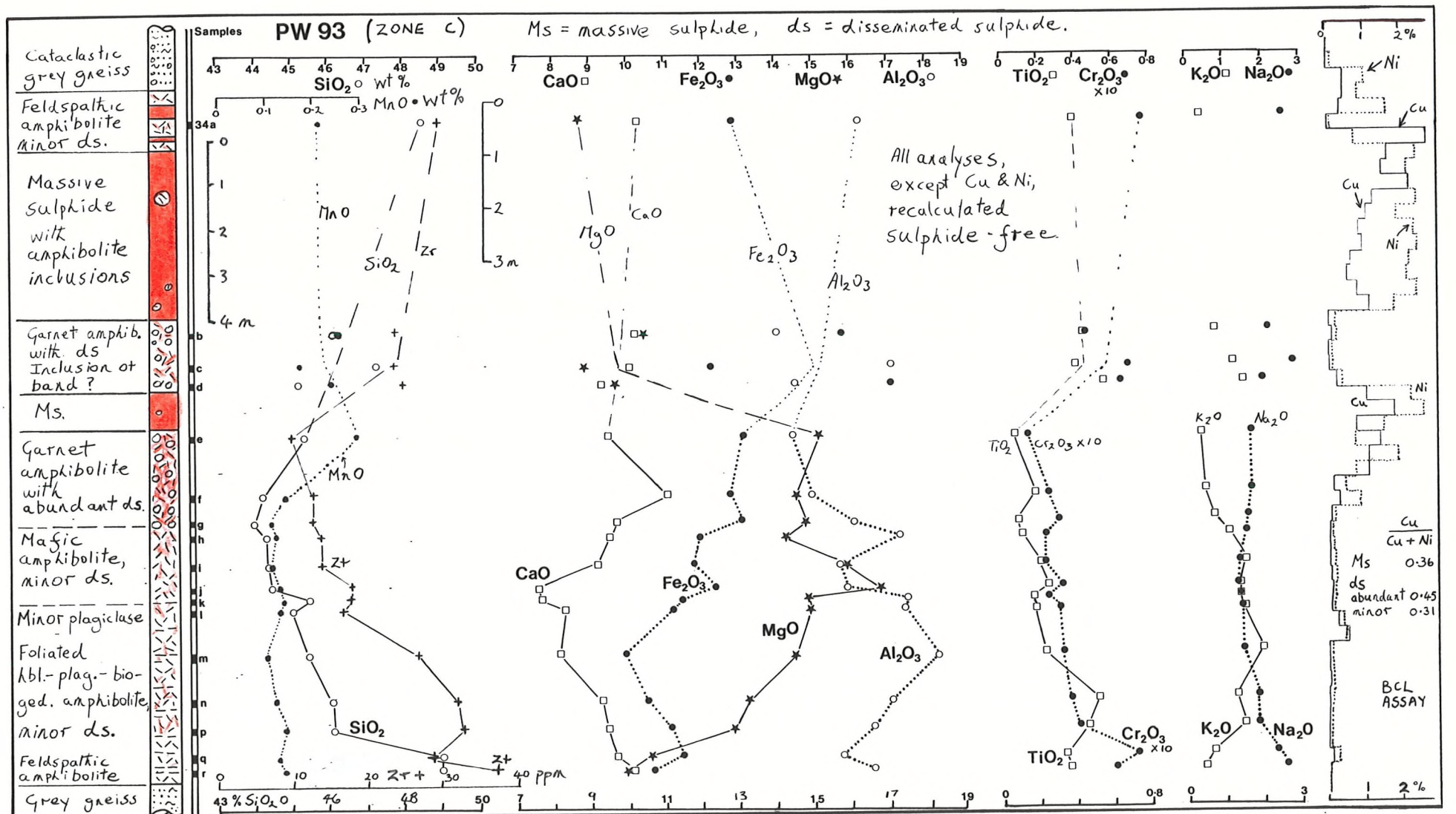

Fig. 7.2 GEOCHEMICAL VARIATION THROUGH PHIKWE HOST AMPHIBOLITE (PW 93) - ZONE C

(Figs 7.1b & 7.2). The highest Mg occurs in the middle of the main body of amphibolite. The highest Al also occurs in the middle of the main body of amphibolite.

(c) The high Si, Ti and Zr content at the top and base of the host amphibolite. The lowest Si, Ti and Zr are in the garnetiferous amphibolite immediately below the massive sulphide. There is a gradual increase in Si, Ti and Zr from immediately below the massive sulphide to the base of the host amphibolite. The trend in the variation of Y (not plotted) is similar to that of Zr, although more variable (possibly because of less precise Y analyses).

(d) Cr is highest at the top of the host amphibolite. In Figure 7.2 there is also a gradual increase in Cr going from immed-iately below the massive sulphide down to the base of the host amphibolite.

(e) There is a weak antithetic relationship between K and Na. The variation in Rb (not plotted) mirrors that of K (Fig. 7.13). The highest Na contents are at the upper and lower margins of the host amphibolite (Figs 7.1b & 7.2).

(f) The highly sheared amphibolite band below the main body of host amphibolite in Figure 7.1b is high in K, Rb, Ti and Zr and particularly low in Ca and Si.

(g) The high Cu (and Ni) contents of the host amphibolite below the main sulphide and the low Cu contents of the amphibolite band or inclusion in the massive sulphide (see Ch. 6.4.2).

The profile shown in Figure 7.3 is from an exploration hole at the approximate margin of Zones C and D at Phikwe. It was chosen for its thickness of host amphibolite. However it is unrepresentative in this thickness and the poor development of massive sulphide. The section consists of a thick upper feldspathic amphibolite and a thin massive sulphide layer. Below the massive sulphide is a zone of interbanded mylonite and sheared amphibolite. The rest of the section consists of variably sheared host amphibolite. The main features are:

(a) The generally lower variability than in Figures 7.1 and 7.2.

(b) The high content of Fe in the garnetiferous amphibolite below the thin massive sulphide and the gradual decrease in Fe and to a lesser extent Mn downwards from garnet amphibolite.

(c) The high K and low Ca in the sheared amphibolite below the garnetiferous amphibolite.

(d) The highest Mg (and Al) contents occur in the middle of the host amphibolite; the lowest Mg is towards the margins.

(e) The highest Cr content at the top of the host amphibolite.

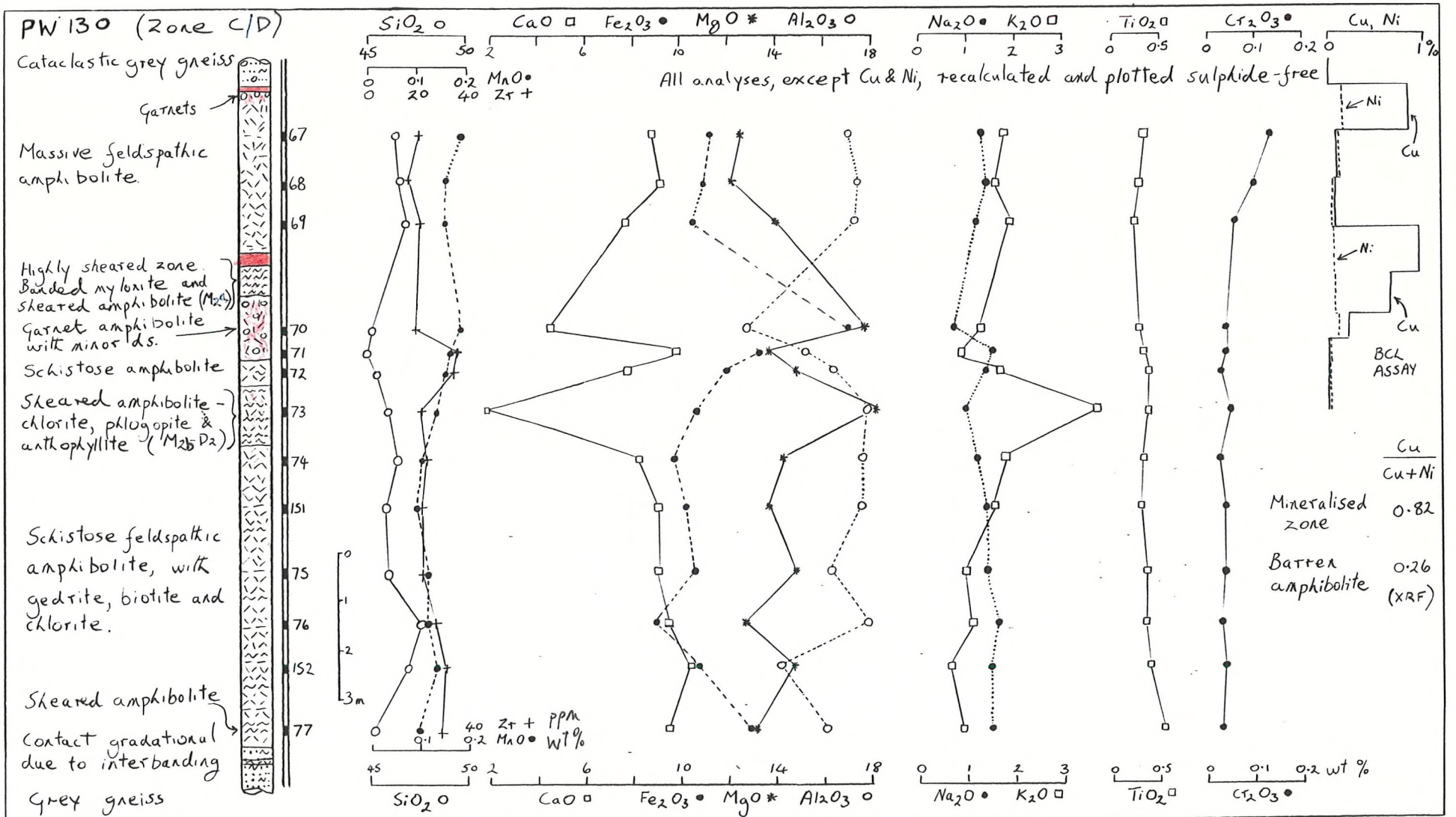

Fig. 7.3 GEOCHEMICAL VARIATION THROUGH PHIKWE HOST AMPHIBOLITE (PW 130) - ZONE C/D

(f) The highest Ti content at the base.
(e) The weak antithetic relationship between Na and K.
(f) The high Cu/(Cu+Ni) ratio of the disseminated sulphides in the highly sheared zone (indicating high mobility of Cu relative to Ni; see Ch. 6.4).

A representative section of thick weakly mineralised of Zone A at Phikwe is shown in Figure 7.4. The whole of the relatively homogeneous amphibolite has been sampled. The main geochemical features are:
(a) The lower variability than in Figures 7.1 and 7.2.
(b) The lack of an Fe and Mn trend.
(c) The higher Ti and Zr contents at the upper and lower margins.
(d) The Mg contents are lowest at the upper and lower margins.
(e) The higher contents of both K and Na at the upper and lower margins.
(g) The asymmetric distribution of Cu and Ni. There is a gradual decrease in Cu and Ni downwards from the Cu-Ni high but a more abrupt decrease upwards.

7.3.1b Selebi

The Selebi ore body was sampled underground. The main reason for this was the complicated structure at Selebi. In exploration holes at Selebi it was difficult to know which of the three sub-divisions (Upper A, Upper B and Lower Bodies) was present. In underground development it was possible to establish without doubt which of the three subdivisions was sampled. The Selebi Upper B and Lower Bodies were sampled in an inclined drive, which was only chosen for ease of access (Fig. 7.5). The Upper B Body was also sampled where it showed a mineralogical gradation from a mafic hornblende-rich top to a feldspathic base (Fig. 7.6).

The main features of the Selebi Upper Body in Figure 7.5a are:
(a) The highly variable nature of the profile.
(b) The general increase in Mg, Fe and Mn towards the top of the host amphibolite.
(c) The general decrease in Al towards the top.
(d) The high Ti and Zr at the upper and lower margins. These high-Ti & Zr marginal amphibolites are also high in P and Y.
(e) The typically "anorthositic" (see Ch. 4.1.6) geochemistry of the plagioclase-rich band in the amphibolite.
(f) The highly variable Cr content.

The main features of the Selebi Lower Body in Figure 7.5a are:

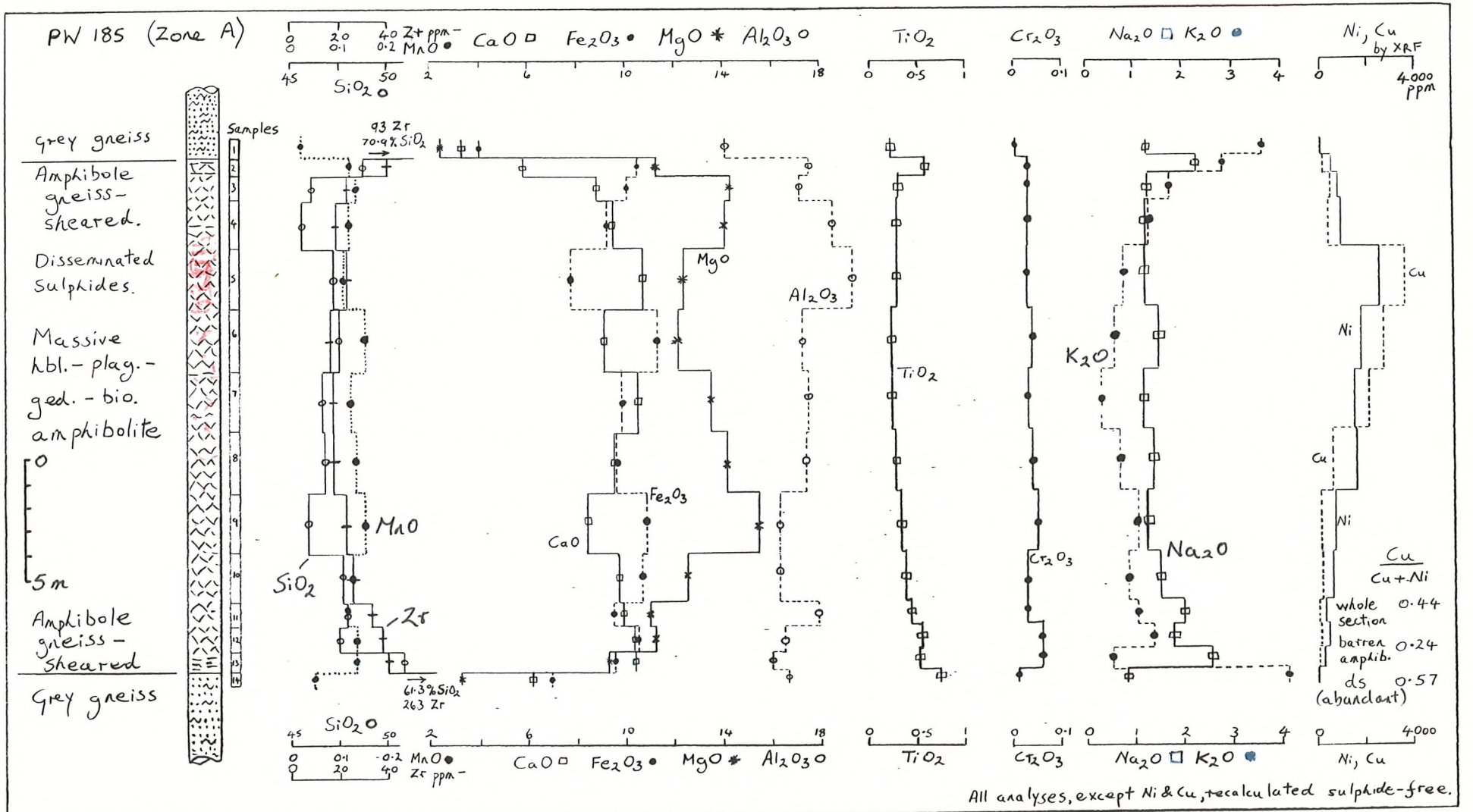

Fig 7.4 GEOCHEMICAL VARIATION THROUGH PHIKNE HOST AMPHIBOLITE (PW 185) - ZONE A.

(a) The more homogeneous nature of the Lower Body compared to the Upper Body.
(b) The high Mg and Cr contents at the top of the host amphibolite. The Cr content also increases at the base.
(c) The low Ca contents at the upper and lower margins. In the lower half of the host amphibolite Ca and K have an antithetic relationship.
(d) The high Ti content at the top of the amphibolite.
(e) The highly variable Zr content which is unrelated to the variation of any major element.

The main features of the Selebi Upper Body in Figure 7.6 are:
(a) The general increase in Mg and Fe towards the top of the host amphibolite.
(b) The general decrease in Al and Ca towards the top.
(c) The highest Cr content near the top.
(d) The weakly antithetic relationship between Ca and K.
(e) The highly variable Zr content which is unrelated to the variation of any major element.

7.3.1c Selebi North

The section chosen for detailed sampling at Selebi North was the exploratory hole with the greatest amount of ultramafic rock associated with host amphibolite. The whole section was sampled and analysed. The section consists of thick amphibole pyroxenite above typical hornblende-plagioclase host amphibolite (see Ch. 5.2.3e). The main features of Figure 7.7 are:
(a) The relatively homogeneous nature of the ultramafic rocks.
(b) The high Ti, Zr, Al, Fe and P and low Ca, Na and Cr contents of the thin serpentinous shear zone and the pyroxenite immediately above this shear zone. The Ti and Zr contents of the rocks above the shear zone gradually increase going down to the shear zone.
(c) The low Ti contents of ultramafic rock (average 0.28 wt%) and the relatively high Ti contents of amphibolite (average 0.80 wt%).
(d) The higher Zr contents of amphibolite compared to those of ultramafic rock.
(b) The gradual decrease in Ca and increase in K going down through the lower portion of the section.
(e) The zone of high Cr (4% Cr_2O_3) in the host amphibolite which is unrelated to the variation of any other major element.
(f) The weakly mineralised ultramafic rocks have a Cu/(Cu+Ni) ratio of 0.24. The amphibolites with even less sulphides have a ratio of 0.08.

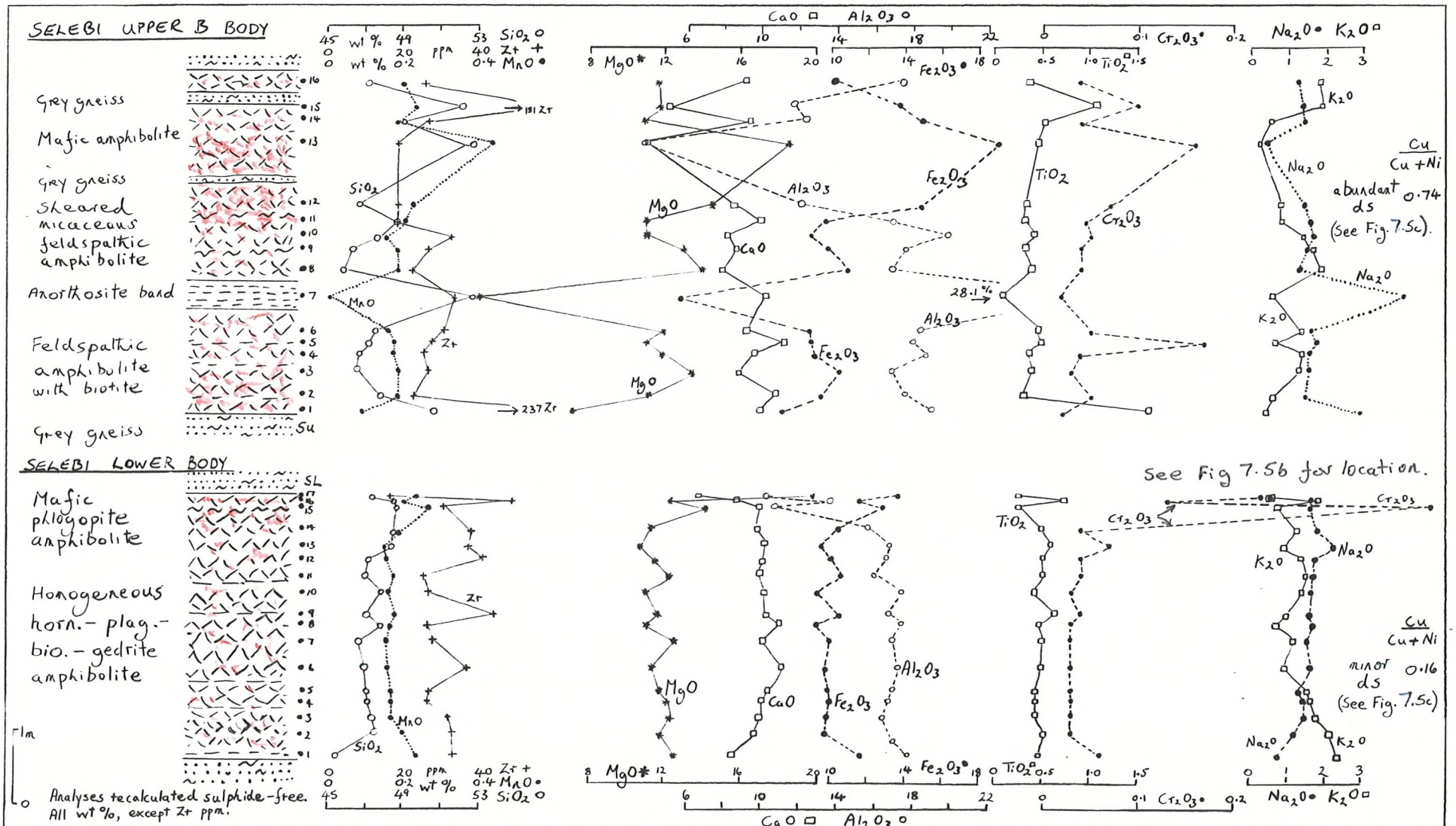

Fig 7.5a GEOCHEMICAL VARIATION THROUGH THE SELEBI LOWER AND UPPER B BODIES (100m SILL DRIVE)

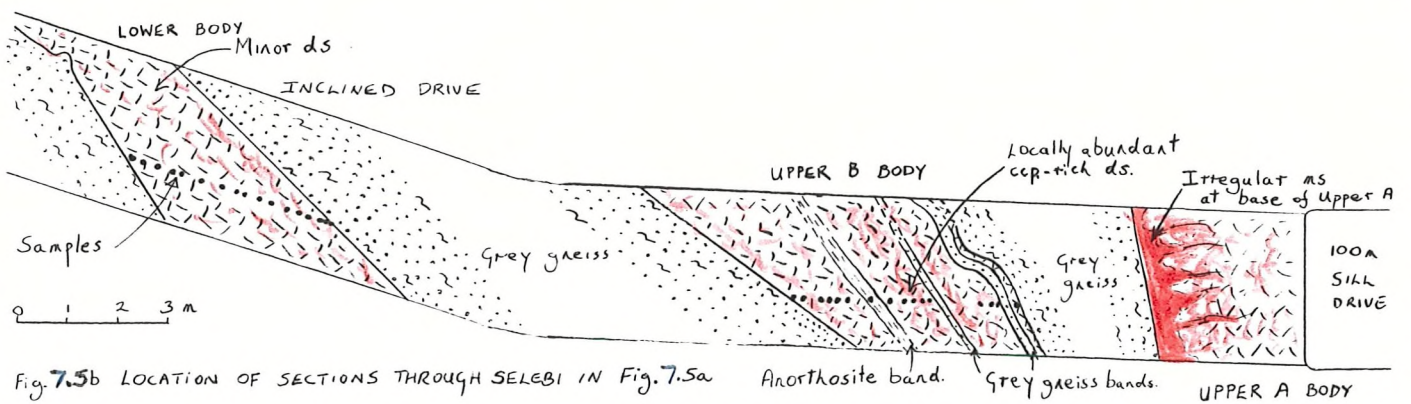

Fig. 7.5b LOCATION OF SECTIONS THROUGH SELEBI IN Fig. 7.5a

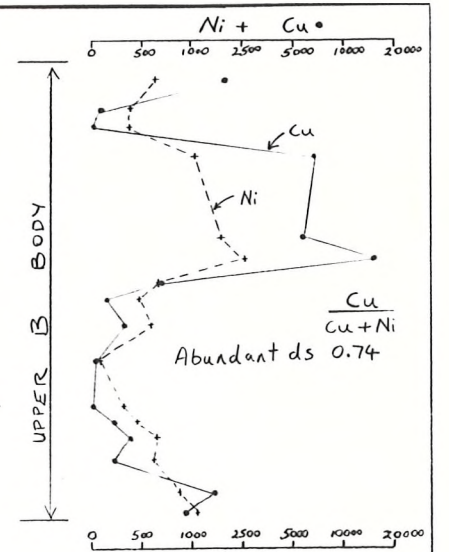

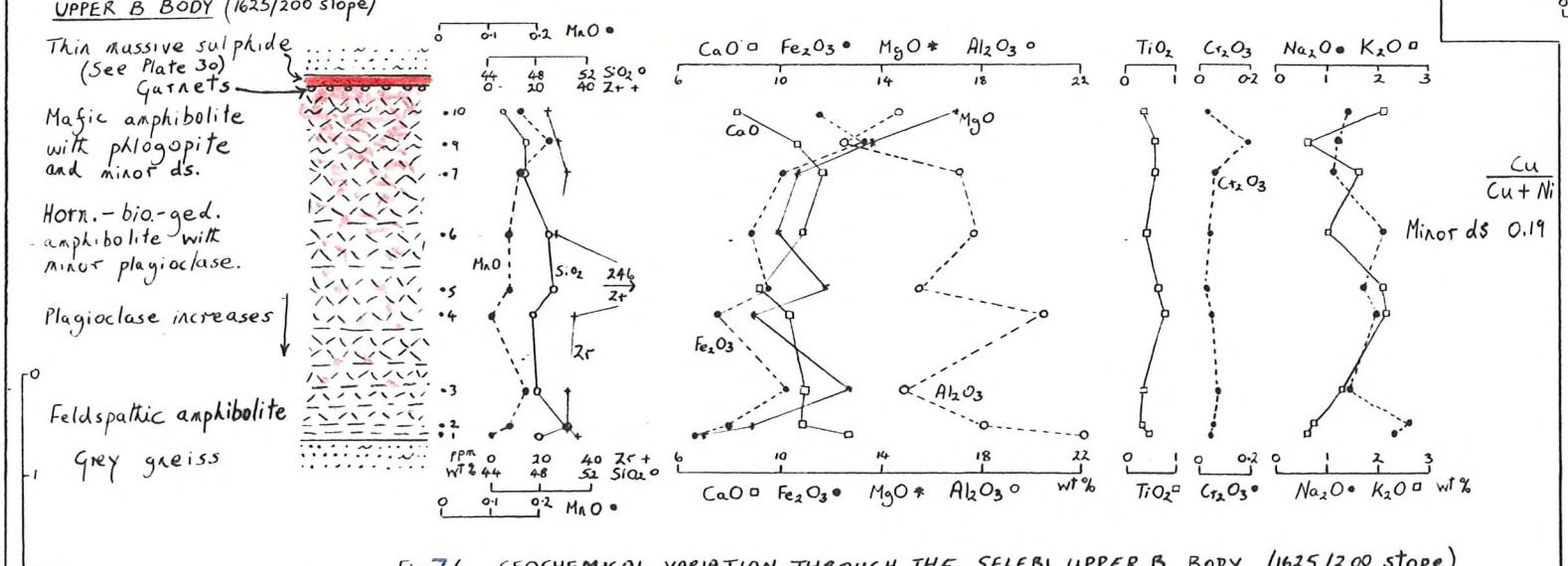

Fig. 7.6 GEOCHEMICAL VARIATION THROUGH THE SELEBI UPPER B BODY (1625/200 stope)

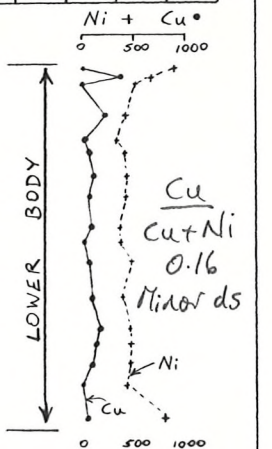

Fig 7.5c Ni - Cu CONTENTS OF UPPER B AND LOWER BODIES IN Fig. 7.5a

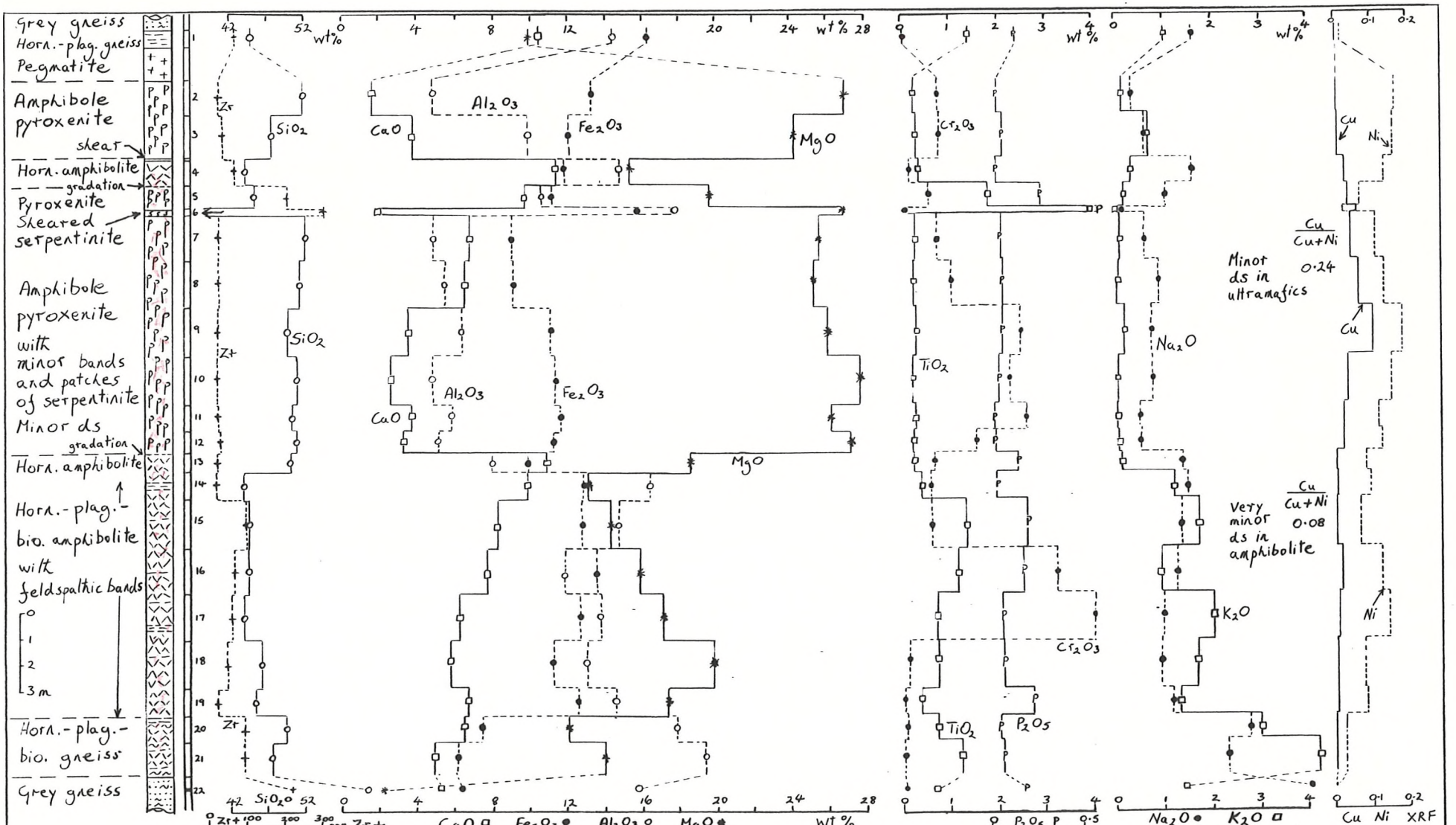

Fig. 7.7 GEOCHEMICAL VARIATION THROUGH THE SELEBI NORTH HOST AMPHIBOLITE AND ULTRAMAFIC (SDN 56)

7.3.2 Two-element Variation Diagrams

Two-element variation diagrams were chosen to show the variation in host rock geochemistry. This was because if the host rocks have a basic-ultrabasic igneous origin (see Ch. 5.2.4), both liquids and minerals can be easily represented on the diagrams (Cox et al. 1979). An indication as to whether an anomolous sample is highly sheared (s) or occurs at the margin of the host body (m) has been made on the diagrams. The highly sheared ultramafic rock from SDN 56 is indicated (u,s).

(a) SiO2 v. MgO (Fig. 7.8) shows the wide range of MgO contents of Selebi-Phikwe host rocks. There appears to be a gap in MgO contents between 20 and 24.5 wt% MgO. The Si-poor nature of the garnetiferous amphibolites is illustrated.

(b) Al2O3 v. MgO (Fig. 7.9a) shows the more aluminous nature of the Selebi host amphibolite and picks out the ultramafic rocks at Selebi North and Phikwe. The more diverse amphibolites and ultramafic rocks define an inverse relationship between Al and Mg. The two amphibolites which lie below this trend are high in Fe and low in Al.

(c) Fe2O3 v. MgO (Fig. 7.9b) shows that Fe is weakly proportional to Mg. However there is also marked enrichment in Fe. This enrichment can be subdivided into two trends: the main one in rocks with average Mg and Al contents (particularly shown by garnet amphibolites) and the other trend in rocks with higher than average Mg but low Al. The serpentinised peridotite at Phikwe is low in Fe.

(d) Cr2O3 v. MgO (Fig. 7.10a) shows a wide variation of Cr contents which are only weakly related to the MgO content. The host amphibolite samples, particularly those of Phikwe, typically have low Cr contents (less than 0.1 wt%). The lowest Cr contents occur in amphibolites with 12-15 wt% MgO. Amphibolites with slightly lower (and higher) MgO than this range have slightly higher Cr contents. This is in agreement with the geochemical profiles in which Cr is typically higher in marginal amphibolite with lower than average MgO contents than in amphibolite from the middle of the section (e.g. Fig. 7.2). The highest Cr contents are at Selebi North, in both ultramafic rocks and amphibolites. The Cr contents of Selebi amphibolites are more variable and commonly higher than those of Phikwe.

(e) Fe2O3 v. TiO2 (Fig. 7.10b) shows that Ti contents are unrelated to Fe contents. TiO2 contents typically range from 0.1 to 0.8 wt%. The Fe-enrichment, particularly of the garnet amphibolites, is well shown. The samples with high TiO2 contents are typically highly

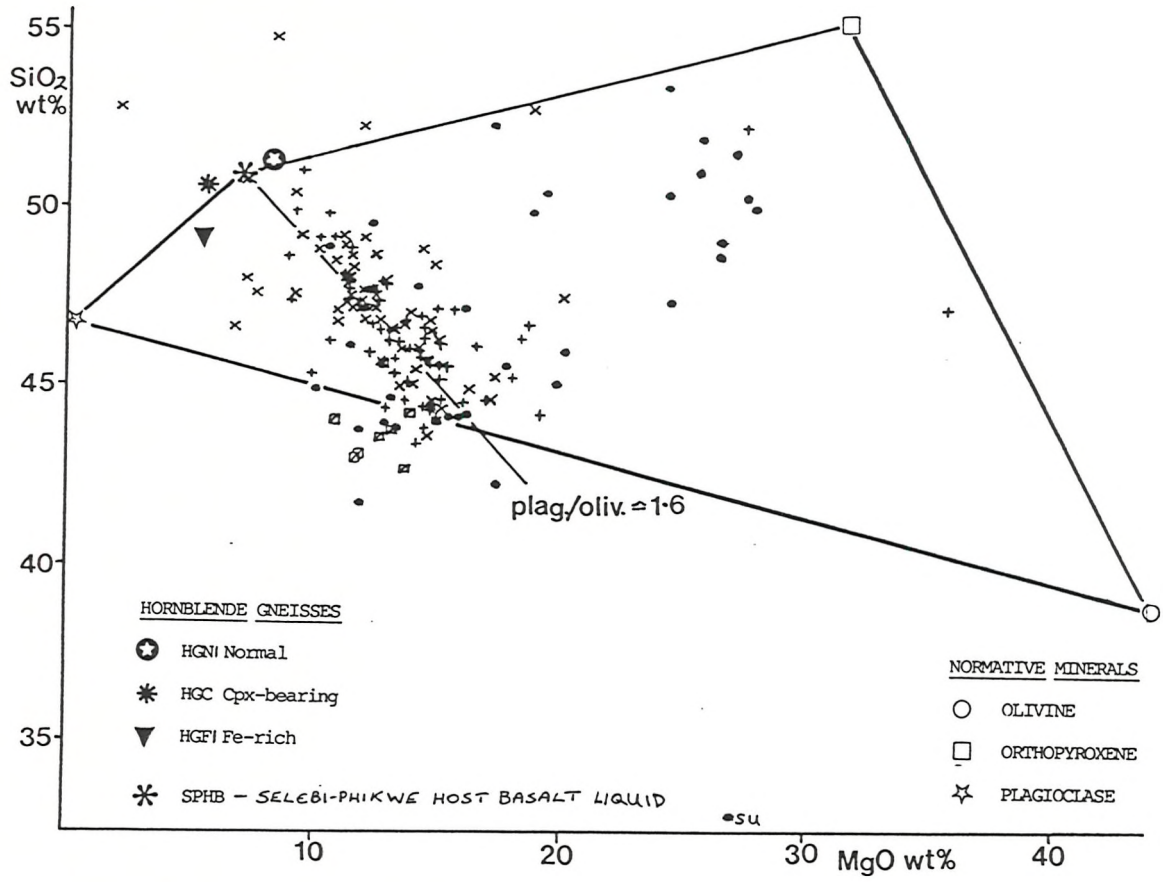

Fig. 7.8 TWO-ELEMENT VARIATION DIAGRAM - THE SELEBI-PHIKWE HOST ROCKS; SiO2 v. MgO.

+ Phikwe Host Rocks, × Selebi Host Rocks, * Selebi North Host Rocks, ø Garnet Amphibolites, su Highly Sheared Ultramafic Rock from SDN 56. All analyses have been recalculated to 100% on an anhydrous and sulphide-free basis.

sheared and/or marginal host rocks. They are mainly from Selebi North. The Selebi North-SDN 56 section (Fig. 7.7) is particularly high in TiO2 and the field of the high-Ti amphibolites in that section is indicated. The highest TiO2 content is in the highly sheared serpentinous ultramafic rock from SDN 56.

(f) TiO2 v. Zr (Fig. 7.11a) shows a diffuse proportional relationship between Ti and Zr. Normal Zr contents are between 15-60 ppm. The majority of host rocks have a Ti/Zr ratio of about 91. Some high-Ti amphibolites have significantly lower Ti/Zr ratios. The samples with high Zr contents are typically highly sheared and/or marginal host rocks, particularly from the Selebi North-SDN 56 section. The high-Ti-Zr amphibolites have higher than average P and Y contents, although relationships are not linear. The highly sheared ultramafic rock from SDN 56 contains 0.61 wt% P2O5 and 34ppm Y. The marginal amphibolites of the Selebi Upper Body (Fig. 7.5a) contain 0.44-0.58 wt% P2O5 and 33-58 ppm Y.

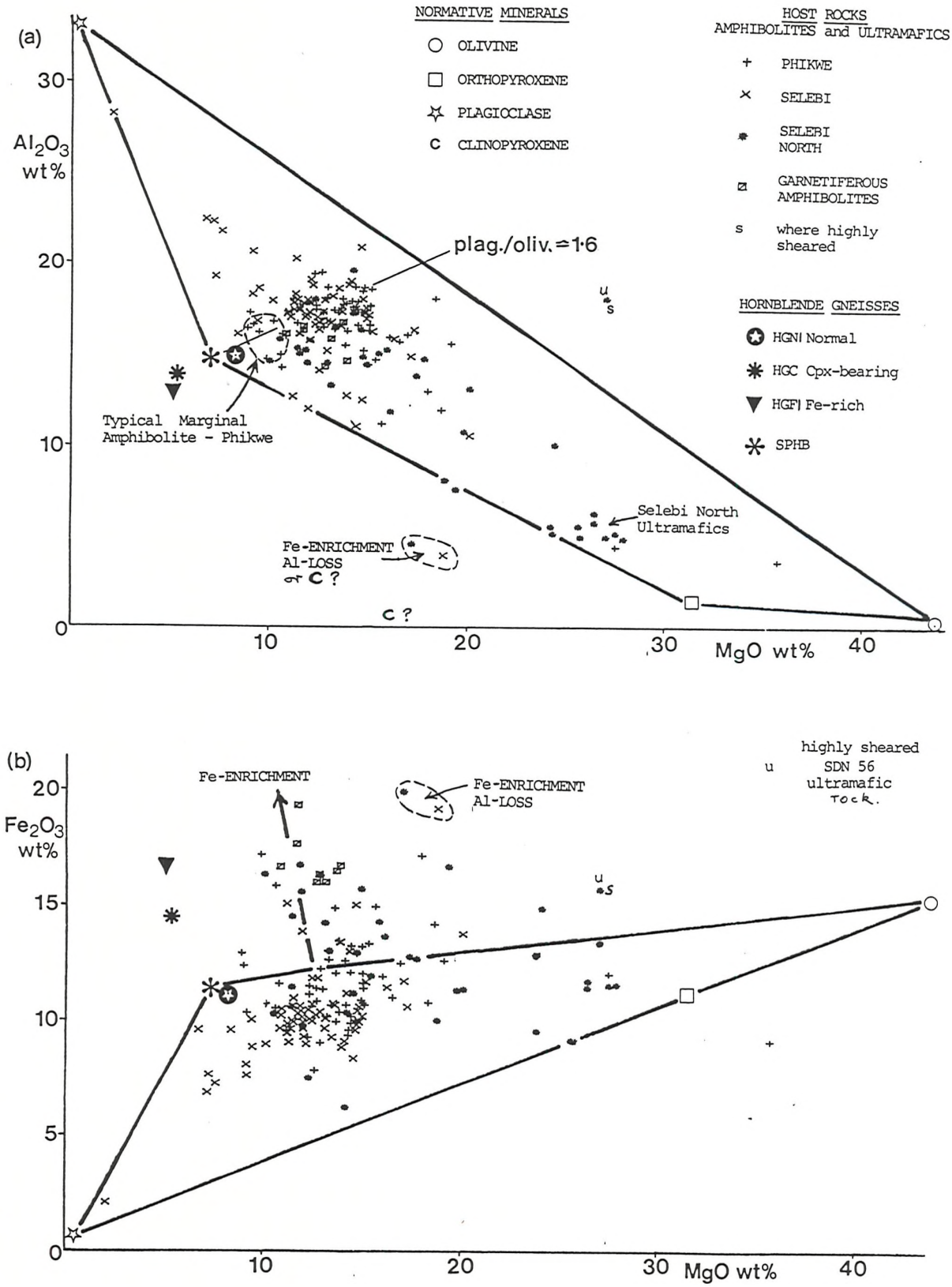

Fig. 7.9 TWO-ELEMENT VARIATION DIAGRAMS - THE SELEBI-PHIKWE HOST ROCKS
(a) Al_2O_3 v. MgO, (b) Fe_2O_3 v. MgO.

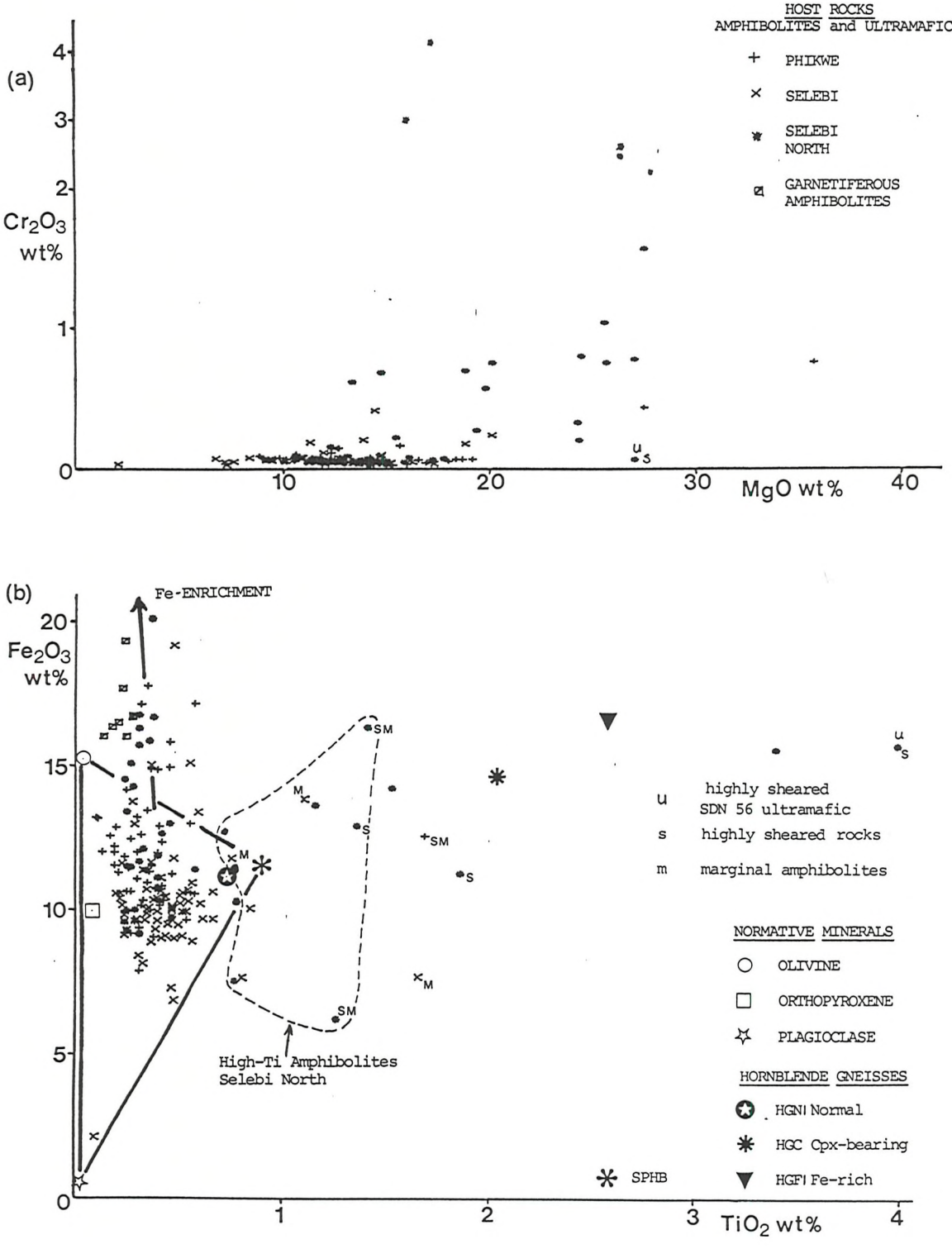

Fig. 7.10 TWO-ELEMENT VARIATION DIAGRAMS - THE SELEBI-PHIKWE HOST ROCKS
(a) Cr_2O_3 v. MgO, (b) Fe_2O_3 v. TiO .

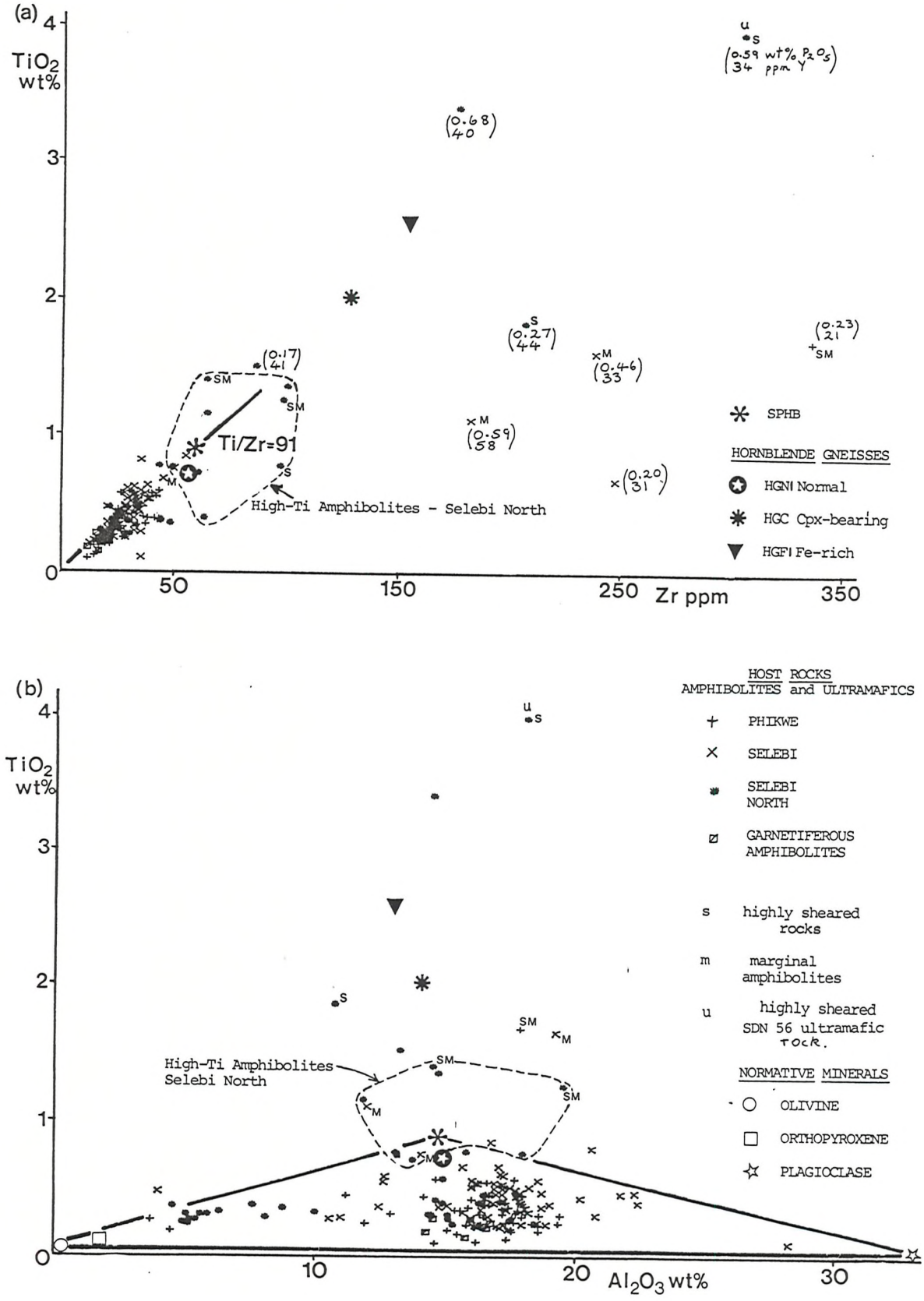

Fig. 7.11 TWO-ELEMENT VARIATION DIAGRAMS - THE SELEBI-PHIKWE HOST ROCKS
(a) TiO_2 v. Zr, (b) TiO_2 v. Al_2O_3.

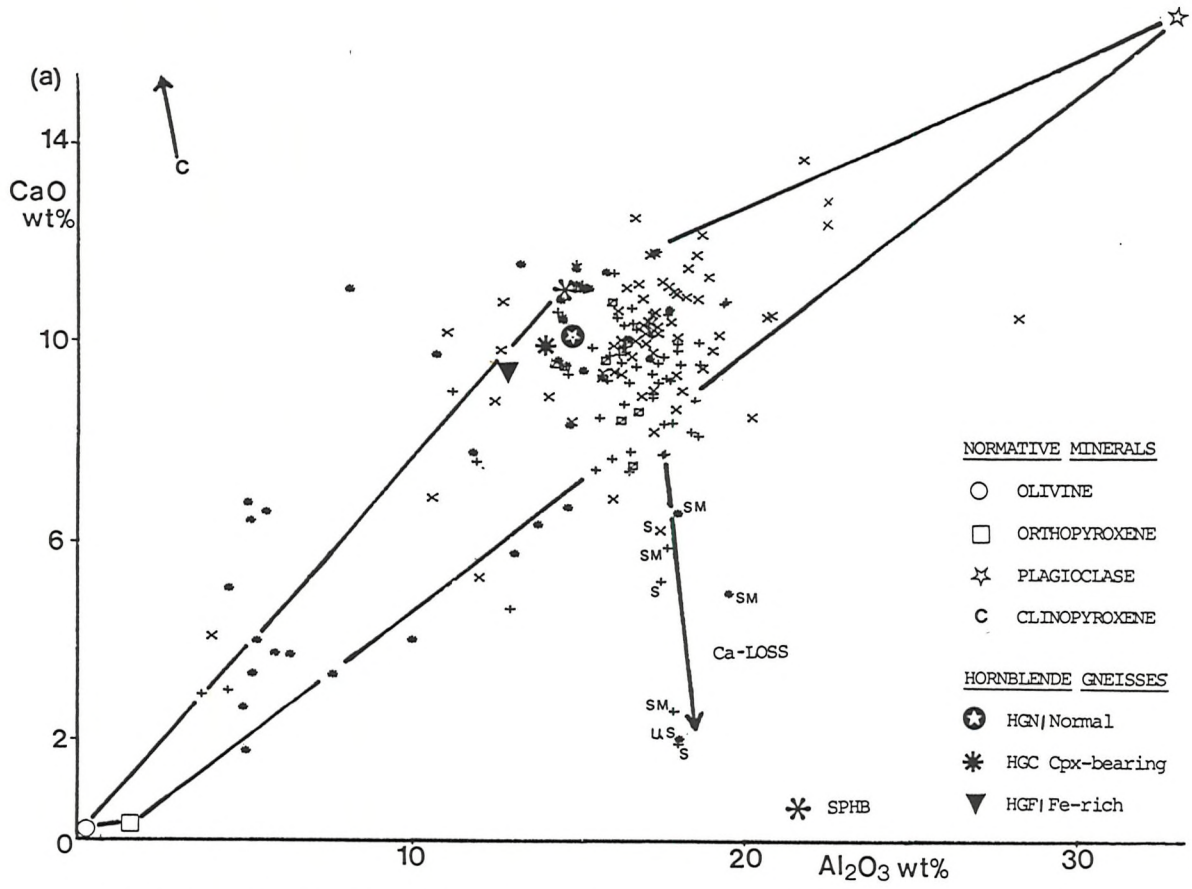

Fig. 7.12a TWO-ELEMENT VARIATION DIAGRAM - THE SELEBI-PHIKWE HOST ROCKS; CaO v. Al_2O_3.

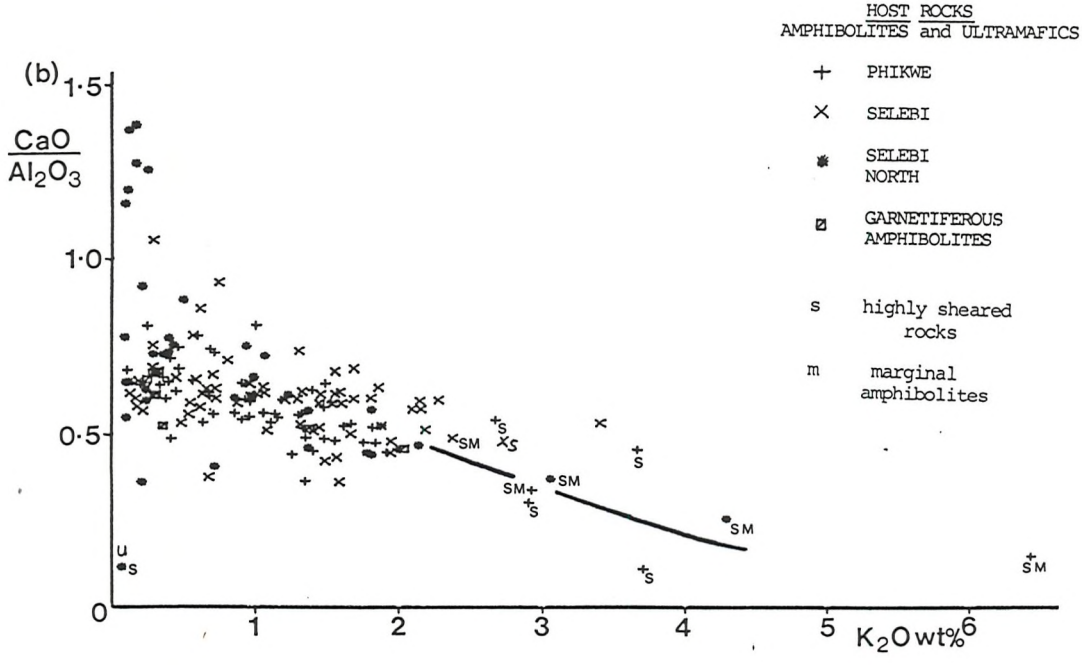

Fig. 7.12b THE SELEBI PHIKWE HOST ROCKS; CaO/Al_2O_3 v. K_2O

Fig. 7.12 THE CaO & Al_2O_3 CONTENTS OF THE SELEBI-PHIKWE HOST ROCKS

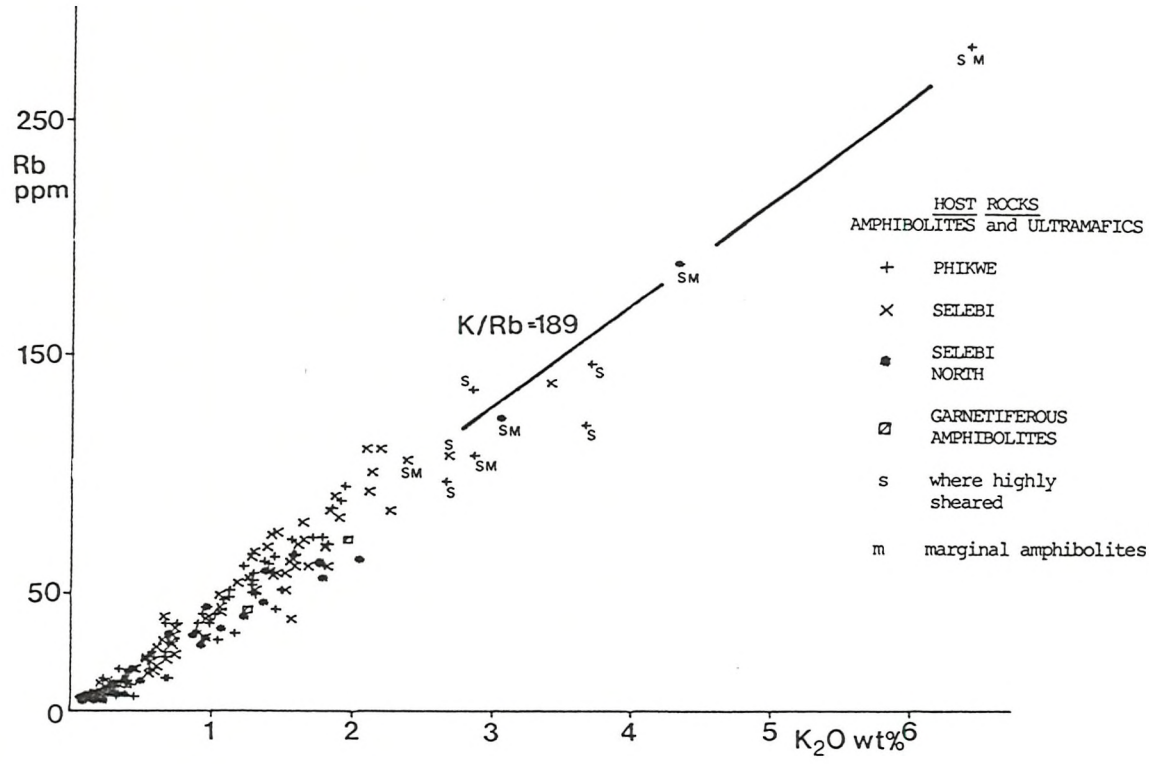

Fig. 7.13 THE Rb & K_2O CONTENTS OF THE SELEBI-PHIKWE HOST ROCKS

(g) TiO2 v. Al2O3 (Fig. 7.11b) further shows that the rocks can be split up into a high TiO2 group (over about 0.9 wt%) and a normal TiO2 group (0.1-0.9 wt%). The highest TiO2 contents of the normal TiO2 group occur in rocks with 15-17 wt% Al2O3. A similar diagram is obtained if TiO2 is plotted against MgO.

(h) CaO v. Al2O3 (Fig. 7.12a) shows a diffuse proportional relationship between CaO and Al2O3. The more aluminous nature of the Selebi amphibolites is illustrated. There is a trend of Ca depletion in amphibolites with normal Al contents. These low-Ca amphibolites are highly sheared.

(i) CaO/Al2O3 v. K2O (Fig. 7.12b) shows that there is a general decrease in the CaO/Al2O3 ratio with increasing K2O. This is in agreement with the geochemical profiles which typically show an antithetic relationship between Ca and K. The high-K amphibolites are typically highly sheared. The CaO/Al2O3 ratio of the majority of the amphibolites is between 0.5 and 0.7. The Selebi North ultramafic rocks typically have high CaO/Al2O3 ratios between 1.2 and 1.4 and low K2O contents. (cf Dikoloti-Lentswe, Ch. 8.5.1)

(j) Rb v K2O (Fig. 7.13) shows a linear relationship between Rb and K2O, with a K/Rb ratio of 189. The host rocks with high K-Rb contents are highly sheared.

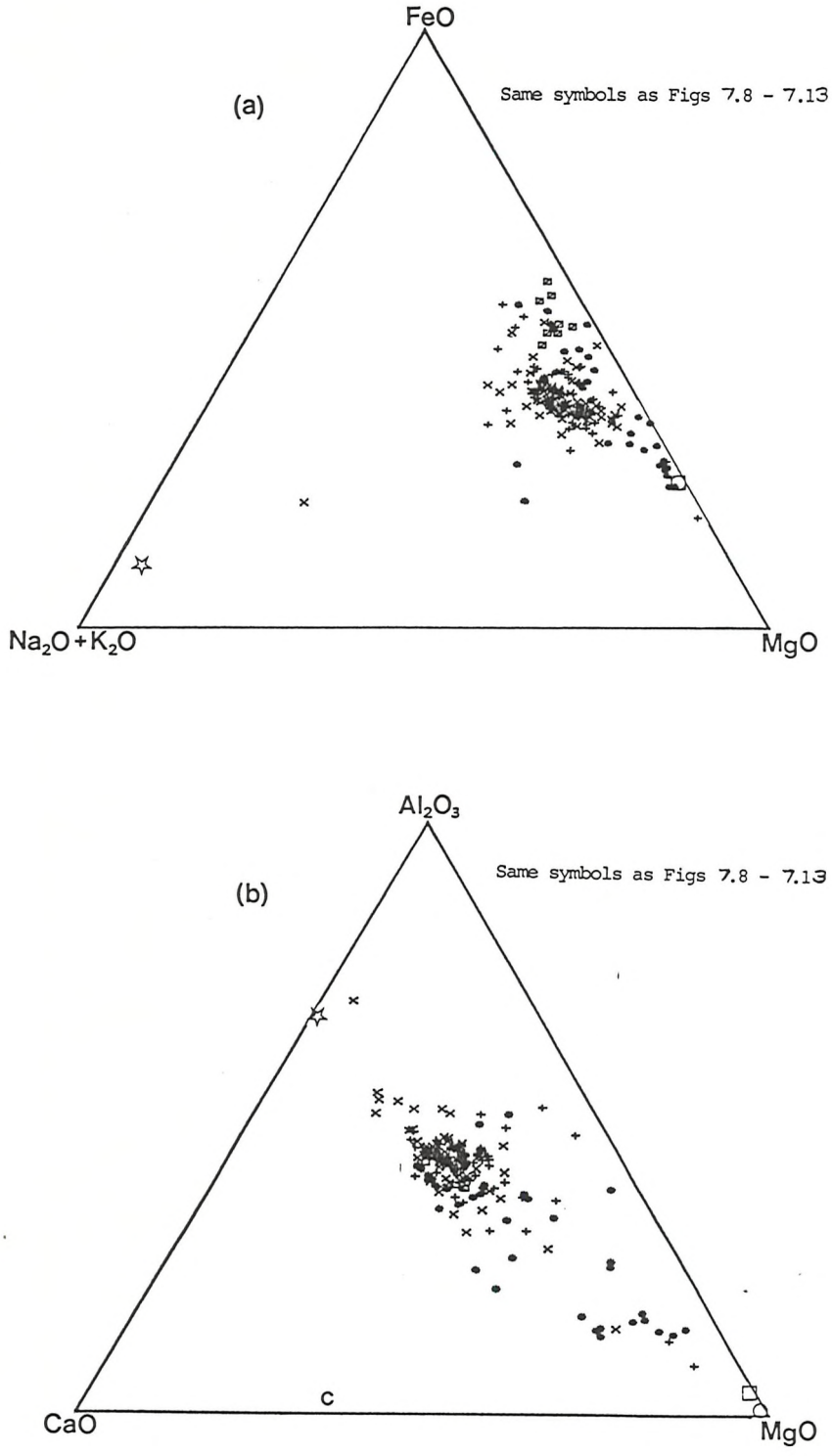

Fig. 7.14 TRIANGULAR DIAGRAMS OF THE SELEBI-PHIKWE HOST ROCKS
(a) AFM and (b) ACM DIAGRAM

7.4 DISCUSSION

7.4.1 Alteration and Element Mobility

Before conclusions as to the original nature of the host rocks can be made, it is necessary to make an estimate of the effects of alteration on the host rock geochemistry. The possible alteration that has been suffered by the host amphibolites can be subdivided into early pretectonic-metamorphic (hydrothermal) alteration, pervasive alteration due to regional metamorphism, localised alteration due to shearing and alteration due to weathering. Fresh samples were collected from recent underground exposures or diamond drill holes. Therefore the effects of recent weathering are assumed to be negligible.

Of the other three alteration effects, that of localised shearing is the simplest to evaluate. The Selebi-Phikwe host rocks have suffered at least two phases of locally superimposed shearing (Ch. 5.1). Highly sheared amphibolites typically have higher than average contents of Ti, K, Rb, P, Y and Zr and lower than average contents of Si, Ca and locally Na. The effect of shearing on the Ti, Zr, Ca, K and Rb contents is shown in Figures 7.10b, 7.11, 7.12 and 7.13. However the effect of shearing is also variable and results, for example, in highly variable contents of Ti, P, Y and Zr (Fig. 7.11a). The geochemical changes that can be brought about during shearing are illustrated by the highly sheared serpentinous zone in the Selebi North section (SDN 56, Fig. 7.7). This ultramafic rock (26.8 wt% MgO) has significantly higher contents of Ti, Al, Fe, P, V, Y (34 ppm), and Zr (303 ppm) and lower contents of Si, Mg, Ca, Na and Cr than enveloping unsheared ultramafic rocks. The high P content is confirmed by the presence of apatite (Plate 33e). Shearing of anorthositic gneisses produced thin mylonitic zones, in some of which Ti, P, Ce, Nb, Y and Zr contents were increased and Al, Mg, Na and Cl were decreased (Fig. 4.14, Ch.4.4.1). It is proposed that shearing has caused significant but variable changes in host rock geochemistry.

The geochemical effects of premetamorphic alteration and regional metamorphism are more difficult to evaluate than those of localised shearing. Regional metamorphism possibly resulted in similar relative changes as localised shearing, but to a much lower degree. The most conspicuous difference in the geochemistry of some unsheared host rocks from the average host rock geochemistry is Fe-

enrichment (Figs 7.9b, 7.10b & 7.14a), particularly in garnet amphibolites.

7.4.2 Garnet Amphibolites

The association of garnet amphibolites with high concentrations of disseminated sulphide (Ch. 5.2.1b & 5.2.3a) and the occurrence of garnets at massive sulphide-host amphibolite contacts (Plate 30) suggest that the garnet amphibolites obtained their excess Fe and Mn (Table 7.3, Figs 7.1-7.3) from sulphides. Apart from the increase in Fe and Mn, the relative changes in the other elements are difficult to evaluate. It is possible that the small differences in Ti, Ca, Al, Na and K between garnet amphibolites and average Phikwe host amphibolite are due to differences in their protoliths rather than desulphurisation. The experiments of Kullerud and Yoder (1965) and MacRae (1974) have demonstrated that silicate minerals may react with S during metamorphism at temperatures above 500°C forming Fe-sulphides, Fe-oxides and Fe-depleted silicates. Macrae (1974) synthesised cordierite and pyrrhotite by the reaction of natural basalt and S. Plimer (1977) has suggested that silicate assemblages associated with the Broken Hill sulphide bodies, New South Wales, underwent desulphurisation reactions, equivalent to the reverse of those above, which produced a silicate fraction enriched in Fe and consumed S.

A possible desulphurisation reaction for the formation of garnet amphibolites (see mineralogy in Ch. 5.2.3) at Selebi-Phikwe is:

Magnesio-
Hornblende + Pyrrhotite + Plagioclase + Ca? =

Almandine + Tshermakitic hornblende + S + (Ti,Na,K,Rb,Sr,Zr ?)

However the occurrence of high-Fe amphibolites (containing a greenschist facies assemblage of chlorite, actinolitic amphibole, epidote, sulphides and minor plagioclase) adjacent to massive sulphide in the gabbroic, Selkirk deposit (Fig. 1.1) in the Tati greenstone belt indicates that the desulphurisation reaction was probably initiated at a low grade of metamorphism and involved greenschist facies minerals (Brown, in prep.).

7.4.3 The Original Components of the Selebi-Phikwe Host Rocks

In Chapter 6.4 it was concluded that the Selebi-Phikwe sulphides

were associated with their host rocks prior to deformation and metamorphism. The mafic hornblende-rich mineralogy of the Selebi-Phikwe host amphibolites, their association with Ni-Cu ores and their gradation into ultramafic rocks suggest an igneous origin for the host rocks. However as observed by Leake (1964) the existence of amphibolites does not always imply that they were derived from igneous rocks. Gallon (1986) suggested that the host amphibolites could be sedimentary in origin, although he does not indicate what type of sediment.

The Selebi-Phikwe host amphibolites are characterised by high Al2O3 and MgO contents and low SiO2/MgO ratios which together are reflected by high normative contents of plagioclase and olivine (Table 7.1). The Selebi North host ultramafic rocks are characterised by high normative hypersthene. The geochemistry suggests an igneous origin for the host amphibolites and ultramafic rocks as troctolitic-noritic gabbros and orthopyroxenites respectively. In the AFM diagram (Fig. 7.14a) the host rocks exhibit a marked tholeiitic fractionation trend towards increasing Fe-content (cf. Myers 1975). The average Ti/Zr ratio of 91 (Fig. 7.11a) is within the range for tholeiitic rocks (Pearce & Cann 1973). However the low contents of imcompatible elements in the host rocks (Table 7.1) are more closely comparable with those of intrusive gabbroic rocks than extrusive basalts (Le Maitre 1976; Coleman 1977). The wide ranging, locally high Cr contents (Fig. 7.10a) suggest a cumulate rather than an extrusive origin. The geochemistry of the average host amphibolites (Al2O3 14-17 wt%, MgO 12-14 wt%) is beyond the compositional limits of known natural melts. It is therefore suggested that the Selebi-Phikwe host rocks are metamorphosed gabbroic and ultramafic cumulates.

In order to test the gabbroic-ultramafic cumulate hypothesis, the compositions of the normative plagioclase, olivine and orthopyroxene (and in a few diagrams, clinopyroxene) have been plotted on the two-element variation diagrams. A composition of An 83 (the average of the norms for the host rocks, corrected for K metasomatism) has been used for the plagioclase. Compositions of Fo 85 and En 85, the normative mineral compositions of the Selebi North ultramafic rocks, have been used for the olivine and orthopyroxene, rather than the less-magnesian normative mineral compositions of the amphibolites, because of the Fe-enrichment in the latter.

If the host rocks were originally gabbroic-ultramafic cumulates, they are possibly related to the hornblende gneisses which are the

major mafic lithology in the Selebi-Phikwe gneiss sequence. The majority of hornblende gneisses have been interpreted in Chapter 4.7 as fractionated tholeiitic lavas and high-level intrusives. The average compositions of the three main types of hornblende gneiss, the dominant type of hornblende gneiss (HGN1), the clinopyroxene-bearing type (HGC) and the high-Fe & incompatibles type (HGF1), have also been also plotted on the two-element variation diagrams.

When the effects of element mobility, particularly the Fe-enrichment and the variable Ca content, are taken into account, the majority of host rock samples lie within fields (Figs 7.8, 7.9, 7.10b, 7.11b & 7.12a) bounded by lines joining the normative plagioclase, olivine and orthopyroxene compositions and SPHB. SPHB has a compositon of about 50.9 wt% SiO_2, 0.9 TiO_2, 14.6 Al_2O_3, 11.6 Fe_2O_3, 7.1 MgO, 11.0 CaO and 59 ppm Zr, i.e. a tholeiitic basalt. SPHB (Selebi-Phikwe Host Basalt liquid) is within the range of HGN1 (Table 4.1). A similar conclusion can be drawn from the ACM diagram (Fig. 7.14b) in which the host rocks lie on a trend between olivine-orthopyroxene and plagioclase. The majority of the host rocks appear to be unrelated to the other main types of hornblende gneiss, HGC and HGF1. It is possible that some of the high-Ti host amphibolites are high-Ti hornblende gneiss (HGC and HGF1-type) of the gneiss sequence that have been incorporated into the host rocks. However these high-Ti amphibolites are commonly sheared which suggests a relationship between high Ti and shearing. The diagrams strongly suggest that the Selebi-Phikwe host rocks are metamorphosed mixtures of Fe-Ni-Cu sulphides, cumulus plagioclase (bytownite), olivine (chrysolite) and orthopyroxene (bronzite) and intercumulus tholeiitic basalt (SPHB). Cumulus clinopyroxene appears to have been a minor phase, mainly at Selebi North.

Plagioclase, olivine and orthopyroxene contain very little Ti (Deer et al. 1963). Therefore if the above hypothesis is correct and the effects of alteration are not too serious in the majority of host rocks, the Ti contents of the host rocks are an indication of the amount of SPHB and hence basaltic liquid in the mixture. For simplicity the following discussion will be of a sulphide-free assemblage. The Phikwe host amphibolites contain an average of 0.33 wt% TiO_2, compared to 0.9 wt% TiO_2 in SPHB. This indicates an average basaltic liquid content of about 39 wt% in the Phikwe host rock protoliths, the remainder having been plagioclase, olivine and orthopyroxene crystals (sulphide-free basis). The average geochemical compositions

(Tables 7.1 & 7.2, corrected for Fe-enrichment and K-metasomatism) of the Selebi-Phikwe host rocks have been modelled in terms of mixtures of intercumulus SPHB basalt and cumulus plagioclase (An 83), olivine (Fo 85), orthoproxene (En 85), clinopyroxene (augite) and chromite (50% Cr2O3). Although it has been concluded that the Selebi-Phikwe sulphides were associated with their host rocks prior to deformation and metamorphism, the results of the modelling are shown for simplicity on a sulphide-free basis in Table 7.4a. The range of the Ti, Al and Mg contents of the Phikwe host amphibolite (Figs 7.8, 7.9a & 7.11b) indicates a wide range of SPHB content from approximately 10 to 69 wt%. The Selebi host amphibolite has an average TiO2 content of 0.44 wt%. The higher average Ti of the Selebi amphibolite compared to that of Phikwe amphibolite is considered to be an original feature rather than due to alteration or shearing. The Selebi host amphibolite is thought to have originally contained an average basaltic liquid content of about 51 wt%. The higher Ti is supported by proportionate increases in the P, Nb, V, Y, Zr and normative diopside contents of average Selebi amphibolite compared to average Phikwe amphibolite (Table 7.1). P, Nb, V, Y and Zr would have remained in the fractionating liquid rather than entering plagioclase, olivine or orthopyroxene crystals.

The Selebi North A amphibolite (without associated ultramafic rocks) has been modelled as originally containing having about the same plagioclase/olivine ratio and SPHB content as the Phikwe and Selebi amphibolites but a higher cumulus clinopyroxene content. The high Ti, P, Y and Zr contents of the Selebi North AU amphibolites (associated with ultramafic rocks) could be fundamental (e.g. a higher basaltic liquid/cumulus crystal ratio or a magma with a significantly higher Ti content than that proposed for the Phikwe and Selebi amphibolites) or imposed (e.g. due to shearing). Although shearing-induced alteration is proposed to have variably mobilised Ti, P, Y and Zr, it is thought that localised shearing could not have been responsible for all the significant differences between the two types of Selebi North host amphibolite. The TiO2 content of the basalt liquid of the Selebi North AU amphibolites is proposed to have been approximately the same as or only slightly higher than that in the Phikwe, Selebi and Selebi North A amphibolites (Figs 7.10b & 7.11), rather than being significantly higher. The Selebi North AU amphibolites have been effectively modelled in terms of a high (70 wt %) content of basaltic liquid content (SPHB), 17 wt% olivine, 6 wt%

clinopyroxene, 1.6 wt% chromite but only 3 wt% plagioclase (Table 7.4a). Other alternatives to partly explain AU geochemistry are that spinel was originally a significant phase or that Si has been depleted in the amphibolites. Taking either of these into account in the modelling would result in higher ratios of orthopyroxene/olivine or intercumulus liquid/cumulus crystals.

The Selebi North ultramafic rocks have been modelled as original mixtures of approximately 27 wt% SPHB, 18 wt% olivine, 47 wt% orthopyroxene and minor plagioclase, clinopyroxene and chromite. They are regarded as an integral part of the host amphibolite body, rather than as a separate intrusion as suggested by Wakefield (1974,1976). The amount of ultramafic rock in the north limb varies from zero to a maximum of about 50% (SDN 56, Fig. 7.7). A combination of Selebi North ultramafic rocks and AU amphibolite in the proportion of 1:3 has therefore been used to give an approximate indication of the original composition of the north limb host rocks (Table 7.4a).

The modelling is very simple and fraught with uncertainties and should only be regarded as an indication of the original components of the host rocks. For example the total amount of cumulus crystals is very dependent on the TiO2 content deduced for SPHB. A higher TiO2 content (>0.9 wt%) content would give significantly different results. However the data appear to fit a TiO2 content of 0.75-1.0 wt% for SPHB (Figs 7.10b & 7.11). The olivine/orthopyroxene ratios obtained in the modelling are very dependant on the Si contents of the host rocks (the average Si contents of which are assumed to have only been significantly altered by Fe-enrichment and K metasomatism) and the Si content of SPHB. The fact that plots of the geochemistry of the majority of the host rocks form trends that can be interpreted in terms of original components and processes indicates that the essential geochemistry of the majority of the host rocks has not been seriously distorted by premetamorphic alteration and regional metamorphism. The two-element variation diagrams (Figs 7.8 & 7.9) suggest that olivine was probably more dominant than orthopyroxene in the majority of host amphibolites and that orthopyroxene was more dominant than olivine in the host ultramafic rocks. The results of the modelling are in agreement with this. The normative compositions of olivine (& opx.), plagioclase and clinopyroxene used in the modelling are generally consistent with the compositions used in the modelling of the evolution of HGC from HGN1 (see Ch. 4.7.2b). It is important to stress that the modelling of the Selebi-Phikwe host rocks was done

(a) SULPHIDE-FREE BASIS

	Cumulus Minerals					Basaltic Liquid	
	Plag. An 83	Oliv. Fo 85	Opx. En 85	Cpx.	Chr.	SPHB	Total
	wt%						
Phikwe	34.1	19.2	9.7	tr.	tr.	39	102.0
Selebi	29.3	16.9	4.3	tr.	0.1	51	101.6
Selebi North Amphibolite A	27.2	18.5	6.5	4.1	0.1	46	102.4
Selebi North Amphibolite AU	3	17	2	6	1.6	c.70	
	(possibly includes spinel & higher opx./oliv. ratio)						
Selebi North Ultramfics	4.2	17.9	47.4	3.0	2.6	27	102.1
Selebi North northern limb	3	17	13	5	2	60	100
	(AU + ultramafics combined in ratio 3:1)						

(b) INCLUDING SULPHIDES

	Cumulus Minerals					Basaltic Liquid	Immiscible Sulphide
	Plag.	Oliv.	Opx.	Cpx.	Chr.		
Phikwe	23	13	6.5	tr.	tr.	26.5	31
Selebi	23.5	13.5	3	tr.	tr.	41	19
Selebi North southern limb	21	14.5	5	3	tr.	35.5	21
Selebi North northern limb	3	15.5	12	4.5	1.5	53.5	10

Table 7.4 The original components (wt%) of the Selebi-Phikwe host rocks: Results of mixing model calculations: (a) on a sulphide-free basis, and (b) including sulphides.
The mixing model consists of cumulus plagioclase, olivine, orthopyroxene, clinopyroxene and chromite mixed with basalt (SPHB). The basalt composition is SiO_2 50.9, TiO_2 0.9, Al_2O_3 14.7, Fe_2O_3 11.6, MgO 7.1, CaO 11.0, K_2O 0.2 & Cr_2O_3 0.05. The host rocks are the averages in Tables 7.1 and 7.2, corrected for Fe-enrichment and K-metasomatism. The host amphibolites have been adjusted for Fe-enrichment by decreasing their Fe/Mg ratios to be equivalent to that of the ultramafics which are assumed to have the lowest Fe-enrichment. The sulphide contents are those in Table 6.1, converted to wt%.

independently (and prior to) the modelling of the evolution of the protoliths of the high-Ca hornblende gneiss suite.

The results of the modelling are also shown with the average Fe-Ni-Cu sulphide contents (Table 6.1) of the ore bodies included (Table 7.4b). The calculation includes the estimations that the ultramafic-bearing host rocks on the northern limb of Selebi North account for

about a third of the total Selebi North host rocks and that the content of sulphides in these weakly mineralised ultramafic-bearing host rocks is approximately half that in the host amphibolites (A) in the core of the antiform and on the southern limb (Ch. 6.1.3).

Amphibolites (garbenschiefer amphibolites) with similar geochemistry (15-20% Al2O3 and 8-19% MgO, depleted in Ti, Zr and P) to the Selebi-Phikwe host amphibolites are found in the Archaean Isua succession of West Greenland. These have been interpreted by Gill et al. (1981) as being metamorphosed basalts, the composition of which is due to the accumulation of olivine in an unusually aluminous basalt (18% Al2O3) with a moderate CaO content. It is suggested here that the geochemistry of the Isua garbenschiefer amphibolites can be more simply interpreted as being due to the accumulation of both olivine and plagioclase in a more typical Archaean tholeiitic basalt liquid. The moderately low Ca contents (CaO/Al2O3 ratios vary from 0.33 to 0.75 in rocks with the same Mg/Fe.) are possibly due to the removal of Ca during alteration.

7.4.4 Igneous Differentiation Within the Selebi-Phikwe Bodies

It is impossible to definitely conclude whether the Phikwe, Selebi North and Selebi bodies were originally connected or were separate intrusions (Ch. 5.1.4). The high strain suffered by the Selebi-Phikwe gneisses means that the original shape of the bodies is difficult to determine. The present form of the Selebi-Phikwe host rocks as discrete layers within unrelated grey gneisses suggests that the bodies were originally sills (or part of one sill), intruded into grey gneiss protoliths. It is feasible however that the bodies were originally stock-like bodies that have been completely flattened. The facts that (a) the three ore bodies are aligned in a NE-SW direction parallel to D1 lineations, and (b) the Phikwe ore body extends down in a SW direction but dies out to the southeast, indicate that either the three ore bodies were originally connected in a single body, the longest dimension of which was orientated in a NE-SW direction or that the the three ore bodies were separate intrusions which were stretched in a NE-SW direction during D1. The latter case is preferred and the Selebi, Selebi North and Phikwe host rocks are considered to have been separate sill-like intrusions of tholeiitic crystal mush. The fact that the host rocks of each ore body can be modelled in terms of different compositons of crystal mush supports this.

In the analysed Phikwe sections (Figs 7.1-7.4), the Ti, Zr (and Cr) contents are typically highest at the top and bottom margins of the host amphibolite. The Mg and Al contents are commonly lower at the margins than in the middle of the host amphibolite. The Phikwe marginal amphibolites plot near the SPHB apex in Figure 7.9. It is thought that the high Ti-Zr contents at the margins could be due to: (a) shearing; (b) Ti-Zr metasomatism during regional metamorphism; (c) contamination from surrounding grey gneisses; or (d) an original feature. Although the host rock body is typically sheared at its margins (hence higher Ti-Zr contents would be expected), some of the high Ti-Zr marginal amphibolites are not obviously sheared. Also the Ti-Zr variations in PW 93 (Fig. 7.2) are gradational over the whole section and independent of the degree of shearing. Therefore localised shearing is not thought to be the main cause of the high Ti-Zr contents at the margins. The same reasoning rules out redistribution of Ti and Zr within the host rock body during regional metamorphism. Marginal amphibolites commonly have higher Ti and Cr but lower Zr contents than the immediately surrounding grey gneiss (Fig. 7.4). The local gradual increase of Ti and Cr out toward the margin of the host amphibolite, with significantly lower values in the surrounding grey gneiss, is inconsistent with contamination of host amphibolite with grey gneiss during intrusion or tectono-metamorphism. The higher Ti, Zr and Cr at the margins are considered to be an original magmatic feature of the host rock body.

The average intercumulus liquid (SPHB) content of the PW 93 section (Fig. 7.2) is estimated as having been about 29 wt%. The average TiO2 (0.41 wt%) and Zr (32 ppm) contents of the marginal amphibolites indicate that they consisted of about 46 wt% SPHB. Ti-Zr contents in the Mg-Al-rich middle portion of the host amphibolite in PW 93 indicate a SPHB content of 10-16 wt%. (The high Cr in the marginal amphibolites is more difficult to explain. It can not be simply accounted for by Cr in intercumulus liquid and the estimate of very low contents of cumulus chromite in the Phikwe crystal mush.) It is proposed that the margins of the host rock body in PW 93 contained less cumulus crystals and more SPHB liquid than the middle. This is consistent with the mechanism of flow differentiation during vertical and later horizontal emplacement of the crystal mush (Bhattacharji & Smith 1964; Bhattacharji 1967; Gibb 1972; Simkin 1967). Phenocrysts are concentrated away from the margins of a flowing body during flow differentiation. Some gravitational crystal settling would be expected to have

occurred at the cessation of flow. However the relatively low contents of intercumulus liquid in the crystal mush and and the rapid cooling and hence viscosity increase of the margins of the sill after emplacement would have limited the degree of crystal settling (Gibb 1972). The small ultramafic lenses which occur in the middle of the thickest Phikwe sections are thought to also have been formed by flow differentiation. The other analysed sections from Phikwe (Figs 7.3 and 7.4) are more homogeneous than that from PW 93. The variation in their Ti and Zr contents indicates flow differentiation, but to lesser extents than that inferred from Figure 7.2. The thickest host amphibolite at Phikwe is in Zone C. Host rocks in Zone C appear to have been the most flow differentiated. The thick amphibolite of Zone C is therefore proposed to be a predeformational feature.

Ti and Zr contents are higher in marginal amphibolites at Selebi (e.g. Selebi Upper B Body, Fig. 7.5a). All three analysed sections from Selebi also show a variation from an Al-rich base to a Mg-Cr-rich top which is consistent with the mineralogical variation (Ch. 5.2.2b, Fig.5.4c). However the middle portions of the sections show fairly uniform Mg/Al ratios. The geochemical variation shown by the Selebi Upper B Body (Fig. 7.5a) is more complex than the other two sections. The location of grey gneiss and anorthosite bands within this section are possibly due to tectonic stacking within the body or may be an original intrusive feature. The Al-Mg variation at Selebi suggests gravitational settling of olivine (& opx.) and chromite and indicates that all three analysed sections are overturned. The geochemical effects of this limited gravitational settling are most marked at the (original) intercumulus liquid-rich base and top of previously flow differentiated sections. In the middle portion of the sections there was less settling of olivine (& opx.) relative to plagioclase. The high Al contents at the original top of the sections reflect that plagioclase will float in static or mildly convecting basaltic magma (Bottinga & Weill 1970; Campbell et al. 1978; McBirney & Noyes 1979). The anorthositic bands within the Selebi host amphibolite are possibly the result of flow differentiation. It is proposed that the geochemical variation shown by the Selebi sections is best explained by flow differentiation that took place during the emplacement of the Selebi crystal mush, followed by variable but limited degrees of gravitational settling of olivine (& opx.) and chromite relative to plagioclase. A higher degree of gravitational crystal settling in the Selebi host rocks compared to those at Phikwe was the result of the higher content of intercumulus liquid

in the crystal mush at Selebi (Table 7.4).

The geometry of the Selebi ore body indicates that D1 shearing has played an important role. The "way-up" derived from the geochemical profiles in the Upper B and Lower bodies suggests that the early D1 structure was of a major D1 synform with a minor synform on the upper limb. It is proposed that D1 shearing attenuated and partly removed the lower limb of the intervening minor antiform.

The mineralogical variation from a mafic margin to a feldspathic margin (Ch. 5.2.3a, Fig.5.6b) in the amphibolites of the Selebi North antiform core and southern limb is similar to that at Selebi and is thought also to have been due to a combination of flow differentiation and later gravitational settling. The occurrence of ultramafic rocks (orthopyroxene-olivine cumulates, Table 7.4) at one margin of the host body (SDN 56, Fig. 7.7) on the northern limb at Selebi North suggests gravitational settling. However the apparent "way-up" is the opposite direction to that deduced above. As noted in Chapter 5.2.3d, this ultramafic-rich section is unrepresentative. Ultramafic rocks typically occur in the middle of the amphibolite body on the north limb. The formation of the orthopyroxene-olivine cumulates within the SPHB-rich protoliths of the AU amphibolites of the Selebi North north limb is proposed to have been due to flow differentiation and concentration of cumulus orthopyroxene plus olivine in a crystal mush with a high content of intercumulus liquid (60 wt%) and only 3 wt% cumulus plagioclase (Table 7.4a). The occurrence of ultramafic rocks at the margin of the body in SDN 56 is possibly due to a localised intrusive feature during flow of the crystal mush or due to deformation.

The conclusion that the ultramafic rocks are an integral part of the host amphibolites and that they formed by flow differentiation is contrary to the conclusion of Wakefield (1974, 1976) that they represent a composite magma of olivine crystal mush and immiscible sulphide magma that was intruded into host amphibolite protoliths. It is proposed that the difference in the host rocks in the antiform core-southern limb and on the northern limb at Selebi North resulted from separate intrusions of significantly different crystal mush. Surface mapping does suggest that the north limb and antiformal core are not connected (Fig. 5.6a), although this could be a tectonic rather than original feature. The difference in geochemistry between the two limbs at Selebi North and the proposal that they represent separate intrusions of crystal mush of significantly different compositons support the proposal that all three ore bodies at Selebi-Phikwe

represent separate intrusions of crystal mush.

7.4.5 The Formation of Massive and Disseminated Sulphides at the Magmatic Stage

In Chapter 6.4 it was proposed that the Selebi-Phikwe sulphides had retained aspects of their original form and Ni-Cu contents. Prior to deformation and metamorphism the Selebi-Phikwe ore bodies consisted of Ni-rich massive sulphides (with a Cu/(Cu+Ni) ratio of c.0.35) and Cu-rich disseminated sulphides (with a ratio of c. 0.65). The association of Fe-Ni-Cu sulphides with tholeitic crystal mushes suggests a "magmatic immiscible sulphide" origin for the sulphides. However Gallon (1986) has suggested that the ore bodies resulted from replacement of sedimentary host rock by sulphide. The high sulphide contents of the ore bodies (Table 6.1) and their virtual restriction to the host rocks indicate that an origin by replacement is highly unlikely, although localised relacement of metamorphic silicate by sulphide has taken place.

The Cu/(Cu+Ni) ratios and the Ni-Cu contents of the massive and disseminated sulphides (Table 6.3) are generally consistent with the theoretical modelling (Duke & Naldrett 1978; Rajamani & Naldrett 1978; Duke 1979) of immiscible sulphides separating progressively from a basalt magma with between 10 and 5 wt% MgO, that is simultaneously crystallising olivine (Fig. 7.15). This is further evidence of a magmatic rather than replacement origin. However the relatively low Ni and Cu contents of the Selebi-Phikwe sulphides (Table 6.3) compared to the major types of Ni-Cu sulphide ore bodies (Fig. 1.4) suggest either relatively low Ni and Cu contents of the magma or relatively low magma/immiscible sulphide ratios (R = c. 63, see Campbell & Naldrett 1979). One method of producing low magma/sulphide ratios is by the assimilation of country rock sulphur. The possibility that calc-silicate gneiss had an evaporitic origin has been mentioned in Chapter 4.4.2. However calc-silicate gneiss forms only a very minor component of the Selebi-Phikwe sequence and is not related to the ore bodies. There are essentially no sulphur-rich country rocks in the Selebi-Phikwe gneisses and there is no evidence that the Selebi-Phikwe ore bodies obtained their sulphur by assimilation of country rock sulphur. It is suggested that saturation of sulphur must have been achieved by magmatic processes. The achievement of magmatic sulphur saturation is discussed in Chapter 8.6.9 along with the formation of the Dikoloti-Lentswe sulphides.

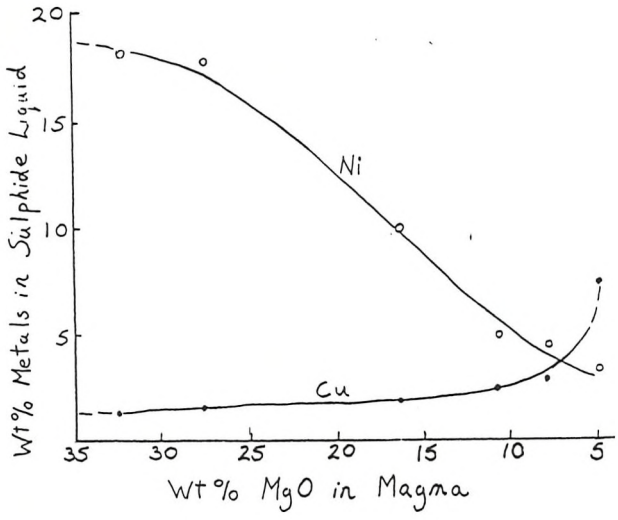

Fig. 7.15a The Ni and Cu contents of typical mafic and ultramafic magmas plotted as a function of their MgO content (from Rajamani & Naldrett 1978).

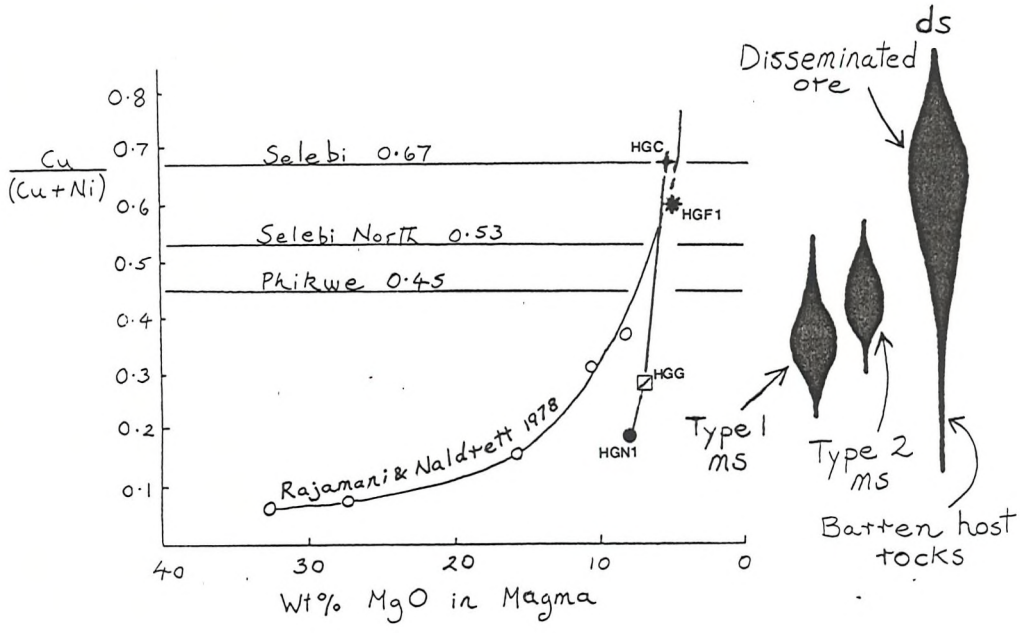

Fig. 7.15b The Cu(Cu+Ni) ratios of the Selebi-Phikwe ore bodies and their main ore types superimposed on the calculated relationship between the Cu(Cu+Ni) ratios of sulphide liquids and the MgO content of magma (from Rajamani & Naldrett 1978).

Fig. 7.15 The "Magmatic" Cu(Cu+Ni) ratio of the Selebi-Phikwe ore bodies.

The sulphide contents of the ore bodies are high (10-25 wt%, Tables 6.1 & 7.4b). Their sulphur contents are much higher than the maximum sulphur content (0.16%) of basalt magma immediately prior to eruption (Moore & Fabbi 1971; Anderson 1974; Czamanske & Moore 1977) or the saturation levels (0.3% S) in basic-ultrabasic determined by Shima & Naldrett (1975). Therefore the sulphides could not have separated out as immiscible sulphides from intercumulus basaltic liquid after the emplacement of the crystal mushes into the Selebi-Phikwe sequence. The crystal mushes must have been emplaced with the great majority of their sulphides already as immiscible sulphide liquid. It is proposed that the immiscible sulphides separated out from a significantly larger body of magma than that represented by the host rocks.

The difference in the Cu/(Cu+Ni) ratios between Type 1 massive sulphide and disseminated sulphide at Selebi-Phikwe could be due to either (a) tectono-metamorphic processes, (b) fractional crystallisation of magmatic immiscible sulphide liquid, or (c) successive separations of magmatic immiscible sulphide liquid. The disseminated sulphides are thought to be the relatively unmobilised metamorphic equivalents of original magmatic disseminated sulphide (see Ch. 6.4). However more work needs to be done on the complex metamorphic sulphide -silicate reactions that may have taken place and the possible physico-chemical affinity of Cu or chalcopyrite for metamorphic silicates rather than metamorphic MSS. It is thought that the difference in Cu/(Cu+Ni) ratios is mainly an original magmatic feature.

Data on the Cu-Fe-Ni-S system (Craig & Kullerud 1969) indicate the co-existence of Cu-enriched liquid with quaternary MSS at temperatures above 850^{o}C. Fractional crystallisation of an accumulated immiscible sulphide liquid is thought to have taken place in some magmatic Ni-Cu sulphide ore bodies (Naldrett 1981). A fractionated Cu-enriched liquid may separate from crystallising MSS (e.g. by filter pressing) to form disseminated sulphide and veins with higher Cu/(Cu+Ni) ratios than massive sulphides formed from the MSS. However the estimated Fe, S, Ni and Cu contents of the Selebi-Phikwe disseminated sulphides and Type 1 massive sulphides (Table 6.3) are such that the the great majority of the Cu would have been incorporated initially in crystallising quaternary MSS (Fig. 6.5e). This excludes the separation of significant Cu-enriched liquid during fractional crystallisation. The disseminated Cu-rich nature of the Selebi ore

body is further evidence against separation of Cu-rich liquid during fractional crystallisation after intrusion of the crystal mush.

In the modelling of a closed tholeiitic system crystallising olivine without magma replenishment (Duke & Naldrett 1978; Rajamani & Naldrett 1978; Duke 1979; Fig. 8.8), early formed immiscible sulphides have lower Cu/(Cu+Ni) ratios than sulphides that separate later. The change in the Cu/(Cu+Ni) ratio from Ni-rich Type 1 massive sulphides to Cu-rich disseminated sulphides is therefore interpreted as indicating that the Ni-rich Type 1 massive sulphides are the eventual products of immiscible sulphides that generally separated out from basalt magma before the Cu-rich disseminated sulphides. It is proposed that Ni-rich immiscible sulphides had already separated and accumulated in a magma chamber prior to their intrusive emplacement along with a crystal mush containing abundant disseminated Cu-rich immiscible sulphides. The previously accumulated Ni-rich immiscible sulphides would have remained segregated from the components of the crystal mush during vertical emplacement, because of viscosity contrasts between the sulphide liquid and the intercumulus liquid-rich margin and the crystal-rich core of the crystal mush. The low viscosity sulphide liquid would have been concentrated towards the margins of the flowing crystal mush (cf. Ross & Hopkins 1975; Groves & Hudson 1981). After intrusion a limited degree of gravitational settling would have resulted in further accumulation of dense immiscible sulphide at the base of the body.

The disseminated Cu-rich immiscible sulphides would not have significantly segregated from their crystal mush during intrusion. After emplacement disseminated Cu-rich immiscible sulphides would possibly have undergone some gravitational settling relative to intercumulus liquid and cumulus crystals. At Selebi and Selebi North the concentration of disseminated sulphides towards the mafic margin of mineralogically graded host amphibolite (Figs 5.4c & 5.6b, Ch. 6.1.2) is possibly due to gravitational settling of disseminated immiscible sulphide liquid. If the conclusion of Wakefield (1974) that the Phikwe ore body is overturned is correct, the distribution of disseminated sulphides in PW 80 (Fig. 6.3), PW 93 (Fig. 7.2) and PW 185 (Fig. 7.4) may possibly indicate limited post-emplacement gravitational settling of disseminated immiscible sulphide liquid. However it has been proposed in Chapter 4.2.1c that Units E and F of the Selebi-Phikwe sequence are the right way-up. The distribution of the dissminated sulphides in these sections is possibly partly

controlled by shearing within the host amphibolite.

It is proposed that flow differentiation of previously separated immiscible sulphide liquid followed by variable degrees of gravitational settling can account for the typical occurrence of massive sulphides either at both top and bottom margins of the host bodies or at one margin that is thought to have been the base of the body (e.g. at Selebi, Fig. 5.4c). The distribution of Type 1 massive sulphides and disseminated sulphides within the Selebi-Phikwe host rocks is consistent with the suggestions that immiscible sulphides separated from a large body of basaltic magma prior to mush emplacement, that Type 1 massive sulphides represent the earliest immiscible sulphides to separate from this large body of magma and that disseminated sulphides separated later.

The crystallisation history of the magmatic sulphides would have been similar to that of the cooling metamorphic MSS, but without the effects of diffusion and mobilisation caused by the deformation (Ch. 6.4). Quaternary MSS would have crystallised until the magnetite-MSS cotectic was intersected, when both quaternary MSS and magnetite would have crystallised. The original massive and disseminated sulphides have retained their respective Ni-rich and Cu-rich nature, although the host rocks and sulphides have been highly deformed and metamorphosed. Strain was concentrated in the low strength original irregular marginal massive sulphide accumulations which moved independently of host rock with disseminated sulphides. Wakefield (1974,1976) has suggested that the occurrence of significant massive sulphide in grey gneiss without host amphibolite at Phikwe (Zone E) was due to the intrusion of a sulphide magma beyond the limits of the host intrusion. Low viscosity immiscible sulphides may have been concentrated at the intrusive front of the crystal mush. However the gross form, mineralogy and textures of the Type 2 massive sulphide in Zones D and E indicate an origin by repeated mobilisation of original magmatic massive and disseminated sulphide. It is possible that Zone D was the original limit of the Phikwe intrusion.

It can be speculated that, if the three host bodies represent a single highly deformed intrusion, the amount and type of sulphide is an indication of proximity to the sill feeder. Phikwe with its high content of low viscosity massive sulphide was possibly further from the feeder than Selebi. The higher content of intercumulus liquid at Selebi however suggests the opposite relationship.

7.4.6 Evolution of Parent Magma

The proposed compositon of the intercumulus liquid (SPHB) of the Selebi-Phikwe crystal mushes is that of moderately evolved HGN1. In Chapter 4.2.5 it was suggested that HGC (the clinopyroxene-bearing hornblende gneiss) was possibly the derivative liquid resulting from the equivalent of about 66% closed system crystallisation of HGN1 (5% olivine, 39% plagioclase and 31% clinopyroxene). Average HGN1 has a Cu/(Cu+Ni) ratio of 0.19 and a sulphur content of 247 ppm (Table 4.1, Figs 4.8 & 8.8). Average HGC has a Cu/(Cu+Ni) ratio of 0.67 and a sulphur content of 912 ppm. The early crystallisation of HGN1 was dominated by olivine and plagioclase which are the main cumulus components of the crystal mushes.

It is proposed that the nature of the Selebi-Phikwe host rocks and the Cu/(Cu+Ni) ratios of the sulphides are consistent with an origin from evolved HGN1 tholeiitic parent magma, the early fractionation of which was controlled by olivine (& opx. ?), plagioclase and minor clinopyroxene. Immiscible sulphides separated from sulphur-saturated evolving HGN1 magma and were accumulated by gravity in the magma chamber. Early immiscible sulphides were Ni-rich. As the magma evolved toward an HGC composition, the immiscible sulphides separating out gradually became Cu-rich. Mushes (Table 7.4b) consisting of plagioclase and olivine (& opx.) crystals, SPHB intercumulus liquid (moderately evolved HGN1), disseminated Cu-rich sulphides and semi-massive accumulated Ni-rich sulphides were expelled from the magma chamber and emplaced into the Selebi-Phikwe sequence. The nature and evolution of the parental HGN1 magma, particularly a mechanism for the achievement of S saturation, are further discussed in Chapter 8.6.9 along with the origin of the sulphides of the Dikoloti-Lentswe prospects.

7.5 SUMMARY OF CONCLUSIONS

The Phikwe, Selebi North and Selebi host amphibolites have similar geochemistries characterised by high normative plagioclase and olivine contents. Shearing has caused significant localised changes in host rock geochemistry. Garnet amphibolites obtained their excess Fe and Mn from sulphides during metamorphic desulphurisation reactions. The fact that the geochemistry can be interpreted in terms of original components and processes suggests that the essentially magmatic geochemistry of the majority of host rocks has not been

seriously distorted by alteration.

The major and trace element geochemistry of the host rocks indicates that they are metamorphosed tholeiitic gabbroic and ultramafic cumulates. The two-element variation diagrams and the modelling indicate that the geochemistry of the Selebi-Phikwe host amphibolites and ultramafic rocks can be interpreted in terms of various mixtures of intercumulus basalt (moderately evolved HGN1) plus cumulus plagioclase, olivine, orthopyroxene, clinopyroxene and chromite and immiscible sulphides, i.e. tholeiitic crystal mushes. The most compelling feature in favour of this hypothesis is that, when combined with the effects of alteration, it can explain all the geochemical variations shown by the Selebi-Phikwe host rocks. The geochemistry of the Selebi-Phikwe host amphibolites (e.g. their high but variable contents of Al, Mg and Cr) is such that the suggestion by Gallon (1986) that they are metamorphosed sediments is completely untenable.

It is proposed that the three ore bodies were originally separate intrusions of crystal mush (at least 4 intrusions). The geochemical variation in profiles through the host bodies is due to a combination of flow differentiation during the intrusion of crystal-rich magma and later gravitational differentiation. The ultramafic host rocks are an integral part of the host amphibolites. They formed by flow differentiation. The Selebi-Phikwe host bodies are considered to be tholeiitic differentiated sills or stocks.

The Selebi-Phikwe sulphides are tectono-metamorphically modified magmatic immiscible sulphides that separated from tholeiitic magma prior to intrusive emplacement within crystal mushes. Ni-rich Type 1 massive sulphides represent the earliest immiscible sulphides to have separated from the parent magma. Cu-rich disseminated sulphides separated later. The distribution of massive and disseminated sulphides is consistent with flow differentiation during emplacement of a crystal-rich mush followed by gravitational settling. The original components of the host bodies, the geochemistry of the tholeiitic intercumulus liquid and the Ni-Cu contents of the sulphides are consistent with the formation of the host rocks and immiscible sulphides from fractionating and evolving tholeiitic HGN1 basalt magma.

CHAPTER 8 THE DIKOLOTI-LENTSWE PROSPECTS

The Dikoloti and Lentswe prospects are located 15 and 22 km respectively southwest of the Phikwe ore body (Figs 1.1 & 8.1).

The ore reserves are shown in Table 8.1.

	Million tonnes	Grade		Cu/(Cu+Ni)
		%Ni	%Cu	
Dikoloti	c. 2.5	0.7	0.5	0.42
Lentswe	c. 1.5	0.5	0.4	0.44

Table 8.1 Dikoloti-Lentswe Ore Reserves

8.1. Gross Form and Structure

The Dikoloti-Lentswe prospects consist of mineralised ultramafic rocks (up to 45 m thick) within a thin unit of hornblende gneiss and minor grey gneiss. The whole unit is enclosed by porphyroblastic granitic gneiss. The mineralised ultramafic rocks consist of amphibole pyroxenites, serpentinised peridotites and minor ultramafic amphibolite and schist.

Hornblende gneiss occurs both in the envelope to the ultramafic rocks and as thin highly sheared bands within and at the margins ofthe ultramafic rocks. Minor magnetite quartzite interbanded with cummingtonite and actinolite ampbolites (Mg-amphibolites) occurs in the unit at Lentswe. Only very thin quartzite occurs at Dikoloti. However elsewhere along strike (e.g. at Phokoje and Mogolodi) the magnetite quartzite and cummingtonite-actinolite amphibolite association is thicker (up to 15 m) and is the most important component of the unit (see Plates 6 & 7). The Dikoloti-Lentswe unit can be traced regionally (Fig. 8.1) by the occurrence of the Mg-amphibolite-magnetite quartzite association along with minor weakly mineralised to unmineralised serpentinite and pyroxenite. It is tentatively suggested from mapping and photogeological interpretation that the Dikoloti-Lentswe unit is the approximate equivalent of Unit A at Phikwe. Alternative interpretations (given the complex structure) is that the Dikoloti-Lentswe unit is the approximate equivalent of

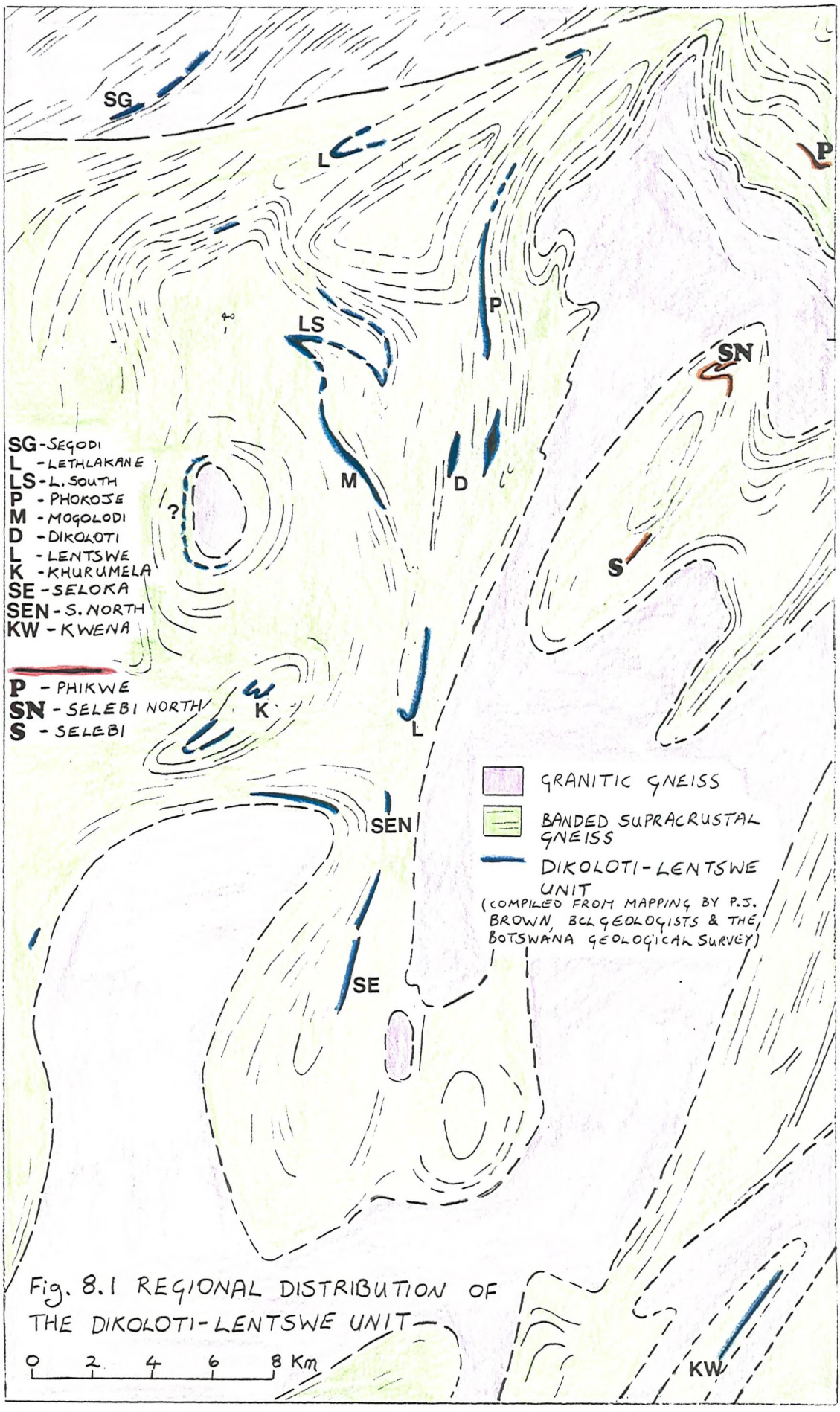

Fig. 8.1 REGIONAL DISTRIBUTION OF THE DIKOLOTI-LENTSWE UNIT

Unit H or that it lies outside the range of the Phikwe sequence (Fig. 2.3). The first alternative is supported by the occurrence of minor marble and magnetite quartzite in Unit H.

At Dikoloti mineralised ultramafic rocks occur in a recumbent antiform plunging to both the north and south (Figs 8.2-8.4). It is uncertain whether this is a D1 structure that has been refolded during D2 or a D2 antiform. Feldspathic amphibolite occurs in the core of the antiform. Anorthositic gneiss occurs about 200 m to the west of Dikoloti. The mineralised amphibole pyroxenites and serpentinised peridotites are interbanded and contacts between them are typically gradational. Pyroxenite slightly predominates over peridotite. Ultramafic schist occurs within the ultramafic rocks and particualrly at their margins (Fig. 8.9). Disseminated sulphides and thin (<1m) irregular massive sulphides occur throughout the ultramafic rocks. Massive sulphide tends to occur near the outer margin of the ultramafic rocks and is commonly associated with ultramafic schists. Minor massive sulphide occurs in the hornblende gneiss-grey gneiss envelope, particularly in the nose of the antiform (Fig. 8.4). Thin quartzite locally occurs in the hornblende gneiss envelope adjacent to the ultramafic rocks. The Mg-amphibolite-magnetite quartzite association was not found at Dikoloti. It is represented by a magnetite-rich facies of grey and intermediate biotite gneiss.

At Lentswe mineralised ultramafic rocks occur in a D2 antiform (?) plunging to the north (Fig. 8.5). The mineralised ultramafic rocks are separated from anorthositic gneiss in the core of the synform by about 8 m of porphyroblastic granitic gneiss with relict bands of hornblende gneiss and grey gneiss. The ultramafic rocks, predominantly interbanded amphibole pyroxenite with serpentinised peridotite (Fig.8.10), are identical to those at Dikoloti. The Dikoloti feldspathic amphibolite does not occur at Lentswe. Hornblende gneiss dominates in the enveloping gneiss immediately above the ultramafic rocks and also occurs as thin sheared bands within the ultramafic rocks (Fig. 8.10). Minor magnetite quartzite and associated Mg-amphibolite occur at both the upper and lower margins of the ultramafic rocks (Fig. 8.6). In a typical section (LT 30, Fig. 8.6), finely laminated magnetite quartzite occurs at the top of the ultramafic rocks (see also LT 31, Fig. 3.2) and thin quartzite with Mg-amphibolite laminae occurs at the base. Disseminated sulphides and irregular massive sulphides occur throughout the ultramafic rocks particularly near their margins. LT 13 (Fig. 8.6) is an atypical

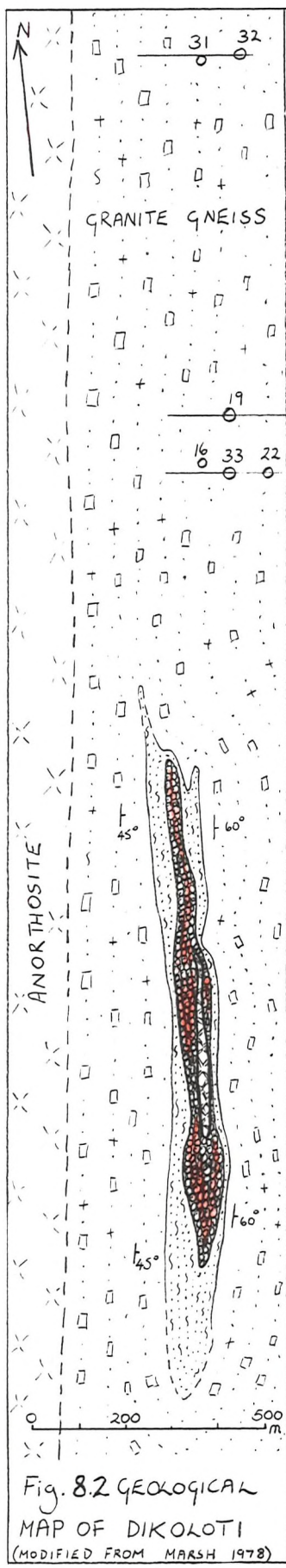

Fig. 8.2 GEOLOGICAL MAP OF DIKOLOTI (MODIFIED FROM MARSH 1978)

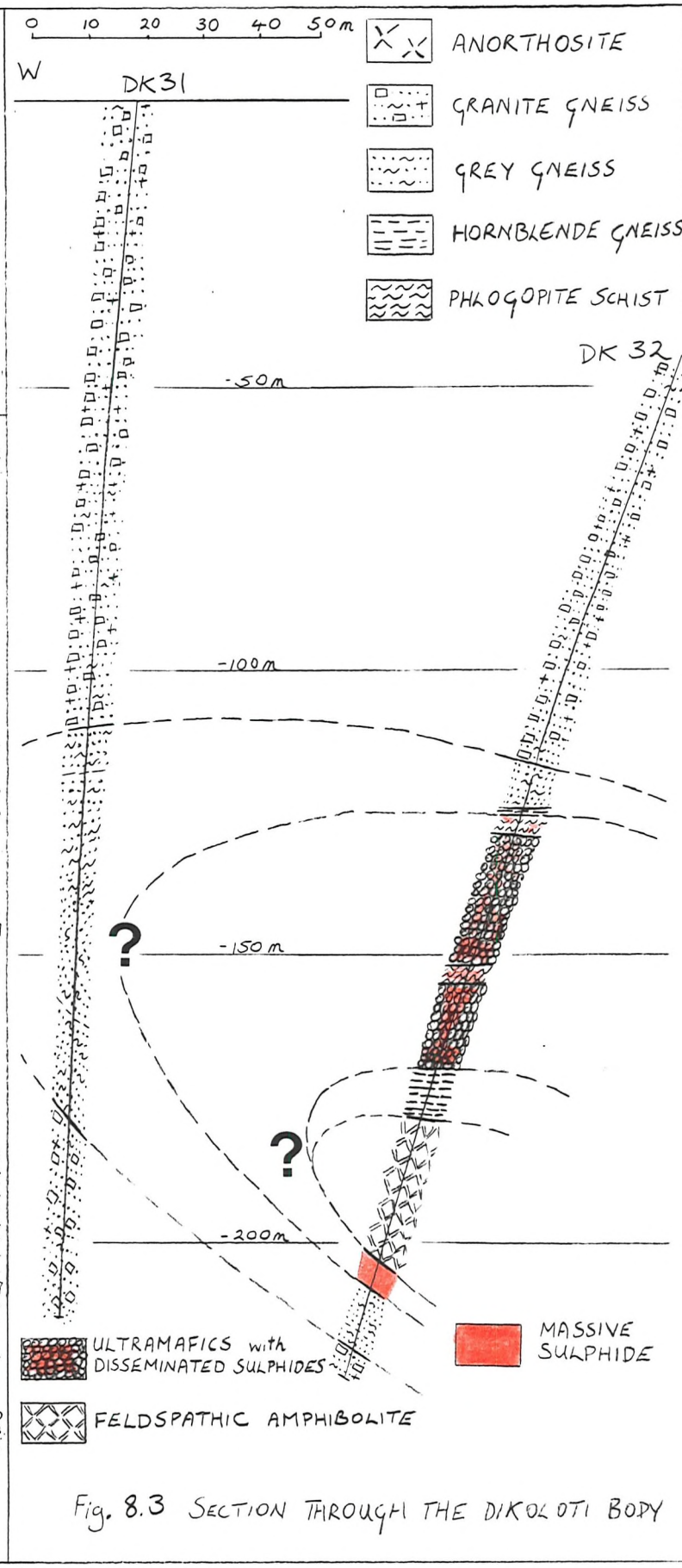

Fig. 8.3 SECTION THROUGH THE DIKOLOTI BODY

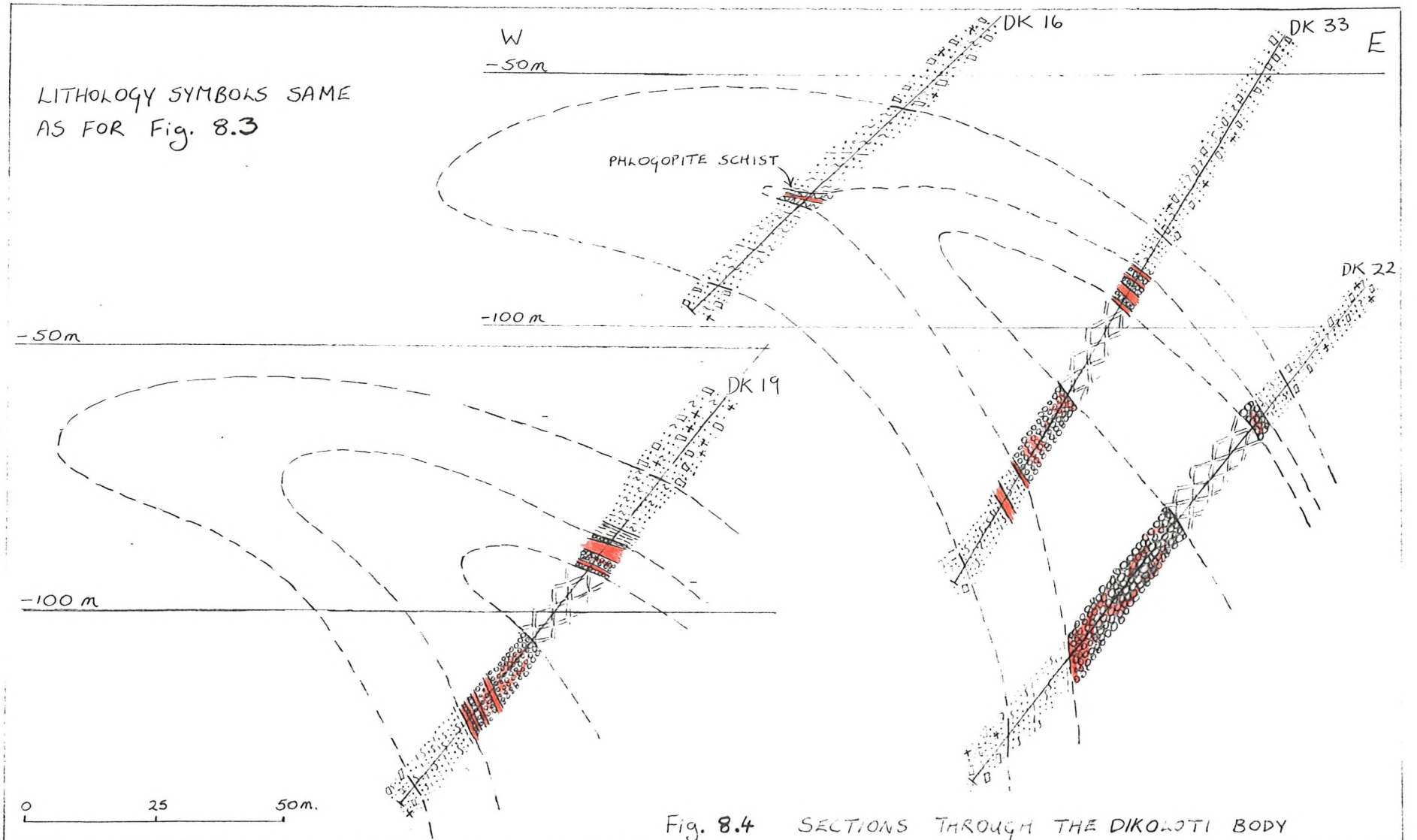

Fig. 8.4 SECTIONS THROUGH THE DIKOLOTI BODY

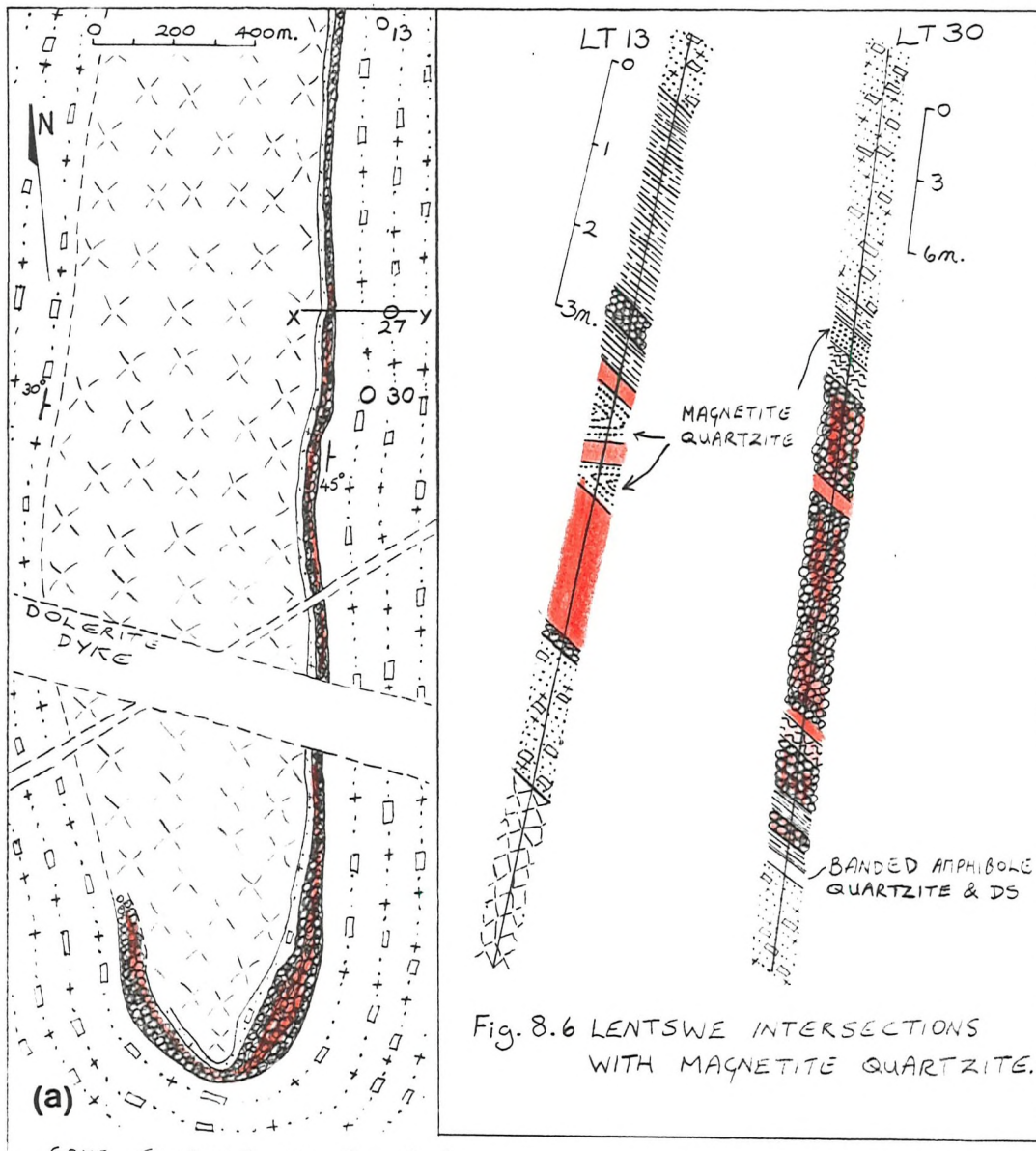

Fig. 8.6 LENTSWE INTERSECTIONS WITH MAGNETITE QUARTZITE.

SAME SYMBOLS AS Fig. 8.3.

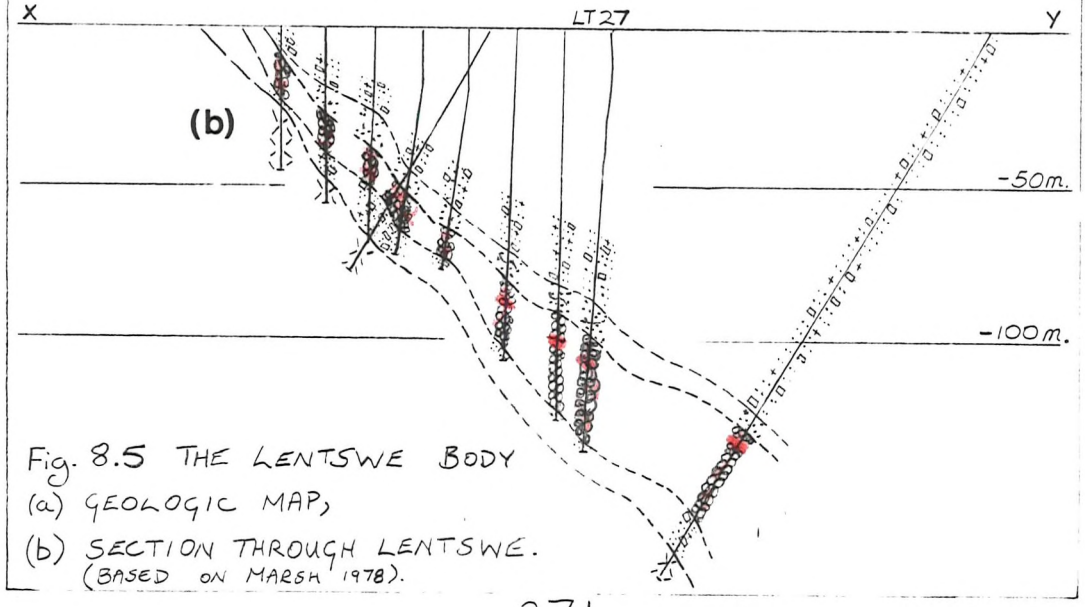

Fig. 8.5 THE LENTSWE BODY
(a) GEOLOGIC MAP,
(b) SECTION THROUGH LENTSWE. (BASED ON MARSH 1978).

section, in which relatively thick massive sulphide is associated with magnetite quartzite but only minor ultramafic rock.

Thinner weakly mineralised ultramafic rocks occur at Phokoje and Mogolodi (Fig. 8.1). They contain a greater proportion of the Mg-amphibolite-magnetite quartzite association (10 m thick), particularly thick cummingtonite amphibolite with lesser finely banded actinolite amphibolite-magnetite quartzite. Minor metagabbroic rocks similar to the Dikoloti feldspathic amphibolite also occur at Phokoje.

8.2 MINERALOGY OF DIKOLOTI-LENTSWE ROCKS

8.2.1 Ultramafic Rocks

The mineralised ultramafic rocks at Dikoloti-Lentswe are similar to those at Phikwe and Selebi North. They consist essentially of serpentinised peridotite and amphibole pyroxenite. There appears to be a complete range of lithologies from serpentinised dunite through olivine-orthopyroxene-calcic amphibole peridotite (harzburgite) and hornblende pyroxenite to cummingtonite-hornblende amphibolite. The olivine-rich rocks consist of fine-grained (0.1-0.5 mm) granoblastic olivine and orthopyroxene with minor idioblastic calcic amphibole (hornblende), green spinel, magnetite and disseminated sulphide (Plate 39a). Minor clinopyroxene was tentatively identified in one sample of olivine-orthopyroxene peridotite. In more orthopyroxene-rich rocks, orthopyroxene is porpyroblastic in a granular olivine-orthopyroxene matrix and includes olivine (Plate 38a). Amphibole pyroxenites consist of coarse porphyroblastic orthopyroxene (typically with abundant hornblende inclusions) in a matrix of hornblende with magnetite and disseminated sulphide (sulphide in both porphyroblasts and matrix) (Plate 38d). The peridotites are typically altered to serpentine-rich assemblages. Fine-grained aggregates (of talc and chlorite ?) after orthopyroxene occur in a matrix of serpentine with chlorite, magnetite and disseminated sulphide (Plate 38e). Pyroxene-rich rocks appear to have been more resistant to alteration.

The amphibolite pyroxenite grades into ultramafic amphibolite with variable proportions of cummingtonite, calcic amphibole (hornblende), biotite-phlogopite, relict orthopyroxene and fine undetermined aggregates (talc, serpentine and chlorite ?) (Plate 38g). With increased mica content these amphibolites become schistose and have been termed ultramafic schists (Plate 38h). The Dikoloti-Lentswe cummingtonite-bearing amphibolites are more common than at Phikwe and

Selebi North. Some sheared amphibole pyroxenite consists of corroded relicts of porphyroblastic orthopyroxene (typically altered to biotite) in an aligned matrix of orthoamphibole (gedrite ?), cummingtonite, biotite and hornblende (Plate 38f).

Analyses of olivine and orthopyroxene in a typical serpentinised peridotite from Dikoloti show that they are chrysolite (Fo 86) and bronzite (En 86) respectively, with very little variation in composition (Table 8.2 & p.A.8). The olivine has a relatively low Ni content (average of 0.07 wt% NiO) compared to those of the upper mantle, high level layered intrusions and basalts (Fleet et al. 1977). One olivine contained 0.05 wt% NiO in the core and 0.25 wt% NiO at the margin (p.A.8). A rare zoned calcic amphibole had a core of edenite and a rim of cummingtonite. Analyses of orthopyroxene in a typical amphibole pyroxenite (Dikoloti) and a spinel pyroxenite (Lentswe) show that it is bronzite (En 84 and En 82 respectively). The calcic amphibole in the amphibole pyroxenite is magnesio-hornblende with 0.4 wt% Cr_2O_3 and an Mg/Mg+Fe ratio of 0.80 (Table 8.2; Fig. 3.1). There is no compositional difference between matrix and included hornblende.

A wide variety of spinel occurs in the Dikoloti-Lentswe ultramafic rocks. Chromite (18-20 wt% Cr_2O_3, Table 8.2, Fig. 8.7) occurs as inclusions in olivine, orthopyroxene and calcic amphibole. Chromian spinel locally forms a fabric in the amphibole pyroxenite (Plate 38b & c). This is interpreted as an early D1-M1a fabric. Green spinel is more common in amphibole pyroxenite than peridotite. It varies from coarse-grained intergranular bright green spinel (Plate 39b & c) to fine-grained dark green inclusions in amphibole and orthopyroxene (Plate 39d). The bright green spinel commonly has coarse-grained magnetite inclusions (0.3-1mm). The green spinel varies in colour. Adjacent to the magnetite inclusions and locally at its margins (particularly if in contact with pyrrhotite) it is bright clear green. Elsewhere it is darker and grades locally to almost opaque. This darkening is due to very fine-grained (<1 micron) inclusions that are thought to be magnetite. Analyses of a bright green spinel in a pyroxenite from Lentswe show that it is a chromian pleonaste with 4.7 wt% Cr_2O_3 (Table 8.2, Fig. 8.7). The coarse magnetite inclusions within the pleonaste are also chromian (3.9 wt% Cr_2O_3). There is no difference in composition within pleonaste grains from bright green areas without very fine-grained inclusions to very dusty, almost opaque areas with abundant inclusions (p.A.8). All the Selebi-Phikwe spinels lie on a linear trend of Cr/(Cr+Al) against

LENTSWE Pyroxenite

	a	b	c	d	e
	opx	spi	mag	chl	cum
SiO2	55.76	0.05	0.08	30.61	55.49
TiO2	0.04	0.03	0.13	0.02	0.04
Al2O3	2.66	57.14	0.34	16.67	1.09
FeO	11.53	21.90	87.78	10.53	16.94
MnO	0.22	0.16	0.11	0.12	0.22
MgO	30.02	14.42	0.16	26.80	21.99
CaO	0.17	0.02	0.04	0.11	1.30
Na2O	0.01	0.09	0.03	0.05	0.48
K2O	0.00			0.01	0.01
Cr2O3	0.05	4.65	3.89		0.07
NiO	0.01	0.04	0.00		0.09
Total	100.47	98.50	92.56	84.92	97.72
	En 82				
No. of analyses	4	7	2	1	5

a Orthopyroxene, average of coarse idioblastic (core and margin) and medium-grained matrix LT 27-25

b Cr-pleonaste, average of clear green, dusty and very dusty spinel LT 27-25

c Cr-magnetite included within Cr-pleonaste LT 27-25

d Chlorite (diabantite) rimming Cr-pleonaste in pyrrhotite LT 27-25

e Cummingtonite of banded quartzite -amphibolite LT 27-30

Samples LT 27-25 - pyroxenite and LT 27-30 - banded quartzite-amphibolite from LT 27

See Fig. 8.10 for LT 27 section

See Plate 39c for LT 27-25

DIKOLOTI

Amphibole Pyroxenite

	f	g	h
	opx	hor	chr
SiO2	56.30	52.12	0.28
TiO2	0.01	0.16	1.08
Al2O3	0.84	5.18	5.70
FeO	10.49	4.76	67.59
MnO	0.21	0.12	0.37
MgO	32.34	20.84	2.81
CaO	0.27	12.03	0.02
Na2O	0.01	1.11	
K2O	0.00	0.15	0.04
Cr2O3	0.06	0.41	20.17
NiO	0.08	0.00	0.11
Total	100.61	96.88	98.17
	En 84		
No. of analyses	2	4	2

Sample 616 - amphibole pyroxenite from DK 32

See Fig. 8.9 for DK 32

f Orthopyroxene, average of core and margin 616

g Hornblende, average of coarse and fine matrix hornblende and inclusion in orthopyroxene 616

h Chromite included in coarse orthopyroxene 616

See appendix A.8 for all analyses

Sample 657 - serpentinised peridotite from DK 17

Serpentinised Peridotite

	i	j	k	l	m	n
	opx	olv	chr	ser	hor	cum
SiO2	55.96	40.07	0.43	41.21	46.85	57.25
TiO2	0.07	0.01	1.20	0.06	0.24	0.02
Al2O3	0.82	0.01	3.15	0.26	9.41	0.29
FeO	9.33	13.73	70.29	1.39	5.75	9.13
MnO	0.17	0.16	0.38	0.05	0.08	0.22
MgO	32.80	46.24	1.79	40.31	18.89	28.69
CaO	0.20	0.02	0.02	0.02	12.09	0.55
Na2O	0.01	0.00			1.68	0.05
K2O	0.02	0.00	0.01	0.03	0.35	0.00
Cr2O3	0.08	0.02	18.24	0.04	0.69	0.07
NiO	0.07	0.07	0.10	0.06	0.03	0.02
Total	99.53	100.33	95.61	83.43	96.06	96.29
	En 86	Fo 86				
No. of analyses	6	6	4	2	3	3

i Orthopyroxene 657

j Olivine, average of core and margin 657

k Chromite, avg. inclusions in olivine and pyrrhotite 657

l Serpentine 657

m Hornblende (edenite), core zoned amphibole 657

n Cummingtonite, rim of zoned amphibole 657

TABLE 8.2 AVERAGE MINERAL ANALYSES -- DIKOLOTI AND LENTSWE ULTRAMAFIC ROCKS

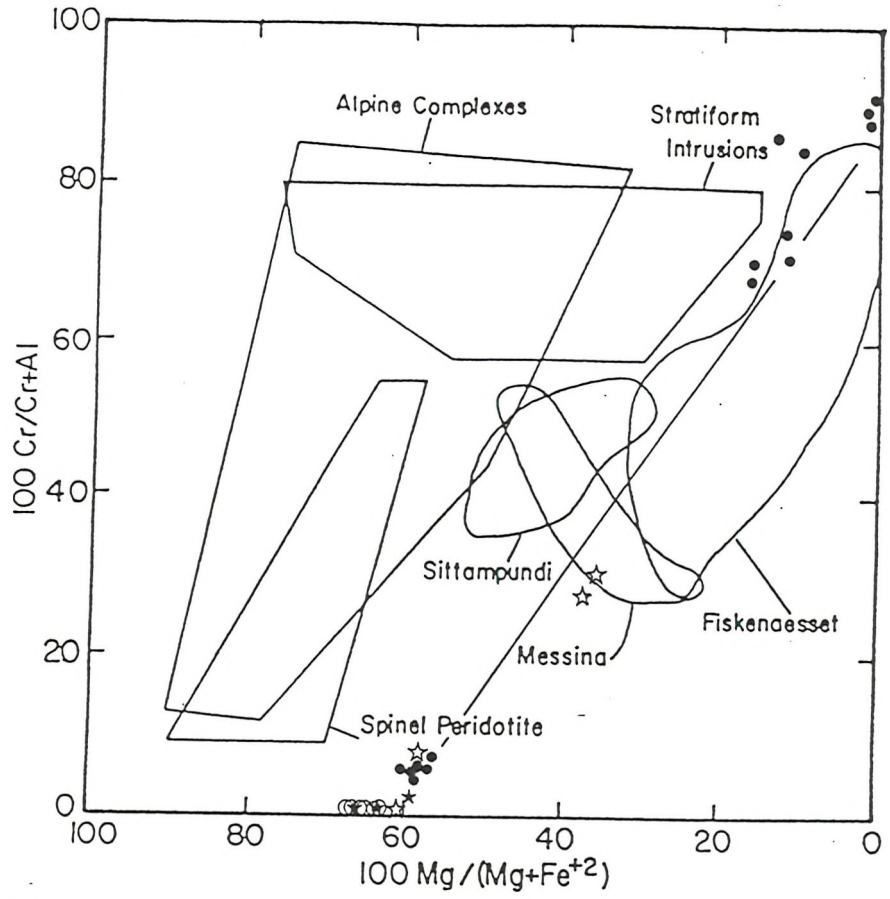

Fig. 8.7 Comparison of Spinel Compositions. Dikoloti-Lentswe Ultramafic Rocks - ●, Dikoloti Feldspathic Amphibolite - O, Selebi Host Amphibolite ★, Selebi North Ultramafic Rocks - ☆. Other data- Irvine (1967) and Windley (1981).

Mg/(Mg+Fe) that is distinct from the compositional fields of spinel from peridotites in ophiolites and stratiform intrusions (Fig. 8.7). The trend is a continuation of the fields for spinels from highly metamorphosed Archaean layered igneous complexes (Windley et al. 1981).

8.2.2 Dikoloti Feldspathic Amphibolite

The mineralogy of the Dikoloti feldspathic amphibolite has been described in Chapter 3.9 because of its importance in the evaluation of the metamorphic history of the Selebi-Phikwe area. It is sufficient to repeat here that the Dikoloti feldspathic amphibolite is a granoblastic (tshermakitic) hornblende-anorthite (An 96) rock (Fig. 3.1, Table 3.2). Included within this are aggregates of corundum-spinel-sapphirine surrounded by mantles of epidote, orthoamphibole and chlorite (Plate 40).

8.2.3 Hornblende Gneiss

The majority of the hornblende gneisses enveloping the ultra-

mafic rocks is similar to those of the Phikwe sequence. They consist of granoblastic hornblende-labradorite-minor biotite gneiss (similar to HGN) that grades with increasing magnetite content into HGF-type hornblende gneiss. Clinopyroxene or garnet-bearing hornblende gneiss is rare. Sheared hornblende gneiss (e.g. at Phokoje) contains abundant chlorite and quartz. Hornblende gneiss immediately adjacent to the ultramafic rocks is locally magnetite, hornblende and pyrrhotite-rich. The contact of the ultramafic rocks is sheared and typically marked by biotite-magnetite-pyrrhotite schists with phacoids of hornblende-plagioclase gneiss. These pass into ultramafic schists and ultramafic amphibolites.

Hornblende gneiss occurs as thin bands within the mineralised ultramafic rocks. They are typically sheared and contain variable proportions of biotite, cummingtonite, quartz, disseminated sulphide, porphyroblastic garnet and minor orthopyroxene as well as hornblende, plagioclase and abundant magnetite. Later chlorite occurs in multiply-sheared zones. Plagioclase is typically recrystallised to a fine aggregate or altered to clinozoisite and replaced by sulphide. Some of the hornblende gneiss has a spotted appearance due to aggregates of plagioclase. As stated in Chapter 3.1, it is impossible to deduce whether these spots represent an original feature (e.g. amygdales in a basalt) or are a metamorphic recrystallisation phenomenon. The latter is preferred because no other original textures appear to have been preserved in these highly strained rocks.

8.2.4 Magnetite Quartzite and Associated Amphibolites

The mineralogy of the magnetite quartzite and associated amphibolites has been described in Ch. 3.5. It is sufficient here to restate that the dominant amphibolite consists of cummingtonite with minor actinolitic calcic amphibole, quartz and magnetite (typically massive thick bands). Of volumetrically lesser importance are actinolite-rich amphibolites with minor cummingtonite, quartz and magnetite (typically thin bands within quartzite) and minor thin hornblende-rich bands.

8.3 Discussion - Igneous or metamorphic ultramafic assemblage ?

The Dikoloti-Lentswe mineralised ultramafic rocks are very similar to the Phikwe and Selebi North host ultramafic rocks. Their mineral compositions are similar and their textures are the same. The question arises as to whether the Dikoloti-Lentswe ultramafic

assemblage and textures are metamorphic or igneous. The same evidence (see Ch.5.2.3d) that was used to show that the Phikwe and Selebi North ultramafic assemblages are metamorphic indicates that the main Dikoloti-Lentswe ultramafic assemblages are also metamorphic (M1p-m) equilibrium assemblages rather than relict igneous assemblages. Additional evidence is provided by the idioblastic nature of the hornblende in olivine-rich rocks Plate 39a), the wide range of spinel compositions (Fig. 8.7) and the low Ni content of the olivine (Simkin & Smith 1977; Binns & Groves 1976; Evans 1977). The assemblage of olivine-green spinel-hornblende-orthopyroxene is the typical assemblage of metaperidotites at the transition between upper amphibolite and granulite facies conditions (Evans 1977, 1982). The Dikoloti-Lentswe ultramafic assemblages are thought to have formed at approximately the same metamorphic temperature as that estimated for the Selebi North ultramafic assemblage (c. 750 ^{o}C). The very fine-grained dusty inclusions in pleonaste are interpreted as magnetite exsolution from metamorphic pleonaste during cooling. The M1 olivine-rich assemblages have retrogressed to M2 serpentine-rich assemblages with lesser chlorite, phlogopite and talc. The M1 amphibole pyroxenites appear to have been more resistant to M2 retrogression. Retrogessed pyroxenites have commonly been sheared with the development of cummingtonite, orthoamphibole (gedrite ?) and biotite.

8.4 DIKOLOTI-LENTSWE SULPHIDES

8.4.1 Morphology, Mineralogy and Bulk Compositon

Fe-Ni-Cu sulphides (dominantly pyrrhotite plus chalcopyrite, pentlandite and minor pyrite) occur thoughout the Dikoloti-Lentswe ultramafic host rocks, mainly as sulphide disseminations and thin irregular bands (typically <1m) of massive sulphide. There is an association of thicker massive sulphide (with sharper contacts) with the development of ultramafic schist. At Dikoloti there is a tendency for massive sulphides to be concentrated near the outer margin of the ultramafic rocks with disseminated sulphides adjacent to them in the ultramafic rocks inside (Figs 8.3 & 8.4). At Lentswe massive sulphides tend to be concentrated towards the upper margin of the ultramafic rocks (Figs 8.5 & 8.6). Minor disseminated sulphide occurs in hornblende gneiss immediately enveloping the ultramafic rocks at Dikoloti and Lentswe. Massive sulphide (typically with higher contents of chalcopyrite than massive sulphide in the ultramafic rocks) also

occurs in the hornblende-grey gneiss envelope (e.g. in the nose of the Dikoloti antiform). There is an inverse relationship between the proportion of massive sulphide to ultramafic rock and the amount of ultramafic rock (e.g. LT 13 & LT 27, Figs 8.6 & 8.10). The Dikoloti feldspathic amphibolite contains only weak Fe-Ni-Cu sulphide disseminations. However it does contain traces of disseminated molybdenite.

The Dikoloti-Lentswe sulphides are similar to those at Selebi-Phikwe in terms of mineralogy and textures. The common massive sulphide in the ultramafic rocks is similar to Type 1 Selebi-Phikwe massive sulphide and consists of granular aggregates of pyrrhotite with granular chalcopyrite (associated with magnetite) and both granular and flame pentlandite. Disseminated sulphides are texturally similar to those in ultramafic host rocks at Phikwe and Selebi North and are particularly associated with the development of M2 assemblages. The Dikoloti-Lentswe sulphides differ from those at Selebi-Phikwe in that:

(a) The Dikoloti-Lentswe sulphides (particularly the typical massive sulphides) have significantly lower pentlandite and chalcopyrite contents than morphologically equivalent sulphides at Selebi-Phikwe. There is approximately half the amount of pentlandite and chalcopyrite at Dikoloti-Lentswe compared to that in Type 1 Selebi-Phikwe massive sulphide. The amount of flame pentlandite to granular pentlandite is about equal. This ratio is significantly higher than that in Type 1 massive sulphide (flame pentlandite only 15% of total pentlandite).

(b) There is little development of Type 2 massive sulphide at Dikoloti -Lentswe. The massive sulphides are texturally similar to Type 1 massive sulphide.

The estimated grade of the Dikoloti and Lentswe prospects is shown in Table 8.1. An estimate of the composition of typical Dikoloti -Lentswe massive sulphide within the ultramafic rocks (recalculated magnetite and silicate inclusion-free) is 1.6 wt% Ni and 0.5wt% Cu with a Cu/(Cu+Ni) ratio of about 0.24 (Table 8.3, Fig. 8.8). Disseminated sulphides have an average Cu/(Cu+Ni) ratio of about 0.48. Massive sulphide in the hornblende gneiss-grey gneiss envelope and at the margins of the ultramafic rocks is Cu-rich and contains up to 3 wt% Cu. The apparently mobilised Cu-rich massive sulphides account for the discrepancy between the Cu/(Cu+Ni) ratios of typical massive sulphide (average 0.28) and the grades from the ore reserve estimates (c. 0.43). Compared to morphologically equivalent Selebi-Phikwe

sulphide, normal Dikoloti-Lentswe massive sulphide has significantly lower Ni and Cu contents (i.e. a maximum of c. 1.6 wt% Ni) and lower Cu/(Cu+Ni) ratios (Table 6.3, Figs 6.5e, 7.15b & 8.8). This is in agreement with the mineralogical observations.

	Ni	Cu	Fe	S	Co	Cu/(Cu+Ni)
Normal massive sulphide	1.6	0.5	60.0	37.8	0.1 wt %	0.24
	1.2	0.3	46.9	51.5	atomic %	
Disseminated sulphide	1.2	1.1	c.60	c.38	tr. wt %	0.48
	0.9	0.8	c.47	c.51.5	atomic %	

Table 8.3 Estimated chemical compositions of the Dikoloti-Lentswe sulphide types. (Recalculated magnetite and inclusion-free.)

8.4.2 Discussion

The great majority of the sulphides at Dikoloti-Lentswe are located within ultramafic rocks. It is thought that sulphides were present within their host ultramafic rocks prior to tectono-metamorphism. The same proposal was made for the sulphides and host amphibolite protoliths at Selebi-Phikwe. The disseminated sulphide in hornblende gneiss immediately adjacent to the mineralised ultramafic rocks appears to have migrated from the ultramafic rocks. The thin irregular massive to semimassive sulphides and the disseminated sulphides within the ultramafic rocks are regarded as only weakly to moderately mobilised pretectonic massive sulphides and disseminated sulphides. The low Ni contents of Dikoloti-Lentswe olivines suggest that the Ni contents of the sulphides have not been reduced from that of the original sulphides by tectonometamorphic processes (e.g. the crystallisation of metamorphic olivine). In fact the reverse has possibly occurred. Their Ni and Cu contents are regarded as generally reflecting the original Ni and Cu contents of pretectono-metamorphic sulphides. The bulk chemical composition of the Dikoloti-Lentswe massive (and disseminated) sulphides are such (Fig. 8.3) that they

would have homogenised at the peak of metamorphism to dominantly quaternary Fe-Ni-Cu-S monosulphide solution (MSS, Fig. 6.5).

Thicker massive sulphides (with sharper contacts) are associated with the development of ultramafic schists (mainly at the margins of the ultramafic rocks) and also occur in the hornblende gneiss-grey gneiss envelope. The inverse relationship of the ratio of massive sulphide/ultramafic rocks to the thickness of ultramafic rocks suggests that some of the massive sulphides have been significantly mobilised relative to the ultramafic rocks during shearing. However highly mobilised Type 2 massive sulphide has not been significantly developed. The mobilised sulphides have been enriched in Cu but not Ni which infers that Cu was more mobile than Ni during shearing-induced mobilisation. (Mobilisation probably also involved mechanical separation of pretectono-metamorphic chalcopyrite from pyrrhotite during initial deformation.)

The typical Dikoloti-Lentswe massive sulphides have significantly lower Ni and Cu contents and slightly lower Cu/(Cu+Ni) ratios than morphologically equivalent sulphides at Selebi-Phikwe (Table 6.3, Figs 7.15b & 8.8). Dikoloti-Lentswe disseminated sulphides also have lower Cu/(Cu+Ni) ratios than Selebi-Phikwe disseminated sulphides. The difference in Ni and Cu contents and hence Cu/(Cu+Ni) ratios of Dikoloti-Lentswe sulphides compared to those at Selebi-Phikwe are thought to reflect original differences. The metamorphic cooling history of the sulphides would have been generally similar to that at Selebi-Phikwe (see Ch. 6.4.4). The higher proportion of flame pentlandite to granular pentlandite at Dikoloti-Lentswe is due to its lower content of Ni. Pentlandite would not have started to exsolve from cooling metamorphic MSS until a temperature of about 300^{o}C had been reached (Fig. 6.5e). A higher proportion of the Ni at Dikoloti-Lentswe than at Selebi-Phikwe remained in cooling quaternary MSS and was exsolved as relatively late flame pentlandite.

8.5 GEOCHEMISTRY OF DIKOLOTI-LENTSWE ROCKS

8.5.1 Ultramafic Rocks

The average chemical compositions of the Dikoloti-Lentswe (& Phokoje) ultramafic rocks are shown in Table 8.4. As with the Selebi-Phikwe host rocks, analyses have been recalculated to 100% on an anhydrous and sulphide-free basis. There are no major differences

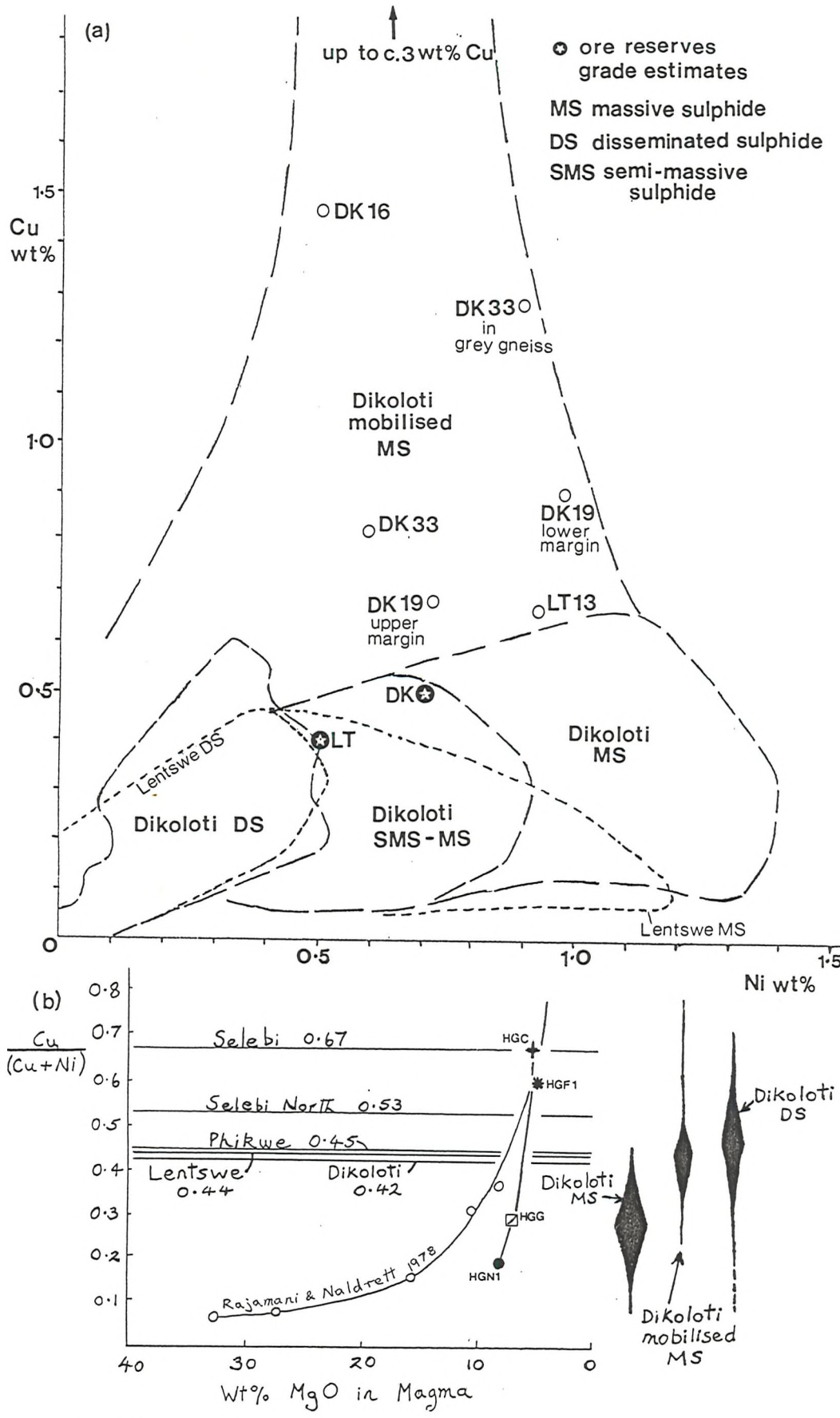

Fig.8.8 Ni and Cu contents and Cu/(Cu+Ni) ratios of the Dikoloti-Lentswe sulphides. See also Fig. 7.15b.

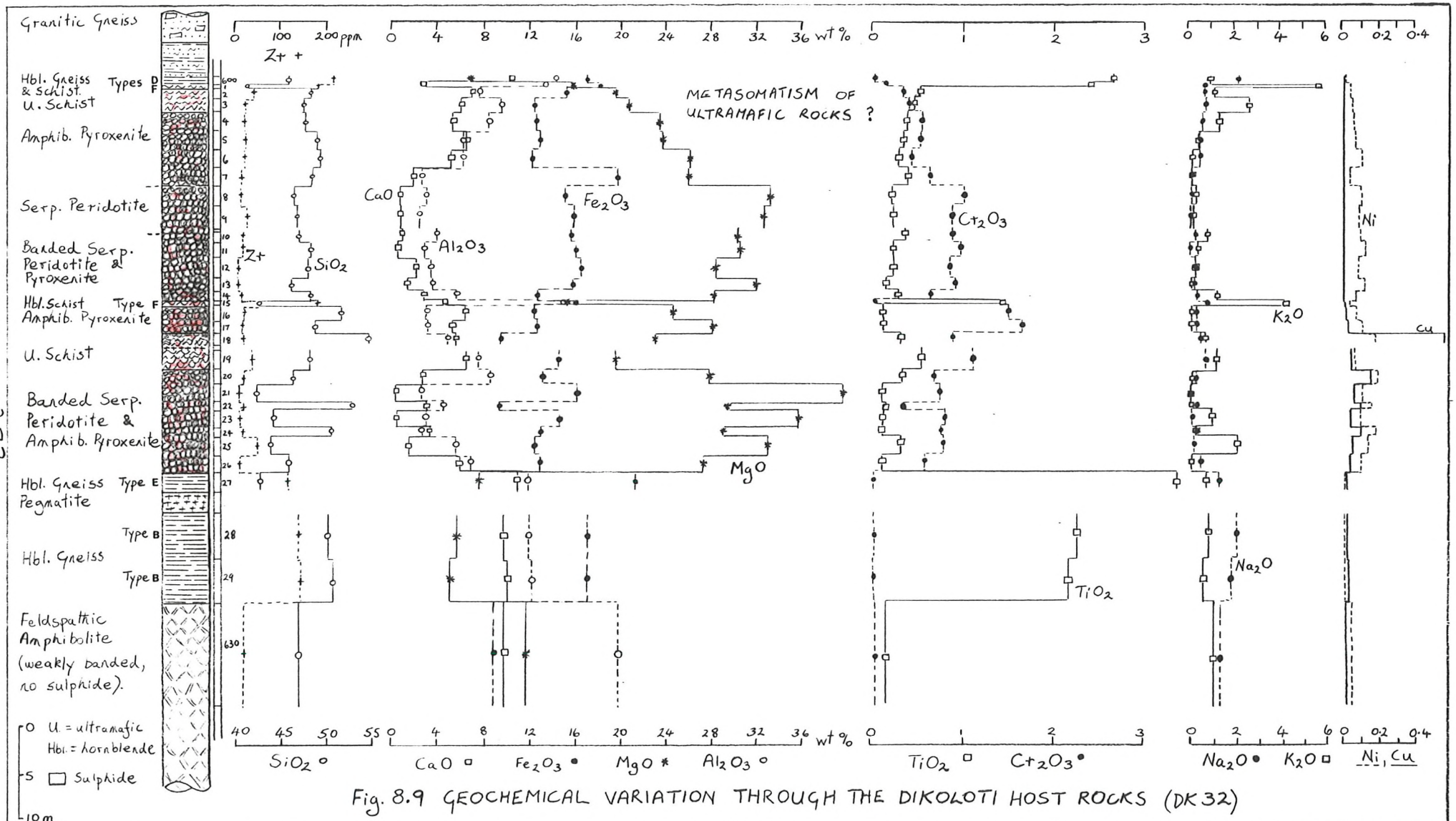

Fig. 8.9 GEOCHEMICAL VARIATION THROUGH THE DIKOLOTI HOST ROCKS (DK32)

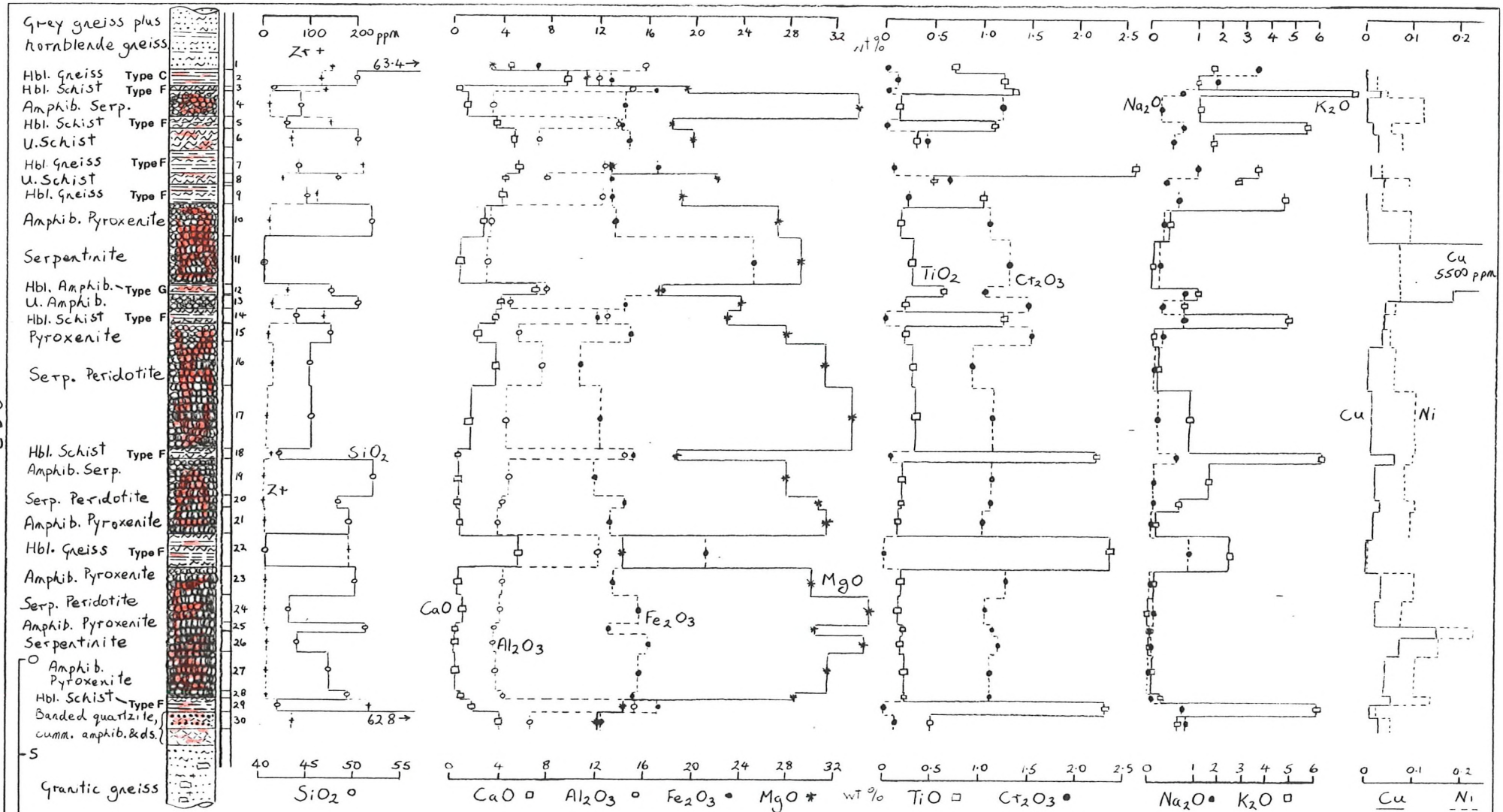

Fig. 8.10 GEOCHEMICAL VARIATION THROUGH THE LENTSWE HOST ROCKS (LT 27)

between the chemical composition of mineralogically similar rocks from Dikoloti and Lentswe (& Phokoje) and they have therefore been grouped together. The ultramafic rocks have been subdivided in order of decreasing Mg content into serpentinised peridotite, amphibole pyroxenite, cummingtonite-calcic amphibole-biotite amphibolite and cummingtonite-biotite-calcic amphibole schist. The four lithologies grade mineralogically and chemically into each other. The serpentinised peridotites and amphibole pyroxenites have been mineralogically separated by the appearance in the former of olivine or serpentine. This occurs at about 30 wt% MgO.

The serpentinised peridotites are characterised by high Mg (31-40 wt% MgO) and Cr (0.7-1.3 wt% Cr_2O_3) and low Si (42-48 wt% SiO_2), Ti (0.1-0.3 wt% TiO_2), Al (2.5-7 wt% Al_2O_3), Ca (0.3-3.6 wt% CaO), Y and Zr (Figs 8.11-8.14). The wide variation in Al reflects locally high spinel and calcic amphibole. They have high normative contents of olivine (Fo 86) and orthopyroxene plus minor plagioclase (Table 8.4). The amphibole pyroxenites are characterised by typically lower contents of Mg (23-31 wt% MgO) and Cr, similar contents of Ti and Fe and higher contents of Si, Ti, Al and Ca than the serpentinised peridotites (Figs 8.11-8.14). Both the serpentinised peridotites and amphibole pyroxenites have a minimum Al content of 2.5 wt% Al_2O_3 (Figs 8.11b & 8.13a). The amphibole pyroxenites have high normative contents of orthopyroxene (En 84) and olivine plus minor plagioclase and clinopyroxene. The Dikoloti-Lentswe amphibole pyroxenites are chemically similar to the amphibole pyroxenites at Selebi North (Table 7.1). However they have higher contents of Mg, Fe, K and Rb and lower contents of Al, Ca and Cr than those at Selebi North.

The ultramafic amphibolites are characterised by typically lower contents of Mg (22-27 wt% MgO), similar Ti, Fe and Cr and higher contents of Al, Ca, K, (Nb) and Rb than the amphibole pyroxenites (Table 8.4, Figs 8.11-8.14). The ultramafic schists are characterised by lower contents of Mg (19-22 wt% MgO) and Cr, similar Fe and higher contents of Ti, Al, Ca, K, Y and Zr than the ultramafic amphibolites.

8.5.2 Dikoloti Feldspathic Amphibolite

The Dikoloti feldspathic amphibolite is characterised by variably high contents of Al (13-26 wt% Al_2O_3), moderate Mg (6-18 wt% MgO) and Ca (10-15 wt% CaO), low Ti (0.0-0.2 wt% TiO_2), Y and Zr and relatively low K/Rb (Table 8.5-A, Figs 8.11-8.14). It has high contents of normative plagioclase (An 86) plus olivine (Fo 79) and

	Serpentinised peridotites		Amphibole pyroxenites	
SiO2	44.81	42.3-48.4	49.53	45.8-53.0
TiO2	0.19	0.12-0.33	0.23	0.08-0.45
Al2O3	3.62	2.5-7.4	4.52	2.5-8.4
Fe2O3	13.78	10.2-17.3	13.30	9.2-19.6
MnO	0.16	0.11-0.23	0.18	0.21-0.29
MgO	34.75	30.7-39.9	27.76	23.4-31.3
CaO	0.93	0.29-3.56	2.96	0.4-6.3
Na2O	0.14	0.05-0.24	0.32	0.06-0.57
K2O	0.54	0.01-2.08	0.34	0.07-1.86
P2O5	0.04	0.02-0.05	0.05	0.02-0.20
Cr2O3	1.04	0.74-1.32	0.81	0.07-1.65
	100.00		100.00	
Cr	6900	4270-8570	5200	500-10700
Nb	3.7	nd-10	3.6	nd-6
Rb	56	5-183	27	4-159
Sr	7	nd-16	6	nd-11
V	94	55-131	110	28-243
Y	6	nd-23	8	nd-13
Zr	16	5-48	13	4-23
or	3.28		2.00	
ab	1.20		2.72	
an	4.42		10.01	
C	1.21			
di			3.63	
hy	34.21		55.91	
ol	51.77		22.04	
mt	2.41		2.32	
il	0.36		0.44	
ap	0.09		0.11	
cr	1.05		0.82	
Fo	86		84	
N-Samples	18		25	

	Ultramafic amphibolites		Ultramafic schists	
SiO2	52.02	50.4-54.1	48.52	47.5-50.4
TiO2	0.19	0.14-0.28	0.47	0.33-0.54
Al2O3	3.90	3.0-4.7	7.78	7.0-9.3
Fe2O3	13.61	8.7-18.2	13.88	12.3-15.1
MnO	0.24	0.16-0.41	0.19	0.12-0.23
MgO	23.89	22.0-26.9	20.28	19.5-21.9
CaO	3.66	1.0-7.5	5.71	4.3-6.9
Na2O	0.35	0.24-0.59	0.58	0.37-0.72
K2O	1.28	0.09-2.05	1.87	1.08-2.75
P2O5	0.03	0.02-0.05	0.08	0.03-0.18
Cr2O3	0.83	0.28-1.49	0.64	0.34-1.35
	100.00		100.00	
Cr	5510	1840-9690	4127	2300-8655
Nb	5.5	3-9	5.4	4-9
Rb	122	7-265	126	75-196
Sr	8	5-12	12	10-16
V	96	58-134	167	104-207
Y	12	6-20	20	13-33
Zr	17	13-25	41	22-63
or	7.56		11.18	
ab	2.94		4.98	
an	5.42		13.26	
di	10.20		11.95	
hy	59.62		29.48	
ol	10.59		25.01	
mt	2.39		2.41	
il	0.37		0.91	
ap	0.07		0.17	
cr	0.84		0.65	
Fo	81		78	
N-Samples	6		5	

Table 8.4 Average chemical and normative compositions of Dikolti-Lentswe ultramafic host rocks.

All analyses have been recalculated to 100% on an anhydrous and sulphur-free basis. The Fe2O3/FeO ratio in the norm calculation is assumed to be 0.15 (Brooks 1976).

	A		B		C
SiO2	46.93	44.9-50.0	44.19	43.5-45.4	36.63
TiO2	0.12	0.04-0.22	0.05	0.04-0.05	0.03
Al2O3	19.27	13.4-26.1	23.00	21.5-24.6	37.20
Fe2O3	7.72	5.4-9.8	7.14	6.8-7.5	4.58
MnO	0.13	0.07-0.16	0.12	0.12-0.13	0.07
MgO	11.89	6.1-18.2	11.88	9.2-14.3	8.34
CaO	12.03	9.8-14.6	11.75	11.2-12.5	11.53
Na2O	1.35	1.1-1.9	1.23	1.0-1.5	0.69
K2O	0.45	0.19-1.13	0.60	0.30-0.84	0.89
P2O5	0.04	0.03-0.05	0.02	0.02-0.03	0.03
Cr2O3	0.07	0.01-0.14	0.02	0.02	0.01
	100.00		100.00		100.00
N-Samples	7		3		1
Cr	491	73-929	140	114-155	46
Cu	162	nd-349	208	28-337	433
Nb	3.0	2-5	3.7	3-5	4
Ni	381	165-612	555	530-580	451
Rb	46	9-123	66	29-106	92
S	1149	29-2381	1305	nd-2361	2954
Sr	97	28-160	123	107-135	305
V	71	18-146	23	17-26	14
Y	5	3-7	<2	nd-2	2
Zr	14	9-18	8	7-9	7
or	2.67				
ab	11.47				
an	45.45				
di	11.56				
hy	6.98				
ol	20.13				
mt	1.35				
il	0.23				
ap	0.09				
cr	0.07				
An	86				
Fo	79				

Table 8.5 Average chemical composition (wt% and ppm) of Dikoloti feldspathic amphibolite.

A - Feldspathic amphibolite without spinel -sapphirine-corundum aggregates;
B - Feldspathic amphibolite with spinel-sapphirine-corundum aggregates;
C - Spinel-sapphirine-corundum aggregate.

Analyses recalculated to 100% on an anhydrous and sulphide-free basis.

clinopyroxene. It is chemically similar (particularly its Al content) to the gabbroic rocks of the anorthosite-metagabbro suite (Table 4.7-B), although the latter have higher Si, Ca and lower Mg, (Cr) and Rb than the Dikoloti feldspathic amphibolite. The corundum-spinel-sapphirine aggregates (and hence the amphibolites containing the aggregates, Table 8.5-B) are characterised by higher contents of Al (37 wt% Al2O3), K, Rb, Sr, S, Cu and Ni and lower Si, Ti, (Fe), Na,

Cr, V, (Y) and (Zr) than the typical feldspathic amphibolite (Table 8.5-C). These chemical differences are similar to those between spinel-bearing host amphibolite at Selebi and average Selebi host amphibolite (see Ch. 7.2). The whole Dikoloti feldsapthic amphibolite suite is characterised by relatively low K/Rb ratios (55-86) and lies along a line of extreme Rb-enrichment (K/Rb slope = 68, Fig. 8.13b).

8.5.3 Hornblende Gneisses

The average composition of the various types of hornblende gneiss at Dikoloti-Lentswe are shown in Table 8.6. They have been subdivided on the basis of geochemistry, mineralogy and location into:

(A) Unsheared hornblende-plagioclase gneiss with only minor clinopyroxene and magnetite, all of which occurs in the hornblende gneiss-grey gneiss envelope to the ultramafic rocks. They are mineralogically and geochemically similar to HGN1 (see Ch.4.1.2 & Table 4.1), although Type-A has higher contents of Fe (13-16 wt% Fe2O3), Ti (0.9-1.2 wt% TiO2), S, V, Y and Zr and lower Mg and Cr compared to average HGN1 (Figs 8.12b, 8.14, 8.15 & 8.16).

(B) Unsheared hornblende-plagioclase-magnetite gneiss, which occurs in the hornblende gneiss-grey gneiss envelope to the ultramafic rocks or between the ultramafic rocks and feldspathic amphibolite at Dikoloti. They are mineralogically and geochemically similar to HGF1, although Type-B has lower contents of Ti, P and Y and higher Cu compared to average HGF1.

(C) A slightly sheared version of Type-A with higher contents of biotite (and locally chlorite), magnetite and quartz, which typically occurs at the sheared margins (Fig. 8.10) and within the ultramafic rocks and locally in the hornblende gneiss-grey gneiss envelope. Type-C has higher contents of Ti, Mg, K, Cr, Cu, Nb, Ni and Rb (Fig. 8.13b) and lower contents of Ca and (Na) than Type-A.

(D) A slightly sheared version of Type-B with high contents of magnetite and locally recrystallised aggregates of plagioclase, which mainly occurs within the ultramafic rocks and at their sheared margins (Fig. 8.9). Type-D has higher contents of Ti, (Al), Mg, P, Cu, Nb, Ni, S, Y and Zr and lower contents of Si than Type-B.

(E) Unsheared hornblende-magnetite-plagioclase amphibolite, which typically occurs adjacent to mineralised ultramafic rock (Fig. 8.9) or massive sulphide. Type-E is characterised by high contents of Fe (> 18.5 wt% Fe2O3, Figs 8.14a & 8.16a) and Ti (> 1.8 wt% TiO2) and low contents of Si (> 42.6 wt% SiO2). Type-E also has relatively high

	A		B		C		D	
SiO2	49.92	47.9-51.6	50.40	50.1-50.7	49.08	45.7-50.6	46.16	44.0-48.5
TiO2	1.08	0.89-1.25	2.22	2.0-2.3	1.43	1.2-1.6	2.70	2.4-3.0
Al2O3	14.41	14.3-14.6	12.15	11.9-12.3	13.65	11.8-14.6	14.05	13.6-14.4
Fe2O3	14.14	12.8-15.7	16.60	15.7-17.1	14.19	13.0-16.7	16.06	13.8-17.6
MnO	0.18	0.15-0.21	0.23	0.21-0.27	0.14	0.09-0.21	0.25	0.19-0.33
MgO	6.40	5.6-7.8	5.46	5.1-5.8	9.66	7.6-10.9	7.35	6.7-8.0
CaO	10.13	8.3-12.0	9.79	9.5-10.3	7.81	4.5-11.7	9.71	9.1-10.3
Na2O	2.45	1.8-3.3	2.10	1.8-2.5	2.05	1.2-2.8	2.42	2.1-3.1
K2O	1.13	0.78-1.38	0.82	0.55-1.09	1.85	1.0-3.7	0.94	0.83-1.07
P2O5	0.13	0.09-0.20	0.21	0.20-0.23	0.10	0.07-0.17	0.34	0.31-0.39
Cr2O3	0.03	0.02-0.04	0.02	0.01-0.02	0.04	0.01-0.12	0.02	0.02
	100.00		100.00		100.00		100.00	
Cr	194	116-255	114	85-125	289	96-788	112	108-117
Cu	37	nd-64	244	195-316	61	4-145	65	43-92
Nb	5.0	3-7	10.6	7-13	8.0	5-12	22 (13)	12-39
Ni	124	89-183	67	63-77	269	110-398	122	111-132
Rb	50	25-64	36	15-49	101	52-182	36	30-40
S	1310	562-2810	693	384-1216	1490	170-4093	2200	936-4162
Sr	109	94-131	134	107-163	96	65-133	126	100-149
V	251	228-286	376	330-418	236	95-386	369	332-429
Y	28	25-34	32	29-35	24	17-36	77 (49)	43-135
Zr	70	58-91	142	129-164	75	45-126	221	212-234
N-Samples	3		5		6		3	

	E		F		G	H	
SiO2	41.26	40.2-42.6	42.80	40.5-46.7	47.57	46.37	45.7-47.0
TiO2	2.70	1.8-3.4	1.78	1.0-2.6	0.60	0.20	0.16-0.24
Al2O3	12.58	11.1-13.8	13.82	12.1-15.2	7.78	14.59	13.4-15.8
Fe2O3	20.99	18.5-22.1	16.39	9.9-23.5	17.12	12.65	11.1-14.2
MnO	0.23	0.19-0.26	0.12	0.03-0.22	0.25	0.17	0.14-0.20
MgO	8.81	7.4-12.3	15.95	8.7-22.8	16.91	12.94	10.2-15.7
CaO	10.72	9.8-12.0	2.99	0.43-5.57	6.81	10.47	10.3-10.7
Na2O	1.59	1.3-2.0	0.73	0.55-1.07	0.76	1.32	1.3-1.4
K2O	0.71	0.41-1.13	5.09	2.5-7.6	1.02	1.13	0.65-1.61
P2O5	0.39	0.29-0.57	0.27	0.04-0.47	0.13	0.04	0.04
Cr2O3	0.02	0.00-0.04	0.06	0.00-0.25	1.05	0.12	0.08-0.16
	100.00		100.00		100.00	100.00	
Cr	149	30-253	387	11-1678	6870	768	570-965
Cu	149	18-286	181	23-649	1873	98	nd-193
Nb	14	7-28	17	7-53	5	2.5	nd-4
Ni	209	85-570	388	79-1008	717	329	266-392
Rb	22	10-39	363	140-567	50	64	49-79
S	4325	nd-14550	3983	630-12780	10650	20	nd-40
Sr	66	50-118	24	11-72	12	40	22-58
V	402	280-479	229	139-318	158	131	100-161
Y	48	34-61	33	5-102	33	8	6-11
Zr	186	115-304	147	23-232	54	17	16-18
N-Samples	6		12		1	2	

Table 8.6 Average chemical composition (wt% and ppm) of Dikolti-Lentswe-Phokoje hornblende gneiss. Analyses recalculated to 100% on an anhydrous and sulphide-free basis.

contents of Ca (10-12 wt% CaO, Figs 8.14b & 8.16b), Nb, Y and Zr and relatively low K (< 1.1 wt% K2O, Figs 8.13b & 8.14a) compared to Type-F and G. In DK 30, typical Type-B (HGF1) hornblende gneiss of the hornblende gneiss-grey gneiss envelope grades over about 4 m into Type -E hornblende-bearing rock as a thick (4 m) inclusion-rich massive sulphide layer at the margin of the mineralised ultramafic rocks is approached. The Type-B hornblende gneiss gradually becomes coarser and less foliated and gradually contains magnetite porphyroblasts and fine disseminated sulphide. In DK32 (Fig. 8.9), Type-E hornblende-rich gneiss occurs in a band adjacent to mineralised ultramafic rocks. The possible gradation of the Type-E gneiss into Type-B below is obscured by a pegmatite band.

(F) Highly sheared hornblende-plagioclase-biotite-magnetite gneiss with minor garnet and orthopyroxene grading into biotite-magnetite schist with phacoids of hornblende gneiss. Type-F typically occurs at the sheared margin of, or within the ultramafic package (Figs 8.9 & 8.10). It is characterised by low contents of Ca (< 5.7 wt% CaO, Figs 8.14b & 8.16b)) and Si (< 46.7 wt% SiO2), high contents of K (> 2.5 wt% K2O), Nb, Rb, Y and Zr and a wide range of typically high Fe and Mg (Fig. 8.16a). Those with the highest Fe/Mg ratios are garnet and magnetite-rich. The average K/Rb ratio is 113 (Fig. 8.13b). The majority of the Dikoloti-Lentswe hornblende-bearing rocks have relatively low K/Rb ratios and lie on a trend of K/Rb = 90-115 (Fig. 8.13b).

(G) A sheared hornblende-cummingtonite-biotite-minor plagioclase gneiss from within the Lentswe ultramafic rocks (Fig. 8.10), characterised by high contents of Fe, Mg and Cr (1.1 wt% Cr2O3) and low Al (7.8 wt% Al2O3, Fig. 8.14b & 8.15b) and total alkalies (Fig. 8.14a).

(H) Coarse-grained granoblastic hornblende-plagioclase amphibolite, mineralogically similar to low-Ti HGN1, from within and at the margin of the ultramafic rocks. Type-H has higher contents of Mg and Cr and lower Si than typical low-Ti HGN1.

8.5.4 Mg-Amphibolites Associated with Magnetite Quartzite

The dominant type of Mg-amphibolite is massive cummingtonite-rich amphibolite which is characterised by high contents of Mg (19-22 wt% MgO), Fe (17-21 wt% Fe2O3) and Mn (0.2-0.6 wt% MnO,) moderate contents of Ni (212-359 ppm) and low contents of Ti, Al (< 1.6 wt% Al2O3), Ca (<4.6 wt% CaO), K (0.01-0.08 wt% K2O), Cr (<201 ppm Cr), Cu

	Cummingtonite-rich amphibolites			
	A	B		C
SiO2	56.83	55.59	54.2-58.6	54.12
TiO2	0.06	0.06	0.04-0.11	0.27
Al2O3	1.64	0.90	0.65-1.10	2.77
Fe2O3	18.46	18.79	17.3-20.6	17.09
MnO	0.34	0.42	0.30-0.60	0.18
MgO	21.02	20.60	18.9-22.1	21.33
CaO	1.31	3.45	2.2-4.6	3.65
Na2O	0.22	0.10	0.06-0.18	0.32
K2O	0.08	0.02	0.01-0.05	0.05
P2O5	0.03	0.06	0.01-0.23	0.03
Cr2O3	0.01	0.01	0.00-0.03	0.19
	100.00	100.00		100.00
Cr	56	74	10-201	1320
Cu	nd	20(5)	nd-125(9)	99
Nb	3	3.8	nd-6	2
Ni	250	285	212-359	628
Rb	6	3	nd-5	5
S	42	nd		3070
Sr	nd	4	nd-10	nd
V	26	63	35-106	89
Y	9	23	6-45	9
Zr	11	9	6-12	12
N-Samples	1	8		1

	Actinolite-rich		Hornblende-rich			
	D		E		F	
SiO2	54.87	54.7-55.0	52.58	50.5-55.6	52.02	50.4-54.1
TiO2	0.04	0.01-0.07	0.46	0.34-0.61	0.19	0.14-0.28
Al2O3	1.63	1.2-2.0	6.55	5.6-7.8	3.90	3.0-4.7
Fe2O3	14.18	11.4-16.5	14.75	12.7-17.0	13.61	8.7-18.2
MnO	0.21	0.17-0.30	0.24	0.19-0.28	0.24	0.16-0.41
MgO	17.69	16.3-20.3	16.46	14.4-18.3	23.89	22.0-26.9
CaO	11.01	9.9-11.5	7.56	4.7-11.1	3.66	1.0-7.5
Na2O	0.25	0.18-0.35	0.76	0.59-1.03	0.35	0.24-0.59
K2O	0.07	0.05-0.09	0.35	0.11-0.82	1.28	0.09-2.05
P2O5	0.05	0.04-0.07	0.08	0.03-0.14	0.03	0.02-0.05
Cr2O3	0.00	0.00-0.01	0.21	0.16-0.24	0.83	0.28-1.49
	100.00		100.00		100.00	
Cr	30	16-39	1450	1120-1665	5510	1840-9690
Cu	34	5-77	105	nd-301		
Nb	3.3	3-4	4.7	3-6	5.5	3-9
Ni	319	163-412	401	229-585		
Rb	3	2-4	14	nd-38	122	7-265
S	nd		10815	nd-21630		
Sr	7	5-10	25	9-50	8	5-12
V	69	49-102	128	93-170	96	58-134
Y	38	35-41	13	13-14	12	6-20
Zr	9	8-9	43	23-70	17	13-25
N-Samples	4		3		6	

Table 8.7 Average chemical composition of amphibolites associated with Dikoloti-Lentswe magnetite quartzite. (F) - ultramafic amphibolite from Table 8.3 for comparison. Analyses recalculated to 100% on an anhydrous and sulphide-free basis.

(typically < 9ppm), Y and Zr and low K/Rb ratios (Table 8.7-A & B). A single sample of cummingtonite-rich amphibolite (Table 8.7-C), interbanded with quartzite 2 m below the ultramafic rocks in LT 26, is characterised by slightly higher contents of Ti, Al, Ca, Ni and particularly Cr (1320 ppm Cr) than typical cummingtonite-rich amphibolite.

The actinolite-rich amphibolites (typically finely banded with magnetite quartzite) are characterised by high contents of Mg (16-20 wt% MgO), Fe (11-16 wt% Fe2O3), Ca (10-12 wt% CaO), K (0.05-0.09) and Y (38 ppm), moderate contents of Ni (163-412) and low contents of Ti, Al (< 2.0 wt% Al2O3), Cr (< 39 ppm Cr) and Zr (Table 8.7-D). There is a general trend of increasing Mg/Fe with increasing Ca content in the cummingtonite-actinolite amphibolites.

The minor hornblende-rich amphibolites are characterised by higher Ti, Al, Cr (1450 ppm Cr) and Zr contents than the cummingtonite and actinolite-rich amphibolites and moderate Ca (5-11 wt% CaO) (Table 8.7-E).

The distinctive geochemistry of the Mg-amphibolites, particularly their low Al, Mg and Cr contents compared to the Dikoloti-Lentswe ultramafic host rocks, is graphically shown in Figures 8.11, 8.12a & c, 8.13a & 8.14b.

8.6 DISCUSSION, THE ORIGINAL NATURE OF THE DIKOLOTI-LENTSWE ROCKS

8.6.1 The Protoliths of the Ultramafic Rocks

The ultrabasic (high Mg & Cr) nature of the Dikoloti-Lentswe serpentinised peridotites and amphibole pyroxenites unequivocally suggests an igneous origin. Their range of Mg and Si contents and low Al and Ca contents (reflected in high normative contents of olivine and orthopyroxene) indicate a complete gradation in composition from dunite and harzburgite to orthopyroxenite. Clinopyroxene and plagioclase appear to have been only minor phases. The low Ti contents and high but variable Cr contents suggests that the ultramafic rocks represent olivine-orthopyroxene-chromite cumulates rather than ultramafic liquids. Serpentinisation has probably resulted in a loss of Fe (Fig. 8.11b) although some unserpentinised peridotites and amphibole pyroxenites are also enriched in Fe. Ca has also probably been depleted in some of the ultramafic rocks (Fig. 8.13a, cf. Challis 1965).

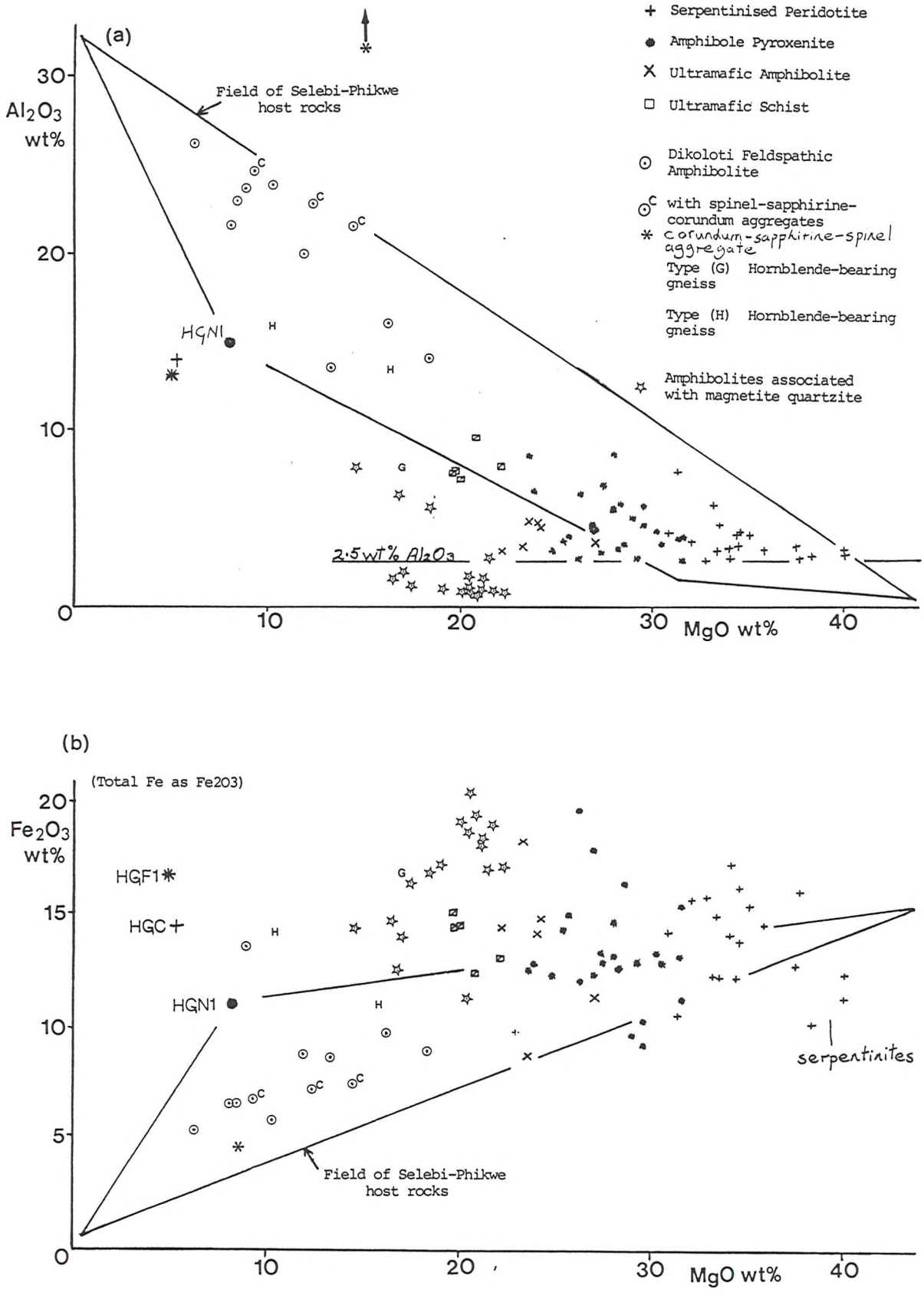

Fig. 8.11 The Dikoloti-Lentswe Host Rocks - mineralised ultramafic rocks and Dikolti feldsapathic amphibolite; Al, Fe and Mg contents.

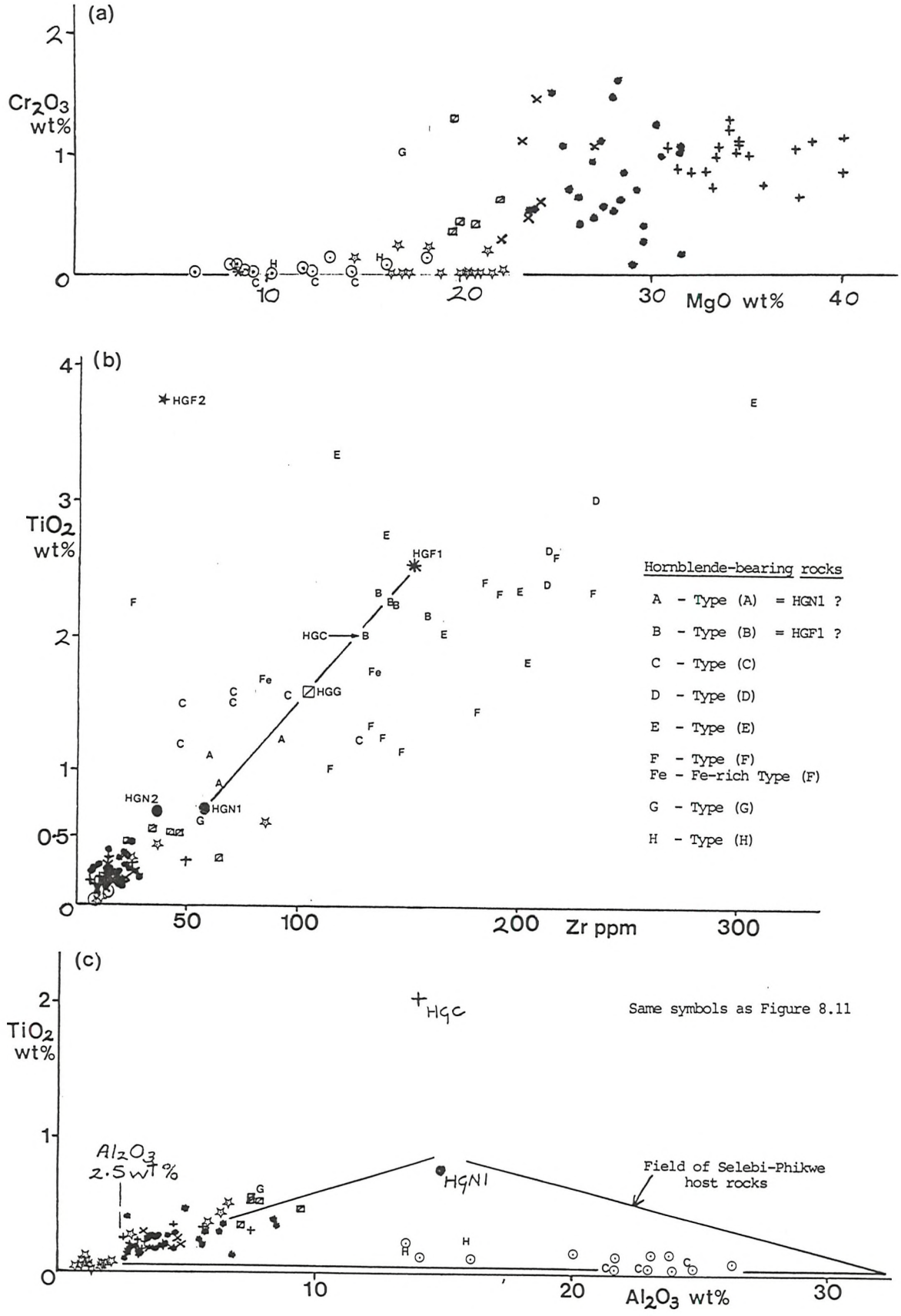

Fig. 8.12 The Dikoloti-Lentswe Host Rocks - mineralised ultramafic rocks and Dikolti feldsapathic amphibolite; Cr, Ti and Zr contents. Ti and Zr contents of Dikoloti-Lentswe hornblende-bearing rocks also plotted in (b).

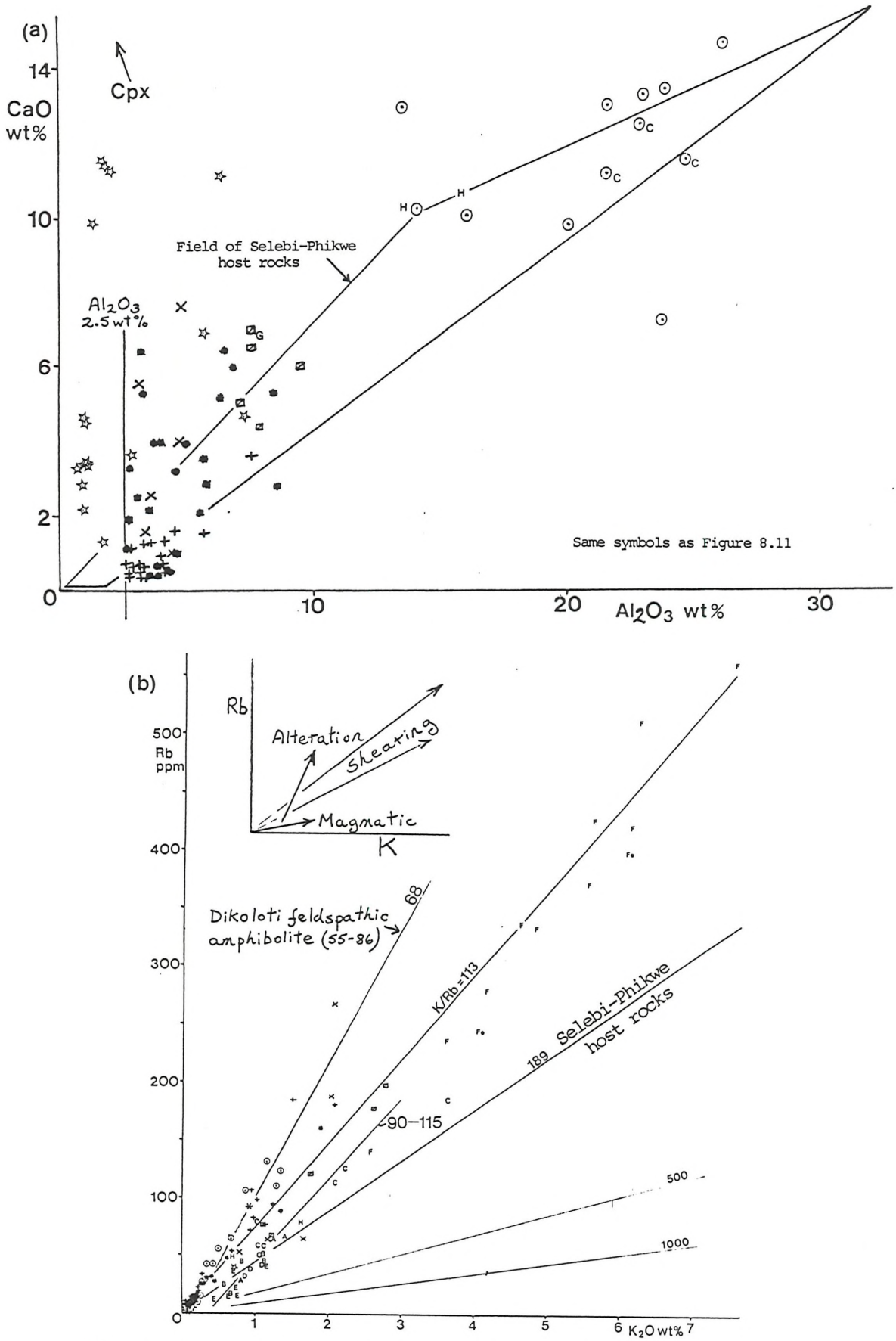

Fig. 8. 13 The Dikoloti-Lentswe Host Rocks - mineralised ultramafic rocks and Dikoloti feldsapathic amphibolite; Ca, K and Rb contents. K and Rb contents of Dikoloti-Lentswe hornblende-bearing rocks also plotted in (b).

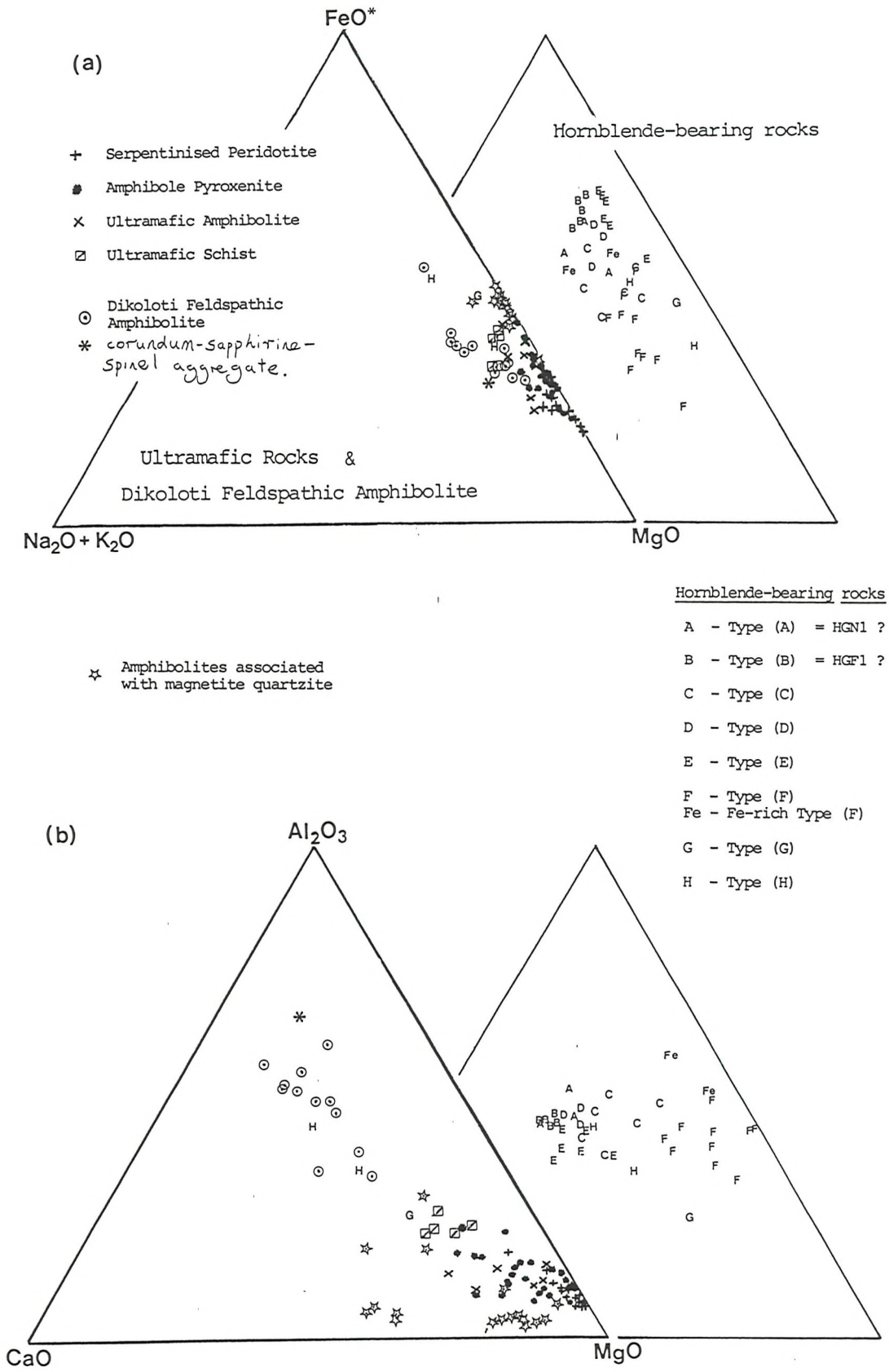

Fig. 8.14 The Dikoloti-Lentswe Host Rocks - mineralised ultramafic rocks, Dikoloti feldsapathic amphibolite and hornblende-bearing rocks: (a) AFM diagram (FeO*-total Fe as FeO); (b) ACM diagram.

The ultramafic amphibolites either represent metasomatised amphibole pyroxenites (i.e. metasomatically increased Si, Ca and K contents and decreased Mg contents) or slightly different ultramafic protoliths to the typical amphibole pyroxenites (i.e. clinopyroxene-bearing orthopyroxenites). The ultramafic schists have a distinctive geochemistry with significantly higher contents of Ti, Al, Ca, K, P, Rb, V, Y and Zr and lower Mg and Cr than the other mineralised ultramafic rocks. The average values of TiO2 (0.47 wt%), P2O5 (0.08 wt%), Y (20 ppm) and Zr (41 ppm) are similar to those of komatiitic basalts (Nesbitt et al. 1979). However the CaO/Al2O3 (0.73), Al2O3/TiO2 (16.5) and TiO2/P2O5 (5.9) ratios are not those of unaltered komatiitic rocks.

In Chapter 7.4.1, it was concluded that shearing had resulted in increased contents of Ti, K, P, Rb, Y and Zr in the Selebi-Phikwe host amphibolite. A highly sheared serpentinous (26.8 wt% MgO) zone at Selebi North has significantly higher Ti, Al, Fe, P, V, Y and Zr and lower Si, Mg, Ca, Na and Cr than the enveloping unsheared ultramafic rocks. It is therefore suggested that much of the geochemical distinctiveness of the ultramafic schists is due to shearing-induced metasomatism, rather than a komatiitic origin. The typical location of the ultramafic schists (and ultramafic amphibolites) at the margins of the ultramafic rocks (Figs 8.9 & 8.10) is further evidence of this. In the top 10 m of the DK 32 section (Fig. 8.9), there is a gradual decrease in Mg and (Cr) and a gradual increase in Ti, Al, Ca, K and (Zr) going upwards from typical amphibole pyroxenite, through ultramafic amphibolite, to ultramafic schist and hornblende schist (Type-F) at the margins. It is suggested that metasomatism and in particular stress-induced diffusion (possibly involving a fluid phase, cf. Sorensen 1967; Sharpe 1979; Pfeifer 1981) at the margins of the ultramafic rocks has resulted in the distinctive geochemistry of the ultramafic schists. A lower degree of metasomatism has modified the geochemistry of the protoliths of the ultramafic amphibolites, some of which probably contained more clinopyroxene than those of the amphibole pyroxenites.

8.6.2 The Protoliths of the Dikoloti Feldspathic Amphibolite

The typical Dikoloti feldspathic amphibolite without corundum-spinel-sapphirine aggregates is characterised by high Al and relatively high Ca and Mg contents which together are reflected in high normative contents of plagioclase (bytownite) and olivine (Table

8.5). The geochemistry suggests an igneous origin for the feldspathic amphibolite as plagioclase-rich olivine gabbro. The low contents of incompatible elements in the feldspathic amphibolite are more closely comparable with those of cumulus gabbros than extrusive basalts (Le Maitre 1976; Coleman 1977). It is concluded that the protolith of the Dikoloti feldspathic amphibolite was a gabbroic plagioclase-olivine cumulate.

The Dikoloti corundum-spinel-sapphirine aggregates present the same problems as to their origin as do the localised occurrence of the corundum-spinel-anorthite assemblage at Selebi (see Ch. 3.9). The Dikoloti feldspathic amphibolite and the spinel-bearing Selebi host amphibolite have similar mineralogies, although simpler retrogression coronas have formed at Selebi. Both appear to have corundum as the earliest preserved phase in the aggregates. The coronas containing spinel, sapphirine and epidote are considered to be M1 and M2 retrogression coronas around an M1p corundum nucleus within a hornblende-anorthite amphibolite. There are also similar changes in geochemistry between between the corundum-spinel-bearing amphibolites and their average host amphibolites (Tables 8.5, 7.1 & 7.2). The corundum-spinel-bearing assemblages are both significantly higher in Al and Sr and lower in Si, Ti, Fe, Na, Cr, V and Zr than their host amphibolites. The volumetrically more important Dikoloti assemblage also has higher K, Rb, S, Cu and Ni and lower Ni than its host amphibolite. It has been concluded that both the Dikoloti feldspathic amphibolite and the Selebi host amphibolite (see Ch. 7.4.3) were originally gabbroic plagioclase-olivine (+ orthopyroxene) cumulates. The origins of the corundum-spinel-bearing aggregates in both lithologies are possibly related.

The aggregates are considered to be either (1) isochemically recrystallised premetamorphic aluminous concentrations in the igneous protolith, (2) metamorphic-metasomatic products (e.g. the restites from partial melting, Droop & Bucher-Nurminen 1984), or (3) the products of a combination of the effects of metasomatism on pre-metamorphic aluminous concentrations. The premetamorhic aluminous concentrations could be aluminous xenoliths (cf. Willemse & Viljoen 1970; Windley et al. 1984), hydrothermally leached veins and patches (cf. Wilson 1971), subaerial weathering products or cumulus plagioclase-rich accumulations. A possible example of the combination of premetamorphic and metamorphic processes is the sapphirine-bearing assemblages of the Fiskenaesset Complex. Metasomatic addition of Si

and K to a suitable high Al-Mg protolith has been suggested (Herd et al. 1969). The high Al-Mg protolith is proposed to have formed by assimilation (Herd 1973) or reaction (Friend & Hughes 1977, 1981) of aluminous ultramafic supracrustal rock with anorthosite magma.

The sole occurrence of the assemblages in completely separate but mineralogically and chemically similar amphibolites suggests a strong bulk chemical control on their formation and a link with the feldspathic cumulate origin of both the Dikoloti feldspathic amphibolite and Selebi host amphibolite that is proposed. Original cumulus labradorite-bytownite would have recrystallised to highly calcic plagioclase during progressive M1 metamorphism. Anorthite melts anhydrously to corundum and liquid at pressures over 9 kbar and temperatures above 1500°C (Hariya & Kennedy 1968; Goldsmith 1980). However at high water pressures the reaction has been found between 9 kbar at 1150°C and 14 kbar at 1025°C (Boettcher 1970) and at 8 kbar and 825°C (Yardley & Blacic 1976). The formation of corundum and sapphirine in the Sittampundi anorthosite intrusion in India by melting of plagioclase at high water pressures has been suggested by Leake et al. (1976). Hariya & Kennedy (1968) and Goldsmith (1980) also found that anorthite exsolves corundum and Al-deficient anorthite at similar high pressures but at temperatures of 350°C below the solidus. The apparent breakdown of the anorthite component of plagioclase to form corundum plus more sodic plagioclase has been noted by Emslie (1983) in coronitic metagabbros from Labrador. Therefore at Dikoloti and Selebi corundum may have formed by exsolution (or partial melting) from calcic plagioclase at the peak of M1 metamorphism at pressures and temperatures above 9kbar and 825°C. A possible metamorphic origin from plagioclase is indicated by the high Al, Ca and Sr of the aggregates. Diffusion and the metasomatic removal of Si, Ti and alkalies would possibly have accompanied the exsolution of corundum from plagioclase. No corundum however has been found in the nearby anorthosites or in anorthosites elsewhere in the Limpopo Belt. The lack of corundum in the anorthosites is possibly due to their anhydrous nature compared to the amphibolites at Dikoloti and Selebi. However it does throw considerable doubt on the hypothesis of exsolved corundum from plagioclase.

There are siliceous sillimanite and cordierite-bearing grey gneisses with approximately 20% Al_2O_3 in the immediately surrounding gneisses at Selebi. However their Si contents would appear to be too high and their Al contents too low to have formed the aggregates.

There are no high-Al gneisses at Dikoloti-Lentswe. Therefore aluminous xenoliths are considered unlikely as precursors for the aggregates. With respect to hydrothermal leaching, sea-floor hydrothermal systems can cause profound alterations involving extreme mobility. Highly aluminous rock compositions may result from these transformations (Hutchinson 1983). Alteration assemblages include Al-rich smectite and chlorite (Velde 1985). Low-high temperature hydrothermal alteration typically results in an increase in Al, Fe, Mg and S and a decrease in Si, Ca and Na (Wilson 1971; Plimer 1979). These changes are similar to those that have taken place in the Dikoloti feldspathic amphibolite. The Dikoloti fedspathic amphibolite suite lies on a line of high Rb-enrichment (K/Rb = 52, Fig. 8.13b). A similar high degree of Rb-enrichment with low K/Rb ratio has taken place in the HGG hornblende gneiss (Fig.4.3b) and has been attributed to preferential adsorption of Rb by smectite formed during submarine alteration prior to regional metamorphism (see Ch. 4.2.1b). The high Rb contents and low K/Rb ratios of the Dikoloti feldspathic amphibolite are possibly due to preferential adsorbtion of Rb by smectite formed during hydrothermal alteration (cf. Dasch 1973; Menzies & Seyfried 1979). It is suggested that the corundum-spinel-sapphirine assemblage at Dikoloti resulted from the metamorphism of veins and patches of hydrothermally altered gabbro. Localised hydrothermal streaming would possibly explain why some sections of Dikoloti fedspathic amphibolite are dominated by corundum-spinel-sapphirine aggregates whereas some sections are unaltered plagioclase-hornblende amphibolite. Hydrothermal alteration also provides the best explanation for the localised molybdenite disseminations in the amphibolite. It is likely that hydrothermal alteration would also have affected the adjacent ultramafic cumulates at Dikoloti but that the metamorphosed results are less obvious. Dikoloti-Lentswe ultramafic rocks have relatively low K/Rb ratios (50-115). It is possible that some of the serpentinites, pleonaste-bearing ultramafic rocks (particularly some of the spinel peridotites with high normative corundum) and ultramafic amphibolites at Dikoloti-Lentswe represent metamorphosed hydrothermally altered ultramafic cumulates. The origin of the Selebi spinel-corundum aggregates is also thought to be localised hydrothermal alteration.

8.6.3 Hornblende Gneiss

The various types (A-H) of Dikoloti-Lentswe hornblende-bearing

rock display significantly different distribution patterns (Figs 8.15 & 8.16) than the common types of hornblende gneiss (HGN, HGG, HGC & HGF) of the Selebi-Phikwe gneiss sequence. This is due mainly to the higher Mg contents and to a lesser extent higher Ti and Fe contents of the Dikoloti-Lentswe hornblende-bearing rocks, compared to HGN-HGF. Ti is generally proportional to Fe (not figured) and Zr (Fig. 8.12b). Al contents of the Dikoloti-Lentswe hornblende-bearing rocks are similar to those of HGN-HGF (Fig. 8.15b). Ca contents are generally similar to the common types of hornblende gneiss, except for Type-C and Type-F (Fig. 8.16b), which are low in Ca. Generally the Ca/Al ratio decreases with increasing K content (not figured). The high-K Type-F has the lowest Ca/Al. Type-A and Type-B plot in the approximate fields of HGN1 and HGF1 respectively and have similar Ti and Zr contents to HGN1 and HGF1. Type-A and Type-B typically occur in the hornblende gneiss-grey gneiss envelope to the ultramafic rocks. It is concluded that they were HGN1 and HGF1 basalts respectively.

When compared to both Type-A (HGN1) and Type-B (HGF1), Type-E has significantly higher Fe and to a lesser extent Mg, and lower Si, Na, (K), Rb and Sr (Table 8.6). Al and Ca are approximately the same. These chemical differences are similar to those between garnetiferous host amphibolite and typical host amphibolite at Selebi-Phikwe (see Ch. 7.4.2). The field relations suggest that Type-E hornblende-bearing rock derived its high Fe-content from the adjacent mineralised ultramafic rocks. It is concluded that Type-E represents HGF1 (and probably HGN1) hornblende gneiss modified by transfer of Fe from the adjacent mineralised ultramafic rocks. The most likely source of the Fe is pyrrhotite. Some mobilisation of sulphur/sulphide from the mineralised ultramafic rocks and massive sulphides into the adjacent hornblende gneiss is indicated by the presence in the hornblende gneiss of disseminated sulphide. It is not known however whether the high Fe content of the Type-E rocks represents mobilisation of pyrrhotite into the hornblende gneiss followed by desulphurisation (e.g. in sulphide-silicate desulphurisation reactions, see Ch. 7.4.2) or whether the majority of the Fe (and lesser Mg) was mobilised from the mineralised ultramafic rocks independently of S. The transfer of the Fe does not appear to have been accompanied by high degrees of shearing. It could have taken place prior to regional metamorphism (e.g. during hydrothermal alteration) or during M1 regional metamorphism.

The geochemistry of Type-F micaceous hornblende-bearing rocks

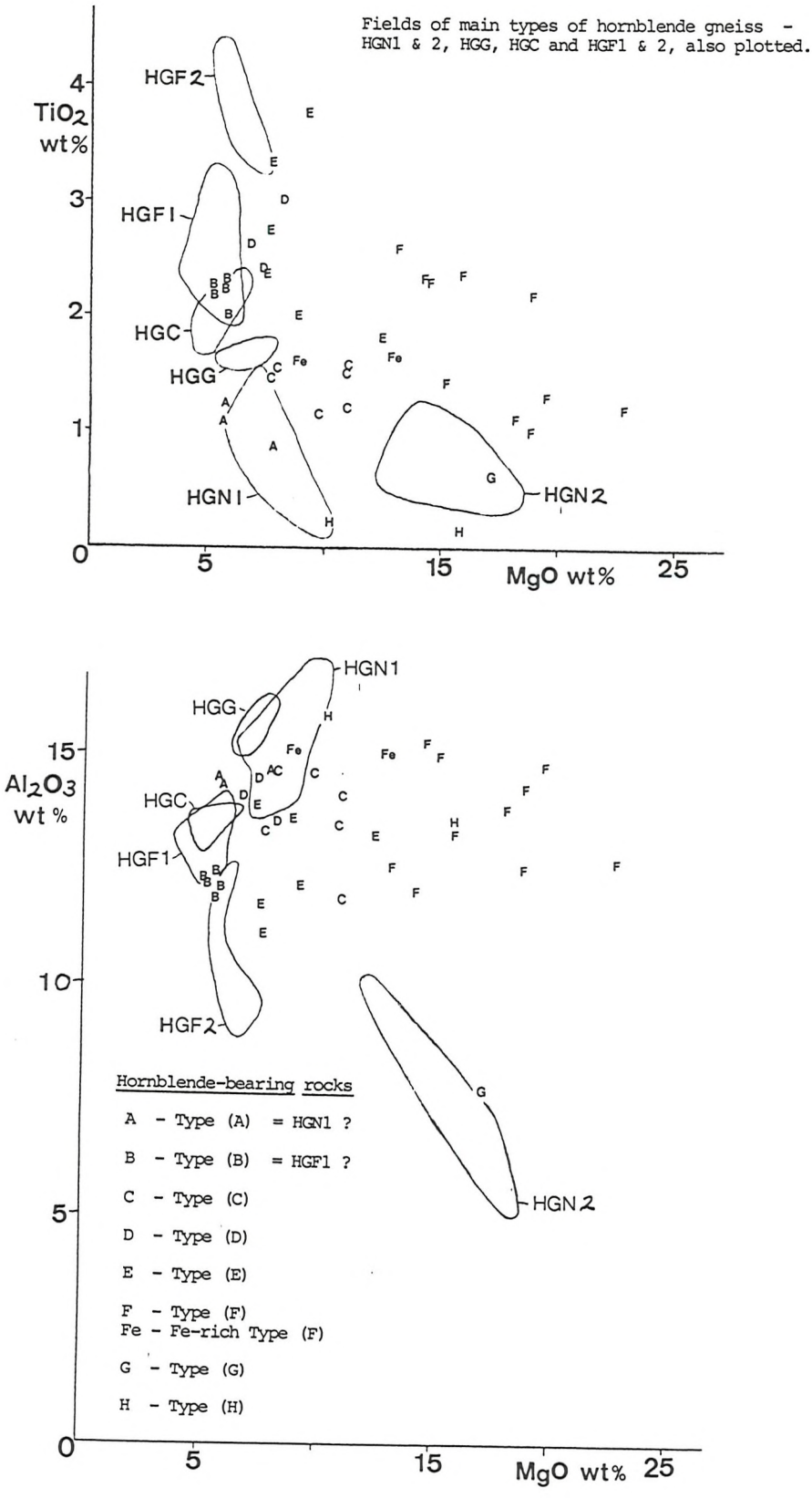

Fig. 8.15 The Dikoloti-Lentswe Host Rocks - hornblende-bearing rocks; Ti, Al and Mg contents.

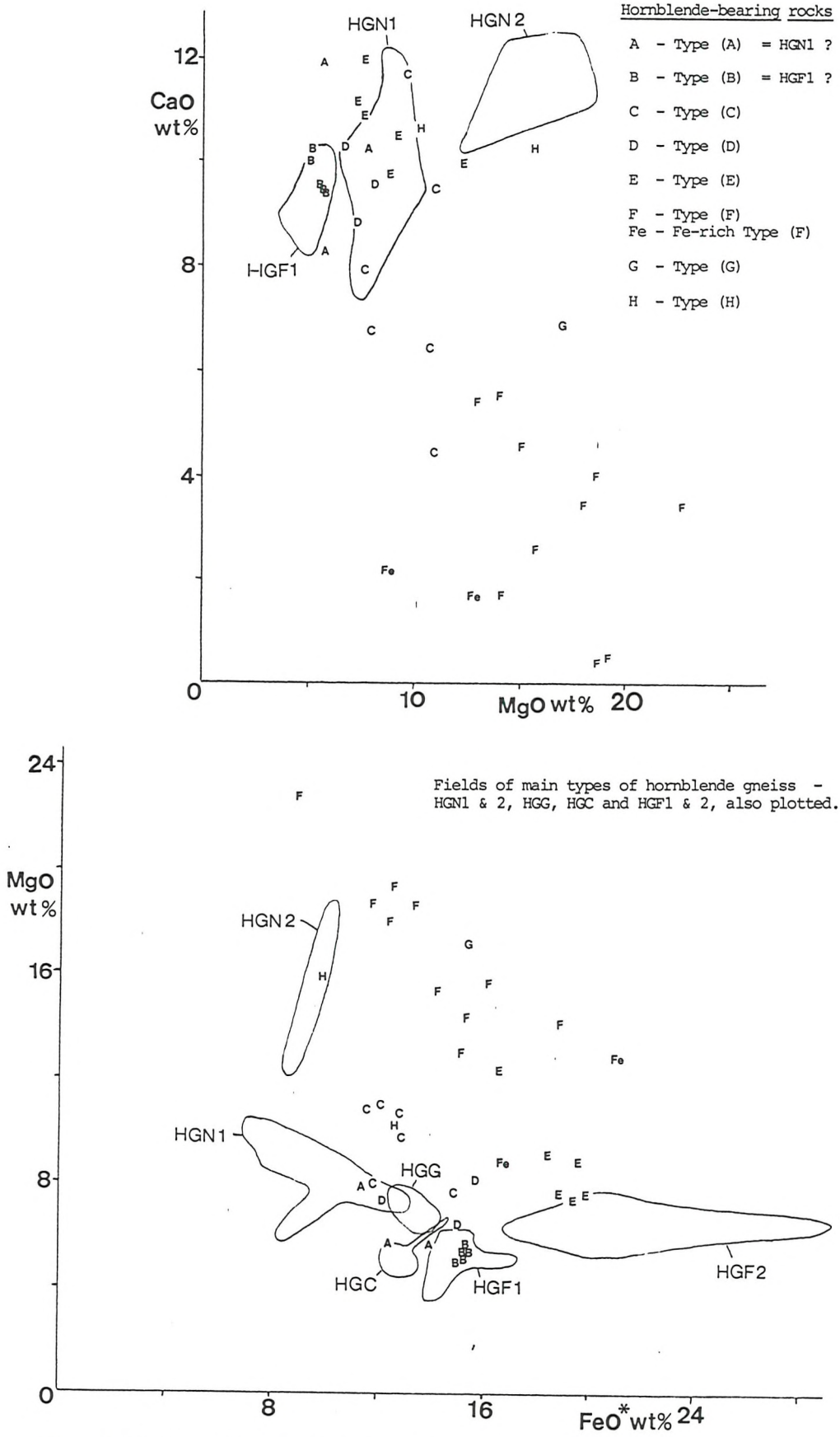

Fig. 8.16 The Dikoloti-Lentswe Host Rocks - hornblende-bearing rocks; Fe, Ca and Mg contents. (* - total Fe as FeO.)

is such (high Ti, Fe, Mg and K and low Ca) that they can not represent unaltered basic-ultrabasic liquid. Their highly sheared nature and their typical occurrence as thin shear-bounded bands within the ultramafic rocks or at their margins suggests that they owe their distinctive geochemistry to shearing. The protoliths of Type-F rock could be typical Type-A & B hornblende-plagioclase gneiss or mineralised ultramafic rock (e.g. amphibole pyroxenite). Despite their high Mg content (average of 15.9 wt% MgO), the presence of phacoids of typical hornblende gneiss within the Type-F bands indicates that the majority are altered hornblende gneiss. There is not a complete geochemical gradation between Type-F rock and ultramafic schist. Although it is not known whether the protoliths were low-Ti Type-A (HGN1) or high-Ti Type-B (HGF1), it can be concluded that shearing has resulted in increased contents of Mg, Fe, K, S, (Cu), Nb, (Ni), Rb, and decresed Ca, Na and Sr in hornblende-plagioclase gneiss. The effect of shearing on the Ti, P, Y and Zr contents can not be directly evaluated. However enrichment in these elements during localised shearing appears to have commonly taken place in the Selebi-Phikwe host amphibolite (see Ch. 7.4.1). The location of the Type-F bands indicates that the source of the Mg, Fe, S, Cu and Ni was the adjacent mineralised ultramafic rocks. The process of their transfer would appear to have been stress-induced diffusion. However some initial tectonic interfingering between Type-F protolith and ultramafic rocks followed by stress-induced diffusion can not be ruled out. The metasomatic formation of the Type-F bands was probably coeval with that of the ultramafic schists.

Type-C and Type-D hornblende gneiss have intermediate compositions between Type-A and Type-F and between Type-B and Type-F rocks respectively (e.g. Ti, Mg, Fe and Ca in Figs 8.15-8.16 and K in Fig. 8.13b). Type-C and Type-D hornblende gneiss typically occur within the ultramafic rocks and at their sheared margins (Figs 8.9 & 8.10). It is therefore tentatively suggested that they respectively represent Type-A and Type-B hornblende gneiss that has been altered by similar processes to those that produced Type-F rock but to a lesser degree.

Type-H hornblende gneiss, characterised by moderately high contents of Al, Fe, Mg and Ca and low contents of Ti, is chemically and mineralogically similar to low-Ti types of HGN1 enriched in cumulus plagioclase and olivine (and orthopyroxene). The low-Ti content of Type-H hornblende gneiss is similar (Fig. 8.12c) to that of

the Dikoloti-Lentswe serpentinised peridotite and amphibole pyroxenite and the Dikoloti feldspathic amphibolite which have been interpreted as cumulus dunites-harzburgites, orthopyroxenites and plagioclase-olivine gabbros respectively. Type-H rock is geochemically similar to the more magnesian samples of the Dikoloti feldspathic amphibolite (Figs 8.11-8.14). The location of Type-H rock only as bands within and at the margin of the ultramafic rocks and not in the hornblende gneiss-grey gneiss envelope strongly indicates that their protoliths were plagioclase-olivine (± orthopyroxene) cumulates and that they are part of the peridotite-pyroxenite-feldspathic amphibolite suite rather than the enveloping hornblende gneiss suite.

Type-G hornblende-cummingtonite amphibolite is a minor component of the Lentswe ultramafic rocks (Fig. 8.10). It is distinguished from the other hornblende-bearing rocks by its low-Al (Fig. 8.15). It is geochemically similar to a high-Fe, low-Ca type of cumulus clinopyroxene-rich HGN2. However Type-G rock can also be described as a low-Mg, high-Fe type of ultramafic schist (Figs 8.11-8.14). The high Cr content of Type-G also indicates that geochemically it is a part of the ultramafic cumulate suite rather than the enveloping hornblende gneiss suite. It is therefore suggested that the Type-G hornblende-rich gneiss is an altered sheared cumulate, possibly originally with a relatively high content of clinopyroxene.

Fe-enrichment is a feature of the Dikoloti-Lentswe host ultramafic rocks and adjacent hornblende gneiss (e.g. the Dikoloti-Lentswe amphibole pyroxenites have higher Fe contents than similar rocks at Selebi North). This Fe-enrichment appears to have been more widespread than at Selebi-Phikwe where significant Fe-enrichment has only taken place in host rocks (garnet amphibolites, see Ch. 7.4.2) with very high contents of disseminated sulphide or at the contacts with massive sulphide. This more widespread Fe-enrichment is regarded as a secondary process rather than a primary igneous feature. It possibly resulted from hydrothermal alteration prior to regional metamorphism. Later shearing resulted in further localised metasomatic alteration (cf. Type-F hornblende gneiss).

8.6.4 The Protoliths of the Mg-amphibolites

The Mg-amphibolites are essentially characterised by high contents of Mg and Fe and low contents of Al and Cr (Table 8.7). There does not appear to be a complete gradation between Ca-poor cummingtonite amphibolite (< 4.6 wt% CaO) and Ca-rich actinolite

amphibolite (9.9-11.5 wt% CaO, Figs 8.13a & 8.14b).

The occurrence of the Mg-rich amphibolites adjacent to the mineralised cumulus ultramafic rocks suggests that they may be related to the latter either as altered olivine-orthopyroxene cumulates (now cummingtonite-rich) and clinopyroxene cumulates (now actinolite-rich) or as metasomatic products. However the association of the Mg-rich amphibolites with magnetite quartzites also suggests that their origin may be linked to that of the magnetite quartzites. The following features are thought to be important in resolving this:

(1) The regional intimate association of the Mg-amphibolite with finely laminated magnetite quartzite. The Dikoloti-Lentswe prospects are somewhat atypical in that cummingtonite-actinolite amphibolite is only a minor component of the unit. Elsewhere ultramafic rocks are a minor component to magnetite quartzite and Mg-amphibolite (dominantly cummingtonite-rich bands up to 5 m thick).

(2) The morphology of the amphibolites which varies from massive thick bands (mainly cummingtonite) with minor amphibole quartzite laminations to finely banded amphibolite-magnetite quartzite (mainly actinolite).

(3) The simple mineralogies (dominantly cummingtonite or actinolite $\pm$ quartz) and textures (granoblastic and unsheared) of the Mg-amphibolites.

(4) The very low Cr contents of the Mg-amphibolites (with the exception of 1 out of 14 samples) which suggest that they can not be directly derived from ultramafic rocks.

(5) The low Al, Ti, K and Rb contents (lower than in the mineralised ultramafic rocks). The Mg-amphibolites appear to have suffered no K-Rb-Ti metasomatism (i.e they have not suffered shearing induced metasomatism). Al appears to have been one of the least mobile elements during shearing and regional metamorphism of Selebi-Phikwe rocks. Therefore it can be concluded that the Mg-amphibolites probably had their low Al contents prior to deformation and metamorphism.

The geochemistry of the Mg-amphibolites, their low Ti, Cr and Al contents and low Mg/Fe ratios, indicates that they can not be unaltered cumulates related to the Dikoloti-Lentswe olivine-orthopyroxene ($\pm$ clinopyroxene) cumulates. As well as a non-ultramafic cumulate origin, the morphology of the Mg-amphibolites and their intimate regional association with magnetite quartzite also suggest that they were not derived from the hydrothermal alteration of a

suitable protolith by the leaching of SiO2 and introduction of Mg and Fe from adjacent ultramafic cumulates undergoing serpentinisation and talc-carbonate alteration (cf. Robinson & Hutchinson 1982). The moderate degree of metasomatism locally shown by the Dikoloti-Lentswe mineralised ultramafic amphibolites and schists is typically associated with shearing particularly at the margins of the mineralised ultramafic rocks which has resulted in variably higher contents of Ti, (Al), K, Ca, Rb, Nb, Y and Zr and lower Mg, Mg/Fe and (Cr). The low Ti, Al, K, Rb and Cr contents of the Mg-amphibolites are distinctively different to the moderately metasomatised ultramafic rocks at Dikoloti-Lentswe. It is thought that the origin of the Mg-amphibolites is related to that of the magnetite quartzites, interpreted as chemical sediments (see Ch. 4.5), rather than to that of the mineralised ultramafic cumulates. Possible protoliths of the Mg-amphibolites are thought to be:

(1) premetamorphically altered ultramafic rocks, not directly related to the mineralised ultramafic cumulates, e.g. komatiitic extrusives,
(2) Mg-rich detrital sediment derived from mafic-ultramafic rocks, or
(3) Mg-rich chemical sediment.

The association of the Mg-amphibolites with magnetite quartzite suggest that they might be komatiitic extrusives. However the amphibolites do not have the chemistry of unaltered basaltic or peridotitic komatiite (extrusives or cumulates) (Nesbitt et al. 1979). It is possible that the amphibolites were derived by a variety of alteration processes (e.g. weathering, serpentinisation or talc-carbonate alteration) from olivine-orthopyroxene-rich rocks (now cummingtonite-rich) and clinopyroxene-rich rocks (now actinolite-rich). For example the in situ products of the saprolitic weathering of ultramafic rocks are typically depleted in Ca and Mg and enriched in Fe (Golightly 1981). Si-Mg-Fe gels with negligible Al, Ca and K, that are locally produced (along with saponite, talc and nontronite) during saprolitic weathering, are chemically similar to the cummingtonite amphibolites (Fontanaud & Meunier 1983; Velde 1985). However saprolitically weathered ultramafic rocks are not homogeneously altered and are typically enriched in residual Al and Cr (Golightly 1981; Velde 1985). The massive cummingtonite amphibolites are homogeneous and have low Al and Cr contents. Serpentinites also have high, typically ultramafic, Cr contents (e.g. serpentinites from

the Mid-Atlantic Ridge, Miyashiro et al. 1969). Talc-carbonate alteration possibly results in a moderate decrease in Cr contents. For example talc-carbonate schists derived from komatiitic extrusives in the Murchison greenstone belt have reduced Cr contents (1700-2100 ppm Cr) and higher Ni/Cr ratios than less altered komatiites (Pearton 1978; Viljoen et al. 1978). Also carbonate-chlorite alteration of tholeiites (with c. 5.8 wt% MgO) in the Barberton greenstone belt (Condie et al. 1977) has resulted in significant loss of Cr. However the average Cr content (92 ppm Cr) of the carbonated tholeiites are higher than the average of the Mg-amphibolites. It is thought unlikely that any alteration process would reduce the Cr content of ultramafic rocks to less than 201 ppm Cr (average of 59 ppm Cr and locally as low as 10 ppm). It is therefore concluded that the low Cr contents of the Mg-amphibolites can not be the result of in situ alteration of ultramafic rocks and that the Mg-amphibolites do not represent in situ altered ultramafic rocks.

Similarly detrital sediments derived from the weathering of ultramafic rocks have higher Cr contents than the Mg-amphibolites, for example the serpentinous tuffs (16-17 wt% MgO, 8-10 wt% Al_2O_3, 5-7 wt% CaO and 1500-2200 ppm Cr) of the Proterozoic Nussir Group in Norway (Pharaoh 1985) and magnesiopelites (10-13 wt% MgO, 14 wt% Al_2O_3, <0.3 wt% CaO and 330 ppm Cr) from the Murchison greenstone belt (Pearton 1978, 1982).

The finely laminated magnetite quartzites with which the Mg-amphibolites are associated have been interpreted as silica-iron oxide chemical sediments (see Ch. 4.5). This raises the possibility that the Mg-amphibolites may have a similar origin. Cummingtonite and actinolite may form by dehydration and decarbonation reactions in silicate and carbonate-facies iron formations undergoing moderate to high-grade metamorphism (Klein 1973). Silicate-facies iron formations are typically low in Al and contain greenalite, minnesotaite (an Fe-rich talc) and stilpnomelane as original sedimentary, diagenetic or very low-grade metamorphic silicate phases (Klein 1973). Higher grades of metamorphism can result in the formation of cummingtonite-grunerite amphibole. Calcic amphibole (tremolite-actinolite) can form by decarbonation and dehydration in metamorphosed carbonate-facies iron formations (and in mixed carbonate-oxide-silicate assemblages) originally containing calcite, members of the dolomite-ankerite series or siderite.

Examples of simplified possible reactions (Klein 1973) are:

$$\underset{\text{greenalite}}{(Fe,Mg)_6Si_4O_{10}(OH)_8} + 4SiO_2 = 2\underset{\text{minnesotaite}}{(Fe,Mg)_3Si_4O_{10}(OH)_2} + 2H_2O$$

$$\underset{\text{minnesotaite}}{(Fe,Mg)_3Si_4O_{10}(OH)_2} = \underset{\text{cummingtonite-grunerite}}{(Fe,Mg)_7Si_8O_{22}(OH)_2} + 4SiO_2 + 4H_2O$$

$$\underset{\text{minnesotaite}}{(Fe,Mg)_3Si_4O_{10}(OH)_2} + \underset{\text{ankerite}}{Ca(Fe,Mg)(CO_3)_2} + SiO_2 = \underset{\text{cummingtonite}}{(Fe,Mg)_7Si_8O_{22}(OH)_2}$$

$$+ \underset{\text{actinolite}}{Ca_2(Fe,Mg)_5Si_8O_{22}(OH)_2} + CO_2 + H_2O$$

Carbonate-facies iron formation that has been metamorphosed to medium or high grade is generally decarbonated relative to less metamorphosed iron formation (Gole & Klein 1981). It is possible that the protolith of the actinolite amphibolite contained carbonate (in order to provide the Ca) and that carbonate has been lost in decarbonation reactions. The increase in Mg/Fe ratio with increasing Ca content in the cummingtonite-actinolite amphibolites suggests that if carbonate were originally present, it was probably dolomite or Mg-rich ankerite. However no carbonate has been observed in the amphibolites. Although high-grade iron formation from the carbonate-bearing Archaean Weld Range in the Yilgarn Block (W.A.) with up to 8 wt% CaO and less than 1 wt% Al2O3 have negligible carbonate contents and appear to have suffered high degrees of decarbonation (Gole 1981), the complete absence of carbonate from the Dikoloti-Lentswe amphibolites remains a problem for the decarbonation hypothesis.

Geochemically the most analogous iron formation to the Dikoloti-Lentswe Mg-amphibolites is the Archaean silicate and carbonate-facies iron formation of Isua, Greenland (Appel 1980). The carbonate facies includes massive Mg-rich siderite (with 10-32% MgO). The silicate facies includes banded magnetite-grunerite-quartz and magnetite-actinolite-quartz and massive grunerite amphibolites. The Mg/Fe ratio of the Isua carbonate and silicate-facies iron formation is typically less than 0.43 (with the exception of localised Mg-rich siderite).

The Mg-amphibolites have morphological and some geochemical (their low Al and relatively high Mn contents, cf. Rona 1978) similarities to metamorphosed silicate and carbonate-facies iron

formation. However they differ in their high MgO/Fe2O3 ratios (>1, total Fe as Fe2O3, Fig. 8.11b). High-Mg iron formations with up to 10 wt% MgO are Fe-rich (MgO/Fe2O3 <0.53) and are typically carbonate facies (Klein 1978; Ewers & Morris 1981; Gole 1981). The Mg-amphibolites just fall outside the definition of iron formation of James (1954) in that they contain less than 15% Fe. They appear to be an Mg-rich version of iron formation.

A possible Mg-rich analogue of the Mg-amphibolites are the Mg-rich, Al-poor chemical sediments that occur in modern oceanic sediments. Although attention has been concentrated on the transition metal sulphides of modern exhalative chemical sediments of the deep-sea floor (Hackett & Bischoff 1973; Hekinian et al. 1980), they also contain a wide variety of exhalative silicates including celadonite (an illite), nontronite (a smectite) and talc. Remarkable among these silicates is the common lack of an Al-bearing phase (Velde 1985). Neoformed talc in hydrothermal aprons has been observed by Spies et al. (1980) in hydrothermal sediment of the East Pacific Rise and by Lonsdale et al. (1980) around sea-floor vents in the Guayamas Basin spreading centre in the Gulf of California. The latter talc deposit is extensive and particularly Fe-rich (51 wt% SiO2, 0.7 wt% Al2O3, 17 wt% total Fe as Fe2O3, 21 wt% MgO and neglible CaO; i.e. very similar to the cummingtonite amphibolite). The talc deposit has been interpreted as a chemical sediment in a turbidite-filled pond at the spreading centre axis, formed from short-lived expulsions of water, perhaps partly as steam, following emplacement of shallow basaltic intrusions. Magnesium silicate was precipitated either from hot, reducing porewater on rapid cooling and mixing as it vented into bottom water or alternatively Mg was derived form the bottom water in the basin and was precipitated as this seawater reacted with siliceous and ferruginous discharges (Lonsdale et al. 1980).

A similar origin by chemical sedimentation of Mg-silicate is thought the most likely for the cummingtonite amphibolite, with Mg derived from leaching of mafic-ultramafic rocks (possibly the Dikoloti -Lentswe gabbroic and ultramafic cumulates) or seawater. Mg is the most important element extracted from seawaterin the Galapagos hydrothermal systems. Natland et al. (1979) show that during the early stages of the Galapagos systems, when the ratio of rock to water was high (rock-dominated), Mg-Fe silicates were deposited over exhalative vents. Fe-Mn oxides have become more abundant in its more recent water-dominated phase. The chemistry of Archaean seawater is problem-

atic. Krynine (1960) and Ronov (1964) have estimated that Archaean seawater was more magnesian than at present. It is therefore feasible that Archaean seawater exchange could have formed the cummingtonite-actinolite amphibolites.

No single hypothesis completely explains all the features of the Mg-amphibolites. Their association with magnetite quartzite, their morphology and their geochemistry (particularly the low-Cr contents) suggest that they were not directly derived from mafic-ultramafic igneous rocks. The most likely protoliths are thought to be chemically precipitated exhalative Mg-silicate (e.g. Fe-rich talc) and mixtures of this Mg-silicate with carbonate (dolomite or Mg-ankerite) that have suffered complete decarbonation (cf. Hutchinson et al. 1980; Hutchinson 1983). The main detraction from this hypothesis is the absence of carbonate in the unit.

The hornblende-bearing amphibolite which forms a minor component of the Mg-amphibolites have higher Ti, Al and Cr contents than the cummingtonite-actinolite amphibolites. It is suggested that it was formed by input of mafic-ultramafic volcanic detritus into the depositional basin of the Mg-rich chemical sediments (cf. Gole 1981). Similarly a mafic-ultramafic detrital component is thought responsible for the geochemistry of the only cummingtonite amphibolite with significant Cr (1320 ppm Cr, Table 8.7-C). It also has the highest Ti, Al and Na and lowest Mn of the cummingtonite amphibolites.

8.6.5 The K/Rb Ratios of the Rocks of the Selebi-Phikwe Area

Rocks in the Selebi-Phikwe area with basic-ultrabasic protoliths have relatively high K and Rb contents but low K/Rb ratios compared to unaltered, unmetamorphosed rocks of approximately the same composition (Condie 1976). K and particularly Rb has commonly been added during alteration. The highest K/Rb ratios of mafic-ultramafic rocks ar Selebi-Phikwe occur in high-Ca hornblende gneisses of the tpes - HGF1 (average K/Rb = 588), HGF2 (566) and HGN2 (446). These are regarded as having been only weakly altered, unsheared tholeiitic rocks for which an intrusive origin is more likely. The majority of the metamorphosed basic-ultrabasic rocks have K/Rb ratios of less than 300, e.g. HGN1 (234) and HGC (253). The lowest K/Rb ratios are thought to have resulted from premetamorphic alteration possibly involving a clay component (smectite), e.g. submarine alteration of the HGG basalts and hydrothermal alteration of the plagioclase-olivine cumulates at Dikoloti. Alteration during regional metamorphism has

resulted in increased K and Rb contents but with higher K/Rb ratios than alteration thought to involve a clay component. Shearing (commonly repeated) has resulted in significant enrichment in K and Rb. However for each group of spatially associated lithologies, sheared rocks have a relatively constant K/Rb ratio, e.g 189 for the Selebi-Phikwe host rocks (Fig. 7.13) and 113 for Dikoloti-Lentswe host rocks (Fig. 8.13b). It would appear that the K/Rb ratios of previously altered rocks (independent of whether the alteration was prior to or during regional metamorphism) have not been changed by shearing (see Fig. 8.13b).

8.6.6 The Original Nature of the Dikoloti-Lentswe Cumulate Body

The protoliths of the Dikoloti-Lentswe mineralised ultramafic rocks were olivine-orthopyroxene (± clinopyroxene) cumulates. The ultramafic schists and to a lesser extent the ultramafic amphibolites represent ultramafic cumulates that have been moderately metasomatised during shearing. The ultramafic cumulates have also possibly suffered hydrothermal alteration. The protolith of the Dikoloti feldspathic amphibolite was a plagioclase-olivine cumulate. This plagioclase-rich cumulate is thought to have been part of the same body as the mineralised ultramafic cumulates at Dikoloti. It is not known whether the Dikoloti and Lentswe bodies represent a single original body or several similar bodies. The widespread occurrence of ultramafic cumulates in the regional Dikoloti-Lentswe unit suggests that there was probably more than one body. The hornblende gneisses of the hornblende gneiss-grey gneiss envelope are regarded as HGN1 (Type-A) and HGF1 (Type-B) basalts that have suffered various types of alteration including Fe-enrichment (Type-E) and shearing-induced metasomatism (Type-F). Type-F hornblende gneiss typically occurs as thin sheared bands at the margins of, and incorporated within, the ultramafic rocks.

The Dikoloti-Lentswe cumulates are thought to represent portions of either (a) a high-level layered sill or layered flow (cf. Arndt 1977), (b) intrusive cumulus mushes (cf. Selebi-Phikwe host rocks), or (c) a slice of a thicker deeper-level cumulus crystal pile.

The relatively high-level nature of the cumulate bodies is indicated by the hydrothermal alteration that has apparently affected the cumulates (e.g. that suffered by the plagioclase-olivine protolith of the corundum-spinel-sapphirine-bearing Dikoloti feldspathic amphibolite). If the Dikoloti-Lentswe bodies represent cumulus

portions of a basic-ultrabasic intrusion (or intrusions) into the Dikoloti-Lentswe unit, virtually all of the evolved liquid must have been expelled from the system (cf. MacRae 1969). The lack of significant clinopyroxene in the cumulates suggests that they do not represent the cumulus minerals from the complete in situ crystallisation of basic-ultrabasic magma (irrespective of whether the magma was komatiitic or tholeiitic). The lack of a gabbroic feldspathic amphibolite at Lentswe could be due to the removal of partly crystallised cumulus plagioclase-rich liquid. The repetition of the olivine-rich and orthopyroxene-rich bands suggests that the system was open to periodic replenishment. The hornblende gneiss of the hornblende gneiss-grey gneiss envelope are predominantly evolved HGF1-type basalts plus lesser HGN1-type basalts. It is possible that they were comagmatic with the cumulates and also that they represent the expelled residual liquids. However the hornblende gneiss in the envelope is intimately associated with minor grey gneiss on all scales and does not appear to be directly related to the cumulates in terms of field relationships. The hornblende gneiss bands within the ultramafic rocks are thought to be slivers of the hornblende gneiss envelope that have been incorporated into the ultramafic rocks and metasomatised during shearing. It is therefore thought that the hornblende gneiss does not represent expelled evolved basaltic liquid that was directly related to the in situ formation of the cumulates. The absence of residual liquids from the cumulate crystallisation suggests that the Dikoloti-Lentswe cumulates could be a tectonically emplaced portion of a thicker cumulus crystal pile rather than a tholeiitic intrusion (that differentiated after intrusion) into the Dikoloti-Lentswe unit.

Tectonic emplacement during late D1 has been suggested for the plagioclase-clinopyroxene cumulates of the thicker anorthosite-metagabbro suite. The Dikoloti-Lentswe rocks show abundant signs of shearing particularly at their margins. Sulphides have been mobilised during shearing. The localised concentration of massive sulphide with only minor ultramafic rock indicates significant relative movement during shearing. The lack of plagioclase-rich cumulates at Lentswe could therefore be due to tectonic dismemberment of a cumulate body rather than an original igneous process. Against significant translation of the Dikoloti-Lentswe cumulates during tectonic emplacement however is the regional nature (Fig. 8.1) of the ultramafic portion of the cumulates (relatively thin compared to the

major anorthosite-metagabbro layers). Further evidence is provided by the very low Ti contents (see below in Ch. 8.6.6) of the cumulates which suggests low intercumulus liquid contents and high degrees of crystal packing (also the minimum Al content of the ultramafic cumulates). The low intercumulus liquid contents also indicate that the cumulates were probably not intruded as cumulus mushes (cf. the Ti contents of Selebi-Phikwe host rocks interpreted as intrusive mushes, see Ch. 7.4.3).

It is tentatively suggested that the Dikoloti-Lentswe cumulate bodies (or body) owe their present morphology and field relationships to tectonic emplacement and dismemberment. It is thought that the cumulate bodies were emplaced as either (a) tectonic slices of a cumulate (olivine-rich, orthopyroxene-rich and plagioclase-olivine cumulates) pile, or (b) high-level layered sills intruded into the tholeiitic basalts and chemical sediments of the Dikoloti-Lentswe unit (separate cumulate portions formed by a combination of igneous and tectonic processes). The Dikoloti-Lentswe cumulates have features that indicate both modes of emplacement. The relatively high-level nature of the Dikoloti-Lentswe cumulate bodies compared to the thicker anorthosite-metagabbro layers is indicated by the hydrothermal alteration that the former have apparently suffered.

8.6.7 The Parent Magma of the Dikoloti-Lentswe Cumulates

The cumulus nature of the Dikoloti-Lentswe host rocks and their highly sheared possibly dismembered nature means that it is very difficult to determine whether the parent magma was komatiitic or tholeiitic. The association of ultramafic rocks with magnetite quartzite led Brown (1981b) to suggest that they were possibly komatiitic extrusives. However it has been shown that there is no direct association with the magnetite quartzites.

The range of compositions of the Dikoloti-Lentse host rocks (metamorphosed cumulates) in terms of Mg and Al similar to that of the Selebi-Phikwe host rocks (Figs 7.9 & 8.11). Although metasomatism of the ultramafic rocks (e.g. the general Fe-enrichment) has altered the compositon of some of the ultramafic rocks, the compositions of the Dikoloti-Lentswe cumulates appears to have been controlled by the same phases as the Selebi-Phikwe host rocks. The controlling phases had approximately the same compositions at Dikoloti-Lentswe and Selebi-Phikwe, i.e plagioclase (bytownite), olivine (chrysolite) and othopyroxene (bronzite). Clinopyroxene was only a minor component.

The ultramafic cumulates lie on a mixing line with low-Ti tholeiitic liquid of the composition of HGN1 (Fig. 8.12c). The Cu/(Cu+Ni) ratios of the sulphides also suggest a tholeiitic rather than high-Mg komatiitic parent magma (Fig. 8.8). The Dikoloti-Lentswe cumulates are therefore thought to be tholeiitic cumulates from HGN1-type tholeiitic basalt magma. A similar origin from HGN1 was concluded for the Selebi-Phikwe host rocks.

The Selebi-Phikwe host rocks are thought to be intrusions of tholeiitic olivine-plagioclase (± orthopyroxene)-immiscible sulphide mush. They have significantly higher Ti contents than the Dikoloti-Lentswe host rocks (Figs 7.11 & 8.12c). The high Ti content of the Selebi-Phikwe host rocks are due to the high contents (39-64 wt%, Table 7.4) of tholeiitic intercumulus liquid in the intrusive mushes, whereas the low Ti content of the Dikoloti-Lentswe cumulates indicate low intercumulus liquid contents. The low Ti contents of the Dikoloti-Lentswe ultramafic cumulates and the common minimum Al content of 2.5 wt% Al_2O_3 are consistent with a low content of tholeiitic HGN1 intercumulus liquid. The average amount of intercumulus liquid in the ultramafic cumulates is estimated as having been about 27% with a common minimum of about 17%. The intercumulus liquid content of the cumulus plagioclase-olivine protolith of the Dikoloti feldspathic amphibolite was possibly lower than that of the ultramafic rocks (average 15 %, minimum <1%). However the low Ti contents of the Dikoloti feldspathic amphibolite are possibly partly due to the hydrothermal alteration. The estimates of the intercumulus liquid contents of the Dikoloti-Lentswe cumulates are similar to the estimates (some based on packing experiments) of the porosity of a cumulus crystal pile (Cox et al. 1979).

It is tentatively suggested that the cumulus host rocks of the Selebi-Phikwe ore bodies and the Dikoloti-Lentswe prospects both formed from differentiating HGN1 tholeiitic basalt magma. The Selebi-Phikwe host rocks are intrusive mushes. The Dikoloti-Lentswe host rocks show features that are consistent with an origin as dismembered layered sills or portions of a cumulate crystal pile which have been thrust into the sequence.

8.6.8 The Origin of the Dikoloti-Lentswe Sulphides

In Chapter 8.4.2 it was concluded that the Dikoloti-Lentswe sulphides were present in their ultramafic host rocks prior to deformation and metamorphism. The virtual restriction of the sulphides

to the ultramafic host rocks suggests a magmatic origin for the sulphides rather than an origin by replacement (cf. Gallon 1986). The possibility exists that the hydrothermal alteration that the host rocks are thought to have suffered played a part in the distribution of the suphides. The Cu/(Cu+Ni) ratios of the Dikoloti-Lentswe sulphides are in general agreement with a magmatic origin from a tholeiitic parent magma rather than a high-Mg komatiitic magma (Wilson et al. 1969; Rajamani & Naldrett 1978; Fig. 8.8). The relatively high proportion of sulphides compared to ultramafic host rocks and the proposed tholeiitic cumulate origin of the ultramafic host rocks exclude the possibility of in situ separation of immiscible sulphide liquid from within the ultramafic rocks alone. The Dikoloti-Lentswe sulphides are thought to have originally formed as magmatic immiscible sulphide liquids in tholeiitic magma. The immiscible sulphides accumulated by gravity along with the formation of the olivine-orthopyroxene cumulates. There are no sulphur-rich country rocks in the Selebi-Phikwe gneisses and there is no evidence that the Dikoloti-Lentswe prospects obtained their sulphur by assimilation of country-rock sulphur. As with the formation of the Selebi-Phikwe ore bodies, the Dikoloti-Lentswe prospects are thought to be concentrations of magmatic sulphur. A process is required however to achieve the sulphur saturation necessary to form a magmatic sulphide deposit.

The Cu/(Cu+Ni) ratios of the Dikoloti and Lentswe prospects (0.42 and 0.44 respectively) are similar to that of Phikwe (Fig. 8.8). However these ratios are made up of a variety of components, thin moderately to weakly mobilised massive and semimassive sulphides in the ultramafic host rocks (average ratio - 0.28), highly mobilised massive sulphides (0.46) and relatively unmobilised disseminated sulphides (0.48). The Ni and Cu contents and Cu/(Cu+Ni) ratios of the relatively unmobilised massive and disseminated sulphides in the ultramafic host rocks are considered to be the best estimates (Table 8.3) of original massive and disseminated sulphides within the ultramafic cumulates.

For the same reasons that were put forward to account for the difference in Cu/(Cu+Ni) ratio between Type 1 massive sulphide and disseminated sulphide at Selebi-Phikwe (see Ch.7.4.5), the difference in the Cu/(Cu+Ni) ratios of typical massive and disseminated sulphide at Dikoloti-Lentswe is tentatively regarded as indicating that the Dikoloti-Lentswe disseminated sulphides were immiscible sulphides that separated from their parent magma after the majority of the

gravitationally concentrated immiscible sulphides that formed the massive sulphides had separated. The alternatives are that the difference is due to fractional crystallisation of an original immiscible sulphide liquid or tectono-metamorphic processes. The lower Cu and Ni contents of the Dikoloti-Lentswe sulphides compared to those at Selebi-Phikwe make the formation of a Cu-enriched liquid during the fractional crystallisation of an immiscible sulphide liquid even less likely (Fig. 6.5e).

Although mobilisation of massive sulphide has partly destroyed the original distribution of the massive and disseminated sulphides, the general occurrence of massive and disseminated sulphides at Dikoloti-Lentswe would appear to be consistent with original gravitational accumulation of earlier immiscible sulphides as massive sulphides towards the base of a subsequently overturned ultramafic cumulate body. Later immiscible sulphides formed more disseminated sulphides within the ultramafic cumulates above the massive sulphides.

8.6.9 The Relationship of the Dikoloti-Lentswe sulphides to those at Phikwe

Normal massive sulphide at Dikoloti-Lentswe differs from morphologically equivalent Selebi-Phikwe Type 1 sulphide in its lower Ni and Cu contents and lower Cu/(Cu+Ni) ratio (Tables 6.3 & 8.3). Although mobilised massive sulphides may have increased Ni and Cu contents (e.g. Type 2 massive sulphide at Selebi-Phikwe), the differences between Dikoloti-Lentswe and Selebi-Phikwe sulphides are significant and are considered to be an original feature. It has been concluded that both the Selebi-Phikwe and Dikoloti-Lentswe host rocks could have formed in tholeiitic magma systems with the approximate magmatic composition of HGN1. In the modelling of a closed tholeiitic system crystallising olivine without magma replenishment (Duke & Naldrett 1978; Rajamani & Naldrett 1978; Duke 1979; Fig. 8.8), early formed immiscible sulphides have higher Ni and Cu contents and lower Cu/(Cu+Ni) ratios than immiscible sulphides that separate later. However Selebi-Phikwe massive sulphides (and disseminated sulphides) have higher Ni and Cu contents and higher Cu/(Cu+Ni) ratios than texturally equivalent Dikoloti-Lentswe sulphides (Figs 7.15 & 8.8). Assuming that the two parent magmas did not have appreciably different major element compositons, it is not possible to model in terms of closed magmatic systems the formation of the Selebi-Phikwe and Dikoloti-Lentswe sulphides as different extracts of immiscible

sulphide liquid from similar differentiating HGN1 magma with initially similar Ni, Cu and S contents.

The difference in the Ni and Cu contents and Cu/(Cu+Ni) ratios between Selebi-Phikwe and Dikoloti-Lentswe sulphides could be because of:

(a) original differences in the Ni, Cu and S contents of the two parent HGN1 magmas; or

(b) processes in two open HGN1 magma systems (with initially similar magmatic Ni, Cu and S contents) which resulted in different Ni, Cu and S contents of the two parent magmas.

If case (a) is correct, the Dikoloti-Lentswe parent HGN1 magma would have had lower Ni and Cu contents and a lower Cu/(Cu+Ni) ratio or a lower magma/immiscible sulphide ratio than the Selebi-Phikwe parent HGN1 magma. A lower magma/immiscible sulphide ratio would cause lower Ni and Cu contents and a lower Cu/(Cu+Ni) ratio of the immiscible sulphides (Campbell & Naldrett 1979). The two parent magmas could have been derived by separate partial melting events from approximately the same level or location in the mantle, as suggested by Marsh 1978. (The lower Ni and Cu contents of the Dikoloti-Lentswe parent magma could have been due to previous extraction of the Selebi-Phikwe parent magma).

The relatively low Ni and Cu contents of the Selebi-Phikwe and particularly the Dikoloti-Lentswe sulphides compared to the main types of magmatic Ni-Cu sulphide deposit (Fig. 1.4) suggest that both parent magmas had relatively low Ni and Cu contents and/or low magma/immiscible sulphide ratios (63 for Selebi-Phikwe and 16 for Dikoloti-Lentswe; see Campbell & Naldrett, 1979). The estimates of the magma/immiscible sulphide ratios, particularly that for Dikoloti-Lentswe, are very low compared to those for other Ni-Cu sulphide deposits (Naldrett 1981). For the Ni-Cu sulphide deposits with low estimated magma/immiscible sulphide ratios, assimilation of country-rock sulphur has been invoked (Campbell & Naldrett 1979). However at Selebi-Phikwe and Dikoloti-Lentswe there is no evidence for assimilation of country-rock sulphur.

With regard to case (b), namely processes in open magmatic systems, it was suggested in Chapter 4.2.5 that the enrichment of incompatible elements in a tholeiitic basalt magma and the formation of Ti-rich ferrobasalt could take place in a differentiating tholeiitic magma system that is open at the top to lava extrusion and at the base to periodic replenishment with tholeiitic magma. The

steeper gradient of MgO content against Cu/(Cu+Ni) ratio (Fig. 8.8) for the Selebi-Phikwe hornblende gneiss suite compared to the closed system experiments of Rajamani and Naldrett (1978) and the sequential increase in S contents in the evolved suite (Table 8.8) is considered to possibly be the result of processes in such an open system. It is thought that enrichment in magmatic S and an increase in the magmatic Cu/(Cu+Ni) ratio could take place in an open tholeiitic magma system provided that (a) olivine is a crystallising phase, and (b) the initial S content of the basalt magma is low (i.e. below saturation levels), so that significant separation of immiscible sulphide does not initially take place prior to replenishment. The rate of increase in the Cu/(Cu+Ni) ratio of the magma would depend on the amount of cumulus olivine that crystallises before replenishment. If the initial S content of the magma is below saturation levels, early cumulate formation followed by replenishment would result in increasing S contents in the magma. Higher Fe contents of the evolving tholeiitic magma would result in an increased sulphur-carrying capacity of the magma (Buchanan & Nolan 1979; Buchanan et al. 1981; Buchanan & Rouse 1984). Eventually sulphur saturation would be achieved and immiscible sulphide liquid would form. Mixing of evolved S-enriched Fe-rich basalt with a new batch of parent basalt would possibly cause rapid immiscible sulphide formation and result locally in low magma/immiscible sulphide ratios.

It is suggested that HGN1-type tholeiitic magma satisfies the two conditions above for the parent magma. HGN1 has a low S content (average of 247 ppm S) and a low Cu/(Cu+Ni) ratio (0.19, Table 8.8). Greater than 10% crystallisation of HGN1 would be dominated by plagioclase and lesser clinopyroxene rather than olivine (see Ch. 4.2.5). The Cu/(Cu+Ni) ratio of HGN1 (0.19) is consistent with the relatively early separation (compared to Selebi-Phikwe massive sulphides) of the Dikoloti-Lentswe low-Ni-Cu massive sulphides (average ratio - 0.28) from an evolving periodically replenished HGN1 magma.

That identical sulphides did not develop in the Dikoloti-Lentswe and Selebi-Phikwe magma systems is because the two systems were not identical. They probably differed in the size of the magma chamber and frequency and amount of replenishment (O'Hara 1977). The Selebi-Phikwe magma system was possibly a more open system than the Dikoloti-Lentswe system and possibly had a longer evolutionary history, more frequent replenishments and only limited formation of

	HGN1	HGG	HGC	HGF1
S	247	338	912	1560
Ni	124	114	93	63
Cu	30	46	187	94
Cu/(Cu+Ni)	0.19	0.29	0.67	0.60

Table 8.8 The S, Ni and Cu contents (ppm) of the Selebi-Phikwe hornblende gneiss suite (from Table 4.1).

early immiscible sulphides.

It has been suggested that the difference in the Ni and Cu contents and Cu/(Cu+Ni) ratios between the Dikoloti-Lentswe and Selebi-Phikwe sulphides can be explained in terms of either (a) differences in the original Ni, Cu and S contents of the two parent HGN1 magmas, or (b) various degrees of crystallisation and replenishment in open evolving HGN1 magmatic systems with initially similar Ni, Cu and S contents. Of the two options, the latter is preferred because (a) it provides a mechanism for achieving sulphur saturation and low magma/sulphide ratios, and (b) it is consistent with the evolution of the country rock basalts (the high-Ca hornblende gneisses).

8.7 SUMMARY OF CONCLUSIONS

The Dikoloti-Lentswe unit is a regionally mappable unit of magnetite quartzite associated with cummingtonite and actinolite amphibolite (Mg-amphibolite), hornblende gneiss with minor grey gneiss and ultramafic-metagabbroic rocks. The ultramafic rocks are commonly weakly mineralised with Fe-Ni-Cu sulphides, the greatest concentrations of which are at Dikoloti and Lentswe. The ultramafic rocks consist of interbanded serpentinised peridotites and amphibole pyroxenites with lesser ultramafic amphibolites and ultramafic schists. The amphibole pyroxenites are mineralogically and geochemically similar to those at Selebi North and Phikwe. The

olivine, orthopyroxene, green spinel and calcic amphibole assemblage of the ultramafic rocks is a metamorphic assemblage of the transiton from upper amphibolite to granulite facies conditons not a relict igneous assemblage.

The Dikoloti-Lentswe sulphides (pyrrhotite, pentlandite and chalcopyrite) consist of weakly mobilised massive and disseminated sulphides in the ultramafic rocks with average Cu/(Cu+Ni) ratios of 0.28 and 0.48 respectively. Mobilised massive sulphides have higher Cu contents. Normal Dikoloti-Lentswe massive sulphide is similar to Selebi-Phikwe Type 1 sulphide but has (a) lower contents of pentlandite and chalcopyrite which are refected in lower Ni and Cu contents, and (b) higher flame pentlandite to granular pentlandite ratios. The Dikoloti-Lentswe sulphides were present in their ultramafic host rocks prior to deformation and metamorphism.

The ultramafic rocks have the geochemistry of olivine-orthopyroxene ($\pm$ clinopyroxene) cumulates. The ultramafic schists and to a lesser extent the ultramafic amphibolites represent cumulates that suffered shearing-induced metasomatism, particularly at the margins of the ultramafic body. The feldspathic amphibolites which locally occur with the ultramafic rocks are regarded as gabbroic plagioclase-olivine cumulates. The corundum-spinel-sapphirine aggregates that occur in the Dikoloti feldspathic amphibolite are thought to be metamorphosed veins and patches of hydrothermally altered gabbro. It is possible that the ultramafic cumulates also suffered hydrothermal alteration.

The hornblende gneiss of the hornblende gneiss-grey gneiss envelope to the ultramafic rocks consists of HGF1 and lesser HGN1-type basalts which have suffered various types of alteration, particularly where they are in contact with or tectonically included in the ultramafic rocks, e.g. Fe-enrichment of possible hydrothermal origin (Type-E) and shearing induced metasomatism (Type-F).

The magnetite quartzites are metamorphosed silica-iron oxide chemical sediments. The associated Mg-amphibolites are geochemically characterised by low contents of Al and Cr and do not appear to be related to the ultramafic cumulates. The Mg-amphibolites are thought to be to be chemically precipitated Mg-silicate (the massive

cummingtonite-rich layers) and mixtures of this Mg-silicate with carbonate (dolomite or Mg-ankerite) that have sufferd complete decarbonation (the actinolite-rich bands finely interbanded with magnetite quartzite).

The Dikoloti-Lentswe cumulate (ultramafic ± gabbroic) bodies (or body) owe their present morphology and field relationships to tectonic emplacement and dismemberment. The cumulate bodies have features that are consistent with an origin as either (a) tectonic slices of thicker olivine-orthopyroxene-plagioclase cumulate piles, or (b) high-level sills into the tholeiitic basalts and chemical sediments. The cumulates are not thought to be intrusive cumulus mushes. The parent magma of the cumulates is considered to be tholeiitic HGN1 basalt, i.e. the same as that for the Selebi-Phikwe host rocks.

The Dikoloti-Lentswe sulphides were magmatic, gravitationally concentrated, immiscible sulphides in ultramafic cumulates that separated from differentiating HGN1 magma. Immiscible sulphides that formed massive sulphides separated before those that formed disseminated sulphides. It is suggested that the S content and Cu/(Cu+Ni) ratio of a magma in an open tholeiitic magma system of the initial composition of HGN1 can been increased by periodic replenishment with HGN1. Periodic replenishment in an open system provides a mechanism for achieving sulphur saturation in the magma and locally low magma/immiscible sulphide ratios. It is thought that the Dikoloti-Lentswe and Selebi-Phikwe sulphides formed in such open systems from initially similar HGN1 magma with similar Ni, Cu and S contents. Differences in the sulphides of the two systems are considered to be the result of differences in such parameters as the size of the magma chamber and the frequency and amount of replenishment. Selebi-Phikwe was a more open system than Dikoloti-Lentswe. The main alternative is that, although the parent magmas of Dikoloti-Lentswe and Selebi-Phikwe probably had similar HGN1 major element compositions, they had significantly different Ni, Cu and S contents.

PLATE 38

Dikoloti-Lentswe ultramafic rocks

(A) Serpentinised peridotite. Porphroblastic orthopyroxene in matrix of granoblastic olivine and orthopyroxene (and minor clinopyroxene ?). Lentswe (LT 27), LT 27-20. FV = 3 mm.

(B) Amphibole pyroxenite. Chromian spinel forming a fabric (M1e) in porphyroblastic orthopyroxene. Dikolti (DK 32), 607. FV =6mm.

(C) Amphibole pyroxenite. Chromian spinel forming fabric (M1e) in granoblastic calcic amphibole (hornblende ?). Dikoloti (DK 32), 607. FV = 6mm.

(D) Amphibole pyroxenite. Coarse intergranular calcic amphibole between orthopyroxene porphroblasts. Dikolti (DK 20), 397. FV = 6 mm.

(E) Serpentinised peridotite. Fine aggregate (talc and chlorite ?) after orthopyroxene in serpentine (after olivine). Dikoloti (DK 32), 613. FV = 6mm.

(F) Sheared amphibole pyroxenite. Relict M1 orthopyroxene porphyroblast and calcic amphibole in M2a matrix of gedrite, cummingtonite and biotite. Lentswe (LT 20), 358. FV = 6mm.

(G) Ultramafic amphibolite. M2 cummingtonite and biotite/phlogopite with small areas of fine talc (or serpentine ?). Phokoje (PJ 1), 333. FV = 3 mm.

(H) Ultramafic schist. Foliated cummingtonite plus calcic amphibole, biotite and pyrrhotite. Dikoloti (DK 32), 619. FV = 6 mm.

PLATE 39

Dikoloti-Lentswe ultramafic rocks

(A) Serpentinised peridotite. Granoblastic olivine, orthopyroxene and minor idioblastic calcic amphibole (hornblende ?). Lentswe (LT 27), LT 27-20. FV = 3mm.

(B) Spinel pyroxenite. Intergranular pleonaste with magnetite inclusions between coarse orthopyroxene. Dikoloti (DK 30), 414. FV = 6 mm.

(C) Spinel pyroxenite. Variably dusty chromian pleonaste with chromian magnetite inclusions in pyrrhotite. Lentswe (LT 27), LT 27-27. FV = 6 mm.

(D) Amphibolite band in serpentinite. Spinel inclusions in calcic amphibole (hornblende). Lentswe (LT 19), 346. FV = 6 mm.

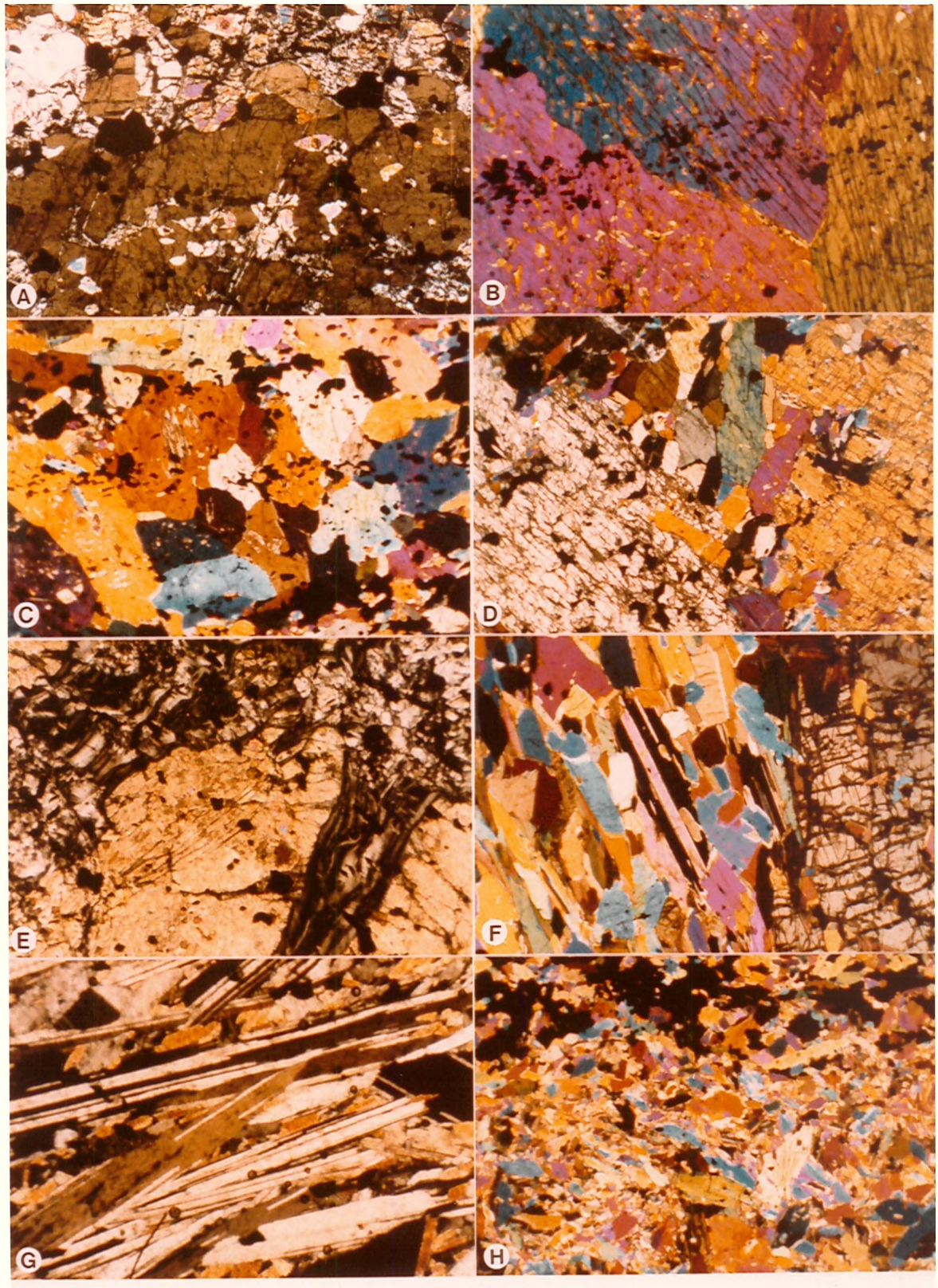

PLATE 38

PLATE 40

Dikoloti feldspathic amphibolite

(A) Corundum-spinel-sapphirine aggregate in feldspathic amphibolite. Epidote-rich rim to aggregate. DK 23, 660.

(B) Foliated feldspathic amphibolite with aggregates of spinel, sapphirine, orthoamphibole and epidote. DK 23, 663.

(C) Feldspathic amphibolite. Typical granoblastic hornblende and anorthite. DK 30, 411. FV = 6 mm.

(D) Pleonaste with minor sapphirine aggregate in feldspathic amphibolite. Aggregate suurounded by epidote and orthoamphibole. Pleonaste surrounded by thin rim (white) of corundophilite. DK 20, 402. FV = 6 mm.

(E) Corundum porphyroblast altering to sapphirine and surrounded by sapphirine plus opaque alteration product. DK 23, 660. FV = 6 mm.

(F) Edge of corundum porphyroblast. Corundum (C) being replaced by sapphirine. Corundum porphyroblast surrounded by opaque alteration product and plenaste grains (P). Pleonaste being replaced by sapphirine. DK 23, 660. FV = 3 mm.

(G) Rim of pleonaste grains (P) mantling relics of corundum porphyroblast (C). Pleonaste being replaced by sapphirine. DK 23, 660. FV = 3 mm.

(H) Foliated feldspathic amphibolite. Band of orthoamphibole with epidote, chlorite with minor sapphirine and trace of kyanite (?). DK 23, 663. FV = 6 mm.

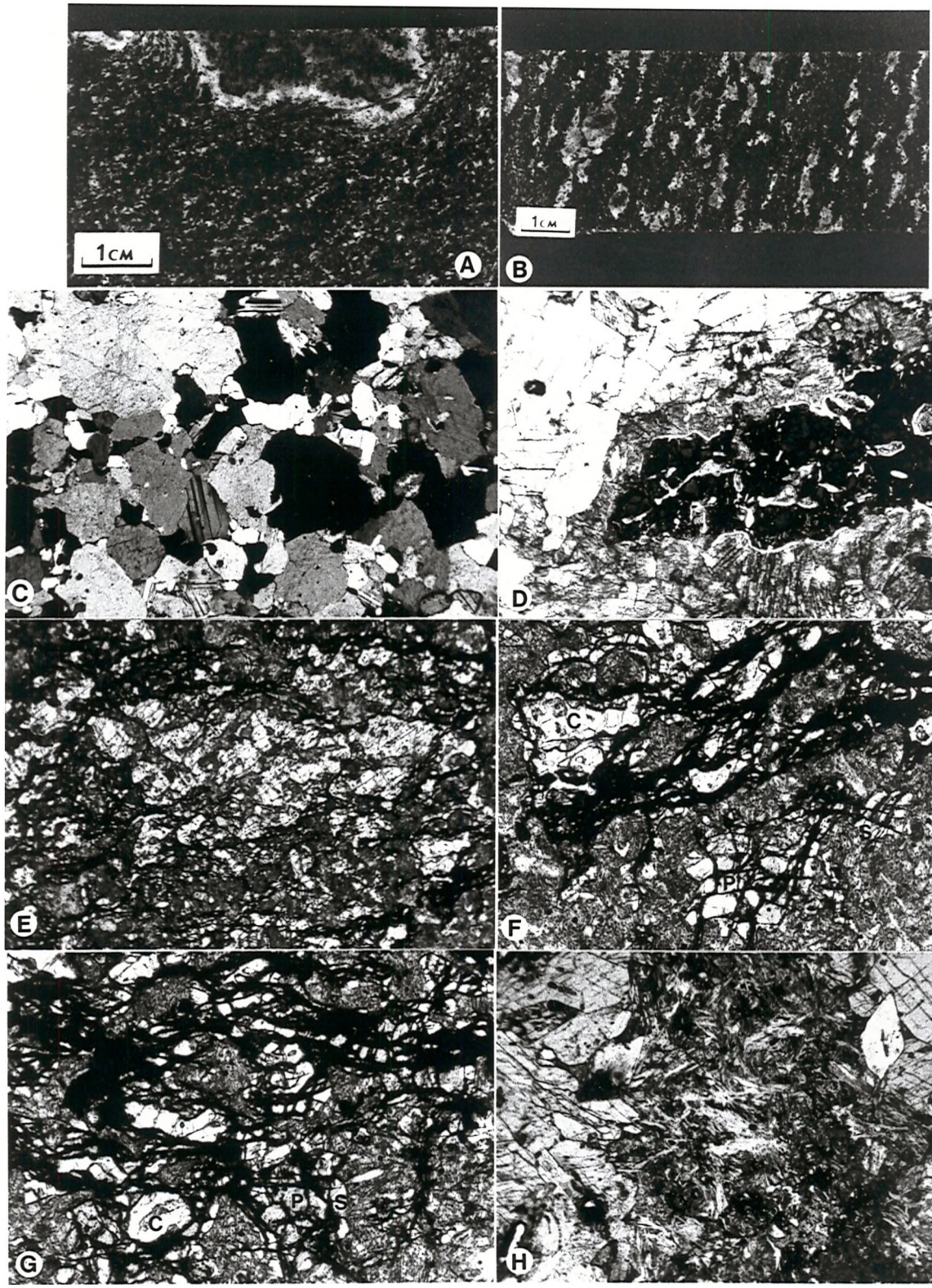

PLATE 40

CHAPTER 9 SUMMARY OF MAIN CONCLUSIONS AND FURTHER SPECULATION ON THE NATURE OF THE SELEBI-PHIKWE MAFIC-ULTRAMAFIC ROCKS AND THEIR TECTONIC SETTING

9.1 SUMMARY OF MAIN CONCLUSIONS

9.1.1 The Protoliths of the Selebi-Phikwe Gneisses

Whole-rock geochemistry of the Selebi-Phikwe gneisses combined with detailed mineralogical data and considerations of the lithological associations in which the gneisses occur have enabled conclusions about the original nature of the gneisses to be made. The most important lithological suites in terms of volume are the hornblende gneiss suite, the grey gneiss suite, the anorthosite-metagabbro suite and the granitic gneiss suite.

The protoliths of the main types of hornblende gneiss (HGN, HGG, HGC and HGF types of high-Ca hornblende gneiss) are proposed to have been both extrusive and intrusive tholeiitic basalts and ferrobasalts. Their original geochemistry has been modified by alteration, some of which is attributed to submarine alteration and some to regional metamorphism. The suite is geochemically characterised by marked Fe and Ti-enrichment. The range in composition of the suite is consistent with low-pressure crystal fractionation dominated by olivine, plagioclase and clinopyroxene in a periodically replenished magma system. Differentiated basalt layers indicate that Units F and E are the right way-up. This is the opposite direction to that proposed by Wakelield (1974) and Wright (1977) from structural data. There is a general increase in the degree of Fe-Ti enrichment going upwards from Unit G. Major replenishment took place between Units D and C.

The typical grey gneiss is a calc-alkaline suite of relatively unaltered andesite to rhyodacite composition, which is tentatively regarded as being volcano-sedimentary rather than intrusive.

The protoliths of the anorthosite-metagabbro suite were plagioclase-clinopyroxene cumulates. Contrary to the proposal of Gallon (1986), they do not represent sediments.

The granitic gneiss suite represents moderately to weakly deformed granitoid intrusions into the Selebi-Phikwe gneiss sequence. They do not represent a basement to the gneisses (as proposed by Wakefield 1974) nor a sandstone unit (as proposed by Gallon 1986).

Of the volumetrically less important lithologies:

The protoliths of the ultramafic lenses that occur throughout the Selebi-Phikwe gneisses and particularly in Unit D are thought to be olivine, orthopyroxene and clinopyroxene-bearing cumulates. They are thought to have been derived from tholeiitic HGN1-type magma rather than komatiitic magma.

The protoliths of the intermediate biotite gneiss, low-Ca hornblende gneiss and diopside-bearing gneiss, all of which are associated with high-Ca hornblende gneiss, were a variety of lithologies derived from the alteration of tholeiitic basalt ranging from in situ altered basalt to volcaniclastic and pelitic sediments.

The protoliths of the quartzites (commonly albite-oligoclase and sillimanite-bearing) associated with hornblende gneiss albite-sillimanite were cherts and aluminous volcaniclastic sediments.

The finely laminated magnetite quartzites associated with cummingtonite and actinolite amphibolites represent chemically precipitated silica-iron oxide sediment. The protoliths of the cummingtonite amphibolite were chemically precipitated Mg-silicate sediment (e.g. talc). The actinolite amphibolite represents decarbonated mixtures of this Mg-silicate chemical sediment with carbonate.

The hornblende-bearing calc-silicate gneiss represent sediments, possibly silicaeous or silicified calcareous argillite.

9.1.2 The Deformation and Metamorphism of the Selebi-Phikwe Gneisses

The Selebi-Phikwe gneisses are highly deformed and metamorphosed. The deformation has been subdivided into two main periods - D1 and D2. D1 is characterised by fold nappes and thrusts. D2 is characterised by open periclinal domes and basins. The temperature and pressure at the peak of metamorphism during late D1 are estimated as having been about 800° C and 10 kbar and are indicative of drastic crustal thickening (about 35 km). A metamorphic assemblage of olivine, orthopyroxene, hornblende and green spinel developed in the ultramafic rocks. Sheets of anorthositic plagioclase-clinopyroxene cumulate were possibly thrust into the Selebi-Phikwe sequence during late D1. Localised partial melting and migmatisation of the Selebi-Phikwe gneisses took place during late D1. Major granitic bodies were intruded into the Selebi-Phikwe sequence after the peak of metamorphism between D1 and D2 and during D2.

9.1.3 The Original Nature of the Selebi-Phikwe Ore Bodies

The Phikwe, Selebi and Selebi North host amphibolites have suffered all the phases of deformation and metamorphism that can be recognised in the Selebi-Phikwe gneisses. Their essential mineralogy consists of hornblende, plagioclase, biotite and Fe-Ni-Cu sulphides. The olivine, orthopyroxene, hornblende and green spinel assemblage of the ultramafic portions of the host amphibolites are equilibrium metamorphic assemblages of the upper amphibolite-granulite facies transition. They are not a relict igneous assemblage.

The host amphibolites are geochemically similar and are characterised by high Al and Mg and hence high normative plagioclase and olivine contents. Field relationships and major and trace element geochemistry indicates that the three host amphibolites were intruded as tholeiitic crystal mushes consisting of different mixtures of intercumulus basalt (of HGN1 compositon), cumulus plagioclase, olivine, orthopyroxene and chromite and syngenetic immiscible sulphides that were all fractionated from tholeiitic HGN1-type magma prior to intrusion. There are no sulphur-rich country rocks in the Selebi-Phikwe country rocks. The excess sulphur to form the deposits is thought to have been derived by internal magmatic processes, rather than by assimilation from country rocks.

The geochemistry of the host amphibolites has been modified during deformation and metamorphism, particularly by sulphide-silicate reactions which produced Fe-rich garnet amphibolites and shearing which resulted in increased contents of Ti, K, Rb, P, Y and Zr and decreased Si, Ca and (Na).

Ni-rich Type 1 massive sulphides represent the tectono-metamorphically modified equivalents of the earliest immiscible sulphides to have separated form the parent magma. Cu-rich disseminated sulphides separated later. The difference in the Cu/(Cu+Ni) ratios between the three ore bodies is essentially due to their differing proportions of massive and disseminated sulphide.

The geochemical variation in profiles through the host amphibolites and the distribution of massive and disseminated sulphides is due to a combination of flow differentiation during the intrusion of crystal-rich magma and post-emplacement gravitational differentiation. The ultramafic portions of the Phikwe and Selebi North host amphibolites formed by flow differentiation. Contrary to the conclusion of Wakefield (1974, 1976), they are not separate intrusions into the host amphibolite protoliths.

9.1.4 The Effects of Deformation and Metamorphism on Selebi-Phikwe Sulphides

The sulphides were physically and chemically mobilised during deformation and metamorphism. Strain was concentrated in the low-strength massive sulphide layers with the eventual formation of inclusion-rich Type-2 massive sulphide. Repeated stress-induced diffusion of Cu, S, (Ni ?) and Co relative to Fe in quaternary metamorphic monosulphide solution (MSS) took place particularly in the mobilised massive sulphides. Later mobilisation was via a fluid phase. However the massive and disseminated sulphides have retained their original Ni-rich and Cu-rich natures.

The sulphide textures formed from cooling metamorphic MSS monosulphide solution and are consistent with the metamorphic and deformation history of the Selebi-Phikwe gneisses.

9.1.5 The Original Nature of the Dikoloti-Lentswe Prospects

The Dikoloti-Lentswe host bodies are metamorphosed tectonically dismembered tholeiitic ultramafic and gabbroic cumulates emplaced into a unit of basalts and chemical sediments. The cumulates were either tectonic slices of thicker cumulate piles or high-level sills. The parent magma of the cumulates was tholeiitic HGN1 basalt, similar to that from which the Selebi-Phikwe host rocks formed. The corundum-spinel-sapphirine assemblage in the Dikoloti metagabbro represent metamorphosed veins and patches of hydrothermally altered gabbro. Ultramafic schists and some of the ultramafic amphibolites represent cumulates that suffered shearing-induced metasomatism particularly at the margins of the ultramafic body. The hornblende gneiss which represent the basalt into which the cumulate bodies were emplaced have suffered hydrothermal or metasomatic enrichment in Fe and Mg derived from the adjacent mineralised ultramafic rocks and shearing-induced metasomatism.

Magmatic Fe-Ni-Cu immiscible sulphides were gravitationally concentrated in the olivine-orthopyroxene cumulates. Immiscible sulphides that concentrated to form the normal massive sulphides with low Cu/(Cu+Ni) ratios separated from parent magma before those that formed the disseminated sulphides with higher Cu/(Cu+Ni) ratios. Tectonically mobilised massive sulphides are enriched in Cu.

9.2 THE COMAGMATIC NATURE OF THE SELEBI-PHIKWE MAFIC AND ULTRAMAFIC ROCKS

The suite of high-Ca hornblende gneisses represent tholeiitic basalts (HGN1, HGG and HGC), Ti-rich ferrobasalts (HGF1) and cumulus-enriched basalts (HGN2 and HGF2). They are thought to be a comagmatic series in that they were all derived from HGN1P by low-pressure fractional crystallisation in the same or related magma systems.

The olivine, orthopyroxene and clinopyroxene cumulates that occur as thin lenses throughout the Selebi-Phikwe sequence are thought to have formed during the evolution of HGC from HGN1.

The thick tectonic slices of plagioclase-clinopyroxene cumulate represented by the anorthosite-metagabbro suite are thought to be the cumulus products of the crystal fractionation of HCG-HGF1 type magma. It is suggested that they are the main cumulus products that formed during the evolution and fractionation of the more evolved types of basalt in the Selebi-Phikwe area, i.e. HGC and HGF1. The main evidence that the anorthositic gneisses were emplaced as tectonic slices is the mylonite zones that bound the anorthositic layers. This does not necessarily mean however that the anorthositic gneisses were translated significant distances prior to emplacement. It could just be due to rheological properties of the anorthositic gneisses.

It is concluded that the geochemistries of the hornblende gneiss suite, the ultramafic lenses and the anorthosite-metagabbro suite are consistent with the formation of their protoliths from evolving HGN1P magma. It is thought that they are comagmatic in that they actually formed in the same magma system or related systems with the initial composition of HGN1. The grey gneiss is geochemically unrelated to the tholeiitic hornblende gneiss suite.

The formation of highly fractionated Fe & Ti-rich tholeiites at mid-ocean ridges has been attributed to fractionation of MORB in both unreplenished closed systems or in frequently replenished open systems. The occurrence of different types of high-Ca hornblende gneiss representing various types of evolved basalt in the same unit indicate that the Selebi-Phikwe magma sytem(s) was not closed and was periodically replenished with HGN1P magma along with expulsion of variably evolved basalt as lava or high-level intrusive.

The protoliths of the host rocks to the Selebi-Phikwe ore bodies were intrusions of tholeiitic crystal mush consisting of cumulus plagioclase and olivine ($\pm$ opx.), intercumulus evolved HGN1-type basalt liquid and immiscible sulphides. The protoliths of the

host rocks to the Dikoloti-Lentswe prospects were olivine, orthopyroxene and plagioclase-olivine cumulates. Both Selebi-Phikwe and Dikoloti-Lentswe protoliths are thought to have fractionated from evolving HGN1-type parental magma.

It is thought that sulphur saturation and separation of significant immiscible Fe-Ni-Cu sulphides could have taken place in the fractionating and evolving, periodically replenished, open tholeiitic HGN1 systems that produced the highly evolved ferrobasalts of the Selebi-Phikwe area. The main requirements to produce immiscible sulphides of the composition that separated in the Selebi-Phikwe and Dikoloti-Lentswe systems is that the magma initially had a low S content and that only limited olivine crystallisation took place before replenishment. HGN1 satisfies these requirements. The higher Ni and Cu contents and Cu/(Cu+Ni) ratios of Selebi-Phikwe sulphides compared to texturally equivalent Dikoloti-Lentswe sulphides are interpreted as indicating that the Selebi-Phikwe system was a more open magma chamber with more frequent HGN1 replenishment than the Dikoloti-Lentswe system. A situation somewhat analogous to that in the Juan de Fuca Ridge of the East Pacific is envisaged in which small short-lived magma chambers, intermediate magma chambers of intermediate duration with periodic magma mixing and long-term steady state magma chambers with continual replenishment coexist (Delaney et al. 1981). It is a paradox of the model described above that a magma with a low sulphur content is initially required in order to form the ore bodies. This situation is somewhat analogous to that of the Bushveld Complex the parent magma of which is considered to have been sulphur-poor (Vermaak 1976).

The metamorphosed and dismembered plagioclase-rich layered complex (including the mineralised crystal mushes) at Selebi-Phikwe has some similarities to larger layered gabbroid intrusions, e.g. the Stillwater and Bushveld Cpmplexes and Sudbury. These complexes would appear to have formed in a continental setting. The most analogous Archaean intrusion to Selebi-Phikwe is possibly the Bird River sill in Manitoba (Karup-Moller & Brummer 1971; Scoates 1971; Coats et al. 1979). The main alternative to a continental setting for the Selebi-Phikwe layered complex is an oceanic setting.

9.3 THE TECTONIC SETTING OF THE SELEBI-PHIKWE GNEISSES AND ORE BODIES

The protoliths of the Selebi-Phikwe rocks are similar to those of the greenschist facies rocks in the Tati greenstone belt (Fig.

1.2), which include tectonically emplaced sheets of gabbroic plagioclase-olivine cumulates with Ni-Cu sulphides (Brown in prep.). However ultramafic rocks are more common in the Tati greenstone belt than in the Selebi-Phikwe sequence. Ultramafic rocks, some of which may have been extrusive, generally occur towards the base of the Tati succession (Key 1976). Although the Ni content of the Phoenix ore body in the Tati belt has been upgraded during tectono-metamorphism (Brown in prep.), the Selkirk ore body has similar Ni and Cu grades to the Selebi-Phikwe ore bodies. The host rocks to the Tati deposits are geochemically similar to the Selebi-Phikwe host rocks, i.e. they were gabbroic plagioclase-olivine cumulates. A genetic link between the Tati deposits and the Selebi-Phikwe ore bodies is thought to be possible, although the latter are probably older. The protoliths of the Selebi-Phikwe rocks and their proportions are similar to those of the Bulawayan Group of the Midlands greenstone belt in Zimbabwe (Fig. 1.2, Table 1.2) (Condie & Harrison 1976; Condie 1981) which contains little ultramafic rock.

The Selebi-Phikwe rocks most obviously differ from those in the Messina-Beit Bridge area (the most studied area of the Limpopo Belt) in their lack of the latter's thick quartzites and carbonates. It is not possible to compare fully the two areas. For example data are not available to evaluate the amount of calc-alkali grey gneiss in the Messina-Beit Bridge area. The value of mineralogically and geochemically analysing complete core sections through all the lithologies of the Selebi-Phikwe area is stressed. Any model of the tectonic setting of the rocks of the Limpopo Belt must take into account the fact that the rocks of the northern part of the Central Zone in Botswana (i.e. the Selebi-Phikwe area) are a different lithological sequence to the carbonate-quartzite-rich sequence of the southern part of the Central Zone (Fig. 9.1), although both sequences contain similar anorthositic complexes.

The rocks of the Selebi-Phikwe area of the Limpopo Belt appear to be more like high-grade analogues of late Archaean greenstone belt to the north in the Rhodesian Craton (Condie 1984) than a separate "high-grade" quartzite, pelitic gneiss, carbonate and anorthosite association (see Ch. 1.3.6; cf. Shackleton 1976; Sutton 1976; Windley 1976, 1977; Condie 1976a). Compared to greenstone belts however the rocks of the Selebi-Phikwe area have more fractionated tholeiites, abundant plagioclase-rich cumulates and no recognised komatiites.

The rocks of the Selebi-Phikwe area are thought to have

formed either in a continental setting or an oceanic setting. Equivalents of the majority of lithologies represented by the Selebi-Phikwe gneisses are found in the modern ocean floor environment (c.f. Dewey & Bird 1970) and in ophiolite complexes (Gass 1977; Coleman 1977). The hornblende gneiss suite have most in common with fractionated oceanic basalts from a mid-ocean ridge or back-arc basin (see Ch. 4.7.3).

The anorthosite-metagabbro suite would appear to have originated in either (1) an oceanic spreading centre, i.e. at an oceanic ridge or back-arc basin, (2) a continental Stillwater-Bushveld setting, or (3) a magmatic arc at a continental margin (Windley & Smith 1976). The oceanic setting as layered cumulates is preferred because of (1) the prevalence of tectonic contacts indicating that the anorthosite-metagabbro suite was emplaced as tectonic slices, and (2) the interpretation that some of the Selebi-Phikwe basalts were submarine extrusives. Anorthosites and anorthositic gabbros form a component of modern oceanic crust (Engel & Fisher 1969; Varne et al. 1969; Hedge et al. 1979), although a smaller component (5% of intrusive rocks in the oceanic crust of the Indian Ocean, Engel & Fisher 1975) than is represented by the Selebi--Phikwe anorthosite-metagabbro suite. Ferrogabbros chemically similar to HGF2 also occur in ocean crust (Engel & Fisher 1975). Some ophiolites, for example the Masirah ophiolite (Oman), contain extensive cumulate gabbroic anorthosite (Moseley 1969). The amount of ultramafic cumulate in the oceanic crust represented by the Samail ophiolite is less than 3% (Pallister & Gregory 1983).

Deep-sea sediments are represented by some of the intermediate biotite gneiss and the Fe-rich grey gneiss (pelitic sediments) and the finely laminated magnetite quartzites and Mg-amphibolites (chemical sediments). Important negative evidence is thought to be the general lack of carbonate and orthoquartzite (shallow water, passive margin lithologies ?) that are significant components of the Limpopo Gneisses of the Messina-Bei Bridge area.

The main ophiolite component missing from the Selebi-Phikwe area are ultramafic rocks representing thick tectonised peridotite below layered cumulates. However this component is always missing in exposures of Archaean rocks. The major ultrabasic complexes with large podiform chromite bodies that occur in a large area south of Buhwa (Fig. 9.1, Mason 1973) possibly represent the basal portion of ophiolitic layered cumulates. The Selebi-Phikwe rocks differ from

typical ophiolite complexes in the highly fractionated incompatible element-enriched nature of the basalts, the plagioclase-rich nature of the layered cumulates and the intermixing of calc-alkaline rocks (the grey gneiss suite) with the basalts.

Shackleton (1986) concluded that the metamorphism (granulite facies and drastic crustal thickening) and structures of the Limpopo Belt suggest collision. He also stated that other criteria to support the proposal for collision, e.g. ophiolites, deep-ocean abyssal sediments and subduction-type calc-alkaline volcanism, have not been recognised. Although it is unlikely that modern-type plate tectonics can be applied without modification to the Archaean, it is tentatively suggested that some of the rocks of the Selebi-Phikwe area have "ophiolitic" affinities. Calc-alkaline volcanism is represented by the grey gneiss suite. They are thought to be fore-arc volcaniclastic sediments derived from an adjacent calc-alkaline arc (the belt of intrusive porphyritic granites between Selebi-Phikwe and the Tati greenstone belt). A reconstruction is shown in Figure 9.1. Convergence of the Rhodesian and Kaapvaal protocontinents resulted in closure of the oceanic basin and collision. The Selebi-Phikwe rocks were deformed and metamorphosed during drastic crustal thickening. Wright (1977) suggested that facing of the recumbent structures implied underthrusting to the north. Granites were the main melts produced by the collision. Closure was possibly oblique to the main trend of the Limpopo belt. Later dextral movement along the collision zone produced the D2 structures.

It is not known whether there was just a single oceanic-type basin between the Rhodesian and Kaapvaal Cratons (protocontinents). The carbonates and quartzites of the Messina-Beit Bridge area represent a passive Atlantic-type margin to the Kaapvaal protocontinent that became tectonically intercalated with oceanic crust (including anorthosites-gabbros). Asymmetry of the Limpopo Belt is also implied by the lack of young (2.6-2.7 Ga) greenstone belts in the Kaapvaal craton. It is suggested that the Sand River Gneiss may not have been a "basement" to the Beit Bridge Gneisses but instead were tectonic slices of the Kaapvaal Craton.

Further work required in the Limpopo Belt includes: (a) the distribution of ferrobasalts within the Belt (Are they a feature of the Selebi-Phikwe area and its Ni-Cu deposits alone ?), (b) the distribution and original nature of the poorly exposed calc-alkaline grey gneiss suite and other leucocratic gneisses.

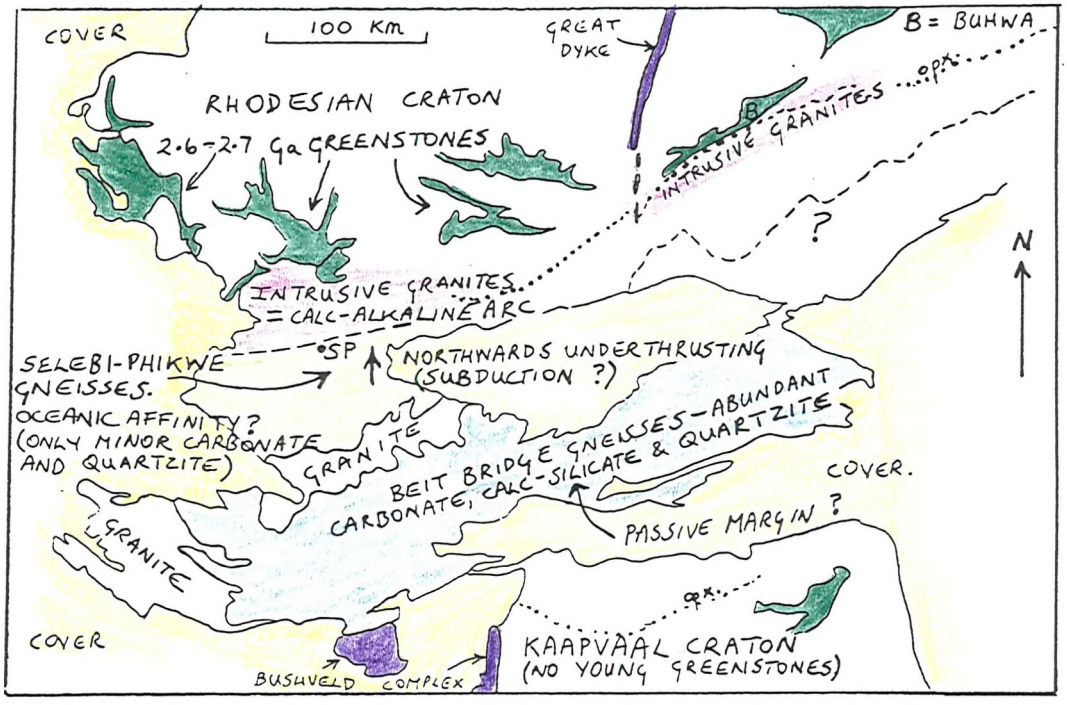

Fig. 9.1 Regional Tectonic Settings within the Limpopo Belt (see Fig. 1.2 and Table 1.2)

The metamorphosed crystal mush intrusions that host the Selebi-Phikwe ore bodies are regarded as analogous to mobilised cumulates in ophiolite complexes that intrude as crystal mushes along faults that penetrate deep into very young, partly consolidated oceanic crust (Karson et al. 1983). These are more prevalent at ridge-transform intersections or "leaky" transform regions. The Dikoloti-Lentswe cumulates are more regional in their occurrence. Whether or not they represent dismembered high-level sills or tectonic slices of a thicker cumulate pile (The latter is preferred.), the Dikoloti-Lentswe unit represents an early (D1) zone of thrusting that was refolded into a dome and basin pattern during D2.

The Selebi-Phikwe Ni-Cu sulphide deposits can be classified as tectonically modified deposits in synvolcanic intrusions associated with a tholeiitic suite of oceanic affinity (cf. Naldrett, IGCP Project, 1979).

BIBLIOGRAPHY

AMSTUTZ, G.C. 1974. Spilites and Spilitic Rocks, Springer Verlag, 482 pp.

ANDERSON, A.T. 1974. Chlorine, sulfur, and water in magmas and oceans. Bull. Geol. Soc. Am., 85, 1485-1492.

ANDERSON R.N., CLAGUE, D.A., KLITGORD, K.D., MARSHALL, M. & MISHIMORI, R.K. 1975. Magnetic and petrological variations along the Galapagos Spreading Center and their relation to the Galapagos melting anomalay. Bull. Geol. Soc. Am., 86, 683-694.

APPEL, P.W.U. 1980. On the Early Archaean Isua iron-formation, West Greenland. Precamb. Res., 11, 73-87.

ARCHER, A.A. 1981. Manganese nodules as a source of nickel, copper, cobalt and manganese. Trans. Instn Min. Metall., 90, A1-6.

ARNDT, N.T. 1977. Ultrabasic magmas and high-degree melting of the mantle. Contrib. Mineral. Petrol., 64, 205-221.

ARNDT, N.T., NALDRETT, A.J. & PYKE, D.R. 1977. Komatiitic and iron-rich tholeiitic lavas of Munro Township, northeast Ontario. J. Petrol., 18, 319-369.

ARTH, J.G., ARNDT, N.T. & NALDRETT, A.J. 1977. Genesis of Archean komatiites from Munro township, Ontario: trace-element evidence. Geology, 5, 590-594.

ATKINSON, B.K. 1974. Experimental deformation of polycrystalline galena, chalcopyrite and pyrrhotite. Trans. Instn Min. Metall., 83, B19-28

ATKINSON, B.K. 1975. A preliminary study of the influence of temperature and strain rate on the rheology of polycrystalline pyrrhotite ores. Neues Jahrb. Mineralogie Monatsh.,11, 483-499.

AUMENTO, F., MITCHELL, W.S. & FRATTA, M. 1976. Interaction between sea water and oceanic layer two as a function of time and depth. 1. Field evidence. Can. Mineral., 14, 269-290.

BAHNEMANN, K.P. 1970. A note on the anorthositic gneiss in the Messina district, Northern Transvaal. Spec. Pub. Geol. Soc. S. Africa, 2, 715-720.

BAHNEMANN, K.P. 1972. A review of the structure, the stratigraphy and the metamorphism of the basement rocks of the Messina district, northern Transvaal. Unpub. D.Sc. thesis, Univ.

Pretoria, 156 pp.

BAHNEMANN, K.P. 1973. The origin of the Singelele granite gneiss near Messina, northern Transvaal. Spec. Pub. geol. Soc. S. Africa, 3, 235-244.

BARKER, R.W. 1975. Metamorphic mass transfer and sulfide genesis, Stillwater Intrusion, Montana. Econ. Geol., 70, 275-298.

BARKER, F. 1979. Trondhjemite: Definition, environment and hypotheses of origin. In: Barker, F., (ed.), Trondhjemites, Dacites and Related Rocks, Elsevier, 659 pp.

BARRETT, F.M., BINNS, R.A., GROVES, D.I., MARSTON, R.J. & McQUEEN, K.G. 1977. Structural history and metamorphic modification of Archean volcanic-type nickel deposits, Yilgarn Block, Western Australia. Econ. Geol., 72, 1195-1224.

BARRETT, F.M., GROVES, D.I. & BINNS, R.A. 1976. Importance of metamorphic processes at the Nepean nickel deposits, Western Australia. Trans. Instn Min. Metall., 85, B252-273.

BARTON, J.M.,Jr 1979. Crustal evolution clues. Nuclear Active, 21, 16-19.

BARTON, J.M.,Jr 1981. Geology of the Limpopo Belt. Excursion guidebook. Geol. Soc. S. Africa, 134 pp.

BARTON, J.M.,Jr 1983a. Our understanding of the Limpopo Belt - A summary with proposals for future research. Spec. Pub. Geol. Soc. S. Africa, 8, 191-203.

BARTON, J.M.,Jr 1983b. Pb-isotopic evidence for the age of the Messina Layered Intrusion, Central Zone, Limpopo Mobile Belt. Spec. Pub. Geol. Soc. S. Africa, 8, 39-41.

BARTON, J.M.,Jr, & KEY, R.M. 1981. The tectonic development of the Limpopo Mobile Belt and the evolution of the Archaean cratons of southern Africa. In: Kroner, A., (ed.), Precambrian Plate Tectonics, Elsevier, 185-212.

BARTON, J.M.,Jr & KEY, R.M. 1983. Rb-Sr ages and geological setting of certain rock units from the Central Zone of the Limpopo Mobile Belt, near Zanzibar, eastern Borswana. Spec. Pub. Geol. Soc. S. Africa, 8, 19-25.

BARTON, J.M.,Jr, FRIPP, R.E.P. & RYAN, B. 1977. Rb/Sr ages and geological setting of ancient dykes in the Sand River area, Limpopo Mobile Belt, South Africa. Nature, 267, 487-490.

BARTON, J.M.,Jr, RYAN, B. & FRIPP, R.E.P. 1978. The relationship between Rb-Sr and U-Th-Pb whole-rock and zircon systems in the greater than 3790 m.y. old Sand River Gneisses, Limpopo Mobile

Belt, southern Africa. U.S. Geol. Surv. Open File Report, 78-701, 27-28.

BARTON, J.M.,Jr, RYAN, B. & FRIPP, R.E.P. 1983b Rb-Sr and U-Th-Pb isotopic studies of the Sand River Gneisses, Central Zone, Limpopo Mobile Belt. Spec. Pub. Geol. Soc. S. Africa, 8, 9-18.

BARTON, J.M.,Jr, DU TOIT, M.C., VAN REENEN, D.D. & RYAN, B. 1983a. Geochronologic studies in the Southern Marginal Zone of the Limpopo Mobile Belt, southern Africa. Spec. Pub. Geol. Soc. S. Africa, 8, 55-64.

BARTON, J.M., Jr, FRIPP, R.E.P, HORROCKS, P. & MCLEAN, N. 1979a. The geology, age and tectonic setting of the Messina Layered Intrusion, Limpopo Mobile Belt, southern Africa. Am. J. Sci., 279, 1108-1134.

BARTON, J.M., Jr, RYAN, B., FRIPP, R.E.P. & HORROCKS, P. 1979b. Effects of metamorphism on the Rb-Sr and U-Pb systematics of the Singelele and Bulai gneisses, Limpopo Mobile Belt, southern Africa. Trans. Geol. Soc. S. Africa, 82, 259-269.

BAVINTON, O.A. 1981. The nature of sulfidic metasediments at Kambalda and their broad relationships with associated ultramafic rocks and nickel ores. Econ. Geol., 76, 1606-1628.

BECCALUVA, L., OHNENSTETTER, D., OHNENSTETTER, M. & VENTURELLI, G. 1979. The trace element geochemistry of Corsican ophiolites. Contrib. Min. Pet., 64, 11-31.

BELL, P.M., ENGLAND, J.L. & KULLERUD, G. 1964. Pentlandite: Pressure effect on breakdown. Carnegie Inst. Wash. Year Book, 63, 206-207.

BENDER, J.F., HODGES, F.N. & BENCE, A.E. 1978. Petrogenesis of basalts from the Project FAMOUS area: experimental study from 0 to 15 kbars. Earth PLanet. Sci. Lett., 41, 277-302.

BENNETT, J.D. 1970. Craton-mobile belt relations with particular reference to the Mosetse-Matsitama area, northeastern Botswana. Geol. Mag., 107, 113-123.

BENNETT, J.D. 1971a. Brief explanation of the geology of the Magogaphate area (accompanying geological map QDS 2128C). Geol. Surv. Botswana.

BENNETT, J.D. 1971b. Map of the tectono-metamorphic complex of eastern Botswana. Geol. Surv. Botswana.

BENNETT, J.D. 1972. Early Precambrian tectogenesis in eastern Botswana. Int. Geol. Cong. Montreal, 24, 317-324.

BENNETT, J.D. 1973. The gneisses and granitoid rocks of northeastern

Botswana. Spec. Pub. Geol. Soc. S. Africa, 3, 245-251.

BHATTACHARJI, S. 1967. Scale model experiments on flowage differentiation in sills. In: Wyllie, P.J., (ed.), Ultramafic and Related Rocks, John Wiley, 69-70.

BHATTACHARJI, S. & SMITH, C.H. 1964. Flowage differentiation. Science, 145, 150-153.

BHATTACHARYYA, C. 1971. An evaluation of the chemical distinction between igneous and metamorphic orthopyroxenes. Am. Mineral., 56, 499-506.

BHATTACHARYYA, P.K. & MUKHERJEE, A.D. 1984. Petrochemistry of metamorphosed pillows and the geochemical status of the amphibolites (Proterozoic) from the Sirohi district, Rajasthan, India. Geol. Mag., 121, 465-473.

BHATTIA, M.R. 1983. Plate tectonics and geochemical composition of sandstones. J. Geol., 91, 611-627.

BHATTIA, M.R. & CROOK, K.A.W. 1986. Trace element characteristics of graywackes and tectonic setting discrimination of sedimentary basins. Contrib. Min. Pet., 92, 181-193.

BICKLE, M.J., FORD, C.E. & NISBET, E.G. 1977. The petrogenesis of peridotitic komatiites: evidence from high-pressure melting experiments. Earth Planet. Sci. Lett., 37, 97-106.

BILLINGTON, L.G. 1984. Geological review of the Agnew nickel deposit, Western Australia. In: Buchanan, D.L. & Jones, M.J. (eds). Sulphide deposits in mafic and ultramafic rocks. Instn Min. Metall., 43-54.

BINNS, R.A. & GROVES, D.I. 1976. Iron-nickel partition in metamorphosed olivine-sulfide assemblages from Perseverance, Western Australia. Am. Mineral., 61, 782-787.

BLATT, H., MIDDLETON, G. & MURRAY, R. 1980. Origin of Sedimentary Rocks, Prentice-Hall, 782 pp.

BOCTOR, N.Z. 1981. Partitioning of nickel between olivine and iron monosulfide melts. Carnegie Inst. Wash. Ybk, 80, 356-359.

BOCTOR, N.Z. 1982. The effect of fO2, fS2 and temperature on Ni partitioning between olivine and iron sulfide melts. Carnegie Inst. Wash. Ybk, 81, 366-369.

BOETTCHER, A.L. 1970. The system CaO-Al2O3-SiO2-H2O at high pressure and temperature. J. Petrol., 11, 337-379.

BONATTI, E. & JOENSUU, O. 1968. Palygorskite form the Atlantic deep sea sediments. Am. Mineral., 53, 975-983.

BOTTINGA, Y. & WEILL, D.F. 1970. Densities of liquid silicate systems

calculated from partial molar volumes of oxide components. Am. J. Sci., 269, 169-182.

BOYD, R. & MATHIESON, C.O. 1979. The nickel mineralization of the Rana mafic intrusion, Nordland, Norway. Can. Mineral., 17, 287-298.

BOWLES, F.A., ANGINO, E.A., HOSTERMAN, J.W. GALLE, O.K. 1971. Precipitation of deep sea palygorskite and sepiolite. Earth Planet. Sci. Lett., 11, 324-332.

BRANDL, G. 1983. Geology and geochemistry of various supracrustal rocks of the Beit Bridge Complex east of Messina. Spec. Pub. Geol. Soc. S. Africa, 8, 103-112.

BROOKS, C. & HART, S.R. 1974. On the significance of komatiite. Geology, 2, 107-110.

BROWN, P.J. 1980. Progress report - the Selebi-Phikwe Ore Bodies. BCL internal report.

BROWN, P.J. 1981a. The genesis of the copper-nickel deposits in eastern Botswana. 11th Colloquium of African Geology, Milton Keynes, Abstracts, p.64.

BROWN, P.J. 1981b. The genesis of the Selebi-Phikwe copper-nickel ore bodies, Botswana. South African Geodynamics Symposium, Abstracts, 32-33.

BRYAN, W.B., THOMPSON, G., FREY, F.A., DICKEY, J.S., ROY, S. & MICHAEL, P.J. 1979. Compositional variation in a steady state zoned magma chamber, Mid-Atlantic Ridge at 36-50'. Tectonophysics, 55, 63-85.

BUCHANAN, D.L. 1982. Nickel: a commodity review. Occasional Papers Instn Min. Metall., 1, 28 pp.

BUCHANAN, D.L. & NOLAN, J. 1979. Solubility of sulfur and sulfide immiscibility in synthetic tholeiitic melts and their relevance to Bushveld-Complex rocks. Can. Mineral., 17, 483-494.

BUCHANAN, D.L., NOLAN, J., SUDDABY, P., ROUSE, J.E., VILJOEN, M.J. & DAVENPORT, J.W.J. 1981. The genesis of sulfide mineralization in a portion of the Potgietersrus limb of the Bushveld Complex. Econ. Geol., 76, 568-579.

BUCHANAN, D.L. & ROUSE, J.E. 1984. Role of contamination in the precipitation of sulphides in the Platreef of the Bushveld Complex. In: Buchanan, D.L. & Jones, M.J., (eds), Sulphide deposits in mafic and ultramafic rocks. Instn Min. Metall., 141-146.

BURKE, K., DEWEY, J.F. & KIDD, W.S.F. 1976. Dominance of horizontal movements, arc and microcontinent collisions during the later

per mobile regime. In: Windley, B.F., (ed.), The Early History of the Earth, John Wiley, 113-130.

BURKE, K., KIDD, W.S.F. & KUSKY, T. 1985. Is the Ventersdorp rift system of southern Africa related to a continental collision between the Kaapvaal and Zimbabawe cratons at 2.64 Ga ago ? Tectonophysics, 115, 1-24.

BURNS, R.G. 1970. Mineralogical applications of crystal field theory, Cambridge University Press.

BURNS, R.G. & FYFE, W.S. 1964. The behaviour of nickel during magmatic crystallization. Nature, London, 210, 1147-1148.

BURT, D.R.L. & SHEPPY, N.R. 1975. Mount Keith nickel sulphide deposit. In: Knight, C.L. (ed.). Economic geology of Australia and Papua New Guinea, I. Metals, Australian Inst. Min. Metall., Mon. 5, 159-168.

BYERLY, G.R., MELSON, W.G. & VOGT, P.R. 1976. Rhyodacites, andesites, ferro-basalts and ocean tholeiites form the Galapagos spreading center. Earth Planet. Sci. Lett., 30, 215-221.

CAMERON, E.M., SIDDELY, G. & DURHAM, C.G. 1971. Distribution of ore elements in rocks for evaluating ore potential: nickel, copper, cobalt and sulphur in ultramafic rocks of the Canadian Shield. Spec. Vol. Can. Inst. Min. Metall., 2, 298-313.

CAMPBELL, I.H. & NALDRETT, A.J. 1979. The influence of silicate-sulfide ratios on the geochemistry of magmatic sulphides. Econ. Geol., 74, 1503-1506.

CAMPBELL, I.H., ROEDER, P.L. & DIXON, J.M. 1978. Plagioclase buoyancy in basaltic liquids as determined with a centifruge surface. Contrib. Min. Pet., 67, 369-377.

CANN, J.R. 1969. Spilites from the Carlsberg Ridge, Indian Ocean. J. Petrol., 10., 1-19.

CANN, J.R. 1970. Rb, Sr, Y, Zr and Nb in some ocean floor basalts. Earth Planet. Sci. Lett., 10, 7-11.

CARD, K.D. & HUTCHINSON, R.W. 1972. The Sudbury structure: Its regional setting. Spec. Pap. Geol. Assoc. Can., 10, 67-78.

CAREY, S.N. & SIGURDSON, H. 1984. A model of volcanogenic sediment-sedimentation in marginal basins. In: Kokelaar, B.P. & Howells, M.F., (eds), Marginal Basin Geology, Spec. Pub. Geol. Soc. London, 16, 37-58.

CARR, S.G. 1974. The geology and geochemistry of the Sherlock Bay nickel-copper deposit, W.A., with special emphasis on the origin of the mineralization. Thesis, B.Sc., Univ. Adelaide.

CARTWRIGHT, I. & BARNICOAT, A.C. 1986. The generation of quartz-normative melts and corundum-bearing restites by crustal anatexis: petrogenetic modelling based on an example from the Lewisian of North-West Scotland. J. Metamorphic Geol., 4,79-99.

CAWTHORN, R.G. & DAVIES, G. 1982. Possible komatiitic affinity of the Bushveld Complex, South Africa. In: Arndt, N.T. & Nisbet, E.G., (eds), Komatiites, George Allen & Unwin, 91-96.

CHALLIS, G.A. 1965. The origin of New Zealand ultramafic intrusions. J. Petrol., 6, 322-364.

CHENEY, E.S. & LANGE, I.M. 1967. Evidence for sulfurization and the origin of some Sudbury-type ores. Mineral. Deposita, 2, 80-94.

CHINNER, G.A. 1961. The origin of sillimanite in Glen Clova, Angus. J. Petrol., 2, 312-323.

CLAGUE, D.A. & BUNCH, T.E. 1976. Formation of ferrobasalt at East Pacific midocean spreading centres. J. Geophys. Res., 81, 4247-4256.

CLARK, B.R. & KELLY, W.C. 1973. Sulphide deformation studies: I. Experimental deformation of pyrrhotite and sphalerite to 2,000 bars and 500C. Econ. Geol., 68, 332-352.

COATS, C.J.A., GREEN, P.W. & WILSON, H.D.B. 1976. Sulphide mobilization in the Manibridge Orebody. CIM Bulletin, 69, 154-159.

COATS, C.J.A., STOCKFORD, H.R. & BUCHAN, R. 1979. Geology of the Maskwa West nickel deposit, Manitoba. Can. Mineral., 17, 309-318.

COLEMAN, A.P. 1926. The magmatic origin of the Sudbury nickel ores. Geol. Mag., 63, 108-112.

COLEMAN, R.G. 1977. Ophiolites, Minerals and Rocks, 12, Springer, 229 pp.

COLEMAN, R.G. & DONATO, M.M. 1979. Oceanic plagiogranite revisited. In: Barker, F., (ed.), Trondhjemites, Dacites and Related Rocks, Elsevier, 659 pp.

COLLERSON, K.D., JESSEAU, C.W. & BRIDGEWATER, D. 1976. Crustal development of the Archaean Gneiss Complex: Eastern Labrador. In: Windley, B.F., (ed.), The Early History of the Earth, John Wiley, 237-253.

CONDIE, K.C. 1976a. Plate Tectonics and Crustal Evolution, Pergamon Press, 288 pp.

CONDIE, K.C. 1976b. Trace-element geochemistry of Archean greenstone belts. Earth Sci. Rev., 12, 393-417.

CONDIE, K.C. 1981. Archean Greenstone Belts, Elsevier, 434 pp.

CONDIE, K.C. 1982. Archaean andesites. In: Thorpe, R.S., (ed.), Andesites, John Wiley, 575-590.

CONDIE, K.C. 1984. Archean geotherms and supracrustal assemblages. Tectonophysics, 105, 29-41.

CONDIE, K.C. & HARRISON, N.M. 1976. Geochemistry of the Archean Bulawayan Group, Midlands greenstone belt, Rhodesia. Precamb. Res., 3, 253-271.

CONDIE, K.C., VILJOEN, M.J. & KABLE, E.J.D. 1977. Effects of alteration on element distributions in Archaean tholeiites from the Barberton greenstone belt, South Africa. Contrib. Min. Pet., 64, 75-89.

CONDIT, R.H., HOBBINS, R.R. & BIRCHENALL, C.E. 1974. Self-diffusion of iron and sulphur in ferrous sulphide. Oxidation of Metals, 8, 409-455.

COOMER, P.G, COWARD, M.P. & LINTERN, B.C. 1977. Stratigraphy, structure and geochronology of ore leads in the Matsitama schist belt of northern Botswana. Precamb. Res., 5, 23-41.

COUTURE, R.A. 1977. Composition and origin of palygorskite-rich and montmorillonite-rich zeolite containing sediments from the Pacific Ocean. Chem. Geol., 19, 113-130.

COWARD, M.P. 1976. Archaean deformation patterns in southern Africa. Phil. Trans. R. Soc., A 283, 313-331.

COWARD, M.P. 1983. Some thoughts on the tectonics of the Limpopo Belt. Spec. Pub. Geol. Soc. S. Africa, 8, 175-180.

COWARD, M.P., GRAHAM, R.H., JAMES, P.R. & WAKEFIELD, J. 1973. A structural interpretation of the northern margin of the Limpopo orogenic belt, southern Africa. Phil. Trans. R. Soc., A 273, 487-492.

COWARD, M.P. & JAMES, P.R. 1974. The deformation patterns of two Archaean greenstone belts in Rhodesia and Botswana. Precamb. Res., 1, 235-258.

COWARD, M.P., JAMES, P.R. & WRIGHT, L. 1976a. Northern margin of the Limpopo mobile belt. Bull. Geol. Soc. Amer., 87, 601-611.

COWARD, M.P., LINTERN, B. & WRIGHT, L. 1976b. The pre-cleavage deformation of the sediments and gneisses of the northern part of the Limpopo Belt. In: Windley, B., (ed.), The Early History of The Earth, John Wiley, 323-330.

COX, K.G., JOHNSON, R.L., MONKMAN, C.J., STILMAN, C.J., VAIL, J.R. & WOOD, D.N. 1965. The geology of the Nuanetsi igneous province.

Phil. Trans. R. Soc., A 257, 71-218.

COX, K.G, BELL, J.D. & PANKHURST, R.J. 1979. The Interpretation of Igneous Rocks. George Allen & Unwin, 450 pp.

CRAIG, J.R. 1973. Pyrite-pentlandite assemblages and other low temperature relations in the Fe-Ni-S system. Am. J. Sci., 273A, 496-510.

CRAIG, J.R. & KULLERUD, G. 1969. Phase relations in the Cu-Fe-Ni-S system and their application to magmatic deposits. In: Wilson, H.D.B. (Ed.), Magmatic Ore Deposits, Econ. Geol. Monograph 4, 344-358.

CZAMANSKE, G.K. & MOORE, J.G. 1977. Composition and phase chemistry of sulfide globules in basalt from the Mid-Atlantic Ridge rift valley near 37 N lat. Bull. Geol. Soc. Am., 88, 587-599.

DASCH, E.J., HEDGE, C.E. & DYMOND, J. 1973. Effect of sea water interaction on strontium isotope composition of deep-sea basalts. Earth Planet. Sci. Lett., 19, 177-183.

DASHER, J. 1976. The energy picture in nickel production. Mining Mag., 134, 379-389.

DEER, W.A., HOWIE, R.A. & ZUSSMAN, J. 1966. An Introduction to the Rock-Forming Minerals, Longman.

DEER, W.A., HOWIE, R.A. & ZUSSMAN, J. 1982. Rock-Forming Minerals, 1A, Orthosilicates, 2nd edition, Longman, 919 pp.

DELANEY, J.R., JOHNSON, H.P., & KARSTEN, J.L. 1981. The Juan de Fuca Ridge hot-spot propagating rift system: new tectonic, geochemical and magnetic data. J. Geophys. Res., 86, 11747-11750.

DESMARAIS, N.R. 1981. Metamorphosed Precambrian ultramafic rocks in the Ruby Range, Montana. Precamb. Res., 16, 67-101.

DESPRAIRIES, A. 1982. Authigenic minerals in volcanogenic sediments cored during DSDP Leg 60. Init. Rep. DSDP, 60, 455-466.

DEWEY, J.F. & BIRD, J.M. 1970. Mountain belts and the new global tectonics. J. Geophys. Res., 3, 363-374.

DIETZ, R.S. 1964. Sudbury structure as an astrobleme. J. Geol., 72, 412-434.

DIETZ, R.S. 1972. Sudbury astrobleme, splash emplaced sub-layer and possible cosmogenic ores. Spec. Pap. Geol. Assoc. Can., 10, 19-28.

DIMROTH, E., COUSINEAU, P., LEDUC, M. & SANSCHAGRIN, Y. 1978. Structure and organization of Archean subaqueous basalt flows, Rouyn-Noranda area, Quebec, Canada. Can. J. Earth Sci., 15, 902-918.

DROOP, G.T.R. & BUCHER-NURMINEN, K. 1984. Reaction textures and metamorphic evolution of sapphirine-bearing granulites from the Graf Complex, Italian Central Alps. J. Petrol., 25, 766-803.

DUKE, J.M. 1979. Computer simulation of the fractionation of olivine and sulfide from mafic and ultramafic magmas. Can. Mineral., 17, 507-514.

DUKE, J.M. 1980. Petrology and economic geology of the Dumont sill, N.W. Quebec. Program with Abstracts, Geol. Assoc. Can. - Mineral. Assoc. Can. Ann. Mtg., 5, p50.

DUKE, J.M. & NALDRETT, A.J. 1978. A numerical model of the fractionation of olivine and molten sulfide from komatiite magma. Earth Planet Sci. Lett., 39, 255-266.

DU TOIT, M.C. & VAN REENEN, D.D. 1977. The southern margin of the Limpopo Mobile belt, northern Transvaal, with special reference to metamorphism and structure. Bull. Geol. Surv. Botswana, 12, 83-97.

DU TOIT, M.C., VAN REENEN, D.D. & ROERING, C. 1983. Some aspects of the geology, structure and metamorphism of the Southern Marginal Zone of the Limpopo Metamorphic Complex. Spec. Pub. Geol. Soc. S. Africa, 8, 121-142.

EALES, H.V. 1965. Mineralogy and petrology of the Empress Nickel-Copper deposit, Southern Rhodesia. Trans. Geol. Soc. S. Africa, 67, 173-202.

ECKSTRAND, O.R. 1975. The Dumont serpentinite: A model for control of opaque nickeliferous mineral assemblages by alteration reactions in ultramafic rocks. Econ. Geol., 70, 183-201.

EHLERS, C. 1976. Homogeneous deformation in Precambrian supracrustal rocks of Kumlinge area, Southwest Finland. Precamb. Res., 3, 481-504.

ELLIOTT, R.B. 1973. The chemistry of gabbro/amphibolite transition in South Norway. Contrib. Min. Pet., 38, 71-79.

EMSLIE, R.F. 1983. The coronitic Michael gabbros, Labrador: Assessment of Grenvillian metamorphism in northeastern Grenville Province. Current Research, Pt.A, Geol. Surv. Can., Paper 83-1A, 139-145.

ENGEL, C.G. & FISHER, R.L. 1969. Lherzolite, anorthosite, gabbro and basalt dredged form the Mid-Indian Ocean Ridge. Science, 166, 1136-1141.

ENGEL, C.G. & FISHER, R.L. 1975. Granitic to ultramafic rock complexes of the Indian Ocean Ridge system, western Indian Ocean. Bull. Geol. Soc. Amer., 86, 1553-1578.

ERMANOVICS, I.F. 1977. Post-tectonic remobilization along the southern margin of the Limpopo Mobile Belt. Bull. Geol. Surv. Botswana, 12, 107-127.

EVANS, B.W. 1977. Metamorphism of alpine peridotite and serpentinite. Annual Rev. Earth Planet. Sci., 5, 397-447.

EVANS, B.W. 1982. Amphiboles in metamorphosed ultramafic rocks. Reviews in Mineralogy, 9B, 98-113.

EVANS, B.W. & FROST, B.R. 1975. Chrome-spinel in progressive metamorphism-a preliminary analysis. Geochim. Cosmochim. Acta, 39, 959-972.

EVANS, B.W. & LEAKE, B.E. 1960. Composition and origin of striped amphibolites of Connemara, Ireland. J. Petrol., 1, 337-363.

EWERS, W.E. 1972. Nickel-iron exchange in pyrrhotite. Proceedings Australasian Inst. Mining Metallurgy, 241, 19-26.

EWERS, W.E. & HUDSON, D.R. 1972. An interpretive study of a nickel-iron sulfide ore intersection, Lunnon Shoot, Kambalda, Western Australia. Econ. Geol., 67, 1075-1092.

EWERS, W.E. & MORRIS. R.C. 1981. Studies of the Dale Gorge Member of the Brockman Iron Formation, Western Australia. Econ. Geol., 76, 1929-1953.

FABRIES, J. 1979. Spinel-olivine geothermometry in peridotites from ultramafic complexes. Contrib. Mineral. Petrol., 69, 329-336.

FERRARA, G. Innocenti, F., Ricci, C.A., & Serri, G. 1976. Ocean-floor affinity of basalts from North Appenine ophiolites: geochemical evidence. Chem. Geol., 17, 101-111.

FIELD, D. & ELLIOTT, R.B. 1974. The chemistry of gabbro/amphibolite transition in South Norway. II Trace elements. Contrib. Min. Pet., 38, 71-79.

FINCHAM, C.J.B. & RICHARDSON, F.D. 1954. The behaviour of sulphur in silicate and aluminate slags. Proc. R. Soc., 223, 40-62.

FISHER, R.V. 1984. A review of submarine volcanism, transport processes and deposits. In: Kokelaar, B.P. & Howells, M.F., (eds), Marginal Basin Geology, Spec. Pub. Geol. Soc. London,16, 5-28.

FLEET, M.E. 1977. Origin of disseminated copper-nickel sulphide ore at Frood, Sudbury. Econ. Geol., 72, 1449-1456.

FLEET, M.E. 1979a. A tectonic origin for the Sudbury shatter cones. Prog. with Abstracts, Geol. Assoc. Can., Mineral Assoc. Can. Ann. Mtg., 4, p50.

FLEET, M.E. 1979b. Partitioning of Fe, Co, Ni, and Cu between sulfide liquid and basaltic melts and the composition of Ni-Cu

sulfide deposits - a discussion. Econ. Geol., 74, 1517-1519.

FLEET, M.E., MACRAE, N.D. & HERZBERG, C.T. 1977. Partition of nickel between olivine and sulfide: A test for immiscible sulfide liquids. Contrib. Mineral. Petrol., 65, 191-197.

FLOWER, M.J.F., ROBINSON, P.T., SCHMINKE, H.U. & OHNMACHT, W. 1977. Magma fractionation systems beneath the Mid-Atlantic Ridge near 36-37 N. Contrib. Min. Pet., 64, 167-195.

FLOWER, M.F.J. 1981. Thermal-kinematic controls on ocean-ridge magma fractionation: Comparisons between Atlantic and Pacific crust. J. Geol. Soc. London, 138, 695-712.

FLOYD, P.A., & WINCHESTER, J.A. 1975. Magma-type and tectonic setting discrimination using immobile elements. Earth Planet. Sci. Lett., 27, 211-218.

FONTANAUD, A. & MEUNIER, A. 1983. Mineralogical facies of a weathered serpentinized lherzolite from the Pyrenees , France. Clay Minerals, 16, 231-243.

FRENCH, B.M. 1967. Sudbury structure, Ontario: Some petrographic evidence for origin by meteorite impact. Science, 156, 1094-1098.

FRENCH, B.M.1972. Shock-metamorphic features in the Sudbury structure, Ontario: a review. Spec. Pap. Geol. Assoc. Can., 10, 19-28.

FRIEND, C.R.L. & HUGHES, D.J.1977. Archaean aluminous ultrabasic rocks with primary igneous textures from the Fiskenaesset region, southern West Greenland. Earth planet. Sci. Lett., 36, 157-167.

FRIEND, C.R.L. & HUGHES, D.J. 1981. Chromium-rich sapphirine from the Bjornesund area, southern West Greenland and its bearing on the conditions of crystallisation of the Fiskenaesset anorthosite complex. Rapp. Gronlands Geol. Unders., 105, 41-44.

FRIPP, R.E.P. 1981. The ancient Sand River Gneisses, Limpopo Mobile Belt, South Africa. Spec. Pub. Geol. Soc. Aust., 7, 329-335.

FRIPP, R.E.P. 1983. The Precambrian geology of the area around the Sand River near Messina, Central Zone, Limpopo Mobile Belt. Spec. Pub. Geol. Soc. S. Africa, 8, 89-102.

FRIPP, R.E.P., LILLY, P.A. & BARTON, J.M.,Jr. 1979. The structure and origin of the Singelele gneiss at the type locality near Messina, Limpopo Mobile Belt. Trans. Geol. Soc. S. Africa, 82, 161-167.

FROST, B.R. 1975. Contact metamorphism of serpentinite, chlorite blackwall and rodingite at Paddy-Go-Easy Pass, Central Cascades, Washington. J. Petrol., 16, 272-313.

FROST, B.R. 1976. Limits to the assemblage forsterite-anorthite as

inferred from peridotite hornfelses, Icicle Creek, Washington. Am. Mineral., 61, 732-750.

GAAL, G. 1980. Geological setting and intrusion tectonics of the Kotalahti nickel-copper deposit, Finland. Bull. Geol. Soc. Finland, 52, 101-128.

GALLON, M. 1986 Structural re-interpretation of the Selebi-Phikwe nickel-copper sulphide deposits. In: Gallagher, M.J., Ixer, R.A., Neary, C.R. & Prichard, H.M.,(eds), Metallogeny of basic and ultrabasic rocks, Instn Min. Metall., 473-485.

GASS, I.G. 1977. Origin and emplacement of ophiolites. In: Gass, I.G. (ed.), Volcanic Processes in Ore Genesis. Spec. Pub. Geol. Soc. London, 7, 72-76.

GATZWEILER, R., LEHNERT-THIEL, K., CLASEN, O., TAN, B., VAULTSIDIS, V., STRNAD, J.G. & RICH, J. 1979. The Key Lake uranium-nickel deposits. Bull. Can. Min. Metall., 72, 73-79.

GELINAS, L., MELLINGER, M. & TRUDEL, P. 1982. Archean mafic metavolcanics from the Rouyn-Noranda district, Abitibi greenstone belt, Quebec. 1.Mobility of major elements. Can. J. Earth Sci., 19, 2258-2275.

GIBB, F.G. 1972. A differentiated ultrabasic sheet on Sgurr-Dearg, Isle of Skye. Min. Mag., 38, 811-818.

GILL, J.B. 1981. Orogenic Andesites and Plate Tectonics. Springer-Verlag, 390 pp.

GILL, J.B. & STORK, A.L. 1979. Miocene low-K dacites and trondhjemites of Fiji. In: Barker, F. (ed.), Trondhjemites, dacites, and related rocks, Elsevier, 629-650.

GILL, J.E. 1960. Solid diffusion of sulphides and ore formation. 21st Int. Geol. Cong., 16, 209-217.

GILL, J.E. 1969. Experimental deformation on annealing of sulphides and interpretation of ore textures. Econ. Geol., 64, 500-508.

GILL, R.C.O. 1979. Comparative petrogenesis of Archaean and modern low-K tholeiites. A critical review of some geochemical aspects. Phys. Chem. Earth, 11, 431-447.

GILL, R.C.O. & BRIDGEWATER, D. 1976. The Ameralik dykes of West Greenland, the earliest known basaltic rocks intruding stable continental crust. Earth Planet. Sci. Lett., 29, 276-282.

GILL, R.C.O., BRIDGEWATER, D. & ALLAART, J.H.1981. The geochemistry of the earliest known basic metavolcanic rocks, at Isua, West Greenland. Spec. Pub. Geol. Soc. Aust., 7, 313-325.

GLASKOVSKY, A.A., GORBUNOV, G.I. & SYSOEV, F.A. 1977. Deposits of

nickel. In: Smirnov, V.I.,(ed.), Ore deposits of the U.S.S.R, Vol. II, (Translated into English by D.A.Brown), 3-79.

GLIKSON, A.Y. 1976. Stratigraphy and evolution of primary and secondary greenstones: significance of data from shields of the southern hemisphere. In: Windley, B.F.,(ed.), The Early History of the Earth, John Wiley, 257-278.

GODLEVSKII, M.N. & GRINENKO, L.N. 1963. Some data on the isotopic composition of sulfur in the sulfides of the Noril'sk deposit. Geochemistry, 1, 35-41.

GOLDSMITH, J.R. 1980. The melting and breakdown reactions of anorthite at high pressures and temperatures. Am. Mineral., 65, 272-284.

GOLE, M.J. 1981. Archean Banded Iron-Formations, Yilgarn Block, Western Australia. Econ. Geol., 76, 1954-1974.

GOLE, M.J. & KLEIN, C. 1981. Banded iron-formations through much of Precambrian time. J. Geology, 89, 169-183.

GOLIGHTLY, J.P. 1981. Nickeliferous laterite deposits. Econ. Geol., Seventy-Fifth Anniversary Volume, 710-735.

GORDON, P.S.L. 1973. The Selebi-Pikwe nickel-copper deposits, Botswana. Spec. Pub. Geol. Soc. S. Africa, 3, 167-187.

GRACHEV, A.F. & FEDOROVSKY, V.S. 1981. On the nature of greenstone belts in the Precambrian. Tectonophysics, 73, 195-212.

GRAF, J.L. & SKINNER, B.J. 1970. Strength and deformation of pyrite and pyrrhotite. Econ. Geol., 65, 206-215.

GRAHAM, R.H. 1974. A structural investigation of the southern part of the Limpopo belt and the adjacent Kaapvaal craton,South Africa. 18th Ann. Rep. Res. Inst. African Geol., Univ. Leeds, 63-69.

GRAHAM, C.M. 1976. Petrochemistry and tectonic significance of Dalradian metabasaltic rocks of the S.W. Scottish Highlands. J. Geol. Soc. London, 132, 61-84.

GREEN, A.H. & NALDRETT, A.J. 1981. The Langmuir volcanic peridotite-associated nickel deposits: Canadian equivalents of the Western Austrlaian occurrences. Econ. Geol., 76, 1503-1523.

GREEN, T.H. 1976. Experimental generation of cordierite- or garnet-bearing granitic liquids from a pelitic composition. Geology, 4, 85-88.

GREEN, D.H. & RINGWOOD, A.E. 1967. An experimental investigation of the gabbro to eclogite transformation and its petrological applications. Geochim. Cosmochim. Acta, 31, 767-833.

GRESHAM, J.J. & LOFTUS-HILLS, G.D. 1981. The geology of the Kambalda nickel field, Western Australia. Econ. Geol., 76, 1373-1416.

GROVES, D.I., BARRETT, F.M., BINNS, R.A., MARSTON, R.J. & MCQUEEN,K.G. 1976. A possible volcanic exhalative origin for lenticular nickel sulfide deposits of volcanic association with special reference to those in Western Australia (Discussion). Can. J. Earth Sci., 13, 1646-1650.

GROVES, D.I., BARRETT, F.M., BINNS, R.A., & MCQUEEN, K.G. 1977. Spinel phases associated with metamorphosed volcanic-type iron-nickel sulfide ores from Western Australia. Econ. Geol.,72, 1224-1244.

GROVES, D.I., BARRETT, F.M. & MCQUEEN, K.G. 1978. Geochemistry and origin of chertu metasediments within ultramafic flow sequences and their relationship to nickel mineralization. In: Glover, J.E. & Groves D.I., (eds), Archaean Cherty Metasediments, Geol. Dep. & Ext. Serv. Univ. W. Aust., 2, 57-69.

GROVES, D.I., BARRETT, F.M. & MCQUEEN, K.G. 1979. The relative roles of magmatic segregation, volcanic exhalation and regional metamorphism in the generation of volcanic-associated nickel ores of Western Australia. Can. Mineral., 17, 319-336.

GROVES, D.I. & HUDSON, D.R. 1981. The nature and origin of Archean stratabound volcanic-associated nickel-iron-copper sulphide deposits. In: Wolfe, K.H., (ed.), Handbook of strata-bound and stratiform ore deposits, 9, Elsevier, 305-410.

GROVES, D.I. & KEAYS, R.R. 1979 Mobilization of ore-forming elements during alteration of dunites, Mt. Keith-Betheno, Western Australia. Can. Mineral., 17, 373-389.

GUY-BRAY, J.V.1972. New developments in Sudbury geology: Introduction. Spec. Pap. Geol. Assoc. Can., 10, 1-5.

HACKETT, J.P.Jr. & BISCHOFF, J.L. 1973. New data on the stratigraphy, extent, and geological historyof the Red Sea geothermal deposits. Econ. Geol., 68, 553-564.

HAMILTON, J. 1977. Sr isotope and trace element studies of the Great Dyke and Bushveld mafic phase and their relation to early Proterozoic magma genesis in Southern Africa. J. Petrol., 18,24-52.

HARIYA, V. & KENNEDY, G.C. 1968. Equilibrium study of anorthite under high pressure and temperature. Am. J. Sci., 266, 193-202.

HART, R. 1970. Chemical exchange between sea water and deep ocean basalts. Earth Planet. Sci. Lett., 9, 269-279.

HART, S.R., Erlank, A.J. & Kable, E.J.D. 1974. Sea floor basalt alteration: some chemical and Sr isotopic effects. Contrib. Mineral. Pet., 44, 219-230.

HATHAWAY, J.C. & SACHS, P.L. 1965. Sepiolite and clinoptilite from the

Mid-Atlantic Ridge. Am. Mineral., 50, 852-867.

HAUGHTON, D.R., ROEDER, P.L. & SKINNER, B.J.1974. Solubility of sulfur in mafic magmas. Econ. Geol., 69, 451-467.

HAWLEY, J.E. 1962. The Sudbury ores. Can. Mineral., 7, 1-207.

HEATH, R.J. 1981. Ferromanganese nodules of the deep sea. Econ. Geol., Seventy-Fifth Anniversary Volume, 736-765.

HEDGE, C.E., FUTA, K., ENGEL, C.G. & FISHER, R.L. 1979. Rare earth abundances and Rb-Sr systematics of basalts, gabbros, anorthosite and minor granitic rocks from the Indian Ocean Ridge system, Western Indian Ocean. Contrib. Min. Pet., 68, 373-376.

HEKINIAN, R. 1982. Petrology of the Ocean Floor, Elsevier, 393 pp.

HEKINIAN, R., FEVRIER, M., BISCHOFF, J.L., PICOT, P. & SHANKS, W.C. 1980. Sulfide deposits from the East Pacific Rise near 21 N. Science, 207, 1433-1444.

HELZ, R.T. 1973. Phase relations of basalts in their melting range at PH2O = 5 kb as a function of oxygen fugacity. J. Petrol., 14, 249-302.

HELZ, R.T. 1976. Phase relations of basalts in their melting ranges at PH2O = 5 kb. Part II. Melt compositions. J. Petrol., 17, 139-193.

HENDERSON, P. 1975. Reaction trends shown by chrome-spinels of the Rhum layered intrusion. Geochim. Cosmochim. Acta, 39,1035-1044.

HERD, R.K. 1973. Sapphirine and kornerupine occurrences within the Fiskenaesset complex. Rapp. Gronlands Geol. Unders., 51, 65-71.

HERD, R.K., Windley, B.F. & Ghisler, M. 1969. The mode of occurrence and petrogenesis of the sapphirine-bearing and associated rocks of West Greenland. Rapp. Gronlands Geol. Unders., 24, 1-44.

HEY, R. & SINTON, J.M. 1979. New observations and implications of propagating rifts. Eos, 60, 957.

HICKMAN, M.H. 1976. Geochronological investigations in the Limpopo belt and part of the adjacent Rhodesian craton. Unpub. Ph.D. thesis, Univ. Leeds.

HICKMAN, M.H. 1978. Isotopic evidence for crustal reworking in the Rhodesian Archaean craton, southern Africa. Geology, 6,214-216.

HICKMAN, M.H. & WAKEFIELD, J. 1975. Tectonic interpretation of new geochronologic data from the Limpopo belt at Pikwe, Botswana, southern Africa. Bull. Geol. Soc. Amer., 86, 1468-1472.

HILL, R.E.T. 1984. Experimental study of phase relations at 600 C in a portion of the Fe-Ni-Cu-S system and its application to natural sulphide assemblages. In: Buchanan, D.L. & Jones, M.J., (eds),

Sulphide deposits in mafic and ultramafic rocks, Instn Min. Metall., 14-21.

HODKINSON, I.P. 1979. Cobalt distribution in the Phikwe and Selebi ore bodies. BCL internal report.

HOLLAND, T.J.B. & NORRIS, R.J. 1979. Deformed pillow lavas from the central Hohe Tauerne, Austria and their bearing on the origin of epidote-banded greenstones. Earth Planet. Sci. Lett., 43, 397-405.

HOPWOOD, T. 1981. The significance of pyritic black shales in the genesis of Archean nickel sulphide deposits. In: Wolfe, K.H., (ed.), Handbook of strata-bound and stratiform ore deposits, 9, Elsevier, 411-467.

HOR, A.K. 1972. The geochemistry of the Phikwe anorthosites, eastern Botswana. Unpub. M.Sc. thesis, Univ. Leeds.

HOR, A.K., HUTT, D.K., SMITH, J.V., WAKEFIELD, J. & WINDLEY, B.F.1975. Petrochemistry and mineralogy of early Precambrian anorthositic rocks of the Limpopo belt, southern Africa. Lithos, 8, 297-310.

HORROCKS, P.C. 1980. Ancient Archaean supracrustal rocks from the Limpopo belt, southern Africa. Nature, 286, 596-599.

HORROCKS, P.C. 1983a. The Precambrian geology of an area between Messina and Tshipise, Limpopo Mobile Belt. Spec. Pub. Geol. Soc. S. Africa, 8, 81-88.

HORROCKS, P.C. 1983b. A corundum and sapphirine paragenesis from the Limpopo Mobile Belt, southern Africa. J. Metamorphic Geol. 1, 13-23.

HUBBARD, F.H. 1968. Exsolution myrmekite - A proposed solid-state transformation model. Geologiska Foreningens I Stockholm Forhandlingar, 89, 410-422.

HUMPHRIS, S.E. & THOMPSON, G. 1978. Trace element mobility during hydrothermal alteration of oceanic basalts. Geochim. Cocmochim. Acta, 42, 127-136.

HUNTER, D.R. 1974. Crustal development in the Kaapvaal Craton. I. The Archaean. Precamb. Res., 1, 259-294.

HUNTER, R.H. & SPARKS, R.S.J. 1987. The differentiation of the Skaergaad intrusion. Contrib. Mineral. Pet., 95, 451-461.

HUPPERT, E.H., SPARKS, R.S.J., TURNER, J.S. & ARNDT, N.T. 1984. Emplacement and cooling of komatiite lavas. Nature, 309, 19-22.

HUTCHINSON, R.W. 1982. Syn-depositional hydrothermal processes and Precambrian sulphide deposits. In: Hutchinson, R.W., Spence, C.D. & Franklin, J.M., (eds), Precambrian sulphide deposits,

Spec. Pap. Geol. Assoc. Can., 25, 761-791.

HUTCHINSON, E.H. 1983. Hydrothermal concepts: The old and the new. Econ. Geol., 78, 1734-1741.

HUTCHINSON, E.H., FYFE, W.S. & KERRICH, R. 1980. Deep fluid penetration and ore deposition. Minerals Sci. Engng, 12, 107-120.

HYNES, A. & FRANCIS, D. 1982. Komatiitic basalts of the Cape Smith foldbelt, New Quebec, Canada. In: Arndt, N.T. & Nisbet, E.G., (eds), Komatiites, George Allen & Unwin, 159-170.

IRVINE, T.N. 1975. Crystallisation sequences in the Muskox intrusion and other layered intrusions - II. Origin of chromitite layers and similar deposits of other magmatic ores. Geochim.Cosmochim. Acta, 39, 991-1020.

IRVINE, T.N. 1977. Origin of chromitite layers in the Muskox intrusion and other stratiform intrusions: A new interpretation. Geology, 5, 273-277.

IRVINE, T.N., KEITH, D.W. & TODD, S.G. 1983. The J-M Platinum-Palladium Reef of the Stillwater Complex, Montana: II. Origin by double-diffusive convective magma mixing and implications for the Bushveld Complex. Econ. Geol., 78, 1287-1334.

IRVINE, T.N. & SHARPE, M.R. 1982. Source-rock compositions and depths of origin of Bushveld and Stillwater magmas. Carnegie Inst. Wash. Ybk, 81, 294-303.

JACOBSEN, J.B.E. 1974. Structure of the copper ore bodies and country rocks at Artonvilla mine, South Africa. Trans. Instn Min. Metall., 83, B60-64.

JAMES, H.L. 1954. Sedimentary facies of iron-formation. Econ. Geol., 49, 235-285.

JANARDHANAN, A.S. & LEAKE, B.E. 1974. Sapphirine in the Sittampundi complex, India. Min. Mag., 39, 901-902.

JANSEN, H. 1975. The Soutpansberg trough (northern Transvaal) - an aulacogen. Trans. Geol. Soc. S. Africa, 78, 129-136.

JEANS, C.V. 1978. The origin of the Triassic clay assemblages of Europe with special reference to the Keuper Marl and Rhaetic of parts of England. Phil. Trans. R. Soc., A289, 549-639.

JOLLY, W.T. 1975. Subdivision of the Archean lavas of the Abitibi area, Canada, from Fe-Mg-Ni-Cr relations. Earth Planet. Sci. Lett., 27, 200-210.

KARSON, J.A., ELTHON, D.L. & DELONG, S.E. 1983. Ultramafic intrusions in the Lewis Hills Massif, Bay of Islands Ophiolite Complex, Newfoundland: implications for igneous processes at oceanic

fracture zones. Bull. Geol. Soc. Amer., 94, 15-29.

KAY, R., HUBBARD, N.J. & GAST, P.W. 1970. Chemical characteristics and origin of oceanic volcanic rocks. J. Geophys. Res., 75, 1585-1613.

KARUP-MOLLER, S. & BRUMMER, J.J. 1971. Geology and sulphide deposits of the Bird River claim group, southeastern Manitoba. Spec. Pap. Geol. Assoc. Can., 9, 143-154.

KELLY, W.C. & CLARK, B.R. 1975. Sulphide deformation studies: III. Experimental deformation of chalcopyrite to 2,000 bars and 500 C. Econ. Geol., 70, 431-452.

KEY, R.M. 1976. The geology of the area around Francistown and Phikwe, northeast and central districts, Botswana. Mem. Geol. Surv. Botswana, 3.

KEY, R.M. 1977. The geological history of the Limpopo Mobile Belt based on the field mapping of the Botswana Geological Survey. Bull. Geol. Surv. Botswana, 12, 41-59.

KEY, R.M. & HUTTON, S.M. 1976. The tectonic generation of the Limpopo Mobile Belt and a definition of its western extremity. Precamb. Res., 3, 79-90.

KEY, R.M., LITHERLAND, M. & HEPWORTH, J.V. 1976. The evolution of the Archaean crust of northeast Botswana. Precamb. Res., 3,375-413.

KISSIN, S.A. & SCOTT, S.D. 1982. Phase relations involving pyrrhotite below 350 C. Econ. Geol., 77, 1739-1754.

KLEIN, C. 1973. Changes in mineral assemblages with metamorphism of some banded Precambrian iron-formations. Econ. Geol., 68, 1075-1088.

KLEIN, C. 1978. Regional metamorphism of Proterozoic iron-formation, Labrador Trough, Canada. Am. Mineral., 63, 898-912.

KLOTSMAN, S.M., TIMOFEYEV, A.N. & TRAKHTENBERG, I.Sh. 1963. Investigation of the diffusion properties of the chalcogenides of transition metals IV. Temperature dependence of the anisotropy of nickel and sulphur self-diffusion in nickel mono-sulphide. Physics Metals Metallography, 16, 92-98.

KRÖNER, A. 1981. Precambrian Plate Tectonics. In: Kröner, A., (ed.), Precambrian Plate Tectonics, Elsevier, 57-90.

KRYNINE, P.D. 1960. Primeval ocean. Bull. Geol. Soc. Amer., 71, p.1911 (Abstr.).

KULLERUD, G. & YODER, H.S. 1965. Sulfide-silicate reactions and their bearing on ore formation under magmatic, postmagmatic and metamorphic conditions. In: Symposium on Problems of Postmagmatic Ore Deposition, II, Geol. Surv. Czechoslavakia, 327-331.

KULLERUD, G., YUND, R.A. & MOH, G.H. 1969. Phase relations in the Cu-Fe-S, Cu-Ni-S, and Fe-Ni-S systems. In: Wilson, H.D.B., (ed.), Magmatic Ore Deposits, Econ. Geol. Monograph 4, 323-343.

LAWRENCE, L.J. 1967. Sulphide neomagmas and highly metamorphosed sulphide deposits. Mineral. Deposita, 2, 5-10.

LEAKE, B.E. 1964. The chemical distinction between ortho- and para-amphibolites. J. Petrol., 5, 238-254.

LEAKE, B.E. 1978. Nomenclature of amphiboles. Am. Mineral., 63, 1023-1052.

LEAKE, B.E., JANARDHANAN, A.S. & KEMP, A. 1976. High P-H2O and hornblende in the Sittampundi complex, India. Min. Mag., 40, 525-526.

LEAR, P.A. 1971. A geological investigation of some Precambrian ultramafic rocks in eastern Botswana. Unpub. M.Sc. thesis, Univ. Manchester.

LEAR, P.A. 1977. Metallogeny of the Limpopo Mobile Belt in Botswana. Bull. Geol. Surv. Botswana, 12, 203-208.

LEAR, P.A. 1979. The ore mineralogy of the phikwe and Selebi Nickel-Copper deposits, Botswana. Spec. Pub. Geol. Soc. S. Africa, 5, 117-132.

LEE, C.A. 1983. Trace and platinum-group element geochemistry and the development of the Merensky Unit of the western Bushveld Complex. Mineral. Deposita, 18, 173-190.

LEE, C.A. & FESQ, H.W. 1985. Au, Ir and trace elements in some chromitites of the East Bushveld Complex. Metallogeny of basic and ultrabasic rocks, British Geological Survey, Edinburgh, Abstracts.

Le MAITRE, R.W. 1976. The chemical variability of some common igneous rocks. J. Petrol., 17, 589-637.

LESHER, C.M., LEE, R.F., GROVES, D.I., BICKLE, M.J. & DONALDSON, M.J. 1981. Geochemistry of komatiites from Kambalda, Western Australia: I. Chalcophile element depletion - a consequence of sulfide liquid separation from komatiitic magmas. Econ. Geol., 76, 1714-1728.

LESHER, C.M. & KEAYS, R.R. 1984. Metamorphically and hydrothermally mobilized Fe-Ni-Cu sulphides at Kambalda, Western Australia. In: Buchanan, D.L. & Jones, M.J., (eds), Sulphide deposits in mafic and ultramafic rocks, Instn Min. Metall., 62-69.

LESHER, C.M., ARNDT, N.T. & GROVES, D.I. 1984. Genesis of komatiite-associated nickel sulphide deposits at Kambalda, Western Australia: a distal volcanic model. In: Buchanan, D.L. & Jones,

M.J., (eds), Sulphide deposits in mafic and ultramafic rocks, Instn Min. Metall., 70-80.

LEYERLOUP, A., LASNIER, B. & MARCHAND, J. 1975. Retrograde corona-forming reactions in high pressure granulite facies rocks. Petrologie, 1, 43-55.

LIEBENBERG, L. 1970. The sulfides in the layered sequence of the Bushveld Igneous Complex. Spec. Pub. Geol. Soc. S. Afr., 1, 108-207.

LIEBERMAN, J.E. & RICE, J.M. 1986. Petrology of marble and peridotite in the Seiad ultramafic complex, northern California, USA. J. Metamorphic Geol., 4, 179-199.

LIGHT, M.P.R. 1982. The Limpopo Mobile Belt: A result of continental collision. Tectonics, 1, 325-342.

LIGHT, M.P.R. & WATKEYS, M.K. 1977. An outline of the Archaean and Proterozoic geological history of the region around Beit Bridge. Ann. Rhod. Geol. Surv., 3, 35-40.

LIGHT, M.P.R., BRODERICK, T.J. & WATKEYS, M.K. 1977. A preliminary report on the central zone of the Limpopo Mobile Belt, Rhodesia. Bull. Geol. Surv. Botswana, 12, 61-73.

LIGHTFOOT, P.C., NALDRETT, A.J. & HAWKESWORTH, C.J. 1984. The geology and geochemistry of the Waterfall Gorge section of the Insizwa Complex with particular reference to the origin of nickel sulfide deposits. Econ. Geol., 74, 1857-1874.

LITHERLAND, M. 1973. Uniformitarian approach to Archaean "schist relics". Nature, 242, 125-127.

LITHERLAND, M. & KEY, R.M. 1974. A preliminary interpretation of the field mapping of the Eastern Geotraverse of Botswana. 18th Ann. Rep. Res. Inst. African Geol., Univ. Leeds, 39-43.

LONSDALE, P.F., BISCHOFF, J.L., BURNS, V.M., KASTNER, M. & SWEENEY, R.E. 1980. A high-temperature hydrothermal deposit on the sea-bed at a Gulf of California spreading center. Earth Planet. Sci. Lett., 49, 8-20.

LUDDEN, J., GELINAS, L. & TRUDEL, P. 1982. Archean metavolcanics from the Rouyn-Noranda district, Abitibi greenstone belt, Quebec. 2. Mobility of trace elements and petrogenetic constraints. Can. J. Earth Sci., 19, 2276-2287.

LUSK, J. 1976a. A possible volcanic-exhalative origin for lenticular nickel sulfide deposits of volcanic association, with reference to Western Australia. Can. J. Earth Sci., 13, 451-458.

LUSK, J. 1976b. A possible volcanic-exhalative origin for lenticular

nickel sulphide deposits of volcanic association, with special reference to those in Western Australia. Can. J. Earth Sci., 13, 1651-1653.

MacDONALD, G.A. & KATSURA, T. 1964. Chemical composition of Hawaiian lavas. J. Petrol., 5, 82-133.

MacGREGOR, A.M. 1953. Precambrian formations of tropical southern Africa. 19th Int. Geol. Cong. Algiers, 39-50.

MacLEAN, W.H. & SHIMAZAKI, H. 1976. The partition of Co, Ni, Cu, and Zn between sulfide and silicate liquids. Econ. Geol., 71, 1049-1057.

MacRAE, N.D. 1974. Sulfurization of basalts under thermal metamorphic conditions to provide cordierite-bearing rocks. Can. J. Earth Sci., 11, 246-253.

MAINWARING, P.R. & NALDRETT, A.J. 1977. Country-rock assimilation and the genesis of Cu-Ni sulfides in the Water Hen intrusion, Duluth Complex, Minnesota. Econ. Geol., 72, 1269-1284.

MARSH, S.C.K. 1978. Nickel-copper occurrences at Dikoloti and Lentswe, Eastern Botswana. In: Verwoerd, W.J., (ed.), Mineralization in Metamorphic Terranes, Spec. Pub. Geol. Soc. S. Africa, 4, 131-148.

MANDER, N.D. 1982. Empress nickel mine. Unpub. RTMZ report.

MARSTON, R.J. & KAY, B.D. 1980. The distribution, petrology, and genesis of nickel ores at the Juan Complex, Kambalda, Western Australia. Econ. Geol., 75, 546-565.

MARSTON, R.J., GROVES, D.I., HUDSON, D.R. & ROSS, J.R. 1981. Nickel sulfide deposits in Western Australia: A review. Econ. Geol., 76, 1330-1363.

MARTIN, J.E. & ALLCHURCH, P.D. 1975. Geology of Perseverance nickel deposit, Western Australia. In: Knight, C.L., (ed.), Economic geology of Australia and Papua New Guinea, I. Metals, Aust. Inst. Min. Metall., Mon. 5, 149-155.

MASON, R. 1967. The geology of the country around Baines Drift - eastern Botswana. Unpub. M.Sc. thesis, Univ. Newcastle.

MASON, R. 1970. The geology of the country between Francistown and Madinare. Unpub. Ph.D. thesis, Univ. Witwatersrand.

MASON, R. 1973. The Limpopo Mobile Belt - southern Africa. Phil. Trans. R. Soc., A 273, 463-485.

MAYNARD, J.B., VALLONI, R. & YU, H. 1982. Composition of modern deep-sea sands from arc-related basins. In: Legget,J.K.(ed.), Trench -Forearc Geology, Geol. Soc. London Spec. Pub., 10, 551-561.

McCALLUM, I.S., RAEDEKE, L.D. & MATHEZ, E.A. 1980. Investigations of the Stillwater Complex: Part 1. Stratigraphy and structure of the Banded zone. Am. J. Sci. 280A, 59-87.

McDONALD, J.A. 1967. Metamorphism and its effects on sulphide assemblages. Mineral. Deposita, 2, 200-220.

McDOUGALL, T.F., MEIKLE, B.K., GUY-BRAY, T.V., SAUL, V.A. & GILL, J.E. 1961. Experimental investigation of solid diffusion and volatization of certain metallic sulfides. Econ. Geol., 56, 362-391.

McKECKNIE, K.R. 1971. The exploration and geology of Selebi North. Unpub. M.Sc. thesis, Imperial College, London.

McLENNAN, S.M., TAYLOR, S.R. & ERIKSSON, K.A. 1983a. Geochemistry of Archean shales from the Pilbara Supergroup, Western Australia. Geochim. Cosmochim. Acta, 74, 1211-1222.

McLENNAN, S.M., TAYLOR, S.R. & KRONER, A. 1983b. Geochemical evolution of Archean shales from South Africa. 1. The Swaziland and Pongola Supergroups. Precamb. Res., 22, 93-124.

McQUEEN, K.G. 1979. Experimental heating and diffusion effects in Fe-Ni sulfide ores from Redros, Western Australia. Econ. Geol., 74, 140-148.

MEDARIS, L.G. 1972. High pressure peridotites in southwestern Oregon. Bull. Geol. Soc. Amer., 83, 41-58.

MEDARIS, L.G. 1975. Coexisting spinel and silicates in alpine peridotites of the granulite facies. Geochim. Cosmochim. Acta, 39, 947-958.

MENZIES, M. & SEYFRIED, W.E.Jr. 1979. Basalt-sea water interaction: Trace element and strontium isotopic variations in experimentally altered glassy basalt. Earth Planet. Sci. Lett., 44, 463-472.

MIKKOLA, A.K. & VAISANEN, S.E. 1972. Remobilization of sulphides in the Outokumpu and Vihanti ore deposits, Finland. 24th Int. Geol. Cong., 4, 488-497.

MILLER, L.J. & SMITH, M.E. 1975. Sherlock Bay nickel-copper. In: Knight, C.L.,(ed.), Economic geology of Australia and Papua New Guinea I. Metals, Aust. Inst. Min. Metall., Mon. 5, 168-174.

MISCH, P. & RICE, J.M. 1975. Micsibility of tremolite and hornblende in progressive Skagit metamorphic suite, North Cascades, Washington. J. Petrol., 16, 1-21.

MIYASHIRO, A. 1975. Classification, characteristics and origin of ophiolites. J. Geology, 83, 249-281.

MIYASHIRO, A., SHIDO, F. & EWING, M. 1969a. Diversity and origin of

abyssal tholeiite from the Mid-Atlantic Ridge near 24 and 30 N latitude. Contrib. Mineral. Petrol., 23, 38-52.

MIYASHIRO, A., SHIDO, F. & EWING, M. 1969b. Compositon and origin of serpentinites from the Mid-Atlantic Ridge near 24 and 30 N latitude. Contrib. Mineral. Petrol., 23, 117-127.

MIYASHIRO, A., SHIDO, F. EWING, M. 1971. Metamorphism in the Mid-Atlantic Ridge near 24 and 30 N. Phil. Trans. R. Soc., A 268, 589-603.

MOORE, J.G. & FABBI, B.P. 1971. An estimate of the juvenile sulfur content of basalt. Contrib. Mineral. Petrol., 33, 118-127.

MURRAY, R.S. 1981. Long range mine planning and ore availability for BCL metallurgical plant. BCL internal report.

MYERS, J.S. 1975. Pseudo-fractionation trend of the Fiskenaesset anorthosite complex, southern West Greenland. Rapport Gronlands Geol. Unders, 75, 77-80.

MYERS, J.S. 1978. Formation of banded gneisses by deformation of igneous rocks. Precamb. Res., 6, 43-64.

MYSEN, B.O. & POPP, R.K. 1980. Solubility of sulfur in CaMgSi2O6 and NaAlSi3O8 melts at high pressure and temperature with controlled FO2 and FS2. Am. J. Sci., 280, 78-92.

NALDRETT, A.J. 1966. The role of sulphurization in the genesis of iron-nickel sulphide deposits of the Porcupine district, Ontario. Trans. Can. Inst. Min. Metall., 69, 147-155.

NALDRETT, A.J. 1969. A portion of the system Fe-S-O between 900 C and 1080 C and its application to sulfide ore magmas. J. Petrol., 10, 171-201.

NALDRETT, A.J. 1973. Nickel sulfide deposits - their classification and genesis, with special emphasis on deposits of volcanic association. Trans. Can. Inst. Min. Metall., 76, 183-201.

NALDRETT, A.J. 1979. Partitioning of Fe, Co, Ni and Cu between sulfide liquid and basaltic melts and the composition of Ni-Cu sulfide deposits - a reply and further discussion. Econ.Geol., 74, 1520-1528.

NALDRETT, A.J., IGCP Project, 1979. IGCP Project No. 161 and a proposed classification of Ni-Cu-PGE sulfide deposits. Can. Mineral., 17, 143-144.

NALDRETT, A.J. 1981. Nickel sulfide deposits: Classification, composition and genesis. Econ. Geol., Seventy-Fifth Anniversary Volume, 628-685.

NALDRETT, A.J. & CABRI, L.J. 1976. Ultramafic and related mafic rocks:

Their classification and genesis with special reference to the concentration of nickel sulfides and platinum-group elements. Econ. Geol., 71, 1131-1158.

NALDRETT, A.J. & GASPARRINI, E.L. 1971. Archean nickel sulfide deposits in Canada, their classification, geological setting and genesis with some suggestions as to exploration. Spec. Pub. Geol. Soc. Aust., 3, 201-226.

NALDRETT, A.J., GUY-BRAY, J.V., GASPARRINI, E.L., PODOLSKY, T. & RUCKLIDGE, J.C. 1970. Cryptic variation and the petrology of the Sudbury Nickel Irruptive. Econ. Geol., 65, 122-155.

NALDRETT, A.J., HOFFMAN, E.L., GREEN, A.H., CHEN-LIN CHOU, NALDRETT, S.R. & ALCOCK, R.A. 1979. The composition of Ni-sulfide ores, with particular reference to their content of PGE and Au. Can. Mineral., 17, 403-415.

NALDRETT, A.J. & KULLERUD, G. 1967. A study of the Strathcona mine and its bearing on the origin of the nickel-copper ores of the Sudbury district, Ontario. J. Petrol., 8, 453-531.

NALDRETT, A.J. & MACDONALD, A.J. 1980. Tectonic settings of some Ni-Cu sulfide ores: Their importance in genesis and exploration. Spec. Pap. Geol. Assoc. Can., 20, 633-657.

NALDRETT, A.J., RAO, B.V. & EVENSEN, N.M. 1986. Contamination of Sudbury and its role in ore formation. In: Gallagher, M.J., Ixer, R.A., Neary, C.R. & Prichard, H.M., (eds), Metallogeny of basic and ultrabasic rocks, Instn Min. Metall., 75-91.

NALDRETT, A.J. & TURNER, A.R. 1977. The geology and petrogenesis of a greenstone belt and related nickel sulfide mineralization at Yakabindie, Western Australia. Precamb. Res., 5, 43-103.

NATLAND,J.H. & MAHONEY, J.J. 1982. Alteration of igneous rocks at DSDP sites 458 and 459, Mariana fore-arc region: relationship to basement structure. Init. Rep. DSDP, 60, 769-788.

NATLAND, J.H., ROSENDAHL, B., HEKINIAN, R., DMITRIEV, Y., FODOR, R.V., GOLL, R.M., HOFFERT, M., HUMPHRIS, S.E., MATTEY, D.P.,PETERSEN, N., ROGGENTHEN, W., SHRADER, E.L., SRIVASTAVA, R.K. & WARREN,N. 1979. Galapagos hydrothermal mounds: stratigraphy and chemistry revealed by deep-sea drilling. Science, 204, 613-616.

NESBITT, R.W., SHEN-SU SUN & PURVIS, A.C. 1979. Komatiites: Geochemistry and genesis. Can. Mineral., 17, 165-186.

NISBET, E.G. & PEARCE, J.A. 1973. TiO2 and a possible guide to past oceanic spreading rates. Nature, 246, 468-469.

NISBET, E.G. 1982. The tectonic setting and petrogenesis of

komatiites. In: Arndt, N.T. & Nisbet, E.G., (eds), Komatiites, George Allen & Unwin, 501-520.

NUTMAN, A.P., BRIDGEWATER, D. & FRYER, B.J. 1984. The iron-rich suite from the Amitsoq gneisses of southern West Greenland: early Archaean plutonic rocks of mixed crustal and mantle origin. Contrib. Min. Pet., 87, 24-34.

O'CONNOR, T.J. 1965. A classification for quartz-rich igneous rocks based on feldspar ratios. U.S. Geol. Surv. Prof. Pap., 525-B, 79-84.

O'HARA, M.J. 1977. Geochemical evolution during fractional crystallization of a periodically refilled magma chamber. Nature, 266, 503-507.

OLIVER, R.L. & JONES, J.B. 1965. A chlorite-corundum rock from Mount Painter, South Australia. Min. Mag., 35, 140-145.

PAGE, N.J. & SIMON, F.O. 1978. Differentiation of the sulfides in the Basal Zone of the Stillwater Complex, Montana. J. Res. U.S. Geol. Surv., 6, 473-482.

PALLISTER, J.S. & GREGORY, R.T. 1983. Composition of the Samail ocean crust. Geology, 11, 638-642.

PAPUNEN, H., HAKLI, T.A. & IDMAN, H. 1979. Geological, geochemical and mineralogical features of sulfide-bearing ultramafic rocks in Finland. Can. Mineral., 17, 217-232.

PATERSON, H.L., DONALDSON, M.J., SMITH, R.N., LENARD, M.F., GRESHAM, J.J., BOYACK, D.J. & KEAYS, R.R. 1984. Nickeliferous sediments and sediment-associated nickel ores at Kambalda, Western Australia. In: Buchanan, D.L. & Jones, M.J., (eds), Sulphide deposits in mafic and ultramafic rocks, Instn Min. Metall., 81-94.

PATTERSON, G.C. & WATKINSON, D.H. 1984a. The geology of the Thierry Cu-Ni mine, Northwestern Ontario. Can. Mineral., 22, 3-11.

PATTERSON, G.C. & WATKINSON, D.H. 1984b. Metamorphism and supergene alteration of Cu-Ni sulfides, Thierry mine, Northwestern Ontario. Can. Mineral., 22, 13-21.

PATTISON, E.F. 1979. The Sudbury sublayer. Can. Mineral. 17, 257-274.

PEARCE, J.A. 1975. Basalt geochemistry used to investigate past tectonic environments on Cyprus. Tectonophysics, 25, 41-67.

PEARCE, J.A. & CANN, J.R. 1973. Tectonic setting of basic volcanic rocks determined using trace element analysis. Earth Planet. Sci. Lett., 19, 290-300.

PEARCE, J.A. & FLOWER, M.F.J. 1977. The relative importance of petro-

genetic variables in magma genesis at accreting plate margins: a preliminary investigation. J. Geol. Soc. London, 134, 103-127.

PEARCE, J.A. & NORRY, M.J. 1979. Petrogenetic implications of Ti, Zr, Y and Nb variations in volcanic rocks. Contrib. Min. Pet., 69, 33-47.

PEARCE, T.H., GORMAN, B.E. & BIRKETT, T.C. 1977. The relationship between major element chemistry and tectonic environment of basic and intermediate volcanic rocks. Earth Planet. Sci. Lett., 36, 121-132.

PEARTON, T.N. 1978. The geology and geochemistry of the Monarch ore body and environs, Murchison Range, north-eastern Transvaal.In: Verwoerd, W.J., (ed.), Mineralization in Metamorphic Terranes, Spec. Pub. Geol. Soc. S. Africa, 4, 77-86.

PEARTON, T.N. 1982. Gold and antimony mineralization in altered komatiites of the Murchison greenstone belt, South Africa. In: Arndt, N.T. & Nisbet, E.G., (eds), Komatiites, George Allen & Unwin, 459-475.

PEREDERY, W.V. 1972. Chemistry of fluidal glasses and melt bodies in the Onaping Formation. Spec. Pap. Geol. Assoc. Can. 10, 49-59.

PEREDERY, W.V. 1979. Relationship of ultramafic amphibolites to metavolcanic rocks and serpentinites in the Thompson belt, Manitoba. Can. Mineral., 17, 187-200.

PEREDERY, W.V. & NALDRETT, A.J. 1975. Petrology of the upper Irruptive rocks, Sudbury, Ontario. Econ. Geol., 70, 164-175.

PEREDERY, W.V. & Geological Staff, 1982. Geology and nickel sulphide deposits of the Thompson Belt, Manitoba. In: Hutchinson, R.W., Spence, C.D. & Franklin, J.M., (eds), Precambrian sulphide deposits, Spec. Pap. Geol. Assoc. Can., 25, 165-209.

PETTIJOHN, F.J. 1963. Chemical composition of sandstones - excluding carbonate and volcanic sands. U.S. Geol. Surv. Prof. Pap., 440-S, 19 pp.

PFEIFFER, H.R. 1981. A model for fluids in metamorphosed ultramafic rocks. III. Mass transfer under amphibolite facies conditions in olivine-enststite rocks of the Central Alps, Switzerland. Bull. Mineral., 104, 834-847.

PHARAOH, T. 1985. Volcanic and geochemical stratigraphy of the Nussir Group of Arctic Norway - an early Proterozoic greenstone suite. J. Geol. Soc. London, 142, 259-278.

PHEMISTER, T.C. 1937. A review of the problems of the Sudbury Irruptive. J. Geol., 45, 1-47.

PLIMER, I.R. 1977. The mineralogy of the high-grade metamorphic rocks enclosing the Broken Hill ore bodies, Australia. N. Jb. Miner. Abh., 131, 115-139.

PLIMER, I.R. 1979. Sulphide rock zonation and hydrothermal alteration at Broken Hill, Australia. Trans. Instn Min. Metall., 88, B161-176.

PRIDER, R.T. 1970. Nickel in Western Australia. Nature, 226, 691-693.

PRINZ, M. 1967. Geochemistry of basaltic rocks: Trace elements. In: Hess, H.H. & Poldervaart, A.,(eds), Basalts, 1, Wiley, 271-323.

PURVIS, A.C., NESBITT, R.W. & HALLBERG, J.A. 1972. The geology of part of the Carr Boyd Rocks complex and its associated nickel mineralization, Western Australia. Econ. Geol., 67, 1093-1113.

RAASE, P. 1974. Al and Ti contents of hornblende, indicators of pressure and temperature of regional metamorphism. Contrib. Min. Pet., 45, 231-236.

RAJAMANI, V. & NALDRETT, A.J. 1978. Partitioning of Fe, Co, Ni, and Cu between sulfide liquid and basaltic melts and the composition of Ni-Cu sulfide deposits. Econ. Geol., 73, 82-93.

RAMSAY,C.R. & DAVIDSON, L.R. 1975. The origin of scapolite in the regionally metamorphosed rocks of Mary Kathleen, Queensland, Australia. Contrib. Min. Pet., 25, 41-51.

RAO, B.V. & RIPLEY, E.M. 1983. Petrochemical studies of the Dunka Road Cu-Ni deposit, Duluth Complex, Minnesota. Econ. Geol., 78, 1222-1238.

REEVES, C.V. & HUTCHINS, D.G. 1975. New data on crustal structures in central southern Africa. Nature, 254, 408-410.

RHODES, J.M., BLANCHARD, D.R., RODGERS, K.V., JACOBS, J.W. & BRANDON, J.C. 1976. Petrology and chemistry of basalts from the Nazca plate, 2. Major and trace element chemistry. Init. Rep. DSDP, 34, 239-244.

RINGWOOD, A.E. 1977. Petrogenesis in island arc systems. Maurice Ewing Series, Am. Geophys. Union, 1, 311-324.

RIPLEY, E.M. 1981. Sulfur isotopic studies of the Dunka Road Cu-Ni deposit, Duluth Complex, Minnesota. Econ. Geol., 76, 610-620.

ROBERTSON, I.D.M. 1968. Granulite metamorphism of the basement complex in the Limpopo metamorphic zone. Trans. Geol. Soc. S. Africa (annex), 71, 125-134.

ROBERTSON, I.D.M. 1973. Potash granites of the southern edge of the Rhodesian craton and the northern granulite zone of the Limpopo Mobile Belt. Spec. Pub. Geol. Soc. S. Africa, 3, 265-276.

ROBERTSON, I.D.M. 1974. Explanation of the country around Mount Towla, Gwanda District. Short Rep. Rhodesian Geol. Surv., 41.

ROBERTSON, I.D.M. 1977. Some granulite facies metasediments of the Rhodesian part of the North Marginal Zone of the Limpopo Mobile Belt. Bull. Geol. Surv. Botswana, 12, 157-176.

ROBERTSON, I.D.M. & DU TOIT, M.C. 1981. The Limpopo Belt. In: Hunter, D.R., (ed.), The Precambrian of The Southern Hemisphere, Elsevier, 641-671.

ROBERTSON, J.M. 1975. Geology and mineralogy of some copper sulfide deposits near Mount Bokemia, Keweenaw County, Michigan. Econ. Geol., 70, 1202-1224.

ROBINSON, D.J. & HUTCHINSON, R.W. 1982. Evidence for a volcanogenic-exhalative origin of a massive nickel sulphide deposit at Redstone, Timmins, Ontario. In: Hutchinson, R.W., Spence, C.D. & Franklin, J.M., (eds), Precambrian sulphide deposits, Spec. Pap. Geol. Assoc. Can., 25, 211-254.

ROGERS, J.J.W. 1982. Criteria for recognizing environments of formation of volcanic suites; Application of these criteria to volcanic suites in the Carolina Slate Belt. Spec. Pap. Geol. Soc. Amer., 191, 99-107.

ROGERS, J.J.W., SUAYAH, I.B., & EDWARDS, J.M. 1984. Trace elements in continental magmatism: Part IV. Geochemical criteria for recognition of two volcanic assemblages near Auburn, western Sierra Nevadas, California. Bull. Geol. Soc. Amer., 95, 1437-1445.

RONA, P.A. 1978. Criteria for the recognition of hydrothermal mineral deposits in oceanic crust. Econ. Geol., 73, 135-160.

RONOV, A.B. 1964. Common tendencies in the chemical evolution of the earth's crust, ocean and atmosphere. Geochem. Int., 1, 713-737.

ROSCOE, W.E. 1975. Experimental deformation of natural chalcopyrite at temperatures up to 300 C over the strain rate range 10-2 to 10-6 sec-1. Econ. Geol., 70, 454-472.

ROSS, J.R. & HOPKINS, G.M.F. 1975. Kambalda nickel sulphide deposits. In: Knight, C.L.,(ed.). Economic geology of Australia and Papua New Guinea, I. Metals, Aust. Inst. Min. Metall. Mon. 5,100-121.

ROSS, J.R. & KEAYS, R.R. 1979. Precious metals in volcanic-type nickel sulfide deposits in Western Australia. I. Relationships with the composition of the ores and their host rocks. Can. Mineral., 17, 417-435.

ROSS, J.R. & TRAVIS, G.A. 1981. The nickel sulfide deposits of Western Australia in global perspective. Econ. Geol., 76, 1291-1329.

RYAN, B.D., KRAMERS, J.D., STACEY, J.S., DELEVAUX, M., BARTON, J.M., Jr, & FRIPP, R.E.P. 1983. Strontium and lead isotopic studies and K/Rb ratio measurements relating to the origin and emplacement of copper deposits near Messina, South Africa. Spec. Pub. Geol. Soc. S. Africa, 8, 47-53.

SAGGERSON, E.P. & TURNER, L.M. 1976. A review of the distribution of metamorphism in the ancient Rhodesian craton. Precamb. Res., 3, 1-53.

SAUNDERS, A.D., TARNEY, J., STERN, C.R. & DALZIEL, I.W.D. 1979. Geochemistry of Mesozoic marginal basin floor igneous rocks from Southern Chile. Bull. Geol. Soc. Amer., 90, 237-258.

SCHEIDEGGER, K.F. 1973. Temperature and composition of magmas ascending along mid-ocean ridges. J. Geophys. Res., 78, 3340-3355.

SCHMULIAN, M.L. 1984. Windarra nickel deposits, Western Australia. In: Buchanan, D.L. & Jones, M.J., (eds), Sulphide deposits in Mafic and ultramafic rocks, Instn Min. Metall., 95-102.

SCHOLTZ, D.L. 1936. The magmatic nickeliferous ore deposits of East Griqualand and Pondoland. Trans. Geol. Soc. S. Africa, 39, 81-210.

SCHREYER, W., HORROCKS, P.C. & ABRAHAM, K. 1984. High-magnesium staurolite in a sapphirine-garnet rock from the Limpopo Belt, Southern Africa. Contrib. Mineral. Petrol., 86, 200-207.

SCOATES, R.F.J. 1971. A description and classficiation of Manitoba ultramafic rocks. Spec. Pap. Geol. Assoc. Can., 9, 89-96.

SCOTT, R.B. & HAJASH, A., Jr, 1976. Initial submarine alteration of basaltic pillow lavas: a microprobe study. Am. J. Sci., 276, 480-501.

SECCOMBE, P.K., GROVES, D.I., BINNS, R.A. & SMITH, J.W. 1977. A sulphur isotope study to test a genetic model for Fe-Ni sulphide mineralization at Mt. Windarra, Western Australia. Bull. New Zealand Dept. Sci. Indus. Res., 220, 187-200.

SECCOMBE, P.K., GROVES, D.I., MARSTON, R.J. & BARRETT, F.M. 1981. Sulfide paragenesis and sulfur mobility in Fe-Ni-Cu sulfide ores at Kambalda: Sulfur isotopic and textural evidence. Econ. Geol., 76, 1675-1685.

SERRI, G. & SAITTA, M. 1980. Fractionation trends of the gabbroic complexes from high-Ti and low-Ti ophiolites and the crust of major oceanic basins: a comparison. Ofioliti, 5, 241-264.

SEYFRIED, W.E., Jr., & BISCHOFF, J.L. 1977. Hydrothermal transport of heavy metals by sea water: the role of sea water/basalt ratio.

Earth Planet. Sci. Lett., 34, 71-77.

SEYFRIED, W.E., Jr., & BISCHOFF, J.L. 1979. Low temperature basalt alteration by sea water: an experimental study at 70 C and 150 C. Geochim. Cosmochim. Acta., 43, 1937-1947.

SHACKLETON, R.M. 1976. Shallow and deep-level exposures of Archaean crust in India and Africa. In: Windley, B.F., (ed.), Early History of The Earth, John Wiley, 317-321.

SHACKLETON, R.M. 1986. Precambrian collision tectonics in Africa. In: Coward, M.P. & Ries, A.C., (eds), Collision Tectonics, Geol. Soc. London Spec. Pub., 19, 329-349.

SHAMAZAKI, H. & CLARK, L.A. 1973. Liquidus relations in the FeS-FeO-SiO2-Na2O system and geological implications. Econ. Geol., 68, 79-96.

SHARPE, M.R. 1979. Metasomatic zonation of an ultramafic lens at Ikatoq, near Faeringehavn, southern West Greenland. Bull. Gronlands Geol. Unders., 135, 4-32.

SHAW, D.M. 1972. The origin of the Apsley gneiss, Ontario. Can. J. Earth Sci., 9, 18-35.

SHERVAIS, J.W. 1982. Ti-V plots and the petrogenesis of modern and ophiolitic lavas. Earth Planet. Sci. Lett., 59, 101-118.

SHIBATA, T., DELONG, S.E. & WALKER, D. 1979. Abyssal tholeiites from the Oceanographer Fracture Zone. Contrib. Min. Pet.,70, 89-102.

SHIDO, F., MIYASHIRO, A. & EWING, M. 1974. Compositional variation in pillow lavas from the Mid-Atlantic Ridge. Marine Geology, 16, 177-190.

SHIMA, H. & NALDRETT, A.J. 1975. Solubility of sulfur in an ultramafic melt and the relevance of the system Fe-S-O. Econ. Geol., 70, 960-967.

SIMKIN, T. 1967. Flow differentiation in the picritic sills of north Skye. In: Wyllie, P.J., (ed.), Ultramafic and Related Rocks, John Wiley, 64-69.

SIMKIN, T. & SMITH, J.V. 1970. Minor element distribution in olivine. J. Geol., 78, 304-325.

SIROKY, F.X., ELTHON, D.L., CASEY, J.F. & BUTLER, J.C. 1985. Major element variations in basalts and diabases from the North Arm Mountain Massif, Bay of Islands ophiolite: Implications for magma chamber processes at mid-ocean ridges. Tectonophysics, 116, 41-61.

SKINNER, B.J. & BARTON, P.B. 1973. Genesis of mineral deposits. Ann. Rev. Earth Planet. Sci., 1, 183-211.

SKINNER, B.J. & PECK, D.L. 1969. An immiscible sulfide melt from Hawaii. Econ. Geol., 64, 310-322.

SOHNGE, P.G. 1945. The geology of the Messina copper mines and surrounding country. Mem. S. African Geol. Surv., 40.

SOHNGE, P.G., Le Roux, H.D. & Nel, H.J. 1948. The geology of the country around Messina. Explanation of sheet 46 (Messina), S. African Geol. Surv. Dept. Mines.

SORENSEN, H. 1967. Metamorphic and metasomatic processes in the formation of ultramafic rocks. In: Wyllie, P.J., (ed.), Ultramafic and Related Rocks, John Wiley, 204-212.

SOUCH, B.E., PODOLSKY, T. & GEOLOGICAL STAFF 1969. The sulfide ores of Sudbury: their particular relationship to a distinctive inclusion-bearing facies of the Nickel Irruptive. Econ. Geol., 4, 252-261.

SPIES, F.N., MacDONALD, K.C., ATWATER, T., BALLARD, R., CARRENZA, D., CORDOBA, D., COX, V., DIAZ GARCIA, V.M., FRANCHETEAU, J., GUERRERO, J., HAWKINS, J., HAYMON, R., HESSLER, R., JUTEAU, T., KASTNER, M., LARSON, R., LUYENDYK, B., MacDOUGALL, J.D., MILLER, S., NORMARK, W., ORCUTT,J. & RANGER, C. 1980. East Pacific Rise: hot springs and geophysical experiments. Science, 207, 1421-1433.

STANTON, R.L. 1964. Mineral interfaces in stratiform ores. Trans. Instn Min. Metall., 74, 45-79.

STANTON, R.L. 1972. Ore Petrology, McGraw-Hill.

STANTON, R.L. 1982a. Metamorphism of a stratiform sulphide orebody at Mount Misery, Einasleigh, Queensland, Australia: 1 - Observations. Trans. Instn Min. Metall., 91, B47-71.

STANTON, R.L. 1982b. Metamorphism of a stratiform sulphide orebody at Mount Misery, Einasleigh, Queensland, Australia: 2 - Implications. Trans. Instn Min. Metall., 91, B72-80.

STEELE, I.M., BISHOP, F.C., SMITH, J.V. & WINDLEY, B.F. 1977. The Fiskenaesset complex, West Greenland,Part 3. Chemistry of silicate and oxide minerals from oxide-bearing rocks, mostly from Qeqertarssuatsiaq. Bull. Gronlands Geol. Unders., 124, 1-38.

STERN, C.R. 1979. Open and closed system igneous fractionation within two Chilean ophiolites and the tectonic implications. Contrib. Min. Pet., 68, 243-259.

STEVENSON, J.S. & STEVENSON, L.S. 1980. Sudbury, Ontario and the meteorite theory. Geoscience Can., 7, 103-109.

STONECIPHER, S.A. 1978. Chemistry of deep-sea phillipsite, clinoptil-

ite, and host sediments. In: Sand, L.B. & Mumpton, F.A., (eds), Natural Zeolites, Pergamon Press, 546 pp.

SUBRAMANIAM, A.P. 1956. Mineralogy and petrology of the Sittampundi complex, Salem district, Madras State, India. Bull. Geol. Soc. Amer., 67, 317-379.

SUN, S.-S. & NESBITT, R.W. & SHARASKIN, A.Y. 1979. Geochemical characteristics of mid-ocean ridge basalts. Earth Planet. Sci. Lett., 44, 119-138.

SUN, S.-S. & NESBITT, R.W. 1978. Geochemical regularities and genetic significance of ophiolitic basalts. Geology, 6, 689-693.

SUTHREN, R.J. 1985. Facies analysis of volcaniclastic sediments: a review. In: Brenchley, P.J. & Williams, B.P.J., (eds), Sedimentology: recent developments and applied aspects, Spec. Pub. Geol. Soc. London, 18, 123-146.

SUTTON, J. 1976. Tectonic relationships in the Archaean. In: Windley, B.F.,(ed.), The Early History of The Earth, John Wiley, 99-104.

SUTTON, J. & WATSON, J. 1959. Metamorphism in deep-seated zones of transcurrent movement at Kungwe Bay, Tanganyika Territory. J. Geol., 67, 1-13.

TANKARD, A.J., JACKSON, M.P.A., ERIKSON, K.A., HOBDAY, D.K., HUNTER, D.R. & MINTER, W.E.L. 1982. Crustal Evolution of Southern Africa, Springer-Verlag.

TARNEY, J. 1976. Geochemistry of Archaean high-grade gneisses, with implications as to the origin and evolution of the Precambrian crust. In: Windley, B.F.,(ed.), The Early History of the Earth, John Wiley, 405-417.

TAYLOR, L.A. 1970. Low-temperature phase relations in the Fe-S system. Carnegie Inst. Wash. Year Book, 68, 259-270.

THOMAS, C.M. 1970. Brief explanation of the geology of the Selebi area (accompanying geological map QSD2227B). Geol. Surv. Bots.

THORNETT, J.R. 1981. The Sally Malay deposit: Gabbroid-associated nickel-copper sulfide mineralization in the Halls Creek Mobile Zone, Western Australia. Econ. Geol., 76, 1565-1580.

TODD, S.G., KEITH, D.W., SCHISSEL, D.J., LEROY, L.L., MANN, E.L. & IRVINE, T.N. 1982. The J-M platinum-palladium reef of the Stillwater Complex, Montana: I. Stratigraphy and petrology. Econ. Geol., 77, 1454-1480.

TROMMSDORF, V. & EVANS, B.W. 1974. Alpine metamorphism of peridotite rocks. Schweiz. Mineral. Petrog. Mitt., 54, 333-352.

VAN BREEMEN, O. 1970. Geochronology of the Limpopo orogenic belt,

southern Africa. J. Earth Sci., 8, 57-62.

VAN BREEMEN, O. & DODSON, M.H. 1972. Metamorphic chronology of the Limpopo belt, southern Africa. Bull. Geol. Soc. Amer., 83, 2005-2018.

VAN BREEMEN, O. DODSON, M.H. & VAIL, J.R. 1966. Isotopic age measurements on the Limpopo orogenic belt, southern Africa. Earth Planet. Sci. Lett., 1, 401-406.

VAN REENEN, D.D. 1983. Cordierite + garnet + hypersthene + biotite-bearing assemblages as a function of changing metamorphic conditions in the Southern Marginal Zone of the Limpopo Metamorphic Complex, South Africa. Spec. Pub. Geol. Soc. S. Africa, 8, 143-167.

VARNE, R., GEE, R.D., QUILTY, P.G. 1969. Macquarie island and the cause of oceanic linear magnetic anomalies. Science, 166, 230-233.

VAUGHAN, D.J., SCHWARZ, E.J. & OWENS, D.R. 1971 . Pyrrhotites from the Strathcona mine, Sudbury, Canada: A thermomagnetic and mineralogical study. Econ. Geol., 66, 1131-1144.

VELDE, B. 1985. Clay Minerals, Developments in Sedimentology, 40, 427 pp.

VERMAAK, C.F. 1976. The Merensky Reef - thoughts on its environment and genesis. Econ. Geol., 71, 1270-1298.

VILJOEN, M.J. & VILJOEN, R. 1969. A collection of 9 papers on many aspects of the Barberton granite-greenstone belt, South Africa. Spec. Pub. Geol. Soc. S. Africa, 2, 295 pp.

VILJOEN, M.J., BERNASCONI, A., VAN COLLER, N., KINLOCH, E. & VILJOEN, R.P. 1976. The geology of the Shangani nickel deposit. Econ. Geol., 71, 76-95.

VILJOEN, M.J., Van VUUREN, C., PEARTON, T.N., MINNITT, R., MUFF, R. & CILLIERS, P. 1978. The regional geological setting of mineralization in the Murchison Range with particular reference to antimony. In: Verwoerd, W.J.,(ed.), Mineralization in Metamorphic Terranes, Spec. Pub. Geol. Soc. S. Africa, 4, 55-76.

VOGT, P.R. & BYERLY, G.R. 1976. Magnetic anomalies and basalt composition in the Juan de Fuca-Gorda Ridge. Earth Planet. Sci. Lett., 33, 185-207.

VOKES, F.M. 1969. A review of the metamorphism of sulphide deposits. Earth Sci. Rev., 5, 99-143.

VOKES, F.M. 1971. Some aspects of the regional metamorphic mobilization of pre-existing sulphide deposits. Mineral. Deposita, 6,

122-129.

VON GRUENEWALDT, G. 1979. A review of some recent concepts of the Bushveld Complex, with particular reference to sulfide mineralization. Can. Mineral., 17, 233-256.

WAGER, L.R. 1960. The major element variation of the layered series of the Skaergaard intrusion and a re-estimation of the average compositon of the Hidden Layered Series and of the successive residual magmas. J. Petrol., 1, 364-398.

WAKEFIELD, J. 1971. Preliminary report on the Pikwe area, Limpopo belt, Botswana. 15th Ann. Rep. Res. Inst. African Geol., Univ. Leeds, 35-38.

WAKEFIELD, J. 1972. Preliminary report on the Lethlakane shear zone, Botswana. 16th Ann. Rep. Res. Inst. African Geol., Univ. Leeds, 35-38.

WAKEFIELD, J. 1973. Origin of the host rocks to the Pikwe ore deposit, Limpopo belt, Botswana. 17th Ann. Rep. Res. Inst. African Geol., Univ. Leeds, 36-38.

WAKEFIELD, J. 1974. The geology of the Pikwe Ni-Cu province, eastern Botswana. Unpub. Ph.D. thesis, Univ. Leeds.

WAKEFIELD, J. 1976. The structural and metamorphic evolution of the Pikwe Ni-Cu sulfide deposit, Selebi-Pikwe, eastern Botswana. Econ. Geol., 71, 988-1005.

WAKEFIELD, J. 1977a. The structural and metamorphic history of the Pikwe area - evidence for post-Great Dyke deformation in the Limpopo Mobile Belt. Bull. Geol. Surv. Botswana, 12, 141-156.

WAKEFIELD, J. 1977b. Mylonitization in the Lethakane shear zone, eastern Botswana. J. Geol. Soc. London, 133, 263-275.

WALKER, D., STOLPER, E.M. & HAYS, J.F. 1980. Komatiite petrogenesis and melt segregation. EOS, 61, 1171-1183.

WALKER, D., SHIBATA, T. & DELONG, S.E. 1979. Abyssal tholeiites from the Oceanographer Fracture Zone. Contrib. Min. Pet.,70,111-125.

WANDKE, A. & HOFFMAN, R. 1924. A study of the Sudbury ore deposits. Econ. Geol., 19, 169-204.

WATKEYS, M. 1983. Brief explanatory notes on the provisional geological map of the Limpopo Belt and environs. Spec. Pub. Geol. Soc. S. Africa, 8, 5-8.

WATKEYS, M., LIGHT, M.P.R. & BRODERICK, T.J. 1983. A retrospective view of the Central Zone of the Limpopo Belt, Zimbabwe. Spec. Pub. Geol. Soc. S. Africa, 8, 65-80.

WEAVER, C.E. & POLLARD, L.D. 1973. The Chemistry of Clay Minerals,

Developments in Sedimentology, 15.

WEAVER, B.L., TARNEY, J. WINBLEY, B.F. 1981. Geochemistry and petrogenesis of the Fiskenaesset anorthosite complex, southern West Greenland: nature of the parent magma. Geochim. Cosmochim. Acta, 45, 711-725.

WEIBLEN, P.W. & MOREY, G.B. 1980. A summary of the stratigraphy, petrology, and structure of the Duluth Complex. Am. J. Sci., 280A, 88-133.

WIEBE, R.A. 1979. Anorthosite and associated plutons, southern Nain Complex, Labrador. Can. J. Earth Sci., 15, 1326-1340.

WIENER, R.W. 1981. Tectonic setting, rock geochemistry and metamorphism of an Archaean gabbro-anorthosite complex, Tessiuyakh Bay, Labrador. Can. J. Earth Sci., 18, 1409-1421.

WILLEMSE, J. 1969. The geology of the Bushveld Complex, the largest repository of magmatic ore deposits in the world. Econ. Geol., Mon. 4, 1-22.

WILLEMSE, J. & VILJOEN, E.A. 1970. The fate of argillaceous material in the gabbroic magmas of the Bushveld Complex. Spec. Pub. Geol. Soc. S. Africa, 1, 336-366.

WILLIAMS, D.A.C. 1979. The association of some nickel sulfide deposits with komatiitic volcanism in Rhodesia. Can. Mineral., 17, 337-349.

WILLIAMS, P.J. 1982. Petrogenesis, metallogenesis and lithogeochemical prospecting of metabasic rocks near Santiago de Compostela,N.W. Spain. Unpub. Ph.D. thesis, Univ. Southampton, 308 pp.

WILSON, A.F. 1971. Some geochemical aspects of the sapphirine-bearing pyroxenites and related highly metamorphosed rocks from the Archaean ultramafic belt of South Quairading, Western Australia. Spec. Pub. Geol. Soc. Aust., 3, 401-411.

WILSON, H.D.B. & ANDERSON, D.T. 1959. The composition of Canadian sulfide ore deposits. Trans. Can. Inst. Min. Metall., 62, 327-339.

WILSON, H.D.B., KILBURN, L.C., GRAHAM, A.R. & RAMBAL, K. 1969. Geology of some Canadian nickeliferous ultrabasic intrusions. Econ. Geol., Mon. 4, 294-309.

WILSON, J.F. 1979. A preliminary reappraisal of the Rhodesian Basement Complex. Spec. Pub. Geol. Soc. S. Africa, 5, 1-23.

WILSON, J.F., BICKLE, M.J., HAWKESWORTH, C.J., MARTIN, A., NISBET, E.G. & ORPEN, J.L. 1978. Granite-greenstone terrains of the Rhodesian Archaean craton. Nature, 271, 23-27.

WINDLEY, B.F. 1976. New tectonic models for the evolution of Archean continents and oceans. In: Windley, B.F., (ed.), The Early History of the Earth, John Wiley, 105-112.

WINDLEY, B.F. 1977. The Evolving Continents, John Wiley, 385 pp.

WINDLEY, B.F. & SMITH, J.V. 1976. Archaean high-grade complexes and modern continental margins. Nature, 260, 671-675.

WINDLEY, B.F., HERD, R.K., BOWDEN, A.A.1973. The Fiskenaesset complex, West Greenland, Part 1. A preliminary study of the stratigraphy petrology and whole-rock chemistry from Qeqertarssuatsiaq. Bull. Gronlands Geol. Unders., 106, 1-80.

WINDLEY, B.F., BISHOP, F.C. & SMITH, J.V. 1981. Metamorphosed layered igneous complexes in Archean granulite-gneiss belts. Ann. Rev. Earth Planet. Sci., 9, 175-198.

WINDLEY, B.F., ACKERMAND, D. & HERD, R.K. 1984. Sapphirine/kornerupine -bearing rocks and crustal uplift history of the Limpopo belt, Southern Africa. Contrib. Mineral. Petrol., 86, 342-358.

WINKLER, H.J.F. 1979. Petrogenesis of metamorphic rocks. Springer-Verlag, 348 pp.

WOODALL, R. & TRAVIS, G.A. 1969. The Kambalda nickel deposits. Proc. 9th Commonwealth Min. Metall. Cong. London, 2, 517-533.

WRIGHT, L. 1973. Preliminary report on the structures present in the Central Zone of the Limpopo belt, eastern Botswana. 17th Ann. Rep. Res. Inst. African Geol., Univ. Leeds, 16-18.

WRIGHT, L. 1974. The structure of the Limpopo belt in eastern Botswana. 18th Ann. Rep. Res. Inst. African Geol., Univ. Leeds, 50-53.

WRIGHT, L. 1977. A structural cross-section across the north margin of the Limpopo Belt. Unpub. Ph.D. thesis, Univ. Leeds.

YARDLEY, B.W.D. & BLACIC, J.D. 1976. Sapphirine in the Sittampundi complex, India: a discussion. Min. Mag., 40, 523-524.

ZURBRIGG, H.F. 1963. Thompson mine geology. Trans. Can. Inst. Min. Metall. 66 227-236.

Addendum

BOSE, M.K. 1979. On the Eastern Ghats precambrian granulite belt and associated anorthosites. Indian J. Earth Sci., 6, 200-219.

McBIRNEY, A.R. & NOYES, R.M. 1979. Crystallization and layering of the Skaergaard Intrusion. J. Pet., 20, 487-554.

MOSELEY, F. 1969. The Upper Cretaceous ophiolite complex of Masirah Island, Oman. J. Geol., 6, 293-306.

APPENDIX

A. Mineral Analyses

All mineral analyses were performed by electron micrpoprobe. Energy dispersive analyses were performed at Imperial College. Wavelength dispersive analyses were performed at the Open University. The analyses are tabulate in pages A.2 to A.8. Only the wavelength energy dispersive (Open University) analyses have been used for the average compositions presented in the thesis.

B. Whole-rock Geochemistry

All the rocks were analysed by X-Ray fluorescence spectrometry. Rock powders were prepared using the normal techniques in operation at Southampton (Cosgrove 1972).

Major Elements

Si, Ti, Al, total Fe, Mg, Ca, Na, K and P were analysed using a Telsec B300 electron excitation X-Ray fluorescence spectrometer (beta-probe). Graphite was added to the rock powders in proportion to give mixtures containning 10 wt% graphite. The mixtures were ground in a tungsten carbide-lined Tema disc mill for 15 minutes. They were then pressed on to lead discs of suitable size for the beta-probe.

The beta-probe was installed in the Department of Geology at the University of Southampton in May 1978. Calibrations based on international rock standards (prepared in the manner described above) were developed under the direction of M. E. Cosgrove during the period 1978-1980. These include separate calibrations for raw basic/ultra-basic igneous rockks, acid igneous rocks, sedimentary rocks (excluding carbonates) and carbonate rocks. A further calibration was developed for fluxed rocks of any composition.

New basic/ultrabasic calibration curves were set up by the writer for both raw and fluxed samples. A secondary calibration of 7 standards was used on each analytical run, instead of the inadequate 2 point calibrations of the standard beta-probe analytical method. A monitor was analysed roughly every 20 samples. Data output was recalculated by hand calculator using the secondary calibration.

Major component totals were generally satisfactory (98-101%). Some low or high totals were obtained outside the above range. If unsatisfactory analyses were obtained on raw samples, then the raw samples were reweighed and remixed. If after repreparation raw samples

MINERAL ANALYSES
ANORTHOSITE

	572 PW 211 ML cpx	GE cpx	GF cpx	MA amp	MB amp	GG amp	MC amp	MD amp	MH plg	MI plg	GI plg	GH plg	GL plg
SiO2	53.60	55.25	53.27	52.88	53.09	53.25	49.44	48.32	52.91	52.24	51.63	54.96	51.89
TiO2	0.08	0.06	0.06	0.15	0.11	0.09	0.31	0.42					
Al2O3	1.35	1.37	0.76	4.42	3.84	4.97	6.95	8.23	30.31	30.33	31.25	29.70	31.21
FeO	7.63	7.45	6.58	10.31	10.16	10.48	11.62	12.17	0.08	0.10			
MnO	0.30	0.28	0.35	0.28	0.27	0.25	0.26	0.25					
MgO	13.64	13.91	13.40	16.41	16.64	15.52	14.63	13.98					
CaO	23.33	23.38	23.27	12.51	12.59	12.49	12.34	12.50	12.82	13.04	14.10	12.37	14.25
Na2O	0.39	0.39	0.29	0.46	0.43	0.58	0.69	0.72	4.31	4.18	3.59	4.53	3.52
K2O	0.00	0.00	0.01	0.30	0.24	0.38	0.56	0.69	0.13	0.13	0.08	0.12	0.10
Cr2O3	0.03	0.02	0.00	0.02	0.03	0.03	0.03	0.05					
NiO		0.00	0.03	0.02	0.03	0.02	0.02	0.00					
TOTAL	100.35	102.11 *	98.02 *	97.76	97.43	98.06	96.85	97.33	100.56	100.02	100.65	101.68	100.97

572 ML Large clinopyroxene rimmed by amphibole-quartz intergrowth
GE Margin of large clinopyroxene rimmed by amphibole-quartz intergrowth
GF Core of large clinopyroxene (GE)
MA Amphibole of quartz-amphibole intergrowth rimming clinopyroxene hornblende
MB as MA GG as MA
MC Amphibole in plagioclase-amphibole matrix MD as MC hornblende
MH Core of unzoned moderate-size plagioclase
MI Margin of plagioclase (MH)
GI Core of large zoned plagioclase
GH Margin of plagioclase (GI)
GL Core of weakly-zoned large plagioclase

	572 continued GK plg	GJ plg	MJ plg	MK plg	549 PW 208 HC cpx	HD cpx	HE cpx	HB amp	HH amp	HF amp	HG amp	HA plg	HM plg
SiO2	53.88	51.19	50.72	53.12	53.77	53.67	53.17	50.39	49.74	49.80	50.99	46.03	47.75
TiO2					0.13	0.13	0.15	0.67	0.72	0.61	0.52		
Al2O3	30.52	32.35	32.38	30.28	1.04	1.19	1.39	6.59	7.03	6.11	5.57	33.24	33.83
FeO			0.07	0.11	6.31	6.27	6.62	9.68	9.66	9.62	9.37	0.13	
MnO					0.11	0.14	0.13	0.09	0.11	0.09	0.08	0.02	
MgO					14.46	14.26	14.00	15.94	15.77	15.91	16.28	0.00	
CaO	13.04	15.27	15.05	13.06	22.61	22.46	22.33	11.67	11.57	11.71	11.79	16.02	17.34
Na2O	4.19	3.10	3.22	4.35	0.31	0.34	0.32	1.01	1.14	0.90	0.77	1.84	1.88
K2O	0.12	0.07	0.06	0.11		0.00	0.00	0.20	0.20	0.20	0.17		0.01
Cr2O3						0.00	0.00	0.02	0.03	0.02	0.02		
NiO					0.00	0.03	0.03	0.09	0.08	0.08	0.06	0.00	
TOTAL	101.75	101.98	101.50	101.03	98.74 **	98.49 **	98.14 **	96.35 **	96.05 **	95.05 **	95.62 **	97.28 **	100.81

GK Margin of weakly-zoned large plagioclase (GL)
GJ Small plagioclase near amphibole-quartz intergrowth MJ as GJ
MK Small matrix plagioclase

549 HC Large clinopyroxene
HD Clinopyroxene adjacent to plagioclase (HA)
HE Clinopyroxene
HB Large amphibole
HH Large idioblastic amphibole
HF Amphibole inclusion in clinopyroxene (HD) HG as HF
HA Matrix plagioclase adjacent to clinopyroxene (HD)
HM Matrix plagioclase

* Instrument fluctuation
** Poor calibration particularly SiO2 and CaO too low

GARNET-QUARTZ ZONES IN ANORTHOSITE

	546 PW 213 BA gnt	BB gnt	BC gnt	BD gnt	BDR gnt	BE gnt	BF gnt	BG gnt	BH gnt	BHR gnt	566 PW 211 BI gnt	BJ gnt
SiO2	39.94	38.55	37.67	38.87	41.15	38.52	37.86	38.30	37.91	38.19	38.62	38.42
TiO2	0.36	0.38	0.41	0.32	0.36	0.45	0.38	0.39	0.37	0.37	0.47	0.45
Al2O3	13.83	14.66	13.36	14.85	13.12	14.56	14.80	14.98	13.82	13.83	15.41	15.57
FeO	13.77	13.51	15.17	13.73	14.13	12.88	12.85	12.02	13.48	13.82	11.32	10.84
MnO	0.08	0.06	0.08	0.06	0.05	0.09	0.09	0.09	0.08	0.08	0.09	0.08
MgO	0.07	0.09	0.05	0.03	0.09	0.09	0.09	0.10	0.07	0.09	0.09	0.10
CaO	31.83	33.04	32.33	30.67	30.85	33.10	33.01	33.27	33.06	31.74	33.89	34.26
Cr2O3	0.00	0.00	0.00	0.00								
TOTAL	99.88	100.59	99.07	98.53 *	99.75	99.69	99.08	99.15 $	98.79	98.12 *	99.89	99.72

546 BA to BD Traverse across zoned garnet from core (BA) to rim (BD) BDR repeat of BD
BE to BH Traverse across zoned garnet from core (BE) to rim (BH) BHR repeat of BH
566 BI to BL Traverse across zoned garnet from core (BI) to rim (BL) grossular-andradite
* Poor analyses instrument fluctuation
$ Filament blew after this analysis

	566 continued BK gnt	BKR gnt	BL gnt	BLR gnt	BM gnt	BN gnt	BO gnt	BP gnt	BQ plg	BS plg	BT cpi
SiO2	38.06	37.94	38.05	37.76	38.05	37.86	38.67	37.70	44.54	45.40	36.68
TiO2	0.47	0.51	0.34	0.36	0.32	0.38	0.36	0.36	0.02	0.02	0.13
Al2O3	15.56	15.69	15.16	15.48	15.20	14.35	14.18	14.08	33.85	33.96	24.53
FeO	10.30	10.26	12.14	10.95	11.42	12.29	13.03	12.94	0.70	0.24	7.42
MnO	0.11	0.11	0.09	0.08	0.11	0.11	0.06	0.09	0.02	0.02	0.00
MgO	0.12	0.10	0.07	0.10	0.09	0.05	0.07	0.07	0.00	0.00	0.08
CaO	34.36	34.16	32.37	33.82	33.64	33.76	33.91	33.56	17.93	17.75	18.59
Na2O									1.16	1.34	0.58
K2O									0.26	0.07	0.16
TOTAL	98.98	98.77	98.22 *	98.55 *	98.83	98.80	100.28	98.80	98.48	98.80	88.17 #

566 BI to BL Zoned garnet from core (BI) to rim (BL) BKR repeat of BK BLR of BL
BM to BP Zoned garnet from core (BM) to rim (BP) grossular
BQ Inclusion in garnet plagioclase
BR Inclusion in garnet plagioclase
BS Inclusion in garnet plagioclase
BT Inclusion in garnet epidote ?

\# Poor analysis possibly instrument fluctuation possibly high contents of Y & Zr

CALC-SILICATE GNEISS

	30-7-1d JH amp	JI amp	JK cpx	JJ cpx	JN plg	JO plg	JP plg	JQ plg	JL sph	JM sph
SiO2	42.63	42.99	51.39	51.19	47.99	48.70	47.54	51.51	29.96	29.58
TiO2	0.66	0.70	0.17	0.17					33.27	33.20
Al2O3	10.59	10.40	2.03	2.14	32.79	31.69	32.85	30.31	3.02	3.04
FeO	14.43	14.14	8.89	9.17					1.46	1.30
MnO	0.14	0.12	0.17	0.19					0.05	0.05
MgO	12.63	12.68	12.49	12.26					0.02	0.03
CaO	12.18	12.31	24.12	24.10	16.78	15.33	16.43	13.47	28.07	27.78
Na2O	1.50	1.34	0.47	0.50	2.15	2.90	2.21	3.87	0.07	0.05
K2O	1.94	1.95	0.00	0.01	0.06	0.05	0.05	0.11	0.00	0.01
Cr2O3		0.00	0.00	0.02						
NiO		0.02								
TOTAL	96.70	96.65	99.73	99.75	99.77	98.67	99.13	99.27	95.92 ***	95.04 ***

30-7-1d Botsabelo
JH Core of large amphibole hornblende
JI Core of large amphibole
JK Clinopyroxene rimming amphibole (JH) salite
JJ Clinopyroxene rimming amphibole (JI)
JN Core of moderate-size twinned plagioclase
JO Margin of plagioclase (JN)
JP Core of moderate-size twinned plagioclase
JQ Margin of plagioclase (JP)
JL Sphene
JM Sphene

*** Low total high Ti calibration ? or unanalysed element ?

BANDED QUARTZITE-AMPHIBOLITE

	LT 27-30 IC Energy Dispersive 1 amp	2b amp	2c amp	4b amp	3d amp	4a bio	3a py	3b po	3c po	
SiO2	55.39	54.93	56.03	55.55	55.34	38.35	0.03	0.18	0.07	Si
TiO2	0.07	0.00	0.02	0.09	0.00	2.06	0.00	0.00	0.07	Ti
Al2O3	0.76	1.06	1.19	1.05	1.40	15.28	0.01	0.04	0.06	Al
FeO	16.80	16.62	17.68	16.67	16.95	10.96	46.63	60.03	59.85	Fe
MnO	0.19	0.21	0.27	0.25	0.18	0.00	0.00	0.00	0.00	Mn
MgO	21.90	22.08	21.84	22.23	21.88	17.92	0.00	0.03	0.07	Mg
CaO	1.18	1.30	1.32	1.07	1.62	0.02	0.00	0.00	0.00	Ca
Na2O	0.51	0.33	0.45	0.52	0.57	0.53	0.27	0.29	0.34	Na
K2O	0.00	0.00	0.03	0.00	0.00	8.39	0.02	0.04	0.00	K
P2O5	0.10	0.00	0.00	0.07	0.00	0.00	0.20	0.06	0.05	P
Cr2O3	0.15	0.01	0.03	0.02	0.14	0.65	0.07	0.00	0.08	Cr
NiO	0.00	0.00	0.30	0.06	0.10	0.26	0.00	0.21	0.35	Ni
CuO	0.00	0.12	0.00	0.06	0.21	0.19	0.01	0.00	0.00	Cu
S	0.00	0.00	0.00	0.04	0.04	0.00	55.07	39.96	40.05	S
ZnO	0.04	0.00	0.07	0.00	0.34	0.06	0.02	0.01	0.14	Zn
CoO					0.00			0.00	0.11	Co
TOTAL	97.09	96.66	99.23	97.68	98.77	98.06	102.33 ***	100.85 ***	101.24 ***	

LT 27-30
1 Clinoamphibole cummingtonite
2b Core of coarse amphibole cummingtonite
2c Margin of amphibole (2b)
4b Amphibole cummingtonite
3d Amphibole cummingtonite
4a Phlogopite
3a Opaque pyrite *** Assumes no O
3b Opaque pyrrhotite
3c Opaque pyrrhotite

DIKOLOTI FELDSPATHIC AMPHIBOLITE

	660 DK 23 BA cor	BF cor	BG cor	BB sap	BC sap	BD sap	BH sap	BE spi	BI spi	BJ spi	TC unk?	TD unk?
SiO2	0.03	0.03	0.03	12.70	12.95	12.29	12.67	0.06	0.09	0.09	39.40	39.54
TiO2	0.02	0.02	0.02	0.04	0.04	0.04	0.04	0.02	0.02	0.02	0.02	0.02
Al2O3	98.11	97.50	97.77	63.63	63.74	64.11	63.62	63.74	63.90	63.92	32.87	32.81
FeO	0.38	0.38	0.39	5.77	5.80	5.25	5.65	17.16	17.56	17.70	0.35	0.44
MnO	0.02	0.02	0.02	0.06	0.09	0.06	0.08	0.12	0.11	0.12	0.05	0.03
MgO	0.00	0.00	0.00	16.80	16.76	16.87	16.88	16.19	16.27	16.17	0.00	0.02
CaO	0.01	0.01	0.01	0.03	0.01	0.01	0.01	0.03	0.03	0.01	24.37	24.51
Na2O		0.01	0.03				0.00				0.08	0.08
K2O											0.01	0.00
Cr2O3	0.00	0.00	0.00	0.00	0.00	0.00	0.00	0.00	0.00	0.02		
NiO	0.00	0.00	0.00	0.07	0.04	0.04	0.06	0.19	0.15	0.15		
TOTAL	98.57	97.97	98.27	99.10	99.16	98.67	99.01	97.51	98.13	98.20	97.15	97.45
660	*	*	*		*		*	*	*	**	**	

BA Large corundum in corundum-sapphirine-spinel aggregate in feldspathic amphibolite
BF as BA BG as BA
BB Sapphirine in corundum-sapphirine-spinel aggregate
BC as BB BD as BB BH as BB
BE Spinel in corundum-sapphirine-spinel aggregate pleonaste
BI as BE BJ as BE
TC Fine-grained aggregate in corona to corundum-sapphirine-spinel (dark) (clino)zoisite?
TD adjacent TC (light) (clino)zoisite?
* Low totals probably poor polish or high Al calibration?
** Low totals poor polish and fine-grained aggregates

	660 continued TE unk?	TF unk?	TG unk?	TH unk?	TI amp	TL amp	TJ plg	TK plg	TM plg	663 DK 23 BI sap	BJ sap	BK sap
SiO2	39.78	39.28	43.93	46.75	45.29	45.30	43.91	44.00	43.86	12.93	12.93	13.33
TiO2	0.02	0.02	0.02	0.02	0.11	0.09				0.02	0.02	0.02
Al2O3	30.36	32.52	35.63	37.72	15.16	15.04	35.53	35.58	35.64	63.36	63.21	62.99
FeO	0.32	0.87	0.10	0.35	7.39	7.39	0.08	0.14	0.06	5.40	5.73	5.43
MnO	0.03	0.05	0.02	0.02	0.14	0.16				0.08	0.06	0.06
MgO	0.06	0.00	0.00	0.04	16.01	16.10				17.37	17.29	17.32
CaO	24.95	24.04	19.46	0.07	11.11	11.08	19.52	19.48	19.52	0.03	0.01	0.03
Na2O	0.03	0.11	0.41	0.20	1.77	1.65	0.40	0.43	0.41			
K2O	0.01	0.05	0.00	11.08	0.24	0.24	0.00	0.00	0.00			
Cr2O3					0.00	0.00				0.02	0.02	0.00
NiO												
TOTAL	95.56	96.94	99.57	96.25	97.22	97.05	99.44	99.63	99.49	99.21	99.27	99.18
	**	**										

660 TE Fine-grained fibrous (bow-tie) aggregate in corona (dark) (clino)zoisite?
TF near TE (light) (clino)zoisite?
TG Fine-grained aggregate near edge of corona adjacent to amphibolite anorthite?
TH Fine-grained aggregate in corona (light) sericite?
TI Amphibole in feldspathic amphibolite hornblende
TL as TI
TJ Plagioclase in feldspathic amphibolite
TK as TJ
TM Core of large plagioclase in amphibolite

663 BI Sapphirine in sapphirine-spinel clot in feldspathic amphibolite
BJ BK as BI

	663 continued BM sap	BA spi	BB spi	BC spi	BH chl	BN chl	BNR chl	BP chl	BPR chl	BL1 unk?	BL2 unk?	BO unk?
SiO2	13.03	0.03	0.03	0.06	25.66	25.93	26.15	25.39	26.10	30.64	38.73	41.72
TiO2	0.02	0.02	0.02	0.02	0.02	0.02	0.02	0.02	0.02	0.02	0.02	0.02
Al2O3	62.77	66.43	66.57	66.80	25.39	26.04	26.18	26.64	25.72	27.01	32.32	32.86
FeO	5.62	17.46	17.17	17.15	4.44	3.32	3.14	5.99	3.84	15.97	1.07	2.43
MnO	0.08	0.14	0.12	0.14	0.03	0.03	0.02	0.03	0.02	0.09	0.03	0.03
MgO	17.36	17.02	17.35	17.57	27.63	28.38	29.14	26.11	28.61	8.95	0.25	0.20
CaO	0.04	0.01	0.01	0.01	0.29	0.26	0.27	0.26	0.32	7.02	24.15	16.63
Na2O						0.00	0.00	0.02	0.00		0.00	0.09
K2O						0.00	0.00	0.00	0.00		0.00	3.13
Cr2O3	0.02	0.00	0.00	0.00	0.00	0.00		0.00		0.00		0.00
NiO		0.27	0.22	0.24								
TOTAL	99.21	101.38	101.49	101.99	83.46	83.98	84.92	84.46	84.63	89.70	96.46	97.11
663		m	m	m	***	***	***	***	***	**	**	**

BM Sapphirine in sapphirine-spinel aggregate in feldspathic amphibolite
BA Spinel in sapphirine-spinel clot in feldspathic amphibolite pleonaste
BB BC as BA m high totals due to mas absorption effect in dense minerals
BH Thin vermicular rim to spinel chlorite (corundophilite)
BN as BH BNR repeat of BN BP as BH BPR repeat of BP
BL1 Fine-gr. aggregate in corona to sap-spin mixture of Fe-Al chlorite (70%) + clzoi (30%)?
BL2 adjacent to BL1 (clino)zoisite ?
BO as BL1 mixture of (clino)zoisite (68%) + sericite (28%) + chlorite (4%) ?
*** Low totals due to H2O content of chlorite plus fine-grained nature and poor polish

	663 continued BQ unk?	BR1 unk?	BR2 unk?	BU unk?	BV unk?	BW unk?	TN unk?	TP unk?	BD amp	BE amp
SiO2	38.74	35.69	45.14	38.74	41.08	33.85	26.97	27.87	45.73	46.03
TiO2	0.02	0.04	0.05	0.02	0.04	0.04	0.05	0.02	0.06	0.06
Al2O3	32.60	18.38	17.26	32.32	22.76	20.81	22.67	22.07	15.85	15.29
FeO	0.51	11.42	10.67	1.07	4.93	8.52	7.38	7.48	6.96	7.02
MnO	0.05	0.22	0.31	0.03	0.03	0.17	0.03	0.03	0.16	0.13
MgO	0.00	21.98	21.17	0.25	20.37	26.18	27.86	28.24	16.02	16.14
CaO	24.08	0.57	0.83	24.15	0.36	0.29	0.09	0.04	11.45	11.55
Na2O	0.05	0.89	1.53	0.00	2.01	0.48	0.02	0.02	1.56	1.50
K2O	0.00	0.01	0.00	0.00	0.01	0.01	0.01	0.00	0.24	0.27
NiO									0.08	0.09
TOTAL	96.05	89.20	96.96	96.58	91.59	90.35	85.08	85.77	98.11	98.08
	** @	***@	**	**	**	**	***	***@	@	@

BQ Fine-grained aggregate near outer margin of corona (clino)zoisite ?
BR1 as BQ Mixture of amphibole and chlorite ?
BR2 as BQ adjacent to BR1 amphibole qedrite ?
BU Fine-grained aggregate in corona adjacent to BL (clino)zoisite ?
BV Coarse str.ex. fibrous min. on outer rim of corona. Amphibole qedrite? + chlorite?
BW as BV Mixture of chlorite + amphibole ?
TN TP as BV Chlorite ? @ Cr2O3 analysed not detected
BD Core of large amphibole of feldspathic amphibolite
BE Typical amphibole in amphibolite hornblende

PHIKWE HOST AMPHIBOLITE

	34e PW 93 BG amp	BY amp	BYR amp	ME amp	MG amp	BF amp	BS amp	BT amp	BTR amp	MF amp
SiO2	43.70	42.72	43.05	44.20	43.86	44.83	43.78	44.44	44.57	45.29
TiO2	0.09	0.09		0.09	0.09	0.05	0.05	0.05		0.07
Al2O3	15.03	14.72	14.81	14.71	15.02	15.90	15.55	15.16	15.21	15.50
FeO	11.66	11.89	12.26	11.88	12.20	16.57	16.42	16.27	16.49	16.66
MnO	0.22	0.20	0.25	0.20	0.20	0.39	0.37	0.39	0.39	0.46
MgO	13.55	13.30	13.41	13.34	13.44	17.67	16.97	17.78	17.97	17.43
CaO	11.30	10.42	10.56	11.09	10.48	1.18	1.06	1.11	1.13	0.96
Na2O	1.64	1.65	1.55	1.62	1.64	1.60	1.69	1.64	1.47	1.67
K2O	0.20	0.32	0.33	0.24	0.33	0.01	0.01	0.01	0.00	0.01
Cr2O3	0.00	0.02		0.00		0.00	0.00	0.00		0.00
NiO	0.01	0.01		0.03		0.03	0.03	0.03		0.01
TOTAL	97.40	95.34 *	96.22 *	97.40	97.26	98.23	95.93 *	96.88	97.23	98.06

34e BG Fine matrix amphibole hornblende adjacent to BF
BY Matrix amphibole hornblende
BYR Repeat of BY
ME Fine green matrix amphibole hornblende
MG Fine green matrix amphibole hornblende

BF Long thin idioblastic amphibole straight extinction gedrite
BS Core of large idioblastic amphibole gedrite
BT Margin of large idioblastic amphibole (BS) gedrite
BTR Repeat of BT gedrite
MF Fine light brown matrix amphibole gedrite
* Poor analyses instrument fluctuation

	34q PW 93 GA plg	GB plg	GM plg	GC amp	GD amp
SiO2	53.92	54.92	55.24	48.23	47.83
TiO2				0.50	0.51
Al2O3	30.93	30.37	30.08	11.62	11.85
FeO				12.42	12.68
MnO				0.17	0.19
MgO				14.14	13.94
CaO	13.43	12.56	12.36	10.42	10.54
Na2O	4.10	4.64	4.77	1.49	1.55
K2O	0.02	0.04	0.02	0.32	0.35
Cr2O3				0.05	0.13
NiO				0.06	0.06
TOTAL	102.40 **	102.53 **	102.47 **	99.42 **	99.63 **

34q GA Matrix plagioclase
GB Matrix plagioclase
GM Typical small matrix plagioclase
GC Moderately coarse amphibole hornblende
GD Moderately coarse amphibole hornblende
** Totals too high spectrometer B counter fluctuating (Si & Al)

SELEBI HOST AMPHIBOLITE

	112 SD 82 FA spi	FB spi	FG plg	FK plg	FL plg	FC	FD	FH	FE	FI	FF	FJ
SiO2	0.09	0.09	44.62	45.39	45.33	40.32	46.83	44.97	36.83	31.43	44.94	45.11
Al2O3	66.37	65.66	35.84	36.30	36.14	32.05	35.26	34.85	29.39	25.52	35.35	35.802
FeO	20.38	19.71										
MnO	0.11	0.11										
MgO	15.36	15.17										
CaO	0.03	0.01	19.92	19.73	19.70	22.25	5.34	8.18	20.80	22.61	16.86	17.97
Na2O	0.08	0.10	0.50	0.94	0.92	0.08	0.54	0.74	0.52	0.68	0.48	0.88
K2O			0.01	0.00	0.01	0.31	7.53	6.23	0.20	0.10	1.55	0.90
TOTAL	102.42 ***	100.85 ***	100.89 **	102.36 **	102.30 **	95.01	95.50	94.97	87.74	80.34	99.18	100.66

112 FA Spinel in spinel aggregate surrounded by altered plagioclase corona pleonaste
FB as FA *** High totals due to mas absorption effect in dense minerals
FG Fine plagioclase associated with spinel anorthite
FK Matrix plagioclase of hornblende-feldspar amphibolite anorthite
FL same plagioclase as FK
FC Alteration product of plagioclase in the corona surrounding spinel aggregate
FD-FJ below alteration products of matrix plagioclases of amphibolite
FD and FH same plagioclase
FE, FI, FF, FJ all same plagioclase
Low totals due to fine-grained nature, H2O content and counter B fluctuating

	113 IC Energy Dispersive SD 82 5a spi	6 spi	5b plg	1 clz	5c clz	8a phl	8b plg	8c amp
SiO2	0.05	0.03	43.48	38.74	39.63	38.24	43.36	44.66
TiO2	0.01	0.06	0.04	0.00	0.02	0.67	0.00	0.18
Al2O3	64.24	63.67	35.88	32.55	33.11	17.88	35.91	17.65
FeO	18.79	18.44	0.39	0.51	0.41	6.14	0.09	11.33
MnO	0.07	0.03	0.03	0.08	0.00	0.05	0.00	0.30
MgO	16.75	16.26	0.15	0.14	0.00	21.33	0.07	21.25
CaO	0.02	0.04	19.62	24.48	24.88	0.00	19.90	0.95
Na2O	0.50	0.43	0.25	0.09	0.05	0.89	0.41	2.10
K2O	0.00	0.01	0.02	0.00	0.00	8.18	0.00	0.00
Cr2O3	0.00	0.05	0.00	0.00	0.02	0.03	0.00	0.09
NiO	0.15	0.21	0.00	0.00	0.00	0.04	0.00	0.09
CuO	0.25	0.00	0.02	0.18	0.00	0.00	0.03	0.06
S	0.01	0.00	0.01	0.01	0.00	0.00	0.00	0.00
CoO	0.01	0.10	0.11	0.00	0.02	0.00	0.00	0.09
TOTAL	100.85	99.33	100.00	96.78	98.14	93.45	99.77	98.75

113 5a Spinel of spinel aggregate pleonaste
6 Spinel of spinel aggregate pleonaste
5b Fine plagioclase inclusion within spinel aggregate anorthite
1 & 5c Clinozoisite after plagioclase retaining twinning in corona surrounding spinel aggregate
8a Coarse phlogopite on outside of corona
8b Coarse plagioclase of amphibolite anorthite
8c Coarse amphibole of amphibolite gedrite

SELEBI-NORTH HOST AMPHIBOLITE

	56-16			56-17		High Cr amphibolite				
	UD	UE	UF	UA	UG	UH	UB	UC	UI	UJ
	amp	amp	amp	amp	amp	amp	amp	amp	amp	amp
SiO2	42.86	42.80	42.83	46.44	46.30	46.62	46.62	46.49	45.48	46.59
TiO2	1.35	1.39	1.21	0.50	0.52	0.50	0.50	0.52	0.53	0.52
Al2O3	14.48	14.47	14.48	11.44	11.50	11.42	11.67	11.59	12.17	11.26
FeO	12.67	12.79	12.78	9.06	8.60	9.01	8.94	9.12	9.25	8.74
MnO	0.22			0.20			0.20	0.22		
MgO	12.73	12.66	12.71	16.05	15.76	16.09	15.91	16.08	15.43	15.80
CaO	10.40	10.38	10.37	10.13	10.78	10.28	10.57	10.36	10.23	10.78
Na2O	2.11	2.25	2.14	1.79	1.72	1.74	1.80	1.82	1.85	1.74
K2O	0.32			0.20			0.19	0.20		
Cr2O3	0.05	0.03	0.03	0.97	0.82	0.78	0.68	0.69	1.08	1.02
NiO	0.00			0.09			0.09	0.11		
TOTAL	97.19	96.77	96.55	96.87	96.00	96.44	97.17	97.20	96.02	96.45

56-16 & 56-17 from SDN 56

56-16 UD Moderate-size amphibole hornblende
UE & UF as UD

56-17 UA Edge of small amphibole Cr hornblende
UG Opposite edge of UA amphibole
UH Core of UA amphibole
UB Core of large amphibole Cr hornblende
UC Small amphibole Cr hornblende
UI Very small amphibole Cr hornblende
UJ Very small amphibole Cr hornblende

	133	Gnt amphibolite			129	Garnet amphibolite				IC Energy Dispersive			
	HI	HIR	HK	HL	4-1	4-2	4-3	4-4	4-5	4-6	4-7	4-8
	amp	amp	gnt	gnt	gnt	gnt	gnt	gnt	gnt	gnt	gnt	gnt
SiO2	41.43	43.57	40.03	40.19	38.66	38.47	39.17	38.91	39.18	38.66	38.88	38.77
TiO2	0.20	0.20	0.04	0.04	0.00	0.00	0.00	0.05	0.00	0.00	0.00	0.00
Al2O3	16.89	16.47	22.32	22.43	21.76	21.75	22.34	21.71	22.10	21.65	21.78	22.18
FeO	13.73	13.69	26.27	26.45	25.47	24.84	24.60	24.78	24.44	25.01	25.09	24.68
MnO	0.25	0.26	2.17	1.49	2.09	1.73	1.69	1.51	1.52	1.31	1.29	1.50
MgO	11.09	11.21	8.33	8.43	7.99	8.37	8.90	8.62	8.87	8.84	8.64	8.99
CaO	10.28	10.51	3.51	3.78	4.01	4.29	4.32	4.33	4.24	4.53	4.43	4.50
Na2O	1.65	1.62	0.04	0.04	0.25	0.16	0.36	0.14	0.24	0.40	0.26	0.38
K2O	0.30	0.32	0.00	0.00	0.03	0.00	0.00	0.00	0.00	0.00	0.00	0.00
Cr2O3	0.02				0.00	0.09	0.00	0.00	0.06	0.02	0.00	0.04
NiO	0.04				0.00	0.13	0.17	0.00	0.04	0.16	0.00	0.08
CuO					0.12	0.02	0.00	0.00	0.17	0.02	0.00	0.00
TOTAL	95.88 *	97.85	102.71 **	102.85 **	100.38	99.85	101.56	100.05	100.88	100.60	100.37	101.12

133 & 129 from SDN 42

133 HI Coarse amphibole w/ 120 cleavage
HIR Repeat of HI after recalibrating Si & Ca hornblende
HK Margin of coarse garnet almandine
HL Core of garnet (HK)
* Low total Si & Ca calibration ?
** Garnets and spinels tend to give high totals because of mass absorption effects in dense minerals. However totals are still too high Si counter drift ?

129 4-1 to 4-8 Traverse across coarse garnet from margin to margin almandine
4-3 0.01 S 4-5 0.02 S No Co detected

	129	continued		Garnet amphibolite			IC Energy Dispersive		
	6-1	6-2	6-3	4a	8c	8m	8s	1-1	1-2
	gnt	gnt	gnt	amp	amp	amp	amp	clz	clz
SiO2	38.90	39.38	39.45	42.78	41.76	42.90	42.77	39.27	38.88
TiO2	0.00	0.00	0.00	0.26	0.19	0.20	0.14	0.05	0.03
Al2O3	21.82	22.33	22.27	14.66	15.18	15.50	15.40	31.72	32.07
FeO	24.83	24.23	24.76	13.44	13.90	13.40	12.93	1.24	1.15
MnO	1.46	1.69	1.59	0.13	0.19	0.25	0.25	0.04	0.12
MgO	8.74	9.03	8.89	12.16	12.13	12.81	12.55	0.08	0.32
CaO	4.71	4.43	4.64	10.72	10.88	10.93	10.71	24.04	24.57
Na2O	0.32	0.30	0.36	1.51	1.54	1.91	1.56	0.06	0.07
K2O	0.02	0.03	0.06	0.22	0.31	0.24	0.29	0.00	0.00
Cr2O3	0.01	0.01	0.04	0.02	0.16	0.16	0.10	0.14	0.07
NiO	0.00	0.00	0.09	0.15	0.02	0.11	0.27	0.12	0.02
CuO	0.35	0.00	0.05	0.21	0.06	0.04	0.25	0.22	0.24
S		0.00	0.04	0.00	0.01	0.00	0.00	0.02	0.00
CoO		0.00	0.00	0.00	0.02	0.00	0.00	0.14	0.03
TOTAL	100.16	101.43	102.24	96.26	96.35	98.45	97.22	97.14	97.57

129 6-1 Coarse garnet near core almandine
6-2 Same coarse garnet near core
6-3 Core of same coarse garnet
4a Margin of amphibole adjacent to coarse garnet 4 hornblende
8c Core of coarse amphibole hornblende
8m Margin of coarse amphibole (8c) hornblende
8s Small amphibole next to 8m amphibole hornblende
1-1 (Clino)zoisite after plagioclase
1-2 (Clino)zoisite after plagioclase

SELEBI-NORTH HOST ULTRAMAFICS

SDN 56-5 OU Wavelength Dispersive

	MS olv	MT olv	MU opx	MO opx	MP opx	MR spi	MV spi	MW spi	MQ mag	MM amp
SiO2	40.09	40.38	56.01	55.68	55.65	0.09	0.08	0.11	0.16	45.31
TiO2	0.02	0.02	0.05	0.05	0.05	0.07	0.39	0.34	0.03	0.50
Al2O3	0.00	0.00	1.64	1.85	1.71	57.64	33.80	35.49	0.00	11.85
FeO	18.93	19.58	12.96	12.87	12.80	22.57	36.36	35.54	77.41	7.17
MnO	0.25	0.26	0.31	0.30	0.31	0.17	0.35	0.34	0.04	0.13
MgO	42.51	41.99	29.38	29.81	29.67	14.58	7.84	8.41	0.00	16.96
CaO	0.01	0.01	0.23	0.20	0.21	0.01	0.01		0.04	11.56
Na2O	0.00	0.00	0.02	0.00	0.02	0.04	0.02		0.00	1.91
K2O	0.00	0.00	0.00	0.00	0.00		0.00			0.23
Cr2O3	0.00	0.00	0.13	0.10	0.12	5.89	20.54	19.97	0.00	0.36
NiO	0.11	0.11	0.00	0.02	0.00		0.04			0.02
TOTAL	101.92	102.35	100.73	100.88	100.54	101.06	99.43	100.20	77.68 **	96.00

** Low total due to Fe2O3

56-5 MS Small olivine relict in serpentine
MT Small olivine relict in serpentine
MU Fine-gr. granoblastic orthopyroxene associated w/ spinel
MO Margin of coarse orthopyroxene
MP Core of orthopyroxene (MO) abundant inclusions of amphibole
MR Green spinel in olivine Cr pleonaste
MV Grey spinel assoc. w/ fine opx (MU) picotite
MW Grey spinel assoc. w/ fine opx (MU) picotite
MQ Magnetite assoc w/ fine opx (MU)
MM Typical fine-grained matrix amphibole hornblende

different grains therefore not intergrowths

56-5 IC Energy Dispersive

	1a apa	1f apa	3d olv	6c opx	9q opx	5b amp	5e amp	D mp
SiO2	0.07	0.15	38.21	54.35	54.35	44.52	44.40	.32
TiO2	0.05	0.04	0.00	0.03	0.05	0.63	0.64	.42
Al2O3	0.03	0.00	0.00	1.33	1.57	12.26	12.37	.23
FeO	0.17	0.16	18.89	12.25	12.51	7.09	7.18	.17
MnO	0.02	0.00	0.22	0.33	0.40	0.05	0.00	.25
MgO	0.17	0.17	41.96	29.90	29.39	17.13	17.42	.98
CaO	55.02	54.23	0.00	0.21	0.28	11.51	11.41	.50
Na2O	0.19	0.03	0.35#	0.12	0.27	1.89	2.16	.72
K2O	0.00	0.02	0.01	0.00	0.00	0.20	0.22	.69
P2O5	47.02	46.80	0.00	0.00	0.00	0.11	0.00	.05
Cr2O3	0.06	0.07	0.06	0.17	0.07	0.34	0.28	.05
NiO	0.07	0.00	0.19	0.05	0.05	0.03	0.12	.00
CuO	0.03	0.09	0.00	0.10	0.17	0.15	0.05	.00
S	0.14	0.04	0.00	0.00	0.00	0.00	0.00	.00
ZnO	0.00	0.00	0.15	0.03	0.11	0.00	0.00	.00
CoO	0.02	0.00	0.00	0.00	0.00	0.01	0.00	.00
TOTAL	103.06 *	101.80 *	100.04	98.87	99.22	95.92	96.25	.33

56-5 1a Apatite associated w/ serpentinised olivine
1f Apatite associated w/ serpentinised olivine
3d Small olivine relicts in serpentine
6c Core of large orthopyroxene
9q Fine-grained granoblastic orthopyroxene
5b Fine-grained amphibole associated w/ serp.olivine, spinel and apatite
5e as 5b

Na - energy dispersive sometimes suspect.

* High totals possibly P calibration no F or Cl included

SDN 56-7 Amphibole orthopyroxenite

	CA opx	CB opx	CE opx	CF opx	CD amp	CC amp	CG amp	CH amp	CI amp	506 JT spi	JU opx	JV chl
SiO2	55.42	56.69	56.58	55.26	47.60	47.00	47.02	47.79	48.69	0.06	54.36	24.84
TiO2	0.07	0.07	0.07	0.07	0.53	0.52	0.52	0.50	0.47	0.05	0.09	0.05
Al2O3	1.76	1.52	1.37	1.65	10.27	10.11	10.00	9.73	9.51	61.49	3.15	24.36
FeO	10.11	9.43	9.45	10.16	5.23	5.52	5.28	5.16	5.27	21.96	13.17	7.05
MnO	0.19	0.22	0.22	0.19	0.08	0.09	0.09	0.09	0.09	0.09	0.12	0.06
MgO	31.80	28.13	28.01	31.96	18.78	18.77	18.71	19.15	19.16	15.46	29.32	26.22
CaO	0.17	0.52	0.50	0.17	11.54	11.30	11.58	11.46	11.28	0.01	0.20	0.17
Na2O	0.00	0.27	0.23	0.00	2.02	1.89	1.94	1.88	1.76	0.02	0.02	0.09
K2O		0.00	0.00	0.00		0.10	0.15	0.13	0.13	0.00	0.00	0.01
Cr2O3	0.15	0.18	0.22	0.13	0.89	0.81	1.03	0.93	0.72	0.16	0.00	
NiO	0.06	0.06	0.08	0.03	0.08	0.11	0.06	0.05	0.12	0.25	0.03	
TOTAL	99.73	97.09	96.73	99.62	97.17	96.22	96.38	96.87	97.20	99.55	100.46	82.85

56-7 CA Core of coarse orthopyroxene w/ abundant inclusions of amphibole
CB Core of coarse orthopyroxene altered ? pyribole
CE Core of coarse orthopyroxene altered ? pyribole
CF Core of coarse orthopyroxene
CD Amphibole inclusion in coarse orthopyroxene hornblende
CC Fine matrix amphibole surrounding coarse orthopyroxene hornblende
CG Fine matrix amphibole surrounding coarse orthopyroxene hornblende
CH Amphibole inclusion in coarse orthopyroxene hornblende
CI Amphibole inclusion in coarse orthopyroxene hornblende

506 JT Coarse green spinel pleonaste
JU Orthopyroxene
JV White rim around spinel chlorite - pennixite

DIKOLOTI-LENTSWE ULTRAMAFICS

LT 27-25

	DA opx	DB opx	DC opx	DG opx	DO amp?	DQ chl	DD spi	DE spi	DI spi	DH spi	DJ spi	DM spi	DN spi
SiO2	55.60	55.96	55.27	56.20	56.05	30.61	0.06	0.03	0.03	0.06	0.06		
TiO2	0.04	0.04	0.04	0.04	0.04	0.02	0.03	0.03	0.03	0.03	0.03		
Al2O3	2.80	2.24	3.22	2.37	2.39	16.67	57.22	57.79	56.95	57.92	55.94	57.15	57.04
FeO	11.70	11.44	11.51	11.36	9.90	10.53	21.91	21.27	22.54	21.94	22.26	21.58	21.81
MnO	0.23	0.22	0.20	0.22	0.28	0.12	0.17	0.15	0.14	0.17	0.17	0.14	0.15
MgO	30.00	30.20	29.65	30.22	26.56	26.80	14.41	14.46	14.28	14.95	13.97	14.45	14.43
CaO	0.16	0.17	0.16	0.17	0.40	0.11	0.03	0.01	0.01	0.01	0.03		
Na2O	0.00	0.02	0.02	0.00	0.25	0.05	0.09	0.09	0.11	0.09	0.07		
K2O	0.00	0.00	0.00	0.00	0.00	0.01							
Cr2O3	0.05	0.05	0.07	0.02			4.21	4.45	4.50	4.47	5.80	4.52	4.63
NiO	0.00	0.00	0.00	0.02			0.03	0.03	0.07	0.03	0.03		
TOTAL	100.58	100.34	100.14	100.62	95.87	84.92	98.16	98.31	98.66	99.67	98.36	97.89	98.09

LT 27-25
DA Near margin of coarse elongate orthopyroxene in large bleb of pyrrhotite
DB Core of orthopyroxene (DA) DC Margin of orthopyroxene (DA)
DG Typical medium-grained matrix orthopyroxene DO Amphibole ? diabantite
DQ Chlorite rim between orthopyroxene (DC) and pyrrhotite
DD Green spinel very dusty DE Green spinel (DD) clear Cr pleonaste
DI Green spinel very dusty DH Green spinel (DI) mod.dusty DJ Green spinel (DI) clear
DM Green spinel very dusty DN Green spinel (DM) relatively clear

27-25 continued

	DF opa	DK opa	DL opa
SiO2	0.08		
TiO2	0.12	4.62	0.13
Al2O3	0.39	0.23	0.29
FeO	87.58	84.50	87.97
MnO	0.11	0.52	0.10
MgO	0.13	0.05	0.18
CaO	0.04		
Na2O	0.03		
K2O			
P2O5			
Cr2O3	4.01	3.64	3.70
NiO	0.00		
CuO			
S			
ZnO			
TOTAL	92.94 *	93.56 *	92.37 *

657 IC Energy Dispersive DK 19

	3a olv	1a olv	1d olv	2a olv	2c olv	3b opx	1b opx	1c opx	1h opx
SiO2	40.20	40.00	39.71	40.01	39.67	57.23	54.81	55.12	55.02
TiO2	0.00	0.00	0.00	0.00	0.04	0.04	0.06	0.16	0.01
Al2O3	0.00	0.01	0.02	0.00	0.00	0.61	0.83	1.10	1.02
FeO	13.69	14.18	13.59	13.76	13.09	9.40	9.28	8.93	9.40
MnO	0.22	0.15	0.03	0.26	0.14	0.10	0.10	0.19	0.29
MgO	46.65	46.17	45.69	46.94	45.78	33.30	33.34	32.78	31.87
CaO	0.03	0.03	0.00	0.04	0.00	0.23	0.03	0.30	0.24
Na2O	0.37					0.48			
K2O	0.01	0.03	0.02	0.00	0.00	0.00	0.03	0.03	0.06
P2O5		0.00	0.16	0.05	0.00		0.05	0.09	0.13
Cr2O3	0.08	0.03	0.00	0.00	0.00	0.02	0.01	0.10	0.10
NiO	0.00	0.04	0.00	0.25	0.05	0.00	0.12	0.14	0.17
CuO	0.00	0.01	0.19	0.10	0.00	0.11	0.04	0.07	0.02
S	0.00	0.00	0.00	0.00	0.02	0.01	0.00	0.07	0.01
ZnO				0.00	0.00				0.11
TOTAL	101.25 @	100.65	99.41	101.41	98.79	101.53 @	98.70	99.18	98.45

27-25 DF Opaque in green spinel (DD/DE) Cr magnetite
DK Opaque in green spinel (DI/DJ) Cr-Ti magnetite (fine exsolution?)
DL Opaque in green spinel (DM/DN) Cr magnetite
* Low totals due to Fe2O3 content ?
657 3a Small olivine embayment into coarse orthopyroxene (3b)
1a Core of olivine 1d Margin of olivine (1a)
2a Margin of olivine 2c Core of olivine (2a)
@ Co analysed not detected
3b Orthopyroxene
1b Margin of orthopyroxene adjacent to olivine (1d)) 1c Core of orthopyroxene (1b)
1h Thin orthopyroxene extension into olivine

657 IC Energy Dispersive continued

	2b opx	1e chr	1f chr	2d chr	4a chr	1g phl	1i ser	1j ser	6e mag	4b po	4c po	
SiO2	56.61	0.26	0.39	0.31	0.77	39.63	41.13	41.29	0.25	0.14	0.34	Si
TiO2	0.14	1.32	1.06	1.32	1.11	0.29	0.11	0.00	0.00	0.00	0.05	Ti
Al2O3	0.82	4.03	4.39	2.22	1.97	14.02	0.08	0.43	0.06	0.00	0.11	Al
FeO	9.48	70.96	67.23	72.02	70.95	3.55	1.25	1.52	93.13	60.95	58.48	Fe
MnO	0.14	0.37	0.41	0.32	0.40	0.00	0.00	0.09	0.00	0.00	0.00	Mn
MgO	32.69	1.50	1.88	1.69	2.07	23.59	40.35	40.26	0.12	0.00	0.14	Mg
CaO	0.16	0.00	0.03	0.01	0.02	0.00	0.03	0.01	0.00	0.00	0.11	Ca
Na2O					0.22					0.16	0.13	Na
K2O	0.00	0.00	0.01	0.02	0.00	7.71	0.03	0.02	0.04	0.00	0.03	K
P2O5	0.01	0.00	0.00	0.00	0.09	0.06	0.19	0.00	0.05	0.02	0.07	P
Cr2O3	0.19	14.89	20.29	18.61	19.18	0.59	0.03	0.05	0.14	0.00	0.13	Cr
NiO	0.00	0.00	0.03	0.17	0.21	0.11	0.00	0.11	0.00	0.61	0.50	Ni
CuO	0.13	0.00	0.42	0.17	0.00	0.03	0.14	0.03	0.00	0.21	0.26	Cu
S	0.02	0.04	0.04	0.00	0.00	0.00	0.04	0.00	0.03	38.63	37.37	S
ZnO	0.00	0.13	0.29	0.01	0.38	0.15	0.03	0.08	0.10	0.10	0.11	Zn
TOTAL	100.39	93.50 *	96.47 *	96.87 *	97.37 *	89.73 **	83.41 **	83.89 **	93.92 *	100.82 ***	97.83 ***	

657 2b Orthopyroxene next to olivine (2a)
1e Idioblastic opaque in olivine Fe chromite (+ Al,Ti,Mg) different grains
1f 2d Opaques in olivine Fe chromite (+ Al,Ti,Mg) therefore not intergrowths
4a Opaque within pyrrhotite Fe chromite (+ Al,Ti,Mg)
1g Phlogopite
1i Serpentine 1j Serpentine ** Low totals due to high H2O content
6e Opaque adjacent to zoned amphibole magnetite
4b Pyrrhotite 4c Pyrrhotite *** Assumes no O

657 OU Wavelength

	JE opx	JR olv	JF amp	JG amp?
SiO2	56.96	40.80	46.85	57.25
TiO2	0.04	0.02	0.24	0.02
Al2O3	0.56	0.00	9.41	0.29
FeO	9.46	14.08	5.75	9.13
MnO	0.19	0.17	0.08	0.22
MgO	32.84	46.21	18.89	28.69
CaO	0.22	0.01	12.09	0.55
Na2O	0.00	0.00	1.68	0.05
K2O	0.00	0.00	0.35	0.00
Cr2O3	0.05	0.00	0.69	0.07
NiO	0.00	0.05	0.03	0.02
CuO				
S				
CoO				
TOTAL	100.32	101.34	96.06	96.29

616 IC Energy Dispersive DK 32

	5-1 opx	1-1 opx	5-2 amp	5-3 amp	1-2 amp	3-1 amp	1-3 chr	1-4 chr
SiO2	56.06	56.54	51.65	51.72	52.38	52.74	0.38	0.18
TiO2	0.01	0.01	0.13	0.10	0.25	0.17	1.04	1.12
Al2O3	0.94	0.75	5.46	5.30	5.13	4.81	6.04	5.36
FeO	10.71	10.28	4.55	5.20	4.72	4.57	66.43	68.75
MnO	0.29	0.14	0.12	0.17	0.08	0.09	0.46	0.27
MgO	32.19	32.49	20.68	20.67	21.00	21.00	2.90	2.72
CaO	0.29	0.26	11.99	12.01	12.11	11.99	0.00	0.05
Na2O	0.30	0.38	1.16	1.18	1.01	1.07	0.41	0.51
K2O	0.00	0.00	0.16	0.15	0.20	0.08	0.02	0.07
Cr2O3	0.06	0.06	0.54	0.43	0.43	0.23	20.30	20.04
NiO	0.09	0.07	0.00	0.00	0.01	0.00	0.18	0.04
CuO	0.00	0.00	0.15	0.00	0.01	0.08	0.00	0.07
S	0.01	0.00	0.01	0.00	0.00	0.05	0.01	0.02
CoO	0.03	0.03	0.00	0.00	0.00	0.00	0.00	0.00
TOTAL	100.98	101.01	96.60	96.93	97.33	96.88	98.17	99.20

657 JE Orthopyroxene
JR Small unaltered olivine relict in serpentine
JF Core of zoned amphibole hornblende JG Rim of zoned amphibole cummingtonite ?
616 5-1 Margin of coarse orthopyroxene 1-1 Coarse orthopyroxene
5-2 Fine amphibole next to orthopyroxene (5-1) hornblende
5-3 and 3-1 Coarse amphibole hornblende
1-2 Amphibole inclusion in orthopyroxene hornblende
1-3 1-4 Opaques Fe chromite (+ Al,Mg,Ti) different grains, therefore not intergrowths

were still unsatisfactory, they were fluxed. On repreparation, satisfactory totals were often obtained. The major cause of errors was thought to be weighing and mixing errors (i.e. dilution) and to a lesser extent inadequate disc preparation. All the individual components of the analyses with low or high totals were reduced or increased (in case of high) in the same proportion with respect to repeat preparations. When recalculated to a constant total (i.e. 100 wt%) both initial and repeat preparation analyses were statistically identical. Therefore because of constraints on time and facilities not all rocks with unsatisfactory totals have been fluxed.

The main example of a litholgy which gave unsatisfactory (too high, c. 102-103 wt%) raw analayses was the highly chloritised metagabbroic host rocks of the Phoenix deposit in the Tati greenstone belt (Brown in prep.). When recalculated to 100 wt%, their analyses (except for higher K contents) were similar to the unchloritised metagabbroic Selkirk host rocks. Because of mainly weighing & mixing because of time not all analyses were fluxed

Trace elements

As, Ba, Cr, Cu, Ga, Mn, Mo, Nb, Ni, Pb, Sc, Sr, S, V Y Zn Zr were analysed at Southampton University using a Philips PW 1212 X-ray fluorescence spectrometer (S1). Departmental sample preparationn and calibration procedures with some modifications were used throughout (Cosgrove 1972). Count times for Zr, Y, Nb and Rb were increased to 100 seconds. V data were improved by correcting for Ti K overlap on the V K line. Better calibration lines for most elements were obtained if the Southampton internal standards (CGM, DLC, GRD, KPL, BMS, PM & MCM) were excluded from the calculations. The practice of forcing calibrations through the origin was discontinued.

The detection limits (ppm) and coefficients of variation (%) for the Southampton 1212 analyses were:- Cr - 4 ppm & 9%, Cu - 5 & 16, Mo -3 & 17, Nb - 2 & 12 (100 sec.), Ni - 2 & 13, Rb - 2 & 7 (100 sec.), Pb - 5 & 15, Sr -4 & 8, S - 20 & 19, Th - 5 & 18, U -5 & 20, V - 5 & 10, Y - 2 & 12 (100 sec.), Zn - 5 & 12, Zr - 2 & 8 (100 sec.)

As a check on accuracy some samples were also analysed using the Philips 1400 spectrometers at Nottingham University (N) and Southampton University (S2) (replaced the Southamptn 1212). Comparative analyses of three samples which were chosen only on the basis of covering a wide range in composition are tabulated in Table A.1. The overall comparison is regarded as good and the Southampton

HORNBLENDE GNEISSES

	UNIT A	UNIT B				UNIT D					
	528	535	544	546	560	HG1	HG2	HG3	HG4	HG5	HG6
SiO2	50.20	52.96	49.03	52.31	49.68	47.00	43.38	50.14	49.09	48.68	51.71
TiO2	3.28	1.72	0.25	1.79	0.81	2.80	3.32	2.29	2.35	0.40	0.71
Al2O3	12.49	13.22	16.62	12.81	13.84	12.22	9.33	13.08	12.26	6.93	14.86
Fe2O3	16.91	14.52	8.69	13.77	11.54	19.38	22.83	14.63	16.81	10.91	10.46
MnO	0.55	0.15	0.15	0.19	0.18	0.25	0.22	0.20	0.23	0.17	0.17
MgO	4.98	4.64	9.27	5.09	8.73	5.11	7.31	5.21	4.67	17.06	6.46
CaO	8.36	9.74	11.50	9.81	11.07	10.11	10.55	9.74	9.39	12.14	9.93
Na2O	1.29	1.61	1.83	1.99	1.88	1.97	1.27	2.59	2.24	1.00	2.72
K2O	1.24	0.71	0.64	0.51	0.60	0.70	0.66	1.30	0.78	0.29	0.56
P2O5	0.77	0.07	0.04	0.06	0.11	0.37	0.07	0.37	0.31	0.06	0.12
Cr2O3	0.01	0.00	0.08	0.00	0.05	0.02	0.01	0.02	0.02	0.39	0.04
LOI	(1.05)	(0.49)	(1.28)	(0.46)	(1.04)	(0.24)	(0.32)	(0.29)	(0.18)	(1.78)	(0.58)
TOTAL	100.40	99.34	98.10	98.33	98.49	99.93	98.95	99.57	98.15	98.03	97.74
As						nd*	nd*	nd*	nd*		nd*
Ba	188	81	39	111	57	138	86	308	150	21	133
Ce	115	198	29	72	21	142	53	174	138	36	60
Cl	566	153	171	100	nd	1462	1091	231	1446	148	369
Co	61	57	51	40	35	72	93	51	50	59	46
Cr	67	39	552	30	320	131	68	154	143	2600	261
Cu	54	199	8	431	21	105	70	297	92	64	49
Ga	21	16	13	18	14	21	13	16	3	8	14
La	44	82	nd	17	7	32	nd	44	45	nd	11
Mo	3	3	12	nd	nd	nd	3	3	4	nd	nd
Nb	9	5	3	5	3	8	2	18	8	3	7
Ni	58	121	138	88	103	63	39	76	64	333	105
Pb	10	7	7	nd	5	6	5	10	6	nd	5
Rb	78	36	43	21	27	8	6	41	8	5	12
S	1700	1270	nd	1180	nd	1950	1360	427	1310	344	412
Sr	80	100	90	107	114	100	41	105	124	34	145
Th	nd	7			10	6	nd	8	6	nd	7
U						nd	nd	nd	nd	nd	nd
V	374	671	115	534	222	362	1200	355	340	113	173
Y	58	31	15	37	16	41	12	35	42	13	21
Zn	133	111	91	98	95	143	146	97	150	96	86
Zr	273	66	19	67	49	157	28	187	144	29	81

528 Fine-grained hornblende gneiss minor garnet Unit A PW 210
535 Pyroxene-hornblende gneiss fairly coarse banded Unit B PW 210
544 Coarse massive hornblende-feldspar rock/gneiss Unit B PW 213
546 Pyroxene-hornblende gneiss well-banded Unit B PW 213
560 Typical hornblende gneiss Unit B LK 2
HG1 Hornblende gneiss Unit D PW 210
HG2 Coarse mafic hornblende-rich gneiss minor diss. sulphides Unit D PW 210
HG3 Pyroxene-hornblende-feldspar gneiss Unit D PW 210
HG4 Hornblende gneiss typical Unit D PW 210
HG5 Hornblende amphibolite Unit D PW 210
HG6 Typical hornblende gneiss Unit D PW 210

	UNIT D continued					UNIT E		UNIT F				
	HG7	23	275	276	277	57	58	17	47	48	49	55
SiO2	42.46	51.06	37.40	45.12	46.51	48.47	53.77	50.30	51.56	50.71	50.43	49.96
TiO2	4.31	0.95	7.16	3.39	2.56	1.98	0.63	1.18	1.08	0.19	1.52	2.01
Al2O3	10.99	18.56	8.92	12.22	13.73	13.43	9.96	6.49	13.84	16.55	13.52	12.98
Fe2O3	23.37	9.69	33.65	21.42	17.18	16.43	9.84	14.45	12.51	8.20	14.61	15.83
MnO	0.24	0.13	0.40	0.20	0.24	0.22	0.21	0.33	0.21	0.20	0.21	0.21
MgO	5.33	6.08	6.41	6.26	5.87	5.98	12.49	13.22	7.53	10.09	7.23	5.53
CaO	9.66	10.14	6.41	10.44	10.07	9.60	10.34	11.32	7.41	9.37	7.98	9.27
Na2O	1.81	3.35	0.90	1.28	2.19	2.16	1.77	0.74	4.02	1.90	2.62	2.96
K2O	0.82	0.33	0.33	0.72	0.75	1.07	0.80	0.42	0.91	2.25	1.08	0.78
P2O5	0.14	0.23	0.13	0.04	0.24	0.23	0.09	0.24	0.11	0.03	0.23	0.25
Cr2O3	0.02	0.02	0.00	0.01	0.01	0.02	0.13	0.08	0.05	0.07	0.05	0.02
LOI	(0.21)	0.89	-0.40	(0.91)	0.50	0.58	1.00	1.60	1.04	1.89	1.49	0.45
TOTAL	99.15	101.43	101.31	101.10	99.85	100.17	101.03	100.37	100.27	101.45	100.97	100.25
As	nd*											
Ba	134			154					nd*			nd*
Ce	239			102					113*			112*
Cl	1348			730					nd*			38*
Co	96			117								
Cr	34	112	8	87	92	153	921	560	317	445	339	154
Cu	246	29	86	353	37	57	nd	348	10	6	41	47
Ga	24			18					16*			19*
La	93			nd					7*			18*
Mo	3	nd	3	4	3	15	nd	4	nd	nd	nd	nd
Nb	13	10	7	4	11	7	5	7	3	4	6	12
Ni	87	118	27	71	60	65	158	279	117	138	109	67
Pb	7	nd	6	8	3	25	23	32	nd	13	5	20
Rb	10	9	5	16	13	17	14	9	34	114	38	7
S	3730		4640	9450	360	1320	65			55	1200	
Sr	71	238	22	78	117	96	54	18	100	108	83	88
Th	7	nd				11		nd	5			nd
U	nd	nd						nd	nd			nd
V	1320	169	153	1180	415	286	165	258	264	126	182	342
Y	38	24	13	12	36	37	21	18	22	7	26	41
Zn	153	88	135	137	125	109	116	165	67	88	101	73
Zr	62	116	30	21	79	124	56	28	72	15	259	129

HG7 Coarse hornblende gneiss with magnetite and apatite minor diss. sulphides Unit D PW 210
23 Feldspathic hornblende gneiss near top of Unit D PW 81
275 Garnet-hornblende gneiss with magnetite diss. sulphides Unit D PW 195
276 Coarse hornblende gneiss diss. sulphides Unit D PW 195
277 Fine-grained, well-foliated hornblende gneiss Unit D PW 195
57 Hornblende gneiss more mafic top of gradational band Unit E PW 149
58 Coarse hornblende-feldspar gneiss more felsic base of gradational band Unit E PW 149
17 Coarse hornblende-feldspar gneiss minor diss. sulphide Unit F PW 193
47 Hornblende gneiss more mafic top of gradational band Unit F PW 177
48 Coarser hornblende-gneiss more felsic base of gradational band Unit F Pw 177
49 Coarse hornblende gneiss/feldspathic amphibolite (cf Phikwe host amph.) Unit F PW 177
55 Fine-grained hornblende gneiss Unit F PW 188

HORNBLENDE GNEISSES continued

	UNIT F continued				UNIT E/F	UNIT G			
	65	156	264	704	511	632	634	636	639
SiO2	50.28	48.26	47.34	46.54	52.55	50.60	46.45	46.96	46.49
TiO2	1.01	2.36	3.10	2.24	0.26	1.57	1.45	1.75	1.61
Al2O3	14.30	13.76	12.48	16.48	15.01	9.99	14.96	15.84	14.99
Fe2O3	13.11	16.41	17.48	13.98	8.94	20.84	15.46	13.98	15.50
MnO	0.14	0.20	0.22	0.18	0.17	0.62	0.20	0.16	0.29
MgO	7.40	6.45	5.83	5.58	8.67	5.24	6.42	7.48	6.78
CaO	9.62	9.63	10.25	10.45	12.13	7.08	10.31	8.84	10.06
Na2O	3.32	2.32	1.98	2.73	1.37	0.96	2.77	3.09	2.76
K2O	1.01	0.43	0.90	0.45	0.51	0.43	0.30	0.32	0.35
P2O5	0.09	0.41	0.91	0.45	0.05	0.52	0.22	0.24	0.24
Cr2O3	0.04	0.03	0.02	0.07	0.02	0.00	0.02	0.03	0.03
LOI	0.48	0.35	(0.34)	(0.46)	0.97	(-0.21)	(0.33)	(0.55)	(0.34)
TOTAL	100.80	100.61	100.51	99.15	100.65	97.85	98.56	98.69	99.10
Ba			186	57		214	74	121	65
Ce			184	85		182	71	48	72
Cl			75	66		nd	nd	nd	nd
Co			41	36		34	63	63	50
Cr	289	173	120	484	122	11	192	172	173
Cu	nd	11	81	32	61	51	89	34	10
Ga			20	19		24	21	19	20
La			61	26		47	12	10	22
Mo	nd	nd	nd	nd	nd	3	4	nd	nd
Nb	6	14	11	8	6	13	6	7	8
Ni	106	118	67	95	162	19	117	114	111
Pb	16	8	Ad	7	13	Ad	nd	5	9
Rb	19	7	15	16	14	30	6	15	12
S	54	737	2720	945		6830	959	49	nd
Sr	116	116	99	184	95	27	149	187	75
Th	6		5	nd		103?	12	7	13
U				nd					
V	203	118	338	274	148	28	220	258	261
Y	27	49	45	34	22	75	28	33	29
Zn	56	83	141	100	113	153	122	123	146
Zr	60	175	130	134	103	272	97	114	113

65 Hornblende gneiss Unit F PW 175
156 Foliated hornblende gneiss with pyroxene? Unit F PW 84
264 Typical hornblende gneiss Unit F PW 195
704 Hornblende gneiss with pyroxene? Unit F PW 208A
511 Coarse massive hornblende-feldspar rock Unit E/F Selebi North SDN 45
632 Banded garnet-hornblende gneiss qnt-plag bands Unit G PW CAM 38/1
634 Fine-grained garnet-hornblende gneiss Unit G PW CAM 38/1
636 Foliated hornblende gneiss w/ minor garnet Unit G PW CAM 38/1
639 Fine-gr. hornblende gneiss w/ minor qnt dark spots Unit G PW CAM 38/1

Biotite Amphibolites

						UNIT B	Low Ca	
	31-7-1a	1e	16-9-6a	6b	532	533	534	557
SiO2	50.30	51.31	51.44	51.80	49.60	51.40	51.61	53.12
TiO2	1.70	2.40	0.70	0.50	2.90	0.75	0.67	0.85
Al2O3	13.24	13.01	14.15	5.10	7.83	11.70	9.49	12.36
Fe2O3	14.62	15.57	11.00	11.23	17.31	14.21	16.30	17.49
MnO	0.21	0.21	0.19	0.19	0.31	0.15	0.22	0.13
MgO	4.72	3.82	8.09	18.22	16.21	11.21	13.40	7.26
CaO	9.59	8.91	10.75	11.13	1.11	3.04	2.25	2.82
Na2O	2.90	2.54	2.12	0.64	0.41	1.79	1.50	1.75
K2O	0.56	0.80	0.54	0.15	3.26	1.29	0.42	0.22
P2O5	0.26	0.32	0.09	0.09	0.09	0.16	0.05	0.78
Cr2O3	0.01	0.01	0.06	0.14	0.09	0.03	0.01	0.00
LOI	(0.09)	(0.20)	(0.91)	(1.47)	1.50	2.39	1.52	1.48
TOTAL	98.11	98.90	99.13	99.19	100.62	98.12	97.44	98.26
As					nd*			
Ba			142		228*	153	62	80
Ce			32		40*	114	59	223
Cl			74			109	nd	nd
Co			50			54	51	46
Cr	84	43	442	961	587	201	63	52
Cu	152	281	68	Ad	12	1280	22	167
Ga			14		15*	15	10	19
La			nd		28*	39	22	68
Mo	nd	nd	nd	nd	nd	126	nd	4
Nb	16	17	6	5	14	6	7	11
Ni	57	56	141	430	239	151	191	235
Pb	Ad	Ad	6	Ad	Ad	26	14	13
Rb	13	12	27	4	342	111	33	26
S			nd			4420	nd	6790
Sr	197	172	117	13	10	66	37	49
Th	11	Ad	11	nd	Ad	nd		
U		nd			nd			
V	323	337	233	141	195	74	94	579
Y	36	39	20	17	33	35	32	76
Zn	115	121	84	58	250	142	156	142
Zr	146	174	54	41	77	119	220	116

31-7-1a Fine -grained hornblende gneiss with altered pyroxene Motloutse River
31-1-7e Coarse hornblende gneiss Motloutse River
16-9-6a Hornblende gneiss Tobane
16-9-6b Coarse hornblende amphibolite Tobane

532 Actinolite-biotite amphibolite Unit B PW 210
533 Well-banded actinolite-biotite-plagioclase gneiss/schist Unit B PW 210
534 Coarse gedrite-plagioclase-biotite gneiss Unit B PW 210
557 Coarse hornblende gneiss diss. sulphide Unit B LK 2
Compare these low-Ca biotite amphibolites with the low-Ca quartz-rich biotite gneisses (1)

GREY QUARTZOFELDSPATHIC GNEISSES

	UNIT D		UNIT E									
	274	278	GG1	GG2	GG3	GG4	GG5	33*	50*	51	63*	185-1
SiO2	59.68	70.37	65.37	55.53	60.83	68.93	66.38	74.09	75.10	57.17	70.29	69.86
TiO2	0.75	0.40	0.79	0.89	0.86	0.35	0.42	0.17	0.16	0.59	0.26	0.22
Al2O3	16.13	13.92	15.69	16.64	16.67	14.75	14.63	13.59	13.11	17.30	13.39	13.74
Fe2O3	12.64	3.86	5.59	8.03	6.97	3.25	4.36	2.21	1.30	7.13	2.98	3.90
MnO	0.14	0.02	0.06	0.09	0.09	0.04	0.05	0.01	0.01	0.08	0.02	0.03
MgO	2.55	0.82	1.31	3.19	1.74	0.97	1.52	0.70	0.46	4.17	0.79	2.32
CaO	3.80	2.66	4.39	6.06	4.81	3.27	4.35	1.18	1.65	6.84	1.57	3.25
Na2O	2.69	3.56	3.72	3.00	3.83	3.91	3.72	3.75	2.59	3.67	3.11	3.58
K2O	0.96	2.56	1.41	1.84	2.05	2.58	1.95	4.21	5.32	1.47	4.77	1.24
P2O5	0.04	0.07	0.16	0.25	0.28	0.08	0.12	0.03	0.03	0.17	0.04	0.05
Cr2O3	0.01	0.00	0.00	0.00	0.00	0.00	0.00	0.00	0.00	0.01	0.00	0.00
LOI	0.05	(0.39)	(0.36)	(0.58)	(0.48)	(0.44)	(0.62)	0.41	0.37	0.97	0.61	(0.78)
TOTAL	99.44	98.24	98.49	99.62	98.43	98.13	98.00	100.35	100.10	99.57	97.83	98.19
As				46*		10*						
Ba		1076	386	481	457	812	671					
Ce		101	34	126	68	95	78					
Cl		nd	63	54	72	nd	nd					
Co		26	25	32	21	25	30					
Cr	76	5	8	33	8	11	29	nd	nd	66	nd	31
Cu	68	15	12	18	27	7	8	18	22	7	6	19
Ga		16	21	22	22	18	19					
La		45	25	62	31	52	44					
Mo	3	3	nd	nd	nd	nd	nd	nd	nd	nd	nd	nd
Nb	6	11	16	12	14	12	13	15	5	13	11	13
Ni	39	20	12	56	11	19	28	13	22	78	3	90
Pb	10	18	20	17	33	27	18	39	41	20	36	33
Rb	29	75	79	76	95	114	73	109	114	591	102	80
S	1730	27	nd	48	137	nd	nd			137	162	149
Sr	239	145	179	202	180	152	147	74	120	195	114	125
Th			13	18	19	39	20	36	32	5	41	6
U				43		5		10	5		8	
V	87	32	35	100	64	28	44	13	17	79	17	26
Y	22	27	64	34	33	21	37	43	12	36	41	12
Zn	85	43	45	87	92	56	45	37	19	60	53	53
Zr	143	242	544	245	243	212	220	120	119	194	234	93

core

274 Garnetiferous quartz-feldspar-biotite gneiss abundant Fe oxide Unit D PW 195
278 Quartz-feldspar-biotite gneiss PW 195
GG1 Banded quartz-feldspar biotite gneiss Unit E PW 210
GG2 Feldspar-quartz-hornblende-biotite gneiss Unit E PW 210
GG3 Quartz-feldspar-biotite-garnet gneiss w/ Fe oxide Unit E PW 210
GG4 Finely banded quartz-feldspar-biotite gneiss Unit E PW 210
GG5 Well-banded quartz-feldspar-biotite gneiss mafic & leuco Unit E PW 210
33* Coarse granitic gneiss w/ biotite minor garnet ? 12 m. above Phikwe amphibolite PW 93
50* Coarse granitic gneiss w/ biotite 17 m. above Phikwe host amphibolite PW 188
51 Banded feldspar-quartz-hornblende-biotite gneiss Unit E PW 188
63* Fine-grained granitic gneiss 9 m. above Phikwe host amphibolite Unit E PW 175
185-1 Coarse porphyroclastic quartz-feldspar-biotite gneiss adjacent to top of Phikwe host amphibolite Unit E PW 185
* Granitic gneiss band up to 15 metres thick, 6-20 metres above the Phikwe ore body

	UNIT F				UNIT E/F SELEBI-SELEBI NORTH					DK-LT	
	185-14	56	64	705	93	101	56-22	525	526	631	LT27-1
SiO2	60.17	59.25	71.61	72.46	70.17	63.59	62.81	72.23	58.85	60.93	62.76
TiO2	0.74	0.90	0.44	0.22	0.39	0.98	0.67	0.28	1.14	0.64	0.70
Al2O3	16.58	16.08	13.99	14.72	13.81	15.26	15.75	13.29	16.91	14.94	15.75
Fe2O3	6.67	7.22	3.78	1.81	4.75	6.92	6.18	2.56	8.13	8.72	6.86
MnO	0.05	0.08	0.04	0.04	0.12	0.09	0.06	0.04	0.13	0.05	0.04
MgO	3.04	3.25	0.97	5.14	1.23	2.79	2.17	5.05	4.23	3.70	3.10
CaO	5.88	6.45	2.63	0.38	2.82	4.39	5.09	0.05	3.97	4.43	4.46
Na2O	4.00	4.35	4.69	0.78	4.07	2.95	3.97	0.62	3.06	3.93	3.51
K2O	0.84	1.16	1.66	2.28	1.11	1.97	1.27	3.74	1.58	1.21	1.66
P2O5	0.17	0.18	0.10	0.03	0.08	0.32	0.17	0.02	0.21	0.14	0.16
Cr2O3	0.01	0.00	0.00	0.00	0.00	0.00	0.01	0.00	0.01	0.01	0.01
LOI	(0.60)	0.50	0.30	1.54	0.28	0.53	(0.59)	(1.92)	(2.50)	(0.66)	(0.62)
TOTAL	98.15	99.42	100.21	99.40	98.83	99.79	99.15	97.88	98.32	98.70	99.01
As			26*		72*				nd*		
Ba			691*	412	515*			735	263	117	254
Ce			68*	nd	67*			53	88	53	32
Cl				nd				nd	nd	123	60
Co				23				17	24	320	38
Cr	45	26	11	5	38	7	38	6	71	49	52
Cu	12	13	20	6	21	162	5	7	nd	55	38
Ga			17*	18	17*			16	21	18	21
La			45*	10	34*			29	32	25	30
Mo	nd	nd	nd	nd	5	4	nd	nd	4	11	nd
Nb	12	9	8	13	9	13	13	8	11	8	10
Ni	38	52	14	11	50	16	43	13	60	65	78
Pb	19	18	22	33	26	19	26	15	12	12	14
Rb	51	43	55	84	46	77	52	140	77	68	107
S	197			nd			104	nd	nd	1170	563
Sr	169	168	146	64	160	201	202	29	141	125	134
Th	25	14	26	28	19	24		25	8	14	11
U		nd	nd		nd	nd			nd		
V	78	103	34	9	30	62	55	14	122	124	78
Y	38	23	24	70	41	35	38	14	41	24	18
Zn	54	53	42	41	45	34	41	32	80	32	22
Zr	263	188	202	154	181	339	213	137	112	118	148

core

185-14 Coarse quart-feldspar-biotite gneiss at base of Phikwe host amphibolite PW 185
56 Feldspar-quartz-hornblende-biotite gneiss Unit F PW 188
64 Quartz-feldspar-biotite gneiss Unit F PW 175
705 Blue quartz-cordierite-biotite-sillimanite gneiss Unit F PW 208A
93 Quartz-plagioclase-microcline-biotite-garnet gneiss Unit E/F SD
101 Garnetiferous quartz-feldspar-biotite gneiss Unit E/F SD
56-22 Coarse grey gneiss w/ hhl. adjacent to Selebi North host amphibolite SDN 56
525 Blue quartz-cordierite-biotite-feldspar gneiss Unit E/F SDN 51
526 Fine-gr. blue quartz-feldspar-hornblende-chlorite gneiss Unit E/F SDN 51
631 Mafic fine-gr. grey gneiss w/ hornblende & Fe oxide above ultramafics DK 32
27-1 as 631 Unit A? LT 27

Analyses of furnace-dried samples give consistently lower totals than 'wet' samples. However no difference in element ratios between wet and dry when recalculated to 100%.

INTERMEDIATE BIOTITE GNEISSES

	UNIT A					UNIT B					
	537	538	540	541	542	529	531	545	547	555	556
SiO2	60.57	60.57	58.89	63.30	62.33	56.57	57.45	54.51	58.38	55.33	56.95
TiO2	0.61	0.60	0.66	0.36	0.58	0.64	1.06	0.36	2.04	0.88	0.75
Al2O3	13.74	14.08	14.20	14.57	14.10	12.82	12.73	16.28	11.59	15.24	14.00
Fe2O3	11.59	11.23	10.78	9.05	10.14	11.09	13.63	10.66	13.82	11.81	10.90
MnO	0.12	0.06	0.07	0.05	0.08	0.07	0.11	0.14	0.14	0.17	0.18
MgO	7.39	7.44	8.84	6.95	7.73	9.33	9.58	3.88	3.50	5.66	5.94
CaO	0.67	0.41	0.64	0.47	0.34	2.95	0.85	8.86	4.95	6.81	6.52
Na2O	0.76	0.25	0.51	0.73	0.29	2.28	0.36	1.46	2.53	1.20	1.42
K2O	3.99	3.83	4.51	3.07	3.57	2.33	0.24	1.66	0.60	0.52	0.54
P2O5	0.04	0.11	0.10	0.05	0.10	0.26	0.13	0.38	0.25	0.14	0.10
Cr2O3	0.03	0.03	0.04	0.06	0.02	0.04	0.02	0.01	0.00	0.01	0.02
LOI	(1.94)	(2.56)	(2.06)	2.29	(1.69)	(0.96)	1.65	(1.11)	(0.75)	(0.42)	0.67
TOTAL	99.51	98.61	99.24	100.95	99.28	98.38	97.81	98.12	97.80	97.77	97.99
	l	l	l	l	l	l	l	h	h?	h	h
Ba	452	382	441		441	252	107	175	191	108	115
Ce	45	29	25		34	83	65	155	75	50	52
Cl	454	585	664		266	175	nd	281	12	nd	11
Co	32	38	45		39	27	71	65	85	41	33
Cr	191	200	237	425	123	253	108	81	21	36	108
Cu	153	120	25	56	5	5	142	224	350	5	6
Ga	24	14	15		16	13	16	17	17	17	14
La	13	13	11		14	26	24	60	24	8	nd
Mo	3	nd	nd	nd	nd	nd	nd	nd	nd	nd	nd
Nb	32	5	5	18	8	9	5	4	6	11	5
Ni	59	60	62	103	58	65	61	101	890	68	68
Pb	17	5	13	5	13	14	nd	21	6	6	6
Rb	269	231	277	181	144	165	14	127	32	31	19
S	1171	955	375		nd	nd	1070	1765	6604	nd	nd
Sr	32	32	27	40	15	75	9	125	94	65	47
Th		9		8	15	5		8			
U				nd							
V	114	104	132	61	97	182	272	178	359	256	189
Y	43	17	9	30	12	34	31	104	26	32	36
Zn	110	113	103	73	78	275	107	88	56	87	84
Zr	105	121	107	78	124	112	96	29	118	82	130

537 Qtz-bio-gnt-plag-cordierite gneiss Unit A PW 213
538 Plag-qtz-amph-bio-gneiss Unit A PW 213
540 Qtz-bio-cordierite-plag-sill schist Unit A PW 213
541 Qtz-bio-cordierite-sill gneiss/schist Unit A PW 213
542 Banded qtz-bio-amph-plag-gnt gneiss Unit A PW 213
529 Fine-grained plag-qtz-bio-cummingtonite gneiss Unit B PW 210
531 Coarse garnet-amph-qtz-bio gneiss Unit B PW 210
545 Well-banded fine-gr. hbl-plag-bio gneiss Unit B PW 213
547 Fine-gr.foliated plag-bio-hbl-qtz pyrox gneiss diss. sulphides Unit B PW 213
555 Fine-gr. plag-hbl-qtz-bio-pyrox gneiss Unit B LK 2
556 Fine-gr. plag-hbl-pyrox-qtz-bio gneiss tuffaceous Unit B LK 2

	UNIT F	UNIT E/F	UNIT G		DK/LT	Coarse Garnets UNIT B		UNIT E/F	
	62	103	633	641	658	145	149	513	514
SiO2	55.38	58.06	54.86	58.11	55.79	43.60	41.97	50.91	47.48
TiO2	1.13	1.43	2.50	0.85	0.45	0.75	1.02	2.84	0.53
Al2O3	17.46	16.27	14.75	16.16	11.88	17.29	17.55	13.05	23.30
Fe2O3	9.96	9.06	11.10	10.09	18.74	22.49	22.96	16.35	11.41
MnO	0.17	0.12	0.24	0.09	0.06	0.19	0.14	0.20	0.12
MgO	4.70	10.25	3.77	5.45	3.33	8.90	9.78	10.70	11.42
CaO	7.21	0.90	6.29	1.46	1.72	2.17	0.83	1.32	0.37
Na2O	2.64	0.46	3.33	1.84	2.74	1.52	0.81	0.33	0.34
K2O	1.91	2.51	1.52	3.14	2.71	1.58	2.30	3.97	6.16
P2O5	0.24	0.32	1.02	0.12	0.14	0.06	0.07	0.45	0.03
Cr2O3	0.01	0.01	0.00	0.04	0.00	0.08	0.05	0.02	0.01
LOI	0.98	1.67	(0.52)	1.36	1.13	1.99	2.57	(1.64)	(3.09)
TOTAL	101.79	101.06	99.38	98.71	98.69	100.62	100.05	100.14	101.17
	h	l	h	l	l	l	l	l	l
As		14*							
Ba		281*	979	504	232			398	1480
Ce		46*	75	57	156			95	10
Cl			nd	nd	431			nd	nd
Co			31	42	14			77	11
Cr	71	65	5	250	28	557	372	168	90
Cu	14	58	84	59	6	441	253	83	6
Ga		29*	28	23	14			19	25
La		22*	46	26	37			29	10
Mo	nd	nd	nd	nd	6	4	3	3	nd
Nb	11	19	14	13	5	13	11	10	8
Ni	76	74	13	139	89	136	148	95	68
Pb	19	13	186	34	18	13	5	6	7
Rb	79	120	129	121	248	122	179	84	229
S			7260	2790	nd	32370	19790	4540	23
Sr	166	24	139	92	71	30	21	9	11
Th	nd	10	nd	11	13				
U	nd	nd							
V	154	130	77	133	64	225	225	259	126
Y	29	37	76	28	8	49	35	69	13
Zn	89	45	245	135	86	204	221	95	93
Zr	145	331	266	149	82	43	48	178	149

62 Fine-grained plag-hbl-bio-qtz gneiss Unit E PW 195
103 Coarse,banded qtz-bio-cordierite-gedrite-plag-gnt gneiss Unit E/F Selebi SD 80
633 Well-foliated fine-gr. plag-bio-hbl-qtz-mag schist/gneiss Unit G PW CAM 38/1
641 Biotite-plag-qtz schist Unit G PW CAM 38/1
658 Fine-gr.dk-grey qtz-bio-mag-plag-gneiss (cf feld.quartzite) Unit A? Dikoloti DK 17

145 Coarse plag-gnt-bio-amph-magnetite gneiss diss. sulphides Unit B PW 195
149 Coarse plag-gnt bio-qtz-amph-mag-cordierite? gneiss diss.sulphides Unit B PW 195
513 Coarse qtz-garnet-bio-magnetite-cordierite? gneiss Unit E/F Selebi North SDN 45
514 Coarse qtz-bio-gnt-cordierite-sill gneiss Unit E/F Selebi North SDN 45

h high calcium quartz-poor biotite gneisses
l low calcium quartz-rich biotite gneisses

CALC-SILICATE GNEISSES and QUARTZ-FELDSPAR GRANULITES

	574	30-7 1b	30-7 1c	30-7 1d	30-7 1f	30-7 4	11-8 3a	11-8 3c	17-8 6a	24-8 3c	4-9 1g
SiO2	71.73	75.90	58.22	71.36	67.93	76.95	85.67	71.60	69.05	61.95	59.94
TiO2	0.01	0.17	0.13	0.13	0.14	0.01	0.04	0.10	0.18	0.24	1.15
Al2O3	14.10	12.91	21.98	15.44	16.94	12.76	7.74	13.54	13.29	19.96	18.56
Fe2O3	4.17	0.48	1.95	0.77	1.03	0.44	0.16	3.34	4.01	2.22	3.04
MnO	1.61	0.01	0.02	0.01	0.01	0.08	0.01	0.01	0.02	0.02	0.04
MgO	0.44	0.01	1.23	0.63	0.58	0.11	0.08	0.06	0.09	0.28	0.07
CaO	0.92	7.84	12.42	8.49	10.99	1.22	2.05	8.71	9.14	12.32	13.25
Na2O	5.32	0.55	1.87	1.26	0.63	5.38	2.24	2.73	2.48	0.96	1.52
K2O	1.24	0.03	0.25	0.17	0.03	0.81	0.18	0.20	0.18	0.08	0.15
P2O5	0.02	0.05	0.07	0.05	0.06	0.03	0.03	0.03	0.08	0.08	0.52
Cr2O3	0.00	0.00	0.00	0.00	0.00	0.00	0.00	0.00	0.00	0.00	0.01
LOI	-0.15	0.32	(0.71)	(0.39)	(0.30)	0.22	0.16	(0.26)	(1.24)	(0.52)	(0.68)
TOTAL	99.41	98.27	98.14	98.31	99.24	98.01	98.36	100.32	98.52	98.11	98.25
As	35*				34*	38*				17*	nd*
Ba	35*	nd			31*	49*	92			22	
Ce	58*	49			48*	nd*	8			223	
Cl		nd					nd			19	
Co		51					43			30	
Cr	11	10	5	nd	5	23	7	12	14	82	37
Cu	27	14	15	12	13	20	14	14	9	17	8
Ga	34*	17			23*	28*	11			28	
La	28*	34			25*	7*	15			133	
Mo	nd	nd	nd	nd	nd	nd	nd	nd	nd	3	nd
Nb	32	15	12	11	11	158	3	6	18	24	35
Ni	34	30	17	25	20	19	35	9	25	19	12
Pb	49	12	23	15	9	37	nd	17	27	26	11
Rb	52	nd	4	5	5	26	nd	9	20	4	11
S		nd	nd	nd	nd		nd	nd	2040	nd	
Sr	12	255	422	302	315	35	216	394	336	403	333
Th	6	49	39	80	44	9	8	5	75	72	6
U	5	12	7	7	14	25			15	15	
V	8	7	11	7	12	nd	6	26	17	36	81
Y	401	39	34	28	24	49	7	24	32	39	94
Zn	21	24	38	26	24	12	24	23	25	28	21
Zr	86	104	216	173	66	17	42	92	199	247	221

574 Quartz-feldspar-garnet granulite (cf 701 & 702 granitic bands) Unit B PW 208
30-7-1b Quartz-feldspar-garnet granulite finely banded mylonite? Botsabelo
30-7-1c Quartz-feldspar-hornblende granulite/calc-silicate gneiss Botsabelo
30-7-1d Quartz-feldspar-hornblende-pyroxene granulite/calc-silicate gneiss Botsabelo
30-7-1f Quartz-feldspar-hornblende granulite/calc-silicate gneiss Botsabelo
30-7-4 Quartz-feldspar-garnet granulite Botsabelo
11-8-3a Siliceous quartz-feldspar-hornblende granulite/csg Selebi North
11-8-3c Qtz-feldspar-hornblende granulite/csg mylonitised? Selebi North
17-8-6a Quartz-feldspar-hornblende granulite/calc-silicate gneiss Phokoje
24-8-3c Qtz-feldspar-hornblende granulite/csg mylonitised? Mogolodi North
4-9-1g Quartz-feldspar-epidote granulite/csg mylonite Lethlakane fault zone

GRANITIC GNEISSES

	31-7-3	16-9-5a	703	700	701	702
SiO2	72.77	71.79	72.78	58.22	72.44	75.12
TiO2	0.17	0.16	0.18	1.00	0.13	0.01
Al2O3	13.78	14.80	13.90	14.88	14.82	14.11
Fe2O3	1.84	1.13	1.57	9.88	1.09	0.11
MnO	0.02	0.02	0.04	0.12	0.03	0.02
MgO	0.29	0.49	0.31	2.67	0.31	0.05
CaO	1.38	1.85	1.45	5.73	3.54	0.58
Na2O	4.22	4.64	3.57	3.25	4.54	2.86
K2O	3.92	3.77	4. 0	1.88	1.59	7.35
P2O5	0.05	0.06	0.04	0.41	0.05	0.01
Cr2O3	0.00		0.00	0.01	0.00	0.00
LOI	0.32	0.68	(0.38)	(0.40)	(0.26)	(0.21)
TOTAL	98.76	99.40	97.94 wm	98.05	98.54	100.22
As	33*	36*				
Ba	610*	796*	599	492	115	439
Ce	55*	nd*	59	133	14	nd
Cl			nd	324	nd	nd
Co			47	32	39	27
Cr	15	12	8	64	9	7
Cu	13	17	17	45	10	8
Ga	21*	18*	17	21	25	19
La	42*	13*	42	59	11	nd
Mo	5	3	6	nd	nd	nd
Nb	14	4	11	15	13	25
Ni	18	21	32	40	26	22
Pb	44	37	28	23	41	79
Rb	150	108	193	89	73	361
S			198	nd	nd	nd
Sr	91	401	79	151	109	58
Th	38	7	35	15	9	6
U	11	nd	19			nd
V	13	17	12	135	10	6
Y	21	3	39	54	18	20
Zn	49	26	53	127	37	22
Zr	160	108	130	263	52	21

METASEDIMENTS

	amphibolite	quartzites	
	31-7-5b	530	539
SiO2	52.54	69.26	76.37
TiO2	0.14	0.57	0.04
Al2O3	10.97	8.06	12.64
Fe2O3	5.97	14.35	0.84
MnO	0.13	0.04	0.01
MgO	11.50	2.89	0.27
CaO	16.34	0.86	1.92
Na2O	0.95	0.59	3.53
K2O	1.54	0.46	0.53
P2O5	0.03	0.05	0.02
Cr2O3	0.03	0.03	0.00
LOI	(2.07)	4.60	(0.47)
TOTAL	100.14	101.56	98.67
As			
Ba		527	47
Ce		13	nd
Cl		nd	nd
Co		53	40
Cr	270	191	4
Cu	15	212	7
Ga		5	15
La		7	nd
Mo	35	nd	33
Nb	5	5	3
Ni	54	166	33
Pb	6	10	30
Rb	54	19	34
S	4690	47020	nd
Sr	146	27	84
Th	14		
U			
V	68	108	9
Y	13	10	9
Zn	100	50	21
Zr	168	43	86

31-7-3 Coarse porphyroblastic granitic gneiss core of body northeast of Phikwe
16-9-5a Medium-gr. weakly porphyroblastic-granoblastic granitic gneiss Tobane
703 Coarse porphyroblastic granitic gneiss PW 208
700 Dk-grey med.-gr.'dioritic' plag-bbl-qtz-bio gneiss assoc. w/ 703 PW 208
701 Cse pink-white 'pegmatitic' granite band assoc w/ 703 PW 208
702 Cse pink-white 'pegmatitic' granite band assoc w/ 703 PW 208
wm definite weighing & mixing error

31-7-5b Diopside-actinolite amphibolite assoc. w/ diop-actin quartzite Phikwe dome
530 Finely banded sillimanite-pyrrhotite quartzite Unit B PW 210
539 Quartz-plagioclase-sillimanite-biotite gneiss/quartzite Unit A PW 213

ANORTHOSITES and RELATED ROCKS

	PW 211				PW 208							
	561	562	563	571	548	552	553	554	28-7 2	30-7 1a	13-8 1a	7-8 3
SiO2	47.50	47.40	48.11	50.71	47.12	78.22	49.29	69.72	50.16	48.51	47.87	48.61
TiO2	0.27	0.01	0.19	0.10	0.32	0.14	0.15	0.39	0.21	0.08	0.35	0.14
Al2O3	24.25	32.06	21.88	26.48	23.09	11.58	17.40	12.90	17.09	28.77	24.06	23.70
Fe2O3	3.88	1.03	5.71	3.38	3.74	0.94	7.78	4.27	6.50	2.70	6.49	4.88
MnO	0.04	0.01	0.08	0.05	0.05	0.01	0.15	0.04	0.14	0.05	0.07	0.10
MgO	5.41	0.31	7.55	2.47	6.57	0.59	8.84	1.20	8.50	1.38	3.53	6.02
CaO	16.78	16.33	14.13	12.19	16.31	3.78	11.74	5.55	15.57	14.03	12.97	14.76
Na2O	1.49	2.21	1.79	3.36	1.15	2.78	2.10	2.80	1.39	2.92	2.43	1.78
K2O	0.09	0.04	0.06	0.45	0.14	0.57	0.72	0.29	0.17	0.25	0.88	0.11
P2O5	0.08	0.12	0.04	0.03	0.13	0.06	0.03	0.04	0.03	0.02	0.05	0.03
Cr2O3	0.02	0.00	0.02	0.01	0.03	0.00	0.04	0.00	0.01	0.00	0.00	0.01
LOI	(0.90)	(0.34)	(0.96)	(0.61)	(1.08)	(0.43)	(1.22)	(0.37)	(0.74)	(0.51)	(1.40)	(0.85)
TOTAL	99.81	99.52	99.56	99.23	98.65	98.67	98.24	97.20	99.77	98.71	98.70	100.14
Ba	nd	28	50	44	nd	125	67	35			164	nd
Ce	52	nd	15	nd	12	nd	nd	nd			nd	nd
Cl	16	nd	26	26	15	nd	241	54			116	nd
Co	19	26	32	23	21	54	44	52			27	30
Cr	150	11	113	65	206	10	238	6	43	28	27	80
Cu	nd	7	10	12	nd	32	36	14	214	11	25	298
Ga	22	26	19	21	13	12	11	13			20	15
La	32	nd	nd	nd	nd	nd	nd	nd			nd	nd
Mo	4	nd	nd	nd	nd	nd	nd	nd	nd	nd	3	nd
Nb	9	9	6	5	10	6	2	5	4	3	3	4
Ni	136	9	218	43	199	32	189	20	104	33	74	115
Pb	17	5	nd	12	nd	9	nd	9	nd	14	5	nd
Rb	7	4	5	12	8	25	27	8	4	11	47	4
S	nd	nd	nd	nd	nd	nd	nd	nd			96	473
Sr	394	455	231	167	381	144	105	146	103	214	151	134
Th		6	8	nd					6	7	8	nd
V	76	nd	70	40	55	13	142	nd	186	23	129	103
Y	24	4	10	32	9	10	7	28	6	26	10	7
Zn	23	15	47	44	21	29	65	54	50	46	41	45
Zr	62	42	16	16	58	29	9	57	11	12	27	11

561 Pyroxene hornblende anorthosite PW 211
562 100% feldspar anorthosite PW 211
563 Gabbroic hornblende anorthosite PW 211
571 Typical coarse hornblende anorthosite PW 211
548 Banded pyroxene hornblende anorthosite (sheared) PW 208
552 Quartz anorthosite PW 208
553 Gabbroic hornblende anorthosite PW 208
554 Foliated quartz hornblende anorthosite PW 208
28-7-2 Gabbroic hornblende anorthosite Dikoloti
30-7-1a Hornblende anorthosite Botsabelo
13-8-1a Hornblende anorthosite Mahalapye Road
17-8-3 Gabbroic hornblende anorthosite Phokoje

	4-9 2a	10-9 1g	LETHLAKANE SECTION 992-1	992-2	992-3	992-4	992-5	992-6	992-7	992-8	992-9	992-10
SiO2	55.16	49.99	56.12	52.02	51.53	51.06	50.21	50.43	46.83	47.18	52.81	52.16
TiO2	0.02	0.20	0.04	0.07	0.36	0.26	0.17	1.65	1.58	1.77	0.10	0.27
Al2O3	28.00	28.54	26.91	28.01	15.48	11.44	19.80	3.56	7.03	5.44	24.02	16.81
Fe2O3	1.51	3.53	1.58	2.61	9.69	9.88	7.29	15.81	14.27	15.57	4.12	8.29
MnO	0.02	0.04	0.01	0.03	0.19	0.21	0.12	0.24	0.20	0.21	0.08	0.16
MgO	0.68	1.71	0.65	1.52	8.60	11.38	7.05	17.33	15.70	17.15	3.31	8.12
CaO	11.48	13.05	9.81	11.79	11.64	12.67	12.80	11.72	11.24	11.94	10.70	11.79
Na2O	3.92	3.50	4.13	3.84	2.27	1.34	2.29	0.27	1.33	1.17	3.66	2.49
K2O	0.45	0.24	1.21	0.41	0.85	0.53	0.56	0.22	0.12	0.12	1.41	0.66
P2O5	0.04	0.04	0.03	0.06	0.03	0.03	0.03	0.04	0.04	0.04	0.03	0.03
Cr2O3	0.00	0.03	0.00	0.00	0.01	0.03	0.02	0.20	0.18	0.18	0.01	0.01
LOI	(0.84)	(0.87)	(1.39)	(0.92)	(1.74)	(1.65)	(1.27)	(0.42)	(0.70)	(-0.10)	(2.14)	(0.87)
TOTAL	101.28	100.87	100.49	100.36	100.65	98.83	100.34	101.47	98.52	100.77	100.25	100.79
Ba			258	114	181	48	63	494	234	177	250	81
Ce			nd	nd	nd	nd	nd	46	64	107	nd	10
Cl			45	nd	62	154	122	nd	67	64	99	126
Co			12	10	51	48	45	90	80	92	17	44
Cr	10	177	6	29	53	187	160	1346	1206	1248	41	68
Cu	14	21	nd	14	48	nd	6	230	167	184	nd	30
Ga			19	19	13	11	15	9	9	9	16	16
La			nd	nd	nd	nd	nd	nd	7	12	nd	nd
Mo	nd	nd	nd	nd	nd	nd	nd	4	nd	nd	nd	3
Nb	5	4	3	4	3	nd	3	6	5	7	5	2
Ni	13	29	15	34	105	149	167	679	688	679	55	95
Pb	19	8	11	15	nd	6	5	6	nd	7	14	4
Rb	18	7	64	19	33	15	16	16	3	5	74	18
S		32	40	106	280	129	42	292	174	175	64	95
Sr	177	241	333	265	137	80	161	88	354	230	272	151
Th	9	5		9								
V	13	66	6	17	203	215	115	257	215	231	47	141
Y	8	9	nd	7	7	9	8	20	17	15	11	7
Zn	28	34	nd	9	55	53	34	100	85	95	28	48
Zr	16	21	13	16	9	9	12	34	38	43	15	9

4-9-2a Altered (green) anorthosite Lethlakane fault zone
10-9-1g Hornblende anorthosite Kurumela

992-1 Anorthosite Lethlakane section
992-2 Hornblende anorthosite Lethlakane section
992-3 Gabbroic hornblende anorthosite Lethlakane section
992-4 Metagabbro Lethlakane section
992-5 Porphyroblastic gabbroic hornblende anorthosite Lethlakane section
992-6 Thin mafic band in anorthosites Lethlakane section
992-7 Thin mafic band in anorthosites Lethlakane section
992-8 Thin mafic band in anorthosites Lethlakane section
992-9 Porphyroblastic hornblended anorthosite Lethlakane section
992-10 Gabbroic hornblende anorthosite Lethlakane section

ANORTHOSITES and RELATED ROCKS continued

PW 208 SHEAR ZONES

	575a	575b	575c	576a	576b	576c
SiO2	50.35	48.07	54.80	62.40	66.71	62.30
TiO2	0.17	0.08	0.06	0.41	0.74	1.14
Al2O3	24.50	26.80	22.76	17.72	13.92	13.73
Fe2O3	5.08	5.72	4.19	4.92	6.30	6.74
MnO	0.04	0.04	0.05	0.04	0.03	0.06
MgO	2.37	1.97	0.25	1.51	0.71	0.34
CaO	13.52	17.36	16.67	9.22	10.39	13.63
Na2O	1.63	1.03	0.64	1.82	0.64	0.43
K2O	0.35	0.16	0.31	0.32	0.27	0.45
P2O5	0.04	0.07	0.05	0.09	0.18	0.58
Cr2O3	0.00	0.01	0.00	0.00	0.00	0.00
LOI	(0.85)	(2.98)	(0.97)	(0.97)	(1.78)	(1.78)
TOTAL	98.05	101.31	99.78	98.45	99.89	99.40
Ba	13	nd	nd	12	35	45
Ce	10	9	nd	60	490	438
Cl	118	73	nd	43	26	9
Co	46	32	47	39	60	82
Cr	33	48	23	25	14	7
Cu	7	10	11	62	242	243
Ga	21	23	23	15	22	23
La	nd	nd	nd	35	283	252
Mo	4	nd	3	nd	nd	nd
Nb	4	5	3	6	10	15
Ni	79	54	21	30	45	62
Pb	7	7	10	nd	6	17
Rb	9	10	15	13	12	13
S	nd	nd	nd	5	1220	2170
Sr	285	424	432	226	236	225
Th	nd	nd	nd	13	22	12
U	nd	nd	nd	nd	nd	nd
V	42	50	26	25	19	40
Y	15	11	14	12	34	58
Zn	34	29	20	30	29	19
Zr	88	14	22	330	1009	961

575a Unsheared hornblende anorthosite PW 208
575b Sheared margin of shear zone PW 208
575c Garnetiferous core of shear zone PW 208
576a Unsheared quartz anorthosite PW 208
576b Sheared margin of shear zone PW 208
576c Garnetiferous core of shear zone PW 208

DYKES
Metamorphosed and deformed

	18-7-1a	567	573	195
SiO2	53.07	50.21	45.73	50.90
TiO2	0.78	1.95	1.48	1.15
Al2O3	18.40	12.15	18.94	14.11
Fe2O3	10.18	17.69	10.71	14.01
MnO	0.15	0.26	0.15	0.21
MgO	3.65	4.56	5.98	6.10
CaO	8.68	8.42	12.02	11.23
Na2O	2.54	1.97	2.40	2.29
K2O	1.93	1.62	0.41	0.35
P2O5	0.43	0.23	0.69	0.11
Cr2O3	0.01	0.01	0.02	0.01
LOI	(0.69)	(0.56)	(0.91)	0.55
TOTAL	99.82	99.07	98.53	101.02
Ba		239	72	
Ce		136	155	
Cl		992	nd	
Co		54	47	
Cr	46	52	145	70
Cu	24	189	205	171
Ga		21	23	
La		47	56	
Mo	nd	5	nd	4
Nb	21	14	13	6
Ni	41	51	120	59
Pb	10	9	7	9
Rb	83	43	8	15
S		211	117	426
Sr	153	90	216	126
Th	13	nd		
U		nd		
V	58	388	178	281
Y	88	40	34	22
Zn	144	147	74	87
Zr	537	129	197	74

18-7-1a Deformed dyke, hornblende feldspar gneiss in anorthosite Selebi North
567 Fine-grained hornblende gneiss in anorthosite PW211
573 Fine-grained hornblende gneiss in anorthosite PW211
195 Deformed dyke, hornblende feldspar gneiss in granitic gneiss Lobala north

ULTRAMAFICS IN THE SELEBI-PHIKWE GNEISSES

	1	14	213-1	213-2	217-1	217-2	157	158
SiO2	50.22	48.24	50.56	42.56	52.46	50.66	44.98	44.64
TiO2	0.32	0.58	0.37	0.13	0.29	0.32	0.62	0.54
Al2O3	4.10	5.07	6.34	2.85	3.30	3.97	10.25	17.89
Fe2O3	8.64	15.86	9.81	11.18	8.11	7.44	13.34	10.33
MnO	0.13	0.20	0.22	0.15	0.12	0.10	0.16	0.14
MgO	20.91	22.29	25.56	39.55	20.53	22.86	24.94	13.44
CaO	12.32	5.00	1.91	2.11	12.08	11.77	5.16	9.53
Na2O	0.64	0.59	0.20	0.32	0.49	0.46	0.64	1.28
K2O	0.24	0.64	3.05	0.26	0.11	0.13	0.13	1.36
P2O5	0.05	0.06	0.05	0.05	0.04	0.05	0.07	0.10
Cr2O3	0.35	0.51	0.89	1.06	0.49	0.60	0.19	0.04
LOI	1.99	1.33	(2.35)	(6.27)	(1.93)	(2.85)	0.50	2.25
TOTAL	99.91	100.37	98.96	100.22	98.06	98.36	100.98	101.54
As			nd*					
Ba			401	42	nd	nd		
Ce			28	59	53	27		
Cl			115	1046	nd	76		
Co			56	98	50	59		
Cr	2420	3460	5960	6830	3300	3980	1320	307
Cu	50	477	14	10	8	11	127	nd
Ga			6	4	3	3		
La			nd	nd	nd	nd		
Mo	nd	nd	nd	nd	3	3	nd	nd
Nb	3	4	4	2	nd	4	3	4
Ni	494	915	998	1550	588	476	1080	594
Pb	nd	5	4	nd	nd	8	nd	nd
Rb	8	21	125	13	4	5	3	83
S		7140	nd	90	nd	nd	3380	30
Sr	14	11	7	10	11	16	6	101
Th	nd		7	nd	nd	5		
U	nd		nd					
V	152	133	62	54	97	124	84	79
Y	5	12	6	3	14	7	6	8
Zn	64	126	118	83	70	61	91	72
Zr	26	43	73	21	32	23	24	29

1 Pyroxenite Unit D PW 166
14 Amphibolitised pyroxenite w/cummingtonite + phlogopite UNIT D PW 193
213-1 Amphibolite (2 clino & ortho) + phlogopite Unit D PW 213
213-2 Serpentinised peridotite Unit D PW 213
217-1 Clinoamphibolite tremolite Unit D PW 217
217-2 Olivine-orthopyroxene clinoamphibolite - tremolite Unit D PW 217
157 Oliv.-pyrox clinoamphibolite-hornbl. 270 m. above Selebi ore body SD 97
158 Hornblende feldspar amphibolite at margins of 157 SD 97 Unit E/F/G?

These ultramafics only include the small ultramafic bands and pods within the Selebi-Phikwe section particularly Unit D. The ultramafics hosting Ni-Cu sulphides at Selebi-Phikwe and Dikoloti-Lentswe are tabulated elsewhere.

DIOPSIDE GNEISSES UNIT G

	635	637	638	640
SiO2	47.40	49.88	47.90	49.35
TiO2	0.47	0.69	1.50	1.79
Al2O3	7.78	10.52	16.12	16.21
Fe2O3	14.76	13.57	13.17	11.89
MnO	0.58	0.53	0.27	0.27
MgO	2.29	2.75	2.94	3.04
CaO	25.53	20.12	13.96	12.84
Na2O	0.40	1.01	3.05	3.54
K2O	0.08	0.14	0.29	0.31
P2O5	0.34	0.36	0.23	0.27
Cr2O3	0.00	0.00	0.04	0.03
LOI	(4.74)	(0.69)	(1.12)	(1.42)
TOTAL	99.63	99.57	99.47	99.54
Ba	13	165	103	169
Ce	110	197	54	40
Cl	244	221	77	9
Co	4	18	67	66
Cr	11	5	270	172
Cu	57	19	89	43
Ga	16	22	22	20
La	43	109	9	14
Mo	4	3	7	3
Nb	12	14	8	8
Ni	10	10	118	98
Pb	12	9	14	25
Rb	7	9	8	9
S	2120	518	3750	2840
Sr	52	59	137	111
Th	78?	102?	8	11
V	11	11	241	261
Y	51	76	35	41
Zn	139	161	113	135
Zr	194	287	109	122

635 Diopside-plagioclase gneiss Unit G PW CAM 38/1
637 Weakly banded diopside-plagioclase gneiss Unit G PW CAM 38/1
638 V.well-banded and size-min.graded hbl-plag & diop-plag gneiss Unit G PW CAM 38/1
640 V.well-banded hornblende-plag and diopside-plag gneiss Unit G FW CAM 38/1

SEFHOPE DIOPSIDE GNEISSES

2-8-4a	4b	Ga	12-8-3a	Ga
45.94	46.71	48.37	50.70	46.08
0.93	0.85	1.08	0.97	2.63
14.64	15.01	15.75	15.45	13.92
9.52	9.70	11.55	11.27	13.62
0.30	0.29	0.20	0.17	0.27
6.04	5.96	6.14	6.98	4.53
23.12	20.81	13.66	11.81	19.13
0.34	0.43	2.31	2.37	0.91
0.07	0.90	0.33	0.33	0.26
0.17	0.24	0.11	0.10	0.29
0.03	0.03	0.05	0.04	0.01
(2.95)	(2.48)	(0.57)	(0.91)	(0.65)
101.10	100.93	99.55	100.19	101.65
	449		172	
	8		38	
	nd		26	
	62		58	
207	207	323	269	46
37	23	25	42	13
	16		16	
	20		8	
5	4	3	3	5
4	7	6	6	11
158	144	135	132	45
6	nd	13	9	9
2	38	8	9	13
	2400		161	
156	112	146	149	262
nd	nd	10	nd	8
166	191	279	244	407
22	21	26	27	45
70	75	90	79	70
73	67	73	76	151

2-8-4a Diopside-altered plagioclase band of graded? diopside amphibolites Sefhope East
2-8-4b as 2-8-4a with minor thin hornblende-plagioclase amphibolite bands Sefhope East
2-8-6a Whole thin graded band from hbl-rich to diop-plag-rich Sefhope East
12-8-3a Mafic hornblende-plagioclase-diopside gneiss Sefhope East
12-8-6a 'Felsic' diopside-plagioclase-hornblende gneiss band Sefhope East

PHIKWE HOST AMPHIBOLITE

PW 185 core section

	185-2	3	4	5	6	7	8	9	10	11	12	13
SiO2	47.75	45.35	44.31	41.39	43.79	44.21	45.00	44.66	46.61	47.81	47.87	50.67
TiO2	0.56	0.30	0.29	0.26	0.22	0.23	0.26	0.33	0.38	0.44	0.54	0.52
Al2O3	17.12	16.76	17.93	16.89	15.48	16.19	16.71	15.01	15.85	17.73	16.56	15.91
Fe2O3	10.56	10.50	9.94	16.94	17.11	13.02	11.62	10.77	11.09	9.54	10.73	9.54
MnO	0.13	0.14	0.13	0.12	0.16	0.13	0.14	0.16	0.13	0.12	0.14	0.14
MgO	11.05	14.01	13.71	10.87	10.92	12.50	13.59	15.88	12.22	10.93	11.26	9.21
CaO	5.69	8.63	9.17	9.38	8.17	9.66	9.22	8.15	9.46	9.81	10.33	10.33
Na2O	2.32	1.30	1.22	1.09	1.35	1.12	1.34	1.25	1.53	2.03	1.83	2.55
K2O	2.82	1.75	1.26	0.72	0.54	0.31	0.64	1.09	0.87	1.09	1.37	0.53
P2O5	0.07	0.05	0.04	0.06	0.04	0.04	0.04	0.04	0.04	0.06	0.07	0.06
Cr2O3	0.03	0.03	0.03	0.03	0.04	0.03	0.04	0.05	0.03	0.03	0.06	0.06
LOI	1.93	2.45	2.08	3.46	3.39	3.19	2.49	3.26	2.11	1.39	1.42	0.99
TOTAL	98.10	98.82	98.03	97.75	97.82	98.44	98.60	98.39	98.21	99.59	100.76	99.52
Cr	233	233	226	195	259	230	251	322	213	200	424	381
Cu	172	409	358	3614	2660	1110	516	170	199	40	72	29
Mo	nd	3	nd	nd	nd	nd	nd	nd	nd	nd	nd	nd
Nb	11	5	3	2	5	3	2	3	5	4	5	5
Ni	506	769	895	2446	1732	1477	1568	654	618	364	454	241
Pb	14	nd	nd	14	16	nd	9	nd	14	17	8	5
Rb	134	72	57	36	24	17	36	50	36	47	61	17
S	1693	2997	4424	44625	29639	17314	11047	1260	2999	453	987	318
Sr	80	89	111	99	65	81	77	30	80	99	82	100
Th	8	nd	5	7	11	nd	5	nd	8	nd	nd	9
V	107	82	60	54	79	55	59	74	85	99	132	125
Y	38	9	9	7	7	10	9	11	22	19	18	20
Zn	105	72	78	80	105	89	77	80	84	68	80	65
Zr	42	25	21	25	18	19	19	24	26	34	39	41

PW 185 Host amphibolite intersection completely sampled and analysed
185-2 Coarse hornblende-biotite-feldspar-quartz gneiss hybrid zone 0-0.63
3 Hornblende-biotite-feldspar amphibolite 0.63-1.63
4 Hornblende-feldspar-biotite amphibolite 1.63-3.63
5 as 4 ds ccp-rich 3.63-6.13
6 as 4 ds minor fold 6.13-8.63
7 as 4 ds 8.63-11.13
8 as 4 11.13-13.63
9 as 4 13.63-16.13
10 Sheared amphibolite porphyroclastic feldspars 16.13-18.13
11 Hornblende-feldspar-biotite amphibolite 18.13-19.13
12 Hornblende-feldspar-biotite amphibolite 19.13-20.13
13 Hornblende-feldspar gneiss
185-1 & 14 grey quartzofeldspathic gneisses immediately above and below host-amphibolite see grey gneisses for analyses

PW 130 core section

	67	68	69	70	71	72	73	74	151	75	76	152	77
SiO2	46.09	44.72	46.84	43.02	44.32	44.41	45.25	46.37	44.68	44.92	46.65	46.25	44.64
TiO2	0.33	0.27	0.24	0.28	0.32	0.37	0.36	0.32	0.30	0.36	0.35	0.39	0.52
Al2O3	16.90	16.72	17.33	12.16	15.01	16.04	17.43	17.60	17.12	15.93	17.50	13.96	15.90
Fe2O3	11.56	13.14	10.58	16.24	13.32	11.90	10.45	9.76	11.15	10.42	9.65	10.99	12.85
MnO	0.19	0.16	0.16	0.19	0.17	0.16	0.14	0.11	0.10	0.12	0.12	0.14	0.11
MgO	12.38	11.64	14.00	16.94	13.41	14.53	17.76	14.21	13.31	14.49	12.42	14.54	12.89
CaO	8.76	8.79	7.65	4.36	9.64	7.55	1.81	8.26	8.88	8.86	9.24	10.32	9.36
Na2O	1.28	1.31	1.18	0.69	1.55	1.42	0.94	1.21	1.38	1.40	1.64	1.48	1.50
K2O	1.82	1.56	1.88	1.25	0.86	1.68	3.59	1.79	1.54	0.99	1.05	0.64	0.92
P2O5	0.04	0.03	0.04	0.05	0.03	0.03	0.03	0.04	0.04	0.03	0.05	0.04	0.04
Cr2O3	0.13	0.10	0.06	0.04	0.04	0.03	0.05	0.03	0.04	0.04	0.03	0.04	0.03
LOI	2.28	2.67	1.64	5.28	1.92	3.54	4.26	1.83	3.41	3.53	2.79	2.12	3.03
TOTAL	101.76	101.11	101.60	100.50	100.59	101.66	102.07	101.53	101.95	101.90	101.49	100.91	101.79
Cr	870	657	435	257	305	228	345	223	260	241	217	263	195
Cu	274	522	37	14	194	96	13	177	380	47	543	340	71
Mo	nd	nd	nd	nd	nd	nd	nd	nd	nd	3	nd	nd	nd
Nb	2	5	2	5	5	5	2	4	3	2	5	3	4
Ni	445	993	820	885	371	491	775	726	973	620	961	805	466
Pb	nd	25	15	18	25	17	32	18	15	12	15	7	8
Rb	84	65	87	49	33	72	145	69	65	40	46	24	43
S	2030	11090	390	151	883	1350	291	153	5340	468	4260	2200	706
Sr	72	86	63	9	35	61	68	87	91	75	103	68	28
Th	nd			nd			nd				nd		
U	nd										nd		
V	112	91	71	63	159	101	80	78	83	81	80	96	116
Y	7	6	9	7	47	38	13	8	23	9	10	12	22
Zn	160	136	159	221	79	64	69	27	30	44	49	47	41
Zr	22	17	22	20	36	35	22	23	22	22	27	32	31

PW 130 not completely sampled only representative samples
67 Hornblende-feldspar-biotite-gedrite amphibolite 93.6
68 Hornblende-feldspar-biotite-gedrite amphibolite ds 94.6
69 Hornblende-feldspar-biotite-gedrite amphibolite 95.4
70 Hornblende-feldspar-gedrite-biotite amphibolite 97.6
71 Hornblende-feldspar-gedrite-biotite amphibolite 98.1
72 Hornblende-gedrite-biotite-chlorite-feldspar amphibolite schistose 98.5
73 Talcy hornblende-gedrite-biotite-chlorite feldspar amphibolite schistose 99.4
74 Hornblende-gedrite-biotite-chlorite feldspar amphibolite schistose 100.3
151 Hornblende-gedrite-biotite-chlorite feldspar amphibolite schistose ds 101.2
75 Hornblende-gedrite-biotite-chlorite-feldspar amphibolite schistose sheared 102.7
76 Hornblende-gedrite-biotite-chlorite feldspar amphibolite schistose ds 103.7
152 Hornblende-gedrite/anthophyllite-chlorite-feldspar amphibolite 104.6
77 Hornblende-gedrite/anthophyllite-chlorite-altered feldspar amphibolite 105.9

PHIKWE HOST AMPHIBOLITE continued

PW 1500 section underground

	178	179	180	181	182	183	184	185
SiO2	46.05	45.15	43.67	41.89	39.59	43.47	44.69	42.20
TiO2	0.43	0.30	0.28	0.12	0.21	0.27	0.23	0.36
Al2O3	10.81	16.18	16.32	15.01	15.14	17.39	18.41	15.86
Fe2O3	14.73	13.44	13.18	17.56	21.44	12.66	10.78	15.47
MnO	0.18	0.15	0.18	0.31	0.41	0.15	0.12	0.13
MgO	15.13	13.09	14.23	12.41	11.35	13.15	15.00	12.05
CaO	8.71	8.65	7.31	9.15	7.75	9.48	8.76	10.81
Na2O	0.90	1.15	1.02	1.52	0.86	1.10	0.94	1.07
K2O	0.95	2.63	3.63	0.26	1.22	0.90	1.53	0.40
P2O5	0.04	0.03	0.04	0.03	0.04	0.03	0.04	0.14
Cr2O3	0.14	0.03	0.04	0.02	0.06	0.03	0.04	0.03
LOI	2.73	(1.99)	(1.19)	1.26	1.87	1.42	1.50	2.00
TOTAL	100.80	100.80	99.90	99.54	99.94	100.05	102.04	100.52
Cr	990	225	245	159	413	224	241	186
Cu	nd	306	40	451	1230	179	74	1123
Mo	nd	12	4	nd	nd	nd	nd	nd
Nb	3	6	4	3	3	nd	3	3
Ni	697	1090	670	857	1300	841	859	1440
Pb	7	19	23	9	68	43	19	23
Rb	36	95	119	6	42	40	71	10
S	1080	4230	520	9350	27600	4630	1220	26240
Sr	10	63	42	41	41	112	119	84
Th		nd	nd					
V	138	89	86	50	45	61	61	72
Y	14	12	14	10	11	10	7	18
Zn	125	108	151	168	125	133	99	101
Zr	28	22	25	15	15	16	19	40

Phikwe 1500 stope underground section large representative samples
178 Thin micaceous amphibolite above massive sulphide
179 Micaceous amphibolite folded inclusion into massive sulphide
180 Micaceous amphibolite with sulphide stringers
181 Hornblende amphibolite with minor garnet inclusion in massive sulphide
182 Hornblende-garnet amphibolite sulphide stringers
183 Coarse hornblende-feldspar-gedrite amphibolite
184 Hornblende-plagioclase-biotite-gedrite amphibolite
185 Hornblende-gedrite-plagioclase-biotite amphibolite

PW 1600 section underground

	186	189	190	191	192	193	44	45	194	54
SiO2	48.96	41.16	43.80	44.74	50.06	43.86	44.42	49.85	44.85	41.78
TiO2	0.41	0.18	0.16	0.21	0.41	1.67	0.33	0.37	0.23	0.25
Al2O3	15.90	15.91	18.22	18.02	16.48	18.30	17.09	14.80	18.81	15.08
Fe2O3	10.43	18.60	13.63	11.02	10.34	12.90	14.65	10.23	10.89	18.28
MnO	0.15	0.38	0.14	0.13	0.11	0.09	0.11	0.11	0.14	0.23
MgO	10.45	13.03	12.56	14.24	9.02	14.43	13.24	10.38	11.82	10.13
CaO	11.29	7.20	9.77	7.85	10.62	2.60	5.09	11.50	10.43	10.18
Na2O	2.00	0.96	1.25	1.66	2.97	1.66	0.98	2.40	1.29	1.35
K2O	0.37	1.93	0.86	1.19	0.36	6.61	2.83	0.56	1.26	0.28
P2O5	0.06	0.04	0.04	0.04	0.05	0.24	0.03	0.04	0.04	0.03
Cr2O3	0.09	0.02	0.02	0.03	0.05	0.02	0.03	0.04	0.06	0.06
LOI	1.12	1.38	2.07	2.71	0.90	(1.69)	3.15	1.56	(1.96)	1.27
TOTAL	101.23	100.79	102.52	101.84	101.37	102.38	101.95	101.84	99.82	98.92
Cr	596	140	161	196	329	101	216	266	422	439
Cu	20	2300	390	761	24	7	6	12	392	767
Mo	nd	nd	3	3	nd	4	nd	nd	3	nd
Nb	3	6	2	nd	4	18	6	7	3	4
Ni	284	826	927	1080	217	91	683	290	703	881
Pb	23	23	30	24	19	25	13	9	23	40
Rb	12	71	32	60	9	279	106	22	54	8
S	79	11750	7090	6330	405	57	275	105	8110	10380
Sr	104	30	165	129	113	98	150	35	138	33
Th						15			6	nd
V	128	53	51	52	137	124	77	111	82	157
Y	21	30	16	7	24	21	15	32	7	4
Zn	89	150	127	80	50	113	76	43	68	223
Zr	25	16	13	20	28	334	23	43	19	14

PW 1600 stope underground large samples
186 Hornblende-plagioclase amphibolite med.grained above massive sulphide
189 Garnet-hornblende amphibolite sulphide stringers
190 Hornblende-feldspar amphibolite
191 Hornblende-plagioclase-orthoamphibole-biotite-chlorite amphibolite sheared
192 Feldspathic amphibolite
193 Biotite amphibolite biotite = biotite/phlogopite

44 Hornblende-feldspar-gedrite-biotite amphibolite PW 177
45 Coarse feldspathic amphibolite PW 177
194 Hornblende-feldspar-gedrite-biotite amphibolite sheared PW 1700 stope ug
54 Garnet-hornblende amphibolite PW 188

PHIKWE HOST AMPHIBOLITE continued

	PW 93 core												
	34a	34b	34c	34d	34e	34f	34g	34h	34i	34j	34k	34l	34m
SiO2	47.72	45.08	46.58	44.23	41.69	43.40	43.45	43.70	43.49	43.60	44.29	44.04	44.43
TiO2	0.39	0.42	0.39	0.54	0.07	0.18	0.09	0.11	0.21	0.25	0.17	0.18	0.22
Al2O3	15.94	13.73	16.81	14.20	13.28	14.69	15.86	17.00	15.37	15.53	17.22	17.01	17.81
Fe2O3	12.60	17.42	12.28	17.57	18.15	13.43	13.38	12.42	12.25	12.62	11.63	11.75	9.70
MnO	0.21	0.24	0.17	0.23	0.27	0.14	0.11	0.12	0.11	0.13	0.14	0.13	0.10
MgO	8.57	10.20	8.68	9.47	13.92	14.28	14.61	14.04	15.53	16.43	14.69	14.56	14.17
CaO	10.07	9.94	9.90	9.05	8.66	10.87	9.52	9.35	8.95	7.43	7.58	8.08	7.93
Na2O	2.44	2.01	2.70	1.92	1.50	1.63	1.49	1.49	1.28	1.25	1.36	1.35	1.42
K2O	0.29	0.66	1.13	1.42	0.29	0.42	0.64	1.01	1.46	1.28	1.34	1.41	1.91
P2O5	0.05	0.05	0.05	0.04	0.04	0.04	0.04	0.04	0.04	0.04	0.03	0.04	0.04
Cr2O3	0.08	0.04	0.07	0.06	0.01	0.02	0.03	0.02	0.02	0.03	0.02	0.03	0.03
LOI	1.22	1.40	1.64	2.02	1.89	1.56	1.59	2.10	2.08	1.36	1.74	2.23	3.57
TOTAL	99.58	101.19	100.40	100.75	99.77	100.66	100.81	101.40	100.79	99.95	100.84	100.81	101.33
As	nd*												
Ba	20	39	93	132	nd	nd	31	18	94	119	82	68	206
Ce	54	62	24	81	31	50	40	41	36	26	16	26	16
Cl	99	165	75	254	66	19	nd	24	nd	nd	nd	nd	nd
Co	42	92	44	57	138	51	51	54	69	59	60	58	69
Cr	521	301	466	431	89	171	205	160	154	217	168	205	216
Cu	46	364	65	181	749	266	100	133	180	148	137	222	37
Ga	15	13	11	10	10	11	13	10	10	10	9	10	11
La	10	nd	nd	nd	nd	nd	nd	nd	nd	nd	nd	nd	nd
Mo	3	nd	nd	nd	nd	nd	nd	nd	nd	nd	nd	nd	nd
Nb	3	4	nd	2	3	2	nd	3	4	3	3	3	nd
Ni	260	1090	434	803	1200	473	557	563	720	630	565	723	701
Pb	24	35	73	30	15	27	24	25	20	13	14	12	50
Rb	6	13	32	42	5	5	13	29	50	48	62	64	93
S	nd	8368	1023	3671	24961	3801	2061	2916	3303	2292	1568	3575	105
Sr	124	63	237	63	33	33	44	80	39	55	128	105	132
Th	nd	nd	46	nd	nd	nd	nd	nd	nd	nd	nd	nd	nd
U	nd	nd	nd	nd	nd	nd	nd	nd	nd	nd	nd	nd	nd
V	130	135	119	161	55	78	34	37	56	61	47	55	58
Y	10	9	11	17	5	5	7	5	7	10	3	5	3
Zn	161	234	217	188	178	161	153	130	107	95	96	93	50
Zr	30	24	24	25	10	13	13	14	14	18	18	17	27

PW 93 core representative samples analysed

34a Feldspar-hornblende amphibolite 1169.1-1169.5 feet
34b Garnet-hornblende-feldspar-biotite amphibolite po stringers 1183.2-1183.5
34c Hornblende-feldspar-biotite amphibolite minor garnet 1185.3-1185.7
34d Hornblende-feldspar-biotite amphibolite po stringres 1186.5-1186.9
34e Hornblende-gedrite amphibolite minor garnet probed po stringers 1190-1190.4
34f Hornblende-phlogopite-spinel amphibolite minor garnet po stringers 1193.9-1194.3
34g Garnet-hornblende-feldspar amphibolite po stringers 1195.7-1196.0
34h Hornblende amphibolite 1196.7-1197.0
34i Hornblende-biotite amphibolite (phlogopite?) schistose 1198.6-1198.8
34j Hornblende-gedrite-pyroxene amphibolite 1200.1-1200.4
34k Hornblende-gedrite-biotite-feldspar amphibolite 1200.8-1201.2
34l Hornblende-gedrite-feldspar amphibolite 1201.7-1201.9
34m Hornblende-biotite-feldspar amphibolite schistose 1204.4-1205.0

PHIKWE ULTRAMAFICS

	PW 34 continued				PW 204a			
	34n	34p	34q	34r	518	519	523	211
SiO2	45.65	44.81	49.04	48.73	42.29	44.74	51.15	44.94
TiO2	0.50	0.43	0.34	0.36	0.14	0.22	0.17	0.23
Al2O3	16.87	16.09	15.76	16.47	14.72	11.30	4.26	3.40
Fe2O3	10.77	12.18	12.12	11.25	12.33	14.87	12.23	8.83
MnO	0.12	0.13	0.13	0.14	0.18	0.20	0.22	0.20
MgO	13.11	12.48	10.61	9.92	18.19	17.73	26.78	33.92
CaO	9.18	9.14	9.63	10.10	7.06	7.21	2.88	2.73
Na2O	1.80	1.73	2.29	2.53	0.98	0.88	0.42	0.40
K2O	1.25	1.40	0.64	0.41	0.36	0.15	0.07	0.20
P2O5	0.06	0.05	0.04	0.05	0.03	0.05	0.04	0.04
Cr2O3	0.04	0.04	0.07	0.06	0.05	0.05	0.42	0.75
LOI	2.47	3.40	1.36	1.61	(4.09)	(1.87)	(0.94)	5.67
TOTAL	101.82	101.88	102.03	101.63	100.42	99.27	99.58	101.31
As				9*				
Ba	169	159	64	30				
Ce	22	31	35	38				
Cl	nd	nd	nd	nd				
Co	71	72	62	72				
Cr	240	264	485	407	350	341	2880	5110
Cu	162	218	151	124	216	605	263	68
Ga	15	13	11	18				
La	nd	nd	nd	nd				
Mo	nd	nd	nd	nd	nd	nd	nd	nd
Nb	5	5	2	8	4	6	3	5
Ni	673	836	490	361	1110	1300	1210	1910
Pb	12	13	17	12	nd	nd	7	nd
Rb	52	57	22	17	14	4	6	13
S	1810	5780	2940	2803				1180
Sr	119	105	120	115	21	13	7	10
Th	nd	nd	nd	nd				
U	nd	nd	nd	nd				
V	113	109	108	139	32	52	55	64
Y	12	23	16	30	7	11	7	3
Zn	83	44	60	62	115	79	104	121
Zr	32	33	29	37	15	26	20	16

34n Hornblende-biotite-feldspar-chlorite amphibolite schistose 1207.6-1207.9
34p Hornblende-biotite-feldspar amphibolite schistose 1209.4-1209.8
34q Feldspathic hornblende amphibolite probed 1211.2-1211.7
34r Feldspathic hornblende amphibolite 1212.2-1212.6

518 Hornblende amphibolite PW 204a
519 Hornblende amphibolite PW 204a
523 Coarse orthopyroxenite weakly amphibolitised PW 204a

211 Orthopyroxene serpentinite w/ anthophyllite & cse bronzites P3122 ug underground hole

SELEBI HOST AMPHIBOLITE

SELEBI SL SECTION underground

	SL-1	2	3	4	5	6	7	8	9	10	11	12	13
SiO2	45.75	46.75	47.30	47.08	47.15	46.65	46.05	47.90	46.41	47.77	47.01	46.43	48.47
TiO2	0.46	0.52	0.45	0.45	0.45	0.50	0.49	0.48	0.65	0.43	0.53	0.53	0.60
Al2O3	17.84	16.78	16.50	16.83	17.09	17.20	16.83	17.57	16.33	17.20	16.09	16.48	17.02
Fe2O3	11.86	9.69	9.96	10.14	10.30	9.83	10.03	9.40	10.21	9.25	10.71	10.06	9.61
MnO	0.24	0.20	0.17	0.17	0.17	0.16	0.16	0.17	0.18	0.16	0.18	0.16	0.15
MgO	12.64	11.60	12.26	12.16	11.80	11.24	12.30	11.01	11.28	10.79	12.28	11.39	10.68
CaO	8.60	9.52	9.91	10.08	10.47	11.02	10.00	11.02	9.97	10.07	9.94	10.06	10.30
Na2O	0.73	1.13	1.48	1.52	1.39	1.62	1.52	1.71	1.56	1.62	1.67	1.76	2.28
K2O	2.35	2.08	1.77	1.65	1.52	0.92	1.15	0.69	0.95	1.38	1.56	1.40	0.93
P2O5	0.07	0.06	0.07	0.07	0.06	0.07	0.06	0.06	0.06	0.05	0.06	0.07	0.08
Cr2O3	0.06	0.03	0.03	0.03	0.03	0.03	0.03	0.03	0.04	0.03	0.04	0.04	0.07
LOI	(4.89)	(2.52)	(2.20)	(2.22)	(2.31)	(1.53)	(2.00)	(1.26)	(1.68)	(1.74)	(2.14)	(2.19)	(1.33)
TOTAL	100.60	98.36	99.90	100.18	100.43	99.24	98.62	100.04	97.64	98.75	100.07	98.38	100.19
Cr	417	213	210	191	191	228	228	233	277	200	259	286	454
Cu	48	18	94	139	176	74	50	26	72	65	101	50	27
Mo	nd	3	nd	nd	nd	3	nd	3	3	nd	nd	nd	nd
Nb	5	4	2	4	4	4	5	4	4	3	3	4	5
Ni	808	437	452	465	453	383	470	372	369	420	432	413	319
Pb	nd	8	14	12	12	16	15	15	13	20	13	6	18
Rb	104	91	68	60	62	30	53	27	39	58	60	56	38
S	692	150	641	936	1225	539	346	227	444	489	746	328	168
Sr	45	80	79	81	90	121	97	125	99	98	83	111	143
V	150	135	131	123	121	139	133	135	165	127	142	141	160
Y	30	13	20	15	9	14	12	12	18	21	18	15	16
Zn	162	93	71	69	60	61	63	74	81	78	67	70	63
Zr	33	33	32	27	27	37	33	32	44	32	31	41	37

SL-1 Highly micaceous schistose amphibolite
SL-2 Banded feldspar biotite amphibolite
SL-3 Banded amphibolite with feldspar and biotite
SL-4 Amphibolite with minor biotite and feldspar
SL-5 Hornblende feldspar amphibolite wth minor biotite
SL-6 Hornblende feldspar amphibolite with minor biotite
SL-7 Hornblende feldspar amphibolite with pyroxene? and minor biotite
SL-8 Hornblende feldspar amphibolite
SL-9 Hornblende feldspar amphibolite with coarse random biotite
SL-10 Hornblende feldspar amphibolite with coarse random biotite
SL-11 Hornblende feldspar amphibolite with increased coarse biotite
SL-12 Feldspathic amphibolite with biotite
SL-13 Feldspathic amphibolite with biotite

SL SECTION continued

	14	15	16	17
SiO2	48.00	48.73	47.81	46.78
TiO2	0.50	0.27	0.73	0.26
Al2O3	15.70	10.86	13.71	10.29
Fe2O3	10.46	12.89	12.31	13.85
MnO	0.18	0.27	0.21	0.24
MgO	11.19	14.19	12.11	19.65
CaO	9.72	10.04	8.65	6.71
Na2O	1.85	1.62	1.66	0.54
K2O	1.28	0.71	1.79	0.54
P2O5	0.07	0.04	0.14	0.04
Cr2O3	0.04	0.41	0.13	0.23
LOI	(1.73)	(1.66)	(1.92)	(4.98)
TOTAL	98.99	100.03	99.25	99.13
Cr	280	2733	886	1515
Cu	219	nd	380	8
Mo	nd	nd	3	nd
Nb	3	6	8	4
Ni	409	515	682	900
Pb	17	14	12	16
Rb	50	23	60	20
S	479	102	3590	1690
Sr	83	29	70	8
Th				
V	136	119	173	100
Y	17	33	20	7
Zn	118	153	137	204
Zr	38	31	49	17

SL-14 Hornblende feldspar amphibolite with biotite and disseminated sulphides
SL-15 Coarse gabbroic hornblende feldspar amphibolite with biotite
SL-16 Coarse hornblende feldspar amphibolite with biotite and disseminated sulphides
SL-17 Highly micaceous amphibolite

SELEBI SU SECTION underground

SU-1	2	3	4	5	6	7
48.98	46.98	45.50	46.00	46.55	47.22	52.33
1.59	0.31	0.40	0.37	0.50	0.46	0.08
18.42	17.06	16.69	18.58	17.84	18.44	27.85
10.20	11.00	10.59	9.84	9.27	8.86	1.99
0.09	0.14	0.14	0.13	0.13	0.11	0.01
6.84	10.78	13.14	11.68	10.95	11.91	1.86
9.69	10.41	8.73	9.56	11.21	9.30	10.30
2.85	1.43	1.52	1.56	1.76	1.58	4.18
0.43	0.58	1.25	1.39	0.62	1.36	0.63
0.44	0.04	0.04	0.05	0.05	0.03	0.02
0.02	0.05	0.03	0.04	0.17	0.05	0.02
(1.55)	(1.91)	(3.39)	(3.46)	(1.50)	(2.53)	(0.87)
99.55	98.78	98.03	99.20	99.05	99.32	99.17
108	369	197	261	1158	338	127
915	1700	229	381	219	9	48
nd	nd	3	nd	nd	nd	nd
14	3	4	4	6	6	3
1055	893	625	657	467	319	62
12	17	9	nd	8	12	30
17	26	64	73	29	68	39
12940	8730	1520	3510	1970	122	200
206	101	87	117	129	154	515
7	16	nd	8	9	nd	nd
175	103	82	81	120	81	13
33	7	10	13	9	27	4
61	71	62	74	78	80	32
237	23	27	26	28	31	34

SU-1 Fine-grained feldspathic amphibolite with disseminated sulphides
SU-2 Hornblende feldspar amphibolite with biotite
SU-3 Sheared feldspathic amphibolite with biotite
SU-4 Highly micaceous sheared feldspathic amphibolite
SU-5 Feldspathic amphibolite with gedrite and biotite
SU-6 Coarse banded micaceous feldspathic amphibolite
SU-7 Hornblende anorthosite

SELEBI HOST AMPHIBOLITE continued

SELEBI SU SECTION continued

	8	9	10	11	12	13	14	15	16
SiO2	46.24	45.86	46.97	42.94	42.98	49.97	47.87	51.12	46.29
TiO2	0.40	0.34	0.42	0.29	0.33	0.44	0.54	1.09	0.38
Al2O3	16.46	17.75	19.74	14.44	11.33	3.60	12.19	11.60	17.42
Fe2O3	11.03	10.10	9.61	19.50	19.50	21.54	14.64	13.58	11.08
MnO	0.14	0.14	0.11	0.16	0.18	0.44	0.14	0.19	0.15
MgO	13.52	12.83	10.95	9.26	13.34	17.39	10.71	11.53	11.47
CaO	7.81	8.81	8.26	8.45	8.01	3.77	9.48	5.12	9.05
Na2O	1.23	1.53	1.62	1.34	1.32	0.36	1.39	1.33	1.24
K2O	1.84	1.61	1.43	0.70	0.71	0.23	0.52	1.87	1.80
P2O5	0.04	0.05	0.04	0.06	0.05	0.04	0.04	0.58	0.06
Cr2O3	0.04	0.04	0.05	0.04	0.07	0.16	0.04	0.10	0.04
LOI	(3.04)	(2.26)	(2.02)	(3.63)	(3.31)	(1.59)	(0.96)	(1.37)	(3.00)
TOTAL	97.75	99.06	99.20	97.18	97.82	97.94	97.56	98.11	98.99
Ba			168						280
Ce			19						65
Cl			nd						83
Co			56						60
Cr	268	266	311	257	493	1097	241	680	294
Cu	310	147	679	16130	5820	7120	34	96	2049
Ga			11						18
La			nd						nd
Mo	nd	nd	3	nd	4	3	nd	nd	nd
Nb	4	3	4	5	6	4	6	15	4
Ni	600	486	654	2590	1870	1090	381	386	642
Pb	5	14	15	15	9	7	13	34	25
Rb	89	78	74	31	34	12	15	80	83
S	2040	1230	3730	55010	25350	17450	259	608	4770
Sr	80	109	180	68	14	9	38	86	99
Th	nd	5	nd	6	6	10	nd	23	10
V	88	74	77	118	102	161	137	149	90
Y	6	13	11	9	5	9	17	58	14
Zn	108	98	104	126	145	268	178	147	126
Zr	23	27	33	19	19	19	27	181	26

SU-8 Sheared micaceous amphibolite
SU-9 Sheared micaceous feldspathic amphibolite with gedrite
SU-10 Feldspathic amphibolite with biotite
SU-11 Hornblende feldspar amphibolite with disseminated sulphides
SU-12 Mafic hornblende biotite amphibolite with disseminated sulphides
SU-13 Mafic hornblende-rich amphibolite
SU-14 Coarse hornblende feldspar amphibolite
SU-15 Fine-grained mafic hornblende feldspar amphibolite with biotite
Su-16 Micaceous hornblende feldspar amphibolite with disseminated sulphides

SELEBI 1625 SECTION underground

	1	2	3	4	5	6	7	9	10
SiO2	47.83	49.46	47.49	47.68	48.87	48.58	45.98	46.31	44.39
TiO2	0.46	0.31	0.36	0.79	0.65	0.40	0.59	0.58	0.34
Al2O3	22.12	17.77	14.53	20.59	15.48	17.67	16.85	12.11	14.61
Fe2O3	6.85	7.87	9.98	7.71	9.70	8.88	9.95	13.05	11.55
MnO	0.10	0.14	0.17	0.10	0.14	0.14	0.17	0.22	0.16
MgO	7.00	8.82	12.35	9.03	11.80	9.93	10.59	13.23	16.91
CaO	12.67	0.62	10.66	10.44	9.15	10.88	11.51	10.31	8.29
Na2O	2.30	2.58	1.34	1.98	1.73	2.12	1.13	1.18	1.44
K2O	0.58	0.68	1.23	2.16	2.10	1.03	1.62	0.56	2.06
P2O5	0.03	0.05	0.05	0.10	0.20	0.06	0.06	0.06	0.04
Cr2O3	0.04	0.05	0.07	0.05	0.02	0.04	0.06	0.19	0.03
LOI	0.84	(1.16)	(2.47)	(2.55)	(2.20)	(1.81)	(2.26)	(1.17)	2.56
TOTAL	100.82	98.35	98.23	100.63	99.84	99.73	98.51	97.80	102.38
Ba	12	61	65			50	75	34	177
Ce	20	14	28			28	20	60	41
Cl	nd	30	79			235	34	9	nd
Co	32	42	63			46	47	46	56
Cr	247	328	440	304	126	273	418	1283	231
Cu	239	38	79	131	134	18	50	218	5
Ga	14	13	11			12	13	14	12
La	nd	nd	nd			nd	nd	nd	nd
Mo	nd	3	nd	3	nd	nd	nd	nd	nd
Nb	5	7	4	7	4	4	3	4	2
Ni	229	286	444	403	607	299	304	544	720
Pb	11	15	9	nd	nd	15	nd	16	11
Rb	18	28	55	109	99	41	71	16	109
S	616	nd	251	849	961	23	23	1206	38
Sr	252	145	73	158	92	140	97	37	27
Th	nd	nd	5	nd	16	nd	6	5	nd
U	nd								nd
V	124	108	133	155	91	113	202	207	78
Y	23	39	13	16	31	17	14	17	8
Zn	78	76	65	67	61	70	93	124	126
Zr	35	31	31	34	246	27	31	28	24

1625-1 Highly feldspathic amphibolite
1625-2 Coarse hornblende feldspar amphibolite with biotite
1625-3 Coarse hornblende feldspar amphibolite with biotite
1625-4 Feldspathic amphibolite with biotite
1625-5 Hornblende feldspar amphibolite with biotite
1625-6 Hornblende feldspar amphibolite with biotite
1625-7 Hornblende feldspar amphibolite with biotite
1625-9 Mafic hornblende feldspar amphibolite
1625-10 Micaceous mafic hornblende amphibolite

SD 82 core

107	109	153a
47.92	43.90	45.01
0.54	0.21	0.22
15.81	15.90	18.62
11.19	11.68	9.01
0.13	0.17	0.13
11.28	14.91	13.83
9.25	10.45	11.13
2.12	1.83	1.19
1.49	0.41	0.13
0.05	0.04	0.04
0.05	0.03	0.05
1.53	1.56	1.13
101.36	101.09	100.49
355	185	369
615	2143	161
3	nd	nd
5	4	4
751	873	592
16	6	17
50	17	7
3874	1434	467
87	72	141
134	60	55
30	5	12
85	159	59
36	17	16

107 Feldspathic amphibolite SD-82
109 Hornblende feldspar amphibolite SD-82
153a Feldspathic amphibolite SD-82

SELEBI HOST AMPHIBOLITE continued

SD 82 continued

	153b	110	153c	153d	111	113	114	153e	116	153f	153g	118
SiO2	45.92	44.57	44.44	44.10	45.35	42.45	46.29	46.58	47.86	45.00	45.17	47.05
TiO2	0.22	0.20	0.34	0.20	0.20	0.28	0.22	0.28	0.44	0.30	0.37	0.41
Al2O3	16.94	15.92	18.37	16.85	16.56	20.17	17.77	16.56	21.88	15.64	16.78	16.58
Fe2O3	9.65	10.87	8.97	10.73	10.39	9.03	9.99	9.60	7.71	11.39	10.10	10.56
MnO	0.15	0.14	0.12	0.15	0.16	0.12	0.14	0.15	0.10	0.14	0.12	0.15
MgO	14.40	16.89	13.64	14.48	14.58	14.04	14.46	12.97	7.50	16.16	14.70	12.25
CaO	10.38	9.15	11.92	11.56	9.70	10.18	9.96	12.42	13.71	9.33	8.84	9.70
Na2O	1.09	1.39	1.23	1.40	1.27	1.21	1.21	1.32	1.90	1.25	0.55	1.71
K2O	0.09	0.14	0.15	0.25	0.50	1.02	0.18	0.25	0.20	1.27	3.38	1.58
P2O5	0.04	0.03	0.04	0.04	0.03	0.06	0.04	0.04	0.06	0.04	0.05	0.05
Cr2O3	0.08	0.02	0.02	0.02	0.02	0.04	0.03	0.04	0.04	0.03	0.02	0.03
LOI	1.03	1.04	1.75	1.59	2.07	2.22	1.13	1.38	0.85	1.38	2.05	1.88
TOTAL	99.99	100.36	100.99	101.37	100.83	100.82	101.42	101.59	102.17	101.93	102.13	101.95
Cr	564	133	143	147	130	269	211	250	254	216	171	190
Cu	62	432	177	651	418	606	450	16	919	36	245	78
Mo	4	nd	3	nd	nd	3	nd	nd	nd	nd	3	nd
Nb	3	2	2	4	3	4	3	4	4	3	2	3
Ni	497	702	573	672	936	929	750	447	327	406	550	476
Pb	11	6	7	nd	6	7	8	7	11	12	8	8
Rb	5	7	7	7	22	48	11	9	6	66	137	69
S	313	2590	1580	2630	2590	4560	2580	57	2640	407	1290	731
Sr	119	46	153	66	116	177	102	123	192	29	43	84
V	66	43	79	66	46	64	52	66	106	73	75	110
Y	15	6	17	16	12	14	15	15	22	11	6	24
Zn	47	38	55	44	105	63	71	54	66	83	67	69
Zr	18	17	29	13	20	26	22	23	27	23	24	33

153b Hornblende feldspar amphibolite SD-82
110 Hornblende feldspar amphibolite SD-82
153c Hornblende feldspar amphibolite with feldspar-spinel patches SD-82
153d Hornblende feldspar amphibolite with spinels rimmed by feldspar SD-82
111 Sheared micaceous amphibolite SD-82
113 Hornblende feldspar amphibolite plus large clots of spinel with feldspar coronas SD-82
114 Gedritic hornblende feldspar amphibolite SD-82
153e Hornblende feldspar amphibolite SD-82
116 Coarse feldspathic amphibolite SD-82
153f Coarse micaceous schistose amphibolite SD-82
153g Fine-grained micaceous amphibolite SD-82
118 Hornblende feldspar amphibolite with biotite SD-82

Selebi host amphibolites

	86	87	203	207	265	279	281	284	1625-8
SiO2	53.39	45.27	46.20	47.30	48.38	46.69	49.70	47.23	47.59
TiO2	0.26	0.22	0.33	0.33	0.18	0.38	0.56	0.49	0.82
Al2O3	15.47	18.57	16.37	17.18	17.33	22.37	18.65	16.85	16.11
Fe2O3	10.21	9.31	10.67	9.88	10.48	9.55	8.89	10.43	10.38
MnO	0.16	0.13	0.15	0.15	0.19	0.11	0.14	0.19	0.17
MgO	7.99	13.42	13.45	11.25	14.73	6.58	9.38	10.82	8.95
CaO	6.62	11.74	11.06	10.19	6.18	12.35	10.89	10.78	10.73
Na2O	2.82	1.20	0.80	1.21	1.09	1.76	1.47	0.92	2.15
K2O	1.49	1.03	1.53	2.23	1.55	0.50	1.43	2.65	0.65
P2O5	0.05	0.03	0.05	0.05	0.06	0.04	0.06	0.05	0.11
Cr2O3	0.06	0.04	0.05	0.04	0.04	0.06	0.04	0.07	0.06
LOI	2.04	1.36	(3.46)	(2.58)	(3.34)	(1.42)	(1.29)	(2.59)	(1.16)
TOTAL	100.56	102.32	100.66	99.81	100.21	100.39	101.21	100.48	97.72
Ba									44
Ce									37
Cl									nd
Co									56
Cr	441	299	302	282	246	408	296	440	396
Cu	1055	33	256	10	61	3595	103	6	582
Ga									16
La									nd
Mo	nd	nd	4	nd	nd	nd	4	3	nd
Nb	7	3	4	4	11	5	5	5	5
Ni	552	435	624	344	861	906	353	382	510
Pb	22	7	nd	9	24	29	13	14	24
Rb	57	43	38	83	63	21	57	106	21
S	4462	228							3505
Sr	117	146	16	96	100	276	150	74	133
Th	10		nd	nd	nd	nd	nd	7	5
U	15								
V	88	61	69	93	42	103	126	120	212
Y	69	8	14	7	4	7	12	13	21
Zn	105	79	79	73	89	89	91	132	103
Zr	34	27	23	21	11	29	34	30	54

86 Quartz feldspar amphibolite SD-89
87 Coarse banded feldspathic amphibolite SD-89
203 Sheared altered fine-grained amphibolite SD-79
207 Retrogressed amphibolite with random orientation amphiboles SD-79
265 Retrogressed felspathic amphibolite SD-91
279 Very feldspathic amphibolite SD-96
281 Sheared feldspathic amphibolite SD-96
284 Sheared micaceous amphibolite SD-95
1625-8 Hornblende feldspar amphibolite 1625/100 underground

SELEBI NORTH HOST AMPHIBOLITE

SDN 56

	SN56-1	56-2	56-3	56-4	56-5	56-6	56-7	56-8	56-9	56-10	56-11	56-12	56-13
SiO2	44.76	49.84	46.42	43.33	44.35	33.84	50.91	50.41	46.89	49.22	48.11	49.43	49.35
TiO2	1.39	0.23	0.31	0.37	1.81	3.92	0.29	0.29	0.31	0.23	0.29	0.25	0.27
Al2O3	14.34	4.72	9.68	14.53	10.43	18.42	4.84	5.43	5.99	4.73	5.53	5.00	7.90
Fe2O3	16.32	13.31	12.35	13.01	12.51	17.12	9.80	10.00	12.56	12.40	11.96	12.06	9.91
MnO	0.20	0.21	0.17	0.16	0.16	0.11	0.16	0.16	0.20	0.22	0.22	0.23	0.18
MgO	9.83	26.00	23.81	15.03	19.34	27.68	25.02	25.14	25.32	27.30	25.25	26.91	18.46
CaO	10.33	1.66	3.89	11.20	9.52	2.02	6.59	6.46	3.55	2.56	3.56	3.23	10.89
Na2O	1.58	0.35	0.60	1.63	1.08	0.15	0.64	0.95	0.74	0.78	0.51	0.55	1.35
K2O	1.03	0.17	0.66	0.35	0.17	0.03	0.08	0.07	0.20	0.06	0.06	0.08	0.13
P2O5	0.14	0.04	0.07	0.04	0.27	0.61	0.06	0.07	0.07	0.05	0.03	0.03	0.15
Cr2O3	0.04	0.78	0.82	0.21	0.57	0.06	0.76	1.06	2.47	2.25	2.61	1.59	0.70
LOI	(1.45)	(1.34)	(3.15)	(1.72)	(2.43)	(9.00)	(1.78)	(1.32)	(1.69)	(1.58)	(0.81)	(0.93)	(1.69)
TOTAL	99.46	97.31	98.78	99.86	100.21	102.96	99.15	100.04	98.30	99.80	98.13	99.36	99.29
Cr	236	5270	5420	1400	3810	350	5100	7110	16620	15130	17680	10750	4690
Cu	10	64	89	281	364	604	452	637	1042	358	256	260	60
Mo	nd	nd	nd	nd	3	3	nd	nd	nd	nd	nd	nd	nd
Nb	7	3	4	5	12	17	4	5	4	4	3	4	nd
Ni	164	1650	1610	1350	698	223	1080	1330	1830	1550	1180	1290	839
Pb	8	nd	5	10	7	nd	nd	9	5	nd	nd	10	6
Rb	34	7	32	6	4	5	6	6	8	3	4	5	3
S	436	2330	2780	6210	6280	3720	4430	4850	7820	5310	3930	4000	544
Sr	59	nd	9	23	14	9	8	11	9	6	7	8	14
V	274	65	115	148	178	224	115	114	133	101	120	95	100
Y	36	8	13	15	44	34	12	8	6	7	7	10	11
Zn	114	114	114	64	67	23	102	119	376	183	231	163	82
Zr	63	21	32	62	205	303	21	23	21	20	22	29	21

SDN 56 core complete intersection sampled and analysed

1 Banded hornblende gneiss/hornblende-feldspar amphibolite 126.07-126.87
2 Amphibolitised orthopyroxenite w/cummingtonite 126.87-128.23 cse qtz-fel-hbl pegmatite
3 Amphibole orthopyroxenite (ABI) w/ serpentinite patches towards base 129.72-131.58
4 Hornblende amphibolite ds 131.58-132.65
5 Amphibolite - hornblende w/ pleonaste, orthopyroxene & olivine ds 132.65-133.60
6 Chlorite serpentinite band w/ apatite shear sulphide stringers - As=nd*, Ga=17* 133.60-133.86
7 ds 133.86-135.86 Ba=52*, Ce=45*, La=24*
8 Amphibole orthopyroxenite. minor serp. ds 135.86-137.86
9 minor serp. ds 137.86-139.86
10 Orthopyroxene porphyroblasts in a w/ thin cse anthophyllite band ds 139.86-141.86
11 hornblende matrix. minor serp. patches ds 141.86-142.96
12 minor serp. patches ds 142.96-143.92
13 Hornblende amphibolite 143.92-144.86

SELEBI NORTH 56 continued

	56-14	56-15	56-16	56-17	56-18	56-19	56-20	56-21
SiO2	43.68	43.53	43.93	41.75	46.00	45.44	49.40	48.16
TiO2	0.44	1.34	1.14	0.70	0.74	0.40	0.75	1.24
Al2O3	16.31	14.32	11.63	13.48	12.94	14.50	17.80	19.56
Fe2O3	12.98	12.65	13.78	12.66	11.38	12.67	7.41	6.19
MnO	0.21	0.20	0.24	0.20	0.16	0.16	0.11	0.05
MgO	13.12	14.29	15.88	17.04	20.00	17.56	12.10	14.13
CaO	9.95	8.12	7.67	6.23	5.73	6.62	6.51	4.96
Na2O	1.47	1.39	1.32	1.00	0.96	1.17	2.66	2.33
K2O	1.19	1.73	0.92	2.01	1.73	1.33	3.02	4.29
P2O5	0.04	0.20	0.17	0.06	0.07	0.23	0.05	0.07
Cr2O3	0.62	0.64	3.27	4.08	0.77	0.06	0.14	0.05
LOI	(1.74)	(1.95)	(1.88)	(3.08)	(3.96)	(5.75)	(2.35)	(4.33)
TOTAL	100.01	98.41	99.95	99.21	100.48	100.14	99.95	101.03
Cr	4160	4270	21970	27090	5090	386	950	393
Cu	88	36	200	105	63	64	nd	7
Mo	nd	nd	19	5	nd	nd	nd	nd
Nb	3	7	7	6	6	4	6	10
Ni	953	571	1250	1490	782	839	264	271
Pb	6	8	5	14	9	8	14	20
Rb	39	61	30	63	62	45	122	188
S	594	208	1680	908	781	761	80	147
Sr	53	60	27	23	36	62	271	191
V	131	218	230	230	166	95	135	205
Y	10	23	20	8	17	19	16	10
Zn	177	130	346	384	81	96	65	54
Zr	20	99	63	58	48	24	96	97

SDN 56

14 Banded hornblende-feldspar-biotite gneiss 144.68-145.82
15 Banded hornblende-feldspar-biotite gneiss 145.82-147.82
16 Hornblende amphibolite minor feldspar 147.82-149.82
17 Hornblende amphibolite minor feldspar 149.82-151.82
18 Hornblende amphibolite w/ gedrite minor feldspar 151.82-153.82
19 Hornblende-feldspar-biotite amphibolite 153.82-155.00
20 Feldspar-hornblende-biotite gneiss feldspar porphyroblasts 155.00-156.04
21 Feldspar-hornblende-biotite gneiss 156.04-157.50
22 Grey quartzofeldspathic gneiss 157.50-158.50 see grey gneisses

SELEBI NORTH HOST AMPHIBOLITE continued

	SDN 41							SDN 45 ultramafics				
	163	164	165	166	167	168	169	502	505	507	509	510
SiO2	45.04	47.47	47.39	48.77	45.06	44.32	49.86	40.97	48.62	51.63	46.59	52.33
TiO2	0.38	0.44	0.55	0.75	0.37	1.49	0.35	3.36	0.24	0.35	0.33	0.22
Al2O3	17.05	17.74	14.62	15.64	15.96	13.03	7.41	14.06	5.11	4.36	8.35	5.02
Fe2O3	10.41	9.81	11.23	10.37	11.10	14.08	16.56	15.47	14.48	19.80	15.26	9.47
MnO	0.14	0.13	0.17	0.15	0.12	0.18	0.34	0.24	0.18	0.33*	0.23	0.19
MgO	14.10	11.94	11.16	10.34	14.22	12.85	19.00	11.51	23.35	16.84	15.41	23.63
CaO	9.61	10.65	10.95	11.30	9.68	11.42	3.23	10.56	3.95	5.02	10.43	6.36
Na2O	1.42	1.94	2.03	2.35	1.49	1.45	0.46	1.42	0.54	0.44	1.00	0.64
K2O	1.34	0.83	0.89	0.35	0.93	0.46	1.75	0.38	0.05	0.05	0.20	0.13
P2O5	0.04	0.06	0.06	0.07	0.04	0.17	0.07	0.67	0.04	0.04	0.03	0.07
Cr2O3	0.04	0.03	0.17	0.07	0.04	0.07	0.26	0.04	0.19	0.05	0.07	0.31
LOI	2.31	1.54	1.24	1.29	3.25	1.43	1.53	(1.23)	0.99	1.04	(1.93)	1.82
TOTAL	101.88	102.58	100.35	101.45	102.26	100.95	100.82	98.68	97.74	99.95	97.90	100.19
As	nd*	nd*		nd*								
Ba	138*	71*		45*								
Ce	15*	nd*		20*				37				nd
Cl								113				28
Co								nd				nd
Cr	256	217	405	474	263	511	1750	80				90
Cu	112	65	29	37	81	nd	66	302	1280	334	440	2140
Ga	12*	13*		14*				312	978	391	719	64
La	nd*	nd*		nd*				22				8
Mo	nd	nd	nd	nd	nd	nd	nd	19				nd
Nb	3	nd	3	5	6	7	3	nd	3	nd	nd	nd
Ni	525	382	412	218	482	198	2170	9	4	4	6	5
Pb	12	11	9	11	10	14	5	306	2510	357	300	1590
Rb	58	31	27	12	43	12	55	8	7	nd	nd	5
S	879	497	249	900	1070	54	840	16	3	3	3	4
Sr	81	85	62	78	62	25	14	1120				1180
V	98	104	144	199	93	382	102	38	6	7	19	11
Y	11	12	16	19	19	37	10	403	53	67	84	63
Zn	44	37	53	49	45	128	272	40	9	21	48	10
Zr	24	28	30	42	24	85	21	69	32	95	63	93
								175	18	43	47	20

163 Foliated feldspar-hornblende-biotite amphibolite sheared upper limb SDN 41
164 Foliated feldspar-hornblende-biotite amphibolite sheared upper limb SDN 41
165 Coarse hornblende-feldspar amphibolite/gneiss w/ minor biotite SDN 41
166 Coarse feldspathic amphibolite lower limb SDN 41
167 Feldspar-hornblende-biotite amphibolite sheared & folded lower limb SDN 41
168 Dark, finer-gr. hornblende-rich amphibolite w/ minor feldspar lower limb SDN 41
169 Dark, finer-gr. hornblende-rich amphibolite w/ phlogopite lower limb SDN 41

502 Spotty hornblende-feldspar ampphibolite w/ abundant opaques spots = altered feldspars
505 Coarse weaklyamphibolitised orthopyroxenite SDN 45 w/ minor cummingtonite & gedrite.
507 Black hornblende-rich amphibolite SDN 45
509 Black hornblende-rich amphibolite SDN 45
510 Amphibolitised orthopyroxenite (3? amphs) hbl, ged, cumm. w/ minor phlogopite & chlorite SDN 45

SELEBI NORTH AMPHIBOLITES continued

	SDN 42 garnet amphibolites								
	128	129	131	132	133	134	139	140	143
SiO2	42.23	39.02	41.26	43.38	39.86	43.70	45.83	42.37	41.97
TiO2	0.25	0.19	0.24	0.28	0.20	0.29	0.22	0.15	0.28
Al2O3	14.40	14.85	13.48	14.05	14.97	14.98	15.10	13.15	13.72
Fe2O3	16.64	22.10	20.18	15.86	23.20	16.81	15.14	20.98	18.09
MnO	0.26	0.49	0.36	0.22	0.50*	0.19	0.17	0.25	0.26
MgO	15.06	10.44	12.79	14.57	10.69	11.36	11.22	11.75	12.13
CaO	8.97	9.00	8.80	9.42	7.74	10.96	10.95	8.81	9.94
Na2O	1.01	0.83	0.83	1.13	0.68	1.25	1.48	1.23	1.55
K2O	0.19	0.24	0.20	0.27	0.30	0.36	0.25	0.23	0.31
P2O5	0.04	0.04	0.04	0.04	0.04	0.03	0.03	0.04	0.04
Cr2O3	0.03	0.03	0.04	0.03	0.06	0.06	0.04	0.05	0.03
LOI	1.68	1.66	1.53	1.59	2.14	1.31	0.94	1.47	1.36
TOTAL	100.86	98.89	99.75	100.84	100.38	101.57	101.42	100.48	99.68
As				nd*		nd*			
Cr	217	233	274	215	396	392	292	366	191
Cu	617	1134	701	131	829	24	193	1083	531
Ga				10*		12*			
Mo	nd	nd	3	3	nd	nd	3	nd	nd
Nb	3	2	3	4	3	2	4	2	5
Ni	1160	1180	1130	720	1200	295	759	1410	749
Pb	89	100	53	67	35	59	22	8	24
Rb	4	8	5	11	11	12	8	8	6
S	12360	24090	18390	1200	20370	649	3250	23210	10440
Sr	67	62	76	95	51	99	26	72	61
V	54	61	77	83	56	102	90	80	148
Y	15	11	10	9	13	12	13	11	10
Zn	573	121	345	385	96	138	105	148	128
Zr	27	16	17	16	20	21	18	10	21

SDN 42
128 Coarse dark hornblende-rich amphibolite ds SDN 42
129 Garnet-hornblende mphibolite probed ds SDN 42
131 Garnet-hornblende amphibolite ds SDN 42
132 Coarse dark hornblende-rich amphibolite SDN 42 Ba 64*, Ce nd*, La nd*.
133 Garnet-hornblende amphibolite ds SDN 42
134 Coarse hornblende-feldspar amphibolite SDN 42 Ba 46*, Ce 15*, La nd*
139 Dark hornblende-rich amphibolite SDN 42
140 Garnet-hornblende amphibolite ds SDN 42
143 Dark hornblende-rich amphibolite ds SDN 42

DIKOLOTI-LENTSWE-PHOKOJE HOST ROCKS TO NI-CU MINERALISATION

	DIKOLOTI			DK 32	core	intersection completely sampled and analysed						
	32-600	601	602	603	604	605	606	607	608	609	610	611	612
SiO2	45.84	41.43	47.30	46.96	47.17	48.30	47.47	48.02	45.92	46.27	46.60	47.55	47.04
TiO2	2.65	2.40	0.52	0.45	0.37	0.34	0.28	0.39	0.21	0.23	0.35	0.22	0.23
Al2O3	14.07	13.33	7.24	9.23	8.23	6.27	6.01	2.57	3.00	2.43	3.86	2.83	3.32
Fe2O3	17.08	18.37	14.83	12.75	12.79	13.02	13.38	19.66	15.18	15.78	15.83	16.80	16.82
MnO	0.19	0.09	0.18	0.12	0.17	0.18	0.16	0.19	0.18	0.16	0.15	0.15	0.14
MgO	6.66	15.78	19.03	20.42	23.24	23.37	25.30	25.77	32.87	32.26	30.03	29.99	27.81
CaO	10.24	2.64	6.74	5.88	5.20	6.27	4.96	1.84	0.64	0.66	0.80	0.53	2.07
Na2O	2.06	0.63	0.63	0.66	0.53	0.44	0.43	0.18	0.12	0.09	0.24	0.06	0.24
K2O	0.91	5.62	1.06	2.56	1.31	0.38	0.12	0.11	0.25	0.19	0.78	0.38	0.23
P2O5	0.31	0.34	0.05	0.03	0.03	0.04	0.19	0.04	0.04	0.04	0.03	0.03	0.03
Cr2O3	0.02	0.15	0.34	0.40	0.53	0.53	0.41	0.63	1.00	0.87	0.88	0.96	0.84
LOI	(0.71)	(1.75)	(1.63)	(1.61)	(0.91)	(0.87)	(1.41)	(0.11)	(4.68)	(3.61)	(2.73)	(6.23)	(2.13)
TOTAL	100.03	100.78	97.92	99.46	99.57	99.14	98.71	99.40	99.41	98.98	99.60	99.50	98.77
Ba	97	729	65	167	69	29	nd	22	14	nd	43	19	13
Ce	174	136	71	53	40	51	24	87	67	60	61	79	70
Cl	640	273	nd	nd	nd	nd	37	nd	305	379	223	365	196
Co	60	80	46	69	57	74	77	56	68	68	73	102	65
Cr	108	979	2300	2710	3560	3610	2800	4310	6520	5720	5880	6150	5650
Cu	43	36	12	52	25	21	100	14	27	14	31	90	58
Ga	25	22	12	8	6	3	7	6	6	6	9	4	5
La	62	38	nd	nd	nd	nd	nd	nd	nd	nd	nd	nd	nd
Mo	3	4	3	nd	nd	nd	4	nd	nd	nd	nd	3	nd
Nb	12	14	4	4	4	4	4	5	3	2	3	3	5
Ni	111	482	461	565	663	684	1040	373	1000	826	953	1220	807
Pb	5	6	nd	4	nd	nd	ńd	6	nd	6	nd	nd	ńd
Rb	44	376	75	176	87	30	9	13	32	21	61	33	24
S	1050	874	379	2350	1680	1750	7170	883	1790	939	1960	4500	3110
Sr	157	23	14	14	9	ńd	9	10	7	2	8	4	5
Th	12	5	5										
V	346	307	207	204	150	164	116	243	121	131	143	137	162
Y	43	21	13	13	11	12	5	4	3	4	10	7	5
Zn	59	74	56	44	50	39	35	55	61	57	63	41	55
Zr	217	182	41	22	20	22	21	13	12	25	16	14	nd

600 Hornblende gneiss becomes more hornblende-rich towards base 132.53-133.40
601 *Phlogopite* schist w/ bands of 2 amp. amphibolite (hornblende + fibrous amp) 133.40-133.73
602 *Amphibole* schist w/ *phlogopite* + thin bands of hornblende amp. 133.73-135.17
603 *Amphibole* schist w/ serpentinite patches base gradational 135.17-136.65
604 } *Amphibole (hbl.) orthopyroxenite - coarse* 136.65-138.65
605 } 138.65-140.65
606 } *coarse orthopyroxenite w/ minor hornblende* & serpeninite patches ds 140.65-142.65
607 } & serpeninite bands 142.65-144.65
608 Coarse orthopyroxenite locally w/ serpentine + olivine matrix ds 144.65-146.65
609 a/a 146.65-149.00 149.00-149.30 serpentinite w/ cse fibrous amphibole
610 Coarse orthopyroxenite w/ serpentinite patches 149.30-150.48
611 Serpentine-olivine orthopyroxenite 150.48-152.30
612 Coarse orthopyroxenite w/ serpentinite patches 152.30-154.40

DIKOLOTI 32 continued

	613	614	615	616	617	618	619	620	621	622	623	624	625
SiO2	45.69	47.01	42.31	49.85	47.52	41.57	45.82	37.13	40.53	45.40	43.93	47.10	42.74
TiO2	0.16	0.28	1.43	0.12	0.12	0.24	0.51	0.27	0.11	0.13	0.12	0.11	0.30
Al2O3	3.47	5.50	14.82	2.95	3.07	3.69	7.07	6.77	2.48	3.81	3.05	2.46	5.56
Fe2O3	16.09	13.10	16.24	13.26	14.12	27.67	19.07	29.30	21.68	21.91	16.34	18.26	15.00
MnO	0.16	0.12	0.15	0.17	0.17	0.16	0.22	0.12	0.12	0.12	0.18	0.23	0.12
MgO	31.57	27.49	14.97	23.84	27.41	17.52	18.63	22.40	35.93	25.28	35.55	27.10	32.99
CaO	1.22	2.73	4.62	6.11	5.09	4.22	6.13	2.20	0.38	2.70	0.44	3.01	1.49
Na2O	0.22	0.32	0.74	0.28	0.29	0.36	0.69	0.27	0.05	0.25	0.08	0.23	0.20
K2O	0.09	1.18	4.15	0.07	0.07	0.52	1.14	0.11	0.02	0.06	1.00	0.25	2.06
P2O5	0.03	0.03	0.28	0.03	0.03	0.08	0.07	0.05	0.04	0.05	0.03	0.04	0.42
Cr2O3	0.90	0.63	0.02	1.48	1.62	0.70	1.28	0.55	0.69	0.28	0.78	0.71	0.76
LOI	(7.76)	(3.94)	(2.60)	(0.89)	(2.95)	(3.20)	(1.32)	(6.90)	(9.07)	(4.94)	(7.39)	(3.50)	(7.66)
TOTAL	99.60	98.39	99.73	98.16	99.51	96.73	100.63	99.17	102.03	99.99	101.50	99.50	101.64
Ba	10	83	628	nd	nd	58	95	12	10	nd	355	83	651
Ce	58	32	106	61	75	176	199	115	84	56	49	101	365
Cl	386	165	427	nd	164	nd	47	246	731	132	275	24	224
Co	114	60	75	57	58	863	113	410	120	219	82	153	92
Cr	5660	4170	164	10040	10730	4640	8660	3530	4270	1810	4930	4670	4820
Cu	45	80	120	139	204	5534	463	1510	576	974	354	989	558
Ga	4	7	18	5	2	4	6	6	nd	3	3	3	4
La	nd	nd	37	nd	nd	19	10	5	nd	nd	nd	nd	153
Mo	nd	nd	3	nd	nd	3	nd	4	nd	nd	nd	nd	nd
Nb	4	5	14	6	3	6	4	5	2	5	3	4	6
Ni	1180	697	397	727	1040	1760	638	1830	1080	1540	993	1820	1300
Pb	5	ńd	14	ńd	13	nd	nd	nd	5	ńd	ńd	ńd	7
Rb	13	93	317	4	5	27	68	11	7	9	645	24	179
S	2450	3330	2080	5740	7690	87800	20700	70770	22030	55960	7040	25070	10570
Sr	6	11	32	ńd	ńd	5	16	9	5	9	4	8	179
V	121	150	199	118	108	88	175	81	55	50	95	112	122
Y	nd	12	32	9	9	4	19	8	2	4	2	13	5
Zn	69	56	66	92	112	90	98	273	86	55	98	88	86
Zr	5	10	180	19	12	16	35	18	8	16	9	12	48

613 Serpentinite w/ olivine relicts top & bottom gradational 154.40-155.80
614 Amphibole (hbl.) orthopyroxenite w/ cse bronzites 155.80-156.89
615 Biotite schist w/ feldspar and 2 amphiboles locally cse hbl. gneiss 156.89-157.39
616 As 614 cse ds hbl + sulphide rim opx 157.39-159.00
617 Sheared, banded amphibole (hbl.) orthopyroxenite and serpentinite cse ds 159.00-160.40
618 As 617 grading down into 2 amphibole-*phlogopite* schist w/ abundant ds 160.40-161.71
161.71-162.28 Quartz-feldspar-biotite pegmatite
619 Banded & folded 2 amphibole-*phlogopite* schist ds shear at base 162.28-164.35
620 As 617 abundant ds & sms 164.35-165.96
621 Banded serpentinite and amphibole (hbl.) orthopyroxenite ds 165.97-167.92
622 Amphibole (hbl.) orthopyroxenite w/ serpentinite patches ds 167.92-168.70
623 Serpentinite w/ minor amphibole (hbl.) orthopyroxenite ds 168.70-170.62
624 Amphibole (hbl.) orthopyroxenite ds 170.62-171.52
625 Serpentinite w/ orthopyroxene ds 171.52-173.62

ds = disseminated sulphides sms = semi-massive sulphides ms = massive sulphide

DIKOLOTI 32 continued

	32-626	627	628	629	630
SiO2	45.01	42.69	49.59	51.05	46.36
TiO2	0.11	3.35	2.26	2.17	0.15
Al2O3	6.59	11.77	11.75	12.29	19.76
Fe2O3	14.56	21.64	17.02	17.52	8.81
MnO	0.13	0.26	0.23	0.24	0.14
MgO	26.81	7.56	5.62	5.21	11.62
CaO	5.81	10.94	9.52	10.12	9.74
Na2O	0.50	1.34	2.06	1.77	1.33
K2O	0.08	0.70	0.77	0.55	1.12
P2O5	0.04	0.31	0.21	0.23	0.04
Cr2O3	0.58	0.03	0.02	0.02	0.05
LOI	(5.37)	(0.60)	(0.49)	(0.30)	(2.51)
TOTAL	100.22	100.52	99.05	101.17	99.12
Ba	nd	69	136	142	103
Ce	63	167	100	115	17
Cl	138	1086	2639	2378	149
Co	75	79	49	50	51
Cr	3770	127	124	124	331
Cu	373	180	195	278	35
Ga	6	22	17	19	11
La	nd	55	21	27	nd
Mo	nd	nd	nd	nd	nd
Nb	2	21	11	13	5
Ni	962	97	65	63	398
Pb	8	5	11	13	9
Rb	7	20	44	24	123
S	7680	1630	540	1220	515
Sr	10	55	114	148	118
Th	7	8	8	8	nd
V	79	479	363	379	52
Y	10	57	31	35	3
Zn	106	111	99	105	76
Zr	8	115	139	141	18

626 Amphibole (Kbl.) orthopyroxenite w/ magnetite veinlets base sheared ds 173.62-175.51
627 Spotty hornblende gneiss 175.51-177.55
177.55-179.96 Cse quartz-feldspar-biotite pegmatite
628 Hornblende gneiss 179.96-184.90
629 Hornblende gneiss 184.90-189.80
630 Weakly banded cse feldspathic amphibolite 189.80-201.00 amphibolite continues

DIKOLOTI FELDSPATHIC AMPHIBOLITE

	400	401	402	403	404	411	412	660a	660b	661	662	663
SiO2	42.61	46.33	43.35	44.25	45.97	50.12	48.12	44.25	36.14	46.66	45.90	43.62
TiO2	0.15	0.12	0.05	0.05	0.09	0.22	0.13	0.04	0.03	0.15	0.11	0.04
Al2O3	23.18	13.86	22.75	24.02	26.22	13.46	21.11	23.48	36.70	23.19	15.27	21.52
Fe2O3	13.35	9.15	7.46	7.07	5.62	8.68	6.83	6.09	5.16	6.63	9.87	7.46
MnO	0.21	0.16	0.12	0.12	0.07	0.14	0.11	0.10	0.07	0.11	0.16	0.13
MgO	8.55	18.02	12.14	8.93	6.10	13.14	8.06	9.97	8.23	8.36	15.37	14.27
CaO	7.07	10.16	12.44	11.28	14.68	13.01	13.20	13.22	11.38	13.39	9.65	11.17
Na2O	1.46	1.25	1.19	1.45	1.41	1.05	1.92	1.27	0.68	0.98	1.17	1.00
K2O	1.23	0.19	0.30	0.82	0.32	0.23	0.48	0.39	0.88	1.33	0.37	0.65
P2O5	0.03	0.03	0.02	0.02	0.03	0.03	0.04	0.03	0.03	0.03	0.05	0.03
Cr2O3	0.03	0.14	0.02	0.02	0.02	0.14	0.11	0.01	0.01	0.08	0.08	0.02
(LOI)	1.33	1.47	2.12	3.08	1.18	0.92	1.69	(2.24)	(4.25)	(2.27)	(1.99)	(3.53)
TOTAL	99.20	100.88	101.96	101.11	101.71	101.14	101.57	98.85	99.31	100.91	98.10	99.91
core												
As		10*	nd*	nd*	nd*	nd*						
Ba		nd*	nd*	85*	49*	17*		nd	70	114	39	38
Ce		nd*	nd*	nd*	nd*	nd*		nd	nd	9	nd	nd
Cl								nd	166	nd	nd	32
Co								47	53	39	101	58
Cr	200	929	155	151	105	930	537	73	46	551	535	114
Cu	nd	157	260	337	180	nd	98	349	433	31	303	23
Ga		9*	13*	12*	13*	10*		10	18	13	13	13
La		nd*	nd*	nd*	nd*	nd*		nd	nd	nd	5	nd
Mo	nd	nd	nd	12	nd	nd	nd	nd	7	nd	nd	nd
Nb	2	2	3	3	2	3	3	3	4	4	3	5
Ni	81	506	530	555	165	195	288	504	451	210	612	580
Pb	9	nd	6	nd	5	nd	11	nd	nd	6	8	nd
Rb	110	9	29	106	42	15	55	42	92	123	33	64
S	155	1270	1550	2360	1120	29	841	1880	2950	27	2380	nd
Sr	100	28	107	135	160	60	131	185	305	146	40	126
Th		nd	nd	nd	nd	nd	nd	nd	nd	8	5	7
U		nd	nd	nd	nd	nd	nd					
V	46	74	17	26	53	146	82	18	14	89	72	25
Y	3	5	2	nd	4	7	6	3	2	7	4	nd
Zn	68	60	80	75	49	51	45	49	138	56	79	67
Zr	14	12	8	9	14	17	17	10	7	13	9	7

400 Garnetiferous hornblende-feldspar gneiss adjacent to DK ultrabasics DK 20
401 Coarse hornblende-rich amphibolite DK 20
402 Feldspathic amphibolite w/ sapphirine-spinel aggregates DK 20
403 Foliated amphibolite w/ laminae of orthoamphibole-chlorite + minor sap-spi. DK 20
404 Feldspathic amphibolite DK 20
411 Coarse amphibolite DK 30
412 Coarse gabbroic feldspathic amphibolite DK 30
660a Feldspathic amphibolite DK 23
660b Large corundum-sapphirine-spinel aggregate in 660a separated out DK 23
661 Feldspathic amphibolite w/ small sapphirine-spinel aggregates DK 23
662 Hornblende-rich amphibolite DK 23
663 Foliated amphibolite w/ laminae of orthoamphibole-clinozoisite + minor sap-spi DK 23

DIKOLOTI-LENTSWE-PHOKOJE HOST ROCKS TO NI-CU MINERALISATION continued

	SERPENTINISED PERIDOTITES								AMPHIBOLE (HBL.) PYROXENITES			
	335	341	349	350	363	380	657a	657b	340	379	392	397
SiO2	41.87	50.58	42.80	38.86	41.23	39.80	45.60	43.47	49.84	48.39	44.41	48.22
TiO2	0.13	0.19	0.16	0.13	0.15	0.11	0.17	0.15	0.08	0.17	0.25	0.42
Al2O3	2.51	4.80	2.52	2.53	3.80	2.78	3.91	3.19	2.38	5.39	4.15	4.55
Fe2O3	17.83	11.53	11.68	11.73	16.42	13.62	13.38	14.37	13.76	11.12	23.02	13.41
MnO	0.14	0.07	0.21	0.17	0.16	0.13	0.16	0.11	0.14	0.15	0.23	0.15
MgO	32.46	28.18	35.55	36.36	32.36	35.89	34.01	37.23	29.84	28.64	24.74	27.03
CaO	0.31	0.23	1.01	0.53	1.20	0.26	0.66	0.59	1.05	3.40	0.88	3.64
Na2O	0.12	0.36	0.15	0.15	0.17	0.06	0.20	0.17	0.28	0.56	0.23	0.49
K2O	0.36	2.08	0.05	0.02	0.89	0.01	1.47	0.92	0.56	0.30	0.17	0.13
P2O5	0.03	0.02	0.04	0.02	0.03	0.03	0.03	0.05	0.04	0.05	0.03	0.06
Cr2O3	1.25	0.83	1.08	1.11	1.09	0.83	1.03	1.11	0.16	0.39	0.91	0.07
LOI	3.82	3.53	6.52	10.53	4.08	6.54	(4.30)	(7.42)	1.54	2.44	1.08	2.00
TOTAL	100.83	102.40	101.77	102.14	101.58	100.06	100.62	101.36	99.67	101.00	100.10	100.17
As					nd*	nd*						
Ba					43*	30*	67	37				
Ce					nd*	nd*	37	49				
Cl							208	324				
Co							59	77				
Cr	8570	5650	7420	7600	7440	5670	6750	7000	1090	2660	6220	507
Cu	103	51	162	21	715	386	150	246	285	137	536	456
Ga					5*	4*	7	3				
La					nd*	nd*	nd	nd				
Mo	3	nd	nd	3	3	4	nd	4	nd	nd	3	3
Nb	nd	3	3	3	5	3	4	5	3	4	nd	4
Ni	337	326	1880	1150	1340	1380	531	755	1170	581	631	1670
Pb	7	7	5	4	5	nd	nd	7	nd	9	nd	5
Rb	30	186	9	9	81	6	183	105	46	29	13	10
S	5060	1320	9730	2470	14040	14590	5120	6500	13030	4730	24670	18690
Sr	6	9	4	6	6	6	8	6	5	6	4	9
V	88	73	83	68	101	60	68	66	28	60	114	81
Y	4	nd	3	4	4	4	4	4	10	9	8	11
Zn	101	66	136	140	70	77	77	73	65	50	183	32
Zr	7	8	14	13	11	8	11	20	8	23	11	19

core

335 Orthopyroxene serpentinite ds PJ 2
341 Phlogopite-orthopyroxenite w/ serp. PJ 2 (A PYROXENITE).
349 Orthopyroxene serpentinite ds LT 19
350 Serpentinite with olivine relicts ds LT 19
363 Orthopyroxene serpentinite ds LT 20
380 Serpentinised peridotite ds LT 33
657a Serpentinised peridotite ds DK 17
657b Serpentinised peridotite ds DK 17

340 Amphibole (Abl) orthopyroxenite ds PJ 2
379 Coarse orthopyroxenite ds LT 33
392 Amphibole (Abl.) orthopyroxenite with magnetite ds Th & U nd, DK 20
397 Orthopyroxenite ds DK 20

	AMPH.	PYROX.	cont.	ULTRAMAFIC assoc. with AMPHIBOLITES – PYROXENITES					AMPHIBOLITES assoc. with MAGNETITE QUARTZITE		
	410	417	655	325	333	348	364	381	331	339	370a
SiO2	45.83	50.54	45.38	53.18	50.60	51.40	53.06	51.87	54.38	55.73	52.37
TiO2	0.23	0.24	0.23	0.14	0.27	0.15	0.18	0.16	0.04	0.06	0.27
Al2O3	3.23	4.01	3.53	2.98	3.24	3.46	4.73	4.30	1.58	1.61	2.62
Fe2O3	20.09	13.94	20.32	14.34	18.91	11.98	8.74	14.84	15.14	18.10	17.20
MnO	0.22	0.28	0.19	0.17	0.20	0.27	0.16	0.40	0.17	0.34	0.18
MgO	22.82	25.59	23.46	21.66	22.98	26.65	23.57	23.88	16.14	20.61	20.71
CaO	3.52	0.44	3.59	5.39	1.52	2.48	7.57	0.96	11.42	1.28	3.56
Na2O	0.44	0.28	0.38	0.26	0.24	0.34	0.60	0.35	0.35	0.22	0.30
K2O	0.11	1.77	0.15	0.09	1.14	2.03	1.65	2.00	0.09	0.08	0.05
P2O5	0.15	0.02	0.65	0.02	0.03	0.02	0.03	0.02	0.07	0.03	0.03
Cr2O3	0.22	0.46	0.70	0.27	1.08	1.04	0.45	0.58	0.00	0.01	0.19
LOI	1.11	2.34	(1.26)	2.21	1.76	2.45	1.42	(1.36)	1.25	0.84	(0.77)
TOTAL	98.79	99.91	98.58	100.71	101.97	102.27	102.16	100.72	100.63	98.91	97.58
As	nd*				nd*						
Ba	39*		nd		76*						nd
Ce	nd*		88		nd*						81
Cl			295								nd
Co			120								51
Cr	7140	3150	4730	1840	7380	7100	3080	3970	16	56	1320
Cu	601	150	451	198	6	70	23	17	77	nd	99
Ga	6*		11		8*						2
La	3*		18		nd*						13
Mo	4	3	3	4	3	4	3	4	3	nd	nd
Nb	4	5	nd	3	5	3	9	8	4	3	2
Ni	1060	767	621	1140	631	603	525	955	412	250	628
Pb	nd	nd	6	nd	nd	6	nd	nd	5	nd	7
Rb	7	159	9	7	62	265	163	186	4	6	5
S	28720	9020	25560	1060	3010	3210	76	574	2068	42	3070
Sr	8	5	5	5	12	6	10	6	5	nd	nd
V	127	42	265	60	156	99	66	58	49	26	89
Y	11	10	6	13	10	12	20	6	41	9	9
Zn	115	149	79	98	77	189	61	182	27	57	47
Zr	19	6	12	15	13	16	21	13	9	11	12

core

410 Amphibole (Abl.) orthopyroxenite ds DK 30
417 Orthopyroxene amphibolite ds DK 30
655 Amphibole (Abl.) orthopyroxenite ds DK 17

325 Mg amphibolite adjacent to ms PJ 1
333 Coarse cummingtonite amphibolite ds PJ 1
348 Phlogopite amphibolite ds LT 19
364 Mg amphibolite LT 20
381 Phlogopite amphibolite Th & U nd, LT 33

331 Actinolite amphibolite within } MAG. QUARTZITE PJ 1
339 Cummingtonite amphibolite within } PJ 2
370a Cummingtonite-hornblende amphibolite within finely banded quartzite-amphibolite LT 26

DIKOLOTI-LENTSWE-PHOKOJE HOST ROCKS TO NI-CU MINERALISATION continued

LENTSWE LT 27 core intersection completely sampled and analysed

	LT27-2	27-3	27-4	27-5	27-6	27-7	27-8	27-9	27-10	27-11	27-12	27-13	27-14
SiO2	50.29	40.73	44.97	42.86	48.33	44.13	45.87	45.66	51.57	38.28	46.25	48.89	43.37
TiO2	1.23	1.28	0.15	1.12	0.32	2.58	0.48	1.02	0.17	0.27	0.59	0.22	1.20
Al2O3	11.86	14.45	3.20	13.79	6.73	12.57	7.35	12.53	2.92	2.65	7.56	4.45	12.53
Fe2O3	13.20	17.04	14.98	14.95	16.55	18.20	18.32	13.52	13.78	31.77	19.21	16.51	12.31
MnO	0.15	0.03	0.15	0.07	0.22	0.16	0.19	0.09	0.13	0.19	0.24	0.18	0.07
MgO	10.96	19.07	34.07	18.02	19.03	13.03	20.85	18.93	26.98	27.32	16.44	23.14	22.50
CaO	9.50	0.53	1.20	3.52	4.76	5.49	4.10	4.06	2.44	0.56	6.62	3.83	3.44
Na2O	1.80	0.64	0.24	0.72	0.47	1.07	0.35	0.63	0.32	0.20	0.74	0.28	0.75
K2O	1.01	7.47	1.11	5.63	1.66	3.57	2.61	4.71	0.42	0.06	0.99	0.74	4.77
P2O5	0.17	0.25	0.04	0.41	0.07	0.30	0.17	0.17	0.05	0.05	0.13	0.05	0.29
Cr2O3	0.12	0.02	1.22	0.02	0.43	0.09	0.63	0.25	1.09	1.19	1.02	1.45	0.00
LOI	(1.07)	(1.98)	(3.76)	(2.41)	(3.09)	(2.06)	(4.87)	(1.79)	(1.09)	(7.47)	(1.45)	(2.28)	(3.48)
TOTAL	100.29	101.51	101.33	101.11	98.57	101.19	100.92	101.57	99.87	102.54	99.79	99.74	101.23
Ba	82	618	54	433	80								
Ce	92	95	72	92	86								
Cl	468	599	450	627	106								
Co	62	100	78	82	89								
Cr	788	150	8030	163	2880	632	4090	1680	7380	7560	6870	9690	20
Cu	23	319	39	197	300	134	405	30	79	5500	1870	421	402
Ga	17	19	5	17	10								
La	31	15	nd	19	nd								
Mo	nd	nd	nd	3	8	nd	6	nd	nd	nd	3	nd	nd
Nb	12	10	3	14	9	29	6	7	4	2	5	5	8
Ni	250	482	1230	552	790	361	961	342	969	713	717	670	435
Pb	10	10	5	15	17	13	12	12	8	17	7	nd	9
Rb	56	567	76	434	119	236	196	341	26	9	50	51	339
S	780	12780	3420	4520	10620	5240	22700	663	2690	27570	10650	11000	10430
Sr	118	12	9	15	10	27	8	23	nd	6	12	6	14
Th	8	8	4			6		9					4
V	217	151	98	139	104	318	144	148	90	291	158	134	157
Y	36	8	10	27	33	102	21	33	8	3	33	13	19
Zn	59	62	95	62	87	59	83	71	86	45	93	83	38
Zr	126	131	14	145	63	215	45	113	18	9	54	25	136

27-2 Hornblende gneiss grading down to hornblende-biotite amphibolite at base 98.58-99.38
3 *Phlogopite*-magnetite schist shear zone ds 99.38-99.51
4 Serpentine-*phlogopite* amphibolite (schist) ds 99.51-100.99
5 *Phlogopite* schist shear zone ds 100.99-101.54
6 2 amphibole-*phlogopite* schist (fibrous + hbl.) ds 101.54-102.62
7 Hornblende-biotite gneiss ds 103.02-103.84
8 Fine-grained, 2 amphibole-*Phlogopite* schist (hbl.-poor) w/ metachert ? ds 103.84-104.27
9 2 amphibole-*phlogopite* gneiss (hbl.-rich) *phlogopite* shears 104.53-105.46
10 Amphibole (*Abl.*) orthopyroxenite ds 105.46-107.14
11 Serpentinite w/ relicts of peridotite abundant magnetite ds 107.14-109.58
12 Hornblende amphibolite (w/ minor fibrous amp. & plag.) ds 109.58-110.19
13 Amphibolite (2 amps hbl.-poor) ds 110.19-110.79
14 *Phlogopite*-magnetite schist ds 110.79-111.66
Lt 27-1 grey quartz-feldspar-biotite gneiss 98.40

LENTSWE 27 continued

	27-15	27-16	27-17	27-18	27-19	27-20	27-21	27-22	27-23	27-24	27-25	27-26
SiO2	46.20	45.81	45.35	43.34	51.44	46.58	47.70	41.16	47.84	42.86	44.82	40.92
TiO2	0.21	0.29	0.33	2.21	0.19	0.18	0.15	2.35	0.18	0.17	0.19	0.18
Al2O3	5.24	7.48	4.39	14.62	4.60	3.86	3.54	12.20	3.91	3.83	2.96	3.06
Fe2O3	17.05	11.23	13.35	15.64	14.03	16.78	14.62	21.40	16.56	17.21	22.77	23.00
MnO	0.19	0.20	0.21	0.12	0.18	0.18	0.18	0.18	0.15	0.15	0.15	0.12
MgO	27.01	31.40	33.15	19.17	27.55	29.55	30.03	14.26	28.67	34.51	26.46	31.88
CaO	1.98	3.58	1.55	0.44	0.49	0.41	0.60	5.62	0.51	0.88	0.32	0.27
Na2O	0.32	0.16	0.19	0.65	0.11	0.11	0.08	0.90	0.06	0.13	0.07	0.07
K2O	0.10	0.20	0.90	6.43	1.61	0.64	0.17	2.56	0.14	0.03	0.06	0.03
P2O5	0.04	0.04	0.03	0.04	0.04	0.03	0.04	0.47	0.05	0.04	0.05	0.05
Cr2O3	1.49	0.90	1.12	0.07	1.09	1.08	1.00	0.00	1.22	1.04	1.00	1.10
LOI	(3.97)	(5.31)	(7.82)	(2.92)	(4.61)	(4.95)	(2.04)	(1.50)	(1.23)	(7.41)	(3.51)	(4.67)
TOTAL	99.83	101.29	100.57	102.73	101.33	99.40	98.11	101.10	99.29	100.85	98.85	100.68
Cr	9780	5850	7090	441	7100	7030	6730	11	8260	6620	6600	7210
Cu	374	84	144	649	222	317	199	23	345	229	1540	738
Mo	nd	3	nd	4	nd	nd	nd	nd	nd	nd	nd	3
Nb	2	3	10	53	4	3	3	12	3	nd	nd	2
Ni	562	647	1070	1010	819	1060	978	79	1030	773	2300	1570
Pb	nd	5	6	24	nd	nd	5	6	nd	nd	7	nd
Rb	12	18	70	518	130	52	16	140	12	7	9	5
S	10780	2700	4830	1720	9880	12050	8490	630	15920	7300	46310	29510
Sr	10	6	6	11	9	7	5	18	4	4	4	nd
Th		6										
V	98	87	88	190	86	98	81	310	93	62	110	81
Y	7	15	23	5	8	2	2	32	5	4	nd	3
Zn	130	83	69	110	68	66	64	43	63	49	40	48
Zr	16	24	13	23	8	9	11	189	12	12	14	15

27-15 Bronzite pyroxenite ds 111.66-112.50
16 Serpentinised peridotite ds 112.50-114.75
17 a/a 114.75-118.07
18 *Phlogopite* schist 118.07-118.55
19 Serpentinite w/ asbestiform amphibole veins ds 118.55-120.40
20 Serpentinised peridotite w/ amphibole veins ds 120.40-121.02
21 Amphibole (*Abl.*) orthopyroxenite w/ serp. patches ds 121.02-122.43
22 Hornblende-biotite amphibolite w/ magnetite & minor plag. 122.43-124.15
23 Amphibole (*Abl.*) orthopyroxenite ds 124.15-125.58
24 Serpentinised peridotite ds 125.58-126.95
25 Amphibole (*Abl.*) orthopyroxenite ds 126.95-127.47
26 Serpentinite w/ amphibole veins ds 127.47-128.43

DIKOLOTI-LENTSWE-PHOKOJE HOST ROCKS TO NI-CU MINERALISATION continued

	LENTSWE 27 continued						
	27-27	27-28	27-29	27-30	327	332	667
SiO2	44.67	46.32	42.09	58.92	84.93	61.50	78.74
TiO2	0.22	0.22	2.30	0.48	0.03	0.02	0.00
Al2O3	3.50	3.97	15.16	6.13	0.66	0.50	1.11
Fe2O3	19.12	19.75	17.93	16.79	8.84	37.34	19.04
MnO	0.14	0.16	0.11	0.18	0.10	0.02	0.04
MgO	29.50	26.75	14.30	11.33	4.79	1.52	1.14
CaO	0.33	0.81	1.71	3.67	1.96	1.27	0.80
Na2O	0.06	0.10	0.77	0.81	0.02	0.12	0.00
K2O	0.11	0.30	6.16	0.65	0.03	0.04	0.00
P2O5	0.04	0.05	0.28	0.11	0.03	0.07	0.08
Cr2O3	1.06	1.05	0.02	0.13	0.00	0.00	0.00
LOI	(2.20)	(2.63)	(1.79)	(1.30)	0.46	-1.11	(0.33)
TOTAL	98.75	99.48	100.83	99.20	101.85	101.30	100.95
Ba	nd	20	660	138			nd
Ce	92	73	127	81			19
Cl	195	166	724	96			nd
Co	104	149	83	73			118
Cr	7110	7020	121	899	16	22	7
Cu	433	571	111	301	100	39	378
Ga	4	5	25	8			2
La	nd	nd	21	23			nd
Mo	nd	nd	3	nd	3	3	3
Nb	3	2	29	3	4	2	nd
Ni	1070	1400	263	585	278	106	475
Pb	6	9	14	8	nd	13	nd
Rb	14	24	428	38	4	8	4
S	18210	22940	3550	21630	3591	554	17500
Sr	6	4	26	50	4	5	4
V	98	119	269	93	24	25	21
Y	4	8	36	13	6	7	6
Zn	50	66	60	43	32	nd	25
Zr	18	18	232	70	6	6	6

27-27 Amphibole (Abl) orthopyroxenite ds 128.43-130.50
28 Amphibolite banded w/ serpentinite ds 130.50-130.87
29 Sheared biotite-hornblende-plagioclase-garnet-magnetite schist ds 130.87-131.63
30 Banded amphibolite and quartzite (2-3 amphiboles) ds 131.63-132.45
132.45-133.36 sms in banded amphibolite-quartzite
after 133.36 pink-grey medium gr. granitic gneiss

327 Finely banded quartz-magnetite w/ amphibole laminae PJ 1
332 Finely banded quartz-magnetite PJ 1
667 Finely banded quartz-magnetite LT 30

OUTCROPPING AMPHIBOLITES ASSOCIATED WITH MAGNETITE QUARTZITE.

	17-8 2a2	24-8 1d	24-8 1j	24-8 3d	24-8 3x	4-9 1c	14-9 1j	14-9 1m	14-9 1o	24-9 1a	24-9 4a	24-9 5b	24-9 5e
SiO2	56.82	54.85	68.72	53.72	54.71	50.03	60.04	55.96	54.52	51.04	54.51	55.56	59.15
TiO2	0.06	0.04	0.01	0.05	0.11	0.34	0.05	0.04	0.07	0.43	0.07	0.05	0.04
Al2O3	0.98	0.62	0.82	0.89	0.92	5.53	1.47	0.81	1.98	6.20	0.84	1.10	0.78
Fe2O3	17.86	18.71	11.17	18.63	17.39	16.86	9.70	17.24	13.92	12.51	20.24	18.78	17.09
MnO	0.32	0.30	0.13	0.41	0.33	0.28	0.16	0.60	0.30	0.22	0.47	0.48	0.40
MgO	18.33	19.78	11.69	20.98	19.99	18.11	17.28	22.05	16.72	16.47	20.03	20.23	17.65
CaO	3.33	3.13	6.60	3.29	4.30	6.82	9.72	2.83	11.13	10.98	2.15	3.30	4.10
Na2O	0.13	0.10	0.12	0.12	0.17	0.66	0.16	0.06	0.29	0.58	0.06	0.13	0.05
K2O	0.02	0.01	0.05	0.02	0.02	0.11	0.04	0.02	0.07	0.11	0.03	0.05	0.02
P2O5	0.06	0.02	0.03	0.22	0.04	0.06	0.04	0.01	0.04	0.03	0.02	0.09	0.02
Cr2O3	0.00	0.01	0.00	0.00	0.01	0.23	0.01	0.01	0.01	0.24	0.01	0.02	0.00
LOI	(0.66)	(0.78)	(0.95)	(0.68)	(0.80)	(0.67)	(0.95)	(0.87)	(0.98)	(0.81)	(0.76)	(0.91)	(0.89)
TOTAL	97.91	97.57	99.34	98.33	97.29	99.03	98.67	99.63	99.05	98.81	98.43	99.79	99.30
As				nd*	nd*	nd*	8*	nd*	nd*				nd*
Cr	10	73	27	26	89	1550	39	72	36	1665	47	127	21
Cu	5	9	19	4	nd	10	5	nd	35	nd	nd	9	9
Ga				1*	2*	8*	4*	2*	4*				2*
La				5*	4*	4*	2*	nd*	nd*				nd*
Mo	3	nd		4	nd	nd	nd	nd	3	nd	nd	nd	nd
Nb	6	3		6	4	6	3	3	3	5	nd	5	3
Ni	339	269	163	285	359	229	392	294	308	390	270	254	212
Pb	10	7	7	14	nd	8	nd	7	5	nd	nd	nd	nd
Rb	2	4		3	5	5	2	5	3	nd	2	2	nd
Sr	nd	nd		10	nd	15	8	nd	10	9	5	5	6
Th	5	nd	nd	6	nd	6	6	6	7				nd
U				nd	nd	nd	nd		nd				nd
V	106	38	69	60	102	122	58	35	102	170	51	57	55
Y	45	18		22	36	13	39	6	35	14	14	21	24
Zn	44	76	66	63	64	82	30	51	52	96	71	80	78
Zr	12	11		7	11	23	9	9	8#	35	7	10	6

17-8-2a2 Massive amphibolite cummingtonite (+ talc?) Phokoje
24-8-1d Massive amphibolite cummingtonite Mogolodi South
24-8-1j Well-banded quartz-amphibole rock actinolite Mogolodi South
24-8-3d Massive amphibolite cummingtonite Mogolodi North Ba 71*, Ce nd*,
24-8-3x Massive amphibolite cummingtonite Mogolodi North Ba nd*, Ce nd*,
4-9-1c Banded amphibolite cummingtonite + thin hornblende bands Lethlakane Ba 81*, Ce nd*,
14-9-1j Amphibolite actinolite with minor quartz bands, Seloka Ba 24*, Ce nd*,
14-9-1m Massive amphibolite cummingtonite Seloka Ba nd*, Ce nd*,
14-9-1o Massive amphibolite actinolite Seloka Ba 58*, Ce nd*,
24-9-1a Massive amphibolite hornblende Lethlakane River South
24-9-4a Massive amphibolite cummingtonite Lethlakane River South
24-9-5b Massive amphibolite cummingtonite Lethlakane River South
24-9-5e Well-banded amphibolite cummingtonite and thin (2mm) quartz bands Let. R. S., Ba 109*, Ce nd*,

DIKOLOTI-LENTSWE-PHOKOJE HORNBLENDE GNEISSES of the Selebi-Phikwe Banded Gneisses, not enclosed within the ultramafic assemblage

	334	351	354	355	372	373	382	390	406	407	666
SiO2	48.01	50.72	47.79	47.65	50.66	40.24	49.56	50.26	49.80	41.57	41.04
TiO2	1.09	1.22	1.49	1.64	2.34	3.72	0.88	2.02	2.27	2.75	1.83
Al2O3	14.39	14.03	13.11	15.43	12.41	11.98	14.39	12.00	12.19	11.04	12.97
Fe2O3	15.89	14.40	16.44	18.94	15.79	21.51	12.71	16.12	16.98	22.32	18.20
MnO	0.21	0.15	0.16	0.09	0.22	0.19	0.17	0.27	0.21	0.24	0.22
MgO	5.66	5.62	7.53	8.88	5.59	9.03	7.73	5.73	5.08	7.57	12.13
CaO	12.01	8.12	7.84	2.27	9.59	10.43	10.02	9.42	10.20	11.95	9.80
Na2O	2.21	3.27	1.97	0.76	2.56	2.00	1.78	2.07	2.02	1.57	1.35
K2O	0.78	1.20	2.04	6.23	1.10	0.72	1.36	1.04	0.63	0.60	0.40
P2O5	0.11	0.20	0.11	0.16	0.21	0.33	0.09	0.20	0.22	0.29	0.39
Cr2O3	0.03	0.02	0.01	0.01	0.01	0.02	0.04	0.02	0.01	0.02	0.04
LOI	0.64	1.34	(1.59)	(1.33)	(0.47)	0.66	1.07	(0.87)	0.36	0.92	(1.79)
TOTAL	101.03	100.29	98.49	102.06	100.48	100.83	99.80	99.15	99.97	100.84	98.37
Ba								208			37
Ce								94			130
Cl								1907			129
Co								56			69
Cr	210	116	96	94	100	122	255	193	85	160	253
Cu	42	64	120	79	316	135	nd	200	233	82	25
Ga								20			22
La								30			24
Mo	5	3	5	5	nd	3	nd	4	3	nd	nd
Nb	7	5	5	7	10	28	3	10	12	12	7
Ni	89	183	398	99	69	149	100	77	63	85	235
Pb	4	16	nd	12	13	13	10	12	8	5	9
Rb	25	62	112	386	42	13	64	48	15	13	10
S	562	2810				4420	562	384	632	1040	nd
Sr	94	131	84	72	152	50	101	107	123	60	56
Th					10				6		
U									nd		
V	286	183	386	303	418	450	228	463	330	454	356
Y	26	34	20	25	34	61	25	29	33	43	40
Zn	54	59	46	45	128	92	46	99	86	116	50
Zr	58	91	45	80	134	304	62	129	140	136	202

334 Well-banded coarse-grained hornblende gneiss (w/ pyroxene ?) PJ 1
351 Fine-grained hornblende gneiss LT 19
354 Mafic hornblende gneiss w/ minor biotite LT 20
355 Biotite-garnet-hornblende-feldspar-magnetite schist assoc. w/ quartzite LT 20
372 Hornblende gneiss LT 31
373 Mafic hornblende gneiss/amphibolite w/ fine ds LT 31
382 Coarse hornblende gneiss w/ minor ds LT 33
390 Hornblende gneiss DK 20
406 Hornblende gneiss DK 30
407 Hornblende gneiss/amphibolite w/ cse magnetite DK 30
Gradation from 406 to 407 adjacent to massive sulphide (ms)
666 Hornblende amphibolite/gneiss LT 25

DIKOLOTI-LENTSWE-PHOKOJE HORNBLENDE GNEISSES enclosed within the ultramafics

	326	328	338	342	362	375	376	409	665	377	399
SiO2	49.40	49.46	49.24	38.38	41.07	48.02	40.08	45.62	43.06	45.52	45.87
TiO2	1.54	1.45	1.55	1.93	2.37	2.40	1.68	1.15	3.01	0.24	0.16
Al2O3	14.27	13.33	13.97	12.94	13.98	14.27	14.72	14.61	13.34	15.69	13.11
Fe2O3	14.01	14.33	13.56	24.93	21.93	13.99	23.61	14.86	18.30	14.15	10.81
MnO	0.09	0.10	0.11	0.19	0.26	0.22	0.22	0.21	0.33	0.14	0.20
MgO	7.81	10.69	10.81	8.46	7.43	7.27	12.69	9.70	7.86	10.14	15.32
CaO	6.62	6.47	4.44	9.31	11.29	8.99	1.65	11.69	9.58	10.63	10.02
Na2O	2.73	2.52	2.00	1.72	1.45	3.10	0.54	1.18	2.02	1.37	1.23
K2O	2.15	1.09	3.70	1.08	0.70	0.83	3.89	1.00	1.05	1.60	0.63
P2O5	0.07	0.08	0.09	0.54	0.46	0.32	0.21	0.10	0.38	0.04	0.04
Cr2O3	0.03	0.03	0.01	0.00	0.03	0.02	0.03	0.05	0.02	0.09	0.14
LOI	1.64	3.02	1.25	1.56	(1.13)	(0.80)	(1.49)	1.78	(1.08)	(2.47)	(1.56)
TOTAL	100.36	102.57	100.73	101.04	100.97	99.43	99.32	101.95	98.95	99.61	97.53
Ba						82	467		155		26
Ce						212	84		157		nd
Cl						631	387		780		165
Co						43	49		87		67
Cr	184	187	91	30	199	130	179	363	152	570	965
Cu	145	6	nd	286	193	61	44	65	92	193	6
Ga						26	17		25		10
La						42	nd		65		nd
Mo	4	nd	nd	nd	4	nd	4	6	4	nd	4
Nb	8	12	10	8	8	39	8	5	15	4	nd
Ni	287	273	296	570	120	122	156	110	132	266	392
Pb	11	7	6	9	26	13	13	nd	10	7	4
Rb	125	53	182	39	37	30	248	78	40	79	49
S	4090	748	170	14550		1510	1330	1650	4160		nd
Sr	133	92	96	54	118	130	16	65	100	58	22
Th							nd		nd	nd	nd
V	232	149	95	323	424	332	355	338	475	161	100
Y	23	26	17	53	34	144	54	22	54	11	6
Zn	36	35	33	112	53	53	38	68	83	34	67
Zr	69	71	91	163	198	212	133	45	234	16	18

326 Foliated felsic hornblende gneiss assoc. w/ Fe formation PJ 1
328 Coarse sheared hornblende-feldspar-chlorite gneiss PJ 1
338 Feldspar-2 amphibole-biotite gneiss PJ 2
342 Hornblende gneiss/amphibolite w/ abundant magnetite adjacent to ms LT 13
362 Mafic hornblende gneiss w/ magnetite & ds LT 20
375 Spotty felsic hornblende gneiss LT 33
376 Coarse garnet-biotite schist LT 33
409 Hornblende gneiss DK 30
665 Hornblende gneiss DK 30

Coarse amphibolites similar to Phikwe host amphibolite
377 Coarse hornblende-feldspar amphibolite LT 33
399 Coarse hornblende-feldspar amphibolite DK 20

1212 data are regarded as satisfatory. The main difference is that the Nottingham Zr data are consistently higher (see Table A.1). There was no correlation between the Southampton 1212 and 1400 As analyses The 1212 As analyses have not been tabulated.

Ba, Ce, Cl, Ga and La were not measured on the Southampton 1212, but on the 1400 spectrometers. Southampton analyses on the 1400 spectrometer (which are listed in pages A.10 to A.31) are indicated - *. Note that only analyses obtained from the Southampton 1212 spectrometer have been used in this thesis. The data has not been mixed up.

	Detection Limits ppm			Repeated Analyses								
	S1	S2	N	S1	S2	N	S1	S2	N	S1	S2	N
				Ultramafic Rock			Grey Gneiss			HG		
As				nd	nd		nd	nd		nd	nd	
Ba		13	10	365	401		460	481		136	133	
Ce		15	8	nd	28		99	126		41	60	
Cr	4	4		5960	5611	5178	33	38	39	261	192	196
Cu	5	1.5		14	nd	8	18	9	25	49	41	49
Ga		1	1		8	6		21	22		15	14
La		5	5		1	nd		55	62		15	11
Mo	3	2		nd	2		nd	2		nd	2	
Nb	2	2		4	4	nd	12	14	14	7	6	4
Ni	2	1.5		998	1087	1135	56	53	57	105	96	98
Pb	5	3		nd	nd	3	17	14	23	5	4	8
Rb	2	2		125	121	127	76	75	76	12	9	8
Sr	4	2		7	5	4	202	193	194	145	143	145
Th	5	3		7	4		18	17		7	4	
U	5	5		nd	2		nd	nd		nd	nd	
V	5	5		62	68	54	100	104	108	173	195	215
Y	2	2		6	3	4	34	31	35	21	21	25
Zn	5	1		118	118	121	87	87	96	86	84	83
Zr	2	2		73	61	82	245	241	244	81	85	88

Table A.1 Analyses at Southampton and Nottingham for comparison. All are in ppm. Detection limits are tabulated at the right; nd = not detected.

Analyses are tabulated in pages A.10 to A.31. Major components

are in wt%. Trace elements are in ppm. If there is a blank space, no analysis has been attempted for that sample. nd means that the element is present in a concentration below the detection limit. LOI = Loss on ignition. If LOI is indicated thus (LOI), a fluxed sample has been used and LOI is not included in the total. All comparative treatment of major component chemistries has been undertaken with analyses recalculated to 100 % excluding LOI and iron sulphide.

Appendix Bibliography

Cosgrove, M.E. 1972. The geochemistry of the red beds of south-east England, including the Permian volcanics. Unpub. Ph.D thesis,, Univ. Southampton, 136pp.